UNIVERSITY OF CALIFORNIA

Los Angeles

Modern Applications of Scattering Amplitudes and Topological Phases

A dissertation submitted in partial satisfaction

of the requirements for the degree

Doctor of Philosophy in Physics

by

Julio Parra Martinez

2020

ABSTRACT OF THE DISSERTATION

Modern Applications of Scattering Amplitudes and Topological Phases

by

Julio Parra Martinez

Doctor of Philosophy in Physics

University of California, Los Angeles, 2020

Professor Zvi Bern, Chair

In this dissertation we discuss some novel applications of the methods of scattering amplitudes and topological phases. First, we describe on-shell tools to calculate anomalous dimensions in effective field theories with higer-dimension operators. Using such tools we prove and apply a new perturbative non-renormalization theorem, and we explore the structure of the two-loop anomalous dimension matrix of dimension-six operators in the Standard Model Effective Theory (SMEFT). Second, we introduce new methods to calculate the classical limit of gravitational scattering amplitudes. Using these methods, in conjunction with eikonal techniques, we calculate the classical gravitational deflection angle of massive and massles particles in a variety of theories, which reveal graviton dominance beyond 't Hooft's. Finally, we point out that different choices of Gliozzi-Scherk-Olive (GSO) projections in superstring theory can be conveniently understood by the inclusion of fermionic invertible topological phases, or equivalently topological superconductors, on the worldsheet. We explain how the classification of fermionic topological phases, recently achieved by the condensed matter community, provides a complete and systematic classification of ten-dimensional superstrings and gives a new perspective on the K-theoretic classification of D-branes.

The dissertation of Julio Parra Martinez is approved.

Clifford Cheung

Eric D'Hoker

Terence Chi-Shen Tao

Zvi Bern, Committee Chair

University of California, Los Angeles

2020

For my mother, the Mathematician, who inspired my life in science.

Para mi madre, la Matemática, quien inspiró mi vida en la ciencia.

Contents

List of Figures

Acknowledgements

I am indebted to my advisor, Zvi Bern, for his support and enthusiasm, for giving me freedom and encouragement to explore my own ideas, and for teaching me how to do physics during many long drives up and down the coast of California. Next I am most grateful to Enrico Herrmann for his continued mentorship and for being a wonderful collaborator; and to Thomas Dumitrescu for setting an example and serving at times as a second advisor. In addition, I wish to express my gratitude to Eric D'Hoker, Per Kraus and Michael Gurperle for all their help and for creating a stimulating atmosphere in the fourth floor of PAB; and to Clifford Cheung, Eric D'Hoker and Terence Tao for serving in my committee. I am also thankful to the postdocs in our group: Weiming Chen, Andrés Luna, Ben Michel and Christoph Uhlemann, and specially Mao Zeng and Chia-Hsien Shen for teaching me lots of physics during many long (and sometimes heated) discussions. I must also acknowledge my collaborators: Zvi Bern, John Joseph Carrasco, Weiming Chen, Alex Edison, Michael Enciso, Johannes Henn, Enrico Herrmann, Harald Ita, Henrik Johansson, Justin Kaidi, David Kosower, Radu Roiban, Michael Ruf, Eric Sawyer, Yuji Tachikawa, Jaroslav Trnka and Mao Zeng. In addition, I should mention many other physicists that have helped me and from whom I have learnt so much: José Adolfo de Azcárraga, José Bernabeu, Jake Bourjaily, Simon Caron-Huot, Lance Dixon, Juanjo Gómez Cadenas, Matt Heydeman, Callum Jones, Ricardo Monteiro, Isobel Nicholson, Donal O'Connel, Shruti Parajanpe, David Skinner, Mikhail Solon and many others that I do not have space to mention here.

My time in graduate school would have been so much worse without my fellow students. I am most grateful to Alex Edison and Michael Enciso for their friendship (and for getting me out of the office), to Allic Sivaranakrishnan for letting me borrow his brains, and to Justin Kaidi for letting be borrow his branes.

Finally, I need to thank my family for their love and everything they have done for me, even from far away; specially Young, who always was there, and here and everywhere.

My work has been supported by the US Deparment of State through a Fulbright Scholarship and by the Mani L. Bhaumik Institute for Theoretical physics.

Contribution of authors

Chapter 1, which serves as an introduction, draws from Refs. [1–6] in collaboration with the authors detailed below. Chapter 2 is adapted from Refs. [1, 2] in collaboration with Zvi Bern and Eric Sawyer. Chapter 3 is adapted from Ref. [3] with Zvi Bern, Harald Ita and Michael Ruf, and Ref. [4] with Michael Ruf and Mao Zeng. Chapter 4 is adapted from Refs. [5, 6] with Justin Kaidi and Yuji Tachikawa. Appendix 4.D, included in Ref. [6], is based on conversations with Edward Witten. Appendix 4.F, also included in Ref. [6], is kindly contributed by Arun Debray. Other works, in collaboration with various authors, completed during the course of my doctoral candidacy (Refs. [7–14]), are not included in this thesis.

Vita

Institution	Position	Year
Universitat de València	Grado en Física	2010-2014
University of Cambridge	MASt in Applied Mathematics	2014-2015
University of California Los Angeles	Fulbright Scholar	2015-2017
University of California Los Angeles	Graduate Student Researcher	2017-2020

Publications

- Z. Bern, J. Parra-Martinez, and E. Sawyer, "Structure of two-loop SMEFT anomalous dimensions via on-shell methods", (2020), arXiv:2005.12917 [hep-ph].
- J. Parra-Martinez, M. S. Ruf, and M. Zeng, "Extremal black hole scattering at $O(G^3)$: graviton dominance, eikonal exponentiation, and differential equations", (2020), arXiv:2005.04236 [hep-th].
- Z. Bern, H. Ita, J. Parra-Martinez, and M. S. Ruf, "Universality in the classical limit of massless gravitational scattering", Phys. Rev. Lett. **125**, 031601 (2020), arXiv:2002.02459 [hep-th].
- J. Kaidi, J. Parra-Martinez, and Y. Tachikawa, "Topological Superconductors on Superstring Worldsheets", SciPost Phys. **9**, 10 (2020), arXiv:1911.11780 [hep-th].
- Z. Bern, J. Parra-Martinez, and E. Sawyer, "Nonrenormalization and Operator Mixing via On-Shell Methods", Phys. Rev. Lett. **124**, 051601 (2020), arXiv:1910.05831 [hep-ph].
- E. Herrmann and J. Parra-Martinez, "Logarithmic forms and differential equations for Feynman integrals", JHEP **02**, 099 (2020), arXiv:1909.04777 [hep-th].
- A. Edison, E. Herrmann, J. Parra-Martinez, and J. Trnka, "Gravity loop integrands from the ultraviolet", (2019), arXiv:1909.02003 [hep-th].

- J. Kaidi, J. Parra-Martinez, and Y. Tachikawa, "Classification of String Theories via Topological Phases", Phys. Rev. Lett. **124**, 121601 (2020), arXiv:1908.04805 [hep-th].
- Z. Bern, D. Kosower, and J. Parra-Martinez, "Two-loop n-point anomalous amplitudes in N=4 supergravity", Proc. Roy. Soc. Lond. A **A476**, 20190722 (2020), arXiv:1905.05151 [hep-th].
- J. Henn, E. Herrmann, and J. Parra-Martinez, "Bootstrapping two-loop Feynman integrals for planar $\mathcal{N} = 4$ sYM", JHEP **10**, 059 (2018), arXiv:1806.06072 [hep-th].
- Z. Bern, J. J. Carrasco, W.-M. Chen, A. Edison, H. Johansson, J. Parra-Martinez, R. Roiban, and M. Zeng, "Ultraviolet Properties of $\mathcal{N} = 8$ Supergravity at Five Loops", Phys. Rev. D **98**, 086021 (2018), arXiv:1804.09311 [hep-th].
- Z. Bern, A. Edison, D. Kosower, and J. Parra-Martinez, "Curvature-squared multiplets, evanescent effects, and the U(1) anomaly in $N = 4$ supergravity", Phys. Rev. D **96**, 066004 (2017), arXiv:1706.01486 [hep-th].
- Z. Bern, J. Parra-Martinez, and R. Roiban, "Canceling the U(1) Anomaly in the S Matrix of N=4 Supergravity", Phys. Rev. Lett. **121**, 101604 (2018), arXiv:1712.03928 [hep-th].
- Z. Bern, M. Enciso, J. Parra-Martinez, and M. Zeng, "Manifesting enhanced cancellations in supergravity: integrands versus integrals", JHEP **05**, 137 (2017), arXiv:1703.08927 [hep-th].

Chapter 1

Introduction

Through the last century, Quantum Field Theory (QFT) has emerged as the mathematical framework that accurately describes most aspects of fundamental physics. QFT has enabled our understanding of all kinds of phenomena: from the interactions of fundamental particles probed at immense colliders, and the large scale structure of the universe we observe in the sky, to the physics of phase transitions in condensed matter systems measured in tabletop experiments. Even our incomplete grasp of string theory and quantum gravity is deeply rooted in worldsheet conformal field theory and low energy effective field theory (EFT) descriptions. Despite many successes and continued progress over the years, the mathematical structure of QFT remains poorly understood. Still a multitude of tools have been developed which have multiple applications and connect different branches of physics and mathematics. Scattering Amplitudes and Topological Phases are two prominent examples of such tools.

Scattering amplitudes describe the probabilities of particle collisions at colliders. Traditionally computed perturbatively using Feyman diagrams, they nowadays are commonly calculated using *on-shell methods*, which recycle physical information from lower-point processes and lower orders in perturbation theory via recursion and unitarity, thus avoiding gauge redundancies and combinatorial explosion. The on-shell mindset for computing physical quantities has found application beyond collision events to other parts of fundamental

physics, as well as unveiled beatiful mathematical structures that point toward a new understanding of QFT.

The study of topological phases has its roots in the low energy descriptions of lattice models commonly used to model condense matter systems. Such low energy descriptions take the form of topological quantum field theories (TQFT), whose mathematical foundation is in firmer ground compared to general QFTs. Among many kinds of TQFTs, Symmetry Protected Topological (SPT) phases have played a prominent role over the last decade, in part because of their connection to anomalies (i.e. obstructions to gauging a symmetry) of interest for high-energy physicists. Anomalies are one of the few available tools for attacking strongly coupled QFTs. 't Hooft anomaly matching has been a general tool succesfully used to investigate phases of QFT and dualities even at strong coupling. Famously, this technique was used to understand the low energy effective field theory of mesons in QCD, and also contributed to the discovery of dualities in QFT. Renewed insight coming both from the high energy and condensed matter communities, has unveiled a widely larger landscape of symmetries, phases and anomalies than was previously known.

This thesis is devoted to several novel applications of the methods of Scattering Amplitudes and Topological Phases. Herein I will describe how on-shell methods can be used to explore the structure of the renormalization group in the Standard Model Effective Field Theory (SMEFT), as well as to compute classical gravitational observables relevant for the study of gravitational waves at LIGO. Furthermore, I will explain how recent insights from condensed matter physics clarify the structure of string worldsheet theories and provide a complete classification of ten-dimensional superstring theories, including new previously unnoticed examples.

On-shell methods for the Standard Model Effective Field Theory

The discovery of the Higgs boson has established the Standard Model of particle physics as the fundamental theory that describes our universe (with the notable exceptions of gravity, dark matter and dark energy). A key challenge in particle physics is to identify physics beyond the Standard Model. Because current experimental data at colliders is well described by the Standard Model, it is unclear which theoretical direction will ultimately prove to be the one chosen by Nature. It is therefore important to quantify new physics beyond the Standard Model in a systematic, model-independent manner. The theoretical framework for doing so is via effective field theories that extend the Standard Model. Such effective theories augment the Standard Model Lagrangian by adding higher-dimension operators [15, 16]:

$$\Delta\mathcal{L} = \sum_i c_i \mathcal{O}_i \,, \tag{1.1}$$

with Wilson coefficients c_i suppressed by powers of the unknown high-energy scale of new physics, Λ, as dictated by the dimension of $\mathcal{O}_i$. The resulting theory, known as the Standard Model Effective Field Theory (SMEFT), is reviewed in Ref. [17].

As for all quantum field theories, renormalization induces mixing of these operators which is parameterized by the renormalization group equation,

$$\frac{\partial c_i}{\partial \log \mu} = \gamma_{ij}^{\mathrm{UV}} c_j \,, \tag{1.2}$$

where $\gamma_{ij}^{\mathrm{UV}}$ is the anomalous-dimension matrix and μ is the renormalization scale. The knowledge of such renormalization effects is key to translate measurements at low energy to bounds on the Wilson coefficients, c_i, and the scale of new physics, Λ.

Usually, $\gamma_{ij}^{\mathrm{UV}}$ is calculated perturbatively in the Standard Model couplings by analyzing

ultraviolet divergences in matrix elements of the higher-dimension operators. The complete one-loop anomalous-dimension matrix for operators up to dimension six has been computed in Refs. [18–21]. These calculations reveal a number of vanishing entries related to supersymmetry [22, 23], which seem surprising at first because there are valid Feynman diagrams that can be written down. These zeros have been elegantly explained [24] using tree-level helicity selection rules [25], which set certain classes of tree-level amplitudes to zero. The tree-level vanishings imply through unitarity that certain logarithms and their associated anomalous dimensions are not present. Although these selection rules are reminiscent of supersymmetric ones, they hold for generic massless quantum field theories in four dimensions. At first sight, it seems rather unlikely that there are new nontrivial zeros beyond one loop because the helicity selection rules fail to hold at loop level.

In Chapter 2 of this thesis, based on Refs. [1, 2], we will describe new on-shell methods to extract anomalous dimension from unitarity cuts. Such methods, instead of relying on ultraviolet divergences in matrix elements, directly target the renormalization group dependence in physical logarithms. This approach will allow us to unveil further structure in the anomalous dimensions beyond one loop. Using on-shell methods we will prove a multi-loop perturbative non-renormalization, theorem which predicts new zeros in the anomalous dimension matrix of dimension-six operators up to four loops. Furthermore, we will calculate full one-loop matrix elements and explain how judicious choices of renormalization schemes at one loop can generate even further zeros in the anomalous dimensions at two loops. Our results make precise predictions about the two-loop anomalous dimension matrix of the SMEFT, which simplify the structure of the renormalization group at this order.

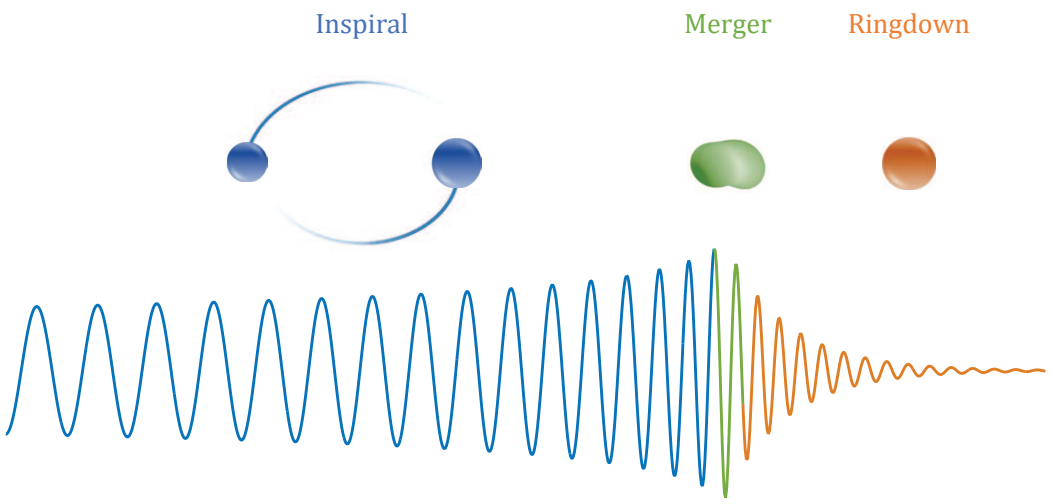

Figure 1.1: Phases of a binary merger. Reproduced from Ref. [28] with permission from the authors.

Scattering Amplitudes and Classical Gravitational Observables

The spectacular observation of gravitational waves by the LIGO/Virgo Collaboration [26, 27] has opened a new window into the universe. It is hard to overstate the discovery prospects of gravitational wave astronomy, from studying the properties and population of black holes, neutron stars to test of General Relativity. The binary merger events observed at LIGO consist of several phases illustrated in Fig. 1.1.

Amongst the different phases of a binary merger, the inspiral phase is amenable to perturbative methods such as the Post-Newtonian (PN) and Post-Minkowskian (PM) expansions (expansions in powers of the velocity in units of the speed of light, v/c, and Newton's gravitational constant, G, respectively). Scattering amplitudes in gravity are also calculated in perturbation theory in G. While scattering processes may seem rather different from the bound-state problem of gravitational-wave generation, the underlying physics is the same. In particular, classical two-body potentials can be extracted from scattering processes [29–40], including new state-of-the-art calculations [41, 42]. This approach leverages the huge

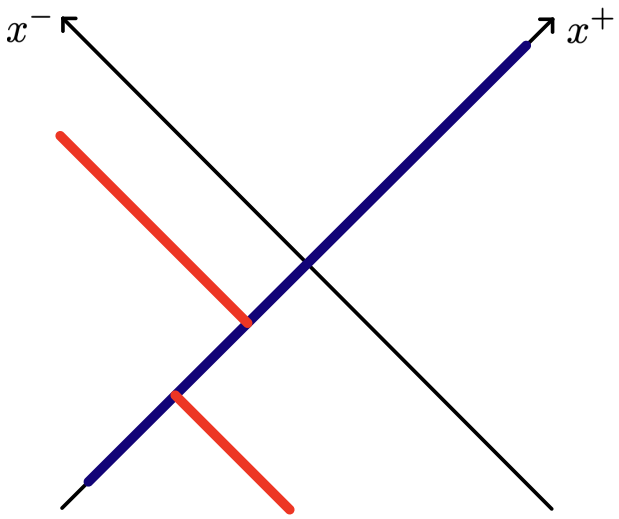

Figure 1.2: Geodesic motion (red line) in shockwave background generated by boosted particle (blue line).

advances in computing quantum scattering amplitudes that stem from the modern unitarity method [43–47] and from double-copy relations [48–52] between gauge and gravity theories.

Beyond its interest for gravitational wave physics, the high-energy behavior of gravitational-scattering processes has a long and interesting history as a fundamental probe of gravitational theories at the classical and quantum level (see e.g. Refs. [53–61]). The simplicity of scattering in the high-energy limit makes it a natural regime to extract information about high-orders in perturbation theory. A famous result by 't Hooft shows that the leading high-energy behaviour or four-point gravitational amplitudes dominated by the exchange of gravitons and takes the form

$$\mathcal{M} \sim \frac{\Gamma(1-iGE^2)}{\Gamma(1+iGE^2)} \frac{GE^2}{q^2} \left(\frac{1}{q^2}\right)^{iGE^2} , \tag{1.3}$$

where q is the momentum transfer, and the exponent is known as the eikonal phase. This result implies that both the amplitude and classical deflection angle are universal and do not depend on the particle content of the theory. The proof of this result relies on two key facts: First, the gravitational coupling grows with two powers of the energy, GE^2, which is faster

than other forces. Second, the gravitational field of a highly boosted particle is described the Aixelburg-Sexl shockwave metric[1]

$$ds^2 = -dx^+dx^- + Gp^+ \log(\boldsymbol{x}_\perp^2)(dx^+)^2 + d\boldsymbol{x}_\perp^2 \tag{1.4}$$

which is an exact solution to Einstein's equations. Thus, at this order any high-energy gravitational proces is described by the semiclassical motion of a geodesic in the shockwave background geometry as illustrated in Fig. 1.2.

Beyond the leading order, such semiclassical description is not valid. Furthermore, by naive power-counting the coupling to other force mediators is comparable to gravity. Because of these reasons, the description of high-energy scattering is more complicated, and one does not expect a universal behavior. Still, using insight from string amplitudes and the analyticity of scattering amplitudes, Amati, Ciafaloni and Veneziano (ACV) [61] worked out the high-energy limit of massless graviton scattering through $O(G^3)$ in General Relativity long before it became technically feasible to compute two-loop scattering amplitudes in quantum field theory directly. Using this they calculated the corresponding correction to the gravitational deflection angle of massless particles in General Relativity.

The possibility of using quantum scattering amplitudes to obtain the classical deflection angle was also recently promoted by Damour [62], who used the ACV result for the conservative scattering angle to impose constraints on classical two-body Hamiltonians of the type used for gravitational-wave template construction [63, 64]. In a very recent paper [65], however, Damour has cast doubt on the program of using quantum scattering amplitudes to extract information on classical dynamics. His central claim is that both the classical scattering angle derived by ACV and the $\mathcal{O}(G^3)$ two-body Hamiltonian derived by Bern *et al.* in Refs. [41, 42] are not correct. His claims, based on information obtained from the self-force (small mass ratio) expansion [66, 67] of the bound-state dynamics as well as struc-

[1]This metric is given in lightcone coordinates $x^\pm = x^0 \pm x^1$, and $\boldsymbol{x}_\perp$ denotes the transverse directions.

tural properties in the results of Ref. [42], provide results with a smooth transition between massive and massless classical scattering. This property is not satisfied by the results of ACV and Bern *et al.*, which are not smoothly connected by the high-energy limit. This has led Damour to criticize the methods of Refs. [39, 41, 42], with particular focus on the velocity resummation and treatment of infrared divergences.

In Chapter 3 of this thesis, based on Refs. [3, 4], we show how the recent computation of two-loop four-graviton scattering amplitudes in General Relativity in conjunction with traditional eikonal resummation methods allows for a first-principles computation of the $\mathcal{O}(G^3)$ massless gravitational scattering angle, which agrees with the result of ACV. The same techniques allow a calculation of the deflection angle for $\mathcal{N} \geq 4$ Supergravity. Furthermore we develop alternative methods to perform the classical expansion of massive amplitudes and to calculate their full velocity dependence via the modern method of differential equations for Feynman integrals. We apply these new methods to study the scattering of extremal black holes in $\mathcal{N} = 8$ Supergravity [68–70]. By comparing both massive and massless results in Supergravity and General Relativity, we find that the high-energy behavior of the classical amplitudes and scattering angle remains universal at $\mathcal{O}(G^3)$. While lacking a proof, this provides overwhelming evidence that, counter to all expectations, 't Hooft's graviton dominance extends to subleading orders. Furthermore it supports the conclusion that both the ACV result and the results of Bern *et al.* are correct.

Topological Phases in String theory

Superstring theory is the only known example of a consistent framework for a theory of quantum gravity. Despite the inherent difficulty in measuring quantum gravitational effects, which put any measurable consequences of any such theory beyond the realm of current experimental verification, the study of string theory has brought many general lessons which have advanced our understanding of fundamental physics and mathematics.

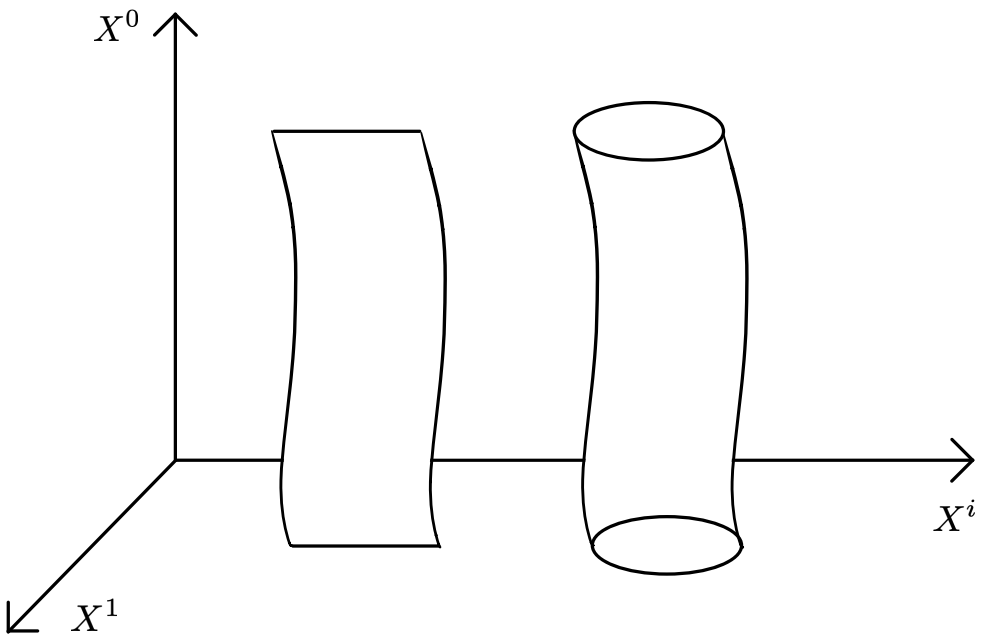

Figure 1.3: Pictorial representation of open and closed string worldsheets.

The most traditional method for studying superstring theory is via superstring perturbation theory. In this setting, the string is described by a worlsheet CFT with bosonic scalar fields X^μ, which describe the motion of the string in a target spacetime, as depicted in Fig. 1.3. In the Neveu-Schwarz-Ramond (NSR) formalism, in addition to the bosonic fields, the worldsheet theory contains fermionic worldsheet spinors, ψ^μ, which are spacetime vectors. Consistency requires that the theory is subjected to a process known as the Gliozzi-Scherk-Olive (GSO) projection [71, 72]. It is well-known that there are various possible choices of consistent GSO projections, which yield different superstring theories such as type IIA and IIB, among others. In the standard textbook presentation e.g. in [73], allowed GSO projections are determined by imposing various consistency conditions, such as the modular invariance of torus amplitudes. That the GSO projections gives consistent results in higher genus amplitudes is not immediately clear in this presentation.

A formulation which works equally well for higher genera was found by Seiberg and Witten in [74]. There, it was pointed out that the GSO projection is a summation over the

spin structures of the worldsheet, and that different GSO projections correspond to different possible phases assigned to spin structures in a way compatible with the cutting and the gluing of the worldsheet. In particular, it was found that the different signs appearing in type IIA and type IIB GSO projections are given by an invariant of the spin structure known as the Arf invariant. The Arf invariant is of order 2, which is closely related to the fact that there are only two type II theories.

Thanks to the developments initiated in condensed matter physics in the last decade, we now have a more physical understanding of this Arf invariant. Namely, it is the partition function of the low-energy limit of the 1+1d symmetry-protected topological (SPT) phase known as the Kitaev chain [75]. In general, the low-energy limit of an SPT phase is known as an invertible phase [76, 77]. An invertible phase is a topological quantum field theory (TQFT) with a unique ground state on any spatial manifold, and whose partition function on a closed manifold is a phase (in the sense of a complex number of absolute value one) which behaves consistently under the cutting and gluing of the spacetime manifold. Conversely, it is now known that any such consistently-assigned phase is given by the partition function of an invertible theory. Furthermore, there is now a general classification of possible invertible phases, or equivalently SPT phases, in terms of bordism groups [77–79]. This means that, with the technology currently available to us, we can now not only understand the consistency of a given GSO projection, but also enumerate all possible GSO projections.

In Chapter 4 of this thesis, based on Refs. [5, 6], we revisit known GSO projections from this modern viewpoint, and also find new ones. We will restrict ourselves to projections which treat all fermions in the same manner – more general projections, which necessarily break spacetime Lorentz invariance, would be interesting to study. We review how the Arf invariant distinguishes the type IIA and IIB theories, and we explain how the same invariant allows for a classification of type 0 superstrings (which do not have spacetime supersymmetry).

The same approach also allows us to clarify the structure of unoriented worldsheet theories. For example, the Kitaev chain is known to be compatible with a parity transformation

Ω such that $\Omega^2 = (-1)^F$, where F is the fermion number operator. Also, it is known that eight copies of the Kitaev chain protected by this symmetry are continuously connected to a completely trivial theory [80]. In this case, the partition function of the low-energy limit of the Kitaev chain is known as the Arf-Brown-Kervaire (ABK) invariant, and is of order 8. If one considers an unoriented NSR wordsheet theory with $\Omega^2 = (-1)^F$, such a worldsheet is said to have a pin$^-$ structure, which is a generalization of the concept of a spin structure to unoriented manifolds (see e.g. Appendix A of [81] for an introduction). The ABK invariant generates the group of invertible phases with pin$^-$ structure. This means that when we perform the GSO projection, or equivalently when we sum over the pin$^-$ structures, we can now include n copies of the ABK invariant. This leads to a series of unoriented type 0 string theories, labeled by n mod 8, some of which have been discussed in the existing literature [82–91]. A similar approach lets us identify worldsheets with $\Omega^2 = 1$ as carrying a pin$^+$ structure, and allows a complete classification. We can also ask whether it is possible to modify the GSO projection of the type I theory. In the type II theory, the left- and right-moving fermions couple to independent spin structures. This means that the worldsheet fermions of the type I theory have neither pin$^+$ nor pin$^-$ structure; rather, one needs to consider the spin structure on the orientation double cover of the worldsheet [90, 91]. We will see below that there are nontrivial invertible phases for this structure, but that they will not lead to any genuinely new type I theory.

We also point out that our viewpoint provides a complementary way to understand the dependence of the K-theoretic classification of D-branes [92] on the choice of the GSO projection. For example, two type II theories differ by the presence of the Arf invariant, or equivalently the Kitaev chain on the worldsheet. Famously, the Kitaev chain has an unpaired fermionic zero mode on its boundary. This explains the fact that the boundary condition for the type IIA non-BPS D9-brane has an unpaired boundary fermion as originally observed in [93]. Mathematically, the presence of n boundary fermions corresponds to the existence of the action of the Clifford algebra $\mathrm{Cl}(n)$, and the K-group $K^n(X)$ is defined in terms of

unitary bundles with a specified action of $\mathrm{Cl}(n)$ [94]. With this observation, we see that the type IIB and type IIA theories have D-branes classified by $K^0(X)$ and $K^1(X)$, respectively. Similarly, when we have n copies of the ABK invariant, we have n boundary fermions, leading to the existence of the action of the Clifford algebra $\mathrm{Cl}(\pm n)$. This means that the unoriented pin$^-$ type 0 theory labeled by n mod 8 has D-branes classified by $KO^{+n}(X) \oplus KO^{-n}(X)$.

Chapter 2

On-shell methods for the Standard Model Effective Theory

2.1 Introduction

Effective Field Theory (EFT) approaches have risen to prominence in recent years as a systematic means for quantifying new physics beyond the Standard Model. The Standard Model Effective Field Theory (SMEFT) incorporates the effects of new physics via higher-dimension operators built from Standard Model fields [15, 17]. The operators are organized according to their dimension, which gives a measure of their importance at low-energy scales. The SMEFT allows exploration of the effects of new physics without requiring a complete understanding of the more fundamental high-energy theory. While systematic, the SMEFT involves a large number of operators and free coefficients [16], making it useful to develop improved techniques for computing quantities of physical interest and for understanding their structure. One such quantity is the anomalous dimension matrix of the higher-dimension operators. The appearance of anomalous dimensions implies that the Wilson coefficients of operators at scales accessible by collider experiments differ from those at the high-energy matching scale to the more fundamental unknown theory. These also control operator mix-

ing, providing important information on how experimental constraints from one operator affect the coefficients of other operators. This makes evaluating the anomalous dimension matrix a crucial aspect of interpreting results within the SMEFT. Towards this goal, here we apply on-shell methods that greatly streamline the computation of anomalous dimensions at one and two loops and expose hidden structure.

A systematic and complete computation of the one-loop anomalous dimension matrix for dimension-six operators in the SMEFT is found in the landmark calculations of Refs. [19–21]. Besides their importance for interpreting experimental data, these calculations reveal a remarkable structure with the appearance of nontrivial zeros in the anomalous dimension matrix [22]. These one-loop zeros have been understood as stemming from selection rules that arise from supersymmetry embeddings [23], helicity [24], operator lengths [1], and angular momentum [95]. Perhaps even more surprisingly, nontrivial zeros in the anomalous dimension matrix of the SMEFT appear at any loop order and for operators of any dimension [1]. In addition, a surprising number of the associated one-loop scattering amplitudes vanish as well [95, 96], suggesting additional zeros may appear in the anomalous dimensions at two loops. Here we apply on-shell methods to identify a new set of vanishing terms in the two-loop anomalous dimension matrix of the SMEFT. As a by product of our two-loop study, we also confirm many one-loop anomalous dimensions computed in Refs. [19–21], via both the generalized unitarity method [43, 44, 97] and an elegant new unitarity-based method due to Caron-Huot and Wilhelm for directly extracting anomalous dimensions from cuts [98], which builds on insight developed in earlier work on $\mathcal{N} = 4$ super-Yang-Mills theory [99, 100].

On-shell methods have proven to be quite useful in a variety of other settings, including collider physics (see e.g. Refs. [101–103]), ultraviolet properties of (super)gravity (see e.g. Refs. [10, 104–106]), theoretical explorations of supersymmetric gauge and gravity theories (see e.g. Refs. [8, 12, 13, 107–111]), cosmological observables (see e.g. Refs. [112–118]), and gravitational-wave physics (see e.g. Refs. [3, 40–42, 119] as well as Refs. [4, 120], which are included in Chapter 3 of this thesis). They have also been used as a convenient means for

classifying interactions in EFTs such as the SMEFT [121–125]. In addition, general properties of the S-matrix, such as unitarity, causality and analyticity have been used to constrain Wilson coefficients of EFTs [126], including the SMEFT [127, 128].

In the context of anomalous dimensions and renormalization-group analyses, unitarity cuts give us direct access to renormalization-scale dependence. After subtracting infrared singularities, the renormalization-scale dependence can be read off from remaining dimensional imbalances in the arguments of logarithms [105]. The direct link between anomalous dimensions at any loop order and unitarity cuts is made explicit in the formulation of Caron-Huot and Wilhelm [98]. In carrying out our two-loop analysis we make extensive use of their formulation. Very recently the same formalism and general set of ideas was applied in Refs. [129–131] to compute certain SMEFT anomalous dimensions.

In general, two-loop unitarity cuts include both three-particle cuts between two tree-level objects, as well as two-particle cuts between tree-level and one-loop objects. Consequently, our exploration of two-loop anomalous dimensions will require computing one-loop matrix elements first. On-shell methods, in particular generalized unitary [43–46, 97, 132, 133], are especially well suited for this task. Because we feed one-loop matrix elements into higher-loop calculations, we find it convenient to use D-dimensional techniques which account for rational terms. To carry out the integration, we decompose the integrands into gauge-invariant tensors along the lines of Refs. [9, 134, 135]. In this form, the integrands can be straightforwardly reduced to a basis of scalar integrals using integration by parts technology (as implemented, e.g., in FIRE [136–138]). These one-loop amplitudes are among the building blocks that feed into the two-loop anomalous dimension calculation.

Using the unitarity-based formalism, we indeed find that many potential contributions to the two-loop anomalous dimension matrix vanish for a variety of reasons, including the appearance of only scaleless integrals [1], color selection rules, vanishing rational terms at one loop, as well as appropriate renormalization scheme choices at one loop. Of the new vanishings, perhaps the most surprising is the finding that additional zeros can be induced

at two loops by slightly adjusting the $\overline{\text{MS}}$ renormalization scheme at one loop. This is tied to the fact that two-loop anomalous dimensions and local rational contributions to one-loop amplitudes are scheme dependent, and can therefore be set to zero by appropriate finite shifts of operator coefficients, or, equivalently, by a finite renormalization of the operators, or the addition of finite local counterterms.

For simplicity, we use a non-chiral version of the Standard Model, with zero quark and Higgs masses and zero Yukawa couplings and without an Abelian sector, but point out overlap with the SMEFT. In particular, our focus is on the mixing between dimension six operators, which by dimensional analysis cannot depend on masses or other dimensionful parameters. In the presence of masses there can be additional mixing between operators of different dimensions, including modifications to the running of the Standard Model couplings, but these correspond to different entries of the anomalous dimension matrix. In summary, our model is a close enough cousin of the SMEFT that we can directly verify a variety of one-loop SMEFT anomalous dimensions calculated in Refs. [19–21], finding full agreement, and make some predictions about the structure of the two-loop anomalous dimension matrix. (See Section 2.6 and in particular Table 2.9.) We note that although we only utilize Dirac fermions here, on-shell methods are well suited for dealing with chiral fermions as well (see e.g. Refs. [45, 101–103]).

This chapter is organized as follows. In Section 2.2, we explain our conventions, list the higher-dimensional operators in our simplified version of the SMEFT, and summarize the on-shell methods that we use to obtain anomalous dimensions. In Section 2.3 we present a new nonrenormalization theorem and its proof using the on-shell formalism, as well as some examples and its application to operators of dimensions six through eight. In Section 2.4 we explain the use of generalized unitarity in constructing full one-loop amplitudes, and we discuss the appearance of numerous zeros in the rational terms of the amplitudes. We also explain how finite counterterms can produce additional zeros in the rational terms of many of the one-loop amplitudes. Examples of additional vanishing contributions to the

two-loop anomalous dimension matrix are presented in Section 2.5, including those that arise from finite counterterms at one-loop. In Section 2.6 we discuss the overlap between our simplified model and the full SMEFT in the basis of operators used in Refs. [19–21], and discus the implications of our results for the latter theory. We give our conclusions in Section 2.7. Appendix 2.A explains the projection method used for integration in detail and lists the gauge invariant basis tensors. The explicit D-dimensional forms of the full one-loop amplitudes, as well as their four-dimensional finite remainders, are relegated to the ancillary files attached to the ArXiV submission of Ref. [2] and Appendix 2.B, respectively.

2.2 Setup and formalism

We now present our conventions and explain the on-shell formalisms that we use for obtaining the anomalous dimensions. One procedure for doing so is to extract them from ultraviolet divergences in amplitudes. This procedure follows the generalized unitarity method for assembling scattering amplitudes from their unitarity cuts [43–45, 97, 101–103]. While we describe the procedure for obtaining the anomalous dimensions in the current section, we leave a more detailed discussion of the generalized unitarity method for Section 2.4, where it will be used to construct full amplitudes.

As a second method, we apply the recent formalism of Caron-Huot and Wilhelm [98], which directly expresses the anomalous dimensions in terms of unitarity cuts. This method is particularly effective for computing anomalous dimensions, and is our preferred method beyond one loop. We show how this method helps clarify the structure of the anomalous dimension matrix at two loops and exposes new nontrivial zeros.

2.2.1 Conventions and basic setup

To illustrate our methods we will consider a model with dimension-four Lagrangian given by

$$\mathcal{L}^{(4)} = -\frac{1}{4}F^a_{\mu\nu}F^{a\mu\nu} + D_\mu\varphi\, D^\mu\overline{\varphi} - \lambda\,(\varphi\overline{\varphi})^2 + i\sum_{m=1}^{N_f}\bar{\psi}_m \not{D}\psi_m\,, \tag{2.1}$$

where the gauge field strength, $F^a_{\mu\nu}$, is in the adjoint representation of $SU(N)$, while ψ_m and φ are fundamental representation Dirac fermions and scalars, respectively. The index m on the fermions denotes the flavor; for simplicity we take a single flavor of scalars. The covariant derivative is given by

$$(D_\mu\psi_m)_i = \Big(\delta_{ij}\partial_\mu + ig\frac{1}{\sqrt{2}}T^a_{ij}A^a_\mu\Big)(\psi_m)_j\,, \tag{2.2}$$

where T^a_{ij} is the $SU(N)$ generator. We normalize the generator in the standard amplitudes convention by $\mathrm{Tr}[T^aT^b] = \delta^{ab}$ which differs from the usual textbook one, and we define $f^{abc} = -i\,\mathrm{Tr}[[T^a,T^b]T^c]$ and $d^{abc} = \mathrm{Tr}[\{T^a,T^b\}T^c]$ for later use.[1]

This model theory has the general structure of the Standard Model, but with all masses and Yukawa couplings set to zero, and with only one gauge group. Here we also use Dirac instead of chiral fermions; the basic methods apply just as well to cases which include chiral fermions in the context of Standard Model calculations, as in Ref. [45].

To mimic the SMEFT we modify this Lagrangian by adding dimension-six operators supressed by a high-energy scale Λ:

$$\mathcal{L} = \mathcal{L}^{(4)} + \frac{1}{\Lambda^2}\sum_k c_i^{(6)}\mathcal{O}_i^{(6)}\,, \tag{2.3}$$

where the list of the operators that we consider here is given in Table 2.1[2]. Note that our

[1] Note that our structure constants, f^{abc}, carry an extra factor of $\sqrt{2}$ relative to standard textbook conventions [139].

[2] We note that $\mathcal{O}_{\varphi^6}$ has no nonzero four-point amplitudes through two-loops, and therefore cannot renormalize any of the other operators [1]. We still include it here for completeness.

simplified model contains representatives from all of the operator classes of the basis used in Refs. [19–21], other than the classes $\psi^2 F\varphi$ and $\psi^2\varphi^3$ ($\psi^2 XH$ and $\psi^2 H^3$ in the notation of Refs. [19–21]), since operators in these classes must always have one uncharged fermion. We defer a comparison to the full SMEFT to Section 2.6.

At first order in c_i/Λ^2, renormalization induces mixing of the dimension-six operators, as parametrized by

$$\dot{c}_i \equiv \frac{\partial c_i}{\partial \log \mu} = c_j \gamma_{ji} \,. \tag{2.4}$$

If the coefficient of operator $\mathcal{O}_j$ appears on the right-hand side of the RG equation for the coefficient of operator $\mathcal{O}_i$, as above, we say that $\mathcal{O}_j$ renormalizes $\mathcal{O}_i$, or that they mix under renormalization. Sometimes we write the corresponding anomalous dimension as $\gamma_{i\leftarrow j}$. In all tables which describe anomalous dimensions we will display $\gamma'_{ij} = \gamma^{\mathrm{T}}_{ij}$ to facilitate comparison with Refs. [19–21]. The anomalous dimension matrix γ_{ij} depends on the dimension-four couplings g and λ, in the combinations

$$\tilde{g}^2 = \frac{g^2}{(4\pi)^2} \,, \qquad\qquad \tilde{\lambda} = \frac{\lambda}{(4\pi)^2} \,, \tag{2.5}$$

which we sometimes refer to collectively as $g^{(4)}$.

We extract anomalous dimensions from both amplitudes and form factors. We define a form factor with an operator insertion as

$$F_i(1^{h_1}, ..., n^{h_n}; q) = \langle k_1^{h_1}, ..., k_n^{h_n} | \mathcal{O}_i(q) | 0 \rangle \,, \tag{2.6}$$

which are matrix elements between an on-shell state $\langle k_1, ..., k_n|$, with particles of momenta $\{k_1 ... k_n\}$ and helicities $\{h_1 ... h_n\}$, and an operator $\mathcal{O}_i$ that injects additional off-shell momentum q. The states might also be dependent on the color and flavor of the particles, but we leave this dependence implicit for the moment. Form factors are especially useful when dealing with on-shell states with fewer than four particles, where kinematics would otherwise

Label	Operator
$\mathcal{O}_{F^3}$	$\frac{1}{3}f^{abc}F^a_{\mu\nu}F^a_{\nu\rho}F^a_{\rho\mu}$
$\mathcal{O}_{(\varphi^2F^2)_1}$	$(\varphi^\dagger\varphi)F^a_{\mu\nu}F^a_{\mu\nu}$
$\mathcal{O}_{(\varphi^2F^2)_2}$	$d^{abc}(\varphi^\dagger T^a\varphi)F^b_{\mu\nu}F^c_{\mu\nu}$
$\mathcal{O}_{(D^2\varphi^4)_1}$	$(\varphi^\dagger D^\mu\varphi)^*(\varphi^\dagger D_\mu\varphi)$
$\mathcal{O}_{(D^2\varphi^4)_2}$	$(\varphi^\dagger\varphi)\Box(\varphi^\dagger\varphi)$
$\mathcal{O}_{\varphi^6}$	$(\varphi^\dagger\varphi)^3$
$\mathcal{O}^{pr}_{(D\varphi^2\psi^2)_1}$	$i(\varphi^\dagger(D_\mu - \overleftarrow{D}_\mu)\varphi)(\bar{\psi}_p\gamma^\mu\psi_r)$
$\mathcal{O}^{pr}_{(D\varphi^2\psi^2)_2}$	$i(\varphi^\dagger(T^aD_\mu - \overleftarrow{D}_\mu T^a)\varphi)(\bar{\psi}_pT^a\gamma^\mu\psi_r)$
$\mathcal{O}^{mnpr}_{(\psi^4)_1}$	$(\bar{\psi}_m\gamma^\mu\psi_n)(\bar{\psi}_p\gamma_\mu\psi_r)$
$\mathcal{O}^{mnpr}_{(\psi^4)_2}$	$(\bar{\psi}_m\gamma^\mu T^a\psi_n)(\bar{\psi}_p\gamma_\mu T^a\psi_r)$

Table 2.1: List of dimension-six operators considered here. For simplicity, we take the fermions to be Dirac. The labels *mnpr* are flavor indices and *abc* color indices. Note the operator $\mathcal{O}_{F^3}$ is normalized slightly differently than in Refs. [19–21], as are the color matrices T^a in the operators $\mathcal{O}_{(D\varphi^2\psi^2)_2}$ and $\mathcal{O}_{(\psi^4)_2}$. We will occasionally drop the $(\,)_1$ and $(\,)_2$ subscripts to refer to pairs of operators collectively.

require the amplitude (with real momenta) to be zero. From the perspective of form factors, we can think of an amplitude with an operator insertion as a form factor, but where the higher-dimension operator injects zero momentum, $q = 0$,

$$A_i(1^{h_1}, ..., n^{h_n}) = \langle k_1^{h_1}, ..., k_n^{h_n}|\mathcal{O}_i(0)|0\rangle\,. \tag{2.7}$$

When the inserted operator is the identity, we recover the usual scattering amplitude, which depends only on the dimension-four couplings. We denote such an amplitude as

$$A(1^{h_1}, ..., n^{h_n}) = \langle k_1^{h_1}, ..., k_n^{h_n}|0\rangle = \langle k_1^{h_1}, ..., k_i^{h_i}|\mathcal{M}|-k_{i+1}^{-h_{i+1}}, \ldots, -k_n^{-h_n}\rangle\,. \tag{2.8}$$

Unless otherwise stated, we use an all outgoing convention where all the particles are crossed to the final state. When crossing fermions there are additional signs on the right-hand side

of Eq. (2.8) that we leave implicit here. In general we can write the form factors (and amplitudes) as color-space vectors,

$$F_i(1,\ldots,n) = \sum_j \mathcal{C}^{[j]} F_{i\,[j]}(1,\ldots,n)\,, \tag{2.9}$$

where the $\mathcal{C}^{[i]}$ are a set of independent color factors. In the context of amplitudes, these correspond to *color-ordered* [52, 140, 141] or, more generally, *primitive* [142] amplitudes. The color factors $\mathcal{C}^{[i]}$ depend on which particles of the amplitude are in the adjoint or fundamental representation of $SU(N)$. Here, we only need the decomposition into a basis of color factors without using special properties of the coefficients. For the various processes we consider, the tree and one-loop amplitudes are listed in Appendix 2.B.

We use the conventional dimensional regularization and $\overline{\text{MS}}$-like schemes throughout, in which the amplitudes and form factors, F_i satisfy the renormalization-group equations

$$\left[(\mu\partial_\mu + \beta\,\partial)\,\delta_{ij} + \left(\gamma^{\text{UV}} - \gamma^{\text{IR}}\right)_{ij}\right] F_j = 0, \tag{2.10}$$

where $\partial_\mu := \partial/\partial\mu$, $\partial := \partial/\partial g^{(4)}$, $\beta := \beta(g^{(4)})$ is the β-function of the collection of marginal couplings, γ_{ij}^{UV} are the anomalous dimensions of the higher-dimension operators, and γ_{ij}^{IR} are the IR anomalous dimensions, arising from soft and/or collinear divergences[3]. For later convenience, we introduce the shorthand

$$\Delta\gamma = \gamma^{\text{UV}} - \gamma^{\text{IR}}\,. \tag{2.11}$$

The appearance of both kinds of anomalous dimensions stems from the fact that there is a single dimensional-regularization parameter, $\epsilon = \epsilon_{\text{UV}} = \epsilon_{\text{IR}}$, and single scale, $\mu = \mu_{\text{UV}} = \mu_{\text{IR}}$, for both the UV and IR divergences. As usual we take $\epsilon = (4-D)/2$.

[3]The relative sign between UV and IR anomalous dimensions is merely a convention.

The perturbative expansion of the different quantities we consider is denoted by

$$\begin{aligned} F_i &= F_i^{(0)} + F_i^{(1)} + F_i^{(2)} + \cdots , \\ A_i &= A_i^{(0)} + A_i^{(1)} + A_i^{(2)} + \cdots , \\ \gamma_{ij} &= \gamma_{ij}^{(1)} + \gamma_{ij}^{(2)} + \cdots , \\ \beta &= \beta^{(1)} + \beta^{(2)} + \cdots , \end{aligned} \tag{2.12}$$

where each order in the expansion includes an additional power of the dimension-four couplings, $g^{(4)}$, as defined in Eq. (2.5), compared to the previous order. Since the operators we consider here have a least four fields, except for the F^3 case, any of the generated four-point tree amplitudes are local, and directly correspond to the operator. The amplitudes generated by the F^3 operator also contain a vertex obtained from the dimension-four operators. Thus, the four-point tree amplitudes have no powers of $g^{(4)}$, with the exception of the four-point amplitudes generated from the F^3 operator.

2.2.2 Anomalous dimensions from UV divergences

Anomalous dimensions are traditionally extracted from countertems associated to UV divergences. For instance, in Refs. [19–21] the full one-loop anomalous dimension matrix of the SMEFT was calculated by extracting the $1/\epsilon$ divergences of the one-particle irreducible (1PI) diagrams that generate the one-loop effective action in the background field method. Alternatively, one might extract the anomalous dimensions from on-shell amplitudes. Here, we use the full one-loop amplitudes to calculate the one-loop anomalous dimension matrix of our model, and thereby verify a representative set of the anomalous dimensions calculated in Refs. [19–21].

An efficient way of determining UV divergences at one loop was presented for the β-function in Ref. [143, 144]. Here we adopt this method to calculate one-loop anomalous

dimensions. In general, the renormalization of $\mathcal{O}_i$ by $\mathcal{O}_j$ at one loop is determined by calculating the matrix element with external particles corresponding to $\mathcal{O}_i$, but with an insertion of $\mathcal{O}_j$. In general, one-loop matrix elements can be expressed in terms of a basis of scalar integrals

$$A_i^{(1)} = \sum_s a^s_{4,\,i}\, I_{4,s} + \sum_s a^s_{3,\,i} I_{3,s} + \sum_s a^s_{2,\,i} I_{2,s}\,, \tag{2.13}$$

comprised of boxes $I_{4,s}$, triangles, $I_{3,s}$, and bubbles, $I_{2,s}$, where the corresponding coefficients, a_i^s, b_i^s and c_i are gauge invariant and generically depend on color and the dimensional regularization parameter ϵ. The integrals can then be expanded in ϵ, producing both UV and IR poles in ϵ. Only the scalar bubble integrals contain UV divergences, so we write a formula for the anomalous dimensions in terms of the bubble coefficients $a^s_{2,\,i}$, whose ϵ dependence can be ignored for this purpose. However, some care is required because of cancellations between UV and IR divergences. We delay a detailed discussion of the infrared structure of the amplitudes to Section 2.4. For the moment, we just recall that the $1/\epsilon$ pole in the bubble integrals in Eq. (2.13) does not contain the full UV divergence of the amplitude. The reason for this is that there is an additional $1/\epsilon$ pole which originates in bubble-on-external-leg diagrams, which are scaleless and set to zero in dimensional regularization because of a cancellation of UV and IR poles,

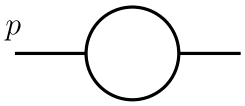

$$\Big|_{p^2=0} \quad \propto \frac{1}{\epsilon_{UV}} - \frac{1}{\epsilon_{IR}} + \log\frac{\mu^2_{UV}}{\mu^2_{IR}}\,. \tag{2.14}$$

Hence the bubbles on external legs give an additional UV contribution,

$$-\frac{1}{2\epsilon}\gamma_{\rm c}^{{\rm IR}\,(1)} A_i^{(0)} := -\frac{1}{2\epsilon}\sum_p \gamma^{\rm IR}_{{\rm c},\,p} A_i^{(0)}\,, \tag{2.15}$$

where γ_p^c is the so-called collinear anomalous dimension of particle p, and the sum is over all external states of the tree amplitude. For the vectors, fermions and scalars in our theory

the collinear anomalous dimensions are given by [145, 146]

$$\gamma_{\mathrm{c},\,v}^{\mathrm{IR}\,(1)} = -\tilde{g}^2 b_0\,, \quad \gamma_{\mathrm{c},\,f}^{\mathrm{IR}\,(1)} = -\tilde{g}^2 3C_F\,, \quad \gamma_{\mathrm{c},\,s}^{\mathrm{IR}\,(1)} = -\tilde{g}^2 4C_F\,, \tag{2.16}$$

where $b_0 = (11N - 2N_f - N_s/2)/3$ is the coefficient in the one-loop β-function of g, and $C_F = (N^2-1)/2N$ is the Casimir of the fundamental representation. While we only consider one flavor of scalar in our model, we include the parameter N_s in the β-function and elsewhere to track contributions from scalar loops.

In addition, there are contributions to the $1/\epsilon$ UV pole proportional to the one-loop β-function of the dimension-four couplings, related to the renormalization of such couplings

$$\frac{1}{2\epsilon}(n - L_i)\tilde{\beta}^{(1)} A_i^{(0)}\,, \tag{2.17}$$

where $\tilde{\beta}^{(1)} = \beta^{(1)}/g^{(4)}$, n is the number of external states and L_i is the length of the operator $\mathcal{O}_i$, i.e., the number of fields it contains. We therefore conclude that the sum over bubble coefficients is related to the UV anomalous dimensions by

$$\frac{1}{(4\pi)^2}\sum_s a_{2\,,i}^s = -\frac{1}{2}\big[\gamma_{ij}^{UV} - \gamma_{\mathrm{c}}^{\mathrm{IR}}\delta_{ij} + (n - L_i)\tilde{\beta}^{(1)}\delta_{ij}\big] A_j^{(0)}\,. \tag{2.18}$$

Similar formulas have recently been used in Ref. [130, 131]. There are multiple methods by which one might calculate these coefficients. We do so by using generalized unitarity. For the purposes of extracting the UV divergences, it suffices to evaluate four-dimensional cuts [24, 143, 144]. However, we are interested in obtaining the full amplitudes, including rational terms, as a stepping stone towards calculating two-loop anomalous dimensions, so we use D-dimensional unitarity cuts as described in Section 2.4.

The approach we outlined is very powerful at one loop, but at higher loops becomes more difficult to use, because it requires two-loop integration. In particular, at higher loops simple decompositions of integrals along the lines of Eq. (2.13) do not exist. One might still

construct the amplitudes using unitarity methods, and then extract their UV divergences by carrying out the loop integration, but one would like a simpler technique that avoids much of the technical complexity. Furthermore, to calculate two-loop divergences, one must also keep track of evanescent one-loop subdivergences, which contaminate the result. By an evanescent subdivergence we mean a subdivergence whose corresponding counterterm vanishes in strictly four dimensions, but which cannot be ignored in dimensional regularization (see e.g. Ref. [147–151]). While not physical, these evanescent subdivergences greatly complicate higher-loop calculations, and it is better to use a method that avoids them, whenever possible. Ref. [105] gives a nontrivial two-loop example for Einstein gravity showing how on-shell methods can efficiently bypass evanescent effects [104] to determine renormalization-scale dependence.

2.2.3 Anomalous dimensions directly from unitarity cuts

A much more direct way to obtain anomalous dimensions is to focus on the renormalization-scale dependence encoded in the logarithms, and not on the divergences. The logarithms are detectable in four-dimensional unitarity cuts. Any dimensional imbalance in the kinematic arguments of the logarithms must be balanced by renormalization-scale dependence, so one can directly determine the renormalization-scale dependence and any anomalous dimensions by collecting the contributions from unitarity cuts. For example, this strategy has been used to greatly simplify the extraction of the two-loop renormalization-scale dependence in Einstein gravity [105].

The formalism of Caron-Huot and Wilhelm [98] gives a rather neat way to carry out this strategy , allowing us to extract the anomalous dimension at L-loops directly from phase-space integrals of lower-loop on-shell form factors and amplitudes. Among other useful features, this makes potential zeros in the anomalous dimension matrix much more transparent than with conventional methods [1].

By considering the analyticity of the form factors with respect to complex shifts in momenta, along with unitarity, Caron-Huot and Wilhelm derived the following compact equation:

$$e^{-i\pi D} F_i^* = S\, F_i^* \,, \tag{2.19}$$

which relates the phase of the S-matrix, S, to the dilatation operator, D (ignoring trivial overall engineering dimensions). The dilation operator acts on the conjugate form factor F_i^*. Writing $S = 1 + i\mathcal{M}$, Eq. (2.19) can be rewritten more practically as

$$(e^{-i\pi D} - 1) F_i^* = i\mathcal{M} F_i^* \,, \tag{2.20}$$

where the scattering amplitude, $\mathcal{M}$, acts as a matrix on the form-factor, yielding its imaginary part via the optical theorem[4]. The right-hand side of this equation is defined to be a unitarity cut. As we discuss below, this equation precisely captures the notion that the scale dependence of F_i is encoded in the coefficients of its logarithms. We note that the use of the complex conjugate form factor, F^*, only affects the imaginary part, which do not affect our calculations through two loops. Therefore, we drop the complex conjugation henceforth.

In dimensional regularization, the dilatation operator is related to the single renormalization scale, μ, as $D = -\mu\partial_\mu$, reflecting the fact that F_i can only depend on dimensionless ratios s_{ij}/μ (ignoring the overall engineering dimensions), and that logarithms in s_{ij} kinematic variables must be balanced either by μ or by each other. The dilatation operator then acts on the form factors as

$$DF_i = -\mu\partial_\mu F_i = [\Delta\gamma_{ij} + \delta_{ij}\beta\,\partial]\, F_j, \tag{2.21}$$

where we have used the renormalization-group equation (2.10). This, together with equation

[4]In our notation the optical theorem states, $2\mathrm{Im}F_i^* = \mathcal{M}F_i^*$ for form factors or $2\mathrm{Im}\mathcal{M} = \mathcal{M}\mathcal{M}$ for amplitudes.

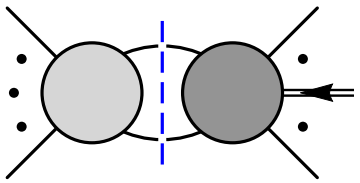

Figure 2.1: Unitarity cut relevant for the extraction of anomalous dimensions from one-loop form factors. The darker blobs indicate a higher-dimension operator insertion. The double-lined arrow indicates the insertion of additional off-shell momentum from the operator. The dashed line indicates the integral over phase space of the particles crossing the cut.

(2.19), gives us a powerful means to extract anomalous dimensions.

While Eqs. (2.19) and (2.21) are valid non-perturbatively, we can expand in perturbation theory to obtain order-by-order expressions for the anomalous dimensions. At one loop the expansion yields

$$\left[\Delta\gamma_{ij}^{(1)} + \delta_{ij}\beta^{(1)}\partial\right] F_j^{(0)} = -\frac{1}{\pi}(\mathcal{M}F_i)^{(1)}\,, \tag{2.22}$$

where the superscript denotes the order in perturbation theory. On the right-hand side $(\mathcal{M}F_i)^{(1)}$ indicates

$$(\mathcal{M}F_i)^{(1)} = \sum_{k=2}^{n}\sum_{c}(\mathcal{M}_{k\to 2}^{c})^{(0)} \otimes F_{n-k+2\,,i}^{(0)}\,, \tag{2.23}$$

where the sums are over all kinematic channels and the $\otimes$ denotes a sum over intermediate two-particle states in the product. For a given kinematic channel this is given by the Lorentz-invariant phase-space integral

$$\begin{aligned}(\mathcal{M}_{k\to 2}^{1\cdots k})^{(0)} \otimes F_{n-k+2\,,i}^{(0)} &= \sum\int d\mathrm{LIPS}_2 \sum_{h_1,h_2}\langle 1\cdots k|\mathcal{M}|\ell_1^{h_1}\ell_2^{h_2}\rangle^{(0)}\langle \ell_1^{h_1}\ell_2^{h_2}\cdots n|\mathcal{O}_i|0\rangle^{(0)} \\ &= \sum\int d\mathrm{LIPS}_2 \sum_{h_1,h_2} A^{(0)}(1,\cdots,k,-\ell_1^{-h_1},-\ell_2^{-h_2})F_i^{(0)}(\ell_1^{h_1},\ell_2^{h_2},\cdots,n)\,,\end{aligned} \tag{2.24}$$

where the sum over helicities also includes a sum over different states crossing the cut. In summary, $(\mathcal{M}F_i)^{(1)}$ corresponds to a sum over all one-loop two-particle unitarity cuts, as depicted schematically in Figure 2.1.

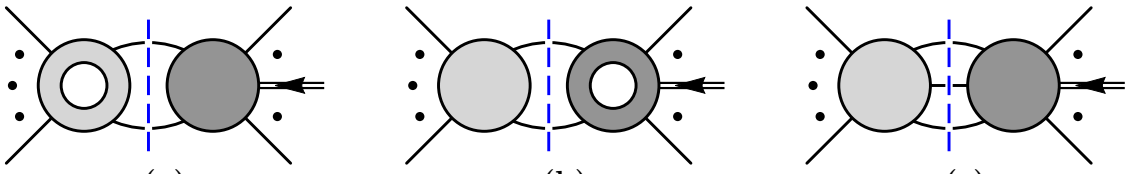

Figure 2.2: Unitarity cuts relevant for the extraction of anomalous dimensions from two-loop form factors, using the same notation as in Figure 2.1. The darker blobs indicate a higher-dimension operator insertion. The blobs with a hole indicate a one-loop form factor or amplitude.

After rewriting the expression in terms of four-dimensional spinors, the two-particle phase-space integrals can be easily evaluated following the discussion of Ref. [98],

$$\begin{pmatrix} \lambda_1' \\ \lambda_2' \end{pmatrix} = \begin{pmatrix} \cos\theta & -\sin\theta\ \mathrm{e}^{i\phi} \\ \sin\theta\ \mathrm{e}^{-i\phi} & \cos\theta \end{pmatrix} \begin{pmatrix} \lambda_1 \\ \lambda_2 \end{pmatrix}, \tag{2.25}$$

where the λ_i and $\tilde{\lambda}_i = \lambda_i^*$ spinors depend on the momenta of the external legs and the λ_i' and $\tilde{\lambda}_i' = \lambda_i'^*$ spinors on the momenta of the cut legs. With this parametrization the integration measure is simply,

$$\int d\mathrm{LIPS}_2 \equiv \frac{1}{16\pi} \int_0^{2\pi} \frac{\mathrm{d}\phi}{2\pi} \int_0^{\frac{\pi}{2}} 2\cos\theta \sin\theta \mathrm{d}\theta\,. \tag{2.26}$$

In the definition of the phase-space measure, here we have included an additional symmetry factor of $1/2$, relative to the usual volume of two-particle phase space, i.e., 8π. This is generally convenient but requires some care when non-identical particles cross the cut, where we will need to multiply by two to cancel the symmetry factor.

Next consider two loops. Expanding Eq. (2.20) through this order, we obtain

$$\begin{aligned} &\left[\Delta\gamma_{ij}^{(1)} + \delta_{ij}\beta^{(1)}\partial\right] F_j^{(1)} + \left[\Delta\gamma_{ij}^{(2)} + \delta_{ij}\beta^{(2)}\partial\right] F_j^{(0)} \\ &\qquad - i\pi\,\frac{1}{2}\left[\Delta\gamma_{ik}^{(1)} + \delta_{ik}\beta^{(1)}\partial\right]\left[\Delta\gamma_{kj}^{(1)} + \delta_{kj}\beta^{(1)}\partial\right] F_j^{(0)} = -\frac{1}{\pi}(\mathcal{M}F_i)^{(2)}\,. \end{aligned} \tag{2.27}$$

On the right-hand side of this equation, $(\mathcal{M}F_i)^{(2)}$ denotes collectively the three two-loop

unitarity cuts displayed in Figure 2.2,

$$(\mathcal{M}F_i)^{(2)} = \sum_{k=2}^{n}\sum_{c}\Big[(\mathcal{M}^{c}_{k\to 2})^{(1)}\otimes F^{(0)}_{n-k+2\,,i} + (\mathcal{M}^{c}_{k\to 2})^{(0)}\otimes F^{(1)}_{n-k+2\,,i} + (\mathcal{M}^{c}_{k\to 3})^{(0)}\otimes F^{(0)}_{n-k+3\,,i}\Big]\,. \tag{2.28}$$

In the first term we find two-particle cuts composed of the one-loop amplitude and the tree-level higher-dimension form factor depicted in Figure 2.2(a). These are

$$\begin{aligned}(\mathcal{M}^{1\cdots k}_{k\to 2})^{(1)}\otimes F^{(0)}_{n-k+2\,,i} &= \int d\mathrm{LIPS}_2 \sum_{h_1,h_2}\langle 1\cdots k|\mathcal{M}|\ell_1^{h_1}\ell_2^{h_2}\rangle^{(1)}\,\langle \ell_1^{h_1}\ell_2^{h_2}\cdots n|\mathcal{O}_i|0\rangle^{(0)}\\ &= \int d\mathrm{LIPS}_2 \sum_{h_1,h_2} A^{(1)}(1,\cdots,k,-\ell_1^{-h_1},-\ell_2^{-h_2})\,F_i^{(0)}(\ell_1^{h_1},\ell_2^{h_2},\cdots,n)\,.\end{aligned} \tag{2.29}$$

Similarly, the second term, shown in Figure 2.2(b), is a combination of cuts composed by the tree-level amplitude and the one-loop higher-dimension operator, which are

$$\begin{aligned}(\mathcal{M}^{1\cdots k}_{k\to 2})^{(0)}\otimes F^{(1)}_{n-k+2\,,i} &= \int d\mathrm{LIPS}_2 \sum_{h_1,h_2}\langle 1\cdots k|\mathcal{M}|\ell_1^{h_1}\ell_2^{h_2}\rangle^{(1)}\,\langle \ell_1^{h_1}\ell_2^{h_2}\cdots n|\mathcal{O}_i|0\rangle^{(0)}\\ &= \int d\mathrm{LIPS}_2 \sum_{h_1,h_2} A^{(0)}(1,\cdots,k,-\ell_1^{-h_1},-\ell_2^{-h_2})\,F_i^{(1)}(\ell_1^{h_1},\ell_2^{h_2},\cdots,n)\,.\end{aligned} \tag{2.30}$$

Finally, the third term is composed of three-particle cuts involving two tree-level objects, as in Figure 2.2(c)

$$\begin{aligned}(\mathcal{M}^{1\cdots k}_{k\to 3})^{(0)}\otimes F^{(1)}_{n-k+3\,,i} &= \int d\mathrm{LIPS}_3 \sum_{h_1,h_2,h_3}\langle 1\cdots k|\mathcal{M}|\ell_1^{h_1}\ell_2^{h_2}\ell_3^{h_3}\rangle^{(0)}\langle \ell_1^{h_1}\ell_2^{h_2}\ell_3^{h_3}\cdots n|\mathcal{O}_i|0\rangle^{(0)}\\ &= \int d\mathrm{LIPS}_3 \sum_{h_1,h_2,h_3} A^{(0)}(1,\cdots,k,-\ell_1^{-h_1},-\ell_2^{-h_2},-\ell_3^{-h_3})F_i^{(0)}(\ell_1^{h_1},\ell_2^{h_2},\ell_3^{h_3},\cdots,n)\,.\end{aligned} \tag{2.31}$$

A parameterization analogous to (2.25) for the three-particle cut is given in Ref. [98]. We will not evaluate any three-particle cuts in the present work, so we refer the reader to the

aformentioned paper for more details.

We can rearrange Eq. (2.27) to put it into a more convenient form for extracting two-loop anomalous dimensions. First, note that the imaginary part of Eq. (2.27)

$$-i\pi\,\frac{1}{2}\left[\Delta\gamma_{ik}^{(1)}+\delta_{ik}\beta^{(1)}\partial\right]\left[\Delta\gamma_{kj}^{(1)}+\delta_{kj}\beta^{(1)}\partial\right]F_j^{(0)}=-\frac{1}{\pi}\mathrm{Im}(\mathcal{M}F_i)^{(2)}\,, \tag{2.32}$$

does not feature the two-loop anomalous dimensions. Using the optical theorem again, we write its right-hand side in terms of unitarity cuts

$$\mathrm{Im}(\mathcal{M}F_i)^{(2)}=(\mathcal{M}\mathcal{M}F_i)^{(2)}\,, \tag{2.33}$$

where the relevant cuts are the iterated two-particle cuts in Fig. 2.3. For instance $(\mathcal{M}\mathcal{M}F_i)^{(2)}$ contains terms of the form

$$\int d\mathrm{LIPS}_2 d\mathrm{LIPS}_2'\sum_{h_1,h_2}\sum_{h_1',h_2'}\langle\cdots|\ell_1^{h_1}\ell_2^{h_2}\rangle^{(0)}\langle\ell_1^{h_1}\ell_2^{h_2}\cdots|\ell_{1'}^{h_1'}\ell_{2'}^{h_2'}\rangle^{(0)}\langle\ell_{1'}^{h_1'}\ell_{2'}^{h_2'}\cdots|\mathcal{O}_i|0\rangle^{(0)}\,, \tag{2.34}$$

which correspond to cuts of the type in Fig. 2.3(a). Note that Eq. (2.33) does not include a factor of 1/2 from the optical theorem because the imaginary part can arise from cutting either the one-loop amplitude or form factor, which give identical contributions.

Eq. (2.32) does not contain the two-loop anomalous dimensions but instead captures the exponentiation of one-loop anomalous dimensions and the associated logarithms. Nonetheless (2.33) can be used to simplify the real part of Eq. (2.27), which yields

$$\begin{aligned}\left[\Delta\gamma_{ij}^{(1)}+\delta_{ij}\beta^{(1)}\partial\right]\mathrm{Re}F_j^{(1)}+\left[\Delta\gamma_{ij}^{(2)}+\delta_{ij}\beta^{(2)}\partial\right]F_j^{(0)} \\ =-\frac{1}{\pi}\mathrm{Re}(\mathcal{M}F_i)^{(2)}=-\frac{1}{\pi}(\mathcal{M}F_i-\mathcal{M}\mathcal{M}F_i)^{(2)}\,.\end{aligned} \tag{2.35}$$

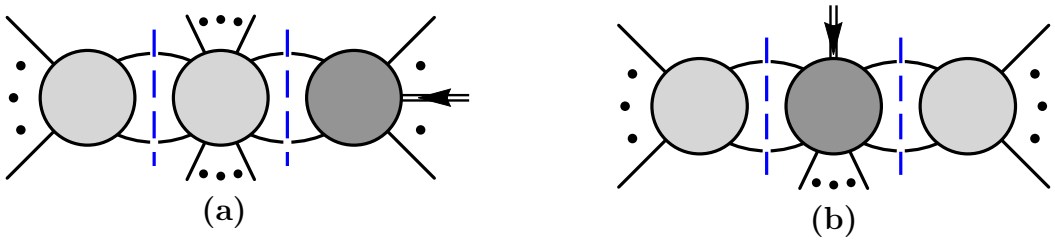

Figure 2.3: Iterated two-particle cuts that appear on the right-hand side of Eq. (2.33).

Note that the right-hand side can be rewritten using

$$(\mathcal{M}F_i - \mathcal{M}\mathcal{M}F_i)^{(2)} = \left[\left(\mathcal{M} - \frac{1}{2}\mathcal{M}\mathcal{M}\right)\left(F_i - \frac{1}{2}\mathcal{M}F_i\right)\right]^{(2)} = [\mathrm{Re}(\mathcal{M})\mathrm{Re}(F_i)]^{(2)} \ , \tag{2.36}$$

and with this we arrive at

$$\left[\Delta\gamma_{ij}^{(1)} + \delta_{ij}\beta^{(1)}\partial\right]\mathrm{Re}F_j^{(1)} + \left[\Delta\gamma_{ij}^{(2)} + \delta_{ij}\beta^{(2)}\partial\right]F_j^{(0)} = -\frac{1}{\pi}\left[\mathrm{Re}(\mathcal{M})\mathrm{Re}(F_i)\right]^{(2)} \ . \tag{2.37}$$

We use this equation to extract two-loop anomalous dimensions. In practice Eq. (2.37) simply instructs us to drop the imaginary parts of the one-loop matrix elements when calculating the cuts in Figs. 2.2(a) and 2.2(b). On the left-hand side, we now see the appearance of one-loop anomalous dimensions and the β-function, as well as the one-loop form factor $F_i^{(1)}$. The two-loop UV anomalous dimension $\gamma_{ij}^{\mathrm{UV}(2)}$ contained in $\Delta\gamma_{ij}^{(2)}$ is the object of interest, but to extract it we first need to remove $\gamma_{ij}^{\mathrm{IR}(2)}$, which requires an understanding of the IR singularities, which we discuss below.

2.2.4 Simplifying strategies

A strategy that greatly simplifies the analysis is to choose an external state with the minimal number of external legs that is sensitive to the operator of interest, i.e. select the operator's minimal form factor. In this way we can avoid terms of the form $\beta^{(n)}\partial F_i^{(0)}$ in Eqs. (2.27) and (2.37), since, under this choice, $F_i^{(0)}$ is local, and thus does not depend on the dimension-four

couplings, $g^{(4)}$.

More generally, the β-function can no longer be eliminated by using minimal form factors whenever the one-loop form factor with an $\mathcal{O}_i$ insertion, $F_i^{(1)}$, produces a nonzero result with the chosen external states. In addition, the β-function acting on the one-loop anomalous-dimension matrix is nonzero if the matrix elements themselves are nonzero. For example, to determine the renormalization of $\mathcal{O}_{F^3}$ by itself at two loops, we would evaluate Eq. (2.37) with the external state $\langle 1^+2^+3^+|$. In this case the term $\beta^{(2)}\partial F^{(0)}_{F^3}$ would vanish, though the term $\beta^{(1)}\partial F^{(1)}_{F^3}$ would remain.

Unlike the β-function, the IR anomalous dimensions are non-trivial to eliminate. Ref. [98] removes them by subtracting, at the integrand level, form factors of global symmetry currents, such as the stress-tensor, which are UV finite but contain the same IR divergences. Alternatively, one can use the same on-shell methods to calculate them and subtract them after integration. At one loop, the structure of infrared divergences is well understood [152–157], and it is straightforward to subtract them after integration. We explain how to carry this out at the level of the amplitudes in the next section. Furthermore, whenever we are interested in a leading off-diagonal element of the anomalous dimension matrix, the IR anomalous dimensions does not appear, since the infrared divergences are diagonal in the operators (excluding color).

Finally, form factors are useful for operators with only two or three external fields, since they allow nonzero results when kinematics would otherwise set amplitudes with fewer than four external particles to zero. Here we generally set the operator momentum insertion $q = 0$ and work in terms of amplitudes whenever possible, i.e. whenever there are four or more external states.

2.2.5 Comments on evanescent operators

When extracting anomalous dimensions from UV divergences in dimensional regularization one must carefully keep track of evanescent operators [147–151]. These operators are non-trivial in D-dimensions, but whose matrix elements vanish for any choice of external four-dimensional states. In the context of the SMEFT an example of an evanescent operator would be the Lorentz–Fierz identities

$$\begin{aligned}\mathcal{O}_{\text{Fierz,L}} &= (\bar{\psi}_L^m \gamma^\mu \psi_L^n)(\bar{\psi}_L^p \gamma_\mu \psi_L^r) + (\bar{\psi}_L^p \gamma^\mu \psi_L^n)(\bar{\psi}_L^m \gamma_\mu \psi_L^r)\,, \\ \mathcal{O}_{\text{Fierz,R}} &= (\bar{\psi}_R^m \gamma^\mu \psi_R^n)(\bar{\psi}_R^p \gamma_\mu \psi_R^r) + (\bar{\psi}_R^p \gamma^\mu \psi_R^n)(\bar{\psi}_R^m \gamma_\mu \psi_R^r)\,,\end{aligned} \tag{2.38}$$

(where we raised the flavor indices for convenience) which are identically zero in four but not in arbitrary dimensions. More generally one can easily construct such operators by antisymmetrizing over five or more Lorentz indices. In the context of our model, an example of such an evanescent operator is

$$(\bar{\psi}\gamma_{[\alpha}\gamma_\mu\gamma_\nu\gamma_\sigma\gamma_{\rho]}\psi)(\bar{\psi}\gamma^{[\alpha}\gamma^\mu\gamma^\nu\gamma^\sigma\gamma^{\rho]}\psi)\,. \tag{2.39}$$

One-loop diagrams might contain a $1/\epsilon$ divergence proportional to the matrix element of an evanescent operator. While this does not affect one-loop anomalous dimensions because we can take the external states to be four-dimensional, when inserted in a higher-loop diagram in the context of dimensional regularization such evanescent operators are activated and can generate both UV divergent and finite contributions. In fact, they are needed to properly subtract subdivergences. These effects must be taken into account in order to correctly extract two-loop UV divergences and their associated anomalous dimension. In practice we can deal with the effects of evanescent operators [147–151], but the number of them grows with dimension and loop order (especially in the presence of fermions). For this reason it would be desirable to avoid them when possible, since they are a technical

complication due to the use of dimensional regularization, and ultimately we would expect that they do not affect the physics [104].

We expect the on-shell methods presented above to completely sidestep the issue of evanescent operators when obtaining anomalous dimension, at least through two loops. Ref. [105] provides a nontrivial demonstration that complications from evanescent operators can be completely sidestepped using on-shell methods and by focusing on renormalization-scale dependence instead of divergences. In the two-loop formulas used here, anomalous dimensions and associated logarithms are given directly in terms of four-dimensional unitarity cuts of tree and one-loop objects. This automatically eliminates most of the evanescent dependence, except for finite shifts in one-loop matrix elements with evanescent operator insertions. We expect that any remaining evanescent dependence in the one-loop amplitudes or form factors to be eliminated by finite renormalizations [151]. Given the usual subtleties of dealing with evanescent operators, it would, of course, be important to explicitly verify that including or not including evanescent operators in the one- and two-loop anomalous dimension matrix amounts to a scheme choice.

2.2.6 Anomalous dimensions and non-interference

As noted in Ref. [158–160] helicity selection rules imply the non-interference of SMEFT tree-level matrix elements when constructing cross sections. This has important consequences in the context of the SMEFT, where the possibility of measuring the coefficient of higher-dimension operators at colliders can be impacted by the vanishings in the interference of the Standard-Model tree amplitudes and those of higher-dimension operators, when computing cross sections. A connection between one-loop anomalous dimension and interference terms can be seen in Eq. (2.22), where, upon setting $q = 0$, the form factors become amplitudes and the right-hand side directly captures the interference of tree-level dimension-four and dimension-six amplitudes. Note that this holds even when the anomalous dimension is not

zero, in which case this equation relates the interference terms to simpler objects, namely the one-loop anomalous dimensions and tree-level matrix elements. Of course, in a realistic cross-section calculation one would not integrate over the full phase space, due to experimental cuts.

At two loops the connection between zeros in the anomalous dimensions and non-interference is not as direct, since it requires cancellations between both sides of Eq. (2.27). Eq. (2.32) shows that, in general, the imaginary part of the interference term is given by the square of one-loop anomalous dimensions times tree-level matrix elements. Instead of non-interference, Eq. (2.35) shows that a vanishing two-loop anomalous dimension would imply that the real part of interference term is simply is related to the product of one-loop anomalous dimensions and one-loop matrix elements. It would be interesting to further investigate the consequences stemming from these observations, even in the presence of experimental cuts.

2.3 Non-renormalization theorem for operator mixing

Having explained the on-shell tools to calculate anomalous dimension we are ready to discuss and prove a new nonrenomalization theorem. To state the theorem we define the length of an operator, $l(\mathcal{O})$, as the number of fundamental field insertions in $\mathcal{O}$. Then the statement of theorem is as follows:

> *Consider operators $\mathcal{O}_s$ and $\mathcal{O}_l$ such that $l(\mathcal{O}_l) > l(\mathcal{O}_s)$. $\mathcal{O}_l$ can renormalize $\mathcal{O}_s$ at L loops only if $L > l(\mathcal{O}_l) - l(\mathcal{O}_s)$.*

At fixed loop order, sufficiently long operators cannot renormalize short operators because there would be too many legs to form a diagram with the right structure. Such zeros in the anomalous-dimension matrix are trivial. As written above the theorem applies non-trivially at $(l(\mathcal{O}_l) - l(\mathcal{O}_s))$-loops, i.e., the first loop order at which there could be renormalization because diagrams exist. However, in a general theory with multiple types of fields, the first

renormalization can be delayed even further, depending on the precise field content of the two operators. We encapsulate this into the more general rule:

If at any given loop order, the only diagrams for a matrix element with the external particle content of $\mathcal{O}_s$ but an insertion of $\mathcal{O}_l$ involve scaleless bubble integrals, there is no renormalization of $\mathcal{O}_s$ by $\mathcal{O}_l$.

What makes them nontrivial is that Feynman diagrams exist that seem as if they should contribute to an anomalous dimension, but fail to do so because the diagrams do not generate the appropriate logarithms. The Feynman-diagram language can obscure this, because individual diagrams are not gauge invariant. While not difficult to disentangle at one loop, at higher loops it becomes more advantageous to work in an on-shell formalism, which only takes gauge-invariant quantities as input. Indeed, modern unitarity methods [43–46, 97] have clarified the structure of loop amplitudes resulting in significant computational advantages for a variety of problems, including the computation of form factors and associated anomalous dimensions [161–164].

2.3.1 Proof of the non-renormalization theorem

We would like to consider the renormalization of a shorter operator $\mathcal{O}_s$ by a longer operator $\mathcal{O}_l$. This could be, for example, the renormalization of $\phi^2 F^2$ by ϕ^6, where ϕ is a scalar and F is a vector field strength. For simplicity we will take $\mathcal{O}_s$ and $\mathcal{O}_l$ to be single operators, though in general they represent collections of operators with the same field content, but differing Lorentz contractions or color factors. Because our arguments rely only on the field content and basic structure of the unitarity cuts, our conclusions will apply just as well to the more general case.

The formalism reviewed above allows us to connect the anomalous dimensions to unitarity cuts of form factors, given knowledge of the β function of the leading couplings and the infrared anomalous dimensions. We now show that for the leading contributions, there is

an even more direct connection between the ultraviolet anomalous dimensions and unitarity cuts.

The appearance of the β function in Eq. (2.22) is avoided simply by extracting the anomalous dimensions from the *minimal* form factor of $\mathcal{O}_s$, which is defined as the one with the minimum number of legs needed to match the operator. Because of its defining property, the minimal tree-level form factor is local and does not depend on the couplings, g. Therefore the dependence of the higher-loop analog of Eq. (2.22) on the β function drops out.

Next, we would need knowledge of the infrared anomalous dimension $\gamma_{\rm IR}$. Infrared singularities are very well understood [146, 152–157, 165]. Our case is special, with a rather simple infrared structure. We are interested in the first loop order at which the higher-dimension operator could be renormalized. This would be the first loop order for which it is possible to write down valid diagrams. The lack of diagrams at lower-loop order means there cannot be any $\log(\mu_{\rm IR})$ terms or corresponding $\gamma_{\rm IR}$ at the given loop order under consideration. In addition, infrared singularities are diagonal for the operators with distinct fields, mixing only via color. Therefore at this order $\gamma_{\rm IR} = 0$. Various examples will be given in later sections.

Thus, application of Eq. (2.19) is particularly simple for our case so that the relation between the first potentially nonvanishing anomalous dimension and unitarity cuts is direct:

$$(\gamma_{sl}^{\rm UV})^{(L)} \langle p_1, ..., p_n | \mathcal{O}_s | 0 \rangle^{(0)} = -\frac{1}{\pi} {}_s\langle p_1, ..., p_n | \mathcal{M} \otimes \mathcal{O}_l | 0 \rangle \,. \tag{2.40}$$

With this relation at hand, it is now straightforward to argue for new non-renormalization zeros by analyzing the allowed unitarity cuts. Eq. (2.40) gives $(\gamma_{sl}^{\rm UV})^{(L)}$ in terms of a sum over cuts of the form illustrated in Figs. 2.1 and 2.2 which in general include multiloop amplitudes and form factors. The left-hand side of any such k-particle cut is a $n_{\mathcal{M}}$-point amplitude, with the number of particles external to the cut equal to $n_{\mathcal{M}} - k$. Similarly the right-hand side is an n_F-point form factor, with $n_F - k$ particles external to the cut. Now, for the minimal form factor, the total number of external particles must match the length

of $\mathcal{O}_s$, so we must have the relation,

$$n_{\mathcal{M}} + n_F - 2k = l(\mathcal{O}_s)\,. \tag{2.41}$$

The number of legs $n_{\mathcal{M}}$ and n_F are both bounded from below. For the unitarity cut to be non-zero, the scattering amplitude on the left must have at least two external particles, that is, $n_{\mathcal{M}} \geq k + 2$. On the other side, n_F is restricted by the requirement that the form factor not include any scaleless bubbles. Since all legs of the form factor, including those crossing the cut, are on shell, any such scaleless bubbles would evaluate to zero. At one loop, for example, this implies $n_F \geq l(\mathcal{O}_l)$, which is the same as the tree level relation. At higher loops the particle count can be reduced depending on the number of loops in the form factor, which produces the relation

$$n_F \geq l(\mathcal{O}_l) - (L_F - 1) - \delta_{L_F,0}\,. \tag{2.42}$$

Here L_F is the number of loops contained in the form factor. $\delta_{L_F,0}$ is unity if the form factor is at tree level and zero otherwise, which accounts for the fact that there is no reduction in particle number between tree level and one loop. By considering the possible placings of the loops in the cut or on either side of the cut, we have $L_F \leq L - (k-1)$, implying $n_F \geq l(\mathcal{O}_l) - L + k - \delta_{L_F,0}$. Combining this with the condition on $n_{\mathcal{M}}$ and plugging in to equation (2.41), we obtain

$$l(\mathcal{O}_l) - L + 2 - \delta_{L_F,0} \leq l(\mathcal{O}_s)\,. \tag{2.43}$$

This inequality shows that the difference in length of the operators can preclude the renormalization unless

$$L > l(\mathcal{O}_l) - l(\mathcal{O}_s)\,, \tag{2.44}$$

and thus completes the proof of the first form of our theorem. In summary, we have shown that at loop orders less than or equal to $l(\mathcal{O}_l) - l(\mathcal{O}_s)$ there are no allowed unitarity cuts that can capture the coefficient of $\log(\mu^2)$, which in turn implies that $\gamma_{sl}^{\rm UV} = 0$. Eq. (2.43) also shows that the contributions to the anomalous dimension at loop order $L = l(\mathcal{O}_l) - l(\mathcal{O}_s) + 1$ are captured by cuts of the type in Figs. 2.1 and 2.2(c), that are given purely in terms of tree-level matrix elements. Cuts of the type in Fig. 2.2(b) are directly ruled out by Eq. (2.43) and cuts of the type in Fig. 2.2(a) are ruled out because $l(O_l) - l(O_s) + 2$ legs need to be sewn across the cut to have a total of $l(O_s)$ external legs, so that all $l(O_l) - l(O_s) + 1$ loops are accounted for in the cut. This observation should help in their computation, for instance by allowing the use of four-dimensional helicity methods to evaluate the cut. It also implies that helicity selection rules can be active beyond one loop, contrary to expectations.

Depending on the particle contents of the two operators, it might happen that there are no allowed unitarity cuts even at a higher loop order than the one predicted by the first form of the theorem. Instead of analyzing the unitarity cuts, this can be explained in the more familiar diagrammatic language. Clearly, if the only diagrams that can be drawn involve scaleless bubbles, there will be no available cut where all loops are included in the cut. Thus, diagrams with fewer cut legs will force the form factor to include the scaleless bubble, and thus to evaluate to zero. Then the corresponding anomalous dimension must also be zero. This explains the more general rule presented in the introduction. As noted above this relies on the absence of infrared singularities whenever corresponding lower-loop form factors vanish.

2.3.2 Examples

Examples of zeros in the SMEFT at one loop are the renormalization of F^3 by $\phi^2 F^2$, and of $D^2\phi^4$, $F\phi\psi^2$, and $D\phi^2\psi^2$ by $\phi^3\psi^2$, which were already explained using the helicity selection rules [24], but also follow from the principles described here. In contrast to the helicity

Table 2.2: Application of the non-renormalization theorem to dimension-five operators. The operators labeling the rows are renormalized by the operators labeling the columns. $\times_L$ indicates the theorem applies at L-loop order. (L) denotes that there are no diagrams before L-loops, but renormalization is possible at that order, since the required cuts can exist. Light-gray shading indicates a zero at one loop due to helicity selection rules, while dark-gray shading indicates the entry is a new zero predicted by our non-renormalization theorem.

	$F^2\phi$	$F\psi^2$	$\phi^2\psi^2$	ϕ^5
$F^2\phi$			(2)	$\times_2$
$F\psi^2$			$\times_1$	$\times_3$
$\phi^2\psi^2$				(2)
ϕ^5				

Table 2.3: Application of the non-renormalization theorem to dimension six. The notation is explained in Table I.

	F^3	ϕ^2F^2	$F\phi\psi^2$	$D^2\phi^4$	$D\phi^2\psi^2$	ψ^4	$\phi^3\psi^2$	ϕ^6
F^3		$\times_1$	(2)	$\times_2$	$\times_2$	$\times_2$	$\times_3$	$\times_3$
ϕ^2F^2							(2)	$\times_2$
$F\phi\psi^2$							$\times_1$	$\times_3$
$D^2\phi^4$							$\times_1$	$\times_2$
$D\phi^2\psi^2$							$\times_1$	(3)
ψ^4							(2)	(4)
$\phi^3\psi^2$								(2)
ϕ^6								

selection rules, however, our theorem can also apply at higher loops. The full set of zeros predicted by our rules for operators of dimensions five, six and seven includes examples at one through four loops and is described in Tables 2.2, 2.3, and 2.4 respectively. The tables also indicate the overlap between our theorem and the one-loop helicity selection rules of [24]. Note we have combined some of the categories of operators of [24], since our theorem does not need to distinguish operators based on their chirality.

Consider now two calculations that show explicit examples, from Table 2.3, of the non-trivial zeros in the anomalous-dimension matrix at two loops. The examples will also demonstrate the vanishing of $\gamma_{\rm IR}$. The first example is the renormalization of $\mathcal{O}_{\phi^2F^2}$ by $\mathcal{O}_{\phi^6}$, which

Table 2.4: Application of the non-renormalization theorem to dimension seven. The notation is explained in Table I. The shortest and longest operators have been dropped from the list of columns and rows, respectively, since our theorem requires a reduction in length of the operators.

	ϕ^3F^2	$D^2\phi^5$	$D\phi^3\psi^2$	$\phi\psi^4$	$F\phi^2\psi^2$	$\phi^4\psi^2$	ϕ^7
$F^3\phi$	$\times_1$	$\times_2$	$\times_2$	$\times_2$	(2)	$\times_3$	$\times_3$
$D^2F\phi^3$	$\times_1$	$\times_1$	$\times_1$	$\times_2$	$\times_1$	$\times_2$	$\times_3$
$DF\phi\psi^2$	(2)	$\times_2$	$\times_1$	$\times_1$	$\times_1$	$\times_2$	$\times_4$
$F^2\psi^2$	(2)	(3)	(2)	(2)	$\times_1$	$\times_2$	$\times_4$
$D^2\phi^2\psi^2$	(2)	(2)	$\times_1$	$\times_1$	$\times_1$	$\times_2$	(4)
$D\psi^4$	(3)	(3)	(2)	$\times_1$	(2)	(3)	(5)
ϕ^3F^2						(2)	$\times_2$
$D^2\phi^5$						$\times_1$	$\times_2$
$D\phi^3\psi^2$						$\times_1$	(3)
$\phi\psi^4$						(2)	(4)
$F\phi^2\psi^2$						$\times_1$	$\times_3$
$\phi^4\psi^2$							(2)

is the entry (2,8) of Table 2.3.

The minimal two-loop form factor for $\mathcal{O}_{\phi^2F^2}$ includes two external scalars and two external gauge bosons. The product $\mathcal{M}F^*$ in Eq. (2.19) at two loops requires either a cut between a five-point amplitude and the tree-level form factor or a four-point amplitude and a one-loop form factor with an insertion of $\mathcal{O}_{\phi^6}$. However, the cut between the five-point amplitude and the tree-level form factor leaves five total external legs, and thus cannot match the minimal form factor for $\mathcal{O}_{\phi^2F^2}$. For the cut between the four-point amplitude and the one-loop form factor to match the minimal form factor for $\mathcal{O}_{\phi^2F^2}$, the one-loop form factor would have to involve a massless tadpole, which would evaluate to zero.

We can also directly check that the (single) diagram—Fig. 2.4(a)—for the $\mathcal{O}_{\phi^6} \to \mathcal{O}_{\phi^2F^2}$ renormalization evaluates to zero. By incorporating an IR regulator $\lambda_{\rm IR}$, we can evaluate the integral while keeping the UV and IR dependences separate and determine the behavior of the form factor in the limit $\lambda_{\rm IR} \to 0$. The integral for this diagram immediately factorizes,

and each of the two loop integrals is of the form

$$\int \frac{d^D\ell_1}{(2\pi)^D} \frac{(2\ell_1 - k_1)\cdot\varepsilon_1}{(\ell_1^2 - \lambda_{\rm IR})((\ell_1 - k_1)^2 - \lambda_{\rm IR})}\,. \tag{2.45}$$

This integral vanishes by the on-shell condition $k_1 \cdot \varepsilon_1 = 0$ and Lorentz invariance, since k_1 is the only available momentum. Therefore $\mathcal{O}_{\phi^6}$ cannot renormalize $\mathcal{O}_{\phi^2 F^2}$ at two loops.

For a slightly more complex example, consider the renormalization of $\mathcal{O}_{F^3}$ by $\mathcal{O}_{\psi^4}$ at two loops, corresponding to entry (1,6) of Table 2.3. Again, for this process the three-particle cut between the five-point amplitude and the tree-level form factor does not produce the correct external-particle state corresponding to the field content of $\mathcal{O}_{F^3}$. The two-particle cut between the four-point amplitude and the one-loop form factor with an insertion of $\mathcal{O}_{\psi^4}$ is shown in Figure 2.4(b). By again adding an IR regulator, the result can be written as

$$\int d\mathrm{LIPS}_{\ell_1} \frac{d^D\ell_2}{(2\pi)^D} \frac{\mathrm{Tr}[X(\ell_1)\not{\ell}_2\not{\varepsilon}_3(\not{\ell}_2 - \not{k}_3)]}{(\ell_2^2 - \lambda_{\rm IR})((\ell_2 - k_3)^2 - \lambda_{\rm IR})}\,, \tag{2.46}$$

where X receives contributions from the multiple possible diagrams of the four-point amplitude and includes the remaining propagators. LIPS indicates that the integration is over the Lorentz-invariant phase space of the particles crossing the cuts.

One can reduce the ℓ_2 tensor integrals using standard techniques to obtain the following result

$$\begin{aligned}\int \frac{d^D\ell_2}{(2\pi)^D} \frac{\ell_2^\mu \ell_2^\nu}{(\ell_2^2 - \lambda_{\rm IR})^2} \int d\mathrm{LIPS}_{\ell_1}\, Y_{\mu\nu}(\ell_1) \\ = -\frac{i\Gamma(-1+\epsilon)}{2(4\pi)^{2-\epsilon}} (\lambda_{\rm IR})^{1-\epsilon} \int d\mathrm{LIPS}_{\ell_1}\, Y^\mu{}_\mu(\ell_1)\,,\end{aligned} \tag{2.47}$$

where $\epsilon = (4-D)/2$, Y contains the rest of the trace in Eq. (2.46), and terms linear in ℓ_2 cancel. Since the phase-space integral can at worst result in a $\log(\lambda_{\rm IR})$ divergence, the factor $(\lambda_{\rm IR})^{1-\epsilon}$ ensures that the expression goes smoothly to zero as $\lambda_{\rm IR}$ approaches zero for

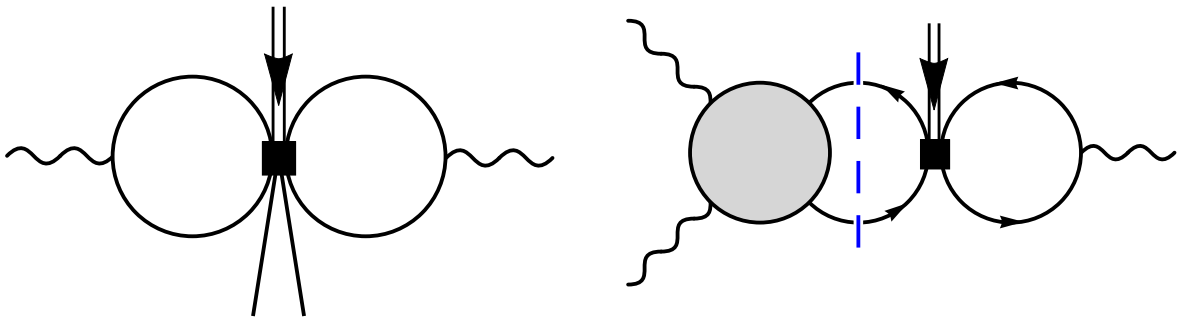

Figure 2.4: (a) Diagram showing the only possible two loop contribution to the renormalization of $\mathcal{O}_{\phi^2 F^2}$ by $\mathcal{O}_{\phi^6}$. (b) Cut of a form factor showing that $\mathcal{O}_{\psi^4}$ cannot renormalize $\mathcal{O}_{F^3}$ at two loops. The solid square indicates the insertion of the ϕ^6 or ψ^4 operator, respectively.

all orders in ϵ. Therefore the cut vanishes, along with the UV anomalous dimension.

2.4 One-loop amplitudes and anomalous dimensions

In this section we describe our generalized unitarity calculation of the one-loop amplitudes with an insertion of a higher-dimensional operator in our simplified model. We then extract the one-loop anomalous dimension matrix of this theory. Finally, we comment on the structure of rational terms in the amplitudes and on the ability to set some of them to zero with a judicious scheme choice. The results in this section are building blocks needed for the two-loop analysis in the next section. In addition, they provide one-loop anomalous dimensions that can be cross-checked against those in Refs. [19–21].

2.4.1 One-loop amplitudes from generalized unitarity

The generalized unitarity method [43–46, 97, 132, 133] for constructing one-loop amplitudes can be found in various reviews, for example see Ref. [166–169], but here we briefly review the procedure for the one-loop case. To construct the full one-loop amplitudes to all orders in the dimensional-regularization parameter ϵ, we begin with the D-dimensional four-point tree-level amplitudes with or without insertions of the dimension-6 operators (given in Appendix

2.B). By using D-dimensional tree amplitudes, we ensure that the cuts appropriately capture the coefficients of the D-dimensional box, triangle, and bubble scalar integrals that form a basis for the full one-loop amplitudes, as in Eq. (2.13). In general, the coefficients have ϵ dependence, and expanding in ϵ produces rational terms that would not automatically be included if a purely four-dimensional approach to the cuts were used [43, 44, 97]. Besides ϵ, the coefficients only depend on the Mandelstam invariants $s = (k_1 + k_2)^2$, $t = (k_2 + k_3)^2$ and $u = (k_1 + k_3)^2$.

We construct the cuts in the standard way. For example, the integrand-level s-channel cut with an $\mathcal{O}_n$ operator insertion is given by

$$\begin{aligned}
&\sum_i \mathcal{C}^{[i]} \left(\left[a^{st}_{4,n[i]} I_{4,st} + a^{su}_{4,n[i]} I_{4,su} + a^{s}_{3,n[i]} I_{3,s} + a^{s}_{2,n[i]} I_{2,s} \right] \Big|_{\ell^2=0} \right) \\
&\quad = \sum_{\text{states}} \sum_j \mathcal{C}^{[j]} A^{(0)}_n(1, 2, \ell_1^{h_1}, \ell_2^{h_2})_{[j]} \sum_k \mathcal{C}^{[k]} A^{(0)}(-\ell_2^{h_2}, -\ell_1^{h_1}, 3, 4)_{[k]} \\
&\qquad + \sum_{\text{states}} \sum_j \mathcal{C}^{[j]} A^{(0)}(1, 2, \ell_1^{h_1}, \ell_2^{h_2})_{[j]} \sum_k \mathcal{C}^{[k]} A^{(0)}_n(-\ell_2^{h_2}, -\ell_1^{h_1}, 3, 4)_{[k]} \,,
\end{aligned} \tag{2.48}$$

where the sum over states includes the helicity and the color, and, for this case, $\ell_2 = -(\ell_1 + k_1 + k_2)$. The $\mathcal{C}^{[i]}$ are the appropriate color factors for the associated amplitudes. Since the cut legs are on-shell, where $\ell_1^2 = \ell_2^2 = 0$. Often, the external particles will restrict $A^{(0)}_n$ to be nonzero only for certain cuts or placements within the cuts, depending on the field content of the operator inserted.

As an example, the cuts of the amplitude $A^{(1)}_{F^3}(1_\psi 2_{\bar{\psi}} 3\, 4)$, are shown in Figure 2.5, where the operator $\mathcal{O}_{F^3}$ should be inserted on either side of the cuts, when the tree amplitudes exist. Other amplitudes with four-point operators require only the cuts corresponding to their correct external particles. The color factors $\mathcal{C}^{[j]}\mathcal{C}^{[k]}$ can be reduced to the appropriate color basis of the full amplitude, $\mathcal{C}^{[i]}$, based on the external particles. Doing so determines the contribution from each color-decomposed cut.

We evaluate the cuts using the D-dimensional state sum completeness relations,

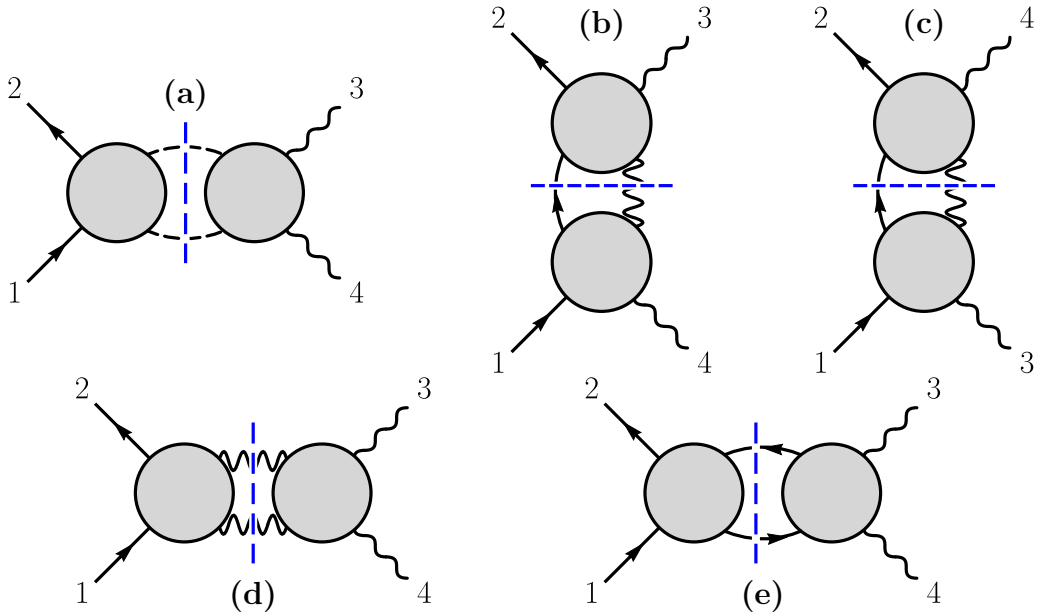

Figure 2.5: The necessary cut for constructing a two-fermion, two-vector amplitude. For an amplitude with an insertion of a higher-dimension operator, one should insert the operator into either side of the diagrams when possible. The wavy lines are vector bosons, the lines with arrows fermions and the dashed lines scalars.

$$\begin{aligned} \epsilon_i^{*\mu} \odot \epsilon_i^{\nu} &= \sum_{\text{states } h} \epsilon_i^{*(h)\mu} \epsilon_i^{(h)\nu} = -g^{\mu\nu} + \frac{q^\mu k_i^\nu + k_i^\mu q^\nu}{q \cdot k_i}\,, \\ \bar{u}_i \odot u_i &= \sum_{\text{states } h} \bar{u}_i^{(h)} u_i^{(h)} = \not{k}_i\,, \end{aligned} \tag{2.49}$$

where q is an arbitrary reference vector with $q^2 = 0$.

The next task is to merge the cuts and to integrate. One can merge the cuts at the level of the integrand to find a single integrand that has the correct cuts in all channels. However, is it is generally simpler to merge the integrated results from each cut, treating each cut as an off-shell object, but dropping contributions that do not have a cut in the given channel. Integration is done by projecting each cut for a given process onto a basis of gauge-invariant tensors, as described in more detail in Appendix 2.A. Although the methods we use to extract anomalous dimensions do not require us to keep track of evanescent divergences, because the projection technique is fully D dimensional, we track them and confirm that they do not enter our calculations of various entries in the two-loop anomalous-dimension matrix. An

alternative is to use spinor-helicity methods [170–172] which are much more powerful when the number of external legs increases. These have been successfully used for both chiral [45] and higher-loop calculations [173], but then additional care is needed to deal with subtleties that arise from using dimensional regularization.

After projection, the cut integrand is rewritten in terms of inverse propagators. We reduce the remaining integrals to the basis of scalar integrals in Eq. (2.13) using integration by parts relations as implemented in FIRE [136–138]. Cut merging is then straightforward, as the coefficients of integrals in the merged amplitude can be read directly off the results from each cut, summed over the possible particles crossing the cut. For example, the s-channel cut in Eq. (2.48) yields the coefficients of the s-channel bubble and triangle, as well as those of the (s,t) and (s,u) boxes in Eq. (2.13).

The full set of D-dimensional four-point one-loop amplitudes for the dimension-six operators in our model are given in the ancillary files attached to the ArXiV submission of Ref. [2]. These expressions are valid to all orders in ϵ, but to obtain the finite, renormalized expressions needed to feed into our calculation of two-loop anomalous dimensions, we need to subtract the UV poles.

The one-loop amplitudes are IR divergent. The IR singularities of gauge theories are well understood [145, 146, 152–157], and can be expressed in terms of lower-loop amplitudes involving the same operator insertion and external particles. The explicit form of the one-loop infrared singularity, for example, is given by

$$A_i^{(1)} = \boldsymbol{I}^{(1)} A_i^{(0)} \,, \tag{2.50}$$

where the IR operator $\boldsymbol{I}^{(1)}$ is given by [145, 146, 152–157][5]

$$\boldsymbol{I}^{(1)} = \frac{e^{\epsilon\gamma_E}}{\Gamma(1-\epsilon)} \sum_{p=1}^{n} \sum_{q\neq p} \frac{\boldsymbol{T}_p \cdot \boldsymbol{T}_q}{2} \left[\frac{\gamma_{\rm cusp}^{\rm IR\,(1)}}{\epsilon^2} - \frac{\gamma_{{\rm c},\,p}^{\rm IR\,(1)}}{\boldsymbol{T}_p^2} \frac{1}{\epsilon} \right] \left(\frac{-\mu^2}{2k_p\cdot k_q} \right)^{\epsilon} \,, \tag{2.51}$$

[5]The difference with the formulas in those references is due to our normalization of the $SU(N)$ generators.

where the sums are over external particles. The color charge $\boldsymbol{T}_p = \{T_p^a\}$ is a vector with respect to the generator label a and a SU(N) matrix with respect to the outgoing particle p. The infrared divergence includes a $1/\epsilon^2$ pole, with coefficient given by the cusp anomalous dimension $\gamma_{\text{cusp}}^{\text{IR}\,(1)} = 4\tilde{g}^2$, and $1/\epsilon$ poles, with coefficient given by the collinear anomalous dimension of particle p given in Eq. (2.16). By obtaining the IR dependence of the one-loop amplitudes from Eq. (2.50), we can subtract it from the full one-loop amplitudes. As always, the definition of the IR-divergent parts carries with it some arbitrariness as to which finite pieces are included.[6]

The remaining poles in ϵ are UV poles, which we then match to the appropriate tree-level counterterm amplitude containing an insertion of the operator $\mathcal{O}_j$. A complication is that there can be multiple operators corresponding to the same external particle content, but with different color structures. Therefore, in these cases the coefficient of a single color factor in the loop amplitude is insufficient for the purpose of determining the anomalous dimensions, and in principle all the color factors for the given process and operator insertion must be considered simultaneously. For example, the one-loop amplitude with an insertion of the $\mathcal{O}_{(D\varphi^2\psi^2)_2}$ operator and four external scalars determines the renormalization of both the $\mathcal{O}_{(D^2\varphi^4)_1}$ and the $\mathcal{O}_{(D^2\varphi^4)_2}$ operators, where the operators are given in Table 2.1.

In some cases the IR structure is trivial, e.g. when the IR anomalous dimensions are zero simply because there are no lower-loop amplitudes for a given operator and given external state. Our examples in Section 2.5 follow this pattern. For instance, in the example of $\mathcal{O}_{(D^2\varphi^4)_1}$ renormalizing $\mathcal{O}_{(\psi^4)_1}$ at two loops, there is no tree level or one-loop amplitude with an insertion of $\mathcal{O}_{(D^2\varphi^4)_1}$ which has an external state of four fermions, simply due to the lack of Feynman diagrams. Since the full IR dependence is proportional to lower-loop amplitudes, this implies there cannot be an IR divergence at two loops. This same reasoning underpinned the non-renormalization theorem proved in the previous section. More generally, one needs to account for the infrared singularities.

[6] In physical quantities this arbitrariness cancels between real emission and virtual contributions.

2.4.2 One-loop UV anomalous dimensions

After subtracting the IR singularities, the only remaining $1/\epsilon$ poles in the amplitudes correspond to the desired one-loop anomalous dimensions,

$$
\begin{aligned}
\dot{c}_{F^3} &= \tilde{g}^2(12N - 3b_0)c_{F^3}\,, \\
\dot{c}_{(\varphi^2F^2)_1} &= \tilde{g}^2\left(-5c_{F_3} - \frac{(3N^2-7)+2Nb_0}{N}c_{(\varphi^2F^2)_1} + \frac{N^2-4}{N^2}c_{(\varphi^2F^2)_2}\right) \\
&\quad + \tilde{\lambda}\,4(1+N)c_{(\varphi^2F^2)_1}\,, \\
\dot{c}_{(\varphi^2F^2)_2} &= \tilde{g}^2\left(-Nc_{F^3} + 2c_{(\varphi^2F^2)_1} + \frac{2N^2-5-2Nb_0}{N}c_{(\varphi^2F^2)_2}\right) + \tilde{\lambda}\,4c_{(\varphi^2F^2)_2}, \\
\dot{c}_{(D^2\varphi^4)_1} &= \tilde{g}^2\left(\frac{3(N+1)}{N}c_{(D^2\varphi^4)_1} + \frac{2(N-2)(N_s+9)}{3N}c_{(D^2\varphi^4)_2} + \frac{4}{3}\frac{N-2}{N}c^{ww}_{(D\varphi^2\psi^2)_2}\right) \\
&\quad + \lambda\,12c_{(D^2\varphi^4)_1}\,, \\
\dot{c}_{(D^2\varphi^4)_2} &= \tilde{g}^2\left(\frac{36NC_F-(2N-1)(N_s+9)}{3N}c_{(D^2\varphi^4)_2} + \frac{3(N-2)(N+1)}{2N}c_{(D^2\varphi^4)_1}\right. \\
&\quad \left. + \frac{2(2N-1)}{3N}c^{ww}_{(D\varphi^2\psi^2)_2}\right) + \tilde{\lambda}\,\left(2(N-2)c_{(D^2\varphi^4)_1} + 8(N+1)c_{(D^2\varphi^4)_2}\right), \\
\dot{c}^{pr}_{(D\varphi^2\psi^2)_1} &= 0\,, \\
\dot{c}^{pr}_{(D\varphi^2\psi^2)_2} &= \tilde{g}^2\left(\frac{1}{3}N_s c_{(D^2\varphi^4)_2}\delta_{pr} + \frac{1}{3}(-9N+N_s)c^{pr}_{(D\varphi^2\psi^2)_2} + \frac{4}{3}N_f c^{ww}_{(D\varphi^2\psi^2)_2}\delta_{pr}\right. \\
&\quad \left. - \frac{2}{3}N_f c^{pwwr}_{(\psi^4)_1} - \frac{2}{3}N_f\left(2c^{prww}_{(\psi^4)_2} - \frac{1}{N}c^{pwwr}_{(\psi^4)_2}\right)\right), \\
\dot{c}^{mnpr}_{(\psi^4)_1} &= \tilde{g}^2\frac{6\,(N^2-1)}{N^2}c^{mnpr}_{(\psi^4)_2}\,, \\
\dot{c}^{mnpr}_{(\psi^4)_2} &= \tilde{g}^2\left(-\frac{N_s}{3}(c^{mn}_{(D\varphi^2\psi^2)_2}\delta_{pr} + c^{pr}_{(D\varphi^2\psi^2)_2}\delta_{mn})\right. \\
&\quad + \frac{2}{3}N_f(\delta_{mn}c^{pwwr}_{(\psi^4)_1} + \delta_{pr}c^{mwwn}_{(\psi^4)_1}) + 6c^{mnpr}_{(\psi^4)_1} - \frac{3}{N}c^{mnpr}_{(\psi^4)_2} \\
&\quad \left. + \frac{2N_f}{3N}(2N(\delta_{pr}c^{mnww}_{(\psi^4)_2} + \delta_{mn}c^{prww}_{(\psi^4)_2}) - (\delta_{pr}c^{mwwn}_{(\psi^4)_2} + \delta_{mn}c^{pwwr}_{(\psi^4)_2}))\right)\,. \qquad (2.52)
\end{aligned}
$$

Here N_s is left as a parameter to track contributions from scalar loops. In our model it should be set to unity. These anomalous dimensions have been extracted directly from the

	F^3	$(\varphi^2F^2)_1$	$(\varphi^2F^2)_2$	$(D^2\varphi^4)_1$	$(D^2\varphi^4)_2$	$(D\varphi^2\psi^2)_1$	$(D\varphi^2\psi^2)_2$	$(\psi^4)_1$	$(\psi^4)_2$
F^3		0	0	$\emptyset$	$\emptyset$	$\emptyset$	$\emptyset$	$\emptyset$	$\emptyset$
$(\varphi^2F^2)_1$				0	0	0	0	$\emptyset$	$\emptyset$
$(\varphi^2F^2)_2$				0	0	0	0	$\emptyset$	$\emptyset$
$(D^2\varphi^4)_1$	0	0	0			0		$\emptyset$	$\emptyset$
$(D^2\varphi^4)_2$	0	0	0			0		$\emptyset$	$\emptyset$
$(D\varphi^2\psi^2)_1$	0	0	0	0	0	0	0	0	0
$(D\varphi^2\psi^2)_2$	0	0	0	0		0			
$(\psi^4)_1$	0	$\emptyset$	$\emptyset$	$\emptyset$	$\emptyset$	0	0	0	
$(\psi^4)_2$	0	$\emptyset$	$\emptyset$	$\emptyset$	$\emptyset$	0			

Table 2.5: Structure of the zeros in the one-loop anomalous dimension matrix. The $\emptyset$ entries indicate there are no contributing one-loop diagrams, whereas a 0 alone indicates that there are one-loop diagrams that could contribute, but actually give a vanishing result. The operators labeling the rows are renormalized by the operators labeling the columns.

scattering amplitudes, and, as a cross-check, we also used the unitarity cut method explained in the previous section [98] for computing directly the anomalous dimensions. The structure of the anomalous dimension matrix is summarized in Table 2.5. It is worth pointing out the simplicity in the renormalization and mixing of $(D\varphi^2\psi^2)_1$ and $(\psi^4)_1$, which is due to these operators being a product of global symmetry currents, which heavily constrains the kind of states they can overlap with. This is special in our model, which does not contain an Abelian gauge field. In the presence of the latter, the operators would be a product of gauge symmetry currents (just like $(D\varphi^2\psi^2)_2$ and $(\psi^4)_2$) which are renormalized [174], so the anomalous dimension matrix will receive contributions proportional to the Abelian gauge coupling.

We use these results to verify a representative set of the one-loop anomalous dimension calculated in Ref. [19–21], including entries from nearly all classes of operators. Additional details about this verification is given in Section 2.6. This provides a nontrivial check on our one-loop results, which we then feed into the two-loop anomalous dimension calculations.

2.4.3 Structure of one-loop amplitudes and rational terms

	$V^+V^+V^+V^+$	$V^+V^+V^+V^-$	$V^+V^+V^-V^-$	ϕV^+V^+	$\phi\phi V^+$	$\phi\phi\phi\phi$	$\psi^-\psi^+V^+V^+$	$\psi^-\psi^+V^+V^-$	$\psi^-\psi^+V^-V^+$	$\psi^+\psi^+V^-V^-$	$\phi\phi\psi^+\psi^-$	$\psi^+\psi^-\psi^+\psi^-$	$\psi^+\psi^-\psi^+\psi^-$	$\psi^+\psi^+\psi^-\psi^-$
F^3	L	L	R	L	R	0	L	R	R	L	0	0	0	0
$(\varphi^2F^2)_1$	R	0	R	L	R	0	0	0	0	0	0	∅	∅	∅
$(\varphi^2F^2)_2$	R	0	R	L	L	0	0	0	0	0	0	∅	∅	∅
$(D^2\varphi^4)_1$	∅	∅	∅	0	0	L_0	∅	∅	∅	∅	0	∅	∅	∅
$(D^2\varphi^4)_2$	∅	∅	∅	R	0	L_0	∅	∅	∅	∅	L_0	∅	∅	∅
$(D\varphi^2\psi^2)_1$	∅	∅	∅	0	0	0	0	0	0	0	L_0	0	0	0
$(D\varphi^2\psi^2)_2$	∅	∅	∅	R	0	L_0	R	0	0	R	L_0	L_0	L_0	L_0
$(\psi^4)_1$	∅	∅	∅	∅	∅	∅	R	0	0	R	L_0	L	L	L
$(\psi^4)_2$	∅	∅	∅	∅	∅	∅	R	0	0	R	L_0	L	L	L

R: rational amplitude
L: amplitude with both logarithms and rational terms
∅: trivial zero, no contributing one-loop diagrams
0: zero explained by angular momentum selection rules [95]
0: zeros "accidental" to our model
0: zero from an appropriate local counterterm
L_0 zero rational term from an appropriate local counterterm, logarithmic terms remain.

Table 2.6: Structure of the zeros, rational terms, and logarithms in the full one-loop helicity amplitudes. In this table each entry indicates whether the operator of its row produces the amplitude with external state corresponding to its column. V denotes a vector boson, ψ a fermion and φ a scalar.

After subtracting the infrared singularities and renormalization, the amplitudes are finite. The full set of results for our renormalized and IR-subtracted amplitudes is given in Appendix 2.B. The renormalized helicity amplitudes include a large number of zeros, including those which would otherwise be rational contributions. A number of these zeros were pointed out in Ref. [96], and explained using angular-momentum selection rules in Ref. [95]. These

selection rules explain most of the observed zeros, leaving some "accidental" zeros, displayed as a blue 0 in Table 2.6. These zeros can be considered an accident of the simplicity of our model, and in a more general theory with an Abelian gauge field, one would expect that such zeros would not occur. In each case, the entry directly below the blue zero shows that while the accident holds for that particular operator, another operator with identical particle content, but different color structure, produces a nonzero result in $\bar{\text{MS}}$. Intuitively this is because only the first of each pair of operators is a product of global symmetry currents in our model (c.f. our discussion in Section 2.4.2). Alternatively, these "accidental" examples can be shown to follow from angular momentum selection rules combined with selection rules for gauge charges (i.e. color selection rules), as described in [95].

Perhaps more interesting is the surprisingly large number of amplitudes—with shaded (red) rectangles around 0 entries in Table 2.6—which do not evaluate to zero in the standard $\bar{\text{MS}}$ renormalization scheme, but which are proportional to a linear combination of the tree-level amplitudes of the dimension-six operators. These amplitudes can therefore be set to zero by an appropriate choice of finite counterterms. This corresponds to a scheme change, showing that these amplitudes are scheme dependent. Explicit examples of how these rational shifts are related to the scheme dependence of the two-loop anomalous dimensions is discussed at length in the next section.

Similarly, for a number of amplitudes (marked L_0 and in a shaded ref rectangle in Table 2.6), all rational terms in the amplitude can be removed with an appropriate choice of finite counterterms, leaving behind logarithmic terms which cannot be subtracted in this way. These logarithmic terms do not appear to be of the right form to produce local results, so we may expect that they also do not produce contributions to the two-loop anomalous dimensions via Eq. (2.37). It would be interesting to investigate this, but we refrain from doing so here. Remarkably, only a small number of the one-loop amplitudes contain rational terms that cannot be removed via finite counterterms.

As expected, however, some amplitudes do contain non-local rational amplitudes, pro-

hibiting such a simple subtraction by a local counterterm. It is interesting to note that all the nonzero rational amplitudes of $(D^2\varphi^4)_2, (D\varphi^2\psi^2)_2, (\psi^4)_1$ and $(\psi^4)_2$ are non-local but can be individually set to zero by the introduction of an F^3ffinite counterterm. This procedure, however, will always introduce new diagrams which make other $\emptyset$ entries in the same row nonzero. For example, since the F^3 tree contains nonzero four-vector tree amplitudes, entries in these columns will no longer be zero. Another interesting observation is that the UV divergence in the only nonzero amplitude of $(D\varphi^2\psi^2)_1$ cancels between terms, but the logarithms remain.

The vanishing one-loop amplitudes strongly suggests that many contributions to the two-loop anomalous dimension matrix should vanish, beyond those identified in Section 2.3. For many of the two-loop anomalous dimensions, these zeros imply that the only contribution to the final result comes from the three-particle cut, making their evaluation much simpler than expected, since only four-dimensional tree-level objects are involved. In a number of cases, including multiple examples in Section 2.5, the three-particle cut also vanishes, thereby immediately implying that the corresponding two-loop anomalous dimension is zero. Of course, the amplitudes corresponding to the entries of Table 2.6 with shaded (red) rectangles are not zero when working strictly in $\bar{\text{MS}}$, so one would need to evaluate the two-particle cuts in order to determine the corresponding anomalous dimensions in this scheme.

Finally, the appearance of many zeros in Table 2.6 suggests that even more zeros in the two-loop anomalous dimension might be found by using the helicity selection rules of Ref. [24] or the angular momentum conservation rules of Ref. [95], given that the remaining three-particle cut only involves four-dimensional tree amplitudes, which are often restricted by these selection rules.

2.5 Two-loop zeros in the anomalous dimension matrix

In this section we use the results of the previous section and the tools in Section 2.2.3 to obtain two-loop anomalous dimensions in our simplified theory. These calculations will unveil a number of mechanisms that give rise to a wealth of new zeros in the two-loop anomalous dimension matrix. As mentioned in the previous section, two-loop anomalous dimensions are scheme dependent[7] This makes the question of whether a two-loop anomalous dimension is zero somewhat ill-defined. We will show explicit examples of anomalous dimensions that are nonzero in the $\overline{\text{MS}}$ scheme, but for which we can find a scheme in which they are zero. In addition, we demonstrate the cancellation of logarithms in the evaluation of Eq. (2.37) when they appear. For simplicitly, throughout this section, we assume the case of a single flavor of fermion, drop the flavor indices, and set $N_f = N_s = 1$. In all the cases we consider here, the one-loop amplitudes required for the two-loop computation are infrared finite, simplifying the discussion.

2.5.1 Zeros from length selection rules

First we summarize the results of a previous section, which points out a set of nontrivial zeros in the two-loop anomalous dimension matrix of generic EFTs: operators with longer length—those with more field insertions—are often restricted from renormalizing operators with shorter length, even if Feynman diagrams exist. Specifically, for operators $\mathcal{O}_l$ and $\mathcal{O}_s$, with lengths $l(\mathcal{O}_l)$ and $l(\mathcal{O}_s)$, $\mathcal{O}_l$ can renormalize $\mathcal{O}_s$ at L loops only if the inequality $L > l(\mathcal{O}_l) - l(\mathcal{O}_s)$ is satisfied. This implies, for example, that the operator $\mathcal{O}_{\varphi^6}$ cannot renormalize any of the other operators in our model (Table 2.1) at two loops. This is due to the fact that any two-loop diagram with an insertion of $\mathcal{O}_{\varphi^6}$ and four external particles must contain a scaleless integral, which evaluates to zero in dimensional regularization. This implies that the anomalous dimensions vanish, if there are no IR divergences. In this case

[7] This is in contrast to the β-function, which is scheme dependent starting at three loops [175].

the lack of infrared singularities follows from the fact that they are proportional to the corresponding lower-loop amplitudes, which vanish due to the lack of diagrams when the bound is not satisfied.

In addition, as shown in Section 2.3, in a theory with multiple types of fields, such as the SMEFT, additional vanishing can occur at loop orders higher than indicated by the above bound. In general, whenever the only diagrams one can draw with an insertion of $\mathcal{O}_l$ and the external particles of $\mathcal{O}_s$ always involve scaleless integrals, then there will be no renormalization of $\mathcal{O}_s$ by $\mathcal{O}_l$. In the language of Section 2.2.3, this happens because there are no nonzero cuts on the right-hand side of Eq. (2.37) or the higher loop analog. Iteration pieces on the left-hand-side of Eq. (2.37)—terms other than $\gamma^{(L)}_{s\leftarrow l}F^{(0)}_s$—are also set to zero by the presence of scaleless integrals. Examples of this form of the rule in effect include the lack of two-loop renormalization of $\mathcal{O}_{F^3}$ by $\mathcal{O}_{D\varphi^2\psi^2}, \mathcal{O}_{D^2\varphi^4}$, or $\mathcal{O}_{\psi^4}$.

Another important consequence of the length selection rule is that, at loop order $L = l(\mathcal{O}_l) - l(\mathcal{O}_s) + 1$, only the $(L+1)$-particle cut can contribute [1]. For example, the three-particle cut depicted in Figure 2.9(a) is the only cut that can contribute to $\gamma^{\mathrm{UV}(2)}_{F^3\leftarrow(\varphi^2F^2)_1}$. The $(L+1)$-particle cut can then be evaluated using a four-dimensional tree-level amplitudes, making the calculation much simpler than that of a generic L-loop anomalous dimension matrix element. This observation, noted in Section 2.3, makes it straightforward to evaluate certain two-loop SMEFT anomalous dimensions solely from three-particle cuts [129].

2.5.2 Zeros from vanishing one-loop rational terms

Next, we show that the vanishing of many one-loop amplitudes and rational terms found in Section 2.4 yields additional zeros in the two-loop anomalous-dimension matrix of our theory. Somewhat surprisingly, this sometimes involves a cancelation between different contributions to the logarithms from one-loop terms in the cut. We will explain how this relates to the scheme dependence of two-loop anomalous dimensions.

$\mathcal{O}_{\psi^4} \leftarrow \mathcal{O}_{D^2\varphi^4}$

We begin by determining the renormalization of $\mathcal{O}_{(\psi^4)_1}$ and $\mathcal{O}_{(\psi^4)_2}$ by $\mathcal{O}_{(D^2\varphi^4)_1}$, which we denote by $\mathcal{O}_{(\psi^4)_1} \leftarrow \mathcal{O}_{(D^2\varphi^4)_1}$ and $\mathcal{O}_{(\psi^4)_2} \leftarrow \mathcal{O}_{(D^2\varphi^4)_1}$. To extract the anomalous dimensions, we examine cuts of amplitudes with four external quarks. We can readily prove that these anomalous dimension matrix elements are zero at two loops in our model. The contributing cuts would be

1. the three-particle cut between the five-point dimension-four tree amplitude and the five-point $(D^2\varphi^4)_1$ amplitude,

2. the two-particle cut between the four-point dimension-four one-loop amplitude and the four-point $(D^2\varphi^4)_1$ tree, and

3. the two-particle cut between the four-point dimension-four tree and the four-point $(D^2\varphi^4)_1$ one-loop amplitude.

In all cases the external particles must be four fermions to match the desired operator.

In case (1), the five point amplitude containing the operator $(D^2\varphi^4)_1$ must have two external fermions, but since the Yukawa couplings are set to zero in our simplified model, the $(D^2\varphi^4)_1$ tree must have at least four scalars, prohibiting the required three-scalar two-fermion amplitude. For case (2), the $(D^2\varphi^4)_1$ tree must again have two fermions, so that there are no valid diagram and the cut vanishes.

The vanishing of case (3) relies on our knowledge of the one-loop amplitudes with an operator insertion$(D^2\varphi^4)_1$, given in Appendix 2.B. In this case, the only $\mathcal{O}_{(D^2\varphi^4)_1}$ one-loop amplitude that can be inserted into the cut is the two-scalar two-fermion amplitude—as in Figure 2.6—which is zero for this operator. Therefore, all possible contributing cuts evaluate to zero. Since $\mathcal{O}_{(D^2\varphi^4)_1}$ does not renormalize $\mathcal{O}_{\varphi^2\psi^2 D}$ or $\mathcal{O}_{\psi^4}$ at one loop, which otherwise produce terms on the left-hand-side of Eq. (2.37), the vanishing of the three types of cuts implies that the two-loop anomalous-dimension matrix element is also zero.

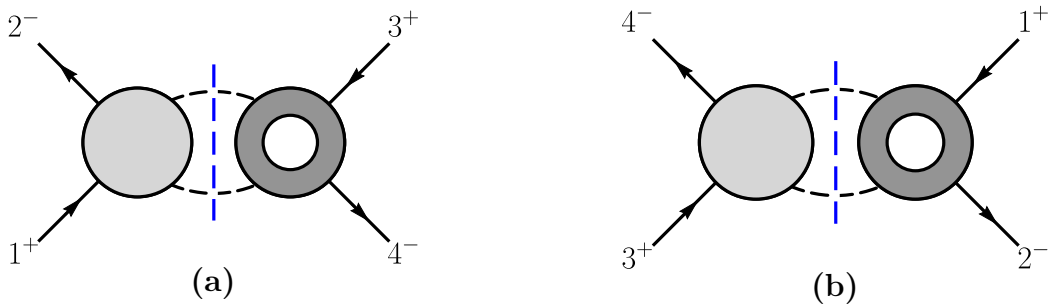

Figure 2.6: The (12)-channel (a) and (34)-channel (b) unitary cuts which determine the renormalization of $\mathcal{O}_{(\psi^4)_1}$ by $\mathcal{O}_{(D^2\varphi^4)_1}$ or $\mathcal{O}_{(D^2\varphi^4)_2}$. The (23)- and (14)-channel cuts are given by the exchange of legs 2 and 4. In each, the darker blobs indicate a higher-dimension operator insertion, and the vertical (blue) dashed line indicates the integral over phase space of the particles crossing the cut.

Next, consider the case $\mathcal{O}_{(\psi^4)_1} \leftarrow \mathcal{O}_{(D^2\varphi^4)_2}$, which we also show has a zero entry in the anomalous dimension matrix of our simplified model. We organize the calculation into the three types of cuts as in the previous case, with the only difference being that, in case (3), the one-loop amplitude with an insertion of $\mathcal{O}_{(D^2\varphi^4)_2}$, and with two scalars and two fermions as external particles is nonzero, and in fact has a UV divergence. While the presence of nonzero cuts, shown diagrammatically in Figure 2.6, might seem to imply that the two-loop anomalous dimension must be nonzero, we will show that it actually evaluates to zero as well.

Using the external state $\langle 1^+_\psi 2^-_{\overline{\psi}} 3^+_\psi 4^-_{\overline{\psi}} |$ and setting $\mathcal{O}_i = \mathcal{O}_{(D^2\varphi^4)_2}$, Eq. (2.37) reduces to

$$\begin{aligned} &\gamma^{\mathrm{UV}(2)}_{\psi^4 \leftarrow (D^2\varphi^4)_2} F^{(0)}_{\psi^4} + \gamma^{\mathrm{UV}(1)}_{(D\varphi^2\psi^2)_2 \leftarrow (D^2\varphi^4)_2} F^{(1)}_{(D\varphi^2\psi^2)_2} \\ &\qquad = -\frac{1}{\pi} (\mathcal{M}^{12}_{2\to 2} + \mathcal{M}^{14}_{2\to 2} + \mathcal{M}^{23}_{2\to 2} + \mathcal{M}^{34}_{2\to 2})^{(0)} \otimes \mathrm{Re} F^{(1)}_{(D^2\varphi^4)_2} \,, \end{aligned} \tag{2.53}$$

where on the right-hand side we only find cuts of the form in Figure 2.6 with an $\mathcal{O}_{(D^2\varphi^4)_2}$ insertion, and the (13) and (24) channels are not allowed. For instance the (12)-channel cut

is

$$
\begin{aligned}
&(\mathcal{M}^{12}_{2\to 2})^{(0)} \otimes \mathrm{Re}F^{(1)}_{(D^2\varphi^4)_2} \\
&\quad = 2\int d\mathrm{LIPS}_2\, \langle 1^+_\psi 2^-_{\overline{\psi}} |\mathcal{M}| \ell_{1\,\varphi} \ell_{2\,\overline{\varphi}} \rangle^{(0)}\, \mathrm{Re}\langle \ell_{1\,\varphi} \ell_{2\,\overline{\varphi}} 3^+_\psi 4^-_{\overline{\psi}} |\mathcal{O}_{(D^2\varphi^4)_2}|0\rangle^{(1)} \,.
\end{aligned}
\tag{2.54}
$$

The factor of 2 is required to cancel the symmetry factor of 1/2 in our definition of the phase-space measure. Other terms in Eq. (2.37) drop out because $\mathcal{O}_{(D^2\varphi^4)_2}$ does not have either a one-loop or tree-level form factor with a four-fermion external state, and does not renormalize $\mathcal{O}_{(D\varphi^2\psi^2)_1}$ or the $\mathcal{O}_{\psi^4}$ operators at one loop. In particular, the β-function also does not appear.

For simplicity, we set the off-shell momentum q to zero, and Eq. (2.53) then reduces to

$$
\begin{aligned}
&\gamma^{\mathrm{UV}(2)}_{\psi^4 \leftarrow (D^2\varphi^4)_2} A^{(0)}_{\psi^4}(1^+_\psi 2^-_{\overline{\psi}}\, 3^+_\psi 4^-_{\overline{\psi}}) + \gamma^{\mathrm{UV}(1)}_{(D\varphi^2\psi^2)_2 \leftarrow (D^2\varphi^4)_2} A^{(1)}_{(D\varphi^2\psi^2)_2}(1^+_\psi 2^-_{\overline{\psi}}\, 3^+_\psi 4^-_{\overline{\psi}}) \\
&\quad = -\frac{2}{\pi}\sum \int d\mathrm{LIPS}_2\, A^{(0)}(1^+_\psi 2^-_{\overline{\psi}}\, -\ell_{2\,\varphi}\, -\ell_{1\,\overline{\varphi}}) \mathrm{Re} A^{(1)}_{(D^2\varphi^4)_2}(\ell_{1\,\varphi} \ell_{2\,\overline{\varphi}} 3^+_\psi 4^-_{\overline{\psi}}) \,,
\end{aligned}
\tag{2.55}
$$

where the sum is over the available channels. The relevant tree and renormalized one-loop amplitudes needed to construct the cut are (including the color factors):

$$
A^{(0)}(1^+_\psi 2^-_{\overline{\psi}}\, 3_\varphi\, 4_{\overline{\varphi}}) = T^a_{i_2 i_1} T^a_{i_4 i_3}\, g^2 \frac{\langle 23\rangle [13]}{s} \,, \tag{2.56}
$$

$$
A^{(1)}_{(D^2\varphi^4)_2}(1^+_\psi 2^-_{\overline{\psi}}\, 3_\varphi\, 4_{\overline{\varphi}}) = T^a_{i_2 i_1} T^a_{i_4 i_3}\, \frac{\tilde{g}^2}{9} \langle 23\rangle [13] (3\log(-s/\mu^2) + 8) \,, \tag{2.57}
$$

where again the flavor indices have been dropped for simplicity. Note the form of Eq. (2.55) provides a nontrivial check on the phase space integral on the right-hand side: $A^{(1)}_{(D^2\varphi^4)_2}$ contains terms proportional to $\log(-s/\mu^2)$, which, after the phase-space integral, must cancel against terms in $A^{(1)}_{(D\varphi^2\psi^2)_2}$.

We can readily evaluate the cut by relabeling the amplitudes (2.56)–(2.57) and applying the spinor parametrization (2.25) to the scalars crossing the cut. This yields an integral

with no poles in $z = \mathrm{e}^{i\phi}$, other than the pole at zero. This can be seen by the fact that all spinor products in $A^{(0)}$ are either proportional to $\mathrm{e}^{\pm i\phi}$ or else have no ϕ dependence under our parametrization, whereas $A^{(1)}_{(D^2\varphi^4)_2}$ only has a pole in s. This makes the ϕ integral trivial to evaluate, resulting in:

$$\int_0^{\frac{\pi}{2}} d\theta\, \frac{\tilde{g}^4}{18}\langle 24\rangle[13]\sin^3(2\theta)(3\log(-s/\mu^2)+8)T^a_{i_2 i_1}T^a_{i_4 i_3} \\ = \frac{\tilde{g}^4}{27}\langle 24\rangle[13](3\log(-s/\mu^2)+8)T^a_{i_2 i_1}T^a_{i_4 i_3}\,, \tag{2.58}$$

for the (12)-channel cut. The (34)-channel cut gives the same result, while the other cuts yield the same result with legs two and four exchanged. Summing over the three other channels, we exactly match the second term on the left-hand side of Eq. (2.53), since $\gamma^{\mathrm{UV}(1)}_{(D\varphi^2\psi^2)_2\leftarrow(D^2\varphi^4)_2} = \tilde{g}^2/3$ and

$$A^{(1)}_{(D\varphi^2\psi^2)_2} = \frac{2\tilde{g}^2}{9}\langle 24\rangle[13](3\log(-s/\mu^2)+8)T^a_{i_2 i_1}T^a_{i_4 i_3} - (2\leftrightarrow 4)\,. \tag{2.59}$$

Therefore the cuts exactly cancel all terms on the left-hand side of Eq. (2.53) involving the one-loop anomalous dimensions and form-factors, leaving $\gamma^{\mathrm{UV}(2)}_{\psi^4\leftarrow(D^2\varphi^4)_2}F^{(0)}_{\psi^4} = 0$. Thus the two-loop anomalous dimension $\gamma^{\mathrm{UV}(2)}_{\psi^4\leftarrow(D^2\varphi^4)_2}$ is zero.

In fact, we could have come to this conclusion simply by examining the form of the one-loop amplitudes in Eqs. (2.57) and (2.59). First, note the two-loop anomalous dimension must be $\tilde{g}^4$ times a number (i.e., it does not have any kinematic dependence). Logarithmic terms resulting from the cut on the right-hand side of (2.53) must therefore cancel against logarithmic terms in $A^{(1)}_{(D\varphi^2\psi^2)_2}$. Since both one-loop form factors are proportional to the factor $(3\log(-s/\mu^2)+8)$, and since this term can be pulled out of the phase-space integral on the right-hand side of Eq. (2.53), the cancellation of the logarithmic terms implies cancellation of the rational term as well. Thus, even though there are nonzero cuts, there can be no remaining rational term that leads to a nonzero two-loop anomalous dimension.

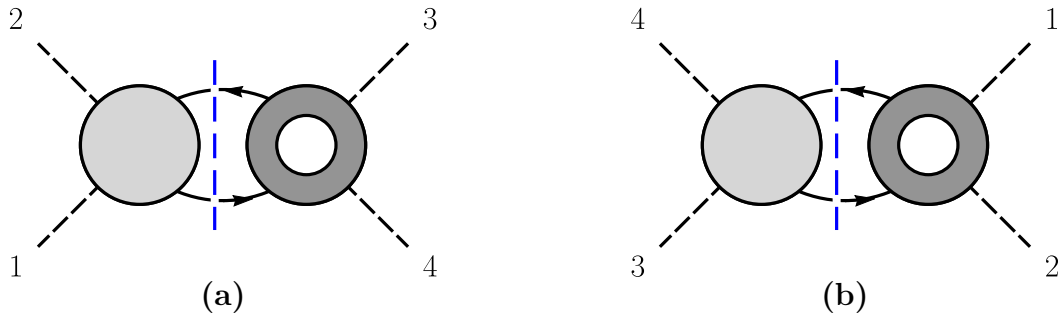

Figure 2.7: The (a) (12)-channel and (b) (34)-channel unitary cuts which determine the renormalization of $\mathcal{O}_{(D^2\varphi^4)_1}$ and $\mathcal{O}_{(D^2\varphi^4)_2}$ by $\mathcal{O}_{(\psi^4)_1}$ or $\mathcal{O}_{(\psi^4)_2}$. The (23)- and (14)-channel cuts are given by exchanging legs 2 and 4. In each, the darker blobs indicate a higher-dimension operator insertion, and the vertical (blue) dashed line indicates the integral over phase space of the particles crossing the cut.

At this point, the vanishing of the two-loop anomalous dimensions due to the cancellation of one-loop rational terms might seem accidental. However, one must remember that such *local* rational pieces are scheme dependent and can be adjusted by adding finite local counter-terms. As described in Section 2.4, the rational terms of both one-loop amplitudes in (2.57) and (2.59) can be set to zero by such finite counterterms, which would also result in $\gamma^{\text{UV}(2)}_{\psi^4\leftarrow(D^2\varphi^4)_2} = 0$. For this particular example, it just so happened that the naive $\bar{\text{MS}}$ scheme has zero anomalous dimension, but next we will see that this is not always the case.

As a cross-check, we have verified that the Eq. (2.32) is also satisfied. The crucial substitution $\log(-s/\mu^2) \to \log(-s/\mu^2) - i\pi$, is required in the right-hand side of that equation, coming from the analytic continuation of the amplitude from the Euclidean region to the correct physical region, which must be carried out for use in Eqs. (2.29)–(2.31).

$\mathcal{O}_{D^2\varphi^4} \leftarrow \mathcal{O}_{(\psi^4)_1}$

This section will provide our first example of nonzero two-loop anomalous dimension matrix elements in $\bar{\text{MS}}$, while demonstrating how an appropriate choice of scheme, i.e. choice of finite local counterterms, can eliminate the two-loop anomalous dimensions of this example.

We will begin with the calculation in $\bar{\text{MS}}$. Again, there is no three-particle cut, due to the particle content of the two types of operators in question. Using the external state

$\langle 1_{\varphi} 2_{\overline{\varphi}} 3_{\varphi} 4_{\overline{\varphi}} |$ and setting $\mathcal{O}_i \to \mathcal{O}_{(\psi^4)_1}$, Eq. (2.37) becomes

$$\begin{aligned}\gamma^{\mathrm{UV}(2)}_{(D^2\varphi^4)_1 \leftarrow (\psi^4)_1} F^{(0)}_{(D^2\varphi^4)_1} + \gamma^{\mathrm{UV}(2)}_{(D^2\varphi^4)_2 \leftarrow (\psi^4)_1} F^{(0)}_{(D^2\varphi^4)_2} + \gamma^{\mathrm{UV}(1)}_{(D\varphi^2\psi^2)_2 \leftarrow (\psi^4)_1} F^{(1)}_{(D\varphi^2\psi^2)_2} \\ = -\frac{1}{\pi}(\mathcal{M}^{12}_{2\to 2} + \mathcal{M}^{14}_{2\to 2} + \mathcal{M}^{23}_{2\to 2} + \mathcal{M}^{34}_{2\to 2})^{(0)} \otimes \mathrm{Re} F^{(1)}_{(\psi^4)_1} \,.\end{aligned} \tag{2.60}$$

As for the previous example, the logarithmic terms in the cuts must cancel against terms in the amplitude $F^{(1)}_{(D\varphi^2\psi^2)_2}$ on the left-hand side of the equation. Since we are dealing with four-point matrix elements we will again set $q = 0$. Then the one-loop amplitudes required for this example are

$$A^{(1)}_{(\psi^4)_1}(1^+_{\psi} 2^-_{\overline{\psi}} 3_{\varphi} 4_{\overline{\varphi}}) = \frac{2\tilde{g}^2}{9}\langle 23\rangle[13](3\log(-s/\mu^2) - 2) T^a_{i_2 i_1} T^a_{i_4 i_3} \,, \tag{2.61}$$

$$A^{(1)}_{(D\varphi^2\psi^2)_2}(1_{\varphi} 2_{\overline{\varphi}} 3_{\varphi} 4_{\overline{\varphi}}) = \frac{2\tilde{g}^2}{9}(t-u)(3\log(-s/\mu^2) - 5) T^a_{i_2 i_1} T^a_{i_4 i_3} + (2 \leftrightarrow 4) \,, \tag{2.62}$$

and the tree-level amplitudes needed are in Eq. (2.56) along with

$$A^{(0)}_{(D^2\varphi^4)_1}(1_{\varphi} 2_{\overline{\varphi}} 3_{\varphi} 4_{\overline{\varphi}}) = \; t\delta_{i_2 i_1}\delta_{i_4 i_3} + s\delta_{i_4 i_1}\delta_{i_2 i_3} \,, \tag{2.63}$$

$$A^{(0)}_{(D^2\varphi^4)_2}(1_{\varphi} 2_{\overline{\varphi}} 3_{\varphi} 4_{\overline{\varphi}}) = \; 2s\delta_{i_2 i_1}\delta_{i_4 i_3} + 2t\delta_{i_4 i_1}\delta_{i_2 i_3} \,, \tag{2.64}$$

which are shown in a slightly different basis of color factors than those shown in the appendix. The phase-space integral is evaluated in the same manner as the previous examples, with the result of the (12)-channel cut being

$$\begin{aligned}-\frac{1}{\pi}\int d\mathrm{LIPS}_2 \sum_{h_1,h_2} A^{(0)}(1_{\varphi} 2_{\overline{\varphi}} -\ell_1{}^{h_1}_{\psi} -\ell_2{}^{h_2}_{\overline{\psi}}) A^{(1)}_{(\psi^4)_1}(\ell_2{}^{h_2}_{\psi}\, \ell_1{}^{h_1}_{\overline{\psi}}\, 3_{\varphi} 4_{\overline{\varphi}}) \\ = -\frac{2}{27}\tilde{g}^4(t-u)(3\log(-s/\mu^2) - 2) T^a_{i_2 i_1} T^a_{i_4 i_3} \,.\end{aligned} \tag{2.65}$$

After summing over all channels and subtracting the contribution of $\gamma^{\mathrm{UV}(1)}_{(D\varphi^2\psi^2)_2 \leftarrow (\psi^4)_1} F^{(1)}_{(D\varphi^2\psi^2)_2}$ in Eq. (2.60)—thus canceling the logarithmic terms—the two-loop anomalous dimensions

are given by

$$\begin{aligned}\gamma^{\mathrm{UV}(2)}_{(D^2\varphi^4)_1\leftarrow(\psi^4)_1}(t\delta_{i_2i_1}\delta_{i_4i_3}+s\delta_{41}\delta_{23})+\gamma^{\mathrm{UV}(2)}_{(D^2\varphi^4)_2\leftarrow(\psi^4)_1}(2s\delta_{i_2i_1}\delta_{i_4i_3}+2t\delta_{i_4i_1}\delta_{i_2i_3}) \\ =-\frac{4}{9}\tilde{g}^4(t-u)T^a_{i_2i_1}T^a_{i_4i_3}+(2\leftrightarrow 4)\,.\end{aligned} \tag{2.66}$$

Applying the color Fierz identity,

$$T^a_{ij}T^a_{kl}=\delta_{il}\delta_{kj}-\frac{1}{N}\delta_{ij}\delta_{kl}\,, \tag{2.67}$$

and solving for the two-loop anomalous dimensions, we find

$$\begin{aligned}\gamma^{\mathrm{UV}(2)}_{(D^2\varphi^4)_1\leftarrow(\psi^4)_1}=&-\frac{4\tilde{g}^4(N-2)}{9N}\,,\\ \gamma^{\mathrm{UV}(2)}_{(D^2\varphi^4)_2\leftarrow(\psi^4)_1}=&\frac{2\tilde{g}^4(2N-1)}{9N}\,,\end{aligned} \tag{2.68}$$

in the $\bar{\mathrm{M}}$S scheme. Although these anomalous dimension matrix elements are nonzero in the $\bar{\mathrm{M}}$S scheme, a simple rational shift of the coefficients $c_{(D^2\varphi^4)_1}, c_{(D^2\varphi^4)_2}$, and $c_{(D\varphi^2\psi^2)_2}$ can set them to zero. This is accomplished by the following shifts in the coefficients:

$$\begin{aligned}c_{(D^2\varphi^4)_1}\longrightarrow\tilde{c}_{(D^2\varphi^4)_1}&=c_{(D^2\varphi^4)_1}+\frac{10\tilde{g}^2(N-2)}{9N}c_{(D\varphi^2\psi^2)_2}\,,\\ c_{(D^2\varphi^4)_2}\longrightarrow\tilde{c}_{(D^2\varphi^4)_2}&=c_{(D^2\varphi^4)_2}+\frac{5\tilde{g}^2(2N-1)}{9N}c_{(D\varphi^2\psi^2)_2}\,,\\ c_{(D\varphi^2\psi^2)_2}\longrightarrow\tilde{c}_{(D\varphi^2\psi^2)_2}&=c_{(D\varphi^2\psi^2)_2}-\frac{2\tilde{g}^2}{9}c_{(\psi^4)_1}\,,\end{aligned} \tag{2.69}$$

which yields

$$\tilde{\gamma}^{\mathrm{UV}(2)}_{(D^2\varphi^4)_1\leftarrow(\psi^4)_1}=0\,,\qquad\qquad\tilde{\gamma}^{\mathrm{UV}(2)}_{(D^2\varphi^4)_2\leftarrow(\psi^4)_1}=0\,, \tag{2.70}$$

where the tilde indicates the modified scheme. The shifts above are equivalent to a finite renormalization of the operator at one loop. Generally this can be achieved by choosing

the rational terms in $\gamma^{\mathrm{UV}(1)}_{(D\varphi^2\psi^2)_2\leftarrow(\psi^4)_1} F^{(1)}_{(D\varphi^2\psi^2)_2}$ to match those of the cuts. In our particular example we set the rational terms of both (2.61) and (2.62) to zero. We briefly comment below on the consequences of this redefinition for the two-loop RG running of the operators involved.

While we do not present the analogous calculation for $\mathcal{O}_{(\psi^4)_2}$ here, by inspecting Table 2.6, we can deduce that the two-loop anomalous dimensions $\gamma^{\mathrm{UV}(2)}_{(D^2\varphi^4)_1\leftarrow(\psi^4)_2}$ and $\gamma^{\mathrm{UV}(2)}_{(D^2\varphi^4)_2\leftarrow(\psi^4)_2}$ can also be set to zero with the appropriate choice of finite counterterms.

2.5.3 General comments about scheme redefinition

As mentioned above, the scheme choice that sets some two-loop anomalous dimensions to zero is equivalent to a finite renormalization of the operators

$$\tilde{\mathcal{O}}_i = Z^{\mathrm{fin}}_{ij}\mathcal{O}_j\,, \quad \text{where} \quad Z^{\mathrm{fin}}_{ij} = \delta_{ij} + f_{ij}(g^{(4)})\,, \tag{2.71}$$

and the quantity f_{ij} is finite and has a perturbative expansion starting at one loop, $f_{ij}(g^{(4)}) = f^{(1)}_{ij} + \cdots$. As usual, the redefinition of the coefficients, $\tilde{c}_i = Z^{\mathrm{fin}\,(c)}_{ij} c_j$ is given by the inverse, $Z^{\mathrm{fin}\,(c)}_{ij} = (Z^{\mathrm{fin}}_{ij})^{-1}$. The effect of such a scheme redefinition can be easily analyzed using the unitarity-based formalism employed in this work. Since the coupling dependence of f_{ij} starts at one loop we have that

$$\tilde{F}^{(0)}_i = F^{(0)}_i\,, \tag{2.72}$$

$$\tilde{F}^{(1)}_i = F^{(1)}_i + f^{(1)}_{ij} F^{(0)}_j\,, \tag{2.73}$$

where the tilde indicates a form factor of the redefined operator $\tilde{\mathcal{O}}_i$. From Eqs. (2.72) and (2.22) we conclude the one-loop anomalous dimensions are unaffected by the finite

renormalization, i.e., $\Delta\tilde{\gamma}_{ij}^{(1)} = \Delta\gamma_{ij}^{(1)}$. Similarly, writing Eq. (2.37) for the redefined operator

$$\left[\Delta\tilde{\gamma}_{ij}^{(1)} + \delta_{ij}\beta^{(1)}\partial\right] \mathrm{Re}\tilde{F}_j^{(1)} + \left[\Delta\tilde{\gamma}_{ij}^{(2)} + \delta_{ij}\beta^{(2)}\partial\right] \tilde{F}_j^{(0)} = -\frac{1}{\pi}\left[\mathrm{Re}(\mathcal{M})\mathrm{Re}(\tilde{F}_i)\right]^{(2)}. \tag{2.74}$$

and using Eqs. (2.72) and (2.73) together with Eqs. (2.22) and (2.37), while keeping in mind that the infrared anomalous dimensions are not changed by redefining the scheme, we find the relation between the two-loop anomalous dimensions in the two schemes,

$$\tilde{\gamma}_{ij}^{\mathrm{UV}(2)} = \gamma_{ij}^{\mathrm{UV}(2)} + f_{ik}^{(1)}\gamma_{kj}^{\mathrm{UV}(1)} - \gamma_{ik}^{\mathrm{UV}(1)} f_{kj}^{(1)} - \beta^{(1)}\partial f_{ij}^{(1)}\,. \tag{2.75}$$

In general, one would like to solve this equation for $f_{ik}^{(1)}$ to get as many vanishing entries as possible in $\tilde{\gamma}_{ij}^{\mathrm{UV}(2)}$.

We have explicitly verified Eq. (2.75) in the examples above, where we set the anomalous dimensions of the form $\tilde{\gamma}^{\mathrm{UV}(2)}_{D^2\varphi^4\leftarrow\psi^4}$ to zero by appropriately choosing $f^{(1)}_{D\varphi^2\psi^2\leftarrow\psi^4}$ and $f^{(1)}_{D^2\varphi^4\leftarrow D\varphi^2\psi^4}$. In addition, $f^{(1)}_{D^2\varphi^4\leftarrow\psi^4}$ vanished, which from Eq. (2.75) implies the the absence of a term induced by the β-function in the new two-loop anomalous dimension. On the other hand, it is clear from Eq. (2.75) that the finite renormalizations will induce some additional running in the two-loop anomalous dimensions $\tilde{\gamma}^{\mathrm{UV}(2)}_{D\varphi^2\psi^2\leftarrow\psi^4}$ and $\tilde{\gamma}^{\mathrm{UV}(2)}_{D^2\varphi^4\leftarrow D\varphi^2\psi^4}$, proportional to the one-loop beta function and $\partial f^{(1)}$. However, this additional running is harmless, since those operators already mix at one loop. Furthermore, the corresponding entries in the two-loop anomalous-dimension matrix receive contributions from both two- and three-particle cuts that have no a priori reason to vanish, so we expect them in any case to run. In summary, our scheme choice prevents certain operators from mixing at two loops at the expense of modifying the running of operators that, in any case, mix at one loop in the original scheme.

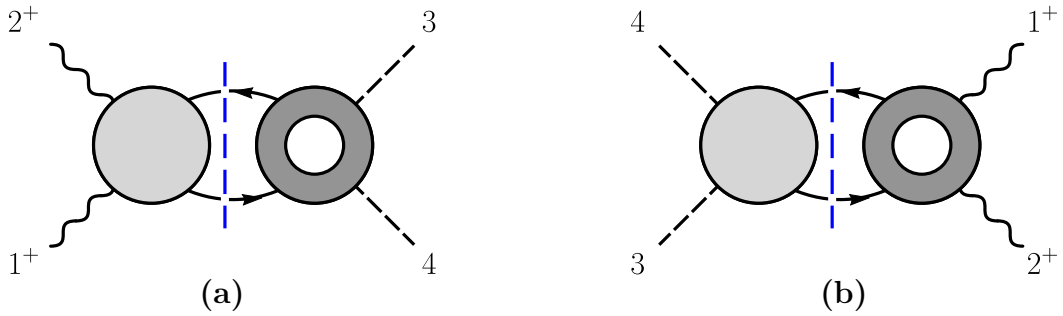

Figure 2.8: (12)-channel (a) and (34)-channel (b) unitary cuts which determine the renormalization of $\mathcal{O}_{(\varphi^2F^2)_1}$ and $\mathcal{O}_{(\varphi^2F^2)_2}$ by $\mathcal{O}_{(\psi^4)_1}$ or $\mathcal{O}_{(\psi^4)_2}$. There are no t-channel cuts for this process. In each diagram, the darker blobs indicate a higher-dimension operator insertion, and the dashed line indicates the integral over phase space of the particles crossing the cut.

2.5.4 Zeros from color selection rules

This section will provide an example of another type of selection rule, wherein a mismatch between the color of the cuts and the color of the target operators prevents renormalization at two loops.

2.5.5 $\mathcal{O}_{\varphi^2F^2} \leftarrow \mathcal{O}_{\psi^4}$

For this example we choose the external state to be $\langle 1_{\varphi} 2_{\overline{\varphi}} 3^+ 4^+|$, under which both $\mathcal{O}_{(\varphi^2F^2)_1}$ and $\mathcal{O}_{(\varphi^2F^2)_2}$ are nonzero. Using this state and setting $\mathcal{O}_i \to \mathcal{O}_{(\psi^4)_1}$, Eq. (2.37) reduces to

$$\begin{aligned}\gamma^{\mathrm{UV}(2)}_{(\varphi^2F^2)_1\leftarrow(\psi^4)_1} F^{(0)}_{(\varphi^2F^2)_1} + \gamma^{\mathrm{UV}(2)}_{(\varphi^2F^2)_2\leftarrow(\psi^4)_1} F^{(0)}_{(\varphi^2F^2)_2} + \gamma^{\mathrm{UV}(1)}_{(D\varphi^2\psi^2)_2\leftarrow(\psi^4)_1} F^{(1)}_{(D\varphi^2\psi^2)_2} \\ = -\frac{1}{\pi}\Big((\mathcal{M}^{12}_{2\to2})^{(0)} \otimes \mathrm{Re}F^{(1)}_{(\psi^4)_1} + (\mathcal{M}^{34}_{2\to2})^{(0)} \otimes \mathrm{Re}F^{(1)}_{(\psi^4)_1} \Big)\,.\end{aligned} \tag{2.76}$$

Naively there would be the additional term $\gamma^{\mathrm{UV}(2)}_{F^3\leftarrow(\psi^4)_1} F^{(0)}_{F^3}$ on the left-hand-side of the equation, since $\mathcal{O}_{F^3}$ produces a nonzero tree amplitude with the state $\langle 1_{\varphi} 2_{\overline{\varphi}} 3^+ 4^+|$. However, as was discussed in Section 2.5.1, the length and particle content of $\mathcal{O}_{(\psi^4)_1}$ requires

$\gamma^{\mathrm{UV}(2)}_{F^3\leftarrow(\psi^4)_1} = 0$. Setting $q = 0$, the (12)-channel cut of the above equation is

$$(\mathcal{M}^{12}_{2\to2})^{(0)} \otimes \mathrm{Re}F^{(1)}_{(\psi^4)_1} = \int d\mathrm{LIPS}_2 \sum_{h_1,h_2} A^{(0)}(1_\varphi 2_{\overline{\varphi}} -\ell_1{}_\psi^{h_1} -\ell_2{}_{\overline{\psi}}^{-h_2}) A^{(1)}_{(\psi^4)_1}(\ell_2{}_\psi^{h_2}\, \ell_1{}_{\overline{\psi}}^{h_1}\, 3^+4^+)\,, \tag{2.77}$$

and the (34)-channel cut is

$$(\mathcal{M}^{34}_{2\to2})^{(0)} \otimes \mathrm{Re}F^{(1)}_{(\psi^4)_1} = \int d\mathrm{LIPS}_2 \sum_{h_1,h_2} A^{(0)}(3^+4^+ -\ell_1{}_\psi^{h_1} -\ell_2{}_{\overline{\psi}}^{h_2}) A^{(1)}_{(\psi^4)_1}(\ell_2{}_\psi^{h_2}\, \ell_1{}_{\overline{\psi}}^{h_1}\, 1_\varphi 2_{\overline{\varphi}})\,. \tag{2.78}$$

The (34)-channel cut vanishes, because the amplitude $A^{(0)}(3^+4^+ -\ell_1{}_\psi -\ell_2{}_{\overline{\psi}})$ is zero for all helicities of the fermions crossing the cut. This vanishing is required for the consistency of the logarithmic terms: $A^{(1)}_{(\psi^4)_1}(\ell_2{}_\psi^{h_2}\, \ell_1{}_{\overline{\psi}}^{h_1}\, 1_\varphi 2_{\overline{\varphi}})$ includes a term proportional to $\log(-s/\mu^2)$, but there is no term on the left-hand side that can cancel it, since $F^{(1)}_{(D\varphi^2\psi^2)_2}(1_\varphi 2_{\overline{\varphi}}\, 3^+4^+)$ is purely rational. The one-loop amplitudes needed for this calculation are

$$A^{(1)}_{(\psi^4)_1}(1^+_\psi\, 2^-_{\overline{\psi}}\, 3^+4^+) = -\frac{\tilde{g}^2 s[14]\langle 24\rangle\, [T^{a_3}, T^{a_4}]_{i_2 i_1}}{3\langle 34\rangle^2}\,, \tag{2.79}$$

$$A^{(1)}_{(\psi^4)_1}(1^-_\psi\, 2^+_{\overline{\psi}}\, 3^+4^+) = -\frac{\tilde{g}^2 \langle 12\rangle[23][24]\, [T^{a_3}, T^{a_4}]_{i_2 i_1}}{3\langle 34\rangle}\,, \tag{2.80}$$

$$A^{(1)}_{(D\varphi^2\psi^2)_2}(1_\varphi 2_{\overline{\varphi}}\, 3^+4^+) = \frac{\tilde{g}^2 s(t-u)\, [T^{a_3}, T^{a_4}]_{i_2 i_1}}{3\langle 34\rangle^2}\,, \tag{2.81}$$

while the tree-level amplitudes needed for the cut calculation are (2.56) and its conjugate. The phase-space integrals are carried out in the same manner as the previous example, with the simplification that the functions are now entirely rational. The result of the phase-space

integral is

$$-\frac{1}{\pi}\int d\text{LIPS}_2 \sum_{h_1,h_2} A^{(0)}(1_\varphi 2_{\overline{\varphi}} -\ell_1{}_\psi^{-h_1} -\ell_2{}_{\overline{\psi}}^{-h_2}) A^{(1)}_{(\psi^4)_1}(\ell_2{}_\psi^{h_2}\, \ell_1{}_{\overline{\psi}}^{h_1}\, 3^+4^+)$$
$$= -\frac{2\tilde{g}^4 s(t-u)\,[T^{a_3},T^{a_4}]_{i_2 i_1}}{9(\langle 34\rangle)^2} = \gamma^{\text{UV}(1)}_{(D\varphi^2\psi^2)_2\leftarrow(\psi^4)_1} A^{(1)}_{(D\varphi^2\psi^2)_2}\,. \tag{2.82}$$

Thus the phase-space integral exactly cancels against this term from the left-hand-side of Eq. (2.76), meaning the two-loop anomalous dimension is again zero.

Interestingly, this can also be seen without looking at the kinematic content of the cuts on the right-hand side of Eq. (2.76). Since the color of both $\mathcal{O}_{(\varphi^2F^2)_1}$ and $\mathcal{O}_{(\varphi^2F^2)_2}$ are symmetric in T^3 and T^4, no combination of the two can produce the color factor $[T^3,T^4]_{i_2i_1}$. Since this is the color of $A^{(1)}_{(D\varphi^2\psi^2)_2}(1_\varphi 2_{\overline{\varphi}}\, 3^+4^+)$, and the color of $A^{(1)}_{(\psi^4)_1}(1^\pm_\psi 2^\mp_{\overline{\psi}}\, 3^+4^+)$ is also anti-symmetric under the exchange of 3 and 4, we can see directly from the color that neither of these terms can contribute to the two-loop anomalous dimension, and therefore must cancel. As in the previous example, we can extend this argument trivially to the operator $\mathcal{O}_{(\psi^4)_2}$, since its two-fermion two-vector-boson amplitude is proportional to that of $\mathcal{O}_{(\psi^4)_1}$. In this case, the only difference on the left-hand side would being the value of $\gamma^{\text{UV}(1)}_{(D\varphi^2\psi^2)_2\leftarrow(\psi^4)_2}$ versus $\gamma^{\text{UV}(1)}_{(D\varphi^2\psi^2)_2\leftarrow(\psi^4)_1}$, but the color again ensures all terms must cancel, leaving

$$\begin{aligned}
\gamma^{\text{UV}(2)}_{(\varphi^2F^2)_1\leftarrow(\psi^4)_1} &= \gamma^{\text{UV}(2)}_{(\varphi^2F^2)_2\leftarrow(\psi^4)_1} = 0\,,\\
\gamma^{\text{UV}(2)}_{(\varphi^2F^2)_1\leftarrow(\psi^4)_2} &= \gamma^{\text{UV}(2)}_{(\varphi^2F^2)_2\leftarrow(\psi^4)_2} = 0\,.
\end{aligned} \tag{2.83}$$

Here we focused on a simple example in which the color can preclude renormalization. In more general cases, one can directly inspect the color of the amplitudes that compose the cuts contributing to a given anomalous dimension and determine whether a given operator can yield a nonzero contribution. Note that this is more efficient than studying the color of individual Feynman diagrams, since the color decomposed amplitudes have fewer color structures.

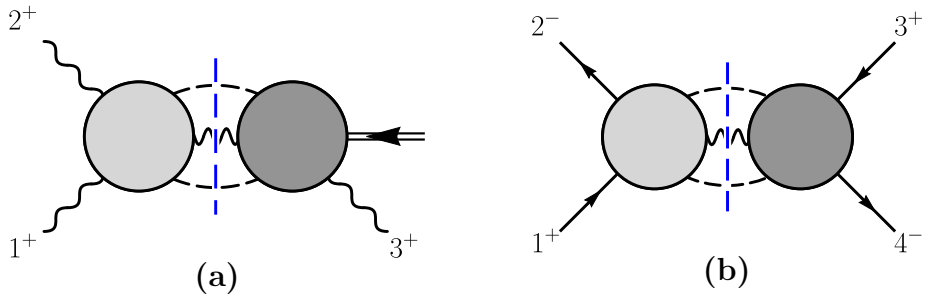

Figure 2.9: (a) Unitary cut which determines the renormalization of $\mathcal{O}_{F^3}$ by $\mathcal{O}_{(\varphi^2F^2)_1}$ or $\mathcal{O}_{(\varphi^2F^2)_2}$. Note this form factor requires $q \neq 0$, and the double-lined arrow indicates this insertion of additional off-shell momentum from the operator. (b) Unitarity cut which determines the renormalization of $\mathcal{O}_{(\psi^4)_1}$ and $\mathcal{O}_{(\psi^4)_2}$ by $\mathcal{O}_{(\varphi^2F^2)_1}$ or $\mathcal{O}_{(\varphi^2F^2)_2}$. In each, the darker blobs indicate a higher-dimension operator insertion, and the dashed line indicates the integral over phase space of the particles crossing the cut.

It is worth noting that, as mentioned in Section 2.4, the nonzero rational amplitudes (2.79)–(2.81) can be set to zero by introducing finite counterterms proportional to $c_{(\psi^4)_1}\mathcal{O}_{F^3}$ and $c_{(D\varphi^2\psi^2)_2}\mathcal{O}_{F^3}$, respectively. However, since these are non-local amplitudes, doing so introduces nonzero terms for other amplitudes, in particular any amplitudes where $\mathcal{O}_{F^3}$ produces a nonzero tree-level amplitude. This would introduce a great deal of confusion—for example, if we were to introduce a counterterm to cancel (2.79), we would then need to include additional cuts on the right-hand side of Eq. (2.76), including three-particle cuts and cuts with nontrivial IR dependence. Canceling either Eq. (2.79) or Eq. (2.81) with such a counterterm would also spoil the argument of Section 2.5.1, as the $\mathcal{O}_{F^3}$ self-renormalization would contribute in a nontrivial way. Therefore we would have to include the term $\gamma^{\text{UV}(2)}_{F^3\leftarrow(\psi^4)_1}F^{(0)}_{F^3}$ on the left-hand side of Eq. (2.76) as well. For all of the above reasons, we choose not to implement these finite shifts. It is interesting however, that even though the rational terms remain in this example, the structure of the color precludes renormalization at two loops.

2.5.6 Outlook on additional zeros

The previous sections have demonstrated numerous zeros in the two-loop anomalous dimension matrix, summarized in Table 2.7. However, the previous examples are by no means

	F^3	$(\varphi^2F^2)_1$	$(\varphi^2F^2)_2$	$(D^2\varphi^4)_1$	$(D^2\varphi^4)_2$	$(D\varphi^2\psi^2)_1$	$(D\varphi^2\psi^2)_2$	$(\psi^4)_1$	$(\psi^4)_2$	φ^6
F^3				0	0	0	0	0	0	$\emptyset$
$(\varphi^2F^2)_1$								0	0	0
$(\varphi^2F^2)_2$								0	0	0
$(D^2\varphi^4)_1$								0^*	0^*	0
$(D^2\varphi^4)_2$								0^*	0^*	0
$(D\varphi^2\psi^2)_1$										$\emptyset$
$(D\varphi^2\psi^2)_2$										$\emptyset$
$(\psi^4)_1$				0	0					$\emptyset$
$(\psi^4)_2$				0	0					$\emptyset$
φ^6										

$\emptyset$: trivial zero, no contributing two-loop diagrams

0 : zero predicted by the selection rules of Section 2.5

: only a three-particle cut is needed to evaluate $\gamma_{ij}^{\mathrm{UV}(2)}$

Table 2.7: Structure of the two-loop anomalous dimension matrix $\gamma_{ij}^{(2)}$ due to the collected rules outlined in this section. A $\emptyset$ indicates there are no contributing two-loop diagrams, whereas 0 alone indicates that there are one-loop diagrams that could contribute, but the anomalous dimension evaluates to zero. A 0^* indicates the result is nonzero in $\overline{\mathrm{MS}}$, but set to zero by introducing the appropriate finite counterterms. Shading indicates the entry depends only on the three-particle cut, due to either the length selection rules of Section 2.5.1 or the vanishing of the relevant one-loop amplitudes. As for Table 2.5, the operators labeling the rows are renormalized by the operators labeling the columns.

exhaustive, and more zeros may exist. The large number of zeros in the one-loop amplitudes (Table 2.6) implies that when calculating two-loop anomalous dimensions, the two-particle cut formed from the dimension-four tree and the dimension-six one-loop amplitude will not contribute. In some cases, the only contribution will come from the three-particle cut. Examples of this include the renormalization of $\mathcal{O}_{F^3}$ by $\mathcal{O}_{(\varphi^2F^2)_1}$ or $\mathcal{O}_{(\varphi^2F^2)_2}$, and the renormalization of $\mathcal{O}_{(\psi^4)_1}$ and $\mathcal{O}_{(\psi^4)_2}$ by $\mathcal{O}_{(\varphi^2F^2)_1}$ or $\mathcal{O}_{(\varphi^2F^2)_2}$. The cuts for these examples are depicted in Figure 2.9. While is may seem that there no reason to expect any given three-particle cut to evaluate to zero, it is possible that a detailed inspection may find that helicity

selection rules [24] or angular momentum selection rules [95] set certain cuts to zero. For a generic entry, the collection of these rules and the rules laid out in the sections above greatly simplify the calculation of the two-loop anomalous dimensions by eliminating one or more required unitary cuts, and one might expect that overlapping rules will conspire to eliminate all possible cuts and set additional entries in Table 2.7 to zero.

2.6 Implications for the SMEFT

The full SMEFT is more intricate than the simplified model adopted in this work, as it includes masses, multiple gauge groups and a number of additional operators. Still many of the results of our calculations provide nontrivial information about the structure of the anomalous dimension matrix of the SMEFT. In this section we describe the overlap of our theory with the SMEFT, and we explain how our results directly confirm a large number of the one-loop anomalous dimensions computed in Refs. [19–21]. We also comment on two-loop zeros and the coupling dependence of a subset of the two-loop anomalous-dimension matrix of the SMEFT.

2.6.1 Mapping our theory to the SMEFT

Let us describe how the differences between our simplified model and SMEFT can be taken into account to import the conclusions of our analysis to the SMEFT.

First, the Standard Model spectrum contains massive particles, notably the Higgs, whose masses can affect the structure of the renomalization group running of both the Standard Model couplings and Wilson coefficients of the SMEFT. However, in this work we have focused on the mixing between dimension six operators, which by dimensional analysis cannot depend on masses or other dimensionful parameters. In the presence of masses there can be additional mixing between operators of different dimensions, including modifications to the running of the Standard Model couplings, but these correspond to entries of the anomalous

dimension matrix different to those studied in this paper. The same holds for the finite renormalizations that were used to cancel certain one-loop matrix elements. Namely, in the presence of masses one might need to introduce finite renormalization of the Standard Model couplings to remove new local contributions to the one-loop matrix elements. Dimensional analysis ensures that this will not affect the structure of the two-loop dimension-six anomalous dimensions. In summary, the structure of the anomalous dimensions in our simplified model directly translates to the the SMEFT, and our comparison and conclusions are not be affected by ignoring masses.

Compared to our simplified model the SMEFT also includes several gauge groups and additional higher-dimension operators. By keeping the gauge group to be a general $SU(N)$, and by leaving the identity of the fermions unspecified, we can still access many of the entries of the anomalous-dimension matrix in the full SMEFT basis of operators used by Refs. [**Manohar123**]. In particular, since the Higgs transforms under $SU(2)$, setting $N = 2$ and the number of scalars $N_s = 1$ allows us to map to anomalous dimensions or four-point amplitudes from representatives of any of the classes of operators in Ref. [**Manohar123**] other than the $\psi^2 F\varphi$ class ($\psi^2 XH$ in the notation of Ref. [**Manohar123**]). Since the scalar is in the fundamental representation that class necessarily involves both a left-handed fermion charged under $SU(2)$, as well as an uncharged right-handed fermion, which does not fit into our framework. By taking $N = 3$, parts of the anomalous dimensions in the SMEFT containing gluons can also be obtained. In principle, one can also compare anomalous dimensions for additional operators using more sophisticated embeddings of the Standard Model into $SU(N)$, including $U(1)$ charges (see e.g, Appendix IV of Ref. [**ConvertToU1**]), but we do not do so here.

By specifying the flavor of the fermions, we can map to a number of operators of the full basis used by Ref. [19–21] via different choices of gauge group and helicity. For example, by taking $N = 2$ and and left-handed helicity on the external states, we access the $SU(2)$ portions of the amplitudes involving the q and $\bar{q}$ quark doublets, and map onto the operators

$(\bar{q}\gamma_\mu q)(\bar{q}\gamma^\mu q)$ and $(\bar{q}\gamma_\mu \tau^I q)(\bar{q}\gamma^\mu \tau^I q)$. One remaining difference in our approach compared to the full SMEFT is that we treat the fermions as Dirac instead of Weyl. This causes factor of 2 differences in the N_f terms of the renormalization of $\mathcal{O}_{(D\varphi^2\psi^2)_2}$ and $\mathcal{O}_{(\psi^4)_2}$ compared to Ref. [19–21], which need to be taken into account when comparing. While our simplified model avoids having to deal with γ_5, the generalized unitarity method has been applied to such cases as well [45]. At one loop, the issue of Weyl versus Dirac fermions is reduced to a question of which helicities to take in the state sum in Eq. (2.24).

Setting aside the issue of Weyl versus Dirac fermions, mapping onto the four-fermion operators of Ref. [19–21], $(\bar{l}\gamma_\mu l)(\bar{l}\gamma^\mu l)$, $(\bar{u}\gamma_\mu u)(\bar{u}\gamma^\mu u)$, and $(\bar{d}\gamma_\mu d)(\bar{d}\gamma^\mu d)$ is possible as well, but requires some care, due to the presence of evanescent effects. In particular, for these cases the operator $\mathcal{O}_{(\psi^4)_2}$ is related to the operator $\mathcal{O}_{(\psi^4)_1}$ due to the $SU(N)$ Fierz identity (2.67)

$$(\bar{\psi}_m\gamma^\mu T^a\psi_n)(\bar{\psi}_p\gamma_\mu T^a\psi_r) = (\bar{\psi}_m\gamma^\mu\psi_n)(\bar{\psi}_p\gamma_\mu\psi_r)\left(\delta_{i_p i_n}\delta_{i_m i_r} - \frac{\delta_{i_m i_n}\delta_{i_p i_r}}{N}\right). \tag{2.84}$$

which, together with the Lorentz–Fierz relations for all left- or right-handed spinors

$$\begin{aligned}(\bar{\psi}^m_L\gamma^\mu\psi^n_L)(\bar{\psi}^p_L\gamma_\mu\psi^r_L) &= -(\bar{\psi}^p_L\gamma^\mu\psi^n_L)(\bar{\psi}^m_L\gamma_\mu\psi^r_L)\,,\\ (\bar{\psi}^m_R\gamma^\mu\psi^n_R)(\bar{\psi}^p_R\gamma_\mu\psi^r_R) &= -(\bar{\psi}^p_R\gamma^\mu\psi^n_R)(\bar{\psi}^m_R\gamma_\mu\psi^r_R)\,,\end{aligned} \tag{2.85}$$

(where we raised the flavor indices for convenience) can be applied to eliminate the need for the $\mathcal{O}_{(\psi^4)_2}$ operator in Table 2.1:

$$\mathcal{O}^{mnpr}_{(\psi^4)_2} = (\bar{\psi}_m\gamma^\mu T^a\psi_n)(\bar{\psi}_p\gamma_\mu T^a\psi_r) = \mathcal{O}^{mrpn}_{(\psi^4)_1} - \frac{1}{N}\mathcal{O}^{mnpr}_{(\psi^4)_1}\,, \tag{2.86}$$

when there are no additional group indices preventing the particle exchange (for example, the additional $SU(3)$ index prevents the reduction of $(\bar{q}\gamma^\mu\tau^I q)(\bar{q}\gamma_\mu\tau^I q)$ operator based on the $SU(2)$ Fierz identity). By choosing to implement Eq. (2.85) or not, we can map onto

either the operators $(\bar{l}\gamma^\mu l)(\bar{l}\gamma_\mu l)$, $(\bar{u}\gamma^\mu u)(\bar{u}\gamma_\mu u)$, or $(\bar{d}\gamma^\mu d)(\bar{d}\gamma_\mu d)$, or onto the set of operators $(\bar{q}\gamma^\mu\tau^I q)(\bar{q}\gamma_\mu\tau^I q)$ and $(\bar{q}\gamma^\mu\tau^I q)(\bar{q}\gamma_\mu\tau^I q)$, respectively. Since we take all the fermions in our operators to be charged under the same gauge group, here we do not map onto the $(\bar{L}R)(\bar{L}R)$ or $(\bar{L}R)(\bar{R}L)$ subsets of the four-fermion operators, which require the presence of multiple gauge groups.

It is worth noting, that there are some simplifications in the SMEFT relative to our model with general gauge group. The symmetric color tensor d^{abc} is zero in $SU(2)$, meaning that the operator $\mathcal{O}_{(\varphi^2F^2)_2}$ is identically zero. In addition, this implies the color factors for the two-vector, two-scalar or two-vector, two-fermion processes are related by $N\{T^{a_1}, T^{a_2}\}_{i_4 i_3} = 2\delta^{a_1 a_2}\delta_{i_4 i_3}$, meaning the number of color-ordered amplitudes is reduced for those processes in the case of $SU(2)$.

2.6.2 Verification of one-loop anomalous dimensions

From our one-loop calculations and the relations described above we have verified entries from numerous classes of operators in the SMEFT, as summarized in Table 2.8, following the notation of Ref. [19–21]. This includes examples proportional to g_3^2, g_2^2, and λ. In this sense our operators are a representative sample of the full SMEFT, despite the simplified nature of our dimension-four Lagrangian. The direct agreement with results of Ref. [19–21] displayed in Table 2.8 provides a highly non-trivial check of the validity and the effectiveness of the approach used here.

2.6.3 Two-loop implications

Next we briefly discuss the implications of the zeros in the two-loop anomalous dimensions of our simplifies model for the SMEFT. The selection rules of Section 2.5 set a number of entries strictly to zero, and restrict the coupling dependence of others. Our findings are summarized in Table 2.9. The full SMEFT anomalous dimensions include dependence

	$\mathcal{O}_G$	$\mathcal{O}_W$	$\mathcal{O}_{HW}$	$\mathcal{O}_{H\Box}$ $\mathcal{O}_{HD}$	$\mathcal{O}_{Hl}^{(1)}$ $\mathcal{O}_{Hl}^{(3)}$	$\mathcal{O}_{Hq}^{(1)}$ $\mathcal{O}_{Hq}^{(3)}$	$\mathcal{O}_{ll}$	$\mathcal{O}_{qq}^{(1)}$ $\mathcal{O}_{qq}^{(3)}$	$\mathcal{O}_{uu}$ $\mathcal{O}_{dd}$
$\mathcal{O}_G$	$\checkmark_3$	$\emptyset$	$\emptyset$	$\emptyset$	$\emptyset$	$\emptyset$	$\emptyset$	$\emptyset$	$\emptyset$
$\mathcal{O}_W$	$\emptyset$	$\checkmark_2$	$\checkmark_2$	$\emptyset$	$\emptyset$	$\emptyset$	$\emptyset$	$\emptyset$	$\emptyset$
$\mathcal{O}_{HW}$	$\emptyset$	$\checkmark_2$	$\checkmark_{2,\lambda}$	$\checkmark_2$	$\checkmark_2$	$\checkmark_2$	$\emptyset$	$\emptyset$	$\emptyset$
$\mathcal{O}_{H\Box}$, $\mathcal{O}_{HD}$	$\emptyset$	$\checkmark_2$	$\checkmark_2$	$\checkmark_{2,\lambda}$	$\checkmark_2$	$\checkmark_2$	$\emptyset$	$\emptyset$	$\emptyset$
$\mathcal{O}_{Hl}^{(1)}$, $\mathcal{O}_{Hl}^{(3)}$	$\emptyset$	$\checkmark_2$	$\checkmark_2$	$\checkmark_2$	$\checkmark_{2,\lambda}$	$\checkmark_2$	$\checkmark_2$	$\emptyset$	$\emptyset$
$\mathcal{O}_{Hq}^{(1)}$, $\mathcal{O}_{Hq}^{(3)}$	$\emptyset$	$\checkmark_2$	$\checkmark_2$	$\checkmark_2$	$\checkmark_2$	$\checkmark_{2,\lambda}$	$\emptyset$	$\checkmark_2$	$\emptyset$
$\mathcal{O}_{ll}$	$\emptyset$	$\checkmark_2$	$\emptyset$	$\emptyset$	$\checkmark_2$	$\emptyset$	$\checkmark_2$	$\emptyset$	$\emptyset$
$\mathcal{O}_{qq}^{(1)}$, $\mathcal{O}_{qq}^{(3)}$	$\checkmark_3$	$\checkmark_2$	$\emptyset$	$\emptyset$	$\emptyset$	$\checkmark_2$	$\emptyset$	$\checkmark_2$	$\emptyset$
$\mathcal{O}_{uu}$, $\mathcal{O}_{dd}$	$\checkmark_3$	$\emptyset$	$\emptyset$	$\emptyset$	$\emptyset$	$\emptyset$	$\emptyset$	$\emptyset$	$\checkmark_3$

Table 2.8: Checks on the one-loop anomalous dimensions calculated in Ref. [19–21] obtained from our calculations. The $\emptyset$ entries correspond to trivial cases were there are no contributing diagrams. The entries $\checkmark_3$ and $\checkmark_2$ are checked by setting the SU(N) group to SU(3) or SU(2), respectively. In both cases, only the pieces of the anomalous dimensions proportional to g_3^2 or g_2^2 are accessed by our amplitudes. The $\checkmark_{2,\lambda}$ cases indicates that both terms proportional to g_2^2 and λ are verified. Operators have been grouped according to whether the gauge dependence of the particle content is the same. As for the other tables, the operators labeling the rows are renormalized by the operators labeling the columns.

on the Yukawa couplings, which are absent in our simplified theory, so some of the zeros uncovered above may be replaced by anomalous dimensions that depend on such couplings. Nevertheless, our results show that the coupling dependence of the anomalous dimensions is simpler than one might have expected, and that some of the entries are zero or do not have pure dependence on the gauge couplings. Though most of the strictly zero examples rely on the length selection rule, which does not depend on the gauge group or the presence of Yukawa couplings, the anomalous-dimension matrix element $\gamma^{(2)}_{HW\leftarrow qq}$ relies solely on the color selection rules. In this case, including Yukawa and U(1) couplings will not affect this zero, as the cuts still cannot match the color of the target operator.

In addition to the zeros, we find that many of the entries only receive contributions from either three- or two-particle cuts, which should greatly simplify their computation. One

interesting example is the element $\gamma^{(2)}_{qq\leftarrow HW}$, which only has a three-particle cut due to the vanishing of the one-loop amplitudes that would contribute to the two-particle cut. For this example, we have also checked the one-loop amplitudes with Yukawa and U(1) couplings do not contribute. As can also be seen in Table 2.9, many entries vanish when the Yukawa couplings are set to zero. Many of these zeros are trivial due to the particle content of the operators involved, but in some cases a closer examination of the diagrams is required to see that only diagrams with Yukawa couplings will produce nonvanishing results.

Note that the operators in Table 2.9 are merely a representative set, in that all of the operators of the SMEFT are restricted by one or more of our selection rules, either in terms of which operators they can renormalize, or vice versa. In particular, the length selection rules apply independently of the gauge group or the presence of Yukawa couplings, which allows us to include operators of the classes $\psi^2 F\varphi$ and $\psi^2\varphi^3$ in Table 2.9. We would also like to stress that our analysis of the structure of the two-loop anomalous dimensions is not an exhaustive study of the SMEFT anomalous dimensions. For this reason, we expect that there could be additional vanishings or structures that can be uncovered under closer scrutiny.

2.7 Conclusions

In this chapter we have applied on-shell methods to investigate the structure of the anomalous dimension matrix in both a simplified model and in the SMEFT. We have derived a new non-renormalization theorem that applies to higher-dimensional operators in quantum field theory. Since the theorem is dependent on only the number and type of fields in each operator, it applies to generic massless theories with no relevant operators. Besides being helpful to find zeros of the anomalous-dimension matrix, the on-shell formalism of Ref. [98] is a good way to compute nonzero entries as well. Whenever an entry is excluded by our theorem, it should be much simpler to compute the entry at the next loop order compared

to computing a generic entry at that loop order, because only tree-level quantities enter the cuts. At one loop, we used both the standard generalized unitarity method [43, 44, 97] and the recently developed approach for extracting non-zero anomalous dimensions directly from unitarity cuts [98]. At two loops, we find the latter method to be especially effective, with the former method providing one-loop amplitudes as inputs. As an initial step, we reorganized the basic equation for the two-loop anomalous dimension in the latter approach so as to simplify one-loop iterations. Using this equation, we revealed a number of vanishing contributions in the two-loop anomalous dimension matrix of the SMEFT. Our analysis was based on a simplified model without U(1) or Yukawa interactions. Nevertheless, as summarized in Table 2.9, by analyzing the overlap of our simplified model with the SMEFT we found that a remarkable number of SMEFT two-loop anomalous dimensions either vanish or have a simpler dependence on the Standard Model couplings than naively expected.

The structure we uncovered has a number of origins, including length selection rules, color selection rules, and zeros in the one-loop amplitudes with dimension-six operator insertions. Additional zeros arise from the choice of an $\bar{\text{M}}$S-like scheme which includes additional finite renormalizations designed to set various rational terms in one-loop amplitudes to zero. This suggests that there exist interesting schemes that make the structure of the renormalization-group running beyond one loop more transparent. The full implications of choosing such schemes clearly deserve further study.

Since one-loop amplitudes are used as input for the two-loop calculation, we have computed the full set of four-point amplitudes with dimension-six operator insertions in our simplified version of the SMEFT. As a byproduct, these amplitudes have allowed us to verify a large subset of the one-loop anomalous dimensions calculated in Refs. [19–21].

The zeros that we found in the two-loop anomalous dimension matrix relied on choosing examples with trivial infrared dependence, as well as a lack of a three-particle cut. However, the methods can be applied just as well to any generic anomalous dimension matrix element at two or higher loops. It would be interesting to investigate whether there are additional

zeros at two loops beyond those we identified. The large number of zeros in the one-loop amplitudes restrict the number of cuts that can contribute, suggesting that other mechanisms, such as helicity or angular-momentum selection rules, may set the remaining cuts to zero in some cases.

The conclusions of the present work are unchanged by the presence of masses, as these only affect different entries in the anomalous dimension matrix, which relate operators of different dimension. Studying such entries will require revisiting the proof of the length selection rules, since formerly scaleless integrals can have a UV divergence proportional to a mass, which generates running for operators of lower dimension. Additionally, masses allow additional logarithms of the form $\log(\mu/m)$, whose coefficient is not captured by traditional unitarity cuts. It would be interesting to study the possibility of extending our formalism to capture these effects and explore the structure of that sector of the anomalous dimension matrix.

In summary, we have demonstrated that the on-shell methods applied here are well suited for computing anomalous dimensions and associated scattering amplitudes at one and two loops. We used these methods to expose new structures in the guise of vanishing terms in the anomalous matrix of the SMEFT beyond one loop. Our analysis here was not exhaustive, so it is likely that further vanishing contributions and new structures exist at two loops and beyond. Our results also suggest that a judicious choice of renormalization scheme can help expose such structures.

The presented methods are quite general, and should be applicable to general EFTs. In addition, while we have focused on ultraviolet anomalous dimensions here, this method could equally be applied to the evaluation of infrared anomalous dimensions, such as the soft anomalous dimension, by the use of ultraviolet protected operators such as the stress-tensor or global symmetry currents. It would also be interesting to understand the implications, if any, of the vanishing of two-loop anomalous dimensions for the interference of Standard Model and higher-dimension operator matrix elements beyond tree level, in the presence of

experimental cuts. Another obvious direction would be to include dimension seven and eight operators into the analysis [**Dim78**].

2.A Integral reduction via gauge-invariant tensors

In this appendix we summarize the projection technique that we use to perform tensor reduction of loop integrals in Section 2.4. The same technique has been previously used in Refs. [9, 134, 135] and is a convenient method for decomposing D-dimensional tensor loop integrands (or cuts) into a basis of scalar master integrals, in a way that makes dimensional regularization, and any associated chiral and evanescent issues relatively straightforward. In particular this technique is well suited to deal with integrals with high-rank numerators, which naturally arise in loop amplitudes with insertions of higher-dimension operators.

We start by noting that scattering amplitudes amplitudes are gauge invariant and can therefore be decomposed into a basis of gauge-invariant tensors, T_m. For a given amplitude labeled by i we have,

$$A_i^{(L)} = \sum_m \mathcal{A}_{i,m}^{(L)}(k_j) T_m(k_j, \epsilon_j, u_j, \bar{u}_j)\,, \tag{2.87}$$

where the coefficients, $\mathcal{A}_{i,m}^{(L)}$, only depend on the external momenta, and all dependence on the polarization vectors or spinors is contained entirely within the basis tensors, T_m. The basis tensors for the various processes we consider in this work are given below and in the supplementary material to the ArXiV submission of Ref. [2]. They are found by writing down the most general polynomials built from Lorentz invariant products of external polarizations, spinor and momenta and then demanding gauge invariance.

The desired coefficient of tensor T_j can be extracted using a projector

$$P_n = c_{nm} T_m^*\,, \tag{2.88}$$

where c_{nm} is the inverse of the matrix

$$m_{nm} = T_n^* \odot T_m \,. \tag{2.89}$$

Here the product $\odot$ corresponds to the state sum in Eq. (2.49), taken over all particles. The coefficient of the tensor is then simply given by

$$\mathcal{A}_{i,m}^{(L)} = P_m \odot A_i^{(L)} \,. \tag{2.90}$$

The projectors for all processes consider in this work are given explicitly in an ancillary file attached to the ArXiV submission of Ref. [2].

Once projected, any gauge invariant quantity can be summarized as a list of the coefficients corresponding to each basis tensor. In the case of a loop integrand or cut thereof, each coefficient is a rational function of scalar propagators and inverse propagators (and irreducible numerators beyond one loop). The integrals corresponding to each term in the projected quantity are then in a form that can be reduced to a basis of master integrals using by integration by parts (IBP) relations. This can be done using by using IBP programs such as FIRE [136–138].

As described in Section 2.4, we can apply this procedure cut by cut to determine the coefficients of each gauge invariant tensor in the full amplitude.

Basis tensors

Basis tensors for the four-vector amplitudes are taken from [9], which we reproduce here. Beginning with the linearized field strength for each external particle:

$$F_{i\,\mu\nu} \equiv k_{i\,\mu}\varepsilon_{i\,\nu} - k_{i\,\nu}\varepsilon_{i\,\mu} \,, \tag{2.91}$$

one can construct the following combinations,

$$\begin{aligned} F_{st}^4 &\equiv (F_1F_2F_3F_4)\,, & F_{tu}^4 &\equiv (F_1F_4F_2F_3)\,, & F_{us}^4 &\equiv (F_1F_3F_4F_2)\,, \\ (F_s^2)^2 &\equiv (F_1F_2)(F_3F_4)\,, & (F_t^2)^2 &\equiv (F_1F_4)(F_2F_3)\,, & (F_u^2)^2 &\equiv (F_1F_3)(F_4F_2)\,, \end{aligned} \tag{2.92}$$

where parentheses one the right-hand side of the above equations indicate taking the trace over adjacent Lorentz indices. The four-vector basis tensors are then given by

$$\begin{aligned} T_{vvvv}^{\rm tree} &= -\frac{1}{2}((F_s^2)^2 + (F_t^2)^2 + (F_u^2)^2) + 2\,(F_{st}^4 + F_{tu}^4 + F_{us}^4)\,, \\ T_{vvvv}^{++++} &= -2\,F_{st}^4 + \frac{1}{2}\,((F_s^2)^2 + (F_t^2)^2 + (F_u^2)^2)\,, \\ T_{vvvv}^{-+++} &= -T_{F^3} - (F_{tu}^4 - F_{us}^4)\,(s-t) + (F_{st}^4 - \frac{1}{4}((F_s^2)^2 + (F_t^2)^2 + (F_u^2)^2))\,(s+t)\,, \\ T_{vvvv}^{--++} &= (F_s^2)^2 - (F_t^2)^2 + 2\,(F_{tu}^4 - F_{us}^4)\,, \\ T_{vvvv}^{-+-+} &= 2\,F_{st}^4 - \frac{1}{2}((F_s^2)^2 + (F_t^2)^2 - (F_u^2)^2)\,, \\ T_{vvvv}^{\rm ev1} &= -(2\,F_{st}^4 + \frac{3}{2}\,((F_s^2)^2 + (F_t^2)^2 + (F_u^2)^2))\,(s+t) + 2\,(F_{us}^4\,(3\,s+t) + F_{tu}^4\,(s+3\,t))\,, \\ T_{vvvv}^{\rm ev2} &= -(2\,F_{st}^4 - \frac{1}{2}((F_s^2)^2 + (F_t^2)^2 + (F_u^2)^2))\,(s-t) + 2\,(F_{tu}^4 - F_{us}^4)\,(s+t)\,, \end{aligned} \tag{2.93}$$

where the v labels signifies that a leg is a vector boson, and T_{F^3} is proportional to the F^3 amplitude [176]:

$$T_{F^3} = -istA_{F^3}^{(0)} = -istu\left(\frac{(F_s^2)^2}{4s^2} + \frac{(F_t^2)^2}{4t^2} + \frac{(F_u^2)^2}{4u^2} - \frac{g_1g_2g_3g_4}{(stu)^2}\right)\,, \tag{2.94}$$

where $g_i \equiv (k_{i+1}F_ik_{i-1})$. We note that we have written this expression in an explicitly gauge-invariant form at the expense of manifest locality. These tensors are nonzero only under the indicated (and parity conjugate) helicity configurations, along with cyclic permutations. $T_{vvvv}^{\rm tree}$ is nonzero for helicities $(1^-2^+3^-4^+)$, $(1^-2^-3^+4^+)$, and cyclic permutations. $T_{vvvv}^{\rm ev1}$ and $T_{vvvv}^{\rm ev2}$ are evanescent, i.e. zero for all helicity configurations in four dimensions. This can be

made manifest by rewriting them as

$$\begin{aligned} T^{\rm ev1}_{vvvv} &= \frac{1}{2} k_4^{[\alpha} F_1^{\mu\nu} F_2^{\sigma\rho]} k_{2\alpha} F_{4\mu\nu} F_{3\sigma\rho} + \frac{1}{2} k_4^{[\alpha} F_3^{\mu\nu} F_2^{\sigma\rho]} k_{2\alpha} F_{4\mu\nu} F_{1\sigma\rho} \,, \\ T^{\rm ev2}_{vvvv} &= \frac{1}{2} k_2^{[\alpha} F_1^{\mu\nu} F_3^{\sigma\rho]} k_{1\alpha} F_{2\mu\nu} F_{4\sigma\rho} \,, \end{aligned} \tag{2.95}$$

where the anti-symmetrization does not include a symmetry factor.

The two-vector, two-scalar tensors are also nonzero under specific helicity combinations, and are given by

$$T^{+-}_{vvss} = 2(k_3 F_1 F_2 k_4) + 2(k_4 F_1 F_2 k_3) - (k_3 \cdot k_4)(F_1 F_2) \,, \quad T^{++}_{vvss} = -(F_1 F_2) \,, \tag{2.96}$$

where the v and s labels specify the corresponding legs are vectors or scalars.

Similarly, the two-vector, two-fermion tensors are linear combinations of those in Ref. [134, 135], chosen to again be nonzero only under specific helicities:

$$\begin{aligned} T^{-+++}_{ffvv} &= -\frac{1}{2^4}(\bar{u}_2 \not{F}_4 \not{F}_3 \not{k}_2 u_1) \,, \qquad T^{-+-+}_{ffvv} = -\frac{1}{2^4}(\bar{u}_2 \not{F}_4 \not{k}_2 \not{F}_3 u_1) \,, \\ T^{-++-}_{ffvv} &= -\frac{1}{2^4}(\bar{u}_2 \not{F}_3 \not{k}_1 \not{F}_4 u_1) \,, \qquad T^{-+--}_{ffvv} = -\frac{1}{2^4}(\bar{u}_2 \not{k}_1 \not{F}_4 \not{F}_3 u_1) \,, \\ T^{\rm ev}_{ffvv} &= \frac{1}{2} k_1^{[\alpha} F_3^{\mu\nu} F_4^{\rho\sigma]} (\bar{u}_2 \gamma_\alpha \gamma_\mu \gamma_\nu \gamma_\rho \gamma_\sigma u_1) \,, \end{aligned} \tag{2.97}$$

where f now indicates a leg as a fermion, $\not{F}_i = F_{i\,\mu\nu} \gamma^\mu \gamma^\nu$, and the antisymmetrization in $T^{\rm ev}$ includes a symmetry factor of $1/5!$. As for the four-vector case, we encounter an evanescent tensor, $T^{\rm ev}_{ffvv}$ which vanishes for all four-dimensional helicities. For the two-fermion two-scalar case there is only a single basis tensor:

$$T_{ffss} = \bar{u}_2 \not{k}_3 u_1 \,. \tag{2.98}$$

Finally, the four-fermion tensors are,

$$
\begin{aligned}
T^1_{ffff} &= (\bar{u}_2\gamma^\mu u_1)(\bar{u}_4\gamma_\mu u_3)\,, \\
T^2_{ffff} &= (\bar{u}_2 \not{k}_4 u_1)(\bar{u}_4 \not{k}_2 u_3)\,, \\
T^3_{ffff} &= (\bar{u}_2\gamma^\mu\gamma^\nu\gamma^\rho u_1)(\bar{u}_4\gamma_\mu\gamma_\nu\gamma_\rho u_3) - 16(\bar{u}_2\gamma^\mu u_1)(\bar{u}_4\gamma_\mu u_3)\,, \\
T^4_{ffff} &= t\,(\bar{u}_2\gamma^\mu \not{k}_4\gamma^\rho u_1)(\bar{u}_4\gamma_\mu \not{k}_2\gamma_\rho u_3) - 4u(\bar{u}_2 \not{k}_4 u_1)(\bar{u}_4 \not{k}_2 u_3)\,,
\end{aligned}
\tag{2.99}
$$

plus those given by the exchange of legs 2 and 4. It should be noted, however, that in practice it is unnecessary to calculate the coefficients of the exchanged tensors, since they are fixed by the symmetry of the contributing diagrams. T^3_{ffff} and T^4_{ffff} are chosen to be zero for the helicity configuration $1^+_\psi 2^-_{\bar{\psi}} 3^+_\psi 4^-_{\bar{\psi}}$ and its conjugate, so that these tensors are evanescent if the spinors are Weyl of the same handedness.

2.B Tree-level and one-loop amplitudes

In this appendix we collect tree- and one-loop amplitudes. In addition to the spinor-helicity amplitudes given below, expressions that are valid to all orders in the dimensional regularization parameter ϵ are provided in a supplementary file to the ArXiV submission of Ref. [2]. While we do not require one-loop amplitudes without higher-dimension operators for our specific examples in Section 2.5, they would be required for the calculation of a generic two-loop anomalous dimension matrix element. These one-loop dimension-4 amplitudes can be found in various references; e.g. Refs. [177, 178] gives the relevant amplitudes which exclude scalars.

The amplitudes and form factors can be written as vectors in color space,

$$
A^{(L)}(\lambda_1\lambda_2\lambda_3\lambda_4) = S_{\lambda_1\lambda_2\lambda_3\lambda_4} \sum_i \mathcal{C}^{[i]}_{\lambda_1\lambda_2\lambda_3\lambda_4} A^{(L)}(\lambda_1\lambda_2\lambda_3\lambda_4)_{[i]}\,,
\tag{2.100}
$$

where $S_{\lambda_1\lambda_2\lambda_3\lambda_4}$ is a helicity-dependent factor which which depending on spinors when evaluated using four-dimensional spinor helicity. These factors are pure phases for the amplitudes with an even number of pairs of external fermions, and for the amplitudes with an odd number of fermions their square is a dimensionless ratio of s, t, or u and powers thereof. The full list of $S_{\lambda_1\lambda_2\lambda_3\lambda_4}$ for each process is listed below.

The IR dependence has been stripped from the amplitudes below, but can be reconstructed, if desired, using the basic IR formulas given in the text, which we reproduce here:

$$A_i^{(1)} = \boldsymbol{I}^{(1)} A_i^{(0)} + A_i^{(1)\text{fin}}\,, \tag{2.101}$$

where the IR operator $\boldsymbol{I}^{(1)}$ is given by

$$\boldsymbol{I}^{(1)} = \frac{e^{\epsilon\gamma_E}}{\Gamma(1-\epsilon)} \sum_{p=1}^{n} \sum_{q\neq p} \frac{\boldsymbol{T}_p \cdot \boldsymbol{T}_q}{2} \left[\frac{\gamma_{\text{cusp}}^{\text{IR}\,(1)}}{\epsilon^2} - \frac{\gamma_{\text{c},\,p}^{\text{IR}\,(1)}}{\boldsymbol{T}_p^2} \frac{1}{\epsilon} \right] \left(\frac{-\mu^2}{2k_p\cdot k_q} \right)^{\epsilon}, \tag{2.102}$$

with

$$\gamma_{\text{cusp}}^{\text{IR}\,(1)} = \tilde{g}^2 4\,, \quad \gamma_{\text{c},\,v}^{\text{IR}\,(1)} = -\tilde{g}^2 b_0\,, \quad \gamma_{\text{c},\,f}^{\text{IR}\,(1)} = -\tilde{g}^2 3C_F\,, \quad \gamma_{\text{c},\,s}^{\text{IR}\,(1)} = -\tilde{g}^2 4C_F\,. \tag{2.103}$$

Explicit evaluations of $\boldsymbol{I}^{(1)}$ for various processes can be found, for example, in Refs. [134, 135, 173]. All results below are reported in the Euclidean region and the $\bar{\text{MS}}$ scheme. As a shorthand, logarithms are given by:

$$\begin{gathered} X^2 = \log\left(\frac{s}{t}\right)^2 + \pi^2, \qquad Y^2 = \log\left(\frac{s}{u}\right)^2 + \pi^2, \qquad Z^2 = \log\left(\frac{u}{t}\right)^2 + \pi^2, \\ X_s = \log\left(\frac{\mu^2}{-s}\right), \qquad X_t = \log\left(\frac{\mu^2}{-t}\right), \qquad X_u = \log\left(\frac{\mu^2}{-u}\right). \end{gathered} \tag{2.104}$$

In general we drop the Wilson coefficients, for example c_{F^3} for amplitudes with an $\mathcal{O}_{F^3}$ insertion, since it is in this form that the amplitudes are used in Eq. (2.37). However we have contracted the Wilson coefficients with the amplitudes for operators which include

fermions, since doing so simplifies the flavor information for these cases.

2.B.1 Four-vector amplitudes

The color factors for the four-vector amplitudes are

$$\begin{aligned}
\mathcal{C}^{[1]}_{vvvv} &= \mathrm{Tr}[T^1T^2T^3T^4]\,, \qquad \mathcal{C}^{[2]}_{vvvv} = \mathrm{Tr}[T^1T^3T^2T^4]\,,\\
\mathcal{C}^{[3]}_{vvvv} &= \mathrm{Tr}[T^1T^2T^4T^3]\,, \qquad \mathcal{C}^{[4]}_{vvvv} = \mathrm{Tr}[T^1T^4T^2T^3]\,,\\
\mathcal{C}^{[5]}_{vvvv} &= \mathrm{Tr}[T^1T^3T^4T^2]\,, \qquad \mathcal{C}^{[6]}_{vvvv} = \mathrm{Tr}[T^1T^4T^3T^2]\,,\\
\mathcal{C}^{[7]}_{vvvv} &= \mathrm{Tr}[T^1T^2]\,\mathrm{Tr}[T^3T^4]\,, \quad \mathcal{C}^{[8]}_{vvvv} = \mathrm{Tr}[T^1T^3]\,\mathrm{Tr}[T^2T^4]\,, \quad \mathcal{C}^{[9]}_{vvvv} = \mathrm{Tr}[T^1T^4]\,\mathrm{Tr}[T^2T^3]\,,
\end{aligned} \tag{2.105}$$

where only two partial amplitudes—one single-trace and one double-trace—are independent in general, and the rest are given by relabelings.

We remove dimensionless prefactors from the helicity amplitudes. These are all phases except for the amplitudes involving only one pair of fermions. For the four-vector amplitudes, the spinor prefactors are are given by

$$\begin{aligned}
S(1^+2^+3^+4^+) &= \frac{[12][34]}{\langle 12\rangle\langle 34\rangle}\,, \qquad S(1^-2^+3^+4^+) = \frac{\langle 12\rangle\langle 14\rangle[24]}{\langle 23\rangle\langle 24\rangle\langle 34\rangle}\,,\\
S(1^-2^-3^+4^+) &= \frac{\langle 12\rangle[34]}{\langle 34\rangle[12]}\,, \qquad S(1^-2^+3^-4^+) = \frac{\langle 13\rangle[24]}{\langle 24\rangle[13]}\,.
\end{aligned} \tag{2.106}$$

The tree-level D-dimensional amplitudes are given by

$$\begin{aligned}
A^{(0)}(1234)_{[1]} &= \frac{-g^2}{st}T^{\mathrm{tree}}_{vvvv}\,,\\
A^{(0)}(1234)_{[7]} &= 0\,,\\
A^{(0)}_{F^3}(1234)_{[1]} &= \frac{g}{2stu}\left(4stT^{++++}_{vvvv} - 2uT^{-+++}_{vvvv} + (s-t)T^{\mathrm{ev2}}_{vvvv}\right)\,,\\
A^{(0)}_{F^3}(1234)_{[7]} &= 0\,,
\end{aligned} \tag{2.107}$$

which have four-dimensional helicity values

$$
\begin{aligned}
&A^{(0)}(1^-2^+3^+4^+)_{[1]} = A^{(0)}(1^=2^+3^+4^+)_{[1]} = 0\,,\\
&A^{(0)}(1^-2^-3^+4^+)_{[1]} = -\frac{g^2 s}{t}\,,\\
&A^{(0)}(1^-2^+3^-4^+)_{[1]} = -\frac{g^2 u^2}{st}\,,\\
&A^{(0)}(1^\pm 2^\pm 3^\pm 4^\pm)_{[7]} = 0\,,
\end{aligned}
\tag{2.108}
$$

$$
\begin{aligned}
&A^{(0)}_{F^3}(1^+2^+3^+4^+)_{[1]} = 2gs\,,\\
&A^{(0)}_{F^3}(1^-2^+3^+4^+)_{[1]} = -gu\,,\\
&A^{(0)}_{F^3}(1^-2^-3^+4^+)_{[1]} = A^{(0)}_{F^3}(1^-2^+3^-4^+)_{[1]} = 0\,,\\
&A^{(0)}_{F^3}(1^\pm 2^\pm 3^\pm 4^\pm)_{[7]} = 0\,.
\end{aligned}
\tag{2.109}
$$

The one-loop amplitudes with one insertion of the F^3 operator are

$$
\begin{aligned}
A^{(1)\text{fin}}_{F^3}(1^+2^+3^+4^+)_{[1]} &= g\tilde{g}^2\big((4N(t-u)+2ub_0)X_s + (4N(s-u)+2ub_0)X_t\\
&\qquad - \frac{1}{2}(44N+2N_f-N_s)u\big)\,,\\
A^{(1)\text{fin}}_{F^3}(1^-2^+3^+4^+)_{[1]} &= g\tilde{g}^2\Big(N\frac{u^2-st}{u}X^2\\
&\qquad + (2N(t-u)+b_0u)X_s + (2N(s-u)+b_0u)X_t - 12u\Big)\,,\\
A^{(1)}_{F^3}(1^-2^+3^-4^+)_{[1]} &= 0\,,\\
A^{(1)}_{F^3}(1^-2^-3^+4^+)_{[1]} &= \frac{g\tilde{g}^2}{6}\left(4N(u-s)-(2N_f-N_s)(u-t)\right)\,,
\end{aligned}
\tag{2.110}
$$

where $\tilde{g}^2 = g^2/(4\pi)$ as defined in Eq.(2.5), and $b_0 = (11N - 2N_f - N_s/2)/3$. The double-trace amplitudes with an $\mathcal{O}_{F^3}$ insertion are given by the $U(1)$ decoupling identity

$$
A^{(1)}_{F^3}(1234)_{[7]} = \frac{1}{N}\left(A^{(1)}_{F^3}(1234)_{[1]} + A^{(1)}_{F^3}(1243)_{[1]} + A^{(1)}_{F^3}(1423)_{[1]}\right)\,. \tag{2.111}
$$

The amplitudes with one insertion of a $\varphi^2 F^2$ operators are

$$
\begin{aligned}
&A^{(1)}_{(\varphi^2F^2)_1}(1^{\pm}2^{\pm}3^{\pm}4^{\pm})_{[1]} = 0\,,\\
&A^{(1)}_{(\varphi^2F^2)_1}(1^{+}2^{+}3^{+}4^{+})_{[7]} = 4\tilde{g}^2N_s s\,,\\
&A^{(1)}_{(\varphi^2F^2)_1}(1^{-}2^{+}3^{+}4^{+})_{[7]} = A^{(1)}_{(\varphi^2F^2)_1}(1^{-}2^{+}3^{-}4^{+})_{[7]} = 0\,,\\
&A^{(1)}_{(\varphi^2F^2)_1}(1^{-}2^{-}3^{+}4^{+})_{[7]} = 4\tilde{g}^2N_s s\,,\\
&A^{(1)}_{(\varphi^2F^2)_2}(1^{+}2^{+}3^{+}4^{+})_{[1]} = -2\tilde{g}^2N_s u\,,\\
&A^{(1)}_{(\varphi^2F^2)_2}(1^{-}2^{+}3^{+}4^{+})_{[1]} = A^{(1)}_{(\varphi^2F^2)_2}(1^{-}2^{+}3^{-}4^{+})_{[1]} = 0\,,\\
&A^{(1)}_{(\varphi^2F^2)_2}(1^{-}2^{-}3^{+}4^{+})_{[1]} = 2\tilde{g}^2N_s s\,,\\
&A^{(1)}_{(\varphi^2F^2)_2}(1^{+}2^{+}3^{+}4^{+})_{[7]} = A^{(1)}_{(\varphi^2F^2)_2}(1^{-}2^{-}3^{+}4^{+})_{[7]} = -\frac{4\tilde{g}^2N_s s}{N}\,,\\
&A^{(1)}_{(\varphi^2F^2)_2}(1^{-}2^{+}3^{+}4^{+})_{[7]} = A^{(1)}_{(\varphi^2F^2)_2}(1^{-}2^{+}3^{-}4^{+})_{[7]} = 0\,.
\end{aligned}
\tag{2.112}
$$

2.B.2 Four-fermion amplitudes

The color structures for the four-fermion amplitudes are

$$
\mathcal{C}^{[1]}_{ffff} = T^a_{i_2 i_1}T^a_{i_4 i_3}\,, \qquad \mathcal{C}^{[2]}_{ffff} = T^a_{i_4 i_1}T^a_{i_2 i_3}\,. \tag{2.113}
$$

Note for any operator, due to the anti-symmetry of the amplitudes under exchange of (anti-)fermions:

$$
\begin{aligned}
&A^{(L)}_{\mathcal{O}}(1^{+}_{\psi_m}2^{-}_{\bar{\psi}_n}3^{+}_{\psi_p}4^{-}_{\bar{\psi}_r})_{[2]} = -A^{(L)}_{\mathcal{O}}(1^{+}_{\psi_m}2^{-}_{\bar{\psi}_r}3^{+}_{\psi_p}4^{-}_{\bar{\psi}_n})_{[1]}\ (s\leftrightarrow t)\,,\\
&A^{(L)}_{\mathcal{O}}(1^{+}_{\psi_m}2^{-}_{\bar{\psi}_n}3^{-}_{\psi_p}4^{+}_{\bar{\psi}_r})_{[2]} = -A^{(L)}_{\mathcal{O}}(1^{+}_{\psi_m}2^{+}_{\bar{\psi}_r}3^{-}_{\psi_p}4^{-}_{\bar{\psi}_n})_{[1]}\ (s\leftrightarrow t)\,,\\
&A^{(L)}_{\mathcal{O}}(1^{+}_{\psi_m}2^{+}_{\bar{\psi}_n}3^{-}_{\psi_p}4^{-}_{\bar{\psi}_r})_{[2]} = -A^{(L)}_{\mathcal{O}}(1^{+}_{\psi_m}2^{-}_{\bar{\psi}_r}3^{-}_{\psi_p}4^{+}_{\bar{\psi}_n})_{[1]}\ (s\leftrightarrow t)\,.
\end{aligned}
\tag{2.114}
$$

The overall spinor phases are

$$S(1^+_\psi 2^-_{\bar\psi} 3^+_\psi 4^-_{\bar\psi}) = \frac{\langle 24\rangle[12]}{\langle 34\rangle[24]}\,, \qquad S(1^+_\psi 2^-_{\bar\psi} 3^-_\psi 4^+_{\bar\psi}) = \frac{\langle 23\rangle[12]}{\langle 34\rangle[23]}\,,$$
$$S(1^+_\psi 2^+_{\bar\psi} 3^-_\psi 4^-_{\bar\psi}) = \frac{[12]}{[34]}\,. \tag{2.115}$$

The tree-level D-dimensional amplitudes are given by

$$\begin{aligned}
A^{(0)}(1_{\psi_m} 2_{\bar\psi_n} 3_{\psi_p} 4_{\bar\psi_r})_{[1]} &= g^2 \frac{u_2\gamma^\mu u_1\ \bar u_4\gamma_\mu u_3}{2s}\delta_{mn}\delta_{pr}\,,\\
A^{(0)}_{(\psi^4)_1}(1_{\psi_m} 2_{\bar\psi_n} 3_{\psi_p} 4_{\bar\psi_r})_{[1]} &= \frac{N}{N^2-1}(c^{nmrp}_{(\psi^4)_1} u_2\gamma^\mu u_1\ \bar u_4\gamma_\mu u_3 - c^{rmnp}_{(\psi^4)_1} N u_4\gamma^\mu u_1\ \bar u_2\gamma_\mu u_3)\,,\\
A^{(0)}_{(\psi^4)_2}(1_{\psi_m} 2_{\bar\psi_n} 3_{\psi_p} 4_{\bar\psi_r})_{[1]} &= c^{nmrp}_{(\psi^4)_2} u_2\gamma^\mu u_1\ \bar u_4\gamma_\mu u_3\,,
\end{aligned} \tag{2.116}$$

which have four-dimensional values

$$\begin{aligned}
A^{(0)}(1^+_{\psi_m} 2^-_{\bar\psi_n} 3^+_{\psi_p} 4^-_{\bar\psi_r})_{[1]} &= \frac{g^2 u}{s}\delta_{mn}\delta_{pr}\,,\\
A^{(0)}(1^+_{\psi_m} 2^-_{\bar\psi_n} 3^-_{\psi_p} 4^+_{\bar\psi_r})_{[1]} &= -\frac{g^2 t}{s}\delta_{mn}\delta_{pr}\,,\\
A^{(0)}(1^+_{\psi_m} 2^+_{\bar\psi_n} 3^-_{\psi_p} 4^-_{\bar\psi_r})_{[1]} &= 0\,,\\
A^{(0)}_{(\psi^4)_1}(1^+_{\psi_m} 2^-_{\bar\psi_n} 3^+_{\psi_p} 4^-_{\bar\psi_r})_{[1]} &= -\frac{2Nu(Nc^{rmnp}_{(\psi^4)_1} + c^{nmrp}_{(\psi^4)_1})}{N^2-1}\,,\\
A^{(0)}_{(\psi^4)_1}(1^+_{\psi_m} 2^-_{\bar\psi_n} 3^-_{\psi_p} 4^+_{\bar\psi_r})_{[1]} &= \frac{2Ntc^{nmrp}_{(\psi^4)_1}}{N^2-1}\,,\\
A^{(0)}_{(\psi^4)_1}(1^+_{\psi_m} 2^+_{\bar\psi_n} 3^-_{\psi_p} 4^-_{\bar\psi_r})_{[1]} &= \frac{2N^2 sc^{nmrp}_{(\psi^4)_1}}{N^2-1}\,,\\
A^{(0)}_{(\psi^4)_2}(1^+_{\psi_m} 2^-_{\bar\psi_n} 3^+_{\psi_p} 4^-_{\bar\psi_r})_{[1]} &= -2uc^{nmrp}_{(\psi^4)_2}\,,\\
A^{(0)}_{(\psi^4)_2}(1^+_{\psi_m} 2^-_{\bar\psi_n} 3^-_{\psi_p} 4^+_{\bar\psi_r})_{[1]} &= 2tc^{nmrp}_{(\psi^4)_2}\,,\\
A^{(0)}_{(\psi^4)_2}(1^+_{\psi_m} 2^+_{\bar\psi_n} 3^-_{\psi_p} 4^-_{\bar\psi_r})_{[1]} &= 0\,.
\end{aligned} \tag{2.117}$$

The amplitudes with one insertion of the F^3 operator are

$$
\begin{aligned}
A^{(1)}_{F^3}(1^+_{\psi_m}2^-_{\bar\psi_n}3^+_{\psi_p}4^-_{\bar\psi_r})_{[1]} &= \frac{1}{3}g\tilde g^2 u\delta_{mn}\delta_{pr}\,,\\
A^{(1)}_{F^3}(1^+_{\psi_m}2^-_{\bar\psi_n}3^-_{\psi_p}4^+_{\bar\psi_r})_{[1]} &= -\frac{1}{3}g\tilde g^2 t\delta_{mn}\delta_{pr}\,,\\
A^{(1)}_{F^3}(1^+_{\psi_m}2^+_{\bar\psi_n}3^-_{\psi_p}4^-_{\bar\psi_r})_{[1]} &= 0\,.
\end{aligned}
\tag{2.118}
$$

The amplitudes with one insertion of a $D\varphi^2\psi^2$ operator are

$$
\begin{aligned}
A^{(1)}_{(D\varphi^2\psi^2)_1}(1^\pm_{\psi_m}2^\pm_{\bar\psi_n}3^\pm_{\psi_p}4^\pm_{\bar\psi_r})_{[1]} &= 0\,,\\
A^{(1)}_{(D\varphi^2\psi^2)_2}(1^+_{\psi_m}2^-_{\bar\psi_n}3^+_{\psi_p}4^-_{\bar\psi_r})_{[1]} &= -\frac{1}{9}\tilde g^2 N_s(3X_s+8)u(c^{rp}_{(D\varphi^2\psi^2)_2}\delta_{mn}+c^{nm}_{(D\varphi^2\psi^2)_2}\delta_{pr})\,,\\
A^{(1)}_{(D\varphi^2\psi^2)_2}(1^+_{\psi_m}2^-_{\bar\psi_n}3^-_{\psi_p}4^+_{\bar\psi_r})_{[1]} &= \frac{1}{9}\tilde g^2 N_s(3X_s+8)t(c^{rp}_{(D\varphi^2\psi^2)_2}\delta_{mn}+c^{nm}_{(D\varphi^2\psi^2)_2}\delta_{pr})\,,\\
A^{(1)}_{(D\varphi^2\psi^2)_2}(1^+_{\psi_m}2^+_{\bar\psi_n}3^-_{\psi_p}4^-_{\bar\psi_r})_{[1]} &= 0\,.
\end{aligned}
\tag{2.119}
$$

The amplitudes with one insertion of a ψ^4 operator are

$$
\begin{aligned}
A^{(1)\text{fin}}_{(\psi^4)_1}(1^+_{\psi_m}2^-_{\bar\psi_n}3^+_{\psi_p}4^-_{\bar\psi_r})_{[1]} &= \frac{2\tilde g^2 u}{9t}\Big(t\big(72N c^{rmnp}_{(\psi^4)_1} \\
&\quad + N_f(3X_s+2)(\delta_{mn}c^{rwwp}_{(\psi^4)_1}+\delta_{pr}c^{nwwm}_{(\psi^4)_1})\big) \\
&\quad + 9(2s+t(3X_u+25))c^{nmrp}_{(\psi^4)_1}\Big)\,, \\
A^{(1)\text{fin}}_{(\psi^4)_1}(1^+_{\psi_m}2^-_{\bar\psi_n}3^-_{\psi_p}4^+_{\bar\psi_r})_{[1]} &= -\frac{2}{9}\tilde g^2(N_f t(3X_s+2)(\delta_{mn}c^{rwwp}_{(\psi^4)_1}+\delta_{pr}c^{nwwm}_{(\psi^4)_1}) \\
&\quad + 9(2s+t(5-3X_t))c^{nmrp}_{(\psi^4)_1})\,, \\
A^{(1)\text{fin}}_{(\psi^4)_1}(1^+_{\psi_m}2^+_{\bar\psi_n}3^-_{\psi_p}4^-_{\bar\psi_r})_{[1]} &= -16\tilde g^2 N s c^{rmnp}_{(\psi^4)_1}\,, \\
A^{(1)\text{fin}}_{(\psi^4)_2}(1^+_{\psi_m}2^-_{\bar\psi_n}3^+_{\psi_p}4^-_{\bar\psi_r})_{[1]} &= \frac{2\tilde g^2 u}{9Nst}\Big(9s\left(2\left(N^2-1\right)s+t\left(13N^2-3X_u-25\right)\right)c^{nmrp}_{(\psi^4)_2} \\
&\quad + t(N_f s(2N(3X_s+5)(\delta_{mn}c^{rpww}_{(\psi^4)_2}+\delta_{pr}c^{nmww}_{(\psi^4)_2}) \\
&\quad - (3X_s+2)(\delta_{mn}c^{rwwp}_{(\psi^4)_2}+\delta_{pr}c^{nwwm}_{(\psi^4)_2})) \\
&\quad + 9N(s(3X_u+17)+2t)c^{rmnp}_{(\psi^4)_2})\Big)\,, \\
A^{(1)\text{fin}}_{(\psi^4)_2}(1^+_{\psi_m}2^-_{\bar\psi_n}3^-_{\psi_p}4^+_{\bar\psi_r})_{[1]} &= -\frac{2\tilde g^2}{9N}\Big(9\left(2\left(N^2-1\right)s-t\left(3(N^2-1)X_t-3N^2+5\right)\right)c^{nmrp}_{(\psi^4)_2} \\
&\quad + N_f t(2N(3X_s+5)(\delta_{mn}c^{rpww}_{(\psi^4)_2}+\delta_{pr}c^{nmww}_{(\psi^4)_2}) \\
&\quad - (3X_s+2)(\delta_{mn}c^{rwwp}_{(\psi^4)_2}+\delta_{pr}c^{nwwm}_{(\psi^4)_2}))\Big)\,, \\
A^{(1)\text{fin}}_{(\psi^4)_2}(1^+_{\psi_m}2^+_{\bar\psi_n}3^-_{\psi_p}4^-_{\bar\psi_r})_{[1]} &= 2\tilde g^2(3s(X_s+1)-2t)c^{rmnp}_{(\psi^4)_2}\,.
\end{aligned}
\tag{2.120}
$$

2.B.3 Four-scalar amplitudes

The color structures for this process are identical to those of the four fermion case:

$$
\mathcal{C}^{[1]}_{ssss} = T^a_{i_2 i_1}T^a_{i_4 i_3}\,, \qquad \mathcal{C}^{[2]}_{ssss} = T^a_{i_4 i_1}T^a_{i_2 i_3}\,. \tag{2.121}
$$

There is no spinor phase in this case, as the scalars do not carry helicity weight. The tree-level amplitudes are

$$\begin{aligned} A^{(0)}(1_\varphi 2_{\bar\varphi} 3_\varphi 4_{\bar\varphi})_{[1]} &= -\frac{g^2(t-u)}{2s} - \frac{2\lambda N}{N-1}\,, \\ A^{(0)}_{(D^2\varphi^4)_1}(1_\varphi 2_{\bar\varphi} 3_\varphi 4_{\bar\varphi})_{[1]} &= \frac{N(Ns+t)}{N^2-1}\,, \\ A^{(0)}_{(D^2\varphi^4)_2}(1_\varphi 2_{\bar\varphi} 3_\varphi 4_{\bar\varphi})_{[1]} &= \frac{2N(Nt+s)}{N^2-1}\,. \end{aligned} \tag{2.122}$$

The one-loop amplitudes with an insertion of the F^3 operator are

$$A^{(1)}_{F^3}(1_\varphi 2_{\bar\varphi} 3_\varphi 4_{\bar\varphi})_{[1]} = -\frac{1}{6} g\tilde{g}^2 N(t-u)\,. \tag{2.123}$$

The one-loop amplitudes with an insertion of a $\varphi^2 F^2$ operator are

$$\begin{aligned} A^{(1)}_{(\varphi^2F^2)_1}(1_\varphi 2_{\bar\varphi} 3_\varphi 4_{\bar\varphi})_{[1]} &= 2\tilde{g}^2(Nt+s)\,, \\ A^{(1)}_{(\varphi^2F^2)_2}(1_\varphi 2_{\bar\varphi} 3_\varphi 4_{\bar\varphi})_{[1]} &= \frac{2\tilde{g}^2\,(N^2-4)\,s}{N}\,. \end{aligned} \tag{2.124}$$

The one-loop amplitudes with an insertion of a $D^2\varphi^4$ operator are

$$\begin{aligned} A^{(1)\text{fin}}_{(D^2\varphi^4)_1}(1_\varphi 2_{\bar\varphi} 3_\varphi 4_{\bar\varphi})_{[1]} &= \frac{\tilde{g}^2}{2}\Big(-4(4N+3)s - 2(3N+5)t \\ &\quad - 3(N-2)tX_t - 3sX_s + 3uX_u\Big) \\ &\quad + \frac{2\tilde{\lambda}}{N-1}\Big(2N((N-3)t-2s) - NsX_s \\ &\quad + (N-2)NtX_t + NuX_u\Big)\,, \\ A^{(1)\text{fin}}_{(D^2\varphi^4)_2}(1_\varphi 2_{\bar\varphi} 3_\varphi 4_{\bar\varphi})_{[1]} &= \frac{\tilde{g}^2}{9}\Big(-2(2t(9N+4N_s+27) + (4N_s+45)s) \\ &\quad + 27(2N-1)tX_t - 3X_s((N_s-18)s + 2N_st) + 27uX_u) \\ &\quad + \frac{4\tilde{\lambda}N}{N-1}(-4(Nt+s) + (1-2N)tX_t - sX_s + uX_u)\,. \end{aligned} \tag{2.125}$$

The one-loop amplitudes with an insertion of a $D\varphi^2\psi^2$ operator are

$$\begin{aligned} A^{(1)}_{(D\varphi^2\psi^2)_1}(1_\varphi 2_{\bar\varphi} 3_\varphi 4_{\bar\varphi})_{[1]} &= 0\,, \\ A^{(1)}_{(D\varphi^2\psi^2)_2}(1_\varphi 2_{\bar\varphi} 3_\varphi 4_{\bar\varphi})_{[1]} &= -\frac{2}{9} c^{ww}_{(D\varphi^2\psi^2)_2} \tilde{g}^2 (3X_s + 5)(t-u)\,. \end{aligned} \tag{2.126}$$

2.B.4 Two-fermion, two-vector amplitudes

The color factors for the two-fermion, two-vector amplitudes are

$$\mathcal{C}^{[1]}_{ffvv} = (T^3T^4)_{i_2 i_1}\,, \qquad \mathcal{C}^{[2]}_{ffvv} = (T^4T^3)_{i_2 i_1}\,, \qquad \mathcal{C}^{[3]}_{ffvv} = \mathrm{Tr}[T^3T^4]\delta_{i_2 i_1}\,. \tag{2.127}$$

In this case the spinor prefactors are not pure phases, but have magnitudes equal to ratios of s, t, and u:

$$\begin{aligned} S(1^-_{\psi_p} 2^+_{\bar\psi_r} 3^+ 4^+) &= \frac{\langle 13\rangle[34]}{\langle 23\rangle\langle 34\rangle}\,, & S(1^-_{\psi_p} 2^+_{\bar\psi_r} 3^- 4^+) &= \frac{\langle 13\rangle^3}{\langle 12\rangle\langle 34\rangle\langle 41\rangle}\,, \\ S(1^-_{\psi_p} 2^+_{\bar\psi_r} 3^+ 4^-) &= \frac{\langle 14\rangle^3}{\langle 12\rangle\langle 31\rangle\langle 43\rangle}\,, & S(1^-_{\psi_p} 2^+_{\bar\psi_r} 3^- 4^-) &= \frac{\langle 34\rangle^3}{\langle 23\rangle\langle 24\rangle[12]}\,. \end{aligned} \tag{2.128}$$

The tree-level amplitudes for this process are

$$\begin{aligned} A^{(0)}(1_{\psi_p} 2_{\bar\psi_r} 34)_{[1]} &= -\frac{g^2}{st}(2T^{-+-+}_{ffvv} - 2T^{-++-}_{ffvv} + T^{\mathrm{ev}}_{ffvv})\delta_{pr}\,, \\ A^{(0)}_{F^3}(1_{\psi_p} 2_{\bar\psi_r} 34)_{[1]} &= -\frac{2g}{s}(T^{-+++}_{ffvv} + T^{-+--}_{ffvv})\delta_{pr}\,, \end{aligned} \tag{2.129}$$

which evaluate in four dimensions as

$$
\begin{aligned}
A^{(0)}(1^-_{\psi_p}2^+_{\bar\psi_r}3^+4^+)_{[1]} &= 0\,,\\
A^{(0)}(1^-_{\psi_p}2^+_{\bar\psi_r}3^+4^-)_{[1]} &= g^2\delta_{pr}\,,\\
A^{(0)}(1^-_{\psi_p}2^+_{\bar\psi_r}3^-4^+)_{[1]} &= \frac{g^2 t}{u}\delta_{pr}\,,\\
A^{(0)}(1^-_{\psi_p}2^+_{\bar\psi_r}3^-4^-)_{[1]} &= 0\,,\\
A^{(0)}_{F^3}(1^-_{\psi_p}2^+_{\bar\psi_r}3^+4^+)_{[1]} &= -gt\delta_{pr}\,,\\
A^{(0)}_{F^3}(1^-_{\psi_p}2^+_{\bar\psi_r}3^+4^-)_{[1]} &= 0\,,\\
A^{(0)}_{F^3}(1^-_{\psi_p}2^+_{\bar\psi_r}3^-4^+)_{[1]} &= 0\,,\\
A^{(0)}_{F^3}(1^-_{\psi_p}2^+_{\bar\psi_r}3^-4^-)_{[1]} &= \frac{gtu}{s}\delta_{pr}\,.
\end{aligned}
\tag{2.130}
$$

The one-loop amplitudes with an insertion of a F^3 operator are

$$
\begin{aligned}
A^{(1)\text{fin}}_{F^3}(1^-_{\psi_p}2^+_{\bar\psi_r}3^+4^+)_{[1]} &= \frac{g\tilde g^2\delta_{pr}}{36Nu}\Big(2tu\big(34N^2+N(5N_f+2N_s)-18\big)\\
&\qquad + 9Ntu((4N_f+N_s)X_s+2(N-b_0)X_t)\\
&\qquad + 18N^2(t-u)tX^2\Big)\,,\\
A^{(1)\text{fin}}_{F^3}(1^-_{\psi_p}2^+_{\bar\psi_r}3^-4^+)_{[1]} &= 0\,,\\
A^{(1)}_{F^3}(1^-_{\psi_p}2^+_{\bar\psi_r}3^+4^-)_{[1]} &= g\tilde g^2\delta_{pr}N\frac{su}{t}\,,\\
A^{(1)\text{fin}}_{F^3}(1^-_{\psi_p}2^+_{\bar\psi_r}3^-4^-)_{[1]} &= -\frac{u}{s}A^{(1)\text{fin}}_{F^3}(1^-_{\psi_p}2^+_{\bar\psi_r}3^+4^+)_{[1]}\,,
\end{aligned}
\tag{2.131}
$$

$$
\begin{aligned}
A^{(1)\text{fin}}_{F^3}(1^-_{\psi_p}2^+_{\bar\psi_r}3^+4^+)_{[3]} &= g\tilde g^2\delta_{pr}\bigg(\frac{(3N+b_0)}{2N}t(X_u-X_t)\\
&\qquad +\frac{(t-u)}{2su}(stX^2+suY^2+utZ^2)\bigg)\,,\\
A^{(1)}_{F^3}(1^-_{\psi_p}2^+_{\bar\psi_r}3^-4^+)_{[3]} &= g\tilde g^2\delta_{pr}2\frac{st}{u}\,,\\
A^{(1)}_{F^3}(1^-_{\psi_p}2^+_{\bar\psi_r}3^+4^-)_{[3]} &= g\tilde g^2\delta_{pr}2\frac{su}{t}\,,\\
A^{(1)\text{fin}}_{F^3}(1^-_{\psi_p}2^+_{\bar\psi_r}3^-4^-)_{[3]} &= -\frac{u}{s}A^{(1)\text{fin}}_{F^3}(1^-_{\psi_p}2^+_{\bar\psi_r}3^+4^+)_{[3]}\,.
\end{aligned}
\tag{2.132}
$$

The one-loop amplitudes with an insertion of a φ^2F^2 operator all evaluate to zero:

$$
\begin{aligned}
A^{(1)}_{(\varphi^2F^2)_1}(1^\pm_{\psi_p}2^\pm_{\bar\psi_r}3^\pm4^\pm)_{[1]} &= A^{(1)}_{(\varphi^2F^2)_1}(1^\pm_{\psi_p}2^\pm_{\bar\psi_r}3^\pm4^\pm)_{[3]} = 0\,,\\
A^{(1)}_{(\varphi^2F^2)_2}(1^\pm_{\psi_p}2^\pm_{\bar\psi_r}3^\pm4^\pm)_{[1]} &= A^{(1)}_{(\varphi^2F^2)_2}(1^\pm_{\psi_p}2^\pm_{\bar\psi_r}3^\pm4^\pm)_{[3]} = 0\,.
\end{aligned}
\tag{2.133}
$$

The one-loop amplitudes with an insertion of a $D\varphi^2\psi^2$ operator are

$$
\begin{aligned}
A^{(1)}_{(D\varphi^2\psi^2)_1}(1^\pm_{\psi_p}2^\pm_{\bar\psi_r}3^\pm4^\pm)_{[1]} &= A^{(1)}_{(D\varphi^2\psi^2)_1}(1^\pm_{\psi_p}2^\pm_{\bar\psi_r}3^\pm4^\pm)_{[3]} = 0\,,\\
A^{(1)}_{(D\varphi^2\psi^2)_2}(1^-_{\psi_p}2^+_{\bar\psi_r}3^+4^+)_{[1]} &= \frac{1}{3}\tilde g^2c^{rp}_{(D\varphi^2\psi^2)_2}N_st\,,\\
A^{(1)}_{(D\varphi^2\psi^2)_2}(1^-_{\psi_p}2^+_{\bar\psi_r}3^+4^-)_{[1]} &= A^{(1)}_{(D\varphi^2\psi^2)_2}(1^-_{\psi_p}2^+_{\bar\psi_r}3^-4^+)_{[1]} = 0\,,\\
A^{(1)}_{(D\varphi^2\psi^2)_2}(1^-_{\psi_p}2^+_{\bar\psi_r}3^-4^-)_{[1]} &= -\frac{1}{3s}\tilde g^2c^{rp}_{(D\varphi^2\psi^2)_2}N_stu\,,\\
A^{(1)}_{(D\varphi^2\psi^2)_2}(1^\pm_{\psi_p}2^\pm_{\bar\psi_r}3^\pm4^\pm)_{[3]} &= 0\,.
\end{aligned}
\tag{2.134}
$$

The one-loop amplitudes with an insertion of a ψ^4 operator are

$$
\begin{aligned}
A^{(1)}_{(\psi^4)_1}(1^\pm_{\psi_p}2^\pm_{\bar\psi_r}3^\pm4^\pm)_{[1],[3]} &= \frac{N_f}{N_s}\frac{c^{rwwp}_{(\psi^4)_1}}{c^{rp}_{(D\varphi^2\psi^2)_2}}A^{(1)}_{(D\varphi^2\psi^2)_2}(1^\pm_{\psi_p}2^\pm_{\bar\psi_r}3^\pm4^\pm)_{[1],[3]}\,,\\
A^{(1)}_{(\psi^4)_2}(1^\pm_{\psi_p}2^\pm_{\bar\psi_r}3^\pm4^\pm)_{[1],[3]} &= \frac{2Nc^{rpww}_{(\psi^4)_2}-c^{rwwp}_{(\psi^4)_2}}{c^{rwwp}_{(\psi^4)_1}}A^{(1)}_{(\psi^4)_1}(1^\pm_{\psi_p}2^\pm_{\bar\psi_r}3^\pm4^\pm)_{[1],[3]}\,.
\end{aligned}
\tag{2.135}
$$

2.B.5 Two-scalar, two-vector amplitudes

The color basis for this process is analogous to the that of the previous:

$$\mathcal{C}^{[1]}_{vvss} = (T^1T^2)_{i_4i_3}\,, \qquad \mathcal{C}^{[2]}_{vvss} = (T^2T^1)_{i_4i_3}\,, \qquad \mathcal{C}^{[3]}_{vvss} = \mathrm{Tr}[T^1T^2]\delta_{i_4i_3}\,. \tag{2.136}$$

The spinor factors are again pure phases:

$$S(1^+2^+3_\varphi 4_{\bar\varphi}) = \frac{[12]}{\langle 12\rangle}\,, \qquad S(1^+2^-3_\varphi 4_{\bar\varphi}) = \frac{\langle 23\rangle\langle 24\rangle[12][34]}{\langle 12\rangle\langle 34\rangle[23][24]}\,. \tag{2.137}$$

The D-dimensional tree-level expressions are given by

$$\begin{aligned}
A^{(1)}(123_\varphi 4_{\bar\varphi})_{[1]} &= -\frac{g^2}{st}T^{+-}_{vvss}\,,\\
A^{(1)}(123_\varphi 4_{\bar\varphi})_{[3]} &= 0\,,\\
A^{(1)}_{F^3}(123_\varphi 4_{\bar\varphi})_{[1]} &= \frac{g(t-u)}{2s}T^{++}_{vvss}\,,\\
A^{(1)}_{F^3}(123_\varphi 4_{\bar\varphi})_{[3]} &= 0\,,\\
A^{(1)}_{(\varphi^2F^2)_1}(123_\varphi 4_{\bar\varphi})_{[1]} &= 0\,,\\
A^{(1)}_{(\varphi^2F^2)_1}(123_\varphi 4_{\bar\varphi})_{[3]} &= -2T^{++}_{vvss}\,,\\
A^{(1)}_{(\varphi^2F^2)_2}(123_\varphi 4_{\bar\varphi})_{[1]} &= -2T^{++}_{vvss}\,,\\
A^{(1)}_{(\varphi^2F^2)_2}(123_\varphi 4_{\bar\varphi})_{[3]} &= -\frac{4}{N}T^{++}_{vvss}\,,
\end{aligned} \tag{2.138}$$

with four-dimensional helicity values

$$
\begin{aligned}
A^{(1)}(1^+2^+3_\varphi 4_{\bar\varphi})_{[1]} &= 0\,,\\
A^{(1)}(1^+2^-3_\varphi 4_{\bar\varphi})_{[1]} &= \frac{g^2 u}{s}\,,\\
A^{(1)}(1^\pm 2^\pm 3_\varphi 4_{\bar\varphi})_{[3]} &= 0\,,\\
A^{(1)}_{F^3}(1^+2^+3_\varphi 4_{\bar\varphi})_{[1]} &= \frac{1}{2} g(t-u)\,,\\
A^{(1)}_{F^3}(1^+2^-3_\varphi 4_{\bar\varphi})_{[1]} &= 0\,,\\
A^{(1)}_{F^3}(1^\pm 2^\pm 3_\varphi 4_{\bar\varphi})_{[3]} &= 0\,,\\
A^{(1)}_{(\varphi^2F^2)_1}(1^\pm 2^\pm 3_\varphi 4_{\bar\varphi})_{[1]} &= 0\,,\\
A^{(1)}_{(\varphi^2F^2)_1}(1^+2^+3_\varphi 4_{\bar\varphi})_{[3]} &= -2s\,,\\
A^{(1)}_{(\varphi^2F^2)_1}(1^+2^-3_\varphi 4_{\bar\varphi})_{[3]} &= 0\,,\\
A^{(1)}_{(\varphi^2F^2)_2}(1^+2^+3_\varphi 4_{\bar\varphi})_{[1]} &= -2s\,,\\
A^{(1)}_{(\varphi^2F^2)_2}(1^+2^-3_\varphi 4_{\bar\varphi})_{[1]} &= 0\,,\\
A^{(1)}_{(\varphi^2F^2)_2}(1^+2^+3_\varphi 4_{\bar\varphi})_{[3]} &= -\frac{4s}{N}\,,\\
A^{(1)}_{(\varphi^2F^2)_2}(1^+2^-3_\varphi 4_{\bar\varphi})_{[3]} &= 0\,.
\end{aligned}
\tag{2.139}
$$

The one-loop amplitudes with an insertion of the F^3 operator are

$$
\begin{aligned}
A^{(1)\text{fin}}_{F^3}(1^+2^+3_\varphi 4_{\bar\varphi})_{[1]} &= -\frac{g\tilde g^2}{72N}\Big(8((52N^2-18)s+(77N^2-36)t+N(t-u)(5N_f+2N_s)) \\
&\quad +18N((2N(5t-7u)-3b_0(t-u))X_t+X_s(2Ns+b_0(u-t))) \\
&\quad -72N^2tX^2\Big)\,, \\
A^{(1)}_{F_3}(1^+2^-3_\varphi 4_{\bar\varphi})_{[1]} &= \frac{1}{2}g\tilde g^2Nu\,, \\
A^{(1)\text{fin}}_{F^3}(1^+2^+3_\varphi 4_{\bar\varphi})_{[3]} &= \frac{g\tilde g^2}{4N}\Big((8Nt+b_0(t-u))X_t+(8Nu+b_0(u-t))X_u-4NsX_s \\
&\quad +\frac{1}{6s}(stX^2+suY^2+tuZ^2)\Big)\,, \\
A^{(1)}_{F_3}(1^+2^-3_\varphi 4_{\bar\varphi})_{[3]} &= -g\tilde g^2 s\,.
\end{aligned}
\tag{2.140}
$$

The one-loop amplitudes with an insertion of a φ^2F^2 operator are

$$
A^{(1)\text{fin}}_{(\varphi^2F^2)_1}(1^+2^+3_\varphi 4_{\bar\varphi})_{[1]} = -\frac{\tilde g^2 s}{N}((b_0-2N)X_t+b_0X_u)+4\tilde g^2 s\,, \tag{2.141}
$$

$$
\begin{aligned}
A^{(1)}_{(\varphi^2F^2)_1}(1^+2^-3_\varphi 4_{\bar\varphi})_{[1]} &= 2\tilde g^2(s+3t)\,, \\
A^{(1)\text{fin}}_{(\varphi^2F^2)_1}(1^+2^+3_\varphi 4_{\bar\varphi})_{[3]} &= \tilde g^2 s\,(4C_F-2(b_0+3C_F)X_s) \\
&\quad +4\tilde\lambda(N+1)s(X_s+2)\,, \\
A^{(1)}_{(\varphi^2F^2)_1}(1^+2^-3_\varphi 4_{\bar\varphi})_{[3]} &= 0\,, \\
A^{(1)\text{fin}}_{(\varphi^2F^2)_2}(1^+2^+3_\varphi 4_{\bar\varphi})_{[1]} &= \frac{\tilde g^2 s}{N^2}\Big(6N\left(2N^2-3\right)+N\left(3-Nb_0\right)X_s+2b_0X_u \\
&\quad +\left(2N(N^2-4)-b_0(N^2-2)\right)X_t\Big) \\
&\quad +4\tilde\lambda s(X_s+2)\,, \\
A^{(1)}_{(\varphi^2F^2)_2}(1^+2^-3_\varphi 4_{\bar\varphi})_{[1]} &= -\frac{2\tilde g^2}{N}\left(N^2u+4t\right)\,, \\
A^{(1)\text{fin}}_{(\varphi^2F^2)_2}(1^+2^+3_\varphi 4_{\bar\varphi})_{[3]} &= \frac{\tilde g^2 s}{N^2}\Big(2\left(b_0N-3\right)X_s+b_0N(X_t+X_u)-3\left(4N^2-1\right)\Big) \\
&\quad -\frac{8}{N}\tilde\lambda s(X_s+2)\,, \\
A^{(1)}_{(\varphi^2F^2)_2}(1^+2^-3_\varphi 4_{\bar\varphi})_{[3]} &= -4\tilde g^2 s\,.
\end{aligned}
\tag{2.142}
$$

The one-loop amplitudes with an insertion of a $D^2\varphi^4$ operator are

$$\begin{aligned}
&A^{(1)}_{(D^2\varphi^4)_1}(1^+2^+3_\varphi 4_{\bar\varphi})_{[1]} = -\frac{1}{2}\tilde g^2 N_s s\,,\\
&A^{(1)}_{(D^2\varphi^4)_1}(1^+2^-3_\varphi 4_{\bar\varphi})_{[1]} = 0\,,\\
&A^{(1)}_{(D^2\varphi^4)_1}(1^\pm2^\pm3_\varphi 4_{\bar\varphi})_{[3]} = -A^{(1)}_{(D^2\varphi^4)_1}(1^\pm2^\pm3_\varphi 4_{\bar\varphi})_{[1]}\,,\\
&A^{(1)}_{(D^2\varphi^4)_2}(1^+2^+3_\varphi 4_{\bar\varphi})_{[1]} = \frac{1}{3}\tilde g^2 N_s (s-t)\,,\\
&A^{(1)}_{(D^2\varphi^4)_2}(1^+2^-3_\varphi 4_{\bar\varphi})_{[1]} = 0\,,\\
&A^{(1)}_{(D^2\varphi^4)_2}(1^\pm2^\pm3_\varphi 4_{\bar\varphi})_{[3]} = 4A^{(1)}_{(D^2\varphi^4)_1}(1^\pm2^\pm3_\varphi 4_{\bar\varphi})_{[1]}\,.
\end{aligned} \tag{2.143}$$

The one-loop amplitudes with an insertion of a $D\varphi^2\psi^2$ operator are

$$\begin{aligned}
&A^{(1)}_{(D\varphi^2\psi^2)_1}(1^\pm2^\pm3_\varphi 4_{\bar\varphi})_{[1]} = A^{(1)}_{(D\varphi^2\psi^2)_1}(1^\pm2^\pm3_\varphi 4_{\bar\varphi})_{[3]} = 0\,,\\
&A^{(1)}_{(D\varphi^2\psi^2)_2}(1^+2^+3_\varphi 4_{\bar\varphi})_{[1]} = \frac{1}{3}\tilde g^2 c^{ww}_{(D\varphi^2\psi^2)_2} N_f (t-u)\,,\\
&A^{(1)}_{(D\varphi^2\psi^2)_2}(1^+2^-3_\varphi 4_{\bar\varphi})_{[1]} = A^{(1)}_{(D\varphi^2\psi^2)_2}(1^\pm2^\pm3_\varphi 4_{\bar\varphi})_{[3]} = 0\,.
\end{aligned} \tag{2.144}$$

2.B.6 Two-fermion, two-scalar amplitudes

The color structures for this process are identical to those of the four fermion case:

$$\mathcal{C}^{[1]}_{ffss} = T^a_{i_2 i_1} T^a_{i_4 i_3}\,, \qquad \mathcal{C}^{[2]}_{ffss} = T^a_{i_4 i_1} T^a_{i_2 i_3}\,. \tag{2.145}$$

There is only one independent spinor prefactor (which again is not a pure phase for this case):

$$S(1_\psi 2_{\bar\psi} 3_\varphi 4_{\bar\varphi}) = \frac{\langle 23\rangle[13]}{s}\,. \tag{2.146}$$

The tree-level amplitudes for this process are given by

$$
\begin{aligned}
A^{(0)}(1_{\psi_p}2_{\bar{\psi}_r}3_{\varphi}4_{\bar{\varphi}})_{[1]} &= g^2\frac{\bar{u}_2\not{k}_3u_1}{s}\delta_{pr}\,,\\
A^{(0)}(1_{\psi_p}2_{\bar{\psi}_r}3_{\varphi}4_{\bar{\varphi}})_{[2]} &= 0\,,\\
A^{(0)}_{(D\varphi^2\psi^2)_1}(1_{\psi_p}2_{\bar{\psi}_r}3_{\varphi}4_{\bar{\varphi}})_{[1]} &= -\frac{2c^{rp}_{(D\varphi^2\psi^2)_1}N(\bar{u}_2\not{k}_3u_1)}{N^2-1}\,,\\
A^{(0)}_{(D\varphi^2\psi^2)_1}(1_{\psi_p}2_{\bar{\psi}_r}3_{\varphi}4_{\bar{\varphi}})_{[2]} &= -\frac{2c^{rp}_{(D\varphi^2\psi^2)_1}N^2(\bar{u}_2\not{k}_3u_1)}{N^2-1}\,,\\
A^{(0)}_{(D\varphi^2\psi^2)_2}(1_{\psi_p}2_{\bar{\psi}_r}3_{\varphi}4_{\bar{\varphi}})_{[1]} &= -2c^{rp}_{(D\varphi^2\psi^2)_2}(\bar{u}_2\not{k}_3u_1)\,,\\
A^{(0)}_{(D\varphi^2\psi^2)_2}(1_{\psi_p}2_{\bar{\psi}_r}3_{\varphi}4_{\bar{\varphi}})_{[2]} &= 0\,,
\end{aligned}
\tag{2.147}
$$

with four-dimensional helicity values

$$
\begin{aligned}
A^{(0)}(1^+_{\psi_p}2^-_{\bar{\psi}_r}3_{\varphi}4_{\bar{\varphi}})_{[1]} &= g^2\delta_{pr}\,,\\
A^{(0)}(1^+_{\psi_p}2^-_{\bar{\psi}_r}3_{\varphi}4_{\bar{\varphi}})_{[2]} &= 0\,,\\
A^{(0)}_{(D\varphi^2\psi^2)_1}(1^+_{\psi_p}2^-_{\bar{\psi}_r}3_{\varphi}4_{\bar{\varphi}})_{[1]} &= -\frac{4c^{rp}_{(D\varphi^2\psi^2)_1}Ns}{N^2-1}\,,\\
A^{(0)}_{(D\varphi^2\psi^2)_1}(1^+_{\psi_p}2^-_{\bar{\psi}_r}3_{\varphi}4_{\bar{\varphi}})_{[2]} &= -\frac{4c^{rp}_{(D\varphi^2\psi^2)_1}N^2s}{N^2-1}\,,\\
A^{(0)}_{(D\varphi^2\psi^2)_2}(1^+_{\psi_p}2^-_{\bar{\psi}_r}3_{\varphi}4_{\bar{\varphi}})_{[1]} &= -4c^{rp}_{(D\varphi^2\psi^2)_2}s\,,\\
A^{(0)}_{(D\varphi^2\psi^2)_2}(1^+_{\psi_p}2^-_{\bar{\psi}_r}3_{\varphi}4_{\bar{\varphi}})_{[2]} &= 0\,.
\end{aligned}
\tag{2.148}
$$

The one-loop amplitudes with an insertion of the F^3 operator are

$$
\begin{aligned}
A^{(1)}_{F^3}(1^+_{\psi_p}2^-_{\bar{\psi}_r}3_{\varphi}4_{\bar{\varphi}})_{[1]} &= \frac{1}{6}g\tilde{g}^2Ns\delta_{pr}\,,\\
A^{(1)}_{F^3}(1^+_{\psi_p}2^-_{\bar{\psi}_r}3_{\varphi}4_{\bar{\varphi}})_{[2]} &= 0\,.
\end{aligned}
\tag{2.149}
$$

The one-loop amplitudes with an insertion of a $\varphi^2 F^2$ operator all evaluate to zero:

$$\begin{aligned}
&A^{(1)}_{(\varphi^2F^2)_1}(1^+_{\psi_p}2^-_{\bar\psi_r}3_\varphi 4_{\bar\varphi})_{[1]} = A^{(1)}_{(\varphi^2F^2)_1}(1^+_{\psi_p}2^-_{\bar\psi_r}3_\varphi 4_{\bar\varphi})_{[2]} = 0\,,\\
&A^{(1)}_{(\varphi^2F^2)_2}(1^+_{\psi_p}2^-_{\bar\psi_r}3_\varphi 4_{\bar\varphi})_{[1]} = A^{(1)}_{(\varphi^2F^2)_2}(1^+_{\psi_p}2^-_{\bar\psi_r}3_\varphi 4_{\bar\varphi})_{[2]} = 0\,.
\end{aligned} \tag{2.150}$$

The one-loop amplitudes with an insertion of a $D^2\varphi^4$ operator are

$$\begin{aligned}
&A^{(1)}_{(D^2\varphi^4)_1}(1^+_{\psi_p}2^-_{\bar\psi_r}3_\varphi 4_{\bar\varphi})_{[1]} = A^{(1)}_{(D^2\varphi^4)_1}(1^+_{\psi_p}2^-_{\bar\psi_r}3_\varphi 4_{\bar\varphi})_{[2]} = 0\,,\\
&A^{(1)}_{(D^2\varphi^4)_2}(1^+_{\psi_p}2^-_{\bar\psi_r}3_\varphi 4_{\bar\varphi})_{[1]} = \frac{1}{9}\tilde g^2 N_s s(3X_s+8)\delta_{pr}\,,\\
&A^{(1)}_{(D^2\varphi^4)_2}(1^+_{\psi_p}2^-_{\bar\psi_r}3_\varphi 4_{\bar\varphi})_{[2]} = 0\,.
\end{aligned} \tag{2.151}$$

The one-loop amplitudes with an insertion of a $D\psi^2\varphi^2$ operator are

$$\begin{aligned}
&A^{(1)\text{fin}}_{(D\varphi^2\psi^2)_1}(1^+_{\psi_p}2^-_{\bar\psi_r}3_\varphi 4_{\bar\varphi})_{[1]} = -\tilde g^2 s(3X_t-3X_u-16)c^{rp}_{(D\varphi^2\psi^2)_1}\,,\\
&A^{(1)\text{fin}}_{(D\varphi^2\psi^2)_1}(1^+_{\psi_p}2^-_{\bar\psi_r}3_\varphi 4_{\bar\varphi})_{[2]} = 16\tilde g^2 N s c^{rp}_{(D\varphi^2\psi^2)_1}\,,\\
&A^{(1)\text{fin}}_{(D\varphi^2\psi^2)_2}(1^+_{\psi_p}2^-_{\bar\psi_r}3_\varphi 4_{\bar\varphi})_{[1]} = \frac{\tilde g^2 s}{9N}c^{rp}_{(D\varphi^2\psi^2)_2}\Big(8\left(9N^2+NN_s-18\right)\\
&\qquad\qquad -27\left(N^2-1\right)X_t+3NN_sX_s-27X_u\Big)\\
&\qquad\qquad +\frac{4}{9}\tilde g^2 N_f s(3X_s+5)c^{ww}_{(D\varphi^2\psi^2)_2}\delta_{pr}\,,\\
&A^{(1)\text{fin}}_{(D\varphi^2\psi^2)_2}(1^+_{\psi_p}2^-_{\bar\psi_r}3_\varphi 4_{\bar\varphi})_{[2]} = -3\tilde g^2 s(X_t-X_u)c^{rp}_{(D\varphi^2\psi^2)_2}\,.
\end{aligned} \tag{2.152}$$

The one-loop amplitudes with an insertion of a ψ^4 operator are

$$
\begin{aligned}
&A^{(1)}_{(\psi^4)_1}(1^+_{\psi_p}2^-_{\bar{\psi}_r}3_\varphi 4_{\bar{\varphi}})_{[1]} = -\frac{2}{9}\tilde{g}^2 N_f s(3X_s+2)c^{rwwp}_{(\psi^4)_1}\,,\\
&A^{(1)}_{(\psi^4)_1}(1^+_{\psi_p}2^-_{\bar{\psi}_r}3_\varphi 4_{\bar{\varphi}})_{[2]} = 0\,,\\
&A^{(1)}_{(\psi^4)_2}(1^+_{\psi_p}2^-_{\bar{\psi}_r}3_\varphi 4_{\bar{\varphi}})_{[1]} = \frac{2\tilde{g}^2 N_f s}{9N}((3X_s+2)c^{rwwp}_{(\psi^4)_2} - 2N(3X_s+5)c^{rpww}_{(\psi^4)_2})\,,\\
&A^{(1)}_{(\psi^4)_2}(1^+_{\psi_p}2^-_{\bar{\psi}_r}3_\varphi 4_{\bar{\varphi}})_{[2]} = 0\,.
\end{aligned}
\tag{2.153}
$$

	$\mathcal{O}_G$	$\mathcal{O}_W$	$\mathcal{O}_{HW}$	$\mathcal{O}_{uW}$	$\mathcal{O}_{H\Box}$ $\mathcal{O}_{HD}$	$\mathcal{O}_{Hq}^{(1)}$ $\mathcal{O}_{Hq}^{(3)}$	$\mathcal{O}_{qq}^{(1)}$ $\mathcal{O}_{qq}^{(3)}$	$\mathcal{O}_{uu}$	$\mathcal{O}_{uH}$	$\mathcal{O}_H$
$\mathcal{O}_G$		$\emptyset$	$\emptyset$	$\emptyset$	$\emptyset$	$\emptyset$	0	0	$\emptyset$	$\emptyset$
$\mathcal{O}_W$	$\emptyset$			0_y	0	0	0	$\emptyset$	$\emptyset$	$\emptyset$
$\mathcal{O}_{HW}$	$\emptyset$			0_y			0	$\emptyset$	0_y	0
$\mathcal{O}_{uW}$	0_y	0_y	0_y		0_y	0_y	0_y	0_y		$\emptyset$
$\mathcal{O}_{H\Box}$, $\mathcal{O}_{HD}$	$\emptyset$			0_y			$0_y(\not{g}_2^{4*})$	0_y	0_y	0
$\mathcal{O}_{Hq}^{(1)}$, $\mathcal{O}_{Hq}^{(3)}$				0_y				0_y	$0_y(\not{y}\not{\lambda})$	$\emptyset$
$\mathcal{O}_{qq}^{(1)}$, $\mathcal{O}_{qq}^{(3)}$				0_y	$0_y(\not{g}_2^4)$				$\emptyset$	$\emptyset$
$\mathcal{O}_{uu}$		$\emptyset$	$\emptyset$	0_y	0_y	0_y			$\emptyset$	$\emptyset$
$\mathcal{O}_{uH}$	0_y	0_y	0_y		0_y	0_y	0_y	0_y		0_y
$\mathcal{O}_H$	$\emptyset$			0_y					0_y	

$\emptyset$	: trivial zero, no contributing two-loop diagrams
0	: zero predicted by the selection rules of Section 2.5
	: only a three-particle cut is needed to evaluate $\gamma_{ij}^{\mathrm{UV}(2)}$
	: only two-particle cuts available for the relevant diagrams
$0(\not{y}\not{\lambda})$, etc.	: the selection rules of Section 2.5 forbid the stated coupling dependence
0_y	: $\gamma_{ij}^{\mathrm{UV}(2)}$ vanishes if Yukawa couplings are set to zero

Table 2.9: Predictions for the zeros and coupling dependences of a representative selection of the SMEFT two-loop anomalous-dimension matrix, $\gamma_{ij}^{\mathrm{UV}(2)}$. The notation for the operator labels follows that of [19–21]. The g_2^4 dependence of the entry labeled $0_y(\not{g}_2^{4*})$ vanishes using the appropriate counterterms at one loop. The operators labeling the rows are renormalized by the operators labeling the columns.

Chapter 3

Scattering Amplitudes and Classical Gravitational Observables

3.1 Introduction

The direct detection of gravitational waves at LIGO/VIRGO [26, 27] has started an exciting new age of gravitational wave astronomy. Scattering amplitudes have emerged as the latest tool in computing the gravitational dynamics of binary systems in the perturbative regime. In contrast to the traditional post-Newtonian expansion, which is a simultaneous expansion in the Newton constant, G, and a relative velocity, v, relativistic scattering amplitudes can naturally lead to results up to a fixed order in G but to all orders in velocity, known as the post-Minkowskian (PM) expansion [37–42, 62, 179–192]. A recent highlight is the result of Bern *et al.* [41, 42] for the conservative dynamics of black hole binary systems at $\mathcal{O}(G^3)$, i.e. the third-post-Minkowskian (3PM) order. The result points to many interesting questions, some of which are explored in the present work.

1. The scattering angle for massive particles in Refs. [41, 42] contains a term that diverges in the high-energy limit. Does the aforementioned term in the massive scattering angle appear in the presence of supersymmetry? And, can we learn something by studying

the high-energy limit of both massive and massless scattering?

2. The computation of the scattering angle in Ref. [41, 42] proceeds by first extracting a classical potential using a non-relativistic effective field theory (EFT) [39], then calculating the scattering trajectory by solving the classical equations of motion. However, there is a well-known alternative method: the eikonal approximation [3, 56–59, 61, 106, 120, 192–204], which calculates the classical scattering angle from suitable Fourier transforms of quantum scattering amplitudes. Do the two methods give equivalent results at $\mathcal{O}(G^3)$ for the scattering of massive scalar particles?

3. Refs. [41, 42] resums the velocity dependence of the $\mathcal{O}(G^3)$ result by first calculating the velocity expansion to the 7th-post-Newtonian order, i.e. $\mathcal{O}(G^3v^{10})$ around the static limit, then fitting the series to an ansatz, which is shown to be unique. Can we instead directly obtain exact velocity dependence, as is common in the calculation of relativistic scattering amplitudes?

The answers to the above three questions are all *yes*, as we will show using several calculation of two-loop, i.e. $\mathcal{O}(G^3)$, scattering in General Relativity and supergravity. The last question about exact velocity dependence is especially of current interest due to two reasons. First, a direct calculation without a series expansion to high orders can be computationally more efficient. Second, Ref. [65] raised questions about the velocity resummation of Refs. [41, 42] in the case of Einstein gravity. Since then, the correctness of the latter result has been verified at high orders in the velocity expansion [205, 206], an alternative method for resummation of the velocity series has been used with identical results [207], and the unitarity cut construction of the loop integrand has been checked against direct Feynman diagram computations [208]. Still, a direct relativistic calculation that bypasses velocity resummation will be a valuable additional confirmation of the result, and will provide a way to streamline future calculations at $\mathcal{O}(G^3)$ and beyond.

Ref. [65] also raised doubts about the validity of the massless conservative scattering

angle computed long ago by Amati, Ciafaloni and Veneziano (ACV) [61]. In this chapter we also confirm from first principles that the conservative scattering angle as determined by ACV [61] is indeed correct. Our confirmation follows as a by-product of studying universality of the classical scattering angle in massless theories. Our study of massless scattering relies on having on hand the explicit expressions for massless two-loop four-point amplitudes for $\mathcal{N} \geq 4$ supergravity [209–212] and pure Einstein gravity [106]. The latter result makes use of the latest advances in evaluating multiloop amplitudes based on numerical unitarity followed by analytic reconstructions [213, 214]. Armed with the fully-evaluated amplitudes we then follow the standard [193] and widely used (see e.g. Refs. [198–204, 215]) extractions of the scattering angle, using both impact parameter space and partial-wave analyses.

For the case of $\mathcal{N} = 8$ supergravity a recent paper [202] analyzes the eikonal phase through $\mathcal{O}(G^4)$ using the two- and three-loop amplitudes from Refs. [212, 216]. The same work [202] observes that the $\mathcal{N} = 8$ scattering angle matches the angle found by ACV through $\mathcal{O}(G^3)$ [61], despite having different matter content. Indeed, as we show here, this is not an accident, but part of a general pattern. Our explicit calculations for the $\mathcal{O}(G^3)$ contributions to the classical scattering angle in $\mathcal{N} \geq 4$ and pure gravity give the identical result as the angle found by ACV, demonstrating its universality.

Remarkably, we find that the massless scattering angle through $\mathcal{O}(G^3)$ is independent of the matter content for a variety of theories, implying graviton dominance in the high-energy limit. This dominance is well known at leading eikonal order [56–60]. Ref. [217] revealed early hints of such dominance via analysis of gravitino contributions at the next nonvanishing order.

The study of classical gravitational scattering for massive particles in $\mathcal{N} = 8$ supergravity was initiated in a beautiful paper by Caron-Huot and Zahraee [119], which we build upon. The large set of symmetries of this theory provides important simplifications, which make it the perfect theoretical laboratory to study various conceptual questions and test the technology to be applied at higher orders in perturbation theory. This is familiar to how

precision QCD practitioners have often sharpened their axes with simpler calculations in $\mathcal{N} = 4$ super-Yang–Mills theory before honing in on the beast. A lot is known about $\mathcal{N} = 8$ supergravity, in particular the complete loop integrands for the quantum four-point amplitude are available through five loops [10, 13, 111, 209, 218–222]. These were constructed using the unitarity method [43–46, 223] and the different incarnations of the double copy [48, 50, 51, 224]. These results, being valid in D-dimensions, can be used to easily obtain massive integrands via Kaluza-Klein reduction, as we will do in this work.[1]

Moving on to integration, we will obtain the part of the amplitude relevant for classical conservative dynamics using the method of regions [225]. In particular, integration in the "soft region" produces the correct small momentum transfer expansion of the amplitude [35, 192], up to contact terms that are irrelevant for long-range classical physics at any order in G. However, conservative classical dynamics actually arises from the "potential region" which is a sub-region contained in the soft region [39]. Strictly speaking, the potential region is defined in the near-static limit and produces an expansion of the Feynman integrals as a series in small velocity. But since the velocity series can be resummed to all orders, the resummed result will be also referred to as the amplitude evaluated in the potential region. In addition to isolating conservative effects, evaluating in the potential region also simplifies the integrals considerably.

Refs. [41, 42] exploits the fact that infrared (IR) divergences cancel when matching the EFT against full theory, and circumvents the evaluation of IR divergent integrals. In this work, all IR divergent integrals will be evaluated explicitly in dimensional regularization (which serves as both UV and IR regulators). This will allows us to check against the predictions from eikonal exponentiation, which expresses the divergent amplitude in an exponentiated form. Additionally, we will evaluate all integrals relativistically with full dependence on velocity, without constructing and resumming a velocity series. This is made possible by employing the method of differential equations for Feynman integrals [226–229],

[1] See also [191] for a recent application of KK reduction in the context of the eikonal approximation.

with a crucial new ingredient being the use of modified boundary conditions that isolate the contributions from the potential region. While Ref. [42] already presented a precursor of our differential equations method as an alternative to the "expansion-resummation method", it was only successfully applied to a subset of the needed integrals that do not involve infrared divergences due to "iteration" of graviton exchanges. This work will use a finer control of boundary conditions to evaluate all integrals using differential equations. We also perform soft expansions prior to the construction of differential equations, resulting in dramatic speedups in computation. Another improvement is that we transform the differential equations into Henn's canonical form [230, 231]. In this form, the differential equations have a simple analytic structure, and can be easily solved to higher orders in the ϵ expansion. (See also [232] for advances in automated solution of generic univariate differential equations that are solvable by iterated integrals.)

In the context of $\mathcal{N} = 8$ supergravity, Ref. [119] put forward a tantalizing conjecture: that the energy levels of a pair of black holes in such theory retain hydrogen-like degeneracies to all orders in perturbation theory. This is tantamount to the classical black hole binary orbits being integrable and showing no precession. Two pieces of evidence were provided in support of this conjecture: first, the absence of precession for the full $\mathcal{O}(G^2)$ dynamics, which directly follows from an analog of the "no-triangle" hypothesis [233–238] for massive scattering; and second, various all-orders-in-G calculations in the probe limit for different charge configurations. It is known that $\mathcal{O}(G^3)$ (or any odd power of G) corrections to the conservative dynamics cannot yield precession [239, 240]. Instead we will use the scattering angle at $\mathcal{O}(G^3)$ to test this conjecture, and see that it deviates from the integrable Newtonian result at this order. We will extract the scattering angle both from appropriate derivatives of the "eikonal phase" and via the EFT techniques of Refs. [41, 42], finding agreement between both methods.

Although we perform our calculations in $\mathcal{N} = 8$ supergravity, we expect the techniques here developed to be directly applicable to Einstein gravity as well. Such application is

beyond the scope of the present work and we leave it for the future.

The rest of this chapter is organized as follows: In section 3.2 we discuss the computation of the classical massless deflection angle using scattering amplitudes in a variety of theories and the implications of our result to universality and graviton dominance. In section 3.3 we discuss the computation of the massive deflection angle using the scattering of extremal black in $\mathcal{N} = 8$ supergravity as a toy model. We present new methods to calculate the classical limit of the scattering amplitude with full velocity dependence using the modern method of differential equations, and compare the results from the eikonal calculation to the effective field theory methods used by Bern *et al.* In section 3.4 we present our conclusions. We include two appendices: Appendix 3.A contains some technical details about the computation of integrals in the near-static limit and Appendix 3.B collects the solution to our two-loop differential equations. The results are provided in computer-readable format in several ancillary files to the ArXiv submission of this work (see comments at the beginning of each file for detailed descriptions).

3.2 Universality in the classical limit of massless gravitational scattering

In this section we study the scattering of massless particles at $\mathcal{O}(G^3)$ in General Relativity and $\mathcal{N} \geq 4$ supergravity, and calculate the classical deflection angle using eikonal methods. In subsection 3.2.1 we discuss the classical limit of the quantum scattering amplitude. In subsection 3.2.2 we discuss how to compute the classical deflection angle via eikonal methods in impact parameter space. In subsection 3.2.3 we use partial wave methods to extract the deflection angle from the scattering phase shifts.

3.2.1 The classical limit of the amplitude

We are interested in extracting the contributions to the conservative classical scattering angle from the two-loop four-point scattering amplitudes of Refs. [106, 209–212]. Four-point scattering amplitudes depend on the kinematic invariants s and $t = -q^2$, which in the center of mass frame correspond to the squared total energy and squared four-momentum transfer, respectively. We consider the amplitude in the physical region $s > 0$, $t < 0$, $u = -s - t < 0$ (using a mostly-minus sign convention for the metric), commonly known as the s-channel. The contributions in the amplitude relevant for the classical angle corresponds to the large angular momentum limit, which for massless particles is $J \sim \sqrt{s}\, b \gg 1$, where b denotes the usual impact parameter. In the absence of any other kinematic scales such as masses in the momentum-space scattering amplitude, the classical limit is equivalent to the Regge or high-energy small-angle limit, $s/q^2 \gg 1$. It is straightforward to argue that the singularity structure of massless scattering amplitudes implies that only even loop orders can give rise to classical contributions (see e.g. Refs. [61, 202] for a detailed argument). At one loop, in particular, this is directly tied to the fact that no term behaves as $1/q$ which would be required to contribute to the classical deflection angle.

Following Ref. [61], we consider external graviton states. For simplicity we focus on the configuration where the incoming and outgoing gravitons in the s-channel have identical helicity; the situation where the incoming and outgoing gravitons have opposite helicity gives the same final classical scattering angle. We extract the classical scattering angle from the

Regge limit of the renormalized scattering amplitudes, which take the following form,

$$\mathcal{M}^{(0)}(s,q^2) = \quad = \mathcal{K} 8\pi G s \left[\frac{s}{q^2}+1\right],$$

$$\mathcal{M}^{(1)}(s,q^2) = \quad = 4\mathcal{K}\, G^2 s^2 r_\Gamma \left(\frac{\bar{\mu}^2}{q^2}\right)^\epsilon \left[-\frac{2\pi i}{\epsilon}\frac{s}{q^2}+\frac{1}{\epsilon}(2L+2-2\pi i)+F^{(1)}\right], \tag{3.1}$$

$$\mathcal{M}^{(2)}(s,q^2) = \quad = 2\mathcal{K}\, G^3 s^3 \frac{r_\Gamma^2}{\pi}\left(\frac{\bar{\mu}^2}{q^2}\right)^{2\epsilon} \left[-\frac{2\pi^2}{\epsilon^2}\frac{s}{q^2}-\frac{2\pi i}{\epsilon^2}(2L+2-i\pi)-\frac{2\pi i}{\epsilon}F^{(1)}+F^{(2)}\right],$$

where we dropped subdominant terms of $\mathcal{O}(q^2/s)$ in the loop amplitudes, and where $\mathcal{K}$ is a local factor depending on the external states, $\bar{\mu}^2 \equiv 4\pi e^{-\gamma_E}\mu^2$ is a rescaled renormalization scale and $r_\Gamma \equiv e^{\epsilon\gamma_E}\Gamma(1+\epsilon)\Gamma(1-\epsilon)^2/\Gamma(1-2\epsilon)$. For convenience we introduced $L = \log(s/q^2)$, and the finite remainders $F^{(i)}$, which depend on the theory and are implicitly defined in Eq. (3.1). This result is given in the conventional dimensional regularization scheme, where all internal states and momenta are analytically continued into $D = 4-2\epsilon$ dimensions. For the purposes of this work we only need $F^{(1)}$ to $\mathcal{O}(\epsilon)$ and $F^{(2)}$ to $\mathcal{O}(\epsilon^0)$. The two-loop infrared singular part is related to the square of the one-loop amplitude via $[\mathcal{M}^{(1)}]^2/2\mathcal{M}^{(0)}$ which follows from the fact that to all loop orders the infrared singularity is given by an exponential of the ratio of the one-loop and tree amplitudes [210, 211, 241, 242].

The pure gravity one-loop amplitudes were originally computed in Ref. [243]. These were recomputed in an intermediate step [244] of the two-loop analysis of Ref. [104, 105]. This is matched by the expressions in Ref. [106] that include the $\mathcal{O}(\epsilon)$ contributions. The latter contributions are needed when extracting the two-loop finite remainders in the presence of

infrared singularities, with the result,

$$
\begin{aligned}
F^{(1)}_{\rm GR} = {} & 2L^2 + 2i\pi L + 4\pi^2 - \frac{87}{10}L + \frac{841}{90} \\
& + \epsilon\bigg[-\frac{2}{3}L^3 - \pi^2 L + 6\zeta_3 + \frac{47}{20}L^2 - 3\pi^2 - \frac{6913}{225}L \\
& + \frac{35597}{1200} + i\pi\Big(-L^2 + \frac{\pi^2}{3} + 10L + \frac{1957}{360}\Big)\bigg] ,
\end{aligned}
\tag{3.2}
$$

where $F^{(1)}_{\rm GR}$ is the pure gravity result for $F^{(1)}$ in Eq. (3.1). The $\mathcal{N} \geq 4$ supergravity amplitudes can be found in Ref. [212, 243, 245] in a scheme that preserves supersymmetry. For these cases, the Regge limit of the $\mathcal{O}(\epsilon^0)$ contributions to the finite remainders can be read off from Eq. (4.6) of Ref. [199].

Ref. [106] provides the complete Einstein-gravity amplitude needed for our analysis, including subdivergence subtractions [104, 105, 246]. We note that these results pass highly nontrivial checks. The amplitude yields the expected IR pole structure [241, 242] and the net ultraviolet poles cancel against the known counterterms [104, 105, 247, 248]. Furthermore the amplitude only has the poles in the Mandelstam variables s, t and u dictated by factorization. The amplitudes have also been validated against results in the literature and independent computations. While not directly relevant for the classical scattering angle, the results of Ref. [106] also match the previously computed [244] identical-helicity amplitude (in an all outgoing momentum convention), corresponding to the case that both incoming gravitons flip helicity.

Starting from the full four-graviton two-loop amplitude in pure Einstein gravity [106], we extract the finite remainder in the Regge limit giving the result,

$$
\begin{aligned}
F^{(2)}_{\rm GR} = {} & -2\pi^2 L^2 + 4\pi^2 L - \frac{\pi^4}{90} + \frac{13403\pi^2}{675} - \frac{13049}{2160} \\
& + i\pi\bigg[\frac{4}{3}L^3 - \frac{47}{10}L^2 + \frac{26159}{450}L - 20\zeta_3 + \frac{2621\pi^2}{210} - \frac{11221}{375}\bigg] .
\end{aligned}
\tag{3.3}
$$

The constant parts are scheme dependent and in any case they do not affect the scattering angle. A detailed discussion of scheme dependence and its effects on the final angle, in the context of IR regulators in $\mathcal{N} = 8$ supergravity is found in Section 6 of Ref. [202].

The two-loop amplitudes for $\mathcal{N} \geq 4$ supergravity are given in Ref. [212]. The $\mathcal{N} = 8$ supergravity result is the simplest of these and was first given in Ref. [210, 211] by combining the integrand of Ref. [209] with the integrals of Ref. [249, 250]. Explicit results for the finite remainders in the Regge limit are found in Eqs. (4.13)–(4.16) of Ref. [199]. Note that the remainders in Ref. [199] are normalized with an extra factor of $q^2 s$ relative to ours.

So far we have presented the classical scattering amplitudes in perturbation theory, which assumes $Gs \ll 1$. Ultimately, we are interested in the limit $Gs \gg 1$, with $Gs/J \ll 1$ corresponding to the classical post-Minkowskian expansion used in classical general relativity [182–185, 187, 188]. Implicitly this assumes that the relevant parts of the perturbative series have been resummed. Standard ways to do so use eikonal or partial wave methods which we utilize in the following.

3.2.2 Scattering angle from eikonal phase

The basic observation that allows eikonal resummation is that, in the classical limit, certain classes of multiloop Feynman diagrams at all orders in perturbation theory are given by momentum space convolutions of lower order diagrams. A Fourier transform to impact parameter space can be used to diagonalize the convolutions, and the result is such the amplitude exponentiates. For the moment let us just direct the reader to the many reviews and references [61, 193, 198, 200–203], where this is described in detail, and delay a detailed discussion of this procedure to the next section. Following such procedure, we obtain the eikonal phase by taking the transverse Fourier transform of the amplitude in the classical limit,

$$-i\left(e^{i2\delta(s,b_{\rm e})}-1\right)=\int\frac{\mu^{2\epsilon}{\rm d}^{2-2\epsilon}q}{(2\pi)^{2-2\epsilon}}\,e^{i\vec{q}\cdot\vec{b_{\rm e}}}\,\frac{\mathcal{M}(s,q^2)}{2s\mathcal{K}}\,, \tag{3.4}$$

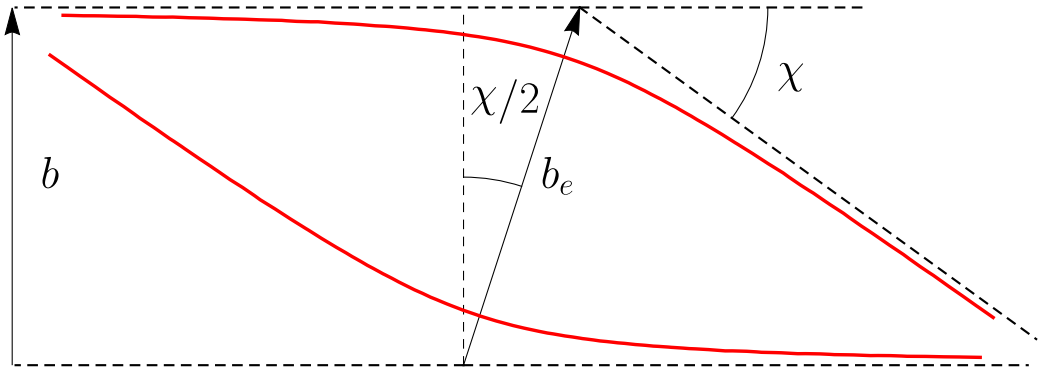

Figure 3.1: The scattering configuration showing the impact parameter, b, eikonal impact parameter, $b_{\rm e}$, and the scattering angle, χ.

where $\delta(s, b_{\rm e})$ is the eikonal phase, which we expand perturbatively in Newton's constant ($\delta = \delta^{(0)} + \delta^{(1)} + \delta^{(2)} + \cdots$), $\vec{q}$ is the $(2-2\epsilon)$-dimensional vector in the scattering plane such that $\vec{q}^{\,2} = q^2$ and $b_{\rm e} \equiv |\vec{b_{\rm e}}|$ is the eikonal impact parameter shown in Fig. 3.1. The basic formula needed for calculating the Fourier transform is given in Eq. (2.11) of Ref. [204].

The full phase shift is generically complex, and be readily obtained from Eqs. (3.1), (3.2) and (3.3). Its imaginary part at a given order captures inelastic (e.g., radiation) effects. Here we are only interested in the conservative part, as in Ref. [61] so we do not display it in the following and focus only on the elastic phase. However, these imaginary parts are needed to extract the elastic contributions at higher orders because of the exponentiation. The Fourier transform of polynomial terms corresponds to short-range contact interactions, which are not relevant for the problem of long-range scattering.

The universal $\mathcal{O}(G)$ result for the eikonal phase extracted from the tree amplitude is

$$\delta^{(0)} = \frac{Gs}{2}\left(\bar{\mu}^2 \tilde{b_{\rm e}}^{\,2}\right)^{\epsilon}\left[-\frac{1}{\epsilon} - \epsilon\frac{\pi^2}{12} - \frac{1}{3}\epsilon^2\zeta_3 + \mathcal{O}(\epsilon^3)\right], \tag{3.5}$$

where we introduced $\tilde{b_{\rm e}} = e^{\gamma_E} b_{\rm e}/2$ for convenience.

As explained above, the pieces relevant for the one-loop scattering angle are given by the

real part of the nonanalytic part,

$$\operatorname{Re} F^{(1)} = -\frac{\mathcal{N}-4}{2} L^2 + cL + \cdots , \tag{3.6}$$

where $\mathcal{N}$ denotes the amount of supersymmetry and c is a constant that takes on the values $0, -1, -87/10$ for $\mathcal{N} > 4$, $\mathcal{N} = 4$ and pure gravity respectively. The leading logarithms (L^2) arise from backward-scattering diagrams [199] and the subleading logarithm (L) from bubble integrals. We conclude that they are nonuniversal and depend on the specific theory. As mentioned above, the $\mathcal{O}(G^2)$ one-loop phase can contribute to the angle only at the quantum level, so this nonuniversality does not affect the classical scattering angle. These contributions, including the $\mathcal{O}(\epsilon)$ parts, are however crucial for extracting the $\mathcal{O}(G^3)$ classical pieces because of cross terms with infrared singularities.

The $\mathcal{O}(G^2)$ phase extracted from the one-loop amplitude is

$$\operatorname{Re} \delta^{(1)} = \frac{2G^2 s}{\pi b_{\rm e}^2} \left(\bar{\mu}^2 \tilde{b_{\rm e}}^2\right)^{2\epsilon} \left[\frac{1}{\epsilon} - \frac{(\mathcal{N}-6)}{2} \log(s\tilde{b_{\rm e}}^2) + \frac{c+2}{2} + \mathcal{O}(\epsilon)\right], \tag{3.7}$$

where c is the same theory-dependent constant appearing in Eq. (3.6). Additionally, there is an imaginary part at $\mathcal{O}(\epsilon)$, needed to obtain the real part of $\delta^{(2)}$, which is not displayed here but is readily obtained from the Fourier transform of the full amplitudes in Eqs. (3.1) and (3.2) as well from Refs. [104, 105, 243, 244].

The relevant terms at two loops arise from the nonanalytic terms in the imaginary part of the remainder at one loop and from the real part at two loops

$$\begin{aligned} \operatorname{Im} F^{(1)} &= 2\pi L - \epsilon \pi L^2 + \cdots , \\ \operatorname{Re} F^{(2)} &= -2\pi^2 L^2 + 4\pi^2 L + \cdots . \end{aligned} \tag{3.8}$$

where the dots indicate non-universal terms which do not contribute to the phase at $\mathcal{O}(\epsilon^0)$. This includes non-universal ϵL terms in $\operatorname{Im} F^{(1)}$ that could naively contribute but ultimately

cancels against the iteration $-2i\delta^{(0)}\delta^{(1)}$ coming from expanding the exponential.

The $\mathcal{O}(G^3)$ terms in the phase can thus be extracted from the two-loop amplitude after subtracting the iteration from the leading and subleading phases in the exponential (3.4). The leading eikonal exponentiation also predicts a universal $\mathcal{O}(\epsilon)$ contribution to the two-loop amplitude which needs to be taken into account. (See the discussion in Ref. [202] near Eq. (3.7)). We obtain the universal result,

$$\mathrm{Re}\,\delta^{(2)} = \frac{2G^3s^2}{b_{\rm e}^2}\left(\bar{\mu}^2\tilde{b}_{\rm e}^2\right)^{3\epsilon} + \mathcal{O}(\epsilon)\,, \tag{3.9}$$

valid for $\mathcal{N} \geq 4$ supergravity as well as pure Einstein gravity. We are not displaying the imaginary parts since they are not universal and do not contribute to the conservative dynamics at this order.

The classical scattering angle is given in terms of the eikonal phase via the usual stationary-phase argument (see e.g. [56–60]),

$$\sin\frac{1}{2}\chi(s,b_{\rm e}) = -\frac{2}{\sqrt{s}}\frac{\partial}{\partial b_{\rm e}}\,\delta(s,b_{\rm e})\,. \tag{3.10}$$

Applying this formula to Eq. (3.9), which holds for all theories evaluated here, we obtain the universal result

$$\sin\frac{1}{2}\chi(s,b_{\rm e}) = \frac{2G\sqrt{s}}{b_{\rm e}} + \frac{(2G\sqrt{s})^3}{b_{\rm e}^3}\,, \tag{3.11}$$

matching the ACV pure gravity angle given in Eq. (5.28) in Ref. [61], as well as the recently obtained angle in $\mathcal{N} = 8$ supergravity [202]. The scheme dependence cancels, as expected. The result above is written in terms of the symmetric impact parameter, $\vec{b_{\rm e}}$ which appears naturally in the eikonal formula. This points in the direction of the momentum transfer $\vec{q}$, while the more familiar impact parameter $\vec{b}$ is perpendicular to the incoming momenta, as shown in Fig. 3.1. (See also Ref. [215].) The relation between their magnitudes is $b = b_{\rm e}\cos(\chi/2)$. Rewriting the universal scattering angle in terms of the usual impact parameter

b gives,

$$\sin\frac{1}{2}\chi(s,b) = \frac{2G\sqrt{s}}{b} + \frac{1}{2}\frac{(2G\sqrt{s})^3}{b^3}\,. \tag{3.12}$$

We note that the quantum corrections to the scattering angle do not display a corresponding universality, analogous to previously observed nonuniversal spin dependence in quantum corrections [251–254].

3.2.3 Scattering angle from partial-wave expansion

Alternatively, we can extract the scattering angle from the partial-wave expansion of the amplitude (see e.g. Ref. [65])

$$\mathcal{M} = \frac{2^d \pi^{\frac{d-2}{2}}}{s^{\frac{d-4}{2}}\,\Gamma\left(\frac{d-2}{2}\right)} \sum_\ell (\ell+1)_{d-4}(2\ell+d-3)\, a_\ell(s)\, \tilde{C}_\ell(x) \tag{3.13}$$

where $x = \cos\chi = 1 + 2t/s$ and the $C_\ell^{\frac{1-2\epsilon}{2}}(x)$ are Gegenbauer polynomials (normalized to take unit value at $x = 1$), which reduce to the more familiar Legendre polynomials when $\epsilon \to 0$. Using the orthogonality properties of the Gegenbauer polynomials

$$\int_{-1}^{1} (1-x^2)^{\frac{d-4}{2}}\, \tilde{C}_\ell(x)\, \tilde{C}_{\ell'}(x) = \delta_{\ell\ell'} \frac{2^{d-3}\Gamma\left(\frac{d-2}{2}\right)^2}{(\ell+1)_{d-4}(2\ell+d-3)} \tag{3.14}$$

the partial waves are given by

$$a_\ell(s) = \frac{(16\pi\mu^2/s)^\epsilon}{\Gamma(1-\epsilon)} \int_{-1}^{1} \mathrm{d}x\, (1-x^2)^{-\epsilon}\, C_\ell^{\frac{1-2\epsilon}{2}}(x)\, \frac{\mathcal{M}(s,x)}{16\pi\,\mathcal{K}}\,. \tag{3.15}$$

If we ignore inelastic contributions, unitarity dictates that the partial waves satisfy the relation $\mathrm{Im}(a_\ell) = |a_\ell|^2$, so they can be parametrized in terms of phase shifts as

$$a_\ell(s) = -i\left(e^{i2\delta_\ell(s)} - 1\right)\,, \tag{3.16}$$

Once again a stationary-phase argument [193] gives the scattering angle as

$$\frac{1}{2}\chi(s,\ell) = -\frac{\partial\delta_\ell(s)}{\partial\ell}\,. \tag{3.17}$$

Using this approach we find the phase shifts,

$$\begin{aligned}
\delta_\ell^{(0)}(s) &= \frac{Gs}{2}\left(\frac{\bar{\mu}^2\tilde{J}^2}{s}\right)^{\epsilon}\left[-\frac{1}{\epsilon} - \frac{1}{3J^2} + \mathcal{O}(\epsilon, J^{-4})\right]\,,\\
\mathrm{Re}\,\delta_\ell^{(1)}(s) &= \frac{G^2s^2}{2\pi J^2}\left(\frac{\bar{\mu}^2\tilde{J}^2}{s}\right)^{2\epsilon}\left[\frac{1}{\epsilon} - \frac{(\mathcal{N}-6)}{2}\log(\tilde{J}^2) + \frac{c+2}{2} + \mathcal{O}(\epsilon, J^{-2})\right]\,,\\
\mathrm{Re}\,\delta_\ell^{(2)}(s) &= \frac{G^3s^3}{3J^2}\left(\frac{\bar{\mu}^2\tilde{J}^2}{s}\right)^{3\epsilon} + \mathcal{O}(\epsilon, J^{-4})\,,
\end{aligned} \tag{3.18}$$

where $\tilde{J}^2 = e^{2\gamma_E}J^2$ and J^2 denotes the Casimir of the rotation group, i.e., $J^2 :\equiv \ell(\ell+1-2\epsilon)$, which has a well defined classical limit. The classical deflection angle is then

$$\frac{1}{2}\chi(s,J) = \frac{Gs}{J} + \frac{2}{3}\frac{G^3s^3}{J^3}\,, \tag{3.19}$$

written in terms of the classical variables, or, equivalently,

$$\sin\frac{1}{2}\chi(s,J) = \frac{Gs}{J} + \frac{1}{2}\frac{G^3s^3}{J^3}\,. \tag{3.20}$$

Using the relation between the angular momentum and the impact parameters

$$J = \frac{\sqrt{s}}{2}b = \frac{\sqrt{s}}{2}b_{\mathrm{e}}\cos\frac{1}{2}\chi\,, \tag{3.21}$$

we find that Eq. (3.20) reproduces Eqs. (3.11) and (3.12).

We can directly compare our results to Damour's conjectured angle given in Eq. (5.37) of Ref. [65],

$$\sin\frac{1}{2}\chi^{\mathrm{D}}(s,J) = \frac{Gs}{J} - \frac{3}{4}\frac{G^3s^3}{J^3}\,. \tag{3.22}$$

As noted in Ref. [65], this disagrees with the angle obtained by ACV, which is matched by Eq. (3.20). As emphasized by Damour [65], because the sign of the G^3 term in Eq. (3.22) is opposite to that of Eq. (3.20) the disagreement between the two formulas is robust.

Here we focused on the scattering of identical-helicity gravitons in the initial state. We have repeated the calculation for the case of opposite-helicity gravitons with the same results for the classical scattering angle. Furthermore, we expect the result to be identical for any massless external states. Indeed, for the supersymmetric cases that we analyzed, supersymmetry identities [255, 256] relate graviton scattering to scattering of other massless states.

3.3 Extremal black hole scattering at $\mathcal{O}(G^3)$: graviton dominance, eikonal exponentiation, and differential equations

In this section we move on to study massive scattering of extremal black holes in $\mathcal{N} = 8$ supergravity. In subsection 3.3.1 we setup our conventions, we review some basic features of extremal black holes in $\mathcal{N} = 8$ supergravity, and discuss the different limits that will be used in this work. In subsection 3.3.2 we construct the tree-level four-point amplitude, as well as the one- and two-loop massive integrands from the known massless integrands via Kaluza-Klein reduction and truncation to the appropriate sector. In subsection 3.3.3 we briefly discuss the integration regions involved in our problem, and introduce our new integration method based on differential equations, which is applied to calculate the full one- and two-loop amplitudes in the potential region. In subsection 3.3.4 we assemble the scattering amplitudes. In subsection 3.3.5 we review the eikonal method, and use it to calculate the order $G^{n\leq 3}$ eikonal phase, while checking exponentiation. Then we use the eikonal phase to calculate the gravitational scattering angle and we compare its high-energy

limit with the result of Refs. [41, 42] in Einstein gravity. In subsection 3.3.6 we cross check our results via the EFT method of Ref. [39], and we comment on the advantages of this approach. We calculate the conservative Hamiltonian by matching, and find the scattering angle by solving the classical equations of motion.

3.3.1 Kinematics and setup

We model the dynamics of two half-BPS black holes in $\mathcal{N} = 8$ supergravity [257, 258] by considering the scattering of two massive point particles in half-BPS multiplets, which interact via the massless supergravity multiplet. We use an all-outgoing convention for the momenta, and the masses of the particles are

$$p_1^2 = p_4^2 = m_1^2\,, \qquad p_2^2 = p_3^2 = m_2^2\,. \tag{3.23}$$

We will parametrize the scattering amplitudes in terms of the usual invariants $s = (p_1+p_2)^2$, $t = (p_1 + p_4)^2 = q^2$ and $u = (p_1 + p_3)^2$, where we introduced the four-momentum transfer $q = p_1 + p_4$ for later convenience. As is common in the study of scattering amplitudes we will cross the incoming particles to the final state, so that all particles are outgoing. The physical scattering configuration corresponds to the region $s > (m_1 + m_2)^2, t = q^2 < 0$ and $u < 0$.[2]

The half-BPS multiplet in $\mathcal{N} = 8$ supergravity contains massive states with spin $0 \leq S \leq 2$. In this work we will focus on particular scalar components, ϕ and $\bar{\phi}$, with $S = 0$ and leave the study of spinning states for later work. The interactions between different half-BPS particles are mediated by the massless supergraviton multiplet. In addition to gravitons the $\mathcal{N} = 8$ supergraviton multiplet contains 28 (vector) graviphotons, A_{IJ}, and 70 scalars ϕ_{IJKL}, as well as fermions which will not be important for our discussion. Black holes in $\mathcal{N} = 8$ supergravity interact with the graviphotons and scalars with charges C_{IJ} given by

[2]We use a mostly minus metric.

an 8×8 matrix. Here $I, J, \ldots$ are SU(8) R-symmetry indices and the vectors a scalars are in SU(8) representations of the appropriate dimension. We will not print the Lagrangian here, because it is lengthy. For our purposes, however, all scattering amplitudes could be built from the three-particle amplitudes:

$$M_3^{\text{tree}}(1_\phi, 2_{\bar{\phi}}, 3_h) = 16\pi G \left(\varepsilon_3 \cdot p_1\right)^2 , \tag{3.24}$$

$$M_3^{\text{tree}}(1_\phi, 2_{\bar{\phi}}, 3_{A_{IJ}}) = 8\pi G \sqrt{2} \left(\varepsilon_3 \cdot p_1\right) C_{IJ} , \tag{3.25}$$

$$M_3^{\text{tree}}(1_\phi, 2_{\bar{\phi}}, 3_{\phi_{IJKL}}) = 16\pi G \left(C_{IJ}\, C_{KL} - C_{IK}\, C_{JL} + C_{IL}\, C_{JK}\right) , \tag{3.26}$$

using factorization and unitarity, as done in Ref. [119]. Here ε are polarization vectors.

In general the charges, C_{IJ} are complex and the black holes are dyonic. The charges are also central charges of the supersymmetry algebra, and the BPS condition requires their magnitude to be equal to the mass

$$C^{IK} C_{KJ} = m^2\, \delta^I{}_J . \tag{3.27}$$

When studying a pair of black holes we need only consider the relative phases in their BPS charges. These are parameterized by three angles along which the charges might be misaligned

$$C_1 = m_1 \begin{pmatrix} 0 & 1_{4\times 4} \\ -1_{4\times 4} & 0 \end{pmatrix} , \qquad C_1 = m_2 \begin{pmatrix} 0 & \Phi \\ -\Phi & 0 \end{pmatrix} , \tag{3.28}$$

with $\Phi = \text{diag}(e^{i\phi_1}, e^{i\phi_2}, e^{i\phi_3}, e^{i\phi_4})$ and $\sum_i \phi_i = 0$. For the two- and one-angle cases, however, there always exist a duality frame where the magnetic charges are zero. We point the reader to Ref. [119] for a more detailed discussion of the charges.

Although we will construct the full (quantum) loop integrands for the scattering amplitudes of these black holes, we are ultimately interested in their classical conservative dynamics. In the classical limit of hyperbolic scattering, the orbital angular momentum of

the black hole binary system is much larger than $\hbar$. Thus, the *classical* limit of the scattering amplitudes simply corresponds to the large angular momentum limit $J \gg 1$ (in natural units), which establishes a hierarchy of scales

$$s, |u|, m_1^2, m_2^2 \sim J^2|t| \gg |t| = |q|^2 \,. \tag{3.29}$$

As a result, we are interested in calculating scattering amplitudes in the limit of small q, or more precisely as an expansion in small q. From a heuristic calculation in the Newtonian limit, the leading-order scattering angle θ is of the order $Gm/(vr) \sim Gmq/v$, where m and r are the total mass and relative transverse distance of the system. So for generic values of v, the quantity Gmq is of order θ, and for each additional order of G, we need to expand the amplitude up to one additional power of q to obtain corrections to the scattering angle of order θ^L, where L is the loop order. Terms that are more subleading in q at the same power of G are quantum corrections that vanish classically. In summary, at $\mathcal{O}(G^n)$, we only need to expand the scattering amplitude of massive particles up to $\mathcal{O}(|q|^{n-2})$ in the small-q expansion [35], in order to extract the classical dynamics. In practice this will imply, among other things, that when we calculate an amplitude some loop integrals can be discarded before any calculation, if they are beyond the classical order.

Furthermore, we will only be interested in the conservative dynamics, so we will restrict the components of the momentum transfer $q = (q^0, \boldsymbol{q})$ to scale as

$$|\boldsymbol{q}| \gg q^0 \,, \tag{3.30}$$

so that the graviton multiplet mediates instantaneous long-range interactions. Note that the latter expansion involves an additional small parameter, a velocity $|\boldsymbol{v}| = q^0/|\boldsymbol{q}| \ll 1$, on top of the classical limit $J \gg 1$. We will refer to this expansion as the *near-static* limit, and we delay a more detailed discussion to subsection 3.3.3.

Finally, in comparing our results to Einstein gravity, it will be useful to take the *high-energy* or ultra-relativistic limit in which the black holes are highly boosted. This simply makes the hierarchy of scales in Eq. (3.29) more strict

$$s, |u| \gg m_1^2, m_2^2 \sim J^2|t| \gg |t| \,. \tag{3.31}$$

In this context, it will be useful to introduce the variable

$$\sigma = \cosh\eta = \frac{s - m_1^2 - m_2^2}{2m_1 m_2} = \frac{p_1 \cdot p_2}{m_1 m_2} \,, \tag{3.32}$$

which is simply the relativistic factor of particle 1 in the rest-frame of particle 2 (or vice versa). In terms of this variable the high-energy limit simply corresponds to taking $\sigma \gg 1$. Note that in our setup it is important that we take the classical limit first, before taking the high-energy limit, so that $J \gg \sigma$. This is equivalent to having the hierarchy of scales in Eq. (3.31). The opposite limit, $J \ll \sigma$, is closely connected to the regime of massless high-energy scattering considered in Ref. [3].

In summary, we will be interested in the three limits

$$\text{Generic classical limit:} \qquad J \gg 1 \,, \tag{3.33}$$

$$\text{near-static classical limit:} \qquad J \gg 1, \quad |\boldsymbol{v}| \ll 1 \,, \tag{3.34}$$

$$\text{high-energy classical limit:} \qquad J \gg 1 \quad \text{then} \quad \sigma \gg 1 \,, \tag{3.35}$$

expressed here in terms of their corresponding dimensionless expansion parameters.

3.3.2 Integrands from Kaluza-Klein reduction

In this subsection we construct the tree amplitude and loop integrands for the scattering of the two black holes via Kaluza-Klein (KK) reduction. Ref. [119] studied the case of three-

angle misalignment in the BPS charges. While such case is the most rich and interesting, we will focus on the single-angle misalignment case, which is the one we can access via KK reduction from the existing integrands. Let us explain this in more detail: we consider Type IIA supergravity in $D = 10$ and perform KK reduction on a six-torus of radius R. When dimensionally reducing the massless integrand we will identify the massive black holes with KK gravitons, with ten-dimensional momenta k_i and masses arising from the components of momenta outside of $D = 4$. The supersymmetry algebra in higher dimensions, upon reduction, identifies the extra-dimensional momenta as BPS charges (see e.g. Appendix B of Ref. [119]). There is only one relative angle between the extra dimensional momenta, so the dimensional reduction only provides the result for one-angle misalignment. Because of this, one might perform a rotation to set the momenta along all but two directions to zero and effectively reduce from $D = 6$. Henceforth, for simplicity, we shall then pretend we are reducing from six dimensions. Then we can write the momenta of the four particles as

$$k_1 = \begin{pmatrix} p_1 \\ 0 \\ m_1 \end{pmatrix}, \qquad k_2 = \begin{pmatrix} p_2 \\ m_2 \sin\phi \\ m_2 \cos\phi \end{pmatrix}, \qquad k_3 = \begin{pmatrix} p_3 \\ -m_2 \sin\phi \\ -m_2 \cos\phi \end{pmatrix}, \qquad k_4 = \begin{pmatrix} p_4 \\ 0 \\ -m_1 \end{pmatrix}. \tag{3.36}$$

The compactness of the extra dimensions requires the extra dimensional momenta to be discrete and of order $\sim R^{-1}$. We will choose the masses m_1 and m_2 to correspond to the two lightest KK modes, ϕ_1, ϕ_2. Depending on the momentum in the extra dimensions the massless six-dimensional scalar, ϕ, will reduce to either of these.

We will see momentarily that the massless integrands for maximal supergravity, have two simplifying features which imply that we just need a few basic rules to perform the KK reduction. First, the loop integrands are proportional to the tree amplitude to all orders. This follows from the supersymmetry Ward identity [209], and implies that the polarization dependence is trivial and factors out of the integrand. Second, through two loops, the

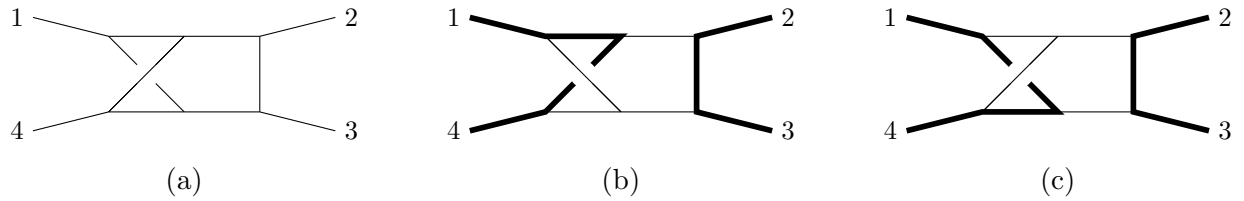

Figure 3.2: Example of KK reduction with massless exchange. The diagram in (a) reduces to the pair of diagrams in (b) and (c). The thin and thick lines denote massless and massive momenta respectively.

integrands are composed only of scalar loop integrals, so we only need to understand how to KK reduce propagators.

Let us first discuss the rules for reducing the massless loop integrand. The integration over loop momentum reduces as

$$\mathrm{d}^6\ell \longrightarrow \frac{1}{(2\pi R)^2} \sum_{\ell^4,\ell^5 \in 2\pi R\mathbb{Z}} \mathrm{d}^4\ell\,, \tag{3.37}$$

where the factors of $(2\pi R)^2$ simply relate the $D = 6$ and $D = 4$ Newton's constant $G = G^{6D}(2\pi R)^{-2}$, and the sum is over all possible ways to assign a KK momentum to each leg in a given diagram, subject to the constraint of momentum conservation in the extra dimensions. Since we are choosing our external legs to be two particular KK modes, this means in practice that we should sum over all the ways the external massive particles could route inside the diagram. We are interested in the diagrams that feature the exchange of massless particle in the graviton multiplet, so we will truncate the full massive integrand to this sector. We delay a discussion about the consistency of this truncation to the end of this subsection. The truncation to massless exchange, together with momentum conservation imposes an additional rule when routing the external particles through the diagram, namely that lines corresponding to different KK modes cannot cross at a three-point vertex.

As an example, consider the massless non-planar double-box integral in Fig. 3.2(a). It is easy to see that there are two alternative ways to route the mass/extra-dimensional momenta through the diagram, shown in Fig. 3.2(b) and (c). So this massless integral will yield two

contributions to the massive integrand. In contrast, there are also examples in which there there is no way to route the masses. We will find several of these when constructing the two loop integrand.

Finally, using the identifications in Eq. (3.36) we find that the reduction of the external invariants is given by the following simple replacement rules

$$s \to s - |m_1 + m_2 e^{i\phi}|^2 \,, \qquad t \to t \,, \qquad u \to u - |m_1 - m_2 e^{i\phi}|^2 \,, \tag{3.38}$$

and similarly for loop momenta

$$(\ell + k_i)^2 \to (\ell + p_i)^2 - m_i^2 \,, \tag{3.39}$$

which follows from the orthogonality of the four-dimensional loop momentum and the extra-dimensional components of the external momentum.

Tree level amplitude

As a warmup let's start with the tree level amplitude. We will write it as

$$M_4^{\text{tree}}(1,2,3,4) = 8\pi G^{6D} \frac{\mathcal{K}}{stu} \,, \tag{3.40}$$

where $\mathcal{K}$ is the four point matrix element of the supersymmetric $t_8 t_8 R^4$ operator (see e.g. Ref. [259], Eq. (9.A.18)). In four dimensions $\mathcal{K} = [3\,4]^4 \,/\, \langle 1\,2\rangle^4 \;\; \delta^{(16)}(Q)$, where Q is the on-shell super-momentum [260]. For simplicity we choose the incoming and outgoing states to be complex conjugate scalars ϕ and $\bar{\phi}$ in the graviton multiplet. The corresponding component of $\mathcal{K}$ is simply s^4 and the D-dimensional scalar amplitude is

$$M_4^{\text{tree}}(1_\phi, 2_\phi, 3_{\bar{\phi}}, 4_{\bar{\phi}}) = 8\pi G^{6D} \, \frac{s^3}{tu} \,. \tag{3.41}$$

(a) Box: $I_{\rm II}$ (b) Non-planar box: $I_{\rm X}$

Figure 3.3: One-loop topologies.

Using our rules for dimensional reduction we find the result

$$M_4^{\rm tree}(1_{\phi_1}, 2_{\phi_2}, 3_{\bar{\phi}_2}, 4_{\bar{\phi}_1}) = 8\pi G \frac{(s - |m_1 + m_2 e^{i\phi}|^2)^3}{t(u - |m_1 - m_2 e^{i\phi}|^2)}\,. \tag{3.42}$$

Although this is the full amplitude we want to restrict to the massless exchange sector. We can partial fraction (3.42) as

$$M_4^{\rm tree}(1_{\phi_1}, 2_{\phi_2}, 3_{\bar{\phi}_2}, 4_{\bar{\phi}_1}) = 8\pi G \frac{(s - |m_1 + m_2 e^{i\phi}|^2)^2}{-t} + \text{massive exchange}\,, \tag{3.43}$$

which using $s - |m_1 + m_2 e^{i\phi}|^2 = 2m_1 m_2(\cosh\eta - \cos\phi)$, where η is the relative rapidity, $\eta = \text{arcosh}(\sigma)$, agrees with Eq. (3.18) of Ref. [119], restricted to the one-angle case.

One-loop integrand

The one-loop massless integrand was constructed long ago in Refs. [209, 218]

$$M_4^{\text{1-loop}}(1,2,3,4) = -i8\pi G^{6D} stu M_4^{\rm tree}(1,2,3,4)\left(\, I^{(1)}_{1234} + I^{(1)}_{1342} + I^{(1)}_{1423}\,\right), \tag{3.44}$$

where all the integrals are one-loop boxes with the specified ordering of the external legs. Using the reduction rules described above

$$stu M_4^{\rm tree}(1_\phi, 2_\phi, 3_{\bar{\phi}}, 4_{\bar{\phi}}) \to 8\pi G(s - |m_1 + m_2 e^{i\phi}|^2)^4\,, \tag{3.45}$$

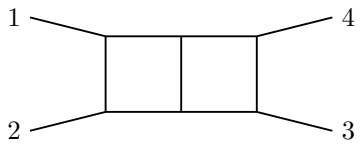

(a) Double box: $I^{(2)\,\mathrm{P}}_{1234}$

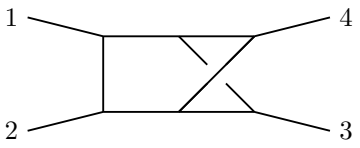

(b) Non-planar double-box: $I^{(2)\,\mathrm{NP}}_{1234}$

Figure 3.4: Massless two-loop topologies.

and KK reduction maps the massless integrals to massive integrals as follows

$$I^{(1)}_{1234} \to I_{\mathrm{II}}\,, \qquad I^{(1)}_{1342} \to 0\,, \qquad I^{(1)}_{1423} \to I_{\mathrm{X}}\,, \tag{3.46}$$

where the integrals are shown in Fig. 3.3, and 0 indicates that there is no way to route the momenta so the reduction yields zero. Putting all together we find the one-loop integrand

$$M_4^{\text{1-loop}}(1_{\phi_1}, 2_{\phi_2}, 3_{\bar{\phi}_2}, 4_{\bar{\phi}_1}) = -i(8\pi G)^2\,(s - |m_1 + m_2 e^{i\phi}|^2)^4\,\big(\,I_{\mathrm{II}} + I_{\mathrm{X}}\,\big)\,, \tag{3.47}$$

where we have truncated to the massless exchange sector. This matches the result in Eqs. (3.33) and (3.34) of Ref. [119].

Two-loop integrand

The massless two loop integrand was constructed in Ref. [209] using the unitarity method. It takes the remarkably simple form

$$\begin{aligned} M_4^{\text{2-loop}}(1,2,3,4) &= -(8\pi G^{6D})^2 stu M_4^{\text{tree}}(1,2,3,4) \\ &\quad \times \big(s^2\, I^{(2)\,\mathrm{P}}_{1234} + s^2\, I^{(2)\,\mathrm{P}}_{3421} + s^2\, I^{(2)\,\mathrm{NP}}_{1234} + s^2\, I^{(2)\,\mathrm{NP}}_{3421} + \text{cyclic}\big)\,, \end{aligned} \tag{3.48}$$

where " + cyclic" means adding the two other cyclic permutations of $(2,3,4)$ and the integrals, which are all scalar, are shown in Fig. 3.4. It is easy to find how the integrals map

under the dimensional reduction. The planar integrals reduce as follows

$$
\begin{aligned}
&I^{(2)\,\mathrm{P}}_{1234} \to I_{\mathrm{III}}\,, \qquad && I^{(2)\,\mathrm{P}}_{1342} \to 0\,, \qquad && I^{(2)\,\mathrm{P}}_{1423} \to I_{\overline{\mathrm{H}}} + I_{\overline{\overset{\frown}{\mathrm{II}}}} + I_{\overline{\underset{\smile}{\mathrm{II}}}}\,, \\
&I^{(2)\,\mathrm{P}}_{3421} \to 0\,, && I^{(2)\,\mathrm{P}}_{4231} \to I_{\overline{\mathrm{III}}}\,, && I^{(2)\,\mathrm{P}}_{2341} \to I_{\mathrm{H}} + I_{\overset{\frown}{\mathrm{II}}} + I_{\underset{\smile}{\mathrm{II}}}\,,
\end{aligned}
\tag{3.49}
$$

where I_{III} is the ladder or double-box integral in Fig. 3.5(a), I_{H} is the H integral in Fig. 3.6(a), $I_{\overset{\frown}{\mathrm{II}}}, I_{\underset{\smile}{\mathrm{II}}}$ are the self-energy diagrams in Fig. 3.7(a-b), and the integrals with a bar denote their crossed versions, obtained by exchanging $p_2 \leftrightarrow -p_3$, which are also shown in the same figures. It is interesting to note that the H and self-energy diagrams come from the dimensional reduction of the same massless diagrams. The non-planar integrals reduce as follows

$$
\begin{aligned}
&I^{(2)\,\mathrm{NP}}_{1234} \to I_{\mathrm{XI}}\,, \qquad && I^{(2)\,\mathrm{NP}}_{1342} \to I_{\overline{\mathrm{XI}}}\,, \qquad && I^{(2)\,\mathrm{NP}}_{1423} \to I_{\mathrm{I\lambda}} + I_{\overline{\mathrm{I\lambda}}}\,, \\
&I^{(2)\,\mathrm{NP}}_{3421} \to I_{\mathrm{IX}}\,, && I^{(2)\,\mathrm{NP}}_{4231} \to I_{\overline{\mathrm{IX}}}\,, && I^{(2)\,\mathrm{NP}}_{2341} \to I_{\mathrm{IY}} + I_{\overline{\mathrm{IY}}}\,,
\end{aligned}
\tag{3.50}
$$

where we will refer to I_{IX} and I_{XI} as non-planar double-boxes, and the rest of the integrals are shown in Figs. 3.5 and 3.6. The KK reduced two-loop integrand is then given by

$$
\begin{aligned}
&M_4^{\text{2-loop}}(1_{\phi_1}, 2_{\phi_2}, 3_{\bar{\phi}_2}, 4_{\bar{\phi}_1}) = (8\pi G)^3 (s - |m_1 + m_2 e^{i\phi}|^2)^4 \\
&\quad \times \Bigg[(s - |m_1 + m_2 e^{i\phi}|^2)^2 (I_{\mathrm{III}} + I_{\mathrm{XI}} + I_{\mathrm{IX}}) + (u - |m_1 - m_2 e^{i\phi}|^2)^2 (I_{\overline{\mathrm{III}}} + I_{\overline{\mathrm{XI}}} + I_{\overline{\mathrm{IX}}}) \\
&\qquad + t^2 (I_{\mathrm{H}} + I_{\overset{\frown}{\mathrm{II}}} + I_{\underset{\smile}{\mathrm{II}}} + I_{\mathrm{IY}} + I_{\mathrm{I\lambda}} + I_{\overline{\mathrm{H}}} + I_{\overline{\overset{\frown}{\mathrm{II}}}} + I_{\overline{\underset{\smile}{\mathrm{II}}}} + I_{\overline{\mathrm{IY}}} + I_{\overline{\mathrm{I\lambda}}}) \Bigg]\,.
\end{aligned}
\tag{3.51}
$$

Comments on the consistency of the integrands

Finally, let us make some brief comments about the consistency of the integrands we have constructed in this subsection. We have focused on the sector of the theory where KK modes with masses m_1, m_2 of order R^{-1} exchange massless particles. This is not a consistent truncation, however, since there is no parametric separation between the masses of the KK

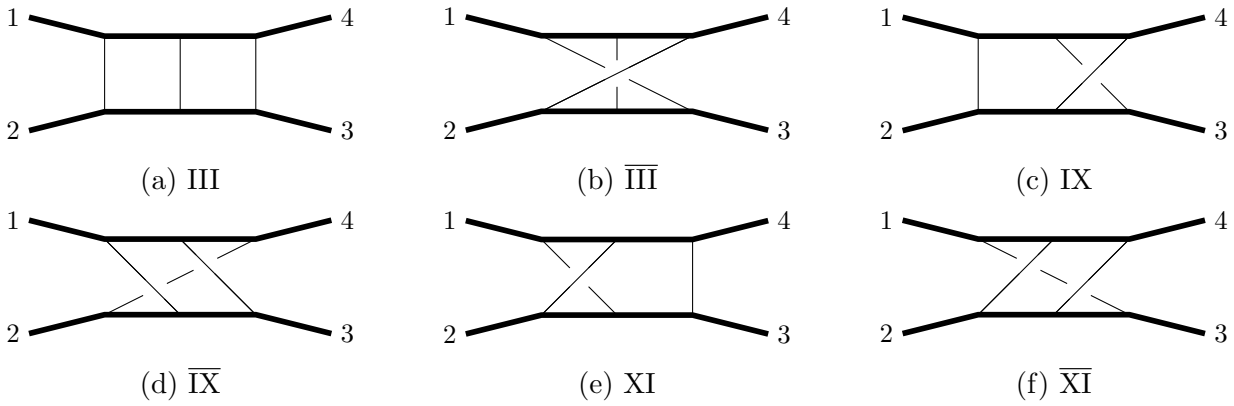

(a) III (b) $\overline{\text{III}}$ (c) IX

(d) $\overline{\text{IX}}$ (e) XI (f) $\overline{\text{XI}}$

Figure 3.5: Two loop integrals that are of the "ladder" type.

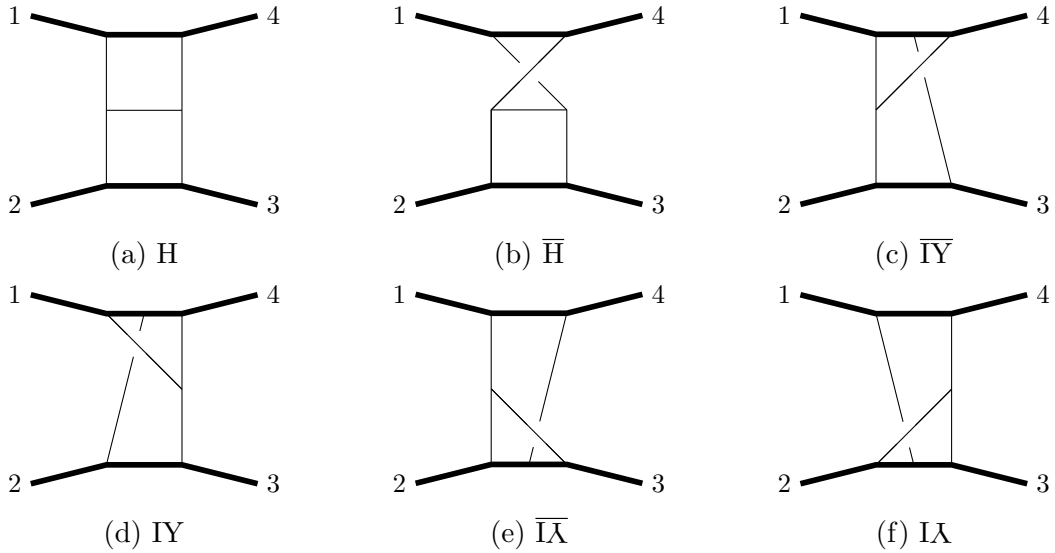

(a) H (b) $\overline{\text{H}}$ (c) $\overline{\text{IY}}$

(d) IY (e) $\overline{\text{I⅄}}$ (f) I⅄

Figure 3.6: Two loop integrals that are not of the "ladder" type.

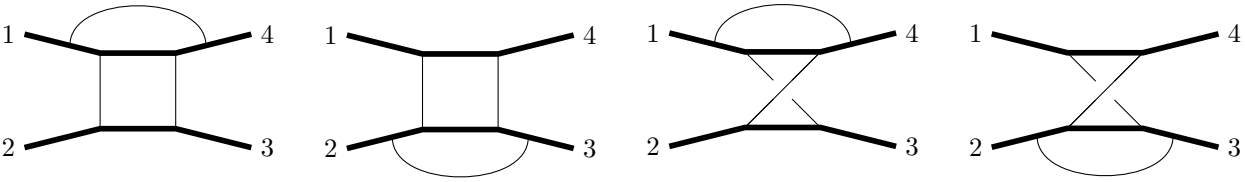

(a) Ш (b) Ш (c) $\overline{\text{Ш}}$ (d) $\overline{\text{Ш}}$

Figure 3.7: Two loop integrals that include a self interaction.

modes which are all of order R^{-1}.[3] This manifests itself in various ways. For instance, the tree amplitude in Eq. 3.42, features the exchange of massive particle of mass $\sim m_1 - m_2$, which is required by crossing symmetry. Similarly, at loop-level, it is known that the sum of the box and crossed-box integrals contains a mass singularity (see e.g. [261]). Consequently, the amplitude in Eq. (3.47) has collinear divergences in violation of the theorem of Ref. [262] which precludes them in quantum gravity.[4] All of these issues are manifestations of the well known fact that there is no consistent quantum theory of a finite number of massive particles coupled to maximal supergravity. In attempting to fix these problems, one is bound to discover the tower of KK modes, which arise from a consistent massless theory in higher dimensions. In spite of these comments, our truncated theory has a well-defined classical Lagrangian and is a useful toy model to explore the questions we are interested in in this work, so we will ignore all of these issues henceforth.

3.3.3 Integration via velocity differential equations

In the previous subsection we have constructed the full quantum integrand for the four-point amplitude through two loops. In this subsection we will calculate the integrals using the method of regions [225, 263] to extract the contributions which are relevant for the conservative dynamics. After briefly reviewing the various regions involved the problem, we introduce a new method to calculate the integrals in the potential region, using single-scale fully relativistic differential equations with modified boundary conditions. We illustrate the method using several examples at one and two loops.

[3] We thank Chia-Hsien Shen for discussions related to this point.

[4] This stands in contrast to Einstein gravity, whose quantum one-loop amplitude was shown in Ref. [42] to lack collinear divergences

Regions and power counting

Following the discussion in Ref. [42], we consider an internal graviton line with four-momentum $\ell = (\omega, \boldsymbol{\ell})$, whose components can scale as

$$\text{hard}: \quad (\omega, \boldsymbol{\ell}) \sim (m, m)\,, \tag{3.52}$$

$$\text{soft}: \quad (\omega, \boldsymbol{\ell}) \sim (|\boldsymbol{q}|, |\boldsymbol{q}|) \sim J^{-1}\,(m|\boldsymbol{v}|, m|\boldsymbol{v}|)\,, \tag{3.53}$$

$$\text{potential}: \quad (\omega, \boldsymbol{\ell}) \sim (|\boldsymbol{q}||\boldsymbol{v}|, |\boldsymbol{q}|) \sim J^{-1}\,(m|\boldsymbol{v}|^2, m|\boldsymbol{v}|)\,, \tag{3.54}$$

$$\text{radiation}: \quad (\omega, \boldsymbol{\ell}) \sim (|\boldsymbol{q}||\boldsymbol{v}|, |\boldsymbol{q}||\boldsymbol{v}|) \sim J^{-1}\,(m|\boldsymbol{v}|^2, m|\boldsymbol{v}|^2)\,, \tag{3.55}$$

where we take as reference scale $m = m_1 + m_2$, and each scaling defines a *region*. Note that the four different regions are defined using two small parameters $|\boldsymbol{q}|$ (or J^{-1}) and the velocity $|\boldsymbol{v}|$, which define the classical and non-relativistic limit respectively. Of the four regions, only the potential region contains off-shell modes, which can be integrated out and yield the conservative part of the dynamics. Their contributions can be captured by a non-relativistic EFT which was introduced and put to use in Refs. [39, 41, 42], and we will utilize in subsection 3.3.6.

The method of regions [225, 263] instructs us to expand the integrand using the scaling corresponding to a given region, and then integrate over the whole space of loop momenta in dimensional regularization. Our goal is to calculate the contributions from the potential region.

Outline of the new method

Ref. [41] introduced a "non-relativistic integration" method by which one must first expand in velocity before expanding in $|\boldsymbol{q}|$. This produces simple integrals akin to those appearing in NRGR [264, 265] at the cost of breaking manifest relativistic invariance in the first step. As explained above the potential region is defined by a double expansion, and we might chose to

expand in the opposite order, first in small $|\boldsymbol{q}|$, and then in velocity. The expansion in small $|\boldsymbol{q}|$ is just the expansion in the *soft region* where all graviton momentum components are uniformly small (of order $|\boldsymbol{q}|$). The result of this expansion is a power series in $|\boldsymbol{q}|$ truncated at an appropriate order, with each term in the expansion given by fully relativistic *soft integrals* with linearized matter propagators. To simplify the expressions, we will apply the well-known method of integration-by-parts reduction [266] to these soft integrals to rewrite them as a linear combination of *master integrals*. Then we will construct differential equations [226–229] in the canonical form [230, 231] for these master integrals. The choice of a *basis* of the master integrals will be an important technical point to be discussed later. The selection of pure basis integrals is also facilitated by automated tools [267, 268].

The upside of the soft expansion is that it keeps the integrals fully relativistic, but here we are only interested in the contributions from the potential region. Thus, in a second step we should *re-expand* the integrals in the potential region where graviton momenta are dominated by spatial components, since the potential region isolates conservative classical effects [39, 41, 42]. After the expansion in the potential region, each term in the previous small-q expansion would be rewritten as a Taylor series in the velocity (ratio of spatial to time components) of external momenta. Unlike the first step, which gives the expansion in small $|q|$ to some finite order, in the second step the velocity expansion can be performed to all orders by using method of differential equations for the soft master integrals. A key observation is that we can construct differential equations for the soft integrals directly before re-expanding in the potential region, as the re-expansion does not change the differential equations, but changes the boundary conditions near the static limit. Thus, it suffices to expand the soft master integrals to leading order in velocity in the potential region, to obtain the boundary conditions that allow us to uniquely solve the differential equations and determine the integrals to all orders in velocity.[5]

[5]The true values of the soft integrals, which will be useful for future calculations beyond conservative classical dynamics, can be obtained by solving differential equations subject to the boundary conditions of the "full" soft integrals near the static limit or another suitable kinematic limit.

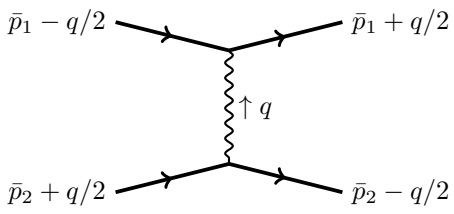

Figure 3.8: Kinematic setup with special variables.

Let us now explain each of these steps in more detail.

Soft expansion using special variables In order to carry out the procedure outline above, it will be useful to parametrize the external kinematics as[6]

$$p_1 = -(\bar{p}_1 - q/2)\,, \quad p_4 = \bar{p}_1 + q/2\,, \tag{3.56}$$

$$p_2 = -(\bar{p}_2 + q/2)\,, \quad p_3 = \bar{p}_2 - q/2\,, \tag{3.57}$$

as displayed in Fig. 3.8. Note that $s = (p_1 + p_2)^2 = (\bar{p}_1 + \bar{p}_2)^2$ so the physical region is still given by $s > (m_1 + m_2)^2$. By construction the $\bar{p}_i$'s are orthogonal to the momentum transfer $q = (p_1 + p_4)$,

$$p_1^2 - p_4^2 = -2\,\bar{p}_1 \cdot q = 0\,, \tag{3.58}$$

$$p_2^2 - p_3^2 = 2\,\bar{p}_2 \cdot q = 0\,. \tag{3.59}$$

We would like expand the full topologies in the *soft region*, which in these variables is characterized by the following hierarchy of scales

$$|\ell| \sim |q| \ll |\bar{p}_i|, m_i, \sqrt{s}\,, \tag{3.60}$$

[6]To our knowledge this parameterization was introduced in [269]. Notice that in our convention all external p_i^μ are outgoing, but $\bar{p}_i$ can be either incoming or outgoing.

where ℓ stands for any combination of graviton momenta $(\ell_1, \ell_2, \ell_1 \pm \ell_2, \cdots)$, or equivalently

$$(\bar{p}_i^0, \bar{\boldsymbol{p}}_i) \sim m(1,1), \tag{3.61}$$

$$(q^0, \boldsymbol{q}) \sim (|\boldsymbol{q}|, |\boldsymbol{q}|), \tag{3.62}$$

$$(\ell^0, \boldsymbol{\ell}) \sim (|\boldsymbol{q}|, |\boldsymbol{q}|). \tag{3.63}$$

The massless graviton propagators typically take the form

$$\frac{1}{\ell^2}, \quad \frac{1}{(\ell - q)^2}, \tag{3.64}$$

so they have uniform power counting $|q|^{-2}$ in the small-$|q|$ limit, without further expansion terms. Meanwhile, the momentum of each matter propagator is the sum of an external matter momentum $\bar{p}_i \pm \frac{1}{2}q$ and the momentum ℓ injected by gravitons (here ℓ is generally some linear combination of one or more graviton momenta). We have to expand these matter propagators in the soft region,

$$\frac{1}{\left(\ell + \bar{p}_i \pm \frac{1}{2}q\right)^2 - m_i^2} = \frac{1}{2\bar{p}_i \cdot \ell} - \frac{\ell^2 \pm \ell \cdot q}{(2\bar{p}_i \cdot \ell)^2} + \cdots . \tag{3.65}$$

That is all massive propagators are replaced by "eikonal" propagators that are linear in loop momenta. We can further define normalized external momenta,

$$u_1^\mu = \frac{\bar{p}_1^\mu}{\bar{m}_1}, \quad u_2^\mu = \frac{\bar{p}_2^\mu}{\bar{m}_2}, \tag{3.66}$$

with

$$\bar{m}_1^2 = \bar{p}_1^2 = m_1^2 - \frac{q^2}{4}, \quad \bar{m}_2^2 = \bar{p}_2^2 = m_2^2 - \frac{q^2}{4}\,. \tag{3.67}$$

We can then rewrite the denominators of Eq. (3.65) by following Eq. (3.66) and factoring out the scale associated to $\bar{p}_i$ from the propagators,

$$\frac{1}{2\bar{p}_i \cdot \ell} = \frac{1}{(2u_i \cdot \ell)\sqrt{m_i^2 - q^2/4}} = \frac{1}{2u_i \cdot \ell}\left(\frac{1}{m_i} + \frac{q^2}{8m_i^3} + \frac{3q^4}{128m_i^5} + \dots\right), \tag{3.68}$$

where the relevant kinematic factor is again expanded in small $|q|$. This choice of variables, has the advantage that each order in the expansion is homogeneous in $|q|$, due to the absence of products between external and graviton momenta in the numerators.

In summary, in the soft region the graviton propagators remain unexpanded, while the matter propagators have the form $1/(2u_i \cdot \ell)$, generally raised to higher powers when we look at terms beyond the leading order in the expansion. Thus, we can write down the following power counting rules applicable at any loop order, before we actually carry out the expansion in the soft region,

$$\begin{aligned} \text{Graviton propagator:} \quad & \sim \frac{1}{|q|^2}, \\ \text{Matter propagator:} \quad & \sim \frac{1}{|q|}, \\ \text{Integration measure per loop:} \quad & \mathrm{d}^4\ell \sim |q|^4. \end{aligned} \tag{3.69}$$

At successively higher orders in the expansion Eq. (3.65), we encounter integrals with propagators raised to higher powers as well as higher-degree polynomials in the numerators. Fortunately, all such integrals can be reduced to a finite number of master integrals via integration by parts [266] automated by the Laporta algorithm [270, 271], and we use the `FIRE6` software package [138] to perform the calculation. This allows the soft expansion result to be expressed in terms of a small number of master integrals, whose values will be calculated by the method of differential equations.

Velocity differential equations for soft integrals Next we want to integrate the master integrals, which we will do by the method of differential equations. Importantly, by virtue of the normalization (3.66) we have

$$u_1^2 = u_2^2 = 1, \quad u_1 \cdot q = u_2 \cdot q = 0. \tag{3.70}$$

Hence, after the soft expansion, the only dimensionful scale of the integrals is q^2. The dependence on q^2 of each integral can be easily fixed by dimensional analysis, and the integrals only depend non-trivially on the following dimensionless parameter,

$$y = u_1 \cdot u_2. \tag{3.71}$$

Hence our differential equations will depend on this single variable, y, which is related to the relativistic Lorentz factor in Eq. (3.32),

$$y = \sigma + \frac{\sigma(m_1^2 + m_2^2) + 2m_1 m_2}{8 m_1^2 m_2^2}\, q^2 + \mathcal{O}(q^4). \tag{3.72}$$

We give this relation to the next-to-leading order in q^2 since it will be used later to convert amplitude results in y to results in σ.

We will construct the differential equations by taking derivatives of the master integrals. The choice of a *basis* master integrals is not unique; we choose a *pure basis* in which each master integral has an ϵ expansion where each term is a generalized polylogarithm [272–274] of uniform transcendentality. This is largely just a technical point, because at the order of ϵ expansion needed, the integrals in this work do not contain any functions more complicated than logarithms (which are a special case of generalized polylogarithms). However, this will yield simple differential equations. A possible form of the differential operator ∂_y, rewritten

as derivatives against normalized external momenta u_i^μ, is

$$\frac{\mathrm{d}}{\mathrm{d}y} = \frac{1}{y^2-1}\left(y u_1^\mu - u_2^\mu\right)\frac{\partial}{\partial u_1^\mu}\,. \tag{3.73}$$

The original form $\mathrm{d}/\mathrm{d}y$ is fine for differentiating the explicit y-dependent factors in the normalization of the master integrals, but the RHS of Eq. (3.73) is needed to differentiate the propagators and numerators expressed in terms of external and internal momenta. After differentiating any of the pure integrals with respect to y, the result can be IBP-reduced back to the basis of master integrals. We will rationalize the square root $\sqrt{y^2-1}$ using the change of variable

$$y = \frac{1+x^2}{2x}, \quad \sqrt{y^2-1} = \frac{1-x^2}{2x}, \quad y \geq 1, \quad 0 < x \leq 1, \tag{3.74}$$

under which

$$\frac{\mathrm{d}}{\mathrm{d}y} = \frac{2x^2}{x^2-1}\frac{\mathrm{d}}{\mathrm{d}x}\,. \tag{3.75}$$

In terms of these variables, the physical region in our scattering processes is given by $1 < y < \infty$, i.e. $0 < x < 1$.

Our differential equations will take the canonical form [230, 231]

$$\mathrm{d}\vec{f} = \epsilon \sum_i A_i \,\mathrm{dlog}\,\alpha_i(x)\,\vec{f}\,, \tag{3.76}$$

where A_i are numerical matrices and each $\alpha_i(x)$, called a *symbol letter*, is a rational functions in x, and $\epsilon = (4-D)/2$ is the dimensional regularization parameter.[7] The set of the α_i is called the symbol alphabet, in the formalism of Ref. [273] which uses "symbols" to elucidate functional identities between generalized polylogarithms.

These differential equations can be easily solved, given appropriate boundary conditions.

[7] Henn's canonical form can also be used for finite integrals without a dimensional regulator, see [14, 275].

While we could use them to calculate the full soft integrals, we will use them to directly extract the values of the integrals evaluated in the potential region. By expanding in the potential region and summing the expansion to all orders, we have localized the loop integration on the poles of matter propagators. We are essentially dealing with a version of cut integrals (see e.g. Refs. [276–281]), which satisfy the same IBP relation and differential equations as original uncut integrals. This is the reason why the only changes are in the boundary conditions, obtained in the near-static limit $y \to 1$ by re-expanding the master integrals in the potential region.

Static boundary conditions from re-expansion in the potential region We are ready to write down the power counting of momentum components in the potential region, in terms of a small velocity parameter v. Since we have first expanded in the soft region and transitioned to normalized external momenta in Eq. (3.68), we will write down the power counting for u_i^μ instead of p_i^μ, and for graviton momenta ℓ^μ,

$$u_i^\mu = (u_i^0, \boldsymbol{u}_i) \sim (1, |\boldsymbol{v}|), \tag{3.77}$$

$$\ell^\mu = (\omega, \boldsymbol{\ell}) \sim |\boldsymbol{q}|(|\boldsymbol{v}|, 1). \tag{3.78}$$

The factor of $|q|$ is unimportant in our two-step expansion procedure, where the integrals are already homogeneous in q^2 (i.e. proportional to a definite power of q^2 without further corrections) after the soft expansion is carried out.

Now we can expand graviton and matter propagators. Recall that graviton propagators $\sim 1/\ell^2$ are unchanged in the soft expansion. Their expansion in the potential region is

$$\frac{1}{\ell^2} = \frac{1}{\omega^2 - \boldsymbol{\ell}^2} = -\left(\frac{1}{\boldsymbol{\ell}^2} + \frac{\omega^2}{(\boldsymbol{\ell}^2)^2} + \frac{\omega^4}{(\boldsymbol{\ell}^2)^3} + \dots\right). \tag{3.79}$$

On the other hand, matter propagators of the form (3.68) are homogeneous in v and the

expansion consists of a single term,

$$\frac{1}{2u_i \cdot \ell} = \frac{1}{2\left(u_i^0\,\omega - \boldsymbol{u}_i\boldsymbol{\ell}\right)}\,. \tag{3.80}$$

The power counting rules for propagators and integration measure in the potential region are

$$\text{Graviton propagator:} \quad \sim 1, \tag{3.81}$$

$$\text{Matter propagator:} \quad \sim \frac{1}{|\boldsymbol{v}|}, \tag{3.82}$$

$$\text{Integration measure:} \quad \mathrm{d}^4\ell \sim |\boldsymbol{v}|. \tag{3.83}$$

We will only need to expand to leading order in $|\boldsymbol{v}|$, since we only wish to obtain the value of the integrals at one point, to supply a boundary condition.

The expanded integrals can be evaluated by residues by performing contour integration over the graviton energies ω. Such energy integrals can be ambiguous until one applies a proper prescription [39, 42]. Such a prescription is effectively part of the *definition* of the potential region which separates it from the larger soft region. Refs. [39, 42] presented the prescription in the absence of double poles, i.e. squared matter propagators, but we will show in our examples that when the energy integral prescription is formulated in terms of residues, double poles can be treated in a natural manner and cause no difficulty. As explained in Ref. [42], this prescription generally implies that an integral in the potential region with less than one massive propagators per loop is necessarily zero. Finally, the resulting $D-1$-dimensional integrals can be easily evaluated using traditional methods, and provide the desired boundary conditions to solve our soft integrals in the potential region.

One-loop integrals

Next we will illustrate the method above with some simple one-loop examples. We will evaluate all the box-type integrals, which appear in the one-loop $\mathcal{N} = 8$ integrand in Eq. (3.47) with scalar numerator. Adopting the convention of Ref. [282], we remove from our integrals an overall factor of

$$\frac{i}{(4\pi)^2}(\bar{\mu}^2)^\epsilon := \frac{i}{(4\pi)^2}\left(\frac{e^{\gamma_{\rm E}}}{4\pi\mu^2}\right)^{-\epsilon} \tag{3.84}$$

per loop, where μ is the dimensional regularization scale, which is to be restored at the end. In other words, we will write the integration measure for each loop as $\mathrm{d}^D\ell/(i\pi^{D/2})$, where $D \equiv 4 - 2\epsilon$, and multiplying by a factor of Eq. (3.84) per loop in the end to recover results defined with the more common normalization $\mathrm{d}^D\ell/(2\pi)^D$.

Box integral The box integral with two opposite masses has been evaluated in Ref. [261] in dimensional regularization up to order ϵ^0. It has also been discussed in detail in Ref. [42]. As show in Fig. 3.9, a generic integral in the box topology is of the form

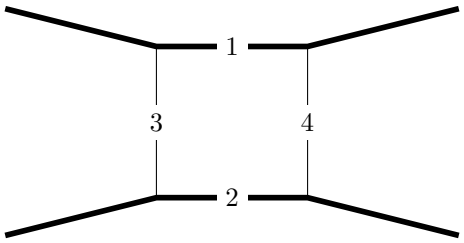

Figure 3.9: Top level topology at one-loop. Indices correspond to the propagators listed in eq. (3.86).

$$\tilde{G}_{i_1,i_2,i_3,i_4} = \int \frac{\mathrm{d}^D\ell\, e^{\gamma_{\rm E}\epsilon}}{i\pi^{D/2}} \frac{1}{\tilde{\rho}_1^{i_1}\tilde{\rho}_2^{i_2}\tilde{\rho}_3^{i_3}\tilde{\rho}_4^{i_4}}\,. \tag{3.85}$$

Where the propagator denominators are explicitly

$$\tilde{\rho}_1 = (\ell - p_1)^2 - m_1^2\,, \quad \tilde{\rho}_2 = (\ell + p_2)^2 - m_2^2\,, \quad \tilde{\rho}_3 = \ell^2\,, \quad \tilde{\rho}_4 = (\ell - q)^2\,. \tag{3.86}$$

The crossed box integral topologies are related to the box integral by the replacement $u_1 \to u_1$, $u_2 \to -u_2$.

Integration-by-parts reduction of soft integrals Using the soft power counting rules explained in the previous subsection we see that the box integrals are $\mathcal{O}(|q|^{-2})$. Thus, classical power counting requires expanding the integral to subleading powers. The box propagators reduce in the soft expansion to

$$\rho_1 = 2u_1 \cdot \ell\,, \quad \rho_2 = -2u_2 \cdot \ell\,, \quad \rho_3 = \ell^2\,, \quad \rho_4 = (\ell - q)^2\,, \tag{3.87}$$

which upon expansion of the integral will generally appear raised to integer powers. The numerators appearing in the expansion are polynomials in ρ_i, so each order in the soft expansion is a sum of integrals of the form

$$G_{i_1,i_2,i_3,i_4} = \int \frac{\mathrm{d}^D \ell\, e^{\gamma_{\mathrm{E}}\epsilon}}{i\pi^{D/2}} \frac{1}{\rho_1^{i_1}\rho_2^{i_2}\rho_3^{i_3}\rho_4^{i_4}}, \tag{3.88}$$

with each such integral multiplied by a rational function of the external kinematic variables m_i^2, q^2, and y. As we already mentioned, q^2 is the only dimensionful scale in such integrals. Whenever i_1 or i_2 is non-positive, the integral will become scaleless and vanish in dimensional regularization.[8]

Using integration-by-parts reduction, all such integrals are rewritten as linear combina-

[8]Physically speaking, this is because the soft expansion only captures the part of the amplitude that is non-analytic in q^2 and relevant for long-range classical physics.

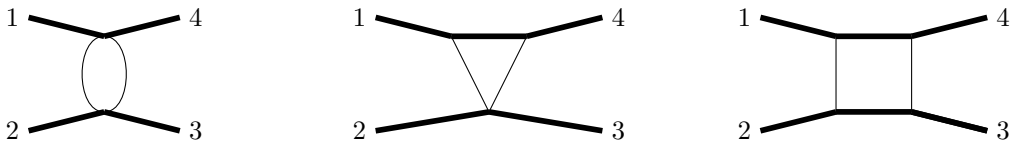

(a) f_1 (b) f_2 (c) f_3

Figure 3.10: Topologies for the box master integrals.

tions of the following three *master integrals*[9]

$$f_1 = \epsilon(-q^2)\, G_{0,0,2,1}\,, \quad f_2 = \epsilon^2\sqrt{-q^2}\, G_{1,0,1,1}\,, \quad f_3 = \epsilon^2\sqrt{y^2-1}\,(-q^2)\, G_{1,1,1,1}\,, \tag{3.89}$$

whose corresponding topologies are depicted in Fig. 3.10. So all integrals given by Eq. (3.88) span not an infinite-dimensional, but a three-dimensional vector space. The above integrals are all proportional to $(-q^2)^{-\epsilon}$ times a q-independent function of the dimensionless parameter y. The basis does not involve the other triangle integral $G_{0,1,1,1}$ with a (linearized) matter propagator on the bottom – this is because with the linearized propagator denominators $2u_i \cdot \ell$ the two triangle integrals are identical and we may freely choose either one as part of the basis of master integrals.

Starting from the original box integral Eq. (3.85) with $a_k = 1$, we expand the propagators as in Eqs. (3.65) and (3.68), and perform integration-by-parts reduction to obtain the small-q expansion of the box integral in terms of the three master integrals in Eq. (3.89),

$$\begin{aligned} I_{\rm II} = \frac{i}{4\pi}(\bar\mu^2)^\epsilon \Bigg[& \frac{1}{\epsilon^2 \bar m_1 \bar m_2 \sqrt{y^2-1}} \frac{1}{(-q^2)} f_3 \\ & + \frac{(\bar m_1 + \bar m_2)}{\epsilon \bar m_1^2 \bar m_2^2 (y-1)} \frac{1}{\sqrt{-q^2}} f_2 \\ & - \frac{(1+2\epsilon)\,(2\bar m_2 \bar m_1 y + \bar m_1^2 + \bar m_2^2)}{8\epsilon^2 \bar m_1^3 \bar m_2^3\,(y^2-1)^{3/2}} f_3 + \frac{(1+2\epsilon)\,[(\bar m_1^2 + \bar m_2^2)\,y + 2\bar m_1 \bar m_2]}{8\epsilon \bar m_1^3 \bar m_2^3 (y^2-1)} f_1 \Bigg], \end{aligned} \tag{3.90}$$

[9] In contrast the full box system has 10 master integrals, see e.g. Ref. [42].

where the 1st, 2nd, and 3rd lines are of order $|q|^{-2}$, $|q|^{-1}$, and $|q|^{0}$, respectively[10]. The bubble integral f_1 will be eventually set to zero because we will evaluate the integrals in the potential region.

Differential equations for soft integrals Now we will construct differential equations for the three pure master integrals in Eq. (3.89). The original form of the differential operator $\mathrm{d}/\mathrm{d}y$ is used for differentiating the explicit y-dependent factors in Eq. (3.89), such as $\sqrt{y^2-1}$, and the RHS of Eq. (3.73) is used to differentiate the propagators in Eqs. (3.87) and (3.88). After differentiating any of the three pure integrals with respect to y, the result is a sum of integrals of the form Eq. (3.88), and can be IBP-reduced back to the basis Eq. (3.89). After IBP-reduction we use the change of variables from y to x in Eq. (3.74), to rationalize the square roots. The resulting differential equation is

$$\frac{\mathrm{d}\vec{f}}{\mathrm{d}x} = \epsilon \frac{A}{x} \vec{f}, \tag{3.91}$$

where the matrix A is explicitly given by

$$A = \begin{pmatrix} 0 & 0 & 0 \\ 0 & 0 & 0 \\ 1 & 0 & 0 \end{pmatrix}. \tag{3.92}$$

This can be written in the form (3.76)

$$\mathrm{d}\vec{f} = \epsilon A_1 \, \mathrm{dlog}(x) \vec{f}, \tag{3.93}$$

so we recognize x as the only *symbol letter* for the integrals relevant at one loop.

[10]This is true up to the factors of $|q|$ hidden in the definition of y and $\bar{m}_i$.

Static boundary conditions from re-expansion in the potential region Finally, we need to obtain the appropriate boundary conditions to solve the differential equation (3.93) in the potential region. As explained above, we proceed by expanding the pure basis of master integrals Eq. (3.89) in the near-static limit $|\boldsymbol{v}| \ll 1$, using the rules in subsection 3.3.3. After expanding in $|\boldsymbol{v}|$, each order in the series consists of a sum of integrals of the form

$$\int \mathrm{d}^{D-1}\boldsymbol{\ell} \int_{-\infty}^{\infty} \mathrm{d}\omega \, \frac{\mathcal{N}(\omega, \boldsymbol{\ell}, u_i^0, \boldsymbol{u}_i)}{(\boldsymbol{\ell}^2 - i0)^{i_1} \left[(\boldsymbol{\ell} - \boldsymbol{q})^2 - i0\right]^{i_2} (2\boldsymbol{u}_1\boldsymbol{\ell} - 2u_1^0\,\omega - i0)^{i_3} (-2\boldsymbol{u}_2\boldsymbol{\ell} + 2u_2^0\,\omega - i0)^{i_4}}, \tag{3.94}$$

with some polynomial numerator $\mathcal{N}$.

These integrals can be evaluated by performing integration over energy ω by residues. We work in a frame where the momentum transfer q^μ has no energy component, so the energy of the two graviton lines are ω and $-\omega$, respectively. For convenience, we can further boost our frame so that particle 1 is at rest[11] and u_2 moves in z-direction

$$u_1 = (1, 0, 0, 0)\,, \quad u_2 = (\sqrt{1+v^2}, 0, 0, v\,)\,. \tag{3.95}$$

The y variable defined in Eq. (3.71) is related to the above parametrization by $v = \sqrt{y^2 - 1}$.

We symmetrize over the energy components of the two graviton lines, and rewrite Eq. (3.94) using the transformation

$$\int_{-\infty}^{\infty} \mathrm{d}\omega\, \mathcal{I}(\omega) \to \int_{-\infty}^{\infty} \mathrm{d}\omega\, \frac{1}{2}\left[\mathcal{I}(\omega) + \mathcal{I}(-\omega)\right]\,. \tag{3.96}$$

Then we perform the ω integral by closing the contour either in the upper half plane or the lower half plane, and pick up contributions from poles at finite values of ω, discarding poles at infinity, i.e. neglecting possible non-zero contributions from the arc of a semi-circle contour whose radius tends to infinity. After the ω integral in Eq. (3.94) is carried out in this

[11] To be precise, particle 1 is only at rest up to $\mathcal{O}(q^2)$, as u_1 only coincides with the four-velocity of particle 1 at leading order in q.

way, we are left with the spatial integral $\mathrm{d}^{D-1}\boldsymbol{\ell}$, and the only denominators left are massless quadratic propagators in three dimensions and linear propagators

$$\frac{1}{\boldsymbol{\ell}^2 - i0}\,, \frac{1}{(\boldsymbol{\ell}-\boldsymbol{q})^2 - i0}\,, \frac{1}{-2\ell^z - i0}\,. \tag{3.97}$$

The resulting spatial integrals only depend on a single scale $\boldsymbol{q}^2$, and are related to standard propagator integrals.

The bubble integral f_1 in Eq. (3.89) trivially vanishes in the potential region, because there are no poles at finite values of ω and poles at infinity are discarded in our integration prescription. Using the power counting rules in the potential region, Eqs. (3.81) to (3.83), we can see that f_2 and f_3, i.e. triangle and box integrals with appropriate prefactors that ensure a canonical form of differential equations, both start at $\mathcal{O}(v^0)$ in the velocity expansion. For example, f_3 has a prefactor $\sqrt{y^2-1} = v$, two matter propagators giving $\mathcal{O}(1/v^2)$, and an integration measure of $\mathcal{O}(v)$, so overall f_3 is of $\mathcal{O}(v^0)$. This is not surprising, since it is well known that integrals of unit leading singularity can have at most logarithmic singularities in any kinematic limit. To obtain f_2 and f_3 evaluated in the potential region at the leading order in v, we keep only the leading term in Eq. (3.79) for each graviton propagator, and then use Eq. (3.96) to perform the energy integral, leaving spatial integrals

$$f_1^{(p)}\big|_{y=1} \equiv 0\,, \tag{3.98}$$

$$f_2^{(p)}\big|_{y=1} = -\frac{\sqrt{\pi}}{2}\epsilon^2\sqrt{-q^2}\int \frac{\mathrm{d}^{D-1}\ell\, e^{\gamma_{\mathrm{E}}\epsilon}}{\pi^{(D-1)/2}} \frac{1}{(\boldsymbol{\ell}^2 - i0)\,[(\boldsymbol{\ell}-\boldsymbol{q})^2 - i0]}\,, \tag{3.99}$$

$$f_3^{(p)}\big|_{y=1} = \sqrt{\pi}\epsilon^2(-q^2)\int \frac{\mathrm{d}^{D-1}\ell\, e^{\gamma_{\mathrm{E}}\epsilon}}{\pi^{(D-1)/2}} \frac{1}{(\boldsymbol{\ell}^2 - i0)[(\boldsymbol{\ell}-\boldsymbol{q})^2 - i0]} \frac{1}{(-2\ell^z - i0)}\,. \tag{3.100}$$

The bubble integral vanishes as the propagator does not have any energy dependence in the potential limit. The $(D-1)$-dimensional integrals are calculated in Appendix 3.A and given

in Eqs. (3.288) and (3.289). The result for the static limit is then

$$f_1^{(p)}\big|_{y=1} = 0, \tag{3.101}$$

$$f_2^{(p)}\big|_{y=1} = -\epsilon^2(-q^2)^{-\epsilon}e^{\gamma_{\rm E}\epsilon}\frac{\sqrt{\pi}\,\Gamma\left(\frac{1}{2}-\epsilon\right)^2\Gamma\left(\epsilon+\frac{1}{2}\right)}{2\Gamma(1-2\epsilon)}\,, \tag{3.102}$$

$$f_3^{(p)}\big|_{y=1} = \epsilon^2(-q^2)^{-\epsilon}e^{\gamma_{\rm E}\epsilon}\frac{i\pi}{2}\frac{\Gamma(-\epsilon)^2\Gamma(1+\epsilon)}{\Gamma(-2\epsilon)}\,. \tag{3.103}$$

Solving the differential equation (3.93) shows that Eqs. (3.101)–(3.103) in fact are correct to all orders in v, i.e. for any values of $y \geq 1$, so they are the final expressions for the pure basis Eq. (3.89) as evaluated in the potential regions to all orders in velocity,

$$f_1^{(p)} = f_1^{(p)}\big|_{y=1}\,, \quad f_2^{(p)} = f_2^{(p)}\big|_{y=1}\,, \quad f_3^{(p)} = f_3^{(p)}\big|_{y=1}\,. \tag{3.104}$$

Looking forward to the next subsections, we will find the solutions to differential equations to be more non-trivial for two-loop integrals.

Result Substituting the results Eqs. (3.101)–(3.103) into Eq. (3.90) and taking into account Eqs. (3.67) and (3.72), we obtain the box integral evaluated in the potential region to all order in velocity, given as a small-$|q|$ expansion,

$$\begin{aligned} I_{\rm II}^{(p)} = \frac{i}{(4\pi)^2}\left(\frac{-q^2}{\bar{\mu}^2}\right)^{-\epsilon}\Bigg\{ & \frac{1}{(-q^2)}\frac{i\pi}{2m_1m_2\sqrt{\sigma^2-1}}\frac{\Gamma(-\epsilon)^2\Gamma(1+\epsilon)}{\Gamma(-2\epsilon)} \\ & - \frac{1}{\sqrt{-q^2}}\frac{\epsilon(m_1+m_2)}{m_1^2m_2^2(\sigma-1)}\frac{\sqrt{\pi}\,\Gamma\left(\frac{1}{2}-\epsilon\right)^2\Gamma\left(\epsilon+\frac{1}{2}\right)}{2\Gamma(1-2\epsilon)} \\ & - \frac{i\pi\epsilon\left(m_1^2+m_2^2+2m_1m_2\sigma\right)}{8m_1^3m_2^3\left(\sigma^2-1\right)^{3/2}}\frac{\Gamma(-\epsilon)^2\Gamma(1+\epsilon)}{\Gamma(-2\epsilon)} \\ & + \mathcal{O}\left(\sqrt{-q^2}\right)\Bigg\}, \quad \sigma > 1\,. \end{aligned} \tag{3.105}$$

Crossed box integral We end with a discussion of the crossed box integrals. As mentioned above, the unexpanded crossed integral is related to the box integral by the crossing

replacement $u_1 \to u_1$, $u_2 \to -u_2$. Therefore, the same soft differential equations (3.93) are satisfied by these integrals, and one only needs to be careful about the boundary conditions.

The specific choice of reference frame Eq. (3.95) is changed by crossing into

$$u_1 = (1,0,0,0)\,, \quad u_2 = (-\sqrt{1+v^2},0,0,-v\,)\,. \tag{3.106}$$

In terms of Lorentz invariants, this is $y \to -y$. However, our results for the box integral at $y > 1$ cannot be analytically continued to negative values of y, because the energy integration prescription produces non-analytic behavior in y. For example, when performing the energy integration for f_3 in Eq. (3.89) in the potential region, the two poles lie on the same side of the contour when $y < 0$, and the contour integration gives zero. The correct result for crossed integrals in the static limit (analogous to Eqs. (3.101)–(3.103) for the box) is

$$f_1^{(p)}\big|_{y=-1} = 0, \tag{3.107}$$

$$f_2^{(p)}\big|_{y=-1} = -\epsilon^2(-q^2)^{-\epsilon}e^{\gamma_{\rm E}\epsilon}\frac{\sqrt{\pi}\,\Gamma\left(\frac{1}{2}-\epsilon\right)^2\Gamma\left(\epsilon+\frac{1}{2}\right)}{2\Gamma(1-2\epsilon)}\,, \tag{3.108}$$

$$f_3^{(p)}\big|_{y=-1} = 0\,. \tag{3.109}$$

Again, the above equations are derived from the static limit but are actually valid to all orders in velocity, because the velocity differential equations have trivial solutions at one loop.

Result To obtain the small-$|q|$ expansion of the crossed box, we also need to make the $y \to -y$ replacement in the coefficients of f_i master integrals in Eq. (3.90). The end result

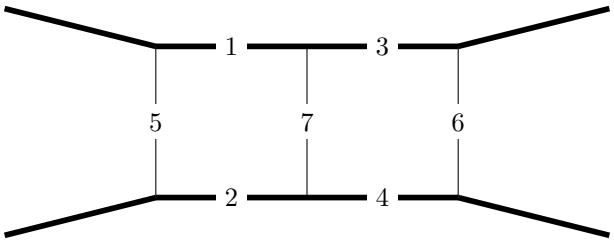

Figure 3.11: III topology. Indices correspond to the propagators listed in eq. (3.112).

for the small-$|q|$ expansion of the crossed box integral is

$$I_{\rm X}^{(p)} = \frac{i}{(4\pi)^2}\left(\frac{-q^2}{\bar{\mu}^2}\right)^{-\epsilon}\left\{\frac{1}{\sqrt{-q^2}}\frac{\epsilon(m_1+m_2)}{m_1^2 m_2^2(\sigma+1)}\frac{\sqrt{\pi}\,\Gamma\left(\frac{1}{2}-\epsilon\right)^2\Gamma\left(\epsilon+\frac{1}{2}\right)}{2\Gamma(1-2\epsilon)}\right.$$
$$\left. + \mathcal{O}\left(\sqrt{-q^2}\right)\right\}, \quad \sigma > 1\,. \tag{3.110}$$

Two-loop integrals

Next we will evaluate the two-loop integrals needed for the two-loop integrand in Eq. (3.51). A simple application of the soft power-counting rules in Eq. (3.69) reveals that all the ladder-type integrals in the second line of Eq. (3.51) contribute in the classical limit with leading power $\mathcal{O}(q^{-2})$ so they need to be expanded to subleading powers. On the other hand, of the integrals in the third line of Eq. (3.51), only the H and $\overline{\rm H}$ integrals at leading power survive the $(q^2)^2$ suppression of the numerator, and the rest do not contribute in the classical limit.[12]

We will describe in detail the computation of the double-box (III) and H-type integrals, and present results for the rest of the integrals. As usual we will strip from our integrals a factor of (3.84) per loop in intermediate steps, to be restored at the end.

[12]The "mushroom" integrals $I_{\overline{\mathfrak{A}}}$ and $I_{\overline{\mathfrak{B}}}$ vanish identically when evaluated in the potential region [41, 42], so cannot contribute even without the $(q^2)^2$ suppression from the integrand numerator.

Double-box (III) We first consider generic integrals of the form

$$\tilde{G}_{i_1,i_2,\ldots,i_9} = \int \frac{\mathrm{d}^D \ell_1 \, e^{\gamma_{\mathbb{E}}\epsilon}}{i\pi^{D/2}} \int \frac{\mathrm{d}^D \ell_2 \, e^{\gamma_{\mathbb{E}}\epsilon}}{i\pi^{D/2}} \frac{1}{\tilde{\rho}_1^{i_1} \tilde{\rho}_2^{i_2} \cdots \tilde{\rho}_9^{i_9}} \,. \tag{3.111}$$

Where the propagators are

$$\begin{aligned}
&\tilde{\rho}_1 = (\ell_1 - p_1)^2 - m_1^2 \,, && \tilde{\rho}_2 = (\ell_1 + p_2)^2 - m_2^2 \,, && \tilde{\rho}_3 = (\ell_2 - p_4)^2 - m_1^2 \,, \\
&\tilde{\rho}_4 = (\ell_2 + p_3)^2 - m_2^2 \,, && \tilde{\rho}_5 = \ell_1^2 \,, && \tilde{\rho}_6 = \ell_2^2 \,, \\
&\tilde{\rho}_7 = (\ell_1 + \ell_2 - q)^2 \,, && \tilde{\rho}_8 = (\ell_1 - q)^2 \,, && \tilde{\rho}_9 = (\ell_2 - q)^2 \,.
\end{aligned} \tag{3.112}$$

The double-box (III) topology can be embedded in this family of integrals, as shown in Fig. 3.11. Later we will see that the H topology can also be embedded in the same family. We note that the equal-mass double-box integral has been evaluated in Refs. [283, 284] without expansion in the soft or potential region, but the case of generic masses has not been discussed in the literature.

Soft expansion and differential equations In the soft region, we construct an expansion of the integrand around small $|\ell_i| \sim |q|$. In the expansion, only the leading order parts of $\tilde{\rho}_i$, denoted by ρ_i and given by

$$\begin{aligned}
&\rho_1 = 2\,\ell_1 \cdot u_1 \,, && \rho_2 = -2\,\ell_1 \cdot u_2 \,, && \rho_3 = -2\,\ell_2 \cdot u_1 \,, \\
&\rho_4 = 2\,\ell_2 \cdot u_2 \,, && \rho_5 = \ell_1^2 \,, && \rho_6 = \ell_2^2 \,, \\
&\rho_7 = (\ell_1 + \ell_2 - q)^2 \,, && \rho_8 = (\ell_1 - q)^2 \,, && \rho_9 = (\ell_2 - q)^2 \,,
\end{aligned} \tag{3.113}$$

appear in the denominators (possibly with raised powers), and subleading corrections all appear in numerators. Such numerators are in turn written as linear combinations ρ_i. The

small-$|q|$ expansion consists of integrals of the form

$$G_{i_1,\,i_2,\ldots,i_9} = \int \frac{\mathrm{d}^D \ell_1\, e^{\gamma_{\mathrm{E}}\epsilon}}{i\pi^{D/2}} \int \frac{\mathrm{d}^D \ell_2\, e^{\gamma_{\mathrm{E}}\epsilon}}{i\pi^{D/2}} \frac{1}{\rho_1^{i_1}\rho_2^{i_2}\ldots\rho_9^{i_9}}, \tag{3.114}$$

where negative indices represent numerators rather than denominators. There are a total of 10 master integrals for the III topology[13] as shown in Figs. 3.12, 3.13. A pure basis is given by

$$f_{\mathrm{III},1} = \epsilon^2(-q^2)G_{0,0,0,0,0,0,1,2,2}\,, \tag{3.115}$$

$$f_{\mathrm{III},2} = \epsilon^4\sqrt{y^2-1}\,G_{0,1,1,0,0,0,1,1,1}\,, \tag{3.116}$$

$$f_{\mathrm{III},3} = \epsilon^3(-q^2)\sqrt{y^2-1}\,G_{0,1,1,0,0,0,2,1,1}\,, \tag{3.117}$$

$$f_{\mathrm{III},4} = -\epsilon^2(-q^2)G_{0,2,2,0,0,0,1,1,1} + \epsilon^3 y\,(-q^2)G_{0,1,1,0,0,0,2,1,1}\,, \tag{3.118}$$

$$f_{\mathrm{III},5} = \epsilon^3\sqrt{y^2-1}\,(-q^2)G_{1,1,0,0,1,1,2,0,0}\,, \tag{3.119}$$

$$f_{\mathrm{III},6} = \epsilon^3(1-6\epsilon)\,G_{1,0,1,0,1,1,1,0,0}\,, \tag{3.120}$$

$$f_{\mathrm{III},7} = \epsilon^4\left(y^2-1\right)(-q^2)G_{1,1,1,1,1,1,1,0,0}\,, \tag{3.121}$$

$$f_{\mathrm{III},8} = \epsilon^3\sqrt{-q^2}G_{1,0,0,0,1,1,2,0,0}\,, \tag{3.122}$$

$$f_{\mathrm{III},9} = \epsilon^3\sqrt{-q^2}G_{0,2,1,0,1,1,1,0,0}\,, \tag{3.123}$$

$$f_{\mathrm{III},10} = \epsilon^4\sqrt{y^2-1}\sqrt{-q^2}G_{1,1,1,0,1,1,1,0,0}\,, \tag{3.124}$$

where all the master integrals are normalized to be proportional to $(-q^2)^{-2\epsilon}$. The corresponding topologies are depicted in Figs. 3.12 and 3.13, where we have separated the integrals which are even and odd in $|q|$.

We perform soft expansion and use IBP-reduction to write the results in terms of the

[13]For reference, in the full equal-mass problem there are 23 master integrals [284].

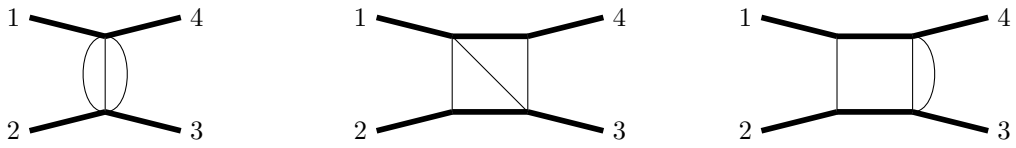

(a) $f_{\text{III},1}$ (b) $f_{\text{III},2}, f_{\text{III},3}, f_{\text{III},4}$ (c) $f_{\text{III},5}$

(d) $f_{\text{III},6}$ (e) $f_{\text{III},7}$

Figure 3.12: Even-$|q|$ topologies relevant for the double-box master integrals.

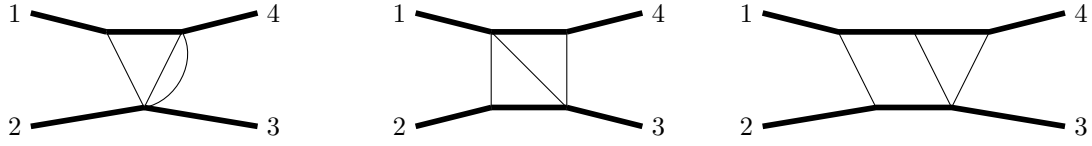

(a) $f_{\text{III},8}$ (b) $f_{\text{III},9}$ (c) $f_{\text{III},10}$

Figure 3.13: Odd-$|q|$ topologies relevant for the double-box master integrals.

master integrals. The double-box integral is given as the following small-$|q|$ expansion,

$$
\begin{aligned}
I_{\text{III}} = -\frac{(\bar{\mu}^2)^{2\epsilon}}{(4\pi)^2}\Bigg\{ & \frac{1}{(-q^2)}\frac{1}{\bar{m}_1^2\bar{m}_2^2\,(y^2-1)\,\epsilon^4} f_{\text{III},7} \\
& + \frac{1}{\sqrt{-q^2}}\frac{16\bar{m}_1^3\bar{m}_2^3(\bar{m}_1+\bar{m}_2)\,(2y^2-1)^3}{(y-1)\sqrt{y^2-1}\,\epsilon^3} f_{\text{III},10} \\
& - \frac{\bar{m}_1^2\,(3\,(y^2+1)\,\epsilon+1)+\bar{m}_2^2\,(3\,(y^2+1)\,\epsilon+1)+2\bar{m}_2\bar{m}_1 y(6\epsilon+1)}{24\bar{m}_1^4\bar{m}_2^4\,(y^2-1)^2\,\epsilon^3} f_{\text{III},1} \\
& + \frac{(2\epsilon+3)\,((\bar{m}_1^2+\bar{m}_2^2)\,y+2\bar{m}_1\bar{m}_2)}{12\bar{m}_1^4\bar{m}_2^4\,(y^2-1)^{3/2}\,\epsilon^3} f_{\text{III},3} \\
& + \frac{-(\bar{m}_1^2+\bar{m}_2^2)\,y-2\bar{m}_1\bar{m}_2}{\bar{m}_1^4\bar{m}_2^4\,(y^2-1)^{3/2}\,\epsilon^2} f_{\text{III},4} \\
& + \frac{-(\bar{m}_1^2+\bar{m}_2^2)\,y-2\bar{m}_1\bar{m}_2}{8\bar{m}_1^4\bar{m}_2^4\,(y^2-1)^{3/2}\,\epsilon^3} f_{\text{III},5} \\
& - \frac{\bar{m}_1^2\,(3\,(y^2+1)\,\epsilon+1)+\bar{m}_2^2\,(3\,(y^2+1)\,\epsilon+1)+2\bar{m}_2\bar{m}_1 y(6\epsilon+1)}{12\bar{m}_1^4\bar{m}_2^4\,(y^2-1)^2\,\epsilon^3} f_{\text{III},2} \\
& - \frac{\bar{m}_1^2\,(3\,(y^2+1)\,\epsilon+1)+\bar{m}_2^2\,(3\,(y^2+1)\,\epsilon+1)+2\bar{m}_2\bar{m}_1 y(6\epsilon+1)}{12\bar{m}_1^4\bar{m}_2^4\,(y^2-1)^2\,\epsilon^3} f_{\text{III},6} \\
& - \frac{(4\epsilon+3)\,(2\bar{m}_2\bar{m}_1 y+\bar{m}_1^2+\bar{m}_2^2)}{12\bar{m}_1^4\bar{m}_2^4\,(y^2-1)^2\,\epsilon^4} f_{\text{III},7}\Bigg\}\,,
\end{aligned}
\tag{3.125}
$$

where the first line is of order $1/q^2$, the second line is of order $1/|q|$, and the remaining lines are of order $|q|^0$, Since integration-by-parts will only produce analytic coefficients for master integrals, e.g. polynomials in q^2 but not $\sqrt{-q^2}$, the master integrals $f_{\mathrm{III},1}$ to $f_{\mathrm{III},7}$ appear in terms that are even in $|q|$ in the small-$|q|$ expansion of the amplitude, while $f_{\mathrm{III},8}$ to $f_{\mathrm{III},10}$ appear in expansion terms that are odd in $|q|$.

The differential equations for the master integrals are

$$\mathrm{d}\vec{f}_{\mathrm{III}} = \epsilon \left[A_{\mathrm{III},0}\,\mathrm{dlog}(x) + A_{\mathrm{III},+1}\,\mathrm{dlog}(x-1) + A_{\mathrm{III},-1}\,\mathrm{dlog}(x+1)\right] \vec{f}_{\mathrm{III}}\,. \tag{3.126}$$

The even- and odd-$|q|$ systems decouple and we can write

$$A_{\mathrm{III},i} = \begin{pmatrix} A^{(\mathrm{e})}_{\mathrm{III},i} & 0 \\ 0 & A^{(\mathrm{o})}_{\mathrm{III},i} \end{pmatrix}, \tag{3.127}$$

where the matrices are given by

$$A^{(\mathrm{e})}_{\mathrm{III},0} = \begin{pmatrix} 0 & 0 & 0 & 0 & 0 & 0 & 0 \\ -\frac{1}{2} & -6 & 0 & -1 & 0 & 0 & 0 \\ -\frac{3}{2} & 0 & 2 & -2 & 0 & 0 & 0 \\ 0 & 12 & 2 & 0 & 0 & 0 & 0 \\ -\frac{3}{4} & 0 & 0 & 0 & 0 & 0 & 0 \\ 0 & 0 & 0 & 0 & 0 & 0 & 0 \\ 0 & 0 & 1 & 0 & -2 & 0 & 0 \end{pmatrix}, \qquad A^{(\mathrm{e})}_{\mathrm{III},\pm1} = \begin{pmatrix} 0 & 0 & 0 & 0 & 0 & 0 & 0 \\ 0 & 6 & 0 & 0 & 0 & 0 & 0 \\ 0 & 0 & -2 & 0 & 0 & 0 & 0 \\ 0 & 0 & 0 & 0 & 0 & 0 & 0 \\ 0 & 0 & 0 & 0 & 0 & 0 & 0 \\ 0 & 0 & 0 & 0 & 0 & 0 & 0 \\ 0 & 0 & 0 & 0 & 0 & 0 & 0 \end{pmatrix}, \tag{3.128}$$

$$A^{(\mathrm{o})}_{\mathrm{III},0} = \begin{pmatrix} 0 & 0 & 0 \\ 0 & -2 & 0 \\ 0 & 1 & 0 \end{pmatrix}, \quad A^{(\mathrm{o})}_{\mathrm{III},+1} = \begin{pmatrix} 0 & 0 & 0 \\ 3 & 6 & 0 \\ 0 & 0 & 0 \end{pmatrix}, \quad A^{(\mathrm{o})}_{\mathrm{III},-1} = \begin{pmatrix} 0 & 0 & 0 \\ -3 & -2 & 0 \\ 0 & 0 & 0 \end{pmatrix}. \tag{3.129}$$

We make a technical observation here. Previously we found that at one loop x, is the only symbol letter. As a consequence only powers of $\log x$ will appear in the solutions to the differential equations. In contrast, at two loops, there are multiple symbol letters appearing in the differential equations in Eq. (3.126): $\{x, 1 \pm x\}$, so the symbol alphabet is larger. This generically results in the solution of the differential equations being (harmonic [285, 286]) polylogarithms, but we will see that at leading order in ϵ all two-loop integrals only contain logarithms.

Re-expansion in the potential region As described in subsection 3.3.3, we obtain boundary conditions for the pure basis of soft integrals by re-expanding the integrals in the potential region following Eqs. (3.79) and (3.80), and then integrate over energy components of loop momenta using an appropriate prescription [42]. The energy components of ℓ_1 and ℓ_2 are written as ω_1 and ω_2, while the spatial components are written as $\boldsymbol{\ell}_1$ and $\boldsymbol{\ell}_2$.

For the Roman III integral and non-planar variants with exactly three graviton propagators, we follow the prescription of Ref. [42], but with slight modifications to simplify the presentation. First, we symmetrize over 3! permutations of the energy components of the three gravitons, in a way that directly extends the one-loop prescription Eq. (3.96),

$$\int_{-\infty}^{\infty} \mathrm{d}\omega_1 \int_{-\infty}^{\infty} \mathrm{d}\omega_2 \, \mathcal{I}(\omega_1, \omega_2) \to \int_{-\infty}^{\infty} \mathrm{d}\omega_1 \int_{-\infty}^{\infty} \mathrm{d}\omega_2 \, \frac{1}{3!} \sum_{\eta \in S_3} \mathcal{I}(\omega_{\eta(1)}, \omega_{\eta(2)}) \,, \tag{3.130}$$

with the definition $\omega_3 = -(\omega_1 + \omega_2)$, and then proceed as usual, i.e. perform the ω_1 and ω_2 contour integrals one by one, closing the contour either above or below the real axis

and always neglecting poles at infinity. As an example, we calculate the static limit of $G_{1,0,1,0,1,1,1,0,0}$, which appears in $f_{\mathrm{III},6}$ in Eq. (3.120) and is shown in Fig. 3.12(d). In the $y=1$ i.e. static limit, the graviton propagators are turned into $(D-1)$-dimensional propagators,

$$\begin{aligned} G_{1,0,1,0,1,1,1,0,0}\big|_{y=1} = &-\int \frac{\mathrm{d}^{D-1}\boldsymbol{\ell}_1\, e^{\gamma_{\mathrm{E}}\epsilon}}{i\pi^{D/2}} \int \frac{\mathrm{d}^{D-1}\boldsymbol{\ell}_2\, e^{\gamma_{\mathrm{E}}\epsilon}}{i\pi^{D/2}} \frac{1}{\boldsymbol{\ell}_1^2 - i0} \frac{1}{\boldsymbol{\ell}_2^2 - i0} \frac{1}{(\boldsymbol{\ell}_1+\boldsymbol{\ell}_2+\boldsymbol{\ell}_3)^2 - i0} \\ &\times \int_{-\infty}^{\infty} \mathrm{d}\omega_1 \int_{-\infty}^{\infty} \mathrm{d}\omega_2 \frac{1}{(2\boldsymbol{\ell}_1\cdot\boldsymbol{u}_1 - 2\omega_1 u_1^0 - i0)} \frac{1}{(-2\boldsymbol{\ell}_2\cdot\boldsymbol{u}_1 + 2\omega_2 u_1^0 - i0)}\,. \end{aligned} \tag{3.131}$$

Again adopting the frame choice Eq. (3.95) with $u_1 = (\omega_1, \boldsymbol{u}_1) = (1, \boldsymbol{0})$, the second line of the above equation becomes

$$\frac{1}{4}\int_{-\infty}^{\infty} \mathrm{d}\omega_1 \int_{-\infty}^{\infty} \mathrm{d}\omega_2 \frac{1}{-\omega_1 - i0} \frac{1}{\omega_2 - i0}\,. \tag{3.132}$$

By the prescription Eq. (3.130), this divergent integral is turned into

$$\begin{aligned} &\frac{1}{4}\cdot\frac{1}{3!}\int_{-\infty}^{\infty} \mathrm{d}\omega_1 \int_{-\infty}^{\infty} \mathrm{d}\omega_2 \left(\frac{1}{-\omega_1 - i0} \frac{1}{\omega_2 - i0} + \frac{1}{-\omega_1 - i0} \frac{1}{-\omega_1 - \omega_2 - i0} \right. \\ &+ \frac{1}{-\omega_2 - i0} \frac{1}{-\omega_1 - \omega_2 - i0} + \frac{1}{-\omega_2 - i0} \frac{1}{\omega_1 - i0} + \frac{1}{\omega_1 + \omega_2 - i0} \frac{1}{\omega_1 - i0} \\ &\left. + \frac{1}{\omega_1 + \omega_2 - i0} \frac{1}{\omega_2 - i0} \right)\,. \end{aligned} \tag{3.133}$$

Now let us perform the ω_1 integral by picking up residues in the upper half plane. Only the 4th, 5th, and 6th terms in the bracket of Eq. (3.133) have ω_1 poles in the upper half plane, and in fact the 5th term contributes two poles whose residues add to zero. The result of ω_1 integration is

$$\frac{1}{4}\cdot\frac{1}{3!}(2\pi i)\int_{-\infty}^{\infty} \mathrm{d}\omega_2 \left(\frac{1}{-\omega_2 - i0} + \frac{1}{\omega_2 - i0} \right)\,. \tag{3.134}$$

Now we integrate over ω_2 by picking up residues in either the upper or lower half plane,

obtaining the same result

$$\frac{1}{4}\cdot\frac{1}{3!}(2\pi i)^2 = -\frac{\pi^2}{6}\,. \tag{3.135}$$

Putting it back into Eq. (3.131), we obtain

$$G_{1,0,1,0,1,1,1,0,0}\big|_{y=1} = \frac{\pi}{6}\int \frac{\mathrm{d}^{D-1}\boldsymbol{\ell}_1\mathrm{d}^{D-1}\boldsymbol{\ell}_2\,(e^{\gamma_{\mathrm{E}}\epsilon})^2}{(i\pi^{(D-1)/2})^2}\frac{1}{\boldsymbol{\ell}_1^2-i0}\,\frac{1}{\boldsymbol{\ell}_2^2-i0}\,\frac{1}{(\boldsymbol{\ell}_1+\boldsymbol{\ell}_2+\boldsymbol{\ell}_3)^2-i0}\,. \tag{3.136}$$

Now we check that the final result is also independent of the contour choice for ω_1. If instead we perform the ω_1 integral in Eq. (3.133) by picking up residues in the lower half plane, we obtain a result identical to Eq. (3.134), so the subsequent ω_2 integration also gives the same result as Eq. (3.135). In conclusion, we have verified in this example that once the S_3 symmetrization over graviton energies are performed, the subsequent energy integration has no dependence on contour choice (in the sense of closing above or below the real axis).

Adopting the frame choice Eq. (3.95), and following this prescription, we find that in the static limit, the only non-vanishing master integrals are equal $f^{(p)}_{\mathrm{III},4}, f^{(p)}_{\mathrm{III},6}, f^{(p)}_{\mathrm{III},7}$ and $f^{(p)}_{\mathrm{III},10}$. The computation of these integrals can be carried out by ordinary methods and is explained in Appendix 3.A. By expanding up to $\mathcal{O}(\epsilon^4)$ they yield the following vector of boundary conditions

$$\begin{aligned}\vec{f}^{(p)}_{\mathrm{III}}\Big|_{y=1} = (-q^2)^{-2\epsilon}\epsilon^2\pi^2\Bigg(&0,0,0,\frac{1}{3}-\frac{7\pi^2\epsilon^2}{18},0,-\frac{1}{6}+\frac{7\pi^2\epsilon^2}{36},\frac{1}{2}-\frac{\pi^2\epsilon^2}{12},\\ &0,0,\frac{i\pi\epsilon}{4}-\frac{i\pi\log(2)\epsilon^2}{2}\Bigg)^T+\mathcal{O}(\epsilon^5)\,.\end{aligned} \tag{3.137}$$

Result The solution of the differential equations (3.126) with the boundary conditions (3.137) and (3.162) is presented in Eqs. (3.313)–(3.318) in Appendix 3.B. Here we just note that all functions have an overall factor of $\pi^2\epsilon^2$ and therefore the transcendental weight of the solutions is effectively reduced by two. Consequently at the order considered, the only polylogarithmic function relevant is $\log(x)$ related to the arcsinh function characteristic of

3PM scattering [41, 42] by the change of variable Eq. (3.74),

$$\log(x) = -\log\left(y+\sqrt{y^2-1}\right) = -2\,\mathrm{arcsinh}\left(\sqrt{\frac{y-1}{2}}\right) = -2\,\mathrm{arcsinh}\left(\sqrt{\frac{\sigma-1}{2}}\right) + \mathcal{O}(q^2)\,. \tag{3.138}$$

Going to $\mathcal{O}(\epsilon^4)$ we find an additional weight-two function

$$\mathrm{Li}_2(1-x^2)\,, \tag{3.139}$$

which has no singularity in the entire range $0 < x < 1$, so has no singularity in either the static limit $y \to 1$ or the high-energy limit $y \to \infty$. Barring cancellations, it is natural to expect that this function will be relevant at $\mathcal{O}(G^4)$ (i.e. at the 4PM order).

Finally, inserting in Eq. (3.125) the values of the master integrals evaluated in the potential region, Eqs. (3.313)–(3.318), and changing variables according to Eqs. (3.67) and (3.72), the end result for the double-box integrals is

$$\begin{aligned} I^{(p)}_{\mathrm{III}} = -\frac{1}{(4\pi)^4}\left(\frac{-q^2}{\bar{\mu}^2}\right)^{-2\epsilon}\Bigg\{ & \frac{1}{(-q^2)}\frac{\pi^2}{2m_1^2m_2^2(\sigma^2-1)}\left[\frac{1}{\epsilon^2}-\frac{\pi^2}{6}+\frac{2}{3}\log^2(x)+\mathcal{O}(\epsilon)\right] \\ & + \frac{1}{\sqrt{-q^2}}\left[\frac{i\pi^3\,(m_1+m_2)}{2m_1^3m_2^3(\sigma-1)\sqrt{\sigma^2-1}}+\mathcal{O}(\epsilon)\right] \\ & + \left[-\frac{\pi^2\,(2m_2m_1\sigma+m_1^2+m_2^2)}{8m_1^4m_2^4\,(\sigma^2-1)^2}\frac{1}{\epsilon}+\mathcal{O}(\epsilon^0)\right]\Bigg\}\,. \end{aligned} \tag{3.140}$$

H and crossed H ($\overline{\mathrm{H}}$) Next we will consider the H integral, which can also be embedded in the family of indices in Eqs. (3.112) and (3.113) as shown in Fig. 3.14. We note that the case of equal masses has been evaluated in [287] without expansion in the soft or potential region. For this topology we only need the leading contribution in $|q|$, which is even in $|q|$. Therefore we only give the pure basis of ten master integrals needed to express the even-$|q|$

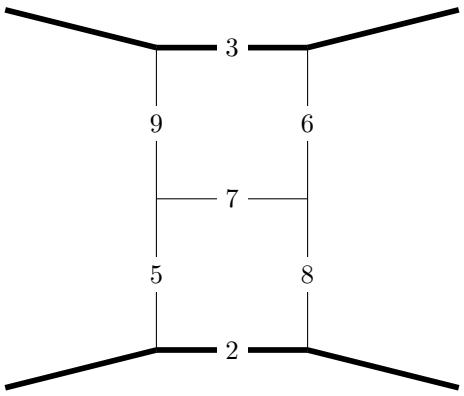

Figure 3.14: H topology. Indices correspond to the propagators listed in eq. (3.112).

terms[14],

$$f_{\mathrm{H},1} = \epsilon^2(-q^2)G_{0,0,0,0,0,0,1,2,2}\,, \tag{3.141}$$

$$f_{\mathrm{H},2} = \epsilon^2(1-4\epsilon)\,G_{0,0,2,0,1,0,1,1,0}\,, \tag{3.142}$$

$$f_{\mathrm{H},3} = \epsilon^2(-q^2)^2G_{0,0,0,0,2,1,0,1,2}\,, \tag{3.143}$$

$$f_{\mathrm{H},4} = \epsilon^4(-q^2)G_{0,1,1,0,1,1,0,1,1}\,, \tag{3.144}$$

$$f_{\mathrm{H},5} = \epsilon^4\sqrt{y^2-1}\,G_{0,1,1,0,0,0,1,1,1}\,, \tag{3.145}$$

$$f_{\mathrm{H},6} = \epsilon^3\sqrt{y^2-1}\,(-q^2)G_{0,1,1,0,0,0,2,1,1}\,, \tag{3.146}$$

$$f_{\mathrm{H},7} = -\epsilon^2(-q^2)G_{0,2,2,0,0,0,1,1,1} + \epsilon^3 y\,(-q^2)G_{0,1,1,0,0,0,2,1,1}\,, \tag{3.147}$$

$$f_{\mathrm{H},8} = \frac{\epsilon^2(4\epsilon-1)}{\sqrt{y^2-1}}\left[(2\epsilon-1)G_{0,1,1,0,0,1,1,0,1} + y\,G_{0,2,0,0,0,1,1,0,1}\right]\,, \tag{3.148}$$

$$f_{\mathrm{H},9} = \epsilon^4\sqrt{y^2-1}\,(-q^2)^2G_{0,1,1,0,1,1,1,1,1}\,, \tag{3.149}$$

$$\begin{aligned} f_{\mathrm{H},10} = {} & -\epsilon^4(-q^2)G_{-1,1,1,-1,1,1,1,1,1} + \frac{1}{2}\epsilon^2(2\epsilon-1)\,G_{0,0,0,0,1,1,0,1,1} \\ & + 2\epsilon^4 y\,(-q^2)G_{0,1,1,0,1,1,0,1,1} + \epsilon(3\epsilon-2)(3\epsilon-1)\,(-q^2)^{-1}G_{0,0,0,0,1,1,1,0,0}\,. \end{aligned} \tag{3.150}$$

[14]For reference, in the full equal-mass problem there are 25 master integrals [287].

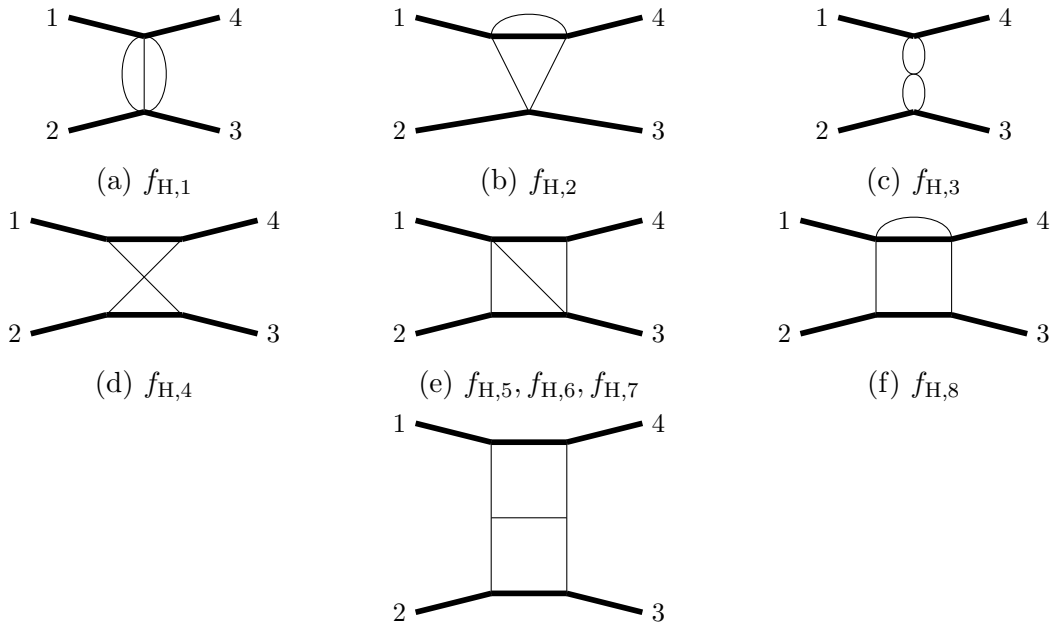

(a) $f_{\mathrm{H},1}$ (b) $f_{\mathrm{H},2}$ (c) $f_{\mathrm{H},3}$

(d) $f_{\mathrm{H},4}$ (e) $f_{\mathrm{H},5}, f_{\mathrm{H},6}, f_{\mathrm{H},7}$ (f) $f_{\mathrm{H},8}$

(g) $f_{\mathrm{H},9}, f_{\mathrm{H},10}$

Figure 3.15: Topologies relevant for the H master integrals.

The corresponding topologies are shown in Fig. 3.15. In terms of these the soft expansion of the H integral is simply given by

$$I_{\mathrm{H}} = -\frac{1}{(4\pi)^4}\left(\frac{1}{\bar{\mu}^2}\right)^{-2\epsilon}\left\{\frac{1}{(-q^2)^2}\frac{1}{\epsilon^4 \bar{m}_1 \bar{m}_2\sqrt{y^2-1}} f_{\mathrm{H},9} + \mathcal{O}\left((-q^2)^{-3/2-2\epsilon}\right)\right\}. \tag{3.151}$$

The differential equations for these master integrals are

$$\mathrm{d}\vec{f}_{\mathrm{H}} = \epsilon\left[A^{(e)}_{\mathrm{H},0}\,\mathrm{dlog}(x) + A^{(e)}_{\mathrm{H},+1}\,\mathrm{dlog}(x-1) + A^{(e)}_{\mathrm{H},-1}\,\mathrm{dlog}(x+1)\right]\vec{f}_{\mathrm{H}}\,, \tag{3.152}$$

where we have only kept the even-$|q|$ sector and the matrices are given by

$$A^{(\mathrm{e})}_{\mathrm{H},0} = \begin{pmatrix} 0 & 0 & 0 & 0 & 0 & 0 & 0 & 0 & 0 & 0 \\ 0 & 0 & 0 & 0 & 0 & 0 & 0 & 0 & 0 & 0 \\ 0 & 0 & 0 & 0 & 0 & 0 & 0 & 0 & 0 & 0 \\ 0 & 0 & 0 & 0 & 0 & 0 & 0 & 0 & 0 & 0 \\ -\frac{1}{2} & 0 & 0 & 0 & -6 & 0 & -1 & 0 & 0 & 0 \\ -\frac{3}{2} & 0 & 0 & 0 & 0 & 2 & -2 & 0 & 0 & 0 \\ 0 & 0 & 0 & 0 & 12 & 2 & 0 & 0 & 0 & 0 \\ 0 & 2 & 0 & 0 & 0 & 0 & 0 & 2 & 0 & 0 \\ 2 & -4 & 0 & 0 & 0 & 4 & 2 & 4 & 2 & -2 \\ -1 & 0 & -1 & 0 & 12 & 8 & 0 & 8 & 2 & -2 \end{pmatrix}, \tag{3.153}$$

$$A^{(\mathrm{e})}_{\mathrm{H},\pm 1} = \begin{pmatrix} 0 & 0 & 0 & 0 & 0 & 0 & 0 & 0 & 0 & 0 \\ 0 & 0 & 0 & 0 & 0 & 0 & 0 & 0 & 0 & 0 \\ 0 & 0 & 0 & 0 & 0 & 0 & 0 & 0 & 0 & 0 \\ 0 & 0 & 0 & 0 & 0 & 0 & 0 & 0 & 0 & 0 \\ 0 & 0 & 0 & 0 & 6 & 0 & 0 & 0 & 0 & 0 \\ 0 & 0 & 0 & 0 & 0 & -2 & 0 & 0 & 0 & 0 \\ 0 & 0 & 0 & 0 & 0 & 0 & 0 & 0 & 0 & 0 \\ 0 & 0 & 0 & 0 & 0 & 0 & 0 & -2 & 0 & 0 \\ 0 & 0 & 0 & 0 & 0 & -4 & 0 & -4 & -2 & 0 \\ 1 & 0 & 1 & \pm 4 & 0 & 0 & 0 & 0 & 0 & 2 \end{pmatrix}. \tag{3.154}$$

We also need to consider the crossed H, or $\overline{\mathrm{H}}$, integral, in Fig. 3.6(b), which is just a crossing of the $\overline{\mathrm{H}}$ integral by $p_2 \leftrightarrow -p_3$. We note, however, that the H and $\overline{\mathrm{H}}$ integrals appear together in the amplitude, with the same coefficient[15]. Thus we can directly evaluate their

[15]This is even true for the pure gravity amplitude [41, 42] with an appropriate alignment of loop momentum labels across the two different diagrams, up to differences that only give quantum corrections.

sum. Since the crossing $p_1 \leftrightarrow -p_4$ is equivalent to $p_2 \leftrightarrow -p_3$, this can be written in the symmetrized form

$$I_{\rm H} + I_{\overline{\rm H}} = \frac{1}{2}\left(I_{\rm H} + I_{\rm H}\big|_{p_2\leftrightarrow -p_3} + I_{\rm H}\big|_{p_1\leftrightarrow -p_4} + I_{\rm H}\big|_{p_2\leftrightarrow -p_3,\, p_1\leftrightarrow -p_4}\right). \tag{3.155}$$

As mentioned above, we only need to perform the soft expansion of H and $\overline{\rm H}$ to the leading order, due to the suppression by $t^2 = q^4$ factor in the numerator, and subleading corrections are not relevant classically. The leading soft expansion of Eq. (3.155) can be obtained from that of the H integral itself by the replacements

$$\frac{1}{\rho_1 + i0} \to \frac{1}{\rho_1 + i0} + \frac{1}{-\rho_1 + i0} = (-2\pi i)\delta(\rho_1), \tag{3.156}$$

$$\frac{1}{\rho_2 + i0} \to \frac{1}{\rho_2 + i0} + \frac{1}{-\rho_2 + i0} = (-2\pi i)\delta(\rho_2), \tag{3.157}$$

followed by multiplying the resulting expression by 1/2. Effectively we have "cut" the matter propagators and turned them into delta functions. However, we still need to define how to "cut" matter propagators raised to higher powers, because integrals with squared matter propagators appear when we construct differential equations, and also appear in our choice of a pure basis of master integrals Eqs. (3.141)–(3.150). An appropriate prescription is

$$G_{i_1,i_2,\ldots,i_9} \to \hat{G}_{i_1,i_2,\ldots,i_9}, \tag{3.158}$$

with the definition

$$\begin{aligned}\hat{G}_{i_1,\,i_2,\ldots,i_9} = \frac{1}{2}\int \mathrm{d}^D\ell_1 \int \mathrm{d}^D\ell_2 \frac{1}{\rho_3^{i_3}\rho_4^{i_4}\cdots\rho_9^{i_9}} \\ \times \left[\frac{1}{(-\rho_1 + i0)^{i_1}} - \frac{1}{(-\rho_1 - i0)^{i_1}}\right]\left[\frac{1}{(-\rho_2 + i0)^{i_2}} - \frac{1}{(-\rho_2 - i0)^{i_2}}\right].\end{aligned} \tag{3.159}$$

Here $\hat{G}_{i_1,\,i_2,\ldots,i_9}$ vanishes whenever the integer i_1 or i_2 is non-positive, because the $i0$ pre-

scription is of no relevance in the numerator, and the terms in one of the square brackets of Eq. (3.159) add to zero. The advantage of this prescription is that it preserves IBP relations and the differential equations Eq. (3.152). In particular, the pure basis of master integrals for the H topology, Eqs. (3.141)–(3.150) can be mapped to the "cut" version

$$f_{\mathrm{H},n} \to f_{\mathrm{cH,n}}, \quad 1 \leq n \leq 10, \tag{3.160}$$

using Eqs. (3.158) and (3.159), and the resulting integrals satisfy differential equations

$$\mathrm{d}\vec{f}_{\mathrm{cH}} = \epsilon \left[A_{\mathrm{cH},0}\, \mathrm{dlog}(x) + A_{\mathrm{cH},+1}\, \mathrm{dlog}(x-1) + A_{\mathrm{cH},-1}\, \mathrm{dlog}(x+1)\right] \vec{f}_{\mathrm{cH}}\,, \tag{3.161}$$

where the matrices, $A_{i,\mathrm{cH}}$, are identical to the ones in Eqs. (3.152) and (3.153) for the differential equations of the original uncut H topology. Hence the solution of the "cut H" differential equations will only differ from the full H in the boundary conditions.

In order to obtain the boundary conditions for the "cut H" integrals, we follow a prescription for performing the energy integrals similar to that in the previous subsection. In this case, the prescription is simply to carry out the ω_1 integral by residues, and then performing the ω_2 integral by residues too. Each of the two integration steps is done by closing the contour either above or below the real axis, picking up residues from poles at finite values and discarding poles at infinity. We find that the only non-vanishing master integrals in the static limit are $f^{(p)}_{\mathrm{cH},4}, f^{(p)}_{\mathrm{cH},7}$ and $f^{(p)}_{\mathrm{cH},10}$. The computation of these integrals is explained in Appendix 3.A. By expanding up to $\mathcal{O}(\epsilon^4)$ they yield the following vector of boundary condition

$$\vec{f}^{(p)}_{\mathrm{cH}}\Big|_{y=1} = (-q^2)^{-2\epsilon}\epsilon^2\pi^2 \left(0,0,0,\frac{\pi^2\epsilon^2}{2},0,0,-\frac{1}{2}+\frac{7\pi^2\epsilon^2}{12},0,0,\pi^2\epsilon^2\right)^T + \mathcal{O}(\epsilon^5)\,. \tag{3.162}$$

The result of solving the differential equation in Eq. (3.161) with the boundary conditions in Eq. (3.162) is given in Eqs. (3.319)–(3.324) in Appendix 3.B. The sum of H and $\overline{\mathrm{H}}$ is given

by Eq. (3.151) with the replacement $f_{\mathrm{H},9} \to f_{\mathrm{cH},9}$, which using the solution of the differential equation yields

$$I_{\mathrm{H}} + I_{\overline{\mathrm{H}}} = -\frac{1}{(4\pi)^4}\left(\frac{-q^2}{\bar{\mu}^2}\right)^{-2\epsilon}\left\{\frac{1}{(-q^2)^2}\left[\frac{2\pi^2}{\epsilon}\frac{\operatorname{arcsinh}\sqrt{\frac{\sigma-1}{2}}}{m_1 m_2\sqrt{\sigma^2-1}} + \mathcal{O}(\epsilon^0)\right] + \mathcal{O}((-q)^{-3/2})\right\}. \tag{3.163}$$

The part of Eq. (3.163), proportional to $\log(-q^2)$, which due to the q^4 suppression in the numerator is the only piece relevant for the classical dynamics, agrees with the result in Refs. [41, 42].

Non-planar double-box (IX) Next we discuss the non-planar ladder integral. We only consider the IX topology, noting that the integral XI is identical. The full integral has been discussed in the equal mass case in Ref. [288]. We first consider generic integrals of the form

$$\tilde{G}_{i_1,i_2,\ldots,i_9} = \int \frac{\mathrm{d}^D\ell_1\, e^{\gamma_{\mathrm{E}}\epsilon}}{i\pi^{D/2}} \int \frac{\mathrm{d}^D\ell_2\, e^{\gamma_{\mathrm{E}}\epsilon}}{i\pi^{D/2}} \frac{1}{\rho_1^{i_1}\rho_2^{i_2}\cdots\rho_9^{i_9}}\,. \tag{3.164}$$

Where the propagators are, as depicted in Fig. 3.16

$$\begin{aligned}
&\tilde{\rho}_1 = (\ell_1 - p_1)^2 - m_1^2\,, && \tilde{\rho}_2 = (\ell_1 + p_2)^2 - m_2^2\,, && \tilde{\rho}_3 = (\ell_2 - p_4)^2 - m_1^2\,,\\
&\tilde{\rho}_4 = (\ell_1 + \ell_2 - q - p_3)^2 - m_2^2\,, && \tilde{\rho}_5 = \ell_1^2\,, && \tilde{\rho}_6 = \ell_2^2\,,\\
&\tilde{\rho}_7 = (\ell_1 + \ell_2 - q)^2\,, && \tilde{\rho}_8 = (\ell_1 - q)^2\,, && \tilde{\rho}_9 = (\ell_2 - q)^2\,.
\end{aligned} \tag{3.165}$$

The small-$|q|$ expansion consists of integrals of the form

$$G_{i_1,\,i_2,\ldots,i_9} = \int \frac{\mathrm{d}^D\ell_1\, e^{\gamma_{\mathrm{E}}\epsilon}}{i\pi^{D/2}} \int \frac{\mathrm{d}^D\ell_2\, e^{\gamma_{\mathrm{E}}\epsilon}}{i\pi^{D/2}} \frac{1}{\rho_1^{i_1}\rho_2^{i_2}\ldots\rho_9^{i_9}}, \tag{3.166}$$

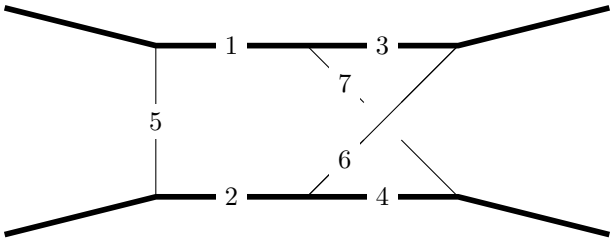

(a) Non-planar double-box topology.

Figure 3.16: Top-level topologies at two-loops. Indices correspond to the propagators listed in eq. (3.165).

where the leading order parts of the propagators are

$$\begin{aligned}
&\rho_1 = 2\,\ell_1 \cdot u_1\,, && \rho_2 = -2\,\ell_1 \cdot u_2\,, && \rho_3 = -2\,\ell_2 \cdot u_1\,,\\
&\rho_4 = -2\,(\ell_1 + \ell_2) \cdot u_2\,, && \rho_5 = \ell_1^2\,, && \rho_6 = \ell_2^2\,,\\
&\rho_7 = (\ell_1 + \ell_2 - q)^2\,, && \rho_8 = (\ell_1 - q)^2\,, && \rho_9 = (\ell_2 - q)^2\,.
\end{aligned} \tag{3.167}$$

A pure basis of master integrals is given by

$$f_{\text{IX},1} = \epsilon^2(-q^2)G_{0,0,0,0,2,2,1,0,0}\,, \tag{3.168}$$

$$f_{\text{IX},2} = \epsilon^4\sqrt{y^2-1}\,G_{0,0,1,1,1,1,1,0,0}\,, \tag{3.169}$$

$$f_{\text{IX},3} = \epsilon^3(-q^2)\sqrt{y^2-1}\,G_{0,0,1,1,2,1,1,0,0}\,, \tag{3.170}$$

$$f_{\text{IX},4} = \epsilon^2(-q^2)G_{0,0,2,2,1,1,1,0,0} + \epsilon^3(-q^2)yG_{0,0,1,1,2,1,1,0,0}\,, \tag{3.171}$$

$$f_{\text{IX},5} = \epsilon^4\sqrt{y^2-1}\,G_{0,1,1,0,1,1,1,0,0}\,, \tag{3.172}$$

$$f_{\text{IX},6} = \epsilon^3(-q^2)\sqrt{y^2-1}\,G_{0,1,1,0,1,1,2,0,0}\,, \tag{3.173}$$

$$f_{\text{IX},7} = \epsilon^2(-q^2)G_{0,2,2,0,1,1,1,0,0} - \epsilon^3(-q^2)y\,G_{0,1,1,0,1,1,2,0,0}\,, \tag{3.174}$$

$$f_{\text{IX},8} = \epsilon^3(1-6\epsilon)G_{1,0,1,0,1,1,1,0,0}\,, \tag{3.175}$$

$$f_{\text{IX},9} = \epsilon^3(-q^2)\sqrt{y^2-1}\,G_{1,1,0,0,1,1,2,0,0}\,, \tag{3.176}$$

$$f_{\text{IX},10} = \epsilon^4(-q^2)(y^2-1)G_{1,1,1,1,1,1,1,0,0}\,, \tag{3.177}$$

$$f_{\text{IX},11} = \epsilon^3\sqrt{-q^2}G_{1,0,0,0,1,1,2,0,0}\,, \tag{3.178}$$

$$f_{\text{IX},12} = \epsilon^3\sqrt{-q^2}G_{0,2,1,0,1,1,1,0,0}\,, \tag{3.179}$$

$$f_{\text{IX},13} = \epsilon^3\sqrt{-q^2}G_{0,0,2,1,1,1,1,0,0}\,, \tag{3.180}$$

$$f_{\text{IX},14} = \epsilon^4\sqrt{-q^2}\sqrt{y^2-1}G_{1,0,1,1,1,1,1,0,0}\,, \tag{3.181}$$

$$f_{\text{IX},15} = \epsilon^4\sqrt{-q^2}\sqrt{y^2-1}G_{1,1,1,0,1,1,1,0,0}\,, \tag{3.182}$$

where the corresponding topologies are shown in Fig. 3.17 and Fig. 3.18. The functions $f_{\text{IX},1}$ to $f_{\text{IX},10}$ are even in $|q|$, while $f_{\text{IX},11}$ to $f_{\text{IX},15}$ are odd. In addition some of the functions are related by $y \to -y$ due to symmetry

$$\{f_{\text{IX},2}, f_{\text{IX},3}, f_{\text{IX},4}, f_{\text{IX},12}\} \overset{y\to -y}{\longrightarrow} \{f_{\text{IX},5}, f_{\text{IX},6}, f_{\text{IX},7}, f_{\text{IX},13}\}\,. \tag{3.183}$$

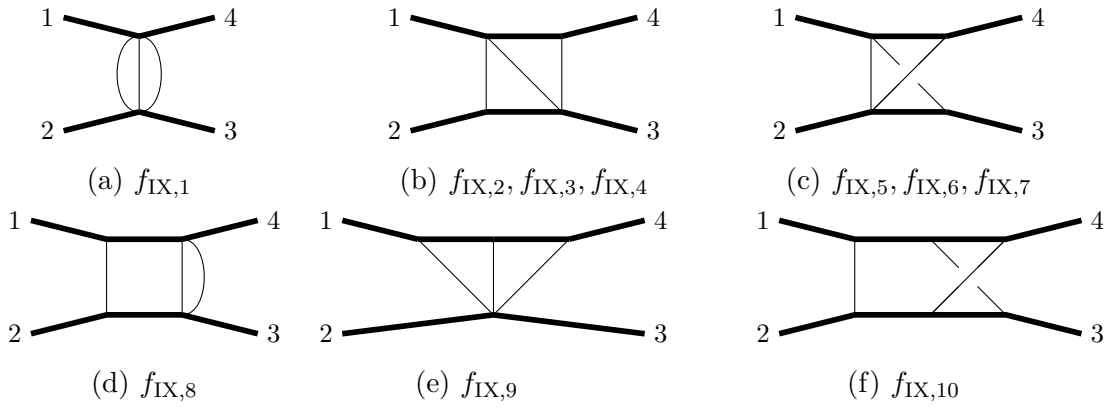

(a) $f_{\text{IX},1}$ (b) $f_{\text{IX},2}, f_{\text{IX},3}, f_{\text{IX},4}$ (c) $f_{\text{IX},5}, f_{\text{IX},6}, f_{\text{IX},7}$

(d) $f_{\text{IX},8}$ (e) $f_{\text{IX},9}$ (f) $f_{\text{IX},10}$

Figure 3.17: Even $|q|$ master integrals relevant for the crossed ladder topology.

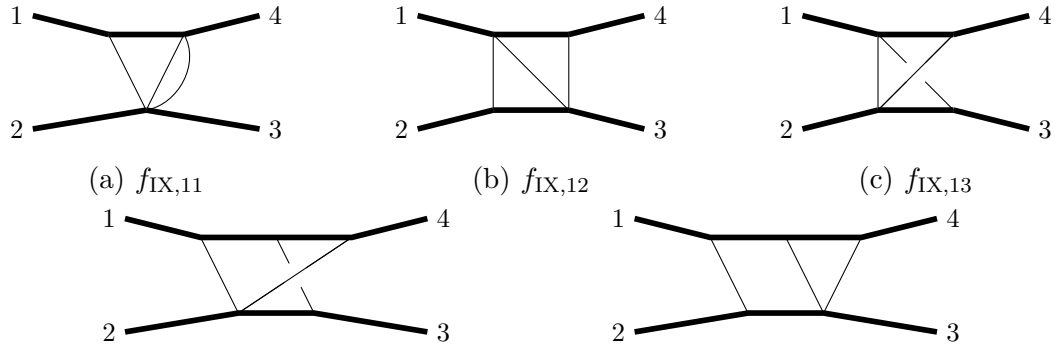

(a) $f_{\text{IX},11}$ (b) $f_{\text{IX},12}$ (c) $f_{\text{IX},13}$

(d) $f_{\text{IX},14}$ (e) $f_{\text{IX},15}$

Figure 3.18: Odd $|q|$ master integrals relevant for the crossed ladder topology.

The differential equations are

$$\mathrm{d}\vec{f}_{\text{IX}} = \epsilon \left[A_{\text{IX},0}\, \mathrm{dlog}(x) + A_{\text{IX},+1}\, \mathrm{dlog}(x-1) + A_{\text{IX},-1}\, \mathrm{dlog}(x+1)\right] \vec{f}_{\text{IX}}. \tag{3.184}$$

The even- and odd-$|q|$ systems decouple and we can write

$$A_{\text{IX},i} = \begin{pmatrix} A^{(\text{e})}_{\text{IX},i} & 0 \\ 0 & A^{(\text{o})}_{\text{IX},i} \end{pmatrix}, \tag{3.185}$$

where the matrices are given by

$$A^{(o)}_{\mathrm{IX},0} = \begin{pmatrix} 0 & 0 & 0 & 0 & 0 \\ 0 & -2 & 0 & 0 & 0 \\ 0 & 0 & -2 & 0 & 0 \\ 0 & -1 & 1 & 0 & 0 \\ 0 & 1 & 0 & 0 & 0 \end{pmatrix}, A^{(o)}_{\mathrm{IX},+1} = \begin{pmatrix} 0 & 0 & 0 & 0 & 0 \\ 3 & 6 & 0 & 0 & 0 \\ -3 & 0 & -2 & 0 & 0 \\ 0 & 0 & 0 & 0 & 0 \\ 0 & 0 & 0 & 0 & 0 \end{pmatrix}, \tag{3.186}$$

$$A^{(o)}_{\mathrm{IX},-1} = \begin{pmatrix} 0 & 0 & 0 & 0 & 0 \\ -3 & -2 & 0 & 0 & 0 \\ 3 & 0 & 6 & 0 & 0 \\ 0 & 0 & 0 & 0 & 0 \\ 0 & 0 & 0 & 0 & 0 \end{pmatrix}, \tag{3.187}$$

$$A^{(\mathrm{e})}_{\mathrm{IX},0} = \begin{pmatrix} 0 & 0 & 0 & 0 & 0 & 0 & 0 & 0 & 0 & 0 \\ \frac{1}{2} & -6 & 0 & -1 & 0 & 0 & 0 & 0 & 0 & 0 \\ \frac{3}{2} & 0 & 2 & -2 & 0 & 0 & 0 & 0 & 0 & 0 \\ 0 & 12 & 2 & 0 & 0 & 0 & 0 & 0 & 0 & 0 \\ -\frac{1}{2} & 0 & 0 & 0 & -6 & 0 & 1 & 0 & 0 & 0 \\ -\frac{3}{2} & 0 & 0 & 0 & 0 & 2 & 2 & 0 & 0 & 0 \\ 0 & 0 & 0 & 0 & -12 & -2 & 0 & 0 & 0 & 0 \\ 0 & 0 & 0 & 0 & 0 & 0 & 0 & 0 & 0 & 0 \\ -\frac{3}{4} & 0 & 0 & 0 & 0 & 0 & 0 & 0 & 0 & 0 \\ 0 & 0 & -\frac{1}{2} & 0 & 0 & -1 & 0 & 0 & 1 & 0 \end{pmatrix}, \tag{3.188}$$

$$A^{(\mathrm{e})}_{\mathrm{IX},\pm1} = \begin{pmatrix} 0 & 0 & 0 & 0 & 0 & 0 & 0 & 0 & 0 & 0 \\ 0 & 6 & 0 & 0 & 0 & 0 & 0 & 0 & 0 & 0 \\ 0 & 0 & -2 & 0 & 0 & 0 & 0 & 0 & 0 & 0 \\ 0 & 0 & 0 & 0 & 0 & 0 & 0 & 0 & 0 & 0 \\ 0 & 0 & 0 & 0 & 6 & 0 & 0 & 0 & 0 & 0 \\ 0 & 0 & 0 & 0 & 0 & -2 & 0 & 0 & 0 & 0 \\ 0 & 0 & 0 & 0 & 0 & 0 & 0 & 0 & 0 & 0 \\ 0 & 0 & 0 & 0 & 0 & 0 & 0 & 0 & 0 & 0 \\ 0 & 0 & 0 & 0 & 0 & 0 & 0 & 0 & 0 & 0 \\ 0 & 0 & 0 & 0 & 0 & 0 & 0 & 0 & 0 & 0 \end{pmatrix}. \tag{3.189}$$

We proceed by computing the boundary condition in the static limit analogously to the planar ladder discussed above. As before the integrals in this limit are evaluated using the residue method, yielding three-dimensional integrals tabulated in Appendix 3.A. Only the

functions f_4, f_7, f_8 and f_{15} are non-vanishing on the boundary and we have

$$\vec{f}^{(p)}_{\rm IX}\Big|_{y=1} = (-q^2)^{-2\epsilon}\epsilon^2\pi^2 \left(0,0,0,-\frac{1}{6}+\frac{7\pi^2\epsilon^2}{36},0,0,\frac{1}{3}-\frac{7\pi^2\epsilon^2}{18},-\frac{1}{6}+\frac{7\pi^2\epsilon^2}{36},0,0, \right. \tag{3.190}$$

$$\left. 0,0,0,0,\frac{i\pi\epsilon}{4}-\frac{i\pi\log(2)\epsilon^2}{2}\right)^T + \mathcal{O}(\epsilon^5)\,. \tag{3.191}$$

Solving the differential equation (3.184) with the boundary conditions (3.191) up to $\mathcal{O}(\epsilon^4)$ gives the result in Eqs. (3.325)–(3.333) in Appendix 3.B. These can be used in the soft expansion of the IX integral to yield the following result for the non-planar double-box integral $I_{\rm IX}$

$$\begin{aligned} I^{(p)}_{\rm IX} = I^{(p)}_{\rm XI} = -\frac{1}{(4\pi)^2}\left(\frac{-q^2}{\bar{\mu}^2}\right)^{-2\epsilon}\Bigg\{ & \frac{1}{(-q^2)}\frac{\pi^2}{2m_1^2m_2^2(\sigma^2-1)}\left[-\frac{5}{6}\log^2(x)+\mathcal{O}(\epsilon)\right] \\ & + \frac{1}{\sqrt{-q^2}}\left[-\frac{i\pi^3\,(m_1+m_2)}{4m_1^3m_2^3(\sigma+1)\sqrt{\sigma^2-1}}+\mathcal{O}(\epsilon)\right] \\ & + (-q^2)^0\Big[0+\mathcal{O}(\epsilon^0)\Big]\Bigg\}\,. \end{aligned} \tag{3.192}$$

Crossed integrals In order to evaluate the integrand (3.51) we also need the integrals that that are obtained from III and IX by $p_2 \to p_3$ crossing (denoted $\overline{\rm III}$ and $\overline{\rm IX}$). Since the energy integration step produces non-analytic behavior, these integrals cannot be directly obtained from analytic continuation, and we have to solve the differential equations again. From Eq. (3.74), we can see that $x \to -x$ corresponds to the change $y \to -y$, $\sqrt{y^2-1} \to -\sqrt{y^2-1}$. The differential equations for the crossed integrals are thus obtained from the differential equations for the original integrals, Eqs. (3.126) and (3.184), when we change the LHS by

$$\vec{f}_{\rm T} \to \vec{f}_{\bar{\rm T}}, \quad u_1^\mu \to u_1^\mu,\, u_2^\mu \to -u_2^\mu,\, y \to -y,\, \sqrt{y^2-1} \to -\sqrt{y^2-1}, \tag{3.193}$$

where $\mathrm{T} \in \mathrm{III}, \mathrm{IX}$ denotes the topology, and change the RHS by

$$\log(x) \to \log(x)\,, \quad \log(1-x) \to \log(1+x)\,, \quad \log(1+x) \to \log(1-x)\,. \tag{3.194}$$

The static boundary conditions for $\overline{\mathrm{III}}$ and $\overline{\mathrm{IX}}$ integrals are obtained by the same energy integration method covered before, and are explicitly given by

$$\vec{f}^{(p)}_{\overline{\mathrm{III}}}\Big|_{y=1} = (-q^2)^{-2\epsilon}\epsilon^2\pi^2 \left(0,0,0,-\frac{1}{6}+\frac{7\pi^2\epsilon^2}{36},0,-\frac{1}{6}+\frac{7\pi^2\epsilon^2}{36},0,0,0,0\right)^T + \mathcal{O}(\epsilon^5)\,, \tag{3.195}$$

$$\begin{aligned}\vec{f}^{(p)}_{\overline{\mathrm{IX}}}\Big|_{y=1} = (-q^2)^{-2\epsilon}\epsilon^2\pi^2 \Bigg(&0,0,0,\frac{1}{3}-\frac{7\pi^2\epsilon^2}{18},0,0,-\frac{1}{6}+\frac{7\pi^2\epsilon^2}{36},-\frac{1}{6}+\frac{7\pi^2\epsilon^2}{36},0,0,\\ &0,0,0,0,0\Bigg)^T + \mathcal{O}(\epsilon^5)\,.\end{aligned} \tag{3.196}$$

Solving the differential equations obtained by crossing of Eqs. (3.126) and (3.184) with the boundary conditions (3.195) and (3.196) gives the result in Eqs. (3.334)–(3.338) and (3.334)–(3.338) in Appendix 3.B. These can be used in the soft expansion of the crossed double-box and non-planar double-box integrals which gives especially simple final results,

$$\begin{aligned}I^{(p)}_{\overline{\mathrm{III}}} = -\frac{1}{(4\pi)^2}\left(\frac{-q^2}{\bar{\mu}^2}\right)^{-2\epsilon}\Bigg\{&\frac{1}{(-q^2)}\frac{\pi^2}{2m_1^2m_2^2(\sigma^2-1)}\left[-\frac{1}{3}\log^2(x)+\mathcal{O}(\epsilon)\right]\\ &+\frac{1}{\sqrt{-q^2}}\left[0+\mathcal{O}(\epsilon)\right]\\ &+(-q^2)^0\left[0+\mathcal{O}(\epsilon^0)\right]\Bigg\}\,,\end{aligned} \tag{3.197}$$

and

$$I^{(p)}_{\overline{\text{IX}}} = I^{(p)}_{\overline{\text{XI}}} = -\frac{1}{(4\pi)^2}\left(\frac{-q^2}{\bar{\mu}^2}\right)^{-2\epsilon}\left\{\frac{1}{(-q^2)}\frac{\pi^2}{2m_1^2m_2^2(\sigma^2-1)}\left[\frac{2}{3}\log^2(x)+\mathcal{O}(\epsilon)\right]\right.$$
$$+\frac{1}{\sqrt{-q^2}}\left[0+\mathcal{O}(\epsilon)\right]$$
$$\left.+(-q^2)^0\left[0+\mathcal{O}(\epsilon^0)\right]\right\}. \tag{3.198}$$

3.3.4 Scattering amplitudes in the potential region

In the previous subsection we calculated the integrals necessary to evaluate the one- and two-loop conservative amplitudes in the potential region, which we will denote by $M_{4,(p)}$. In this subsection we will put together the integrals to construct such scattering amplitudes.

Tree-level amplitude

For completeness, let us start by considering the tree-level amplitude in Eq. (3.43). In this case the restriction to the potential region is trivial and we simply have

$$M^{\text{tree}}_{4,(p)} = 32\pi G m_1^2 m_2^2(\sigma-\cos\phi)^2\frac{1}{-q^2}\,, \tag{3.199}$$

which we have written in a form which will be convenient later.

One-loop amplitude

The one-loop integrand for the conservative black-hole amplitude in $\mathcal{N}=8$ supergravity is given in terms of the sum of the box and crossed box integrals in the potential region,

$$M^{\text{1-loop}}_{4,(p)} = -i(8\pi G)^2\,(s-|m_1+m_2e^{i\phi}|^2)^4\,\big(\,I^{(p)}_{\text{II}}+I^{(p)}_{\text{X}}\,\big)\,. \tag{3.200}$$

From the results in Eqs. (3.105) and (3.110) we find

$$
\begin{aligned}
I_{\rm II}^{(p)} + I_{\rm X}^{(p)} = \frac{i}{(4\pi)^2}\left(\frac{-q^2}{\bar{\mu}^2}\right)^{-\epsilon}\Bigg\{ & \frac{1}{(-q^2)}\frac{i\pi}{2m_1m_2\sqrt{\sigma^2-1}}\frac{e^{\epsilon\gamma_{\rm E}}\Gamma(-\epsilon)^2\Gamma(1+\epsilon)}{\Gamma(-2\epsilon)} \\
& - \epsilon\frac{1}{\sqrt{-q^2}}\frac{\sqrt{\pi}(m_1+m_2)}{m_1^2m_2^2(\sigma^2-1)}\frac{e^{\epsilon\gamma_{\rm E}}\Gamma\left(\frac{1}{2}-\epsilon\right)^2\Gamma\left(\epsilon+\frac{1}{2}\right)}{\Gamma(1-2\epsilon)} \\
& - \epsilon\frac{i\pi\left(m_1^2+m_2^2+2m_1m_2\sigma\right)}{8m_1^3m_2^3\left(\sigma^2-1\right)^{3/2}}\frac{e^{\epsilon\gamma_{\rm E}}\Gamma(-\epsilon)^2\Gamma(1+\epsilon)}{\Gamma(-2\epsilon)} \\
& + \mathcal{O}\left(\sqrt{-q^2}\right)\Bigg\}.
\end{aligned}
\tag{3.201}
$$

Note that this formula is valid in arbitrary dimension. In particular it agrees with the soft-integrals in Eqs. (B.36) and (B.40) of Ref. [192]. This reference also calculated the contribution in the potential region at leading order in velocity, which, as expected, did not match the full soft integrals away from the static limit. It is well known that the contributions of soft and potential region coincide at one loop in $D = 4$, up to differences that are suppressed in the classical limit. Our result shows that this is also true in arbitrary dimensions. As a cross-check we have also calculated the result directly in the soft region, by solving the differential equations for the soft integrals subject to their full boundary conditions without restricting to the potential region, and found agreement to $\mathcal{O}(\epsilon^0)$ for both the $1/(-q^2)$ coefficient and the $1/\sqrt{-q^2}$ coefficient. Details will be given elsewhere.

With the sum of the boxes at hand we can evaluate the one-loop amplitude (3.47) with the result

$$
\begin{aligned}
M_{4,(p)}^{\text{1-loop}} = 64G^2\, m_1^3m_2^3(\sigma-\cos\phi)^4\left(\frac{-q^2}{\bar{\mu}^2}\right)^{-\epsilon}\Bigg\{ & \frac{1}{(-q^2)}\frac{i\pi}{2\sqrt{\sigma^2-1}}\frac{e^{\epsilon\gamma_{\rm E}}\Gamma(-\epsilon)^2\Gamma(1+\epsilon)}{\Gamma(-2\epsilon)} \\
& - \epsilon\frac{1}{\sqrt{-q^2}}\frac{\sqrt{\pi}(m_1+m_2)}{m_1m_2(\sigma^2-1)}\frac{e^{\epsilon\gamma_{\rm E}}\Gamma\left(\frac{1}{2}-\epsilon\right)^2\Gamma\left(\epsilon+\frac{1}{2}\right)}{\Gamma(1-2\epsilon)} \\
& - \epsilon\frac{i\pi\left(m_1^2+m_2^2+2m_1m_2\sigma\right)}{8m_1^2m_2^2\left(\sigma^2-1\right)^{3/2}}\frac{e^{\epsilon\gamma_{\rm E}}\Gamma(-\epsilon)^2\Gamma(1+\epsilon)}{\Gamma(-2\epsilon)} + \mathcal{O}\left(\sqrt{-q^2}\right)\Bigg\}.
\end{aligned}
\tag{3.202}
$$

Two-loop amplitude

Next we use the integrals in subsection 3.3.3 to assemble the two-loop amplitude. The two-loop amplitude in the potential region is given by

$$M_{4,(p)}^{\text{2-loop}} = (8\pi G)^3 (s - |m_1 + m_2 e^{i\phi}|^2)^4 \times \left[(s - |m_1 + m_2 e^{i\phi}|^2)^2 (I_{\text{III}}^{(p)} + I_{\text{XI}}^{(p)} + I_{\text{IX}}^{(p)} + I_{\overline{\text{III}}}^{(p)} + I_{\overline{\text{XI}}}^{(p)} + I_{\overline{\text{IX}}}^{(p)}) + (-q^2)^2 (I_{\text{H}}^{(p)} + I_{\overline{\text{H}}}^{(p)}) \right]. \tag{3.203}$$

where the remaining integrals are suppressed in the classical limit. Naively, the ladders and crossed ladders appear with different prefactor in (3.51). We have

$$u - |m_1 - m_2 e^{i\phi}|^2 = -s + |m_1 + m_2 e^{i\phi}|^2 - q^2 \,, \tag{3.204}$$

so the $\mathcal{O}(|q|^2)$ mismatch could in principle combine with the leading order of the crossed ladders which are of $\mathcal{O}(|q|^{-2})$. The explicit results for this integrals in Eqs. (3.197) and (3.198) shows however that these do not contribute to the classical part of the amplitude and all the ladders contribute with the same coefficient. Using Eqs. (3.140), (3.192), (3.197), and (3.198) the relevant combination of ladders is then

$$\begin{aligned}
&I_{\text{III}}^{(p)} + I_{\text{XI}}^{(p)} + I_{\text{IX}}^{(p)} + I_{\overline{\text{III}}}^{(p)} + I_{\overline{\text{XI}}}^{(p)} + I_{\overline{\text{IX}}}^{(p)} \\
&= -\frac{1}{(4\pi)^4} \left(\frac{-q^2}{\bar{\mu}^2} \right)^{-2\epsilon} \left\{ \frac{1}{(-q^2)} \frac{\pi^2}{2 m_1^2 m_2^2 (\sigma^2 - 1)} \left[\frac{1}{\epsilon^2} - \frac{\pi^2}{6} + \mathcal{O}(\epsilon^1) \right] \right. \\
&\quad + \frac{1}{\sqrt{-q^2}} \frac{i\pi^3 (m_1 + m_2)}{m_1^3 m_2^3 (\sigma^2 - 1)^{3/2}} \left[1 + \mathcal{O}(\epsilon^1) \right] \\
&\quad - \frac{\pi^2 (m_1^2 + m_2^2 + 2\sigma m_1 m_2)}{8 m_1^4 m_2^4 (\sigma^2 - 1)^2} \left[\frac{1}{\epsilon} + \mathcal{O}(\epsilon^0) \right] \\
&\quad \left. + \mathcal{O}\left(\sqrt{-q^2} \right) \right\} + \text{analytic terms} \,,
\end{aligned} \tag{3.205}$$

where "analytic terms" stand for terms with polynomial (including constant) dependence on q^2, with or without poles in ϵ. Such analytic terms give contact terms after Fourier transform

to impact parameter space, and are irrelevant for long-range classical physics. Note that the classical $\log(-q^2)$ arises from the Taylor expansion of $(-q^2)^{-2\epsilon}$. With these, together with the H-type integrals in Eq. (3.163), we can evaluate the conservative two-loop amplitude

$$\begin{aligned} M_{4,(p)}^{\text{2-loop}} = & -32\pi G^3 m_1^4 m_2^4 (\sigma-\cos\phi)^4 \left(\frac{-q^2}{\bar{\mu}^2}\right)^{-2\epsilon} \left\{ \frac{1}{(-q^2)} \frac{2(\sigma-\cos\phi)^2}{(\sigma^2-1)} \left[\frac{1}{\epsilon^2} - \frac{\pi^2}{6}\right] \right. \\ & + \frac{1}{\sqrt{-q^2}} \frac{4i\pi(m_1+m_2)(\sigma-\cos\phi)^2}{m_1 m_2 (\sigma^2-1)^{3/2}} \\ & - \frac{1}{\epsilon} \left[\frac{(m_1^2+m_2^2+2\sigma m_1 m_2)(\sigma-\cos\phi)^2}{2m_1^2 m_2^2 (\sigma^2-1)^2} - 2\frac{\operatorname{arcsinh}\left(\sqrt{\frac{\sigma-1}{2}}\right)}{m_1 m_2 \sqrt{\sigma^2-1}} \right] \\ & \left. + \mathcal{O}\left(\sqrt{-q^2}\right) \right\} + \text{analytic terms}\,. \end{aligned} \tag{3.206}$$

3.3.5 Eikonal phase, scattering angle and graviton dominance

In this subsection we will study eikonal exponentiation of the conservative amplitudes directly in momentum space. We will check the exponentiation of the leading and subleading eikonal in the two-loop amplitude. Then we will use the eikonal phase to evaluate the scattering angle in $\mathcal{N}=8$ supergravity. Finally we will compare the high-energy limit of our result to that of Einstein gravity.

The eikonal phase in $\mathcal{N}=8$ supergravity

In traditional treatments of eikonal exponentiation, it is customary to Fourier transform the scattering amplitudes to impact parameter space in order to extract the eikonal phase. Here we will take a slightly different approach and study eikonal exponentiation directly in momentum space. There is a simple reason why we prefer this approach: First, in the presence of a Coulomb-like tree-level interaction, such as graviton exchange, the Fourier transform has the side effect of introducing an additional infrared divergence, which in dimensional regularization gives the appearance that one needs to carefully analyze the

scattering amplitude at $\mathcal{O}(\epsilon)$ and keep track of ϵ/ϵ contributions to extract the eikonal phase at a fixed order. The momentum space approach has the advantage that the Coulomb-like singularities directly cancel, making clear that the $\mathcal{O}(\epsilon)$ pieces of the L-loop amplitude cannot contribute to the L-loop phase.[16] Working in momentum space comes at a cost nevertheless: simple products in impact parameter space become convolutions in momentum space. However, all convolutions can be easily evaluated as they are equivalent to iterated bubble integrals.

As usual in the eikonal approach, we will consider the amplitude as a function of a $D-2$-dimensional vector, $\boldsymbol{q}_\perp$, transverse to the scattering plane, which has the same magnitude as the four-momentum exchange, i.e., $\boldsymbol{q}_\perp^2 = -q^2$ (see e.g. Ref. [61]). The conservative amplitude only depends on powers of q, so this poses no problem. The statement of eikonal exponentiation is that one can write the scattering amplitude in the potential region as a convolutional exponential of the eikonal phase

$$\begin{aligned} iM_{(p)}(\sigma, \boldsymbol{q}_\perp) &= \operatorname{cexp}\left(i\delta(\sigma, \boldsymbol{q}_\perp)\right) - 1 \\ &\coloneqq i\delta(\sigma, \boldsymbol{q}_\perp) - \frac{1}{2!}\delta(\sigma, \boldsymbol{q}_\perp) \otimes \delta(\sigma, \boldsymbol{q}_\perp) - i\frac{1}{3!}\delta(\sigma, \boldsymbol{q}_\perp) \otimes \delta(s, \boldsymbol{q}_\perp) \otimes \delta(\sigma, \boldsymbol{q}_\perp) + \cdots , \end{aligned} \tag{3.207}$$

where we defined the convolution as integral over the $D-2$ dimensional transverse space

$$f_1(\boldsymbol{q}_\perp) \otimes f_2(\boldsymbol{q}_\perp) = \frac{1}{N} \int \frac{\mathrm{d}^{D-2}\boldsymbol{\ell}_\perp}{(2\pi)^{D-2}} f_1(\boldsymbol{\ell}_\perp)\, f_2(\boldsymbol{q}_\perp - \boldsymbol{\ell}_\perp)\,, \tag{3.208}$$

with a normalization factor $N = 4m_1 m_2 \sqrt{\sigma^2 - 1}$. Equivalently, one can write the inverse

[16] Unfortunately, one still needs to calculate $\mathcal{O}(\epsilon)$ parts of the lower loop amplitudes to extract the phase at a given order.

relation,

$$\begin{aligned}\delta(\sigma,\boldsymbol{q}_\perp) &= -i\,\mathrm{clog}(1+iM_{(p)}(\sigma,\boldsymbol{q}_\perp))\\ &:= M_{(p)}(\sigma,\boldsymbol{q}_\perp) - \frac{i}{2}M_{(p)}(\sigma,\boldsymbol{q}_\perp)\otimes M_{(p)}(\sigma,\boldsymbol{q}_\perp)\\ &\quad - \frac{1}{3}M_{(p)}(\sigma,\boldsymbol{q}_\perp)\otimes M_{(p)}(\sigma,\boldsymbol{q}_\perp)\otimes M_{(p)}(\sigma,\boldsymbol{q}_\perp)+\cdots\,.\end{aligned} \tag{3.209}$$

We expand δ perturbatively

$$\delta = \delta^{(0)} + \delta^{(1)} + \delta^{(2)} + \cdots\,, \tag{3.210}$$

where $\delta^{(L)}$ is $\mathcal{O}(G^{L+1})$. Then, from the discussion above we can write the phase in terms of the amplitudes

$$\delta^{(0)} = M^{\text{tree}}_{4,(p)}\,, \tag{3.211}$$

$$\delta^{(1)} = M^{\text{1-loop}}_{4,(p)} - \frac{i}{2}M^{\text{tree}}_{4,(p)}\otimes M^{\text{tree}}_{4,(p)}\,, \tag{3.212}$$

$$\delta^{(2)} = M^{\text{2-loop}}_{4,(p)} - iM^{\text{tree}}_{4,(p)}\otimes M^{\text{1-loop}}_{4,(p)} - \frac{1}{3}M^{\text{tree}}_{4,(p)}\otimes M^{\text{tree}}_{4,(p)}\otimes M^{\text{tree}}_{4,(p)}\,. \tag{3.213}$$

Looking at Eqs. (3.199)-(3.206), we see that to calculate the right-hand side of these equations we need the following convolutions

$$\frac{1}{\boldsymbol{q}_\perp^2}\otimes\frac{1}{\boldsymbol{q}_\perp^2} = \frac{1}{N}\frac{1}{4\pi\boldsymbol{q}_\perp^2}\left(\frac{\boldsymbol{q}_\perp^2}{\bar\mu^2}\right)^{-\epsilon}\frac{e^{\epsilon\gamma_{\text{E}}}\Gamma(-\epsilon)^2\Gamma(1+\epsilon)}{\Gamma(-2\epsilon)}\,, \tag{3.214}$$

$$\frac{1}{\boldsymbol{q}_\perp^2}\otimes\frac{1}{(\boldsymbol{q}_\perp^2)^{1+\epsilon}} = \frac{1}{N}\left(\frac{\boldsymbol{q}_\perp^2}{\bar\mu^2}\right)^{-2\epsilon}\left(\frac{e^{\gamma_{\text{E}}}}{4\pi}\right)^{\epsilon}\left[-\frac{1}{\epsilon}\frac{3}{8\pi\boldsymbol{q}_\perp^2}+\mathcal{O}(\epsilon)\right]\,, \tag{3.215}$$

$$\frac{1}{\boldsymbol{q}_\perp^2}\otimes\frac{1}{\boldsymbol{q}_\perp^2}\otimes\frac{1}{\boldsymbol{q}_\perp^2} = \frac{1}{N^2}\left(\frac{\boldsymbol{q}_\perp^2}{\bar\mu^2}\right)^{-2\epsilon}\left[\frac{1}{\epsilon^2}\frac{3}{16\pi^2\boldsymbol{q}_\perp^2}-\frac{1}{32\boldsymbol{q}_\perp^2}+\mathcal{O}(\epsilon)\right]\,, \tag{3.216}$$

$$\frac{1}{\boldsymbol{q}_\perp^2}\otimes\frac{1}{(\boldsymbol{q}_\perp^2)^{\frac{1}{2}+\epsilon}} = \frac{1}{N}\left(\frac{\boldsymbol{q}_\perp^2}{\bar\mu^2}\right)^{-2\epsilon}\left(\frac{e^{\gamma_{\text{E}}}}{4\pi}\right)^{\epsilon}\left[-\frac{1}{\epsilon}\frac{1}{4\pi|\boldsymbol{q}_\perp|}+\frac{\log(2)}{\pi|\boldsymbol{q}_\perp|}+\mathcal{O}(\epsilon)\right]\,, \tag{3.217}$$

$$\frac{1}{\boldsymbol{q}_\perp^2}\otimes\frac{1}{(\boldsymbol{q}_\perp^2)^{\epsilon}} = \frac{1}{N}\left(\frac{\boldsymbol{q}_\perp^2}{\bar\mu^2}\right)^{-2\epsilon}\left(\frac{e^{\gamma_{\text{E}}}}{4\pi}\right)^{\epsilon}\left[-\frac{1}{\epsilon}\frac{1}{8\pi}+\mathcal{O}(\epsilon)\right]\,, \tag{3.218}$$

which can all be evaluated by using Eq. (3.286) in Appendix 3.A with $c = 0$ and $\epsilon \to \epsilon - 1/2$. Using the first convolution, Eq. (3.214), we find

$$-\frac{i}{2} M^{\text{tree}}_{4,(p)} \otimes M^{\text{tree}}_{4,(p)} = -i32\pi G^2 m_1^3 m_2^3 \left(\frac{\boldsymbol{q}_\perp^2}{\bar{\mu}^2}\right)^{-\epsilon} \frac{1}{\boldsymbol{q}_\perp^2} \frac{(\sigma - \cos\phi)^4}{\sqrt{\sigma^2-1}} \frac{\Gamma(-\epsilon)^2 \Gamma(1+\epsilon)}{\Gamma(-2\epsilon)}\,, \tag{3.219}$$

which exactly cancels the $\mathcal{O}(|q|^{-2})$ of the one-loop amplitude in Eq. (3.202) to all orders in ϵ. Similarly, using Eqs. (3.215) and (3.216) we find[17]

$$\begin{aligned} -iM^{\text{tree}}_{4,(p)} \otimes M^{\text{1-loop}}_{4,(p)}\Big|_{\mathcal{O}(|q|^{-2})} - \frac{1}{3} M^{\text{tree}}_{4,(p)} \otimes M^{\text{tree}}_{4,(p)} \otimes M^{\text{tree}}_{4,(p)} \\ = 64\pi G^3 m_1^4 m_2^4 \frac{(\sigma - \cos\phi)^4}{\sigma^2-1} \left(\frac{\boldsymbol{q}_\perp^2}{\bar{\mu}^2}\right)^{-\epsilon} \frac{1}{\boldsymbol{q}_\perp^2} \left[\frac{1}{\epsilon^2} - \frac{\pi^2}{6} + \mathcal{O}(\epsilon)\right], \end{aligned} \tag{3.220}$$

using Eq. (3.217)

$$\begin{aligned} -iM^{\text{tree}}_{4,(p)} \otimes M^{\text{1-loop}}_{4,(p)}\Big|_{\mathcal{O}(|q|^{-1})} = -128i\pi^2 G^3 m_1^3 m_2^3 (m_1+m_2) \\ \times \frac{(\sigma - \cos\phi)^6}{(\sigma^2-1)^{3/2}} \left(\frac{\boldsymbol{q}_\perp^2}{\bar{\mu}^2}\right)^{-\epsilon} \frac{1}{|\boldsymbol{q}_\perp|} \left[1 + \mathcal{O}(\epsilon)\right], \end{aligned} \tag{3.221}$$

and using Eq. (3.218)

$$\begin{aligned} -iM^{\text{tree}}_{4,(p)} \otimes M^{\text{1-loop}}_{4,(p)}\Big|_{\mathcal{O}(|q|^{0})} = -16\pi G^3 m_1^2 m_2^2 (2m_1 m_2 \sigma + m_1^2 + m_2^2) \\ \times \frac{(\sigma - \cos\phi)^6}{(\sigma^2-1)^2} \left(\frac{\boldsymbol{q}_\perp^2}{\bar{\mu}^2}\right)^{-\epsilon} \left[\frac{1}{\epsilon} + \mathcal{O}(\epsilon)\right]. \end{aligned} \tag{3.222}$$

These expressions respectively cancel the $\mathcal{O}(|q|^{-2})$, the $\mathcal{O}(|q|^{-1})$ and the $\mathcal{O}(|q|^{0})$ contributions to the two-loop amplitude Eq. (3.206), which arise from the ladder-type diagrams. Therefore, the ladder-type diagrams at two loops give exactly zero contribution to the eikonal exponent, up to the order of q relevant for classical dynamics at $\mathcal{O}(G^3)$. This cancellation is a check of

[17] Note that exponentiation at one loop implies $M^{\text{1-loop}}_{4,(p)}\Big|_{\mathcal{O}(|q|^{-2})} = \frac{i}{2} M^{\text{tree}}_{4,(p)} \otimes M^{\text{tree}}_{4,(p)}$, so the first line can also be written as $\frac{1}{3!} M^{\text{tree}}_{4,(p)} \otimes M^{\text{tree}}_{4,(p)} \otimes M^{\text{tree}}_{4,(p)}$.

the exponentiation of the leading and subleading eikonal phase in the two-loop amplitude. Henceforth we will assume exponentiation of the two-loop phase and leave a proof for further work. We note that this zero result relies on delicate cancellations between *all six* ladder diagrams which leave only the contributions of the H-type diagrams to the two-loop eikonal phase.

In summary, putting together Eqs. (3.199)–(3.206) and (3.219)–(3.222) in (3.211)–(3.213) the result of calculation our of the eikonal phase is

$$\delta^{(0)}(\sigma, \boldsymbol{q}_\perp) = 32\pi G m_1^2 m_2^2 (\sigma - \cos\phi)^2 \frac{1}{\boldsymbol{q}_\perp^2}\,, \tag{3.223}$$

$$\delta^{(1)}(\sigma, \boldsymbol{q}_\perp) = 0 + \mathcal{O}(\epsilon |\boldsymbol{q}_\perp|^0)\,, \tag{3.224}$$

$$\delta^{(2)}(\sigma, \boldsymbol{q}_\perp) = -64\pi (G m_1 m_2)^3 \frac{(\sigma - \cos\phi)^4}{\sqrt{\sigma^2 - 1}} \operatorname{arcsinh}\sqrt{\frac{\sigma - 1}{2}} \frac{1}{\epsilon} \left(\frac{\boldsymbol{q}_\perp^2}{\bar{\mu}^2}\right)^{-2\epsilon} + \mathcal{O}(\epsilon^0 |\boldsymbol{q}_\perp|)\,. \tag{3.225}$$

Note that $\delta^{(2)}$ includes an $\mathcal{O}(\epsilon^0|\boldsymbol{q}_\perp|)$ which we have not calculated. This however goes beyond the classical power counting and so is a quantum correction to the phase. Finally, we can readily perform the Fourier transform to obtain the more familiar eikonal phase in impact parameter space

$$\delta(\sigma, \boldsymbol{b}_{\rm e}) = \frac{1}{N} \int \frac{\mathrm{d}^{D-2}\boldsymbol{q}_\perp}{(2\pi)^{D-2}}\, e^{i\boldsymbol{b}_{\rm e}\cdot\boldsymbol{q}_\perp}\, \delta(\sigma, \boldsymbol{q}_\perp)\,, \tag{3.226}$$

with the result

$$\delta^{(0)}(\sigma, \boldsymbol{b}_{\rm e}) = -2G m_1 m_2 \frac{(\sigma - \cos\phi)^2}{\sqrt{\sigma^2 - 1}} \left(\frac{1}{\epsilon} + \log \boldsymbol{b}_{\rm e}^2\right)\,, \tag{3.227}$$

$$\delta^{(1)}(\sigma, \boldsymbol{b}_{\rm e}) = 0\,, \tag{3.228}$$

$$\delta^{(2)}(\sigma, \boldsymbol{b}_{\rm e}) = -32 G^3 m_1^2 m_2^2 \frac{(\sigma - \cos\phi)^4}{\sigma^2 - 1} \operatorname{arcsinh}\sqrt{\frac{\sigma - 1}{2}} \frac{1}{\boldsymbol{b}_{\rm e}^2}\,, \tag{3.229}$$

where we have dropped $\mathcal{O}(\epsilon)$ and quantum parts. As a cross-check we have verified that the same result is obtained by using the more common approach in which one directly transforms the amplitudes to impact parameter space.

Soft vs. potential and exponentiation Let us stress that it was very important that we evaluated the amplitude in the potential region to extract the conservative piece. For the one-loop amplitude, the expansion in the soft region differs from that of the potential region at $\mathcal{O}(\epsilon\,|\boldsymbol{q}|^0)$, which, in addition to the ϵ suppression, is a quantum correction since the classical dynamics arises from $\mathcal{O}(1/|\boldsymbol{q}|)$ terms. For the two-loop amplitude, however, the two expansions still differ from each other at $\mathcal{O}(|\boldsymbol{q}|^0)$, which is at the same order as the terms responsible for the classical dynamics at two loops, and the difference is also no longer suppressed by ϵ. In fact, when we directly evaluate the integrals in the soft region at two loops we find non-exponentiating effects which cause infrared divergences that are not canceled by either matching to non-relativistic EFT or by extracting the eikonal exponent, signaling the appearance of contributions that cannot be interpreted as arising from a conservative potential.[18] The evaluation of the soft integrals using the differential equations above and a detailed discussion of this point will be presented elsewhere.

Scattering angle from eikonal phase

Let us now calculate the gravitational scattering angle from the eikonal phase. The formula relating the two can be derived from the stationary phase approximation of the Fourier transform of the exponentiated impact-parameter amplitude back to momentum space [58], which yields the relation

$$\boldsymbol{q} = -\frac{\partial}{\partial \boldsymbol{b}_{\rm e}}\delta(\sigma, \boldsymbol{b}_{\rm e})\,. \tag{3.230}$$

The magnitude of $\boldsymbol{q}$ is related to the scattering angle χ and the magnitude of the three-momentum $\boldsymbol{p}$ in the center of mass by

$$|\boldsymbol{q}| = 2|\boldsymbol{p}|\sin\frac{\chi}{2}\,, \tag{3.231}$$

[18] This is reminiscent of the situation in the EFT formulation of the Regge limit of massless scattering [289], where contributions from the Glauber region exponentiate while the full soft regions contain non-exponentiating effects.

where in terms of the center of mass energy $E = \sqrt{s}$ and/or σ

$$|\boldsymbol{p}| = \frac{m_1 m_2 \sqrt{\sigma^2 - 1}}{E} = \frac{m_1 m_2 \sqrt{\sigma^2 - 1}}{\sqrt{m_1^2 + m_2^2 + 2 m_1 m_2 \sigma}} \,. \tag{3.232}$$

From Eqs. (3.230) and (3.231) we can derive the formula for the scattering angle

$$\sin \frac{\chi}{2} = -\frac{1}{2|\boldsymbol{p}|} \frac{\partial}{\partial |\boldsymbol{b}_{\rm e}|} \delta(\sigma, \boldsymbol{b}_{\rm e}) \,. \tag{3.233}$$

Using this formula we find the following result for the scattering angle

$$\sin \frac{\chi}{2} = \frac{G m_1 m_2}{|\boldsymbol{p}||\boldsymbol{b}_{\rm e}|} \frac{2(\sigma - \cos\phi)^2}{\sqrt{\sigma^2 - 1}} - \frac{G^3 m_1^3 m_2^3}{|\boldsymbol{p}|^3 |\boldsymbol{b}_{\rm e}|^3} \frac{32 m_1 m_2 (\sigma - \cos\phi)^4}{m_1^2 + m_2^2 + 2 m_1 m_2 \sigma} \text{arcsinh} \sqrt{\frac{\sigma - 1}{2}} \,. \tag{3.234}$$

or separating the different orders

$$\chi_{\rm eik}^{\rm 1PM} = \frac{G m_1 m_2}{|\boldsymbol{p}||\boldsymbol{b}_{\rm e}|} \frac{4(\sigma - \cos\phi)^2}{\sqrt{\sigma^2 - 1}} \,, \tag{3.235}$$

$$\chi_{\rm eik}^{\rm 2PM} = 0 \,, \tag{3.236}$$

$$\chi_{\rm eik}^{\rm 3PM} = -\frac{G^3 m_1^3 m_2^3}{|\boldsymbol{p}|^3 |\boldsymbol{b}_{\rm e}|^3} 16 \left[-\frac{(\sigma - \cos\phi)^6}{6(\sigma^2 - 1)^{3/2}} + \frac{4 m_1 m_2 (\sigma - \cos\phi)^4}{m_1^2 + m_2^2 + 2 m_1 m_2 \sigma} \text{arcsinh} \sqrt{\frac{\sigma - 1}{2}} \right] . \tag{3.237}$$

Looking ahead, in order to more easily to compare with the results from EFT in the next subsection, we will write the formula in terms of the angular momentum, J. The angular momentum is defined as

$$J = |\boldsymbol{b} \times \boldsymbol{p}| = |\boldsymbol{b}||\boldsymbol{p}| \,, \tag{3.238}$$

where $\boldsymbol{b}$ is an impact parameter perpendicular the incoming center of mass momentum $\boldsymbol{p}$. This is however not the impact parameter, $\boldsymbol{b}_{\rm e}$, which arises naturally from the eikonal phase. Eq. (3.230) shows that $\boldsymbol{b}_{\rm e}$ points in the direction of the momentum transfer. The magnitude of $\boldsymbol{b}$ and $\boldsymbol{b}_{\rm e}$ are then related by

$$|\boldsymbol{b}| = |\boldsymbol{b}_{\rm e}| \cos \frac{\chi}{2} \,, \tag{3.239}$$

so that the angular momentum is

$$J = |\boldsymbol{b}_{\rm e}||\boldsymbol{p}| \cos\frac{\chi}{2} \,. \tag{3.240}$$

For small angle scattering $|\boldsymbol{b}| \sim |\boldsymbol{b}_{\rm e}|$, and the difference is unimportant at leading order. Our results, however, go beyond the leading order and the difference matters. Using the relation (3.240) we find the scattering angle in terms of the angular momentum

$$\chi_{\rm eik}^{\rm 1PM} = \frac{G m_1 m_2}{J} \frac{4(\sigma - \cos\phi)^2}{\sqrt{\sigma^2 - 1}} \,, \tag{3.241}$$

$$\chi_{\rm eik}^{\rm 2PM} = 0 \,, \tag{3.242}$$

$$\chi_{\rm eik}^{\rm 3PM} = -\frac{G^3 m_1^3 m_2^3}{J^3} 16 \left[\frac{(\sigma - \cos\phi)^6}{3(\sigma^2-1)^{3/2}} + \frac{4 m_1 m_2 (\sigma - \cos\phi)^4}{m_1^2 + m_2^2 + 2 m_1 m_2 \sigma} \text{arcsinh} \sqrt{\frac{\sigma - 1}{2}} \right] . \tag{3.243}$$

For later convenience we can rewrite this in terms of the total mass, m, and symmetric mass ratio, ν,

$$m = m_1 + m_2 \,, \quad \nu = \frac{m_1 m_2}{(m_1 + m_2)^2} \,, \tag{3.244}$$

as follows

$$\chi_{\rm eik}^{\rm 1PM} = \frac{G m^2 \nu}{J} \frac{4(\sigma - \cos\phi)^2}{\sqrt{\sigma^2 - 1}} \,, \tag{3.245}$$

$$\chi_{\rm eik}^{\rm 2PM} = 0 \,, \tag{3.246}$$

$$\chi_{\rm eik}^{\rm 3PM} = -\frac{G^3 m^6 \nu^3}{J^3} 16 \left[\frac{(\sigma - \cos\phi)^6}{3(\sigma^2-1)^{3/2}} + \nu \frac{4(\sigma - \cos\phi)^4}{2(\sigma-1)\nu + 1} \text{arcsinh} \sqrt{\frac{\sigma - 1}{2}} \right] , \tag{3.247}$$

Probe limit As a cross-check we can compare the probe limit $\nu \to 0$ of our result with the scattering angle of a particle of mass μ moving along geodesics in the background of the half-BPS black hole of mass M [257, 258]. Ref. [119] studied the precession of the periastron,

which is given by

$$\frac{1}{2}\Delta\Phi = \int_{r_{\min}}^{r_{\max}} \mathrm{d}r\, \frac{\mathrm{d}\chi}{\mathrm{d}r} = J \int_{r_{\min}}^{r_{\max}} \frac{\mathrm{d}r}{r^2\sqrt{p_r(r)^2}}\,, \tag{3.248}$$

where p_r is the radial momentum of the probe particle, related to its three-momentum by $\boldsymbol{p}_{\rm p}^2 = p_r^2 + J^2/r^2$. The scattering angle is given by the same integral with different limits

$$\frac{1}{2}(\chi + \pi) = J \int_{r_{\min}}^{\infty} \frac{\mathrm{d}r}{r^2\sqrt{p_r(r)^2}}\,, \tag{3.249}$$

so their calculation can be easily adapted to obtain this quantity. Let us spare the details to the reader and just give the result

$$\begin{aligned}\frac{1}{2}\chi_{\rm p} &= \arctan\left[\frac{GM^2\nu_{\rm p}}{J}\frac{2(\sigma_{\rm p}-\cos\phi_{\rm p})^2}{(\sigma_{\rm p}^2-1)^{1/2}}\right] \\ &= \frac{GM^2\nu_{\rm p}}{J}\frac{4(\sigma_{\rm p}-\cos\phi_{\rm p})^2}{(\sigma_{\rm p}^2-1)^{1/2}} - \frac{G^3M^6\nu_{\rm p}^3}{J^3}\frac{16(\sigma_{\rm p}-\cos\phi_{\rm p})^6}{3(\sigma_{\rm p}^2-1)^{3/2}}\,,\end{aligned} \tag{3.250}$$

where $\sigma_{\rm p}$ and $\phi_{\rm p}$ are the relativistic factor and charge misalignment of the probe particle respectively, and $\nu_{\rm p} = \mu/M$. Interestingly the structure of the result is the same of that for a Newtonian potential (see e.g Ref. [239], Eq. (4.34)), which could be expected from the fact that Ref. [119] found no precession. Finally, it is easy to check that with the identifications

$$\sigma \leftrightarrow \sigma_{\rm p}\,, \quad \phi \leftrightarrow \phi_{\rm p}\,, \quad M \leftrightarrow m\,, \quad \nu \leftrightarrow \nu_{\rm p}\,, \tag{3.251}$$

this matches Eqs. (3.245)–(3.247) in the limit $\nu \to 0$, in which the term with the arcsinh is suppressed by its coefficient, thus providing a check of our result.

High-energy limit and graviton dominance

At this point we would like to compare our result for the scattering angle with that of Einstein gravity obtained in Refs. [41, 42]. Famously, the high-energy limit of scattering amplitudes in a theory with gravity is dominated by the exchange of gravitons [57]. This is proven at

leading order in Gm_1m_2/J but not beyond that. Recently, in Ref. [3], a similar result was found by explicit calculation at order G^3 for the case of massless scattering. Although a general proof of graviton dominance at this order is lacking, this reference calculated from first principles the scattering angle for $\mathcal{N} \leq 4$ supergravity and Einstein gravity using eikonal and partial wave techniques, and found that it coincides in all such theories.[19] In addition, the result for Einstein gravity was found to agree with an earlier result by Amati, Ciafaloni and Veneziano [61] and contradicts a modified proposal by Damour [65].

Motivated by the universality in the massless case, we will study the high-energy limit of our result by taking $\sigma \to \infty$ in our result for the scattering angle at order G^3, which yields

$$\chi^{\text{3PM}}_{\mathcal{N}=8} \overset{\sigma\to\infty}{=} -\frac{16G^3m^6\nu^3\sigma^3\log(\sigma)}{J^3} + \cdots . \tag{3.252}$$

This can be compared with the high-energy limit of the Einstein gravity result in Ref. [42] Eq. (11.32)

$$\chi^{\text{3PM}}_{\text{EG}} \overset{\sigma\to\infty}{=} -\frac{16G^3m^6\nu^3\sigma^3\log(\sigma)}{J^3} + \cdots , \tag{3.253}$$

finding perfect agreement. This strongly suggests that the coefficient of the arcsinh term features graviton dominance, and universality also holds in the case of massive scattering. Note that this result does not trivially follow from the massless one since here we impose the limits $J \gg 1$ and then $\sigma \gg 1$ in this order (or equivalently $|\boldsymbol{q}| \ll m$). The limits do not commute, so the high energy limit of classical massive scattering is distinct from the Regge limit of massless scattering. Admittedly, our calculation provides is only one point of comparison with Einstein gravity, so the question of graviton dominance merits further investigation, either by calculating the scattering angle in other supergravity theories or by directly proving universality. We leave this for future work.

[19] In massless theories the classical limit and the high-energy limit are not distinct, so the full classical angle agrees.

3.3.6 Consistency check from effective field theory

In this subsection we will calculate the conservative amplitudes using the non-relativistic integration method of Refs. [39, 41, 42], which is optimized for EFT matching. This method avoids explicit computation of infrared divergent integrals in dimensional regularization, by canceling such integrals between the full theory and the effective field theory using a four-dimensional matching procedure. We will use the EFT Hamiltonian to calculate the scattering angle solving the classical dynamics. Finally, we will compare to our predictions for the amplitude and the angle from the previous subsection.

The EFT is defined in the center of mass frame

$$p_1 = (-E_1, \boldsymbol{p}) \,, \quad p_2 = (-E_2, -\boldsymbol{p}) \,, \quad p_3 = (E_2, \boldsymbol{p}') \,, \quad p_4 = (E_1, -\boldsymbol{p}') \,, \tag{3.254}$$

where the magnitude of the three-momenta, $|\boldsymbol{p}| = |\boldsymbol{p}'|$, is unchanged in the scattering and the energies are $E_i = \sqrt{m_i^2 + \boldsymbol{p}^2}$. In this frame the momentum transfer is purely spatial and given by $\boldsymbol{q} = \boldsymbol{p} - \boldsymbol{p}'$, and the usual Mandelstam invariants are

$$s = (p_1 + p_2)^2 = (E_1 + E_2)^2 = E^2 \,, \tag{3.255}$$

$$t = (p_1 + p_4)^2 = -(\boldsymbol{p} - \boldsymbol{p}')^2 = -\boldsymbol{q}^2 = -4\boldsymbol{p}^2 \frac{1 - \cos\chi}{2} = -4\boldsymbol{p}^2 \sin^2 \frac{\chi}{2} \,, \tag{3.256}$$

$$u = (p_1 + p_3)^2 = (E_1 - E_2)^2 - (\boldsymbol{p} + \boldsymbol{p}')^2 = E^2(1 - 4\xi) - 4\boldsymbol{p}^2 \cos^2 \frac{\chi}{2} \,, \tag{3.257}$$

where χ is the scattering angle and we introduced the total center of mass energy, E, and the symmetric energy ratio, ξ, defined as

$$E = E_1 + E_2, \quad \xi = \frac{E_1 E_2}{(E_1 + E_2)^2} \,. \tag{3.258}$$

We will use these variables throughout this subsection.

Scattering amplitude with IR subtractions optimized for EFT matching

Here we will use the method of Refs. [41, 42], which first expand in the small-velocity limit in the potential region to produce three-dimensional integrals, and then expand in the limit of small q. Divergent integrals will be kept unevaluated, to be canceled against EFT amplitudes in the matching procedure.

First let us calculate the scattering amplitudes optimized for EFT matching. At tree level the relevant piece comes from the $1/t$ pole

$$\mathcal{M}_1 = \frac{8\pi G m_1^2 m_2^2}{E_1 E_2} \frac{(\sigma - \cos\phi)^2}{\boldsymbol{q}^2}\,, \tag{3.259}$$

where we have divided by the non-relativistic normalization $4E_1E_2$. We will use the notation in Refs. [41, 42] and denote the conservative amplitudes in this subsection with calligraphic $\mathcal{M}$ to distinguish them from those evaluated in dimensional regularization in previous subsections. The one-loop amplitude can be easily obtained from the one-loop integrand in Eq. (3.47). As explained in Ref. [42], Sec. 7.2.2 and 7.3.3, the scalar crossed box gives a vanishing contribution in the potential region (in strictly four dimensions), and the box yields the following three dimensional integral

$$I_{\rm II}^{(p)} = \int \frac{\mathrm{d}^{D-1}\boldsymbol{\ell}}{(2\pi)^{D-1}} \frac{1}{2E\boldsymbol{\ell}^2(\boldsymbol{\ell}+\boldsymbol{q})^2(\boldsymbol{\ell}^2+2\boldsymbol{p}\boldsymbol{\ell})} + \text{evanescent terms.} \tag{3.260}$$

Here *evanescent terms* refer to two classes of terms: (1) terms that are suppressed in ϵ or $|q|$ after loop integration, (2) terms that arise from EFT diagrams with insertions of EFT operators suppressed by ϵ or $|q|$ omitted from Eq. (3.270). Due to divergences associated with loop integration, terms of class (2) may be naively of the same order of ϵ and $|q|$ as terms that directly correspond to four-dimensional classical dynamics, but nevertheless such evanescent terms cancel in the EFT matching procedure and do not contribute to the final

results. The one-loop amplitude optimized for EFT matching is then

$$\mathcal{M}_2 = \frac{(16\pi G)^2 m_1^4 m_2^4}{2E_1E_2(E_1+E_2)}(\sigma-\cos\phi)^4 \int \frac{\mathrm{d}^{D-1}\boldsymbol{\ell}}{(2\pi)^{D-1}} \frac{1}{\boldsymbol{\ell}^2(\boldsymbol{\ell}+\boldsymbol{q})^2(\boldsymbol{\ell}^2+2\boldsymbol{p}\boldsymbol{\ell})} + \text{evanescent terms.} \tag{3.261}$$

Finally, we extract the two-loop conservative amplitude optimized for EFT matching from the two-loop integrand in Eq. (3.51). Let us first consider the integrals in the first line of such an equation. As explained in Ref. [42], when using the non-relativistic integration method all the non-planar scalar ladders vanish. Intuitively this is because the energy flow would require the propagation of an antiparticle, which is not allowed, so only the planar double-box contributes in the potential region as [42]

$$I_{\text{III}}^{(p)} = \frac{1}{4E^2}\int \frac{\mathrm{d}^{D-1}\boldsymbol{\ell}_1}{(2\pi)^{D-1}} \frac{\mathrm{d}^{D-1}\boldsymbol{\ell}_2}{(2\pi)^{D-1}} \frac{1}{\boldsymbol{\ell}_1^2(\boldsymbol{\ell}_2-\boldsymbol{\ell}_1)^2(\boldsymbol{\ell}_2+\boldsymbol{q})^2(\boldsymbol{\ell}_1^2+2\boldsymbol{p}\boldsymbol{\ell}_1)(\boldsymbol{\ell}_2^2+2\boldsymbol{p}\boldsymbol{\ell}_2)} + \text{evanescent terms}\,. \tag{3.262}$$

We must note that the vanishing of the non-planar integrals is a consequence of the loop-by-loop integration procedure used in Ref. [42], which at every stage drops evanescent contributions. In a two-loop integral these can hit at $1/\epsilon$ or $1/|q|$ pole coming from a different loop and generate finite contributions with classical power-counting such as those calculated in subsection 3.3.3. These contributions arising from evanescent terms are scheme dependent, and, as mentioned above, their ultimate fate is to cancel in the EFT matching procedure. In particular, they will not affect any physical quantity. Thus, as long as the integration in full theory and EFT is done consistently one might drop such evanescent terms. This effectively gives us a four-dimensional regularization method which, in contrast to our eikonal calculation based on dimensional regularization, does not need quantum corrections of $\mathcal{O}(|q|^0)$, and $\mathcal{O}(\epsilon)$ contributions at one-loop in order to extract the classical dynamics at two loops.

Next we consider the integrals in the second line of Eq. (3.51). As explained in previous

subsections only $I_{\rm H}$ and $I_{\overline{\rm H}}$ contribute with value given by Eq. (3.163), which we reprint here

$$I_{\rm H}^{(p)} + I_{\overline{\rm H}}^{(p)} = \frac{\log \boldsymbol{q}^2}{64\pi^2 m_1 m_2 \boldsymbol{q}^4} \frac{\operatorname{arcsinh}\sqrt{\frac{\sigma-1}{2}}}{\sqrt{\sigma^2-1}} + \text{evanescent terms}\,, \tag{3.263}$$

where we dropped $1/\epsilon$ pole terms that do not generate non-analytic dependence on q^2. Putting the pieces together we find the full two-loop amplitude optimized for EFT matching

$$\begin{aligned}\mathcal{M}_3 = \frac{32\pi G^3 m_1^3 m_2^3\,(\sigma-\cos\phi)^4}{E_1 E_2}\Bigg[&\log \boldsymbol{q}^2 \frac{\operatorname{arcsinh}\sqrt{\frac{\sigma-1}{2}}}{\sqrt{\sigma^2-1}} + \frac{64\pi^2 m_1^3 m_2^3 (\sigma-\cos\phi)^2}{(E_1+E_2)^2} \\ &\times \int \frac{\mathrm{d}^{D-1}\boldsymbol{\ell}_1}{(2\pi)^{D-1}} \frac{\mathrm{d}^{D-1}\boldsymbol{\ell}_2}{(2\pi)^{D-1}} \frac{1}{\boldsymbol{\ell}_1^2 (\boldsymbol{\ell}_2-\boldsymbol{\ell}_1)^2 (\boldsymbol{\ell}_2+\boldsymbol{q})^2 (\boldsymbol{\ell}_1^2+2\boldsymbol{p}\boldsymbol{\ell}_1)(\boldsymbol{\ell}_2^2+2\boldsymbol{p}\boldsymbol{\ell}_2)}\Bigg] \\ &+ \text{evanescent terms}.\end{aligned} \tag{3.264}$$

For later convenience we rewrite the conservative amplitudes in terms of the total energy, mass and cross ratios as

$$\mathcal{M}_1 = \frac{8\pi G \nu^2 m^4}{E^2 \xi} \frac{(\sigma-\cos\phi)^2}{\boldsymbol{q}^2}\,, \tag{3.265}$$

$$\mathcal{M}_2 = \frac{(16\pi G)^2 \nu^4 m^8}{2E^3\xi} (\sigma-\cos\phi)^4 \int \frac{\mathrm{d}^{D-1}\boldsymbol{\ell}}{(2\pi)^{D-1}} \frac{1}{\boldsymbol{\ell}^2 (\boldsymbol{\ell}+\boldsymbol{q})^2 (\boldsymbol{\ell}^2+2\boldsymbol{p}\boldsymbol{\ell})} + \text{evanescent terms}\,, \tag{3.266}$$

$$\begin{aligned}\mathcal{M}_3 = \frac{32\pi G^3 \nu^3 m^6\,(\sigma-\cos\phi)^4}{\xi E^2}\Bigg[&\log \boldsymbol{q}^2 \frac{\operatorname{arcsinh}\sqrt{\frac{\sigma-1}{2}}}{\sqrt{\sigma^2-1}} + \frac{64\pi^2 \nu^3 m^6 (\sigma-\cos\phi)^2}{E^2} \\ &\times \int \frac{\mathrm{d}^{D-1}\boldsymbol{\ell}_1}{(2\pi)^{D-1}} \frac{\mathrm{d}^{D-1}\boldsymbol{\ell}_2}{(2\pi)^{D-1}} \frac{1}{\boldsymbol{\ell}_1^2 (\boldsymbol{\ell}_2-\boldsymbol{\ell}_1)^2 (\boldsymbol{\ell}_2+\boldsymbol{q})^2 (\boldsymbol{\ell}_1^2+2\boldsymbol{p}\boldsymbol{\ell}_1)(\boldsymbol{\ell}_2^2+2\boldsymbol{p}\boldsymbol{\ell}_2)}\Bigg] \\ &+ \text{evanescent terms}.\end{aligned} \tag{3.267}$$

EFT matching and classical Hamiltonian

Following Ref. [39], we want to match the amplitudes above to an EFT with an ordinary Hamiltonian with a potential, which we later will use to solve for the classical dynamics.

The EFT describes two massive scalars interacting with momentum space Lagrangian given by

$$\begin{aligned}\mathcal{L} = &\int \frac{\mathrm{d}^{D-1}\boldsymbol{p}}{(2\pi)^{D-1}}\,\phi_1^\dagger(-\boldsymbol{p})\left(i\partial_t - \sqrt{\boldsymbol{p}^2+m_1^2}\right)\phi_1(\boldsymbol{p}) \\ &+ \int \frac{\mathrm{d}^{D-1}\boldsymbol{p}}{(2\pi)^{D-1}}\,\phi_2^\dagger(-\boldsymbol{p})\left(i\partial_t - \sqrt{\boldsymbol{p}^2+m_2^2}\right)\phi_2(\boldsymbol{p}) \\ &- \int \frac{\mathrm{d}^{D-1}\boldsymbol{p}}{(2\pi)^{D-1}}\frac{\mathrm{d}^{D-1}\boldsymbol{p}'}{(2\pi)^{D-1}}\,V(\boldsymbol{p},\boldsymbol{p}')\,\phi_1^\dagger(\boldsymbol{p}')\phi_1(\boldsymbol{p})\phi_2^\dagger(-\boldsymbol{p}')\phi_2(-\boldsymbol{p})\,, \end{aligned} \tag{3.268}$$

where the form of the kinetic term manifests the absence of anti-particles. The potential is given by

$$V(\boldsymbol{p},\boldsymbol{p}+\boldsymbol{q}) = \sum_{n=1}^{\infty}\frac{(G/2)^n(4\pi)^{(D-1)/2}}{|\boldsymbol{q}|^{D-1-n}}\frac{\Gamma\left[(D-1-n)/2\right]}{\Gamma\left[n/2\right]}\,c_n\big(\boldsymbol{p}^2\big) \tag{3.269}$$

$$= \frac{4\pi G}{\boldsymbol{q}^2}\,c_1\big(\boldsymbol{p}^2\big) + \frac{2\pi^2 G^2}{|\boldsymbol{q}|}\,c_2\big(\boldsymbol{p}^2\big) - 2\pi G^3\log\boldsymbol{q}^2\,c_3\big(\boldsymbol{p}^2\big) + \cdots\,, \tag{3.270}$$

where for conciseness we have put the external legs on-shell. As in the full theory, here we have also dropped evanescent terms suppressed by ϵ or q^2 at each order in G, which can affect the scattering amplitudes but do not have physical effects. If we Fourier transform $\boldsymbol{q}$ back to position space this yields the more familiar potential with an expansion in $G/|\boldsymbol{r}|$.

The EFT amplitudes calculated with the Lagrangian above are very simple. Due to the absence of anti-particles they are given by iterated bubble diagrams. The results up to order

G^3 are given by Ref. [42],

$$
\begin{aligned}
\mathcal{M}_1^{\rm EFT} &= -\frac{4\pi G c_1}{\boldsymbol{q}^2}\,,\\
\mathcal{M}_2^{\rm EFT} &= -\frac{2\pi^2 G^2 c_2}{|\boldsymbol{q}|} + \frac{\pi^2 G^2}{E\xi|\boldsymbol{q}|}\left[(1-3\xi)c_1^2 + 4\xi^2 E^2 c_1 c_1'\right] + \int \frac{\mathrm{d}^{D-1}\boldsymbol{\ell}}{(2\pi)^{D-1}} \frac{32 E\xi \pi^2 G^2 c_1^2}{\boldsymbol{\ell}^2(\boldsymbol{\ell}+\boldsymbol{q})^2(\boldsymbol{\ell}^2+2\boldsymbol{p}\boldsymbol{\ell})}\,,\\
\mathcal{M}_3^{\rm EFT} &= 2\pi G^3 \log \boldsymbol{q}^2 c_3 - \frac{\pi G^3 \log \boldsymbol{q}^2}{E^2\xi}\Big[(1-4\xi)c_1^3 - 8\xi^3 E^4 c_1 {c_1'}^2 - 4\xi^3 E^4 c_1^2 c_1'' + 4\xi^2 E^3 c_2 c_1'\\
&\qquad + 4\xi^2 E^3 c_1 c_2' - 2(3-9\xi)\xi E^2 c_1^2 c_1' + 2E(1-3\xi)c_1 c_2\Big]\\
&\quad + \int \frac{\mathrm{d}^{D-1}\boldsymbol{\ell}}{(2\pi)^{D-1}} \frac{16\pi^3 G^3 c_1\left[2E\xi c_2 - (1-3\xi)c_1^2 - 4\xi^2 E^2 c_1 c_1'\right]}{\boldsymbol{\ell}^2|\boldsymbol{\ell}+\boldsymbol{q}|(\boldsymbol{\ell}^2+2\boldsymbol{p}\boldsymbol{\ell})}\\
&\quad - \int \frac{\mathrm{d}^{D-1}\boldsymbol{\ell}_1}{(2\pi)^{D-1}} \frac{\mathrm{d}^{D-1}\boldsymbol{\ell}_2}{(2\pi)^{D-1}} \frac{256 E^2\xi^2\pi^3 G^3 c_1^3}{\boldsymbol{\ell}_1^2(\boldsymbol{\ell}_1+\boldsymbol{\ell}_2)^2(\boldsymbol{\ell}_2+\boldsymbol{q})^2(\boldsymbol{\ell}_1^2+2\boldsymbol{p}\boldsymbol{\ell}_1)(\boldsymbol{\ell}_2^2+2\boldsymbol{p}\boldsymbol{\ell}_2)}\,,
\end{aligned}
\tag{3.271}
$$

where $c_i = c_i(\boldsymbol{p}^2)$ and the primes denote derivatives. The EFT matching is performed by requiring $\mathcal{M}_n = \mathcal{M}_n^{\rm EFT}$, which yields the following coefficients for the potential

$$
c_1(\boldsymbol{p}^2) = -\frac{m^4\nu^2}{E^2\xi} 2(\sigma-\cos\phi)^2\,, \tag{3.272}
$$

$$
c_2(\boldsymbol{p}^2) = \frac{m^6\nu^3}{E^3\xi^2}\left[-8(\sigma-\cos\phi)^3 + \frac{2\nu(\sigma-\cos\phi)^4}{E^2\xi}\right]\,, \tag{3.273}
$$

$$
\begin{aligned}
c_3(\boldsymbol{p}^2) = \frac{m^6\nu^3}{E^2\xi}\Bigg[&\frac{16(\sigma-\cos\phi)^4 \mathrm{arcsinh}\sqrt{\frac{\sigma-1}{2}}}{\sqrt{\sigma^2-1}} - \frac{40m^2\nu(\sigma-\cos\phi)^4}{E^2\xi^2}\\
&+\frac{8m^4\nu^2(3-4\xi)(\sigma-\cos\phi)^5}{E^4\xi^3} - \frac{4m^6\nu^3(1-2\xi)(\sigma-\cos\phi)^6}{E^6\xi^4}\Bigg]\,.
\end{aligned}
\tag{3.274}
$$

A simple check is that for $\phi = 0$ the potential should vanish in the static limit, $\sigma \to 1$ because the black holes are extremal. At higher loops this will continue to hold because the amplitude is proportional $stuM^{\rm tree}$, which vanishes as $(1-\cos\phi)^4$. Note that at one loop there are no triangles so the result is pure iteration

$$
c_2(\boldsymbol{p}^2) = \left[\frac{(1-3\xi)}{2E\xi} + E\xi\partial_{\boldsymbol{p}^2}\right] c_1(\boldsymbol{p}^2)^2\,. \tag{3.275}
$$

We note that in the high-energy limit $\sigma \to \infty$, the potential also matches the result from Einstein gravity in Refs. [41, 42].

Scattering angle from the classical Hamiltonian

The scattering angle can be calculated from the Hamiltonian

$$H(\boldsymbol{p}, \boldsymbol{r}) = \sqrt{\boldsymbol{p}^2 + m_1^2} + \sqrt{\boldsymbol{p}^2 + m_2^2} + V(\boldsymbol{p}, \boldsymbol{r})\,, \tag{3.276}$$

by solving the classical equations of motion. As shown in Ref. [41], this yields a formula that expresses the scattering angle directly in terms the IR finite part of the PM amplitudes, $\mathcal{M}_i'$, which are defined by dropping the unevaluated integrals in the expressions above

$$2\pi\chi = \frac{d_1}{J} + \frac{d_2}{J^2} + \frac{1}{J^3}\left(-4d_3 + \frac{d_1 d_2}{\pi^2} - \frac{d_1^3}{48\pi^2}\right), \tag{3.277}$$

where d_i are defined in terms of $\mathcal{M}_i'$ as

$$d_1 = E\xi\boldsymbol{q}^2\mathcal{M}_1'/|\boldsymbol{p}|\,, \qquad d_2 = E\xi|\boldsymbol{q}|\mathcal{M}_2'\,, \qquad d_3 = E\xi|\boldsymbol{p}|\mathcal{M}_3'/\log\boldsymbol{q}^2\,. \tag{3.278}$$

Using our results for $\mathcal{N} = 8$ supergravity we find

$$d_1 = 8\pi G m^2 \nu \frac{(\sigma - \cos\phi)^2}{\sqrt{\sigma^2 - 1}}\,, \qquad d_2 = 0\,, \tag{3.279}$$

$$d_3 = \frac{32\pi G^3 m^6 \nu^4 (\sigma - \cos\phi)^4}{2(\sigma - 1)\nu + 1} \operatorname{arcsinh}\sqrt{\frac{\sigma - 1}{2}}\,, \tag{3.280}$$

so the scattering angle calculated from the EFT is

$$\chi^{\text{1PM}} = \frac{Gm^2\nu}{J}\frac{4(\sigma-\cos\phi)^2}{\sqrt{\sigma^2-1}}\,, \tag{3.281}$$

$$\chi^{\text{2PM}} = 0\,, \tag{3.282}$$

$$\chi^{\text{3PM}} = -\frac{G^3m^6\nu^3}{J^3}16\left[\frac{(\sigma-\cos\phi)^6}{3(\sigma^2-1)^{3/2}} + \nu\frac{4(\sigma-\cos\phi)^4}{2(\sigma-1)\nu+1}\text{arcsinh}\sqrt{\frac{\sigma-1}{2}}\right], \tag{3.283}$$

which precisely matches our results in Eqs. (3.245)–(3.247) from the eikonal analysis.

One might be tempted to use the Hamiltonian to also calculate the precession of the periastron, $\Delta\Phi$, but as explained in Refs. [239, 240], there is a simple relation between this quantity and the scattering angle

$$\Delta\Phi = \chi(J) + \chi(-J)\,, \tag{3.284}$$

which implies that odd orders in G (i.e. odd PM orders), which are also odd in J, do not produce a precession, which can be confirmed by explicit calculation using the Hamiltonian. This means that the absence of precession observed in Ref. [119] extends to $\mathcal{O}(G^3)$, although for trivial reasons, and a calculation at the next order will be needed to test their conjecture of no precession to all orders. The precise statement of the conjecture of in Ref. [119] is that the quantum energy levels of the bound system, which we have not explored in this work, remain exactly degenerate. However, the fact that there is a correction to the classical scattering angle at $\mathcal{O}(G^3)$, although suppressed in the probe limit, makes us less optimistic about the possibility of the orbits remaining integrable at this and higher orders.

3.4 Conclusions

In this chapter, by studying massless gravitational scattering amplitudes through $\mathcal{O}(G^3)$ in a variety of theories, we found the classical scattering angle to be independent of their matter

content, thus demonstrating graviton dominance at a higher order than had been previously understood [56–60]. In addition, we confirmed that the classical scattering angle found by ACV [61] is indeed correct. The results of our calculation are, however, in conflict with Damour's recent conjecture [65].

In the context of massive scattering, we computed the conservative classical dynamics for the scattering of two spinless extremal black holes in $\mathcal{N} = 8$ supergravity at $\mathcal{O}(G^3)$. In Refs. [41, 42] the $\mathcal{O}(G^3)$ (or 3rd-post-Minkowskian) conservative potential in Einstein gravity was calculated using an EFT matching procedure that avoids evaluation of infrared divergent integrals and provides a velocity expansion to high orders. Here, in contrast, we have directly calculated the IR-divergent scattering amplitude in dimensional regularization, and have directly obtained exact velocity dependence using differential equations, without the need to resum a series expansion.

This has allowed us to probe the delicate IR structure of eikonal exponentiation, where terms that vanish in four dimensions or vanish in the classical limit have to be evaluated explicitly at one loop, in order to construct IR subtraction terms at two loops to isolate genuine classical contributions at $O(G^3)$. Our novel integration method paves the way to a rigorous verification of the velocity resummation of Refs. [41, 42], and to streamline further calculations. The ability to evaluate the divergent two-loop amplitudes in dimensional regularization also opens the door to applying the method of Refs. [40, 189] which computes classical observables directly from appropriate phase space integrations of the S-matrix. Our differential equations method is highly flexible as the only difference between the soft region and the potential region is in the boundary conditions. The evaluation of the amplitude in the soft region at two loops and the emergence of non-exponentiating terms will be discussed elsewhere.

By computing the classical gravitational scattering angle in both the eikonal approximation and EFT formalism, we have explicitly established their equivalence at $\mathcal{O}(G^3)$ for the scattering of massive particles for the first time. While the EFT formalism gives a

more direct connection to the classical Hamiltonian, the eikonal approximation provides a more direct relation between two gauge-invariant quantities, the scattering amplitude and the scattering angle. It would be interesting to prove the all-order eikonal exponentiation structure for massive scattering from first principles beyond the one-loop case [38], perhaps by generalizing the partially massive case studied at two loops in Ref. [262], and to prove the validity of the eikonal angle formula beyond two loops.

Remarkably, we found that the classical scattering angle of two extremal black holes in $\mathcal{N} = 8$ supergravity coincides in the limit of high energy with that of two Schwarzschild black holes in Einstein gravity [41, 42]. Since the classical limit satisfies $|\boldsymbol{q}| \ll M$ and does not commute with the massless limit $M \to 0$, our result is reminiscent of, but not a direct consequence of, the universality of massless gravitational scattering in the Regge limit recently unveiled in Ref. [3], and strongly suggests graviton dominance, whose mechanism still needs to be understood, is generic at this order.

There are a number of interesting directions to pursue. First and foremost, it would be desirable to systematically complete a proof of universality through $\mathcal{O}(G^3)$ for any gravitational theory. An obvious, if nontrivial, next step would be to check whether some form of universality remains at higher orders as well. It would also be important to understand the constraints that the high-energy behavior of scattering amplitudes imposes on classical binary black hole interactions [62]. The recent advances [213, 214, 290, 291] that make it possible to obtain the complete four-graviton two-loop amplitude of pure Einstein gravity [106] can be expected to lead to further insight.

Beyond universality, several aspects of the scattering of black holes in $\mathcal{N} = 8$ supergravity deserve further study. For instance, it would be very interesting to re-analyze the two-loop calculation for dyonic black holes with generic charge misalignments. This might require an improved understanding of the structure of the S-matrix for mutually non-local particles. Furthermore, it would be interesting to calculate the exact quantum energy levels of the bound system and their decay rates to explore the precise integrability conjecture of

Ref. [119]. More generally, this conjecture should be investigated at the next order, where precession can arise. Given the simplicity of loop integrands in $\mathcal{N} = 8$ supergravity, we expect this highly symmetric theory to be an excellent theoretical laboratory for other aspects of black hole binary dynamics, such as spin-dependent scattering at $\mathcal{O}(G^3)$ and spinless scattering at $\mathcal{O}(G^4)$, both of which are unexplored frontiers in post-Minkowskian expansion of black hole binary dynamics, but are amenable to treatment by our techniques.[20] We hope to explore some of these questions in the near future.

3.A Dimensionally regularized integrals for the potential region

In this appendix we present results for dimensionally regularized Feynman integrals in $D - 1 = 3 - 2\epsilon$ spatial dimensions, needed for re-expanding the "soft integrals" in the potential region. All of these integrals are the result of evaluating the energy integrals using the residue prescriptions explained in the main text.

Following widely used conventions in the literature on Feynman integrals, the integrals are presented with the following normalization,

$$\frac{\mathrm{d}^{D-1}\boldsymbol{\ell}}{\pi^{(D-1)/2}} = 8\pi^{3/2}\,(4\pi)^{-\epsilon}\frac{\mathrm{d}^{D-1}\boldsymbol{\ell}}{(2\pi)^{(D-1)}}\,. \tag{3.285}$$

In the frame chosen the external three-momentum transfer $\boldsymbol{q}$ is in the transverse (x, y) direction, while some integrals have linear propagators of the form $1/\ell_z = 1/(\boldsymbol{\ell}\cdot\boldsymbol{n}_z)$, where $\boldsymbol{n}_z$ is the unit vector in the z-direction. The final results are fully relativistic and functions of $\boldsymbol{q}^2 = -q^2$. Unless otherwise shown, we will consider the $-i0$ prescription to be implicitly present in every propagator.

[20] See Refs. [206, 292, 293] for some related recent results in the post-Newtonian expansion. Also see Refs. [120, 189, 294–302] for spin-dependence in the post-Minkowskian expansion up to $\mathcal{O}(G^2)$.

3.A.1 One-loop integrals

At one loop we need to evaluate the linearized triangle and bubble integrals in Eqs. (3.100) and (3.99). These can evaluated using traditional methods. Concrete the general linearized triangle integral is given by [282]

$$\begin{aligned}&\int \frac{\mathrm{d}^{D-1}\boldsymbol{\ell}}{\pi^{(D-1)/2}} \frac{1}{(\boldsymbol{\ell}^2 - i0)^a [(\boldsymbol{\ell}-\boldsymbol{q})^2 - i0]^b (2\ell^z - i0)^c} \\ &= e^{\frac{i\pi c}{2}} (\boldsymbol{q}^2)^{\frac{3}{2}-a-b-\frac{c}{2}-\epsilon} \frac{\Gamma\left(\frac{c}{2}\right)\Gamma\left(\frac{3}{2}-a-\frac{c}{2}-\epsilon\right)\Gamma\left(\frac{3}{2}-b-\frac{c}{2}-\epsilon\right)\Gamma\left(a+b+\frac{c}{2}+\epsilon-\frac{3}{2}\right)}{2\Gamma(a)\Gamma(b)\Gamma(c)\Gamma(3-a-b-c-2\epsilon)}\,.\end{aligned} \tag{3.286}$$

The usual bubble integrals with $c = 0$ can be recovered by

$$\lim_{c\to 0} \frac{\Gamma(c/2)}{2\Gamma(c)} = 1\,. \tag{3.287}$$

In particular, for $a = b = 1$, $c \to 0$, Eq. (3.286) gives

$$\int \frac{\mathrm{d}^{D-1}\boldsymbol{\ell}}{\pi^{(D-1)/2}} \frac{1}{\boldsymbol{\ell}^2 (\boldsymbol{\ell}-\boldsymbol{q})^2} = \left(-q^2\right)^{-\epsilon} \frac{1}{\sqrt{-q^2}} \frac{\Gamma\left(\frac{1}{2}-\epsilon\right)^2 \Gamma\left(\frac{1}{2}+\epsilon\right)}{\Gamma(1-2\epsilon)}\,. \tag{3.288}$$

Setting $a = b = c = 1$ in Eq. (3.286) gives

$$\int \frac{\mathrm{d}^{D-1}\boldsymbol{\ell}}{\pi^{(D-1)/2}} \frac{1}{\boldsymbol{\ell}^2 (\boldsymbol{\ell}-\boldsymbol{q})^2 (2\ell^z)} = \left(-q^2\right)^{-\epsilon} \frac{1}{-q^2} \frac{i\sqrt{\pi}\,\Gamma(-\epsilon)^2\Gamma(1+\epsilon)}{2\Gamma(-2\epsilon)}\,. \tag{3.289}$$

Another way to evaluate this integral is by using symmetrization over the possible assignments of loop momenta

$$\begin{aligned}&\int \frac{\mathrm{d}^{D-1}\boldsymbol{\ell}}{\pi^{(D-1)/2}} \frac{1}{\boldsymbol{\ell}^2 (\boldsymbol{\ell}-\boldsymbol{q})^2 (2\ell_1^z - i0)} \\ &= \int \frac{\mathrm{d}^{D-1}\boldsymbol{\ell}_1}{\pi^{(D-1)/2}} \mathrm{d}^{D-1}\boldsymbol{\ell}_2 \frac{1}{(2\ell_1^z - i0)\prod_i \boldsymbol{\ell}_i^2} \delta\Big(\sum \ell_i^z\Big) \delta^{(D-2)}\Big(\sum \boldsymbol{\ell}_i^\perp - \boldsymbol{q}^\perp\Big)\,.\end{aligned} \tag{3.290}$$

Where the $\boldsymbol{\ell}_i^\perp$ and $\boldsymbol{q}^\perp$ are the components of $\boldsymbol{\ell}_i$ and $\boldsymbol{q}$ in the plane orthogonal to $\boldsymbol{n}_z$, respectively. Now we symmetrize over the two loop momenta, using

$$\frac{1}{2!}\left[\frac{1}{2\ell_1^z - i0} + \frac{1}{2\ell_2^z - i0}\right]\delta(\sum \ell_i^z) = \frac{i\pi}{2}\delta(\ell_1^z)\delta(\ell_2^z)\,. \tag{3.291}$$

Using $q^z = 0$, we can trivially preform the z-integration to obtain a $(D-2)$-dimensional bubble integral

$$\begin{aligned}\int \frac{\mathrm{d}^{D-1}\boldsymbol{\ell}}{\pi^{(D-1)/2}}\frac{1}{\boldsymbol{\ell}^2(\boldsymbol{\ell}-\boldsymbol{q})^2(2\ell_1^z - i0)} &= \frac{i\sqrt{\pi}}{2}\int \frac{\mathrm{d}^{D-2}\boldsymbol{\ell}_1}{\pi^{(D-2)/2}}\frac{1}{\boldsymbol{\ell}^2(\boldsymbol{\ell}-\boldsymbol{q})^2} \\ &= \left(-q^2\right)^{-\epsilon}\frac{1}{-q^2}\frac{i\sqrt{\pi}\Gamma(-\epsilon)^2\Gamma(\epsilon+1)}{2\Gamma(-2\epsilon)}\,,\end{aligned} \tag{3.292}$$

in agreement with Eq. (3.289).

3.A.2 Two-loop integrals

Double box (III) Adopting the frame choice Eq. (3.95), and after energy integration, we find that in the static limit, the pure basis of master integrals, Eqs. (3.115)–(3.124), for the Roman III family are equal to

$$f^{(p)}_{\mathrm{III},4}\big|_{y=1} = \frac{\pi}{6}\epsilon^2(1+2\epsilon)(-q^2)\int \frac{\mathrm{d}^{D-1}\boldsymbol{\ell}_1\mathrm{d}^{D-1}\boldsymbol{\ell}_2\,(e^{\gamma_{\mathbb{E}}\epsilon})^2}{(i\pi^{(D-1)/2})^2\,(\boldsymbol{\ell}_1^2)^2\boldsymbol{\ell}_2^2(\boldsymbol{\ell}_1+\boldsymbol{\ell}_2-\boldsymbol{q})^2}\,, \tag{3.293}$$

$$f^{(p)}_{\mathrm{III},6}\big|_{y=1} = \frac{\pi}{6}\epsilon^3(1-6\epsilon)\int \frac{\mathrm{d}^{D-1}\boldsymbol{\ell}_1\mathrm{d}^{D-1}\boldsymbol{\ell}_2\,(e^{\gamma_{\mathbb{E}}\epsilon})^2}{(i\pi^{(D-1)/2})^2\,\boldsymbol{\ell}_1^2\boldsymbol{\ell}_2^2(\boldsymbol{\ell}_1+\boldsymbol{\ell}_2-\boldsymbol{q})^2}\,, \tag{3.294}$$

$$f^{(p)}_{\mathrm{III},7}\big|_{y=1} = \pi\epsilon^4(-q^2)\int \frac{\mathrm{d}^{D-1}\boldsymbol{\ell}_1\mathrm{d}^{D-1}\boldsymbol{\ell}_2\,(e^{\gamma_{\mathbb{E}}\epsilon})^2}{(i\pi^{(D-1)/2})^2\,\boldsymbol{\ell}_1^2\boldsymbol{\ell}_2^2(\boldsymbol{\ell}_1+\boldsymbol{\ell}_2-\boldsymbol{q})^2(2\ell_1^z)(-2\ell_2^z)}\,, \tag{3.295}$$

$$f^{(p)}_{\mathrm{III},10}\big|_{y=1} = -\frac{\epsilon^4}{8}\sqrt{-q^2}\int \frac{\mathrm{d}^{D-1}\boldsymbol{\ell}_1\mathrm{d}^{D-1}\boldsymbol{\ell}_2\,(e^{\gamma_{\mathbb{E}}\epsilon})^2}{(i\pi^{(D-1)/2})^2\,\boldsymbol{\ell}_1^2\boldsymbol{\ell}_2^2(\boldsymbol{\ell}_1+\boldsymbol{\ell}_2-\boldsymbol{q})^2(2\ell_1^z)}\,, \tag{3.296}$$

where we have omitted the other integrals in the basis which vanish in the static limit. The first, second and fourth of these integrals can be evaluated by first performing a sub-loop integral over $\boldsymbol{\ell}_2$ using Eq. (3.286), and then evaluating the resulting $\boldsymbol{\ell}_1$ integral again using

Eq. (3.286) with non-integer propagator powers,

$$\int \frac{\mathrm{d}^{D-1}\boldsymbol{\ell}_1}{\pi^{(D-1)/2}} \frac{\mathrm{d}^{D-1}\boldsymbol{\ell}_2}{\pi^{(D-1)/2}} \frac{1}{(\boldsymbol{\ell}_1^2)^2 \boldsymbol{\ell}_2^2 (\boldsymbol{\ell}_1+\boldsymbol{\ell}_2-\boldsymbol{q})^2}$$
$$= \left(-q^2\right)^{-2\epsilon} \frac{1}{(-q^2)} \frac{\Gamma\left(-\epsilon-\frac{1}{2}\right)\Gamma\left(\frac{1}{2}-\epsilon\right)^2\Gamma(2\epsilon+1)}{\Gamma\left(\frac{1}{2}-3\epsilon\right)}\,, \tag{3.297}$$

$$\int \frac{\mathrm{d}^{D-1}\boldsymbol{\ell}_1}{\pi^{(D-1)/2}} \frac{\mathrm{d}^{D-1}\boldsymbol{\ell}_2}{\pi^{(D-1)/2}} \frac{1}{\boldsymbol{\ell}_1^2 \boldsymbol{\ell}_2^2 (\boldsymbol{\ell}_1+\boldsymbol{\ell}_2-\boldsymbol{q})^2}$$
$$= \left(-q^2\right)^{-2\epsilon} \frac{\Gamma\left(\frac{1}{2}-\epsilon\right)^3\Gamma(2\epsilon)}{\Gamma\left(\frac{3}{2}-3\epsilon\right)}\,, \tag{3.298}$$

$$\int \frac{\mathrm{d}^{D-1}\boldsymbol{\ell}_1}{\pi^{(D-1)/2}} \frac{\mathrm{d}^{D-1}\boldsymbol{\ell}_2}{\pi^{(D-1)/2}} \frac{1}{\boldsymbol{\ell}_1^2 \boldsymbol{\ell}_2^2 (\boldsymbol{\ell}_1+\boldsymbol{\ell}_2-\boldsymbol{q})^2 (2\ell_1^z)}$$
$$= \left(-q^2\right)^{-2\epsilon} \frac{1}{\sqrt{-q^2}} \frac{i\sqrt{\pi}\Gamma\left(\frac{1}{2}-2\epsilon\right)\Gamma\left(\frac{1}{2}-\epsilon\right)^2\Gamma(-\epsilon)\Gamma\left(2\epsilon+\frac{1}{2}\right)}{2\Gamma\left(\frac{1}{2}-3\epsilon\right)\Gamma(1-2\epsilon)}\,. \tag{3.299}$$

The evaluation of the remaining integral follows closely the evaluation of the one-loop triangle integral by symmetrization. We first rewrite

$$\int \frac{\mathrm{d}^{D-1}\boldsymbol{\ell}_1}{\pi^{(D-1)/2}} \frac{\mathrm{d}^{D-1}\boldsymbol{\ell}_2}{\pi^{(D-1)/2}} \frac{1}{\boldsymbol{\ell}_1^2 \boldsymbol{\ell}_2^2 (\boldsymbol{\ell}_1+\boldsymbol{\ell}_2-\boldsymbol{q})^2 (2\ell_1^z - i0)(-2\ell_2^z - i0)} \tag{3.300}$$
$$= \int \frac{\mathrm{d}^{D-1}\boldsymbol{\ell}_1}{\pi^{(D-1)/2}} \frac{\mathrm{d}^{D-1}\boldsymbol{\ell}_2}{\pi^{(D-1)/2}} \mathrm{d}^{D-1}\boldsymbol{\ell}_3 \frac{1}{(2\ell_1^z - i0)(-2\ell_2^z - i0)\prod_i \boldsymbol{\ell}_i^2} \delta(\sum \ell_i^z)\delta^{(D-2)}(\sum \boldsymbol{\ell}_i^\perp - \boldsymbol{q}^\perp)\,.$$

Symmetrizing over all loop momenta, results in the identity similar to Eq. (3.291),

$$\frac{1}{3!}\left[\frac{1}{(2\ell_1^z - i0)(-2\ell_2^z - i0)} + \text{perms.}\right]\delta\left(\sum \ell_i^z\right) = -\frac{\pi^2}{6}\delta(\ell_1^z)\delta(\ell_2^z)\delta(\ell_3^z)\,. \tag{3.301}$$

Using $q^z = 0$, we can trivially preform the z-integration to obtain a $(D-2)$-dimensional integral

$$\int \frac{\mathrm{d}^{D-1}\boldsymbol{\ell}_1}{\pi^{(D-1)/2}} \frac{\mathrm{d}^{D-1}\boldsymbol{\ell}_2}{\pi^{(D-1)/2}} \frac{1}{\boldsymbol{\ell}_1^2 \boldsymbol{\ell}_2^2 (\boldsymbol{\ell}_1+\boldsymbol{\ell}_2-\boldsymbol{q})^2 (2\ell_1^z - i0)(-2\ell_2^z - i0)} \tag{3.302}$$
$$= -\frac{\pi}{6}\int \frac{\mathrm{d}^{D-2}\boldsymbol{\ell}_1}{\pi^{(D-2)/2}} \frac{\mathrm{d}^{D-2}\boldsymbol{\ell}_2}{\pi^{(D-2)/2}} \frac{1}{\boldsymbol{\ell}_1^2 \boldsymbol{\ell}_2^2 (\boldsymbol{\ell}_1+\boldsymbol{\ell}_2-\boldsymbol{q})^2} = -\frac{\pi}{6}\left(-q^2\right)^{-2\epsilon} \frac{1}{(-q^2)} \frac{\Gamma(-\epsilon)^3\Gamma(2\epsilon+1)}{\Gamma(-3\epsilon)}\,.$$

Therefore, the integrals with nonzero values in the static limit are

$$f^{(p)}_{\text{III},4}\big|_{y=1} = -2f^{(p)}_{\text{III},6}\big|_{y=1} = \frac{2\pi}{3}\epsilon^3(-q^2)^{-2\epsilon}e^{2\gamma_{\text{E}}\epsilon}\frac{\Gamma\left(\frac{1}{2}-\epsilon\right)^3\Gamma(2\epsilon)}{\Gamma\left(\frac{1}{2}-3\epsilon\right)}\,, \tag{3.303}$$

$$f^{(p)}_{\text{III},7}\big|_{y=1} = \frac{\pi^2}{6}\epsilon^4(-q^2)^{-2\epsilon}e^{2\gamma_{\text{E}}\epsilon}\frac{\Gamma(-\epsilon)^3\Gamma(2\epsilon+1)}{\Gamma(-3\epsilon)}\,, \tag{3.304}$$

$$f^{(p)}_{\text{III},10}\big|_{y=1} = -\frac{i\epsilon^4\pi^{3/2}}{4}(-q^2)^{-2\epsilon}e^{2\gamma_{\text{E}}\epsilon}\frac{\Gamma\left(\frac{1}{2}-2\epsilon\right)\Gamma\left(\frac{1}{2}-\epsilon\right)^2\Gamma(-\epsilon)\Gamma\left(\frac{1}{2}+2\epsilon\right)}{\Gamma\left(\frac{1}{2}-3\epsilon\right)\Gamma(1-2\epsilon)}\,. \tag{3.305}$$

By expanding in ϵ one can check that such boundary conditions (3.311)–(3.304) are of uniform transcendental weight, and yield the boundary vector (3.137) used in the text.

H and $\overline{\text{H}}$ The integrals for the sum of H and $\overline{\text{H}}$ topologies with non-vanishing static limits are

$$f^{(p)}_{\text{cH},4}\big|_{y=1} = -\frac{\pi}{2}\epsilon^4(-q^2)\int\frac{\mathrm{d}^{D-1}\boldsymbol{\ell}_1\mathrm{d}^{D-1}\boldsymbol{\ell}_2\,(e^{\gamma_{\text{E}}\epsilon})^2}{(i\pi^{(D-1)/2})^2\boldsymbol{\ell}_1^2\boldsymbol{\ell}_2^2(\boldsymbol{\ell}_1-\boldsymbol{q})^2(\boldsymbol{\ell}_2-\boldsymbol{q})^2}\,, \tag{3.306}$$

$$f^{(p)}_{\text{cH},7}\big|_{y=1} = -\frac{\pi}{4}\epsilon^2(1+2\epsilon)\int\frac{\mathrm{d}^{D-1}\boldsymbol{\ell}_1\mathrm{d}^{D-1}\boldsymbol{\ell}_2\,(e^{\gamma_{\text{E}}\epsilon})^2}{(i\pi^{(D-1)/2})^2(\boldsymbol{\ell}_1^2)^2\boldsymbol{\ell}_2^2(\boldsymbol{\ell}_1+\boldsymbol{\ell}_2-\boldsymbol{q})^2}\,, \tag{3.307}$$

$$f^{(p)}_{\text{cH},10}\big|_{y=1} = -\pi\epsilon^4(-q^2)\int\frac{\mathrm{d}^{D-1}\boldsymbol{\ell}_1\mathrm{d}^{D-1}\boldsymbol{\ell}_2\,(e^{\gamma_{\text{E}}\epsilon})^2}{(i\pi^{(D-1)/2})^2\boldsymbol{\ell}_1^2\boldsymbol{\ell}_2^2(\boldsymbol{\ell}_1-\boldsymbol{q})^2(\boldsymbol{\ell}_2-\boldsymbol{q})^2}\,. \tag{3.308}$$

The second integral has already been evaluated, and equals to

$$f^{(p)}_{\text{cH},7}\big|_{y=1} = -\frac{3}{2}f^{(p)}_{\text{III},4}\big|_{y=1}\,. \tag{3.309}$$

The remaining integrals are proportional to a two-loop double-bubble integral which factorizes and is trivially the square of the one-loop bubble integral (3.288)

$$\int\frac{\mathrm{d}^{D-1}\boldsymbol{\ell}_1}{\pi^{(D-1)/2}}\frac{\mathrm{d}^{D-1}\boldsymbol{\ell}_2}{\pi^{(D-1)/2}}\frac{1}{\boldsymbol{\ell}_1^2\boldsymbol{\ell}_2^2(\boldsymbol{\ell}_1-\boldsymbol{q})^2(\boldsymbol{\ell}_2-\boldsymbol{q})^2} = \left(-q^2\right)^{-2\epsilon}\frac{1}{(-q^2)}\frac{\Gamma\left(\frac{1}{2}-\epsilon\right)^4\Gamma\left(\frac{1}{2}+\epsilon\right)^2}{\Gamma(1-2\epsilon)^2}\,. \tag{3.310}$$

In summary we find the following result for the static integrals

$$f^{(p)}_{\text{cH},4}\big|_{y=1} = \frac{1}{2} f^{(p)}_{\text{cH},10}\big|_{y=1} = \frac{\pi}{2}\epsilon^4(-q^2)^{-2\epsilon}e^{2\gamma_{\text{E}}\epsilon}\left[\frac{\Gamma\left(\frac{1}{2}-\epsilon\right)^2\Gamma\left(\epsilon+\frac{1}{2}\right)}{\Gamma(1-2\epsilon)}\right]^2, \tag{3.311}$$

$$f^{(p)}_{\text{cH},7}\big|_{y=1} = -\pi\epsilon^3(-q^2)^{-2\epsilon}e^{2\gamma_{\text{E}}\epsilon}\frac{\Gamma\left(\frac{1}{2}-\epsilon\right)^3\Gamma(2\epsilon)}{\Gamma\left(\frac{1}{2}-3\epsilon\right)}, \tag{3.312}$$

which yields the boundary vector in Eq. (3.162).

IX **and crossed integrals** The evaluation of the boundary vector for the IX and crossed integrals proceeds analogously to the computations in the previous subsubsections. In particular all three-dimensional integrals necessary have already been computed therein. The values for the boundary conditions can be extracted from the full results provided in the ancillary files accompanying the ArXiv submission of this work.

3.B Solution of the differential equations

Having the canonical form of the differential equations at hand the systems can be straightforwardly solved order-by-order in ϵ, yielding harmonic polylogarithms. In this appendix we present the solution of the differential equations for two-loop master integrals in the potential region up to $\mathcal{O}(\epsilon^4)$. All the functions not shown vanish. The solution of the differential equations in Eq. (3.126) with the matrices in Eqs. (3.128) and (3.129) and boundary conditions

in Eq. (3.137) is

$$f^{(p)}_{\text{III},2} = (-q^2)^{-2\epsilon}\epsilon^2\pi^2\left[-\frac{1}{3}\epsilon\log(x) + \epsilon^2\left(\text{Li}_2(1-x^2) + \log^2(x)\right)\right], \tag{3.313}$$

$$f^{(p)}_{\text{III},3} = (-q^2)^{-2\epsilon}\epsilon^2\pi^2\left[-\frac{2}{3}\epsilon\log(x) - \frac{2}{3}\epsilon^2\left(\text{Li}_2(1-x^2) + \log^2(x)\right)\right], \tag{3.314}$$

$$f^{(p)}_{\text{III},4} = (-q^2)^{-2\epsilon}\epsilon^2\pi^2\left[\frac{1}{3} + \frac{1}{18}\epsilon^2\left(-7\pi^2 - 48\log^2(x)\right)\right], \tag{3.315}$$

$$f^{(p)}_{\text{III},6} = (-q^2)^{-2\epsilon}\epsilon^2\pi^2\left[-\frac{1}{6} + \frac{7\epsilon^2\pi^2}{36}\right], \tag{3.316}$$

$$f^{(p)}_{\text{III},7} = (-q^2)^{-2\epsilon}\epsilon^2\pi^2\left[\frac{1}{2} - \frac{1}{12}\left(4\log^2(x) + \pi^2\right)\right], \tag{3.317}$$

$$f^{(p)}_{\text{III},10} = (-q^2)^{-2\epsilon}\epsilon^2\pi^2\left[\frac{i\pi\epsilon}{4} - \frac{i\pi\log(2)\epsilon^2}{2}\right]. \tag{3.318}$$

The solution of the differential equations in Eq. (3.152) with the matrices in Eq. (3.153) and boundary conditions in Eq. (3.162) is

$$f^{(p)}_{\text{cH},4} = (-q^2)^{-2\epsilon}\epsilon^2\pi^2\left[\frac{\epsilon^2\pi^2}{2}\right], \tag{3.319}$$

$$f^{(p)}_{\text{cH},5} = (-q^2)^{-2\epsilon}\epsilon^2\pi^2\left[\frac{1}{2}\epsilon\log(x) - \frac{3}{2}\epsilon^2\left(\text{Li}_2(1-x^2) + \log^2(x)\right)\right], \tag{3.320}$$

$$f^{(p)}_{\text{cH},6} = (-q^2)^{-2\epsilon}\epsilon^2\pi^2\left[\epsilon\log(x) + \epsilon^2\left(\text{Li}_2(1-x^2) + \log^2(x)\right)\right], \tag{3.321}$$

$$f^{(p)}_{\text{cH},7} = (-q^2)^{-2\epsilon}\epsilon^2\pi^2\left[-\frac{1}{2} + \epsilon^2\left(\frac{7\pi^2}{12} + 4\log^2(x)\right)\right], \tag{3.322}$$

$$f^{(p)}_{\text{cH},9} = (-q^2)^{-2\epsilon}\epsilon^2\pi^2\left[-\epsilon\log(x) + \epsilon^2\left(\text{Li}_2(1-x^2) + \log^2(x)\right)\right], \tag{3.323}$$

$$f^{(p)}_{\text{cH},10} = (-q^2)^{-2\epsilon}\epsilon^2\pi^2\left[\epsilon^2\left(\pi^2 + 6\log^2(x)\right)\right]. \tag{3.324}$$

The solution of the differential equations in Eq. (3.184) with the matrices in Eqs. (3.188) and (3.186) boundary conditions in Eq. (3.191) is

$$f^{(p)}_{\text{IX},2} = (-q^2)^{-2\epsilon}\epsilon^2\pi^2\left[-\frac{1}{6}\epsilon\log(x) - \frac{1}{2}\epsilon^2\left(\text{Li}_2(1-x^2) + \log^2(x)\right)\right], \tag{3.325}$$

$$f^{(p)}_{\text{IX},3} = (-q^2)^{-2\epsilon}\epsilon^2\pi^2\left[\frac{1}{3}\epsilon\log(x) + \frac{1}{3}\epsilon^2\left(\text{Li}_2(1-x^2) + \log^2(x)\right)\right], \tag{3.326}$$

$$f^{(p)}_{\text{IX},4} = (-q^2)^{-2\epsilon}\epsilon^2\pi^2\left[-\frac{1}{6} + \frac{1}{36}\epsilon^2\left(7\pi^2 + 48\log^2(x)\right)\right], \tag{3.327}$$

$$f^{(p)}_{\text{IX},5} = (-q^2)^{-2\epsilon}\epsilon^2\pi^2\left[\frac{1}{3}\epsilon\log(x) - \epsilon^2\left(\text{Li}_2(1-x^2) + \log^2(x)\right)\right], \tag{3.328}$$

$$f^{(p)}_{\text{IX},6} = (-q^2)^{-2\epsilon}\epsilon^2\pi^2\left[\frac{2}{3}\epsilon\log(x) + \frac{2}{3}\epsilon^2\left(\text{Li}_2(1-x^2) + \log^2(x)\right)\right], \tag{3.329}$$

$$f^{(p)}_{\text{IX},7} = (-q^2)^{-2\epsilon}\epsilon^2\pi^2\left[\frac{1}{3} - \frac{1}{18}\epsilon^2\left(7\pi^2 + 48\log^2(x)\right)\right], \tag{3.330}$$

$$f^{(p)}_{\text{IX},8} = (-q^2)^{-2\epsilon}\epsilon^2\pi^2\left[-\frac{1}{6} + \frac{7\pi^2\epsilon^2}{36}\right], \tag{3.331}$$

$$f^{(p)}_{\text{IX},10} = (-q^2)^{-2\epsilon}\epsilon^2\pi^2\left[-\frac{5}{12}\epsilon^2\log^2(x)\right], \tag{3.332}$$

$$f^{(p)}_{\text{IX},15} = (-q^2)^{-2\epsilon}\epsilon^2\pi^2\left[\frac{i\pi\epsilon}{4} - \frac{i\pi\log(2)\epsilon^2}{2}\right]. \tag{3.333}$$

The differential equation for the $\overline{\text{III}}$ topology is obtained by crossing from the differential equation for the III topology in Eq. (3.126) with the matrices in Eqs. (3.128) and (3.129). Using the boundary conditions in Eq. (3.195), we find the solutions

$$f^{(p)}_{\overline{\text{III}},3} = (-q^2)^{-2\epsilon}\epsilon^2\pi^2\left[\frac{1}{6}\epsilon\log(x) - \frac{1}{2}\epsilon^2\left(\text{Li}_2(1-x^2) + \log^2(x)\right)\right], \tag{3.334}$$

$$f^{(p)}_{\overline{\text{III}},4} = (-q^2)^{-2\epsilon}\epsilon^2\pi^2\left[-\frac{1}{6} + \frac{1}{36}\epsilon^2\left(7\pi^2 + 48\log^2(x)\right)\right], \tag{3.335}$$

$$f^{(p)}_{\overline{\text{III}},5} = (-q^2)^{-2\epsilon}\epsilon^2\pi^2\left[\frac{1}{3}\epsilon\log(x) + \frac{1}{3}\epsilon^2\left(\text{Li}_2(1-x^2) + \log^2(x)\right)\right], \tag{3.336}$$

$$f^{(p)}_{\overline{\text{III}},6} = (-q^2)^{-2\epsilon}\epsilon^2\pi^2\left[-\frac{1}{6} + \frac{7\epsilon^2\pi^2}{36}\right], \tag{3.337}$$

$$f^{(p)}_{\overline{\text{III}},7} = (-q^2)^{-2\epsilon}\epsilon^2\pi^2\left[-\frac{1}{6}\epsilon^2\log^2(x)\right]. \tag{3.338}$$

The differential equation for the $\overline{\text{IX}}$ topology is obtained by crossing from the differential equation for the IX topology in Eq. (3.126) with the matrices in Eqs. (3.188) and (3.186). Using the boundary conditions in Eq. (3.196), we find the solutions

$$f^{(p)}_{\overline{\text{IX}},2} = (-q^2)^{-2\epsilon}\epsilon^2\pi^2 \left[\frac{1}{3}\epsilon \log(x) - \epsilon^2 \left(\text{Li}_2(1-x^2) + \log^2(x)\right)\right], \tag{3.339}$$

$$f^{(p)}_{\overline{\text{IX}},3} = (-q^2)^{-2\epsilon}\epsilon^2\pi^2 \left[\frac{2}{3}\epsilon \log(x) + \frac{2}{3}\epsilon^2 \left(\text{Li}_2(1-x^2) + \log^2(x)\right)\right], \tag{3.340}$$

$$f^{(p)}_{\overline{\text{IX}},4} = (-q^2)^{-2\epsilon}\epsilon^2\pi^2 \left[\frac{1}{3} + \frac{1}{18}\epsilon^2 \left(7\pi^2 + 48\log^2(x)\right)\right], \tag{3.341}$$

$$f^{(p)}_{\overline{\text{IX}},5} = (-q^2)^{-2\epsilon}\epsilon^2\pi^2 \left[\frac{1}{6}\epsilon \log(x) - \frac{1}{2}\epsilon^2 \left(\text{Li}_2(1-x^2) + \log^2(x)\right)\right], \tag{3.342}$$

$$f^{(p)}_{\overline{\text{IX}},6} = (-q^2)^{-2\epsilon}\epsilon^2\pi^2 \left[\frac{1}{3}\epsilon \log(x) - \frac{1}{3}\epsilon^2 \left(\text{Li}_2(1-x^2) + \log^2(x)\right)\right], \tag{3.343}$$

$$f^{(p)}_{\overline{\text{IX}},7} = (-q^2)^{-2\epsilon}\epsilon^2\pi^2 \left[-\frac{1}{6} + \frac{1}{36}\epsilon^2 \left(7\pi^2 + 48\log^2(x)\right)\right], \tag{3.344}$$

$$f^{(p)}_{\overline{\text{IX}},8} = (-q^2)^{-2\epsilon}\epsilon^2\pi^2 \left[-\frac{1}{6} + \frac{7\pi^2\epsilon^2}{36}\right], \tag{3.345}$$

$$f^{(p)}_{\overline{\text{IX}},10} = (-q^2)^{-2\epsilon}\epsilon^2\pi^2 \left[\frac{1}{3}\epsilon^2 \log^2(x)\right]. \tag{3.346}$$

Chapter 4

Topological Phases in String Theory

4.1 Introduction and summary

4.1.1 Generalities

In perturbative formulations of superstring theories, one treats the 2d worldsheets of strings as 2d quantum field theories with fermions. The most common treatment is the one due to Neveu-Schwarz [303] and Ramond [304], often called the NSR formalism. There, one starts with ten bosonic fields $X^{\mu=0,\ldots,9}$ and ten left- and right-moving fermionic fields $\psi^{\mu=0,\ldots,9}$ and $\tilde{\psi}^{\mu=0,\ldots,9}$. To remove the closed-string tachyon and at the same time obtain spacetime spinors, one must perform a crucial step called the Gliozzi-Scherk-Olive (GSO) projection [71, 72]. The two Type II superstring theories, Type IIA and Type IIB, arise due to a difference in the specifics of this projection.

It was pointed out in [74, 305] that the GSO projection can be interpreted as a sum over the possible spin structures on the worldsheet, with different consistent GSO projections corresponding to different ways of assigning complex phases to spin structures, in a manner consistent with cutting and gluing of the worldsheet. This point of view makes manifest the all-genus consistency of known GSO projections, which is not evident in the one-loop

analysis often presented to beginners of string theory e.g. in [73]. It does not, however, tell us whether we have found all possible GSO projections. Indeed, possible consistent GSO projections for unoriented superstring theories have not been studied systematically in the past.

One approach to the enumeration of all consistent GSO projections comes from a rather unexpected place, namely from the study of symmetry-protected topological (SPT) and invertible phases of matter in condensed matter physics.[1] For the purposes of this work, an invertible phase for a symmetry G can be defined as a system which has a one-dimensional gapped vacuum on any closed spatial manifold with a background field for G. By taking the infrared limit, one can then isolate a quantum system whose entire Hilbert space on any closed spatial manifold with any background field is one-dimensional and contains the vacuum only, with its partition function simply a complex phase. We note that for an internal symmetry, the background field is simply a non-dynamical gauge field for the symmetry. On the other hand, for fermion number symmetry the background field is the spin structure, while for time-reversal symmetry the background field is the "un-oriented-ness" of the spacetime.

An invertible phase provides a method for assigning complex phases to spin and other structures on a manifold, in a manner consistent with cutting and gluing. Conversely, any such assignment corresponds to an invertible phase. Therefore, if one can classify invertible phases, one can classify all consistent GSO projections. Invertible phases with fermion number symmetry and some additional discrete symmetries are usually called topological superconductors in the condensed matter literature. Therefore, the classification of GSO projections is equivalent to the classification of topological superconductors in $(1+1)$ dimensions.

The classification of invertible phases has been an important topic of recent research in theoretical condensed matter physics. As will be reviewed below, a general answer in terms

[1] In the literature of high-energy physics, the terms SPT and invertible phase are often used interchangeably. In condensed matter physics they have subtly different connotations. In this work we stick to the terminology of invertible phases, which are more directly relevant for our purposes.

of bordism groups has been obtained, see e.g. [77–79]. The upshot is that with this result, we can now carry out the classification of possible GSO projections on a given worldsheet, once the structure on said worldsheet is specified.

One important feature of a nontrivial invertible phase in d dimensions for a symmetry G is that, if it is put on a spacetime with boundary, the $(d-1)$-dimensional boundary theory necessarily hosts nontrivial degrees of freedom. In particular, if G is unbroken on the boundary, the G-symmetric boundary theory carries a corresponding G-anomaly. One familiar case is that of the chiral anomaly of a fermion in spacetime dimension $2n$, which is captured by a Chern-Simons term in $2n+1$ dimensions. This is known as anomaly inflow [306, 307]. The current understanding is that all anomalies[2] in $(d-1)$ dimensions, both local and global, can be characterized in terms of invertible phases in d dimensions.

Applying this observation to the worldsheets of superstrings, we conclude that different invertible phases, i.e. different GSO projections, will require different boundary conditions on the edges of worldsheets. Since the boundaries of worldsheets describe the D-branes to which strings attach, this means that the properties of D-branes reflect the choice of GSO projection. The discussions up to this point can be summarized schematically as follows:

$$\begin{aligned} \text{boundary anomaly} \quad &: \quad \text{bulk invertible phase} \\ \sim \ \text{properties of D-branes} \quad &: \quad \text{choice of GSO projection.} \end{aligned} \tag{4.1}$$

[2]Some qualifications need to be added to this blanket statement. First, this framework is mostly about the anomalies of partition functions, and therefore does not immediately describe the conformal anomaly. Second, anomalies of supersymmetry are less well understood, and it is not clear whether they can be described by bulk invertible phases. That said, neither is conclusively outside of this framework. As for the first, the anomaly described by the Kitaev chain is about the impossibility of quantizing a single Majorana fermion, which is also not directly about the phase of the partition function. As for the second, the supersymmetry anomaly recently found in [308, 309], which is a superpartner of the anomaly in R-symmetry, was first found in the context of AdS/CFT [310]. We also note that the shortening anomaly of [311] is related to the fact that the scalar target space of the holographic supergravity dual is often not Kähler. All this suggests that these anomalies might also be described in a suitable generalization of the current framework. It would be interesting to work this out.

4.1.2 GSO projections and K-theory classification of D-branes

Let us now be more concrete. First, we recall the classification of invertible phases in terms of bordism groups.[3] Let X denote collectively the structure on the spacetime, appropriate for the systems we would like to classify. For example, X consists of a spin structure and a G gauge field for systems with fermion number symmetry and an internal symmetry G. We define the X-bordism group Ω_d^X in dimension d to be

$$\Omega_d^X := \{d\text{-dimensional manifolds with } X \text{ structure}\}/\sim, \tag{4.2}$$

where the equivalence relation is introduced so that $M_d \sim M_d'$ if and only if there exists N_{d+1} with the structure X such that ∂N_{d+1} has M_d as the incoming boundary and M_d' as the outgoing boundary. The group structure is given by the disjoint union. Then, the topological invertible phases in spacetime dimension d are classified by [77–79]

$$\mho_X^d := \mathrm{Hom}(\Omega_d^X, U(1)). \tag{4.3}$$

This simply means that the topological invertible phase for an element $\alpha \in \mho_X^d$ assigns the partition function $\alpha(M_d) \in U(1)$ in such a way that it only depends on the bordism class $[M_d] \in \Omega_d^X$.[4]

In this work we will encounter the following structures on the worldsheet: spin structure

[3] For other recent applications of bordism groups to high-energy theory, see [312–320].

[4] More precisely, $\mho_X^d$ as defined here classifies invertible phases whose partition functions do not depend continuously on the background fields. Therefore it includes e.g. the 2d theta term $\int \theta F/(2\pi)$, which only depends on topological data, but it does not include e.g. the 3d gravitational Chern-Simons term, which does depend continuously on the metric. The latter is accounted for by considering $(D\Omega^X)^{d+1}$ instead, where D denotes the Anderson dual. This group classifies the deformation classes of invertible phases which can depend continuously on the background fields. Since we take the deformation classes, $(D\Omega^X)^{d+1}$ does not include the theta term, which can be continuously varied. The torsion parts of both groups coincide: $\mathrm{Tors}\,\mathrm{Hom}(\Omega_d^X, U(1)) = \mathrm{Tors}(D\Omega^X)^{d+1}$, since torsion invertible phases are discrete and cannot depend continuously on the background data. Both $\mathrm{Hom}(\Omega_d^X, U(1))$ and $(D\Omega^X)^{d+1}$ are generalized cohomology theories, but their common torsion part is not. This unfortunately makes the torsion part less mathematically natural. For all the cases of interest to us in this work, all bordism groups are finite, so these subtle differences can and will be ignored.

d	$\mathfrak{O}^d_{\text{Spin}}(pt)$	$\mathfrak{O}^d_{\text{Spin}}(B\mathbb{Z}_2)$	$\mathfrak{O}^d_{\text{Pin}^-}(pt)$	$\mathfrak{O}^d_{\text{Pin}^+}(pt)$	$\mathfrak{O}^d_{\text{DPin}}(pt)$
2	$\mathbb{Z}_2$	$\mathbb{Z}_2^2$	$\mathbb{Z}_8$	$\mathbb{Z}_2$	$\mathbb{Z}_2^2$
3	0	$\mathbb{Z}_8$	0	$\mathbb{Z}_2$	$\mathbb{Z}_8$

Table 4.1: Dual bordism groups relevant to our analysis. The first four columns are classic [78, 321]. The last column is new.

for oriented Type 0 strings, Spin $\times \mathbb{Z}_2$ structure for oriented Type II strings, $\text{Pin}^{\pm}$ structure for two types of unoriented Type 0 strings, and "double pin" or DPin structure for Type I strings. We remark here that originally the II, I, 0 in Type II, I, 0 strings referred to the number of supersymmetries in ten dimensions. Contrary to this usage, in this work we refer to any NSR strings with independent GSO projections on left- and right-moving spin structures as Type II, and to any NSR strings with diagonal GSO projections as Type 0. Type I strings will then be defined as Type II NSR strings on unoriented worldsheets.

The relevant dual bordism groups are listed in Table 4.1. There we have used a slightly more general notation, with $\Omega^X_d(Y)$ representing the bordism group of d-dimensional manifolds with X structure equipped with a map to Y. Then for example a structure X' consisting of spin structure and a $\mathbb{Z}_2$ gauge field can equivalently be thought of as having $(X, Y) = (\text{spin structure}, B\mathbb{Z}_2)$, where $B\mathbb{Z}_2$ is the classifying space of $\mathbb{Z}_2$ gauge fields, and therefore $\Omega^{X'}_d = \Omega^{\text{Spin}}_d(B\mathbb{Z}_2)$. Similarly, letting pt stands for a point, we have $\Omega^X_d = \Omega^X_d(pt)$.

Let us begin by discussing the group $\mathfrak{O}^2_{\text{Spin}}(pt) = \mathbb{Z}_2$. The nontrivial element is mathematically known as the Arf invariant, and assigns to a surface Σ with a choice of spin structure σ a sign $(-1)^{\text{Arf}(\Sigma,\sigma)}$. A spin structure is called even or odd depending on whether this sign is $+1$ or -1. There are many mathematical and physical definitions of the Arf invariant, one of which is as the number modulo two of zero modes of the Dirac operator on the surface Σ with spin structure σ [322]. From this definition, we see easily that $(-1)^{\text{Arf}(T^2,\sigma)}$ is -1 if and only if the spin structure σ is periodic along both cycles of the torus T^2. There is also a combinatorial definition [323, 324], which we will recall below.

In the continuum quantum field theory language, the Arf invariant may be written in

terms of the partition function of a mass m Majorana fermion on (Σ, σ) as $Z_{\text{ferm}}(m \gg 0; \Sigma, \sigma)/Z_{\text{ferm}}(m \ll 0; \Sigma, \sigma)$. In general, the infinite-mass limit of a fermion partition function is known as an η-invariant in the mathematics literature, meaning that the Arf invariant is an example of an η-invariant. There is also a discretized Hamiltonian version of this massive Majorana fermion defined on a spin chain — this is known as the Kitaev chain [75]. In both of these descriptions, it is easy to argue that one needs a single Majorana fermion on the $(0+1)$d boundary of the $(1+1)$d system hosting the Arf invariant theory.

A single Majorana fermion cannot be consistently quantized, since two Majorana fermions act on a two-dimensional Hilbert space irreducibly. This means that, assuming that this Hilbert space is the tensor product of two copies of the Hilbert space for a single fermion, the single-fermion Hilbert space would need to have dimension $\sqrt{2}$. This is one manifestation of the anomaly of the boundary theory, and will turn out to explain the difference by a factor of $\sqrt{2}$ between the tensions of D9-branes in Type IIA and Type IIB theories, originally found in [325].

Without the Arf invariant on the worldsheet, as will be the case for Type IIB strings, the endpoints of open strings will naturally couple to unitary bundles. Consideration of tachyon condensation motivates one to introduce an equivalence relation on unitary bundles, leading to the statement that stable D-branes on X are classified by complex K-theory $K^0(X)$ [92]. On the other hand, in the presence of the Arf invariant the boundary of the worldsheet needs unitary bundles together with an additional Majorana fermion, or equivalently with an action of the complex Clifford algebra $\text{Cl}(1, \mathbb{C})$. Unitary bundles with an action of $\text{Cl}(1, \mathbb{C})$, under a suitable equivalence relation implementing tachyon condensation, are classified by $K^1(X)$, thus reproducing the known classification of the D-branes in the Type IIA theory [92, 93].

We next discuss the effects of including the topological superconductor corresponding to the group $\mathfrak{V}^2_{\text{Pin}^-}(pt) = \mathbb{Z}_8$ on worldsheets. The worldsheets can now be nonorientable and are equipped with a Pin^- structure. This structure will be seen to be compatible with the Type 0 string, but not with the Type I string. The generator of the group $\mathbb{Z}_8$ of time-reversal

invariant topological superconductors is again the Kitaev chain, but now with the added assumption of time-reversal invariance. The invertible phase corresponding to n modulo 8 is simply n copies of the Kitaev chain, and has n time-reversal symmetric Majorana fermions on the boundary. Physically, the reason that we need only consider n modulo 8 is that one can introduce a four-fermi interaction to the $n = 8$ theory which gives rise to a theory with unique ground state [80]. In continuum field theory language, the effective action describing the basic non-trivial phase is the Arf-Brown-Kervaire (ABK) invariant, to be discussed below.

Roughly speaking, with n copies of the time-reversal-symmetric Kitaev chain on the worldsheet, open string endpoints can now couple to orthogonal bundles with an action of n time-reversal invariant Majorana fermions, or equivalently with an action of the real Clifford algebra $\mathrm{Cl}(n, \mathbb{R})$. Tachyon condensation then leads to the classification of D-branes by $KO^n(X)$. As we will see, a more careful analysis reveals that the classification is in fact by $KO^n(X) \oplus KO^{-n}(X)$.

In the case of Type I strings, the natural way to specify the worldsheet fermions is to consider chiral fermions on the orientation double cover of the worldsheet. This leads to a structure which we call "double pin" structure, since it will be shown to contain both $\mathrm{Pin}^{\pm}$ as subgroups. We will find by a standard algebraic topology computation that any invertible phase one can add on the worldsheet is either the Arf invariant associated to the orientation double cover, or a continuum version of the Haldane chain. We will find that the Arf invariant on the double cover can be removed by performing a spacetime parity transformation along one direction, meaning that it does not give rise to physically distinct theories. On the other hand, the invertible phase corresponding to the low energy limit of the $S = 1$ Haldane chain[326, 327], whose partition function counts the number of $\mathbb{RP}^2$ modulo 2, gives rise to the difference between $\mathrm{O9}^{\pm}$-orientifold planes, thus differentiating between Type I and $\tilde{\mathrm{I}}$ worldsheet theories.

We note in passing that Ryu and Takayanagi have pointed out in [328, 329] that the periodic table [330, 331] of free topological superconductors and topological insulators, based

on K-theory and KO-theory, can be naturally realized by considering D-branes in string theory. In those works the topological superconductors were realized on brane worldvolumes, whereas here we consider the topological superconductors on string worldsheets.

Organization

The aim of the rest of this chapter is to give details on the results presented thus far in this introduction. It is organized as follows: In Sec. 4.2, we begin by reviewing the necessary preliminary material concerning topological superconductors with several variants of spin structure. In Sec. 4.3, we study the effects of worldsheet invertible phases on massless closed string and D-brane spectra. In the next two sections, we give a more detailed analysis of the classification of D-branes. This is done from two different perspectives: in Sec. 4.4 we study D-branes via boundary fermions and tachyon condensation, while in Sec. 4.5 we utilize the boundary state formalism. The final section Sec. 4.6 is devoted to the algebraic-topological study of the possible invertible phases on the Type I worldsheet.

Additional background information and details of calculations are given in the appendices. In Appendix 4.A, we briefly review the NSR formulation of superstring theory. In Appendix 4.B, we provide a short review of the boundary state formalism necessary for calculations in Sec. 4.5. The results of this appendix are also utilized in Appendix 4.C, in which we discuss the issue of tadpole cancellation for some of the Type 0 theories discussed in this work. The final three appendices are more mathematical. In Appendix 4.D we reobtain many of our results for Arf and ABK invariants by means of index theory. Much of this appendix is due to Edward Witten [332]. In Appendix 4.E we provide the technical details of the algebraic-topological computation used in Sec. 4.6, which uses the Atiyah-Hirzebruch spectral sequence. In Appendix 4.F, written by Arun Debray, we explain another computation of the same bordism group via the Adams spectral sequence.

4.2 The (1+1)d topological superconductors

The main topic of this chapter is the addition of fermionic invertible phases to oriented and unoriented string worldsheets. In this section we begin by reviewing some basic facts about fermions and (s)pin structures (see [74, 81] for more detailed reviews), as well as about the known invertible phases for Spin, Spin $\times \mathbb{Z}_2$, Pin^-, and Pin^+ structures [78]. Also of importance to us will be "double pin" or DPin structure, though we postpone a discussion of this to Section 4.6.

Many of the results that we obtain via combinatoric methods in this section can also be obtained via index theory, i.e. by studying the properties of free fermions. For completeness, we discuss this approach in Appendix 4.D.

4.2.1 Oriented invertible phases

On an oriented d-manifold M the structure group of the tangent bundle TM is $\text{SO}(d)$. In order to consider fermions on M, we need to lift $\text{SO}(d)$ to its double cover $\text{Spin}(d)$ as specified by the short exact sequence

$$0 \to \mathbb{Z}_2 \to \text{Spin}(d) \to \text{SO}(d) \to 0\,. \tag{4.4}$$

There might be an obstruction to doing so, which is captured by the second Stiefel-Whitney class of TM, i.e. $w_2(TM) \in H^2(M, \mathbb{Z}_2)$. If this class is trivial, we say that the manifold admits a spin structure. Such a spin structure is generically not unique. Given a spin structure, we can obtain another one by twisting by an element of $H^1(M, \mathbb{Z}_2)$.

In this work, we focus on two-dimensional manifolds Σ, which we take to be the worldsheet of a string. Any orientable two-manifold admits a spin structure since $w_2(T\Sigma) = w_1^2(T\Sigma)$ mod 2. For notational simplicity, from now on we write $w_i := w_i(T\Sigma)$.

Invertible phase for Spin

Our primary interest is in fermionic invertible phases, i.e. phases which depend on a choice of spin structure σ on Σ. In the absence of any symmetry besides fermion number $(-1)^{\mathsf{f}}$, the group capturing such phases is $\mathcal{U}^2_{\text{Spin}}(pt) = \mathbb{Z}_2$. The effective action for the corresponding fermionic invertible phase can be written in terms of the Arf invariant [78],

$$e^{2i\pi S_{\text{eff}}(\Sigma,\,\sigma)} = (-1)^{\text{Arf}(\Sigma,\,\sigma)} \tag{4.5}$$

where $\text{Arf}(\Sigma, \sigma)$ is defined modulo 2. For simplicity, we will often leave the dependence on σ implicit.

As discussed in the Introduction, this phase is a continuum version of the Kitaev chain [75]. In the continuum field theory language, this corresponds to the definition [81]

$$(-1)^{\text{Arf}(\Sigma,\,\sigma)} := \frac{Z_{\text{ferm}}(m \gg 0; \Sigma, \sigma)}{Z_{\text{ferm}}(m \ll 0; \Sigma, \sigma)}, \tag{4.6}$$

where $Z_{\text{ferm}}(m; \Sigma, \sigma)$ is the partition function of a free massive Majorana fermion of mass m. To see that the right-hand side is ± 1, we note that the non-zero eigenvalues E of the Dirac operator D comes in pairs $\pm E$, since $\Gamma := \gamma^1\gamma^2$ is globally well-defined on an oriented spin surface and $D\Gamma = -\Gamma D$. Therefore,

$$\frac{Z_{\text{ferm}}(+m)}{Z_{\text{ferm}}(-m)} = \prod_{E=0}\left(\frac{iE+m}{iE-m}\right)\prod_{E>0}\frac{(iE+m)(-iE+m)}{(iE-m)(-iE-m)} = (-1)^{\text{index}\,D}. \tag{4.7}$$

The Arf invariant can also be defined combinatorially. To do so, given a spin structure σ on Σ, we define $\tilde{q}(a) \in \mathbb{Z}_2$ for each $\mathbb{Z}_2$-valued 1-cocycle a on Σ by taking a non-self-intersecting

1-cycle A Poincaré dual to it and declaring

$$\tilde{q}(a) = \begin{cases} 0 & \text{if the spin structure around } A \text{ is NS,} \\ 1 & \text{if the spin structure around } A \text{ is R .} \end{cases} \tag{4.8}$$

This function $\tilde{q}(a)$ is known as a quadratic form and satisfies

$$\tilde{q}(a+b) - \tilde{q}(a) - \tilde{q}(b) = \int_\Sigma a \cup b. \tag{4.9}$$

There is a one-to-one correspondence between such quadratic forms and spin structures [324].

The Arf invariant can be defined in terms of this quadratic form as follows,

$$(-1)^{\mathrm{Arf}(\Sigma,\sigma)} := \frac{1}{\sqrt{|H^1(\Sigma,\mathbb{Z}_2)|}} \sum_{a \in H^1(\Sigma,\mathbb{Z}_2)} (-1)^{\tilde{q}(a)}. \tag{4.10}$$

To see that the right-hand side is ± 1, we consider its square:

$$\begin{aligned} \mathrm{RHS}^2 &= \frac{1}{|H^1(\Sigma,\mathbb{Z}_2)|} \sum_{a,b \in H^1(\Sigma,\mathbb{Z}_2)} (-1)^{\tilde{q}(a)+\tilde{q}(b)} \\ &= \frac{1}{|H^1(\Sigma,\mathbb{Z}_2)|} \sum_{a,b \in H^1(\Sigma,\mathbb{Z}_2)} (-1)^{\tilde{q}(a+b)+\int_\Sigma a\cup b} \\ &= \frac{1}{|H^1(\Sigma,\mathbb{Z}_2)|} \sum_{a,c \in H^1(\Sigma,\mathbb{Z}_2)} (-1)^{\tilde{q}(c)+\int_\Sigma a\cup c} \end{aligned} \tag{4.11}$$

where we have defined $c = a + b \in H^1(\Sigma,\mathbb{Z}_2)$ and used that $\int_\Sigma a \cup a = 0$ for an orientable manifold. When $c = 0$, the summand is 1 and the sum contributes a factor of $|H^1(\Sigma,\mathbb{Z}_2)|$. When $c \neq 0$ there are equally many $\int_\Sigma a \cup c = 0, 1$ contributions by assumption of a non-degenerate intersection pairing, and hence these contributions cancel out. Thus we find that $\mathrm{RHS}^2 = 1$.

We now focus on the torus T^2, which admits four spin structures. We begin by listing all elements of $H^1(T^2,\mathbb{Z}_2)$, which is an order four group containing $\{0, a, b, a+b\}$. Here a and

b are mod 2 Poincaré duals of the A- and B-cycles of the torus, respectively. Then using formula (4.10), we have

$$\begin{aligned}(-1)^{\mathrm{Arf}(T^2)} &= \frac{1}{\sqrt{4}}\left(1+e^{i\pi\tilde{q}(a)}+e^{i\pi\tilde{q}(b)}+e^{i\pi\tilde{q}(a+b)}\right)\\ &= \frac{1}{2}\left(1+e^{i\pi\tilde{q}(a)}+e^{i\pi\tilde{q}(b)}-e^{i\pi\tilde{q}(a)}e^{i\pi\tilde{q}(b)}\right),\end{aligned} \tag{4.12}$$

where we have made use of (4.9) and noted that $\int a\cup b = 1$ for the two 1-cycles of the torus. Depending on the spin structure, one has $(\tilde{q}(a),\tilde{q}(b))\in\{(0,0),(0,1),(1,0),(1,1)\}$, for which we find that $(-1)^{\mathrm{Arf}(T^2)}$ assigns

$(0,0):$ 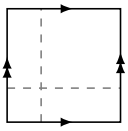 $\mapsto +1,$ $(0,1):$ 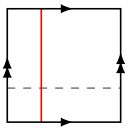 $\mapsto +1,$

$(1,0):$ 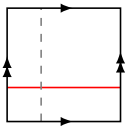 $\mapsto +1,$ $(1,1):$ 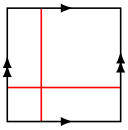 $\mapsto -1.$ (4.13)

Here, we have represented the spin structure by lines on the torus — a grey dashed line means that fermions are anti-periodic i.e. NS in the normal direction, whereas solid red lines means that fermions are periodic i.e. R in the normal direction. From the perspective of canonical quantization the red lines can be interpreted as insertions of $(-1)^{\mathsf{f}}$ symmetry defects/operators.

On a manifold with boundary, the bulk invertible phase requires the presence of an odd number of Majorana fermions on each boundary. As reviewed in Section 4.4.1, there is no canonical way to quantize an odd-dimensional Clifford algebra. This can be thought of as an anomaly of the boundary system, which is compensated by the presence of the bulk invertible phase.

Invertible phase for Spin $\times \mathbb{Z}_2$

We will also need to consider Spin $\times \mathbb{Z}_2$-structures on Σ. These are given by a choice of spin structure σ and a $\mathbb{Z}_2$ bundle with background gauge field $a \in H^1(\Sigma, \mathbb{Z}_2)$. As mentioned above, $H^1(\Sigma, \mathbb{Z}_2)$ acts on the space of spin structures, so the choice of (σ, a) is equivalent to a choice of two separate spin structures $(\sigma_L, \sigma_R) := (\sigma, \sigma + a)$, where we take σ_L and σ_R to be the left- and right-moving spin structures. The corresponding invertible phases are classified by $\mathfrak{O}^2_{\text{Spin}}(B\mathbb{Z}_2) = \mathbb{Z}_2^2$, which is generated by the separate Arf invariants for σ_L and σ_R:

$$(-1)^{\text{Arf}(\Sigma, \sigma_L)}, \quad (-1)^{\text{Arf}(\Sigma, \sigma_R)}. \tag{4.14}$$

The discussion of each of these phases is identical to that in the previous section.

4.2.2 Unoriented invertible phases

We would now like to discuss invertible phases which can be formulated on unoriented manifolds. They can be thought of as phases protected by the action of time-reversal T.

Invertible phase for orientation

Before considering fermionic phases protected by T, let us discuss bosonic phases protected by T. The structure group of the tangent bundle of an unoriented d-manifold M is $\mathrm{O}(d)$, which cannot be reduced to $\mathrm{SO}(d)$. The obstruction to doing so is given by the first Stiefel-Whitney class of the tangent bundle $w_1 \in H^1(M, \mathbb{Z}_2)$. For a 1-cycle C, we have

$$\oint_C w_1 = \begin{cases} 0 & \text{if going around } C \text{ preserves orientation,} \\ 1 & \text{if going around } C \text{ reverses orientation.} \end{cases} \tag{4.15}$$

Bosonic unoriented phases on the worldsheet are classified by $\mathfrak{O}^2_O(pt) = \mathbb{Z}_2$, the generator

of which is the low-energy limit of the $S = 1$ Haldane chain [326, 327]. In the continuum field theory language, the effective action for this phase is[5]

$$e^{2\pi i S_{\text{eff}}(\Sigma)} = (-1)^{\int_\Sigma w_1^2} \,. \tag{4.16}$$

The generator of the bordism group $\Omega_2^O(pt)$ is the projective plane $\mathbb{RP}^2$, i.e. $e^{2\pi i S_{\text{eff}}(\mathbb{RP}^2)} = -1$. One can easily calculate the value of the action on any other manifold by counting the number of constituent $\mathbb{RP}^2$ appearing in its connected sum decomposition (mod 2). For instance, the Möbius strip M_2 is a connected sum of the disc and the projective plane, i.e. $M_2 \cong D_2 \# \mathbb{RP}^2$. Hence

$$e^{2\pi i S_{\text{eff}}(M_2)} = -1. \tag{4.17}$$

On the other hand the Klein Bottle K_2 is a connected sum of two copies of the projective plane, i.e. $K_2 \cong \mathbb{RP}^2 \# \mathbb{RP}^2$, and

$$e^{2\pi i S_{\text{eff}}(K_2)} = 1. \tag{4.18}$$

When considered on a manifold with boundary, this phase captures the time-reversal anomaly of the $(0+1)$d boundary theory. This anomaly can be carried by a bosonic Kramers doublet on the boundary, i.e. we have $\mathsf{T}^2 = -1$ instead of $\mathsf{T}^2 = +1$.

Pin structures

In order to describe fermionic invertible phases protected by T, we need to briefly review how to put fermions on an unoriented manifold. There exist two different lifts of the $\mathrm{O}(d)$ bundle, known as $\mathrm{Pin}^{\pm}(d)$, which fit into the short exact sequence

$$0 \to \mathbb{Z}_2 \to \mathrm{Pin}^{\pm}(d) \to \mathrm{O}(d) \to 0\,. \tag{4.19}$$

[5] This is also occasionally written as $(-1)^{\chi(\Sigma)}$, where $\chi(\Sigma)$ is the Euler characteristic of Σ. The reason for this is that w_1^2 is equal to the mod-two reduction of the Euler class e, which satisfies $\int_\Sigma e = \chi(\Sigma)$. We prefer writing this phase in terms of Stiefel-Whitney classes in order to make bordism invariance manifest.

Both $\mathrm{Pin}^{\pm}(d)$ contain $\mathrm{Spin}(d)$ as their component connected to the identity, and their difference lies in how time-reversal T and spatial reflection R lift,

$$\begin{aligned} \mathrm{Pin}^{+}: &\quad \mathsf{T}^2 = (-1)^{\mathsf{f}}\,, &&\quad \mathsf{R}^2 = 1\,. \\ \mathrm{Pin}^{-}: &\quad \mathsf{T}^2 = 1\,, &&\quad \mathsf{R}^2 = (-1)^{\mathsf{f}}\,. \end{aligned} \tag{4.20}$$

The corresponding obstruction classes are

$$\mathrm{Pin}^{+}: \quad w_2\,, \qquad\qquad \mathrm{Pin}^{-}: \quad w_2 + w_1^2\,. \tag{4.21}$$

Every two-manifold Σ has $w_2 + w_1^2 = 0 \mod 2$, and hence admits a Pin^{-} structure. However, the same is not true for Pin^{+}. For instance, the real projective plane $\mathbb{RP}^2$ has $w_2 \neq 0$, and so it does not admit a Pin^{+} structure.

The action of $\mathrm{Pin}^{\pm}$ on fermions Ψ can be given in terms of gamma matrices. In particular, reflection of the i-th coordinate acts on Ψ by the gamma matrix γ_i. The reflection squared is trivial in $\mathrm{O}(d)$, and therefore its lift when applied to a fermion is ± 1. Then we have

$$\{\gamma_i, \gamma_j\} = \pm 2\eta_{ij}, \tag{4.22}$$

for $\mathrm{Pin}^{\pm}$ structure, respectively, where we temporarily use the Lorentzian signature and the metric η_{ij} is mostly plus. This explains why T squares to $(-1)^{\mathsf{f}}$ when R squares to 1 and vice versa, as written in (4.20). The fermion fields Ψ transforming in this manner are sometimes called "pinors."

In our study of unoriented string amplitudes, the behavior of pinors on the boundary of the Möbius strip with $\mathrm{Pin}^{\pm}$ structure will be particularly important. Recall that on a circle, one can consistently define both anti-periodic and periodic fermions, i.e. fermions in the NS and R sectors. In contrast, the choice of NS or R on the boundary of the Möbius strip is fixed by the choice of $\mathrm{Pin}^{\pm}$. We may see this as follows. Note that the Möbius strip can be

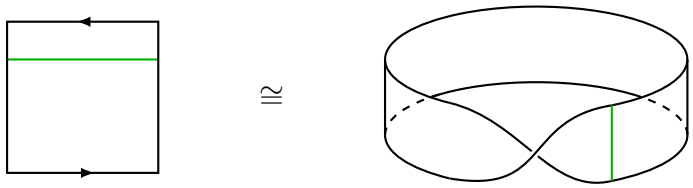

Figure 4.1: Möbius strip with an orientation-reversing line (in green).

constructed by taking a strip and gluing its ends together along an orientation-reversing line (Fig. 4.1) — upon crossing this line, we pick up an action of γ_i on fermions. Traversing the boundary of the Möbius strip involves crossing this line twice, and this picks up an action of $\gamma_i^2 = \pm 1$ on fermions. Thus we conclude that boundary fermions on the Pin^+ Möbius strip are in the R sector, while those on the Pin^- Möbius strip are in the NS sector.

Invertible phase for Pin^- structure

We now study fermionic invertible phases protected by T such that $\mathsf{T}^2 = +1$. Such phases are classified by $\mathcal{U}^2_{\mathrm{Pin}^-}(pt) = \mathbb{Z}_8$, which is generated by the Arf-Brown-Kervaire (ABK) invariant [333]. For recent work on this invertible phase, see e.g. [334–336]. The ABK invariant can be thought of as the effective action of the Kitaev chain protected by time-reversal. In the continuum version, we have:

$$e^{2\pi i S_{\mathrm{eff}}(\Sigma,\sigma)} = e^{\pi i \mathrm{ABK}(\Sigma,\sigma)/4} = \frac{Z_{\mathrm{ferm}}(m \gg 0; \Sigma, \sigma)}{Z_{\mathrm{ferm}}(m \ll 0; \Sigma, \sigma)} \,. \tag{4.23}$$

Here σ represents a choice of Pin^- structure, which we will often omit from the argument of ABK for brevity. Alternatively, the ABK invariant can be defined combinatorially as

$$e^{\pi i \mathrm{ABK}(\Sigma)/4} = \frac{1}{\sqrt{|H^1(\Sigma, \mathbb{Z}_2)|}} \sum_{a \in H^1(\Sigma,\mathbb{Z}_2)} e^{\pi i q(a)/2} \,, \tag{4.24}$$

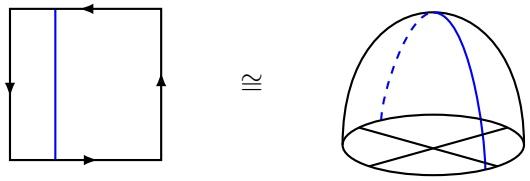

Figure 4.2: Projective plane with the single generator Z of its first homology class (in blue). To the right this is drawn as a sphere with a crosscap.

where q is a quadratic enhancement $q : H^1(\Sigma, \mathbb{Z}_2) \to \mathbb{Z}_4$ satisfying

$$q(a+b) - q(a) - q(b) = 2 \int_\Sigma a \cup b \ . \tag{4.25}$$

One may think of this q as a sort of doubling of the spin structure quadratic form $\tilde{q} : H^1(\Sigma, \mathbb{Z}_2) \to \mathbb{Z}_2$ introduced earlier. Indeed, if the worldsheet is orientable then $q = 2\,\tilde{q} \pmod 4$. In that case one finds $\mathrm{ABK}(\Sigma) = 4\,\mathrm{Arf}(\Sigma) \pmod 8$, and (4.23) reduces to (4.5) as expected.

To see that the right-hand side of (4.24) is an eighth root of unity, again we consider its square:

$$\begin{aligned}
\mathrm{RHS}^2 &= \frac{1}{|H^1(\Sigma,\mathbb{Z}_2)|} \sum_{a,b \in H^1(\Sigma,\mathbb{Z}_2)} i^{q(a)+q(b)} \\
&= \frac{1}{|H^1(\Sigma,\mathbb{Z}_2)|} \sum_{a,b \in H^1(\Sigma,\mathbb{Z}_2)} i^{q(a+b)} (-1)^{\int_\Sigma a\cup b} \\
&= \frac{1}{|H^1(\Sigma,\mathbb{Z}_2)|} \sum_{a,c \in H^1(\Sigma,\mathbb{Z}_2)} i^{q(c)} (-1)^{\int_\Sigma (a\cup c + a\cup a)} \\
&= \frac{1}{|H^1(\Sigma,\mathbb{Z}_2)|} \sum_{a,c \in H^1(\Sigma,\mathbb{Z}_2)} i^{q(c)} (-1)^{\int_\Sigma (a\cup c + a\cup w_1)} \\
&= i^{q(w_1)},
\end{aligned} \tag{4.26}$$

where we used $\int a \cup a = \int a \cup w_1$.

We will need some basic values for the ABK invariant. We begin by reviewing the case

of $\mathbb{RP}^2$, for which there is a single generator Z of $H_1(\mathbb{RP}^2, \mathbb{Z}_2)$, as depicted in Fig. 4.2. Its Poincaré dual, z, is an unoriented cocycle with $\int_{\mathbb{RP}^2} z \cup z = 1$. Then using (4.25) and $q(0) = 0$, we conclude that $2q(z) + 2 = 0 \mod 4$ and hence $q(z) = 1$ or 3. These label the two distinct Pin^- structures on $\mathbb{RP}^2$. The corresponding ABK invariants are easily calculated,

$$\begin{aligned} 1: \qquad e^{\pi i \mathrm{ABK}(\mathbb{RP}^2)/4} &= \frac{1}{\sqrt{2}}\left(1 + e^{i\pi/2}\right) = e^{i\pi/4}, \\ 3: \qquad e^{\pi i \mathrm{ABK}(\mathbb{RP}^2)/4} &= \frac{1}{\sqrt{2}}\left(1 + e^{i3\pi/2}\right) = e^{-i\pi/4}. \end{aligned} \tag{4.27}$$

We will also need the value of the ABK invariant on the Klein bottle. Because K_2 is a connected sum of two copies of $\mathbb{RP}^2$, it admits four choices of quadratic enhancement. Taking z_1 and z_2 to be the basis naturally adapted to the connected sum gives $(q(z_1), q(z_2)) \in \{(1,1), (1,3), (3,1), (3,3)\}$. However, it will behoove us to switch to the more familiar basis of $H_1(K_2, \mathbb{Z}_2)$, for which $a := z_1 + z_2$ is Poincaré dual to the orientation-preserving A-cycle while $b := z_2$ is dual to the orientation-reversing B-cycle. The quadratic enhancements are then $(q(a), q(b)) \in \{(0,1), (0,3), (2,1), (2,3)\}$. For each of these Pin^- structures we compute the following values for the ABK invariant,

$$\begin{aligned} (0,1): \qquad e^{\pi i \mathrm{ABK}(K_2)/4} &= \frac{1}{2}(1 + 1 + i - i) = 1, \\ (0,3): \qquad e^{\pi i \mathrm{ABK}(K_2)/4} &= \frac{1}{2}(1 + 1 - i + i) = 1, \\ (2,1): \qquad e^{\pi i \mathrm{ABK}(K_2)/4} &= \frac{1}{2}(1 - 1 + i + i) = i, \\ (2,3): \qquad e^{\pi i \mathrm{ABK}(K_2)/4} &= \frac{1}{2}(1 - 1 - i - i) = -i. \end{aligned} \tag{4.28}$$

It is useful to note that

$$e^{\pi i (4\mathrm{ABK}(\Sigma))/4} = (-1)^{\int w_1^2}, \tag{4.29}$$

namely that four copies of the ABK theory is the same as the nontrivial bosonic unoriented phase discussed in Section 4.2.2.

The boundary theory of n copies of the ABK theory is detailed in Section 4.4.1. When $n = 4$, we have a system of four Majorana fermions χ_i. We can then introduce a T-invariant interaction term $\chi_1\chi_2\chi_3\chi_4$. The ground state with this interaction is bosonic, two-fold degenerate, and has the projective anomaly $\mathsf{T}^2 = -1$, thus manifesting the equality (4.29) on the boundary. Similarly, when $n = 8$, we can consider a suitable quartic interaction under which the ground state is unique [80].

Invertible phase for Pin^+ structure

We now study fermionic invertible phases protected by T such that $\mathsf{T}^2 = (-1)^{\mathsf{f}}$. Such phases are classified by $\mathcal{O}^2_{\mathrm{Pin}^+}(pt) = \mathbb{Z}_2$, which is generated by the Arf invariant (4.10) on the orientation double cover $\hat{\Sigma}$ of the worldsheet, i.e. $(-1)^{\mathrm{Arf}(\hat{\Sigma})}$ [78]. This gives ± 1 on the Klein bottle, depending on the spin structure of its double cover torus. Concretely, the Klein bottle admits four Pin^+ structures, two of which have NS sector fermions along the oriented A-cycle of K_2, and two of which have R sector fermions along the A-cycle. For each of these Pin^+ structures, we must determine the corresponding spin structure on the orientation double cover, i.e. the torus. To do so, let us consider for simplicity a rectangular torus with real coordinates x, y satisfying $x \sim x + 2\pi$, $y \sim y + 2L$ for some L. The original Klein bottle is obtained by imposing the identification $(x, y) \sim (-x, y + L)$. The cycle in the x-direction is the oriented A-cycle on K_2, while the cycle in the y-direction is twice the unoriented B-cycle. From this we learn that the choice of Pin^+ structure along the B-cycle is irrelevant on the double cover — the fermion is always periodic along the cycle in the y-direction. Thus we conclude that the four Pin^+ structures are assigned phases $(-1)^{\mathrm{Arf}(\hat{\Sigma})} = 1, 1, -1, -1$.

4.3 GSO projections

In this section, we consider the addition of fermionic invertible phases to the worldsheet theories of various superstrings. This will allow us to enumerate all possible GSO projections.

We will focus on oriented Type II and Type 0 theories, as well as unoriented Type 0 theories. The case of unoriented Type II (i.e. Type I) strings will be treated in Section 4.6. In our discussion we will work in the NSR formalism, which is briefly reviewed in Appendix 4.A. The properties of the low-lying states in this formalism are summarized in Table 4.2 for convenience.

State	$(-1)^{\mathsf{f}}$	$(-1)^{\mathsf{f}_{\mathsf{L}}}$	$(-1)^{\mathsf{f}_{\mathsf{R}}}$	Little group rep.
$(\mathrm{NS}-,\mathrm{NS}-)$	$+1$	-1	-1	$\mathbf{1}$
$(\mathrm{NS}+,\mathrm{NS}+)$	$+1$	$+1$	$+1$	$\mathbf{8}_v \otimes \mathbf{8}_v = \mathbf{1} \oplus \mathbf{28} \oplus \mathbf{35}$
$(\mathrm{R}+,\mathrm{R}+)$	$+1$	$+1$	$+1$	$\mathbf{8}_s \otimes \mathbf{8}_s = \mathbf{1} \oplus \mathbf{28} \oplus \mathbf{35}_-$
$(\mathrm{R}-,\mathrm{R}-)$	$+1$	-1	-1	$\mathbf{8}_c \otimes \mathbf{8}_c = \mathbf{1} \oplus \mathbf{28} \oplus \mathbf{35}_+$
$(\mathrm{R}+,\mathrm{R}-)$	-1	$+1$	-1	$\mathbf{8}_s \otimes \mathbf{8}_c = \mathbf{8}_v \oplus \mathbf{56}$
$(\mathrm{R}-,\mathrm{R}+)$	-1	-1	$+1$	$\mathbf{8}_c \otimes \mathbf{8}_s = \mathbf{8}_v \oplus \mathbf{56}$
$(\mathrm{NS}+,\mathrm{R}+)$	$+1$	$+1$	$+1$	$\mathbf{8}_v \otimes \mathbf{8}_s = \mathbf{8}_c \oplus \mathbf{56}_s$
$(\mathrm{NS}+,\mathrm{R}-)$	-1	$+1$	-1	$\mathbf{8}_v \otimes \mathbf{8}_c = \mathbf{8}_s \oplus \mathbf{56}_c$

Table 4.2: Fermion parity and representations of the low-lying states of the closed NSR superstring.

4.3.1 Oriented strings

Type 0

Let us begin by studying oriented Type 0 superstrings, which differ from Type II strings in that there is a single spin structure for both left- and right-movers [74, 337]. The SPT phases which can be consistently realized on the Type 0 worldsheets are classified by $\mathcal{O}^2_{\mathrm{Spin}}(pt) = \mathbb{Z}_2$. As we have seen above, the effective action for the non-trivial phase can be written in terms of the Arf invariant (4.5). Depending on whether or not one allows for this non-trivial phase on the worldsheet, one expects to arrive at two different Type 0 theories, with torus partition

functions

$$Z^{(n)} = \frac{1}{2}\sum_{\sigma}(-1)^{n\,\mathrm{Arf}(T^2,\sigma)} Z[\sigma]\overline{Z}[\sigma] \ , \qquad n = 0, 1 \ , \tag{4.30}$$

where $Z[\sigma], \overline{Z}[\sigma]$ are the standard left- and right-moving worldsheet torus partition functions with spin structure σ. The two theories obtained in this way are Type 0B ($n = 0$) and Type 0A ($n = 1$),

$$\begin{aligned} \text{0A}: \quad Z^{(1)} &= \frac{1}{2}\left(|Z[\sigma_{00}]|^2 + |Z[\sigma_{01}]|^2 + |Z[\sigma_{10}]|^2 - |Z[\sigma_{11}]|^2\right) \ , \\ \text{0B}: \quad Z^{(0)} &= \frac{1}{2}\left(|Z[\sigma_{00}]|^2 + |Z[\sigma_{01}]|^2 + |Z[\sigma_{10}]|^2 + |Z[\sigma_{11}]|^2\right) \ , \end{aligned} \tag{4.31}$$

and their massless RR states are found to be

$$\begin{aligned} \text{0A}: \quad & |0\rangle^{a\dot{b}}_{\mathrm{RR}}, |0\rangle^{\dot{a}b}_{\mathrm{RR}} \in (\mathbf{8}_s \otimes \mathbf{8}_c) \oplus (\mathbf{8}_c \otimes \mathbf{8}_s) = (2 \cdot \mathbf{8}_v) \oplus (2 \cdot \mathbf{56}) \ , \\ \text{0B}: \quad & |0\rangle^{ab}_{\mathrm{RR}}, |0\rangle^{\dot{a}\dot{b}}_{\mathrm{RR}} \in (\mathbf{8}_s \otimes \mathbf{8}_s) \oplus (\mathbf{8}_c \otimes \mathbf{8}_c) = (2 \cdot \mathbf{1}) \oplus (2 \cdot \mathbf{28}) \oplus \mathbf{70} \ . \end{aligned} \tag{4.32}$$

The massless RR sector for Type 0A contains two 1-forms and two 3-form fields, while that of Type 0B contains two scalars, two 2-forms, and a 4-form with no self-duality constraint. This is exactly double the RR content of the corresponding Type II theories. This leads one to expect a doubled brane spectrum, where for each p we have both Dp and Dp' branes. This will be discussed further in Section 4.3.3.

Type II

We now proceed to discuss the more familiar Type II superstrings. A characteristic feature of these strings is that they have separate spin structures for left- and right-movers, which means that the worldsheet is endowed with a Spin $\times\, \mathbb{Z}_2$ structure. The anomalies and invertible phases on such worldsheets are captured by $\mathfrak{V}^3_{\mathrm{Spin}}(B\mathbb{Z}_2)$ and $\mathfrak{V}^2_{\mathrm{Spin}}(B\mathbb{Z}_2)$, respectively. These groups are listed in Table 4.1. As discussed in [338, 339], the fact that $\mathfrak{V}^3_{\mathrm{Spin}}(B\mathbb{Z}_2) = \mathbb{Z}_8$

implies that the number of physical pairs of left- and right-movers needs to be a multiple of eight to have a non-anomalous GSO projection. This is indeed the case if the physical string lives in ten dimensions.

On the other hand, the SPT phases on the worldsheet are classified by $\mathfrak{V}^2_{\text{Spin}}(B\mathbb{Z}_2) = (\mathbb{Z}_2)^2$. The two $\mathbb{Z}_2$ can be interpreted as separate left- and right-moving fermionic invertible phases, as discussed in Section 4.2.1. In other words, the partition functions for these phases are given by

$$(-1)^{n_L \,\text{Arf}(\Sigma,\,\sigma_L)+n_R\,\text{Arf}(\Sigma\,,\sigma_R)}\ , \qquad n_{L,R}=0,1\ , \tag{4.33}$$

where $\sigma_{L(R)}$ is the left(right)-moving spin structure on the worldsheet Σ. The corresponding torus partition functions for these theories are given by

$$Z^{(n_L,n_R)} \;=\; \frac{1}{4}\left(\sum_{\sigma_L}(-1)^{n_L\,\text{Arf}(T^2,\,\sigma_L)}Z[\sigma_L]\right)\times\left(\sum_{\sigma_R}(-1)^{n_R\,\text{Arf}(T^2,\,\sigma_R)}\overline{Z}[\sigma_R]\right)\ , \tag{4.34}$$

For instance, two cases are

$$\begin{aligned} Z^{(0,0)} &= \frac{1}{4}\left(Z[\sigma_{00}]+Z[\sigma_{01}]+Z[\sigma_{10}]+Z[\sigma_{11}]\right)\left(\overline{Z}[\sigma_{00}]+\overline{Z}[\sigma_{01}]+\overline{Z}[\sigma_{10}]+\overline{Z}[\sigma_{11}]\right),\\ Z^{(0,1)} &= \frac{1}{4}\left(Z[\sigma_{00}]+Z[\sigma_{01}]+Z[\sigma_{10}]+Z[\sigma_{11}]\right)\left(\overline{Z}[\sigma_{00}]+\overline{Z}[\sigma_{01}]+\overline{Z}[\sigma_{10}]-\overline{Z}[\sigma_{11}]\right). \end{aligned} \tag{4.35}$$

While there are seemingly four distinct SPT phases, there are in fact only two physically distinct Type II theories. To see this, recall the continuum definition of the Arf invariant:

$$(-1)^{\text{Arf}(\Sigma,\,\sigma)}=\frac{Z_{\text{ferm}}(m\gg 0;\Sigma,\sigma)}{Z_{\text{ferm}}(m\ll 0;\Sigma,\sigma)}\ , \tag{4.36}$$

where $Z_{\text{ferm}}(m;\Sigma,\sigma)$ is the partition function of a free massive Majorana fermion of mass m.

We note this formula holds at finite mass as well,

$$(-1)^{\mathrm{Arf}(\Sigma,\sigma)} = \frac{Z_{\mathrm{ferm}}(+m;\Sigma,\sigma)}{Z_{\mathrm{ferm}}(-m;\Sigma,\sigma)} \ , \tag{4.37}$$

which was already used in (4.7). In other words, upon flipping the sign of a mass term, $m \to -m$, one generates a factor of $(-1)^{\mathrm{Arf}(\Sigma,\sigma)}$ in the partition function. Note that such a flip of the mass term can be performed by $(\psi, \tilde{\psi}) \to (\psi, -\tilde{\psi})$. Taking the limit $m \to 0$, we find that a Majorana-Weyl fermion $\tilde{\psi}$ has an anomaly under $\tilde{\psi} \to -\tilde{\psi}$, and generates $(-1)^{\mathrm{Arf}(\Sigma,\sigma_R)}$. This in particular means that the parity transformation along a single spacetime direction, say $(\psi^{\mu=9}, \tilde{\psi}^{\mu=9}) \to (-\psi^9, -\tilde{\psi}^9)$, produces $(-1)^{\mathrm{Arf}(\Sigma,\sigma_L)+\mathrm{Arf}(\Sigma,\sigma_R)}$, i.e. $n_L = n_R = 1$ in (4.33). Therefore, there are only essentially two distinct Type II GSO projections, with the others being related by spacetime parity transformation. The cases $(n_L, n_R) = (0,0), (1,1)$ are traditionally called Type IIB while the cases $(n_L, n_R) = (0,1), (1,0)$ are called Type IIA.

The reasoning above also explains why T-duality exchanges Type IIA/B. Recall that T-duality along a spacetime direction keeps $(\partial X, \psi)$ fixed and implements $(\bar{\partial} X, \tilde{\psi}) \to (-\bar{\partial} X, -\tilde{\psi})$. Then by the previous paragraph, this generates $(-1)^{\mathrm{Arf}(\Sigma,\sigma_R)}$, exchanging Type IIA/B. By the same arguments, the two Type 0 theories are also exchanged by T-duality.

Comments on the two points of view on the effect of invertible phases

There are two ways of understanding the gauging of a global symmetry in the presence of a non-trivial invertible phase. The point of view which we have taken so far is to take the tensor product of the original theory and the invertible phase, and to then gauge the relevant symmetry. The Hilbert space of the invertible phase is one-dimensional, and therefore this changes the way the global symmetry acts on the states of the original theory. For example, in the case of Type 0 strings, we used the projectors

$$P_{0\mathrm{A}} = \frac{1}{2}(1 + (-1)^{\mathsf{f}}|_{0\mathrm{A}}), \qquad P_{0\mathrm{B}} = \frac{1}{2}(1 + (-1)^{\mathsf{f}}|_{0\mathrm{B}}) \tag{4.38}$$

and what produced the difference between the two was that on the RR sector, we had

$$(-1)^{\mathsf{f}}|_{0\mathrm{A}} = -(-1)^{\mathsf{f}}|_{0\mathrm{B}} \tag{4.39}$$

due to the presence of the Arf theory.

More traditionally, the action of $(-1)^{\mathsf{f}}$ was fixed once and for all, for example to be equal to $(-1)^{\mathsf{f}}|_{0\mathrm{B}}$, and different GSO projections were said to correspond to different projectors. For example, in the RR sector, one would have written

$$P_{0\mathrm{A}}^{\mathrm{RR}} = \frac{1}{2}(1-(-1)^{\mathsf{f}}), \qquad P_{0\mathrm{B}}^{\mathrm{RR}} = \frac{1}{2}(1+(-1)^{\mathsf{f}}). \tag{4.40}$$

These two points of view clearly lead to the same results, and similar statements will be seen to hold for unoriented strings. Though we will briefly discuss this traditional viewpoint when we compare to the existing literature, we will mostly use the first point of view.

4.3.2 Unoriented strings

Orientation reversal on fermions and ground states

We now consider unoriented string theories. One way to obtain such theories is to gauge time-reversal symmetry T on the worldsheet. T is an antiunitary symmetry that acts on worldsheet fermions as

$$\mathsf{T}\psi(t,\sigma)\mathsf{T}^{-1} = \tilde{\psi}(-t,\sigma)\ , \qquad \mathsf{T}\tilde{\psi}(t,\sigma)\mathsf{T}^{-1} = \psi(-t,\sigma) \tag{4.41}$$

with $\mathsf{T}^2 = 1$. In string theory, it is often more common to describe this in terms of worldsheet parity Ω, which is a unitary symmetry whose action is given by

$$\Omega\psi(t,\sigma)\Omega^{-1} = -\tilde{\psi}(t,2\pi-\sigma)\ , \qquad \Omega\tilde{\psi}(t,\sigma)\Omega^{-1} = \psi(t,2\pi-\sigma)\,. \tag{4.42}$$

From this definition it is clear that $\Omega^2 = (-1)^{\mathsf{f}}$. The ability to choose between T or Ω is a consequence of the CPT theorem. The fact that $\mathsf{T}^2 = 1$, or equivalently that $\Omega^2 = (-1)^{\mathsf{f}}$, means that we are working with a Pin^- structure on the worldsheet. In this case the action of Ω on the ground states in the NSNS and RR sectors can be taken to be

$$\Omega\,|0\rangle_{\mathrm{NSNS}} = |0\rangle_{\mathrm{NSNS}}\ , \qquad \Omega\,|0\rangle_{\mathrm{R}} \otimes |\tilde{0}\rangle_{\mathrm{R}} = \begin{cases} -\,|\tilde{0}\rangle_{\mathrm{R}} \otimes |0\rangle_{\mathrm{R}} & \text{for} \quad (\mathrm{R}\pm, \mathrm{R}\pm), \\ -i|\tilde{0}\rangle_{\mathrm{R}} \otimes |0\rangle_{\mathrm{R}} & \text{for} \quad (\mathrm{R}\pm, \mathrm{R}\mp). \end{cases} \tag{4.43}$$

One can also consider gauging Ω twisted by some $\mathbb{Z}_2$ symmetry. Here we consider $\Omega_{\mathsf{f}} := \Omega(-1)^{\mathsf{f}_{\mathsf{L}}}$. We find

$$(\Omega_{\mathsf{f}})^2 = \Omega(-1)^{\mathsf{f}_{\mathsf{L}}}\Omega(-1)^{\mathsf{f}_{\mathsf{L}}} = \Omega(-1)^{\mathsf{f}_{\mathsf{L}}+\mathsf{f}_{\mathsf{R}}}\Omega = (-1)^{\mathsf{f}}\Omega^2 = 1 \tag{4.44}$$

and hence gauging this operator gives Pin^+ structure on worldsheets. In this case parity acts on the NSNS and RR ground states as

$$\Omega_{\mathsf{f}}\,|0\rangle_{\mathrm{NSNS}} = -|0\rangle_{\mathrm{NSNS}}\ , \qquad \Omega_{\mathsf{f}}\,|0\rangle_{\mathrm{R}} \otimes |\tilde{0}\rangle_{\mathrm{R}} = \begin{cases} \mp\,|\tilde{0}\rangle_{\mathrm{R}} \otimes |0\rangle_{\mathrm{R}} & \text{for} \quad (\mathrm{R}\pm, \mathrm{R}\pm), \\ \mp i|\tilde{0}\rangle_{\mathrm{R}} \otimes |0\rangle_{\mathrm{R}} & \text{for} \quad (\mathrm{R}\pm, \mathrm{R}\mp). \end{cases} \tag{4.45}$$

Unlike for Type II strings where Ω is a symmetry of only Type IIB, for Type 0 strings Ω is a symmetry of both Type 0A and 0B. Hence we can obtain Pin^- Type 0 theories by starting from either Type 0A or 0B and gauging Ω. Likewise, one might expect that we can obtain Pin^+ Type 0 theories by starting from either Type 0A or 0B and gauging Ω_{f}. However, it turns out that Ω_{f} cannot be consistently gauged in Type 0A, since it is incompatible with the Type 0A spin structure projection [82–84].

In the rest of this section we study the consistent unoriented Type 0 strings in more detail. We begin by analyzing the Pin^- strings in Section 4.3.2, and then proceed to a discussion of the Pin^+ strings in Section 4.3.2. To the best of our knowledge, many of these

theories have not been discussed in the literature — some preliminary works include [82–91]. For a condensed matter perspective, see e.g. [340, 341].

Pin^- Type 0 Strings

Let us begin by discussing Pin^- Type 0 strings. The group classifying the relevant invertible phases is $\mathfrak{O}^2_{\mathrm{Pin}^-}(pt) = \mathbb{Z}_8$, which is generated by the ABK invariant. We are thus led to predict the existence of eight Pin^- theories, each distinguished by the presence of $n = 0, \ldots, 7$ copies of ABK on the worldsheet.

In unoriented theories, the presence of a non-trivial invertible phase manifests itself in the action of Ω on the different closed string ground states. In order to understand this action, we make use of the values of the ABK invariant on the Klein bottle K_2 obtained in Section 4.2.2. In particular, it was found there that the Klein bottle admits four Pin^- structures labelled by quadratic enhancements $(q(a), q(b)) \in \{(0,1), (0,3), (2,1), (2,3)\}$ with respective values $e^{i\pi \mathrm{ABK}(K_2)/4} = 1, 1, i, -i$. Recall that the first entry a corresponds to the orientation-preserving cycle on K_2, while the second entry b corresponds to the orientation-reversing cycle.

We now want to interpret these results as the action of Ω and $(-1)^{\mathsf{f}}$ on the closed string Hilbert space. This can be done as follows. We begin by cutting K_2 along the orientation-preserving cycle A to obtain a cylinder with an insertion of an Ω symmetry line. Since A is orientation-preserving, we know that $q = 2\,\tilde{q} \mod 4$, where $\tilde{q}(a)$ is the spin structure along A. Consequently, the first and second Pin^- structures correspond to NS structure along the A-cycle, while the third and fourth correspond to R structure along the A-cycle. We may then interpret the partition function for each Pin^- structure as the following traces on the

torus. We have:

$$
\begin{aligned}
(0,1): &\quad \leftrightarrow \quad \frac{1}{4}\mathrm{Tr}_{\mathrm{NSNS}}\left[\Omega\, e^{-2\pi l H_{\mathrm{cl}}}\right] \\
(0,3): &\quad \leftrightarrow \quad \frac{1}{4}\mathrm{Tr}_{\mathrm{NSNS}}\left[\Omega\,(-1)^{\mathsf{f}}\, e^{-2\pi l H_{\mathrm{cl}}}\right] \\
(2,1): &\quad \leftrightarrow \quad \frac{1}{4}\mathrm{Tr}_{\mathrm{RR}}\left[\Omega\, e^{-2\pi l H_{\mathrm{cl}}}\right] \\
(2,3): &\quad \leftrightarrow \quad \frac{1}{4}\mathrm{Tr}_{\mathrm{RR}}\left[\Omega\,(-1)^{\mathsf{f}}\, e^{-2\pi l H_{\mathrm{cl}}}\right]
\end{aligned}
\tag{4.46}
$$

where green lines represent orientation-reversal lines and red lines represent spin lines. In this way, the value of the ABK invariant on K_2 with Pin^- structure labeled by $(q(a), q(b))$ can be assigned to the action of Ω on the ground states with the appropriate cylinder spin structures. In particular, we conclude that Ω acts trivially on NS ground states, whereas it acts with an extra factor of i on R ground states. This implies that the presence of n copies of ABK changes the action of Ω on the RR sector ground states by a factor of i^n relative to (4.43), giving

$$
\Omega|0\rangle_{\mathrm{NSNS}} = |0\rangle_{\mathrm{NSNS}}\ , \qquad \Omega|0\rangle_{\mathrm{R}} \otimes |\tilde{0}\rangle_{\mathrm{R}} = \begin{cases} -i^n \quad |\tilde{0}\rangle_{\mathrm{R}} \otimes |0\rangle_{\mathrm{R}} \quad \text{for} \quad (\mathrm{R}\pm, \mathrm{R}\pm), \\ -i^{n+1}|\tilde{0}\rangle_{\mathrm{R}} \otimes |0\rangle_{\mathrm{R}} \quad \text{for} \quad (\mathrm{R}\pm, \mathrm{R}\mp). \end{cases} \tag{4.47}
$$

Note that upon shifting $n \to n+1$, the additional factor of i changes the fermion-parity of the RR ground state, since $\Omega^2 = (-1)^{\mathsf{f}}$. Since the Type 0A/B theories differ by a projection onto states of worldsheet fermion number $(-1)^{\mathsf{f}} = \pm 1$, we see that theories with even n correspond to orientifolds of Type 0B, while theories with odd n correspond to orientifolds of Type 0A. This is also supported by recalling that on oriented manifolds Σ, the

ABK invariant reduces to $\mathrm{ABK}(\Sigma) = 4\,\mathrm{Arf}(\Sigma)$ (mod 8), and hence the partition function becomes $e^{in\pi\mathrm{ABK}(\Sigma)/4} = (-1)^{n\,\mathrm{Arf}(\Sigma)}$, which is precisely what distinguished the oriented Type 0A/B theories.

As far as the action of Ω on the vacuum (4.47) is concerned, theories differing by four copies of ABK are indistinguishable. The reason for this is that only data about the Klein bottle K_2 was used to obtain (4.47). However, the manifold that generates the bordism group $\Omega_2^{\mathrm{Pin}^-}(pt)$ is the projective plane $\mathbb{RP}^2$, while K_2 is a connected sum of two copies thereof, i.e. $K_2 \cong \mathbb{RP}^2 \# \mathbb{RP}^2$. Consequently, the partition function on K_2 is insensitive to an additional sign that can arise on manifolds whose decompositions contain an odd number of copies of $\mathbb{RP}^2$. Indeed, four copies of the ABK theory is not trivial and gives partition function $e^{4\pi i\mathrm{ABK}(\Sigma)/4} = (-1)^{\int_\Sigma w_1^2}$, as discussed in Section 4.2.2. As described in Section 4.2.2, unlike for the Klein bottle the Möbius strip amplitude *is* sensitive to this sign. This sign turns out to give precisely the difference between $\mathrm{O9}^\pm$ orientifolds. More detail on this will be given in Section 4.5.1.

We may now study the closed string spectra of these theories. The action of Ω proposed in (4.47) does not project out the closed string tachyon in the NSNS sector, but has the following implications for the spectra of RR fields. For n even, Ω projects out all $(\mathrm{R}\pm, \mathrm{R}\mp)$ states. The cases $n = 0 \mod 4$ and $n = 2 \mod 4$ differ by a sign in the action of Ω, which projects out the symmetric or antisymmetric combinations of $(\mathrm{R}\pm, \mathrm{R}\pm)$ states. Then upon gauging Ω we obtain the following RR spectra,

$$\begin{aligned}
n = 0, 4: &\qquad |0\rangle_{\mathrm{RR}}^{[ab]} \in \mathbf{28} \subset \mathbf{8}_s \otimes \mathbf{8}_s, &&\qquad |0\rangle_{\mathrm{RR}}^{[\dot{a}\dot{b}]} \in \mathbf{28} \subset \mathbf{8}_c \otimes \mathbf{8}_c\ , \\
n = 2, 6: &\qquad |0\rangle_{\mathrm{RR}}^{(ab)} \in \mathbf{1} \oplus \mathbf{35}_- \subset \mathbf{8}_s \otimes \mathbf{8}_s, &&\qquad |0\rangle_{\mathrm{RR}}^{(\dot{a}\dot{b})} \in \mathbf{1} \oplus \mathbf{35}_+ \subset \mathbf{8}_c \otimes \mathbf{8}_c\ .
\end{aligned} \tag{4.48}$$

In the $n = 0 \mod 4$ cases, only the two 2-forms survive the projection, while for $n = 2$ mod 4 only the two scalars and the 4-form survive. These spectra of RR fields are indeed a projection of the Type 0B ones. For n odd, the extra factor of i in (4.47) projects out all

the $(\mathrm{R}\pm,\mathrm{R}\pm)$ states, while the $(\mathrm{R}\pm,\mathrm{R}\mp)$ combinations

$$\begin{aligned} n=1,5: &\qquad \frac{1}{\sqrt{2}}(|0\rangle^{a\dot{b}}_{\mathrm{RR}}+|0\rangle^{\dot{b}a}_{\mathrm{RR}})\in \mathbf{8}_v\oplus\mathbf{56}\subset(\mathbf{8}_s\otimes\mathbf{8}_c)\oplus(\mathbf{8}_c\otimes\mathbf{8}_s)\,,\\ n=3,7: &\qquad \frac{1}{\sqrt{2}}(|0\rangle^{a\dot{b}}_{\mathrm{RR}}-|0\rangle^{\dot{b}a}_{\mathrm{RR}})\in \mathbf{8}_v\oplus\mathbf{56}\subset(\mathbf{8}_s\otimes\mathbf{8}_c)\oplus(\mathbf{8}_c\otimes\mathbf{8}_s)\,, \end{aligned} \tag{4.49}$$

survive the projection. This leaves a single set of 1- and 3-form fields. These states are part of the Type 0A spectrum.

It is worth mentioning that because these theories possess neither spacetime fermions nor (anti-)self-dual form fields, they are all free of perturbative gravitational anomalies.

Finally, let us give a more traditional orientifold interpretation to the theories studied in this section. In perturbative string theory we often refer not only to left/right-moving worldsheet fermion number $(-1)^{\mathsf{f}_\mathsf{L},\mathsf{f}_\mathsf{R}}$ but also to left/right-moving spacetime fermion number $(-1)^{\mathsf{F}_\mathsf{L},\mathsf{F}_\mathsf{R}}$. We recall that $(-1)^{\mathsf{F}}$ acts by $+1$ on the NS sector and by -1 on the R sector. We now consider $\Omega_\mathsf{F}:=\Omega(-1)^{\mathsf{F}_\mathsf{L}}$, which acts with an extra minus sign on the left-moving R sector. Above, we saw that gauging Ω with two copies of the ABK theory gives the same minus sign. This suggests the following identifications,

$$\begin{aligned} n &= 0,4: \quad (0\mathrm{B},\Omega) & \qquad n &= 1,5: \quad (0\mathrm{A},\Omega)\\ n &= 2,6: \quad (0\mathrm{B},\Omega_\mathsf{F}) & \qquad n &= 3,7: \quad (0\mathrm{A},\Omega_\mathsf{F}) \end{aligned} \tag{4.50}$$

where the first element in parenthesis denotes the starting theory, and the second element denotes the operator being gauged. The difference between theories differing by 4 copies of ABK is the action of Ω or Ω_F on Chan-Paton factors. This correspondence between the ABK viewpoint and the orientifold viewpoint will be discussed further in Section 4.5.1.

Pin^+ Type 0 Strings

We finally proceed to the case of Pin^+ Type 0 strings, which were studied in [342, 343]. The group capturing potential invertible phases on the Pin^+ worldsheet is $\mathcal{O}^2_{\text{Pin}^+}(pt) = \mathbb{Z}_2$. As reviewed in Section 4.2.2, the effective action for this invertible phase is given by the Arf invariant of the oriented double cover $\hat{\Sigma}$ of the worldsheet, i.e. $(-1)^{\text{Arf}(\hat{\Sigma})}$, whose generating manifold is the Klein bottle. The Klein bottle was seen to admit four Pin^+ structures, which we now label as $(0,1),(0,3),(2,1),(2,3)$ in analogy to the Pin^- notation.[6] By examining the spin structure on the double cover torus, these were assigned respective phases $(-1)^{\text{Arf}(\hat{\Sigma})} = 1, 1, -1, -1$.

We now proceed as in the Pin^- case above. First, we recast the Klein bottle partition functions for the four Pin^+ structures in terms of traces on the torus. This gives

$$\begin{aligned}
(0,1) &\leftrightarrow \frac{1}{4}\text{Tr}_{\text{NSNS}}\left[\Omega_{\mathsf{f}}\, e^{-2\pi l H_{\text{cl}}}\right] , \qquad & (0,3) &\leftrightarrow \frac{1}{4}\text{Tr}_{\text{NSNS}}\left[\Omega_{\mathsf{f}}\,(-1)^{\mathsf{f}}\, e^{-2\pi l H_{\text{cl}}}\right] , \\
(2,1) &\leftrightarrow \frac{1}{4}\text{Tr}_{\text{RR}}\left[\Omega_{\mathsf{f}}\, e^{-2\pi l H_{\text{cl}}}\right] , \qquad & (2,3) &\leftrightarrow \frac{1}{4}\text{Tr}_{\text{RR}}\left[\Omega_{\mathsf{f}}\,(-1)^{\mathsf{f}}\, e^{-2\pi l H_{\text{cl}}}\right] .
\end{aligned} \tag{4.51}$$

The $\text{Arf}(\hat{\Sigma})$ invertible phase assigns -1 to the Klein bottle with Pin^+ structure $(2,1)$ and $(2,3)$, and $+1$ to the other Pin^+ structures. This means that the presence of the non-trivial invertible phase changes the action of Ω_{f} on R sector ground states by a sign relative to (4.45), but does not change the action of $(-1)^{\mathsf{f}}$.

With this information, we may turn towards the analysis of the massless closed string spectra of the theories. For the trivial phase, the orientifold projection keeps the symmetric combinations of (R−,R−) and antisymmetric contributions of (R+,R+) in the Type 0B spectra. In the non-trivial phase, one instead keeps the antisymmetric combinations of

[6] We do this for notational convenience only. There is no correspondence between quadratic enhancements and Pin^+ structures in general.

(R−,R−) and symmetric contributions of (R+,R+),

$$\begin{aligned} n=0: &\qquad |0\rangle_{\rm RR}^{[ab]} \in \mathbf{28} \subset \mathbf{8}_s \otimes \mathbf{8}_s\,, &&\qquad |0\rangle_{\rm RR}^{(\dot{a}\dot{b})} \in \mathbf{1} \oplus \mathbf{35}_+ \subset \mathbf{8}_c \otimes \mathbf{8}_c\,, \\ n=1: &\qquad |0\rangle_{\rm RR}^{(ab)} \in \mathbf{1} \oplus \mathbf{35}_- \subset \mathbf{8}_s \otimes \mathbf{8}_s\,, &&\qquad |0\rangle_{\rm RR}^{[\dot{a}\dot{b}]} \in \mathbf{28} \subset \mathbf{8}_c \otimes \mathbf{8}_c\,. \end{aligned} \tag{4.52}$$

We note that these spectra are the same up to a spacetime parity transformation which exchanges the self-dual and anti-self-dual 4-forms. This observation can also be explained from the fact that the spacetime parity transformation generates $(-1)^{\mathrm{Arf}(\hat{\Sigma})}$ on the world-sheet. Indeed, in the Type II case, the same operation generated $(-1)^{\mathrm{Arf}(\Sigma,\sigma_L)+\mathrm{Arf}(\Sigma,\sigma_R)}$ as we saw before, which is equal to $(-1)^{\mathrm{Arf}(\hat{\Sigma})}$ when Σ is oriented.

We note that the RR spectra are equivalent to that of Type IIB, and the theory has a gravitational anomaly from the anti-self-dual 4-form, with no fermions to cancel it. As we discuss briefly in Appendix 4.C, consistency requires the theory to be coupled to fermionic open strings, giving a $U(32)$ gauge group [85, 89].

4.3.3 Branes and K-theory

In the above analysis we identified two oriented Type II strings, two oriented Type 0 strings, and a number of unoriented Type 0 strings. In this subsection we discuss their spectra of stable branes. To do so, we begin by briefly reviewing the well-known K-theory classification of stable branes for oriented theories.

Recall that oriented Type IIB on a spacetime X has stable D-branes which are classified by the K-group $K(X)$ [92, 93]. This is the group of pairs of vector bundles (E, F) over X subject to an equivalence relation $(E \oplus H, F \oplus H) \sim (E, F)$. More precisely, one should consider the reduced K-group $\widetilde{K}(X)$, for which the bundles E and F are required to have the same rank. Physically, the idea is to begin with a stack of equal numbers of D9- and $\overline{\text{D9}}$-branes, and then to consider annihilation amongst these stacks. When the vector bundles over these stacks are unequal this annihilation is not complete, and a residual brane of lower

dimension is left over [92, 325, 344]. It is expected that all branes can be obtained in this way.

For Type IIA, stable branes are classified by the higher K-group $K^1(X) = \widetilde{K}(X \times S^1)$. One might entertain the possibility of allowing for even higher K-groups $\widetilde{K}^n(X)$ for $n > 1$. However, Bott periodicity states that for complex K-groups,

$$\widetilde{K}^n(X) = \widetilde{K}^{n+2}(X) \ . \tag{4.53}$$

Thus the only distinct complex K-groups are those mentioned above, and both are realized by string theories. The stable Dp-branes are captured by the groups $\widetilde{K}^n(S^{9-p})$, as listed in the first two rows of Table 4.3.

As discussed in Section 4.3.1, the spectrum of massless RR fields in oriented Type 0A/B theories is precisely double that of Type IIA/B. As such, one expects the spectrum of branes in Type 0A/B to be doubled as well; the two branes of given worldvolume dimension $(p+1)$ are typically denoted as Dp- and Dp'-branes. It follows that the classification of stable branes is via two copies of the complex K-groups just described. In other words, because there now exist both D9- and D9$'$-branes, we must consider two separate pairs of vector bundles corresponding to D9-$\overline{\text{D9}}$ and D9$'$-$\overline{\text{D9}'}$ stacks. So the branes in the Type 0 theories are classified by

$$\widetilde{K}^n(X) \oplus \widetilde{K}^n(X) \cong \widetilde{K}^n(X) \oplus \widetilde{K}^{-n}(X) \ . \tag{4.54}$$

The equality above follows from the mod 2 periodicity of complex K-theory. As we now discuss, it is the latter form which generalizes to the unoriented case.

It has long been known that stable branes in unoriented Type I string theory are classified by real K-theory $\widetilde{KO}(X)$ [92, 345]. Crucially, the reduced real K-groups have a mod 8

periodicity [346],

$$\widetilde{KO}^n(X) \cong \widetilde{KO}^{n+8}(X) \ . \tag{4.55}$$

It is thus natural to guess that the eight Pin^- Type 0 strings labeled by n mod 8 have stable branes captured by $\widetilde{KO}^n(X)$. More precisely, because one again expects a doubled spectrum from these Type 0 theories, the relevant group will be found to be

$$\widetilde{KO}^n(X) \oplus \widetilde{KO}^{-n}(X) \ . \tag{4.56}$$

In Sections 4.4 and 4.5, this group will be confirmed to classify the stable p-brane spectrum of the Pin^- Type 0 theory with n copies of ABK. Concretely, this spectrum is obtained by evaluating $KO^{\pm n}(X)$ on $X = S^{9-p}$, with the results listed in Table 4.3. The entries in this table can be obtained by noting that $\widetilde{KO}^n(S^k) = KO^{n-k}(pt)$, and then using the following values for real K-groups of points:

$$\begin{aligned} KO^0(pt) = \mathbb{Z}, \quad KO^{-1}(pt) = \mathbb{Z}_2, \quad KO^{-2}(pt) = \mathbb{Z}_2, \quad KO^{-3}(pt) = 0, \\ KO^{-4}(pt) = \mathbb{Z}, \quad KO^{-5}(pt) = 0, \quad KO^{-6}(pt) = 0, \quad KO^{-7}(pt) = 0. \end{aligned} \tag{4.57}$$

At this point we can check that the RR spectra we determined above agree with the non-torsion part of $\widetilde{KO}^n(S^{9-p}) \oplus \widetilde{KO}^{-n}(S^{9-p})$. The aim of the next two sections is to establish the agreement including the torsion parts.

For Pin^+ Type 0 strings, we saw in Section 4.3.2 that these theories have the same RR spectra as oriented Type IIB. As such, we expect to have the same classification via complex K-theory as in that case. Since the Pin^+ strings have less features not found previously than their Pin^- counterparts, we will be very brief about them in what follows.

It is worth noting that whenever tadpole cancellation requires the addition of D9-branes, the question of stability of Dp-branes must be revisited to account for the possibility of

tachyonic modes of the strings stretched between the Dp- and D9-branes. In this case, the K-theory classification outlined above may be modified, though we will not address these modifications.

	-1	0	1	2	3	4	5	6	7	8	9
$\widetilde{K}$	$\mathbb{Z}$	0	$\mathbb{Z}$	0	$\mathbb{Z}$	0	$\mathbb{Z}$	0	$\mathbb{Z}$	0	$\mathbb{Z}$
$\widetilde{K}^1$	0	$\mathbb{Z}$	0	$\mathbb{Z}$	0	$\mathbb{Z}$	0	$\mathbb{Z}$	0	$\mathbb{Z}$	0
$\widetilde{KO}^0 \oplus \widetilde{KO}^{-0}$	$2\mathbb{Z}_2$	$2\mathbb{Z}_2$	$2\mathbb{Z}$	0	0	0	$2\mathbb{Z}$	0	$2\mathbb{Z}_2$	$2\mathbb{Z}_2$	$2\mathbb{Z}$
$\widetilde{KO}^1 \oplus \widetilde{KO}^{-1}$	$\mathbb{Z}_2$	$\mathbb{Z} \oplus \mathbb{Z}_2$	$\mathbb{Z}_2$	$\mathbb{Z}$	0	$\mathbb{Z}$	0	$\mathbb{Z} \oplus \mathbb{Z}_2$	$\mathbb{Z}_2$	$\mathbb{Z} \oplus \mathbb{Z}_2$	$\mathbb{Z}_2$
$\widetilde{KO}^2 \oplus \widetilde{KO}^{-2}$	$2\mathbb{Z}$	0	$\mathbb{Z}_2$	$\mathbb{Z}_2$	$2\mathbb{Z}$	0	$\mathbb{Z}_2$	$\mathbb{Z}_2$	$2\mathbb{Z}$	0	$\mathbb{Z}_2$
$\widetilde{KO}^3 \oplus \widetilde{KO}^{-3}$	0	$\mathbb{Z}$	0	$\mathbb{Z} \oplus \mathbb{Z}_2$	$\mathbb{Z}_2$	$\mathbb{Z} \oplus \mathbb{Z}_2$	$\mathbb{Z}_2$	$\mathbb{Z}$	0	$\mathbb{Z}$	0
$\widetilde{KO}^4 \oplus \widetilde{KO}^{-4}$	0	0	$2\mathbb{Z}$	0	$2\mathbb{Z}_2$	$2\mathbb{Z}_2$	$2\mathbb{Z}$	0	0	0	$2\mathbb{Z}$
$\widetilde{KO}^5 \oplus \widetilde{KO}^{-5}$	0	$\mathbb{Z}$	0	$\mathbb{Z} \oplus \mathbb{Z}_2$	$\mathbb{Z}_2$	$\mathbb{Z} \oplus \mathbb{Z}_2$	$\mathbb{Z}_2$	$\mathbb{Z}$	0	$\mathbb{Z}$	0
$\widetilde{KO}^6 \oplus \widetilde{KO}^{-6}$	$2\mathbb{Z}$	0	$\mathbb{Z}_2$	$\mathbb{Z}_2$	$2\mathbb{Z}$	0	$\mathbb{Z}_2$	$\mathbb{Z}_2$	$2\mathbb{Z}$	0	$\mathbb{Z}_2$
$\widetilde{KO}^7 \oplus \widetilde{KO}^{-7}$	$\mathbb{Z}_2$	$\mathbb{Z} \oplus \mathbb{Z}_2$	$\mathbb{Z}_2$	$\mathbb{Z}$	0	$\mathbb{Z}$	0	$\mathbb{Z} \oplus \mathbb{Z}_2$	$\mathbb{Z}_2$	$\mathbb{Z} \oplus \mathbb{Z}_2$	$\mathbb{Z}_2$

Table 4.3: The ten K-groups capturing stable branes in the oriented Type II and (un)oriented Type 0 theories discussed above.

4.4 D-brane spectra via boundary fermions

In this section, we demonstrate the $KO^n \oplus KO^{-n}$ classification of stable branes for the Pin^- Type 0 theory with n copies of ABK. This is done by analyzing the Clifford modules carried by open string endpoints. After doing so, we also study the spectra of non-stable branes in these theories, including the gauge groups supported on their worldvolumes and the representations of their open string tachyons.

4.4.1 (0+1)d Majorana fermions and their anomalies

Fermions and Clifford algebras

We begin by considering systems of (0+1)d Majorana fermions, which appear on the boundary of n copies of the ABK theory. Let us say we have $r + s$ hermitian fermion operators

$\xi_a = (\xi_a)^\dagger$, $a = 1, \ldots, r+s$, satisfying

$$\xi_a^2 = +1 \qquad a = 1, \ldots, r+s \tag{4.58}$$

and

$$\mathsf{T}\xi_a\mathsf{T}^{-1} = \begin{cases} +\xi_a & a = 1, \ldots, r, \\ -\xi_a & a = r+1, \ldots, r+s. \end{cases} \tag{4.59}$$

In the mathematics literature it is more common to consider operators invariant under T. This can be achieved by defining

$$\begin{cases} \gamma_a = \xi_a & i = 1, \ldots, r, \\ \gamma_a = i\xi_a & i = r+1, \ldots, r+s. \end{cases} \tag{4.60}$$

The γ_a are no longer hermitian in general, but satisfy $\mathsf{T}\gamma_a\mathsf{T}^{-1} = \gamma_a$. They generate the real Clifford algebra $\mathrm{Cl}(r,s)$. We often use the abbreviations $\mathrm{Cl}(+n) := \mathrm{Cl}(n,0)$ and $\mathrm{Cl}(-n) := \mathrm{Cl}(0,n)$.[7]

The system of $r+s$ fermions giving rise to $\mathrm{Cl}(r,s)$ can have anomalies in the realization of T and $(-1)^{\mathsf{f}}$, which will be the topic of the next subsection. Before proceeding, we now give a rough argument for why these anomalies depend only on $r-s$ modulo 8. First we argue that only $r-s$ is relevant for the anomaly. The reason is that a pair of fermions with opposite T transformations allow a T-invariant mass term, so they cannot be anomalous. For example, when $(r,s) = (1,1)$, we can simply add a T-invariant mass term $i\xi_1\xi_2$, which would trivialize the vacuum, precluding any anomaly.

We next argue that only $r - s \mod 8$ matters. This can be understood in two steps. As the first step, we consider $\mathrm{Cl}(4)$. For this we can introduce a T-invariant quartic hermitian

[7] Our convention is that $\mathrm{Cl}(-n) = C_n$ and $\mathrm{Cl}(+n) = C'_n$ in the notation of Atiyah-Bott-Shapiro [347].

interaction term

$$H = \xi_1\xi_2\xi_3\xi_4 \tag{4.61}$$

to the system, for which the vacuum is two-dimensional, purely bosonic, and $\mathsf{T}^2 = -1$. This realizes a Kramers doublet, on which

$$\sigma_x := i\xi_1\xi_2, \qquad \sigma_y := i\xi_1\xi_3, \qquad \sigma_z := i\xi_1\xi_4 \tag{4.62}$$

act as Pauli matrices.

As the second step, we combine two such Kramers doublets obtained from two copies of Cl(4), and make a single bosonic system with $\mathsf{T}^2 = +1$ and a unique vacuum. This can be done by introducing a T-invariant term

$$H' := \sigma_x \otimes \sigma_x + \sigma_y \otimes \sigma_y + \sigma_z \otimes \sigma_z, \tag{4.63}$$

which we note can be realized as a four-fermi operator using (4.62).

In other words, we can introduce to Cl(8) a four-fermion term $c_{ijk\ell}\xi^i\xi^j\xi^k\xi^\ell$ which is hermitian and T-invariant, such that its addition leads to a non-degenerate vacuum [80]. Therefore, eight Majorana fermions with the same time-reversal properties can be removed without affecting the anomaly.

More general (0+1)d systems and anomalies

We do not necessarily have to couple n boundary Majorana fermions to n copies of the ABK theory. We only have to couple a boundary system which has the *same* anomaly as n Majorana fermions. We thus need to understand the possible anomalies concerning the realizations of T and $(-1)^\mathsf{f}$. In the mathematical literature this analysis was first done in [348], in which the following eight-fold classification in terms of three signs was given.

The first sign is the most subtle to define. We ask whether $(-1)^\mathsf{f}$ can be realized in an

irreducible ungraded representation of the algebra. If this is possible, the representation is of type +, and if not, it is of type −. As an example, consider Cl(+1). There are two ungraded irreducible representations, which are real one-dimensional such that $\xi_1 = \pm 1$. Clearly there is no $(-1)^{\mathsf{f}}$ operator that anticommutes with ξ_1, meaning that Cl(+1) is of type −.

In the following, for representations of type −, we adjoin $(-1)^{\mathsf{f}}$ to the algebra and consider the resulting irreducible graded representations. Again take Cl(+1) as an example. Then we consider a representation given by

$$\xi_1 = \begin{pmatrix} 0 & 1 \\ 1 & 0 \end{pmatrix}, \qquad (-1)^{\mathsf{f}} = \begin{pmatrix} 1 & 0 \\ 0 & -1 \end{pmatrix}. \tag{4.64}$$

This is not irreducible as an ungraded representation but is irreducible as a graded representation.

The other two signs specifying the anomaly type are easier to define. The second sign is the one appearing in

$$\mathsf{T}(-1)^{\mathsf{f}} = \pm(-1)^{\mathsf{f}}\mathsf{T}, \tag{4.65}$$

while the third sign is the one appearing in

$$(\mathsf{T})^2 = \pm 1. \tag{4.66}$$

The eight types, labeled by $n = 0, \ldots, 7$, are summarized in the left portion of Table 4.4. There, we showed $\mathsf{T}^2 = \pm 1$ in terms of the corresponding division algebras $\mathbb{R}$ and $\mathbb{H}$. In [348] it was shown that the tensor product of a representation of type n and another of type n' has the type $n + n'$ modulo 8. A very explicit analysis of Cl($+n$) was given in Sec. 2.5.1 and 2.5.2 of [349], from which one can find that Cl($+n$) is indeed of type n. Similarly, Cl($-n$) is of type $-n$.

In [348] it was also shown that any graded irreducible representation of type n automati-

n	type	T and $(-1)^{\mathsf{f}}$	T^2
0	$+$	commute	$\mathbb{R}$
1	$-$	anticommute	$\mathbb{R}$
2	$+$	anticommute	$\mathbb{R}$
3	$-$	commute	$\mathbb{H}$
4	$+$	commute	$\mathbb{H}$
5	$-$	anticommute	$\mathbb{H}$
6	$+$	anticommute	$\mathbb{H}$
7	$-$	commute	$\mathbb{R}$

n	$\mathcal{A}$		$\mathcal{A}_0$	$\mathcal{A}_1^+$	$\mathcal{A}_1^-$	$\sqrt{\dim_{\mathbb{R}}}$
0	$\mathrm{Cl}(+0) =$	$\mathbb{R}$	$\mathbb{R}$			1
1	$\mathrm{Cl}(+1) =$	$\mathbb{R}\oplus\mathbb{R}$	$\mathbb{R}$	$\mathbb{R}$		$\sqrt{2}$
2	$\mathrm{Cl}(+2) =$	$\mathbb{R}[2]$	$\mathbb{C}$	$\mathbb{C}$		2
3	$\mathrm{Cl}(+3) =$	$\mathbb{C}[2]$	$\mathbb{H}$	$\mathbb{R}^3$	$\mathbb{R}^1$	$2\sqrt{2}$
4		$\mathbb{H}$	$\mathbb{H}$			2
5	$\mathrm{Cl}(-3) =$	$\mathbb{H}\oplus\mathbb{H}$	$\mathbb{H}$	$\mathbb{R}^1$	$\mathbb{R}^3$	$2\sqrt{2}$
6	$\mathrm{Cl}(-2) =$	$\mathbb{H}$	$\mathbb{C}$		$\mathbb{C}$	2
7	$\mathrm{Cl}(-1) =$	$\mathbb{C}$	$\mathbb{R}$		$\mathbb{R}$	$\sqrt{2}$

Table 4.4: The properties of T and $(-1)^{\mathsf{f}}$ for the eight anomaly types $n = 0, \ldots, 7$. The corresponding graded division algebras $\mathcal{A} = \mathcal{A}_0 \oplus \mathcal{A}_1$, $\mathcal{A}_1 = \mathcal{A}_1^+ \oplus \mathcal{A}_1^-$ are also given.

cally contains an action of the minimal algebra $\mathcal{A}$ for that type. This information is shown in the right portion of Table 4.4. There, $\mathbb{F}[n]$ stands for the $n \times n$ matrix algebra over the field $\mathbb{F}$, $\mathcal{A}_0$ and $\mathcal{A}_1$ are the bosonic and fermionic parts of the algebra, and $\mathcal{A}_1^\pm$ are the subspaces of $\mathcal{A}_1$ which are hermitian and anti-hermitian, respectively.[8] These eight graded algebras are known to exhaust the graded division algebras over $\mathbb{R}$, i.e. graded algebras such that any homogeneous element has an inverse.

On the boundary Hilbert space

Consider n copies of the Kitaev chain on a segment $\sigma \in [0, \pi]$. We call $\sigma = 0$ the left boundary and $\sigma = \pi$ the right boundary. The Majoranas ξ on the left and ξ' on the right must have opposite transformation properties under time-reversal [80, 81]. This can be seen by imagining a process in which the endpoints of the segment join to give a closed circle. Once the endpoints come together, the T-invariant mass term involving ξ and ξ' should be able to gap the system, so ξ and ξ' needs to have opposite T-transformation properties.

We work in the convention[9] that we have n fermions ξ_i with $\mathsf{T}\xi_i\mathsf{T}^{-1} = +\xi_i$ on the left and n fermions ξ_i' with $\mathsf{T}\xi_i'\mathsf{T}^{-1} = -\xi_i'$ on the right. They form $\mathrm{Cl}(n)$ and $\mathrm{Cl}(-n)$, respectively. The

[8] Note that the hermitian conjugate on a real algebra is simply an involution satisfying $(ab)^* = b^*a^*$.

[9] In Section 4.5, the choice of the convention here will correspond to a choice of definition of the O9-plane state.

Hilbert space associated to the open string segment, including the bulk and two boundaries, can be identified with $\mathrm{Cl}(n)$ itself, on which $\mathrm{Cl}(n)$ acts from the left and $\mathrm{Cl}(-n)$ acts from the right. That the Hilbert space on the segment should naturally be equal to the boundary algebra $\mathrm{Cl}(n)$ itself is clear from the state-operator correspondence. If we have other degrees of freedom on the worldsheet, the Hilbert space on the segment is of the form

$$\mathcal{H}_{\text{phys}} = \mathrm{Cl}(n) \otimes \mathcal{H}_{\text{other dof}}. \tag{4.67}$$

Naively, one would like to say that this Hilbert space is the tensor product of the Hilbert spaces on the two boundaries. The square root $\sqrt{\dim_{\mathbb{R}} \mathcal{A}}$, listed in Table 4.4, is then what would be taken as the dimension of the boundary Hilbert spaces. Note that this is not always an integer. It is sometimes useful to have a well-defined, non-anomalous boundary Hilbert space with integer dimension. This can be done by introducing n auxiliary boundary fermions Ξ_i with $\mathsf{T}\Xi_i\mathsf{T}^{-1} = -\Xi_i$ on the left and n auxiliary boundary fermions Ξ'_i with $\mathsf{T}\Xi'_i\mathsf{T}^{-1} = +\Xi'_i$ on the right; this technique was used in e.g. [350] in the Type II setting. We note that auxiliary boundary fermions have opposite T-transformation rules as compared to the physical boundary fermions. The fermions on the left boundary now form $\mathrm{Cl}(n, n)$ and can be quantized without anomaly. This can be represented on a space V, thus providing Chan-Paton indices to the boundary. We can do the same on the right. The Hilbert space on the segment, including both the physical and auxiliary boundary fermions, is then of the form

$$V \otimes V^* \otimes \mathcal{H}_{\text{other dof}} = \mathcal{H}_{\text{aux}} \otimes \mathcal{H}_{\text{phys}} \tag{4.68}$$

where $\mathcal{H}_{\text{aux}} = \mathrm{Cl}(-n)$ and $\mathcal{H}_{\text{phys}}$ was defined in (4.67). Note that the elements of $\mathcal{H}_{\text{phys}}$ can be found by finding operators (anti)commuting with all the auxiliary boundary fermions Ξ.

Below, when we say that "a boundary carries a representation of $\mathrm{Cl}(n)$," we mean that there are physical boundary fermions forming $\mathrm{Cl}(n)$, where n is taken modulo 8. If we use the auxiliary boundary fermions, they form $\mathrm{Cl}(-n)$.

4.4.2 D-branes and boundary fermions

Let us now study the boundary fermions in the context of the worldsheet theory of Pin^- Type 0 strings, with n copies of the ABK theory. We first consider open strings ending on 9-branes. We then have n boundary fermions on the left forming $\text{Cl}(n)$ and n boundary fermions on the right forming $\text{Cl}(-n)$, as discussed above. The open-string Hilbert space, before GSO projection, is of the form

$$\text{Cl}(n) \otimes \mathcal{H}_0 \tag{4.69}$$

where $\mathcal{H}_0$ is the open string Hilbert space of the massless worldsheet fields. Also as discussed above, we can replace $\text{Cl}(n)$ with any graded algebra having the same anomaly.

The restriction to 9-branes above meant that the only boundary fermions required were those needed to cancel the anomaly of n copies of ABK. However, for branes of higher codimension there will be additional anomalies from bulk fermion zero-modes, which should be accompanied by additional boundary fermions ζ_i. Let us set $n = 0 \mod 8$ for the moment, since the ABK boundary fermions can be easily reinstated later. In order to understand the additional boundary Majoranas ζ_i, we must first understand when zero-modes can appear in the bulk of the string. As reviewed in Appendix 4.A, this depends on whether the ends of the string have Dirichlet (D) or Neumann (N) boundary conditions. The NN, DD, and ND strings satisfy the following boundary conditions,

$$\begin{aligned}
\text{NN}: \quad & \psi^\mu(t,0) = -\eta_1 \tilde{\psi}^\mu(t,0), & \psi^\mu(t,\pi) &= +\eta_2 \tilde{\psi}^\mu(t,\pi), \\
\text{DD}: \quad & \psi^\mu(t,0) = +\eta_1 \tilde{\psi}^\mu(t,0), & \psi^\mu(t,\pi) &= -\eta_2 \tilde{\psi}^\mu(t,\pi), \\
\text{ND}: \quad & \psi^\mu(t,0) = -\eta_1 \tilde{\psi}^\mu(t,0), & \psi^\mu(t,\pi) &= -\eta_2 \tilde{\psi}^\mu(t,\pi),
\end{aligned} \tag{4.70}$$

where $\psi, \tilde{\psi}$ are left- and right-moving bulk fermions and $\eta_{1,2} = \pm 1$ specifies the boundary conditions at $\sigma = 0, \pi$. Though only the relative sign in these conditions is ultimately

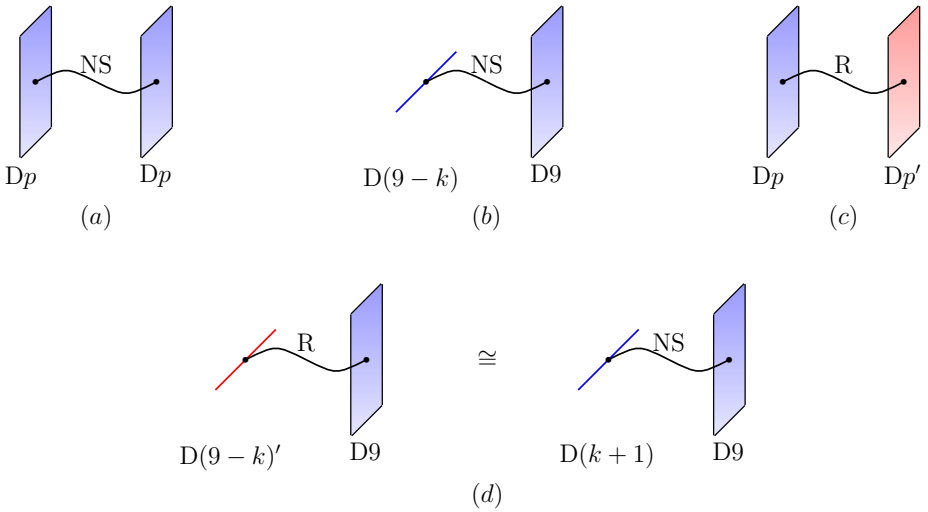

Figure 4.3: (a) A pair of Dp-branes with an NS sector string stretched between them; (b) an NS sector string stretched between a D$(9-k)$- and D9-brane; (c) an R sector string stretched between a Dp- and Dp'-brane; (d) an R sector string stretched between a D$(9-k)'$- and D9-brane, which can be thought of as an NS sector string stretched between a D$(k+1)$- and D9-brane, as far as the behavior of the fermion zero modes is concerned.

important, our current conventions are such that $\eta_{1,2} = +1$ represents a Dp-brane at $\sigma = 0, \pi$, while $\eta_{1,2} = -1$ represents a Dp'-brane at $\sigma = 0, \pi$. This is described in more detail in Appendices 4.A and 4.B.

The presence of zero-modes depends on the relative choice of $\eta_{1,2}$. This choice is in turn related to the choice of NS or R sectors on the open string; we declare that the string is in the NS sector for $\eta_1 = \eta_2$ and in the R sector for $\eta_1 = -\eta_2$; see Appendix 4.A. From (4.70) we then conclude that NS sector fermions can have zero-modes along ND and DN directions, whereas R sector fermions can have zero-modes along NN and DD directions.

Consider now a coincident pair of 9-branes of type η (Fig. 4.3(a)). In light-cone gauge, there are zero ND directions and a total of 8 NN + DD directions. Since open strings stretching between branes of the same type are in the NS sector, any potential zero-modes would be in ND directions, of which there are none. Hence there are no bulk zero-modes, and thus no boundary fermions. The same holds more generally for coincident pairs of p-branes of type η.

We now consider a 9-brane coincident with a $(9-k)$-brane, both of type η (Fig. 4.3(b)). We consider an open string between them, which is again in the NS sector since the branes are still of the same type. However, there are now k DN directions, and hence k zero-modes. We denote the restriction of these zero modes to the boundary at the $(9-k)$-brane by ψ_0^i. As in (4.41), the boundary time-reversal operator T acts on these by $\mathsf{T}\psi_0^i\mathsf{T}^{-1} = \tilde{\psi}_0^i$. By (4.70), if the $(9-k)$-brane is at $\sigma = 0$ then we have $\psi_0^i = \eta\tilde{\psi}_0^i$, whereas if it is at $\sigma = \pi$ we have $\psi_0^i = -\eta\tilde{\psi}_0^i$. Together we conclude that

$$\mathsf{T}\psi_0^i\mathsf{T}^{-1} = \begin{cases} +\eta\psi_0^i & \sigma = 0, \\ -\eta\psi_0^i & \sigma = \pi. \end{cases} \tag{4.71}$$

When $k \neq 0 \mod 8$, these zero-modes will lead to anomalies in T and $(-1)^{\mathsf{f}}$, and in order to cancel them we must add extra boundary fermions. At $\sigma = 0$ there are two options: we may add k boundary fermions ζ_i satisfying $\mathsf{T}\zeta_i\mathsf{T}^{-1} = -\eta\zeta_i$, or $8-k$ boundary fermions satisfying $\mathsf{T}\zeta_i\mathsf{T}^{-1} = +\eta\zeta_i$. These two choices are effectively identical, as they both behave as $\mathrm{Cl}(-\eta k)$. On the boundary at $\sigma = \pi$, one likewise requires a representation of $\mathrm{Cl}(+\eta k)$.

For full consistency, we must check that the same additional boundary fermions also cancel tentative anomalies in mixed strings stretching between Dp- and Dq'-branes. To begin, consider coincident Dp- and Dp'-branes (Fig. 4.3(c)). There are then zero ND directions and a total of 8 NN+DD directions. Since the branes are now of opposite types, the open strings stretched between them are in the R sector. Recall that in the R sector, there are zero-modes not from ND directions, but rather from NN and DD directions. Hence in this case there are a total of 8 bulk zero-modes. But because there are eight of them, there is no time-reversal anomaly, and no boundary fermions are necessary. This is consistent with the fact that the strings stretching from the Dp-branes to themselves, or from the Dp'-branes to themselves, were shown to not require any boundary fermions.

Another way to analyze this setup is to note that, insofar as counting zero-modes is

concerned, switching $\eta \to -\eta$ is equivalent to switching Neumann and Dirichlet boundary conditions in all directions, as is evident from (4.70). Then the Dp'-brane can be replaced by a D$(10-p)$-brane, and we now have a setup with 8 ND directions and zero NN and DD directions (in light-cone gauge). Since the branes are of the same type now, the open string stretched between them is in the NS sector, and we can again conclude that we have 8 zero-modes. This method of replacing the Dp'-brane with a D$(10-p)$-brane is useful in analyzing e.g. the case of a D$(9-k)'$- and D9-brane, which can be replaced by a D$(k+1)$- and D9-brane (Fig. 4.3(d)). By our above analysis, this then has $8-k$ bulk zero-modes which satisfy $\mathsf{T}\psi_0\mathsf{T}^{-1} = -(-1)\psi_0 = +\psi_0$ at $\sigma = 0$. These can be cancelled by adding $8-k$ boundary fermions ζ_i satisfying $\mathsf{T}\zeta_i\mathsf{T}^{-1} = -\zeta_i$, or k boundary fermions satisfying $\mathsf{T}\zeta_i\mathsf{T}^{-1} = \zeta_i$, both of which give a representation of Cl(k). This matches the results found before for a D$(9-k)'$-brane. Using these techniques, one can easily check that the more general mixed strings between Dp- and Dq'-branes have vanishing anomaly when one makes the above assignments of boundary fermions.

Finally, we may reintroduce non-zero n. As discussed above, this gives a representation of Cl(n) on the boundary at $\sigma = 0$ and of Cl$(-n)$ on the boundary at $\sigma = \pi$. Let us now consider an open string stretched between a $(9-k)$-brane of type η at $\sigma = 0$ and a D$(9-k)$-brane at $\sigma = \pi$. In the theory with n copies of ABK, the endpoint at $\sigma = 0$ carries a representation of Cl$(n - \eta k)$, while the endpoint at $\sigma = \pi$ carries a representation of Cl$(-n + \eta k)$.

4.4.3 K-theory classification of branes

We can now study the stability of D-branes in these theories. The analogous results in Type I were obtained in [350–352]. We first note that the tachyon vertex operator ζ is a fermionic,

hermitian boundary operator such that the boundary interaction

$$\int dt\, i\psi_0^\mu \zeta D_\mu \mathcal{T}(X). \tag{4.72}$$

is T-invariant. Here ψ_0^μ is the restriction of the bulk fermion field to the boundary and $\mathcal{T}(X)$ is the spacetime tachyon profile. In particular, the ψ_0^μ appearing here should be those associated to the Neumann directions, which have opposite T transformations as those given in (4.71). Thus for the coupling to be T-invariant, we need ζ to have the *same* T transformations as those given in (4.71),

$$\mathsf{T}\zeta\mathsf{T}^{-1} = \begin{cases} +\eta\zeta & \sigma = 0, \\ -\eta\zeta & \sigma = \pi. \end{cases} \tag{4.73}$$

Stable branes are those for which such ζ does not exist.

It is cumbersome to carry out the analysis below for the two cases $\eta = \pm 1$ separately. This can be circumvented by analyzing the $\sigma = 0$ end when $\eta = +1$ and the $\sigma = \pi$ end when $\eta = -1$. This means that we work with the Clifford algebra $\mathrm{Cl}(n - \eta k)$ for $\eta = +1$ and $\mathrm{Cl}(-n + \eta k)$ for $\eta = -1$, or in other words just $\mathrm{Cl}(\eta n - k)$ for both cases. Therefore, below we simply analyze $\mathrm{Cl}(\eta n - k)$ and look for a tachyon vertex operator satisfying

$$\mathsf{T}\zeta\mathsf{T}^{-1} = \zeta, \tag{4.74}$$

for both cases $\eta = \pm 1$. This means that the results to be obtained depend only on

$$\nu := \eta n - k. \tag{4.75}$$

When $\nu = 0 \mod 8$, the minimal choice of Chan-Paton algebra is simply $\mathbb{R}$, as can be seen from Table 4.4. We can enlarge the Chan-Paton algebra by introducing N bosonic

indices and N' fermionic indices. Then the Chan-Paton algebra has the bosonic part $\mathbb{R}[N] \oplus \mathbb{R}[N']$ and the fermionic part $\mathbb{R}^N \otimes \mathbb{R}^{N'} \oplus \mathbb{R}^{N'} \otimes \mathbb{R}^N$, where we recall that the algebra $\mathbb{F}[N]$ stands for the $N \times N$ matrix algebra with entries in $\mathbb{F}$. The T-invariant fermionic part is then $\mathbb{R}^N \otimes \mathbb{R}^{N'}$. This means that the gauge group is $O(N) \times O(N')$ and the tachyon field is in the bifundamental. The stable branes are those such that the tachyon representation is empty, which occurs for $N \geq 0$ and $N' = 0$ or $N = 0$ and $N' \geq 0$. These can be labeled by $\mathbb{Z}$. The case $\nu = 4$ is similar; one simply replaces $\mathbb{R}$ by $\mathbb{H}$ and O by Sp.

In the other six cases, the minimal choice of Chan-Paton algebra $\mathcal{A}$ already contains both the bosonic and the fermionic part. We can introduce additional Chan-Paton indices $i = 1, \ldots, N$, thus enlarging the Chan-Paton algebra to $\mathcal{A}[N] := \mathcal{A} \otimes \mathbb{R}[N]$. From Table 4.4, we see that $\mathcal{A}[N]$ has the following structure:

ν	$\mathcal{A}[N]_0$	$\mathcal{A}[N]_1^+$	$\mathcal{A}[N]_1^-$
1	$\mathbb{R}[N]$	$\mathbb{R}[N]^{\text{symm.}}$	$\mathbb{R}[N]^{\text{anti.}}$
2	$\mathbb{C}[N]$	$\mathbb{C}[N]^{\text{symm.}}$	$\mathbb{C}[N]^{\text{anti.}}$
3	$\mathbb{H}[N]$	$\mathbb{H}[N]^{\text{symm.}}$	$\mathbb{H}[N]^{\text{anti.}}$
5	$\mathbb{H}[N]$	$\mathbb{H}[N]^{\text{anti.}}$	$\mathbb{H}[N]^{\text{symm.}}$
6	$\mathbb{C}[N]$	$\mathbb{C}[N]^{\text{anti.}}$	$\mathbb{C}[N]^{\text{symm.}}$
7	$\mathbb{R}[N]$	$\mathbb{R}[N]^{\text{anti.}}$	$\mathbb{R}[N]^{\text{symm.}}$

(4.76)

where $\mathcal{A}[N]_{0,1}$ denotes the bosonic and fermionic parts and $\mathcal{A}[N]_1^{\pm}$ denotes the hermitian and anti-hermitian parts. The symmetrization and antisymmetrization are defined as usual for $\mathbb{R}$ and $\mathbb{C}$, and as the symmetric and antisymmetric tensor square for the fundamental representation of $Sp(N)$ for $\mathbb{H}$. It is instructive to check that the table above reduces to Table 4.4 when $N = 1$. From this it is easy to read off the gauge group and the representation of the tachyons for the D-branes, which is given in Table 4.5. One may check that by setting $n = 0$ in Table 4.5 we get back the results of [350–352] for Type I.

The stable branes are those for which the tachyons are absent. For $\nu = 0, 4$ we already discussed that they are classified by $\mathbb{Z}$. For $\nu = 1, 2, 3, 5$ the tachyon field is always present. Finally, for $\nu = 6, 7$ the tachyon field is absent when $N = 1$ but appears when $N = 2$, and hence the classification is by $\mathbb{Z}_2$. These results match with $KO^\nu(pt)$.

Let us reanalyze this setup using the auxiliary boundary fermions discussed in Section 4.4.1. Our physical boundary fermions form an algebra $\mathcal{A}$ whose anomaly is of type ν. We introduce auxiliary boundary fermions $\mathrm{Cl}(-\nu)$ to cancel the anomaly, so $\mathrm{Cl}(-\nu) \otimes \mathcal{A}$ is non-anomalous, acting on the Chan-Paton vector space V. The tachyon field corresponds to a hermitian fermionic element ζ in $\mathcal{A}$. This means that if such a tachyon field is present, the $\mathrm{Cl}(-\nu)$ action on V is extended to a $\mathrm{Cl}(1-\nu)$ action on V. In other words, on the D-brane characterized by ν, a Chan-Paton space V with an action of $\mathrm{Cl}(-\nu)$ is necessary, and it is unstable if and only if this $\mathrm{Cl}(-\nu)$ action can be extended to an action of $\mathrm{Cl}(1-\nu)$. Using the result in [347], this can be directly connected to $KO^\nu(pt)$. To see this, recall that in [347] Atiyah, Bott, and Shapiro considered

$$M_{-n} := \text{free } \mathbb{Z}\text{-modules generated by graded irreducible representations of } \mathrm{Cl}(-n) \quad (4.77)$$

and considered the natural map $i^* : M_{-n-1} \to M_{-n}$ induced by $i : \mathrm{Cl}(-n) \to \mathrm{Cl}(-n-1)$. It was then shown that

$$KO^{-n}(pt) = M_{-n}/i^*(M_{-n-1}). \quad (4.78)$$

We note that by replacing Ξ by $\hat{\Xi} = \Xi(-1)^{\mathsf{f}}$, a graded representation of $\mathrm{Cl}(n)$ can be converted to a graded representation of $\mathrm{Cl}(-n)$ and vice versa. Therefore we also have

$$KO^{-n}(pt) = M_n/j^*(M_{n+1}) \quad (4.79)$$

where $j^* : M_{n+1} \to M_n$ is now induced by $j : \mathrm{Cl}(n) \to \mathrm{Cl}(n+1)$. Then, Chan-Paton spaces with $\mathrm{Cl}(-\nu)$ action modulo those with $\mathrm{Cl}(-\nu+1)$ action are clearly classified by $KO^\nu(pt)$.

ν	0	1	2	3	4	5	6	7
G_ν	$O(N) \times O(N')$	$O(N)$	$U(N)$	$Sp\left(\frac{N}{2}\right)$	$Sp\left(\frac{N}{2}\right) \times Sp\left(\frac{N'}{2}\right)$	$Sp\left(\frac{N}{2}\right)$	$U(N)$	$O(N)$
ρ_ζ	bifund.	symm.	symm.	symm.	bifund.	anti.	anti.	anti.
λ_ν	1	$\sqrt{2}$	2	$2\sqrt{2}$	2	$2\sqrt{2}$	2	$\sqrt{2}$
$KO^\nu(pt)$	$\mathbb{Z}$	0	0	0	$\mathbb{Z}$	0	$\mathbb{Z}_2$	$\mathbb{Z}_2$

Table 4.5: Gauge groups G_ν and tachyon representations ρ_ζ on the worldvolume of N $(9-k)$-branes of type η in the theory with n copies of ABK. Note that $\nu = \eta n - k = \eta n + p - 1$ mod 8. "Bifund." refers to the bifundamental representation, whereas "symm." ("anti.") refer to the symmetric (anti-symmetric) rank 2 tensor representations. We also listed the tensions of these branes, as well as their K-theory classifications, which can be found by considering when the tachyon field is empty.

We note that this restatement also shows that the brane of type ν can naturally host an orthogonal bundle with an additional action of $\mathrm{Cl}(-\nu)$. It would be interesting to connect this observation to the definition of KO-theories in terms of Clifford bundles, which can be found e.g. in [94].

Brane tension from boundary fermions

Finally, let us comment on the tensions of the various branes, both stable and unstable, identified thus far. In order to obtain the tension one computes a disc path integral, with the boundary of the disc anchored on the brane — this may be interpreted as the one-point function of the brane with a graviton in the closed string picture. If there are Majorana fermions present on the boundary of the disc, these will give a contribution to the path integral. In particular, as mentioned in the Introduction the contribution of a $(0+1)$d Majorana fermion to the path integral is an overall factor of $\sqrt{2}$. This holds in all cases, including Type II and Type 0 strings.

We begin by discussing the more familiar case of Type II, for which there are branes of only a single type $\eta = 1$. As we have discussed, the Type IIB and IIA theories are distinguished by the presence of respectively $n = 0, 1$ Majorana fermions on the boundary. For this reason, the non-BPS D9-branes in Type IIA have a tension which is $\sqrt{2}$ times

that of their BPS counterparts in Type IIB. However, it is not the case that *all* branes in Type IIA have tensions which are larger by this factor. Indeed, let us consider branes of codimension k. By considering open strings stretched between such branes and D9-branes, we may conclude that strings ending on such branes must have k bulk zero modes — this is argued for as above, by noting that a change in codimension leads to a change in the number of DN or ND directions for the open string endpoints. It is then possible for the anomalies of the invertible phase and bulk zero modes to cancel. In fact, since in this case the anomaly is only $\mathbb{Z}_2$ we can conclude that the number of boundary fermions is only $|n-k| \mod 2$. As such, we conclude that Dp branes in Type IIA/B have tensions $(\sqrt{2})^{|n-k| \bmod 2} T_p^{\mathrm{II}}$, where T_p^{II} is the tension of the corresponding stable non-torsion p-brane. In particular, this tells us that for Type IIB, branes with p odd have tensions T_p^{II} (essentially by definition) while for p even the branes have tensions $\sqrt{2}T_p^{\mathrm{II}}$. Likewise for Type IIA, branes with p even have tensions T_p^{II}, while branes with p odd have tensions $\sqrt{2}T_p^{\mathrm{II}}$.

We now generalize this to the case of Type 0 strings. As explained above, in this case the bulk theory carries the same anomaly as ν boundary Majorana fermions. It is natural to choose the minimal realization of the anomaly in the boundary system, which is a system of Majorana fermions in a representation of $\mathrm{Cl}(+\nu)$ if $\nu < 4$ and of $\mathrm{Cl}(-\nu)$ if $\nu > 4$. Then the tension of the corresponding branes is weighted by the path integral over the system of fermions, yielding the result $\lambda_\nu T_p^0$ where $\lambda_\nu := \sqrt{\dim_{\mathbb{R}} \mathcal{A}}$ as given in Table 4.4. For example, in the case of a D9- or D9′-brane in the theory with 1 or 7 copies of ABK, we find that the tension is $\sqrt{2}$ times that in the theory with no copies of ABK. The values λ_ν are tabulated in Table 4.5, and will be reproduced for stable branes via the boundary state formalism in Section 4.5.

4.4.4 Vacuum manifolds of tachyons as classifying spaces

We now reinterpret the results of this section in terms of tachyon condensation on the worldvolume of 9-branes. In the string theory literature, this is referred to as the Atiyah-Bott-Shapiro (ABS) construction [92, 93, 347].

We start from the 9-brane of type η. As before we use the trick of analyzing the $\sigma = 0$ boundary when $\eta = +1$ and the $\sigma = \pi$ boundary when $\eta = -1$. The boundary then carries an action of $\mathrm{Cl}(\eta n)$. To construct a $(9-k)$-brane located at $X^1 = \cdots = X^k = 0$, we choose a set of time-reversal invariant Majorana fermion operators $\zeta_{i=1,\ldots,k}$ in $\mathrm{Cl}(\eta n)$ (for this purpose one might need to replace ηn by $\eta n + 8m$ for some integer m) and use them to assemble the tachyon field

$$\mathcal{T}(X) = f(|X|) \sum_{i=1}^{k} X^i \zeta_i \ , \tag{4.80}$$

with $f(|X|)$ some convergence factor chosen such that $\mathcal{T}(X)$ obtains its vacuum value as $|X| \to \infty$ and such that $f(|X|)^2 \sum_{i=1}^{k} (X^i)^2 = 1$. Upon condensation this tachyon gives rise to the desired $(9-k)$-brane. As we used up k out of ηn Majorana fermions we originally had on the 9-brane, we end up with the residual action of $\mathrm{Cl}(\eta n - k)$, as argued before in a different manner.

We now discuss the connection between tachyon profiles and KO-theory. Consider the usual 9-$\overline{9}$ stack, supporting an $O(N) \times O(N)$ gauge group for $n = 0 \mod 8$. We now follow Sen's construction and consider a domain wall configuration of the tachyon such that it condenses to produce a D8-brane [325]. This involves assignment of a vacuum value of $\zeta(X)$ to each point on the "sphere" S^0 at infinity. Thus such domain wall configurations are classified by $\pi_0(\mathcal{V}_9)$, where $\mathcal{V}_9$ is the vacuum manifold for the tachyon on D9-brane. The tachyon potential should be such that it breaks $O(N) \times O(N)$ to the $O(N)$ supported on

the resulting D8. A minimal assumption is then

$$\mathcal{V}_9 = \frac{O(\infty) \times O(\infty)}{O(\infty)} \cong O(\infty) \tag{4.81}$$

where we took the formal limit in which the number of original D9-branes is infinite. We can repeat the argument for lower Dp-branes, and find that they would similarly be classified by $\pi_{8-p}(\mathcal{V}_9)$.

The Dp-brane can also be obtained from tachyon condensation on Dq-branes with $p < q < 9$. The vacuum manifold $\mathcal{V}_q$ for the tachyon field on the Dq-brane can be determined from Table 4.5:

$$\begin{aligned}
&\mathcal{V}_2 = \frac{O(\infty)}{O(\infty) \times O(\infty)} \times \mathbb{Z} \ , \quad \mathcal{V}_3 = \frac{U(\infty)}{O(\infty)} \ , \quad \mathcal{V}_4 = \frac{Sp(\infty)}{U(\infty)} \ , \quad \mathcal{V}_5 = \frac{Sp(\infty) \times Sp(\infty)}{Sp(\infty)} \ , \\
&\mathcal{V}_6 = \frac{Sp(\infty)}{Sp(\infty) \times Sp(\infty)} \times \mathbb{Z} \ , \quad \mathcal{V}_7 = \frac{U(\infty)}{Sp(\infty)} \ , \quad \mathcal{V}_8 = \frac{O(\infty)}{U(\infty)} \ , \quad \mathcal{V}_9 = \frac{O(\infty) \times O(\infty)}{O(\infty)}
\end{aligned} \tag{4.82}$$

where the subscript is defined modulo 8. One then expects that Dp-branes can be classified by $\pi_{q-p-1}(\mathcal{V}_q)$.

All of this is compatible with the statement that the Dp-branes are classified by $\widetilde{KO}^0(S^{9-p})$ thanks to the mathematical fact [94] that $KO_n := \mathcal{V}_{n+2}$ is the classifying space of KO-theory, in the sense that

$$\widetilde{KO}^n(X) = [X, KO_n]. \tag{4.83}$$

The KO_n form an Ω-spectrum, which entails the relation $KO_n \simeq \Omega KO_{n+1}$. We then have

$$\pi_{q-p-1}(\mathcal{V}_q) = [S^{q-p-1}, KO_{q-2}] = [pt, \Omega^{q-p-1} KO_{q-2}] = [pt, KO_{p-1}] = \widetilde{KO}^0(S^{9-p}). \tag{4.84}$$

4.5 D-brane spectra via boundary states

In the previous section, we were able to verify the K-theory classification of Pin^- Type 0 strings from the open string perspective. In this section, we rederive these results from a closed string perspective. In addition to gaining more intuition about the behavior of invertible phases on worldsheets, we will use the closed string perspective to verify our earlier results on the tensions of stable branes appearing in each theory. These tools will also be used to address the issue of tadpole cancellation in Appendix 4.C.

From the closed string point of view, D-branes correspond to states in the closed string Hilbert space. The basic idea is to define these states by imposing the open string boundary conditions (4.70) as gluing conditions. Upon appropriate rotation of the Euclidean worldsheet, one finds that the correct conditions to impose on boundary states $|\text{B}p,\eta\rangle$ are

$$\begin{aligned} \text{N}: \quad & (\alpha_n^\mu - \tilde{\alpha}_{-n}^\mu)|\text{B}p,\eta\rangle = (\psi_r^\mu - i\eta\tilde{\psi}_{-r}^\mu)|\text{B}p,\eta\rangle = 0 \ , \\ \text{D}: \quad & (\alpha_n^\mu + \tilde{\alpha}_{-n}^\mu)|\text{B}p,\eta\rangle = (\psi_r^\mu + i\eta\tilde{\psi}_{-r}^\mu)|\text{B}p,\eta\rangle = 0 \ , \end{aligned} \tag{4.85}$$

as reviewed in Appendix 4.B. Here r is integer/half-integer for the R/NS sector. The solution to these equations ends up being the coherent state defined in (4.136). Furthermore, in Appendix 4.B it is shown that the physical D-brane states in Type 0 theories are in fact linear combinations of these $|\text{B}p,\eta\rangle$, of the form

$$|\text{D}p,\eta\rangle = \frac{1}{\mathcal{N}_{\text{B}p}}\frac{1}{\sqrt{2}}(\eta|\text{B}p,\eta\rangle_{\text{NSNS}} + |\text{B}p,\eta\rangle_{\text{RR}}) \ , \qquad \eta = \pm 1 \tag{4.86}$$

where $|\text{D}p,+\rangle$ represents a Dp-brane, $|\text{D}p,-\rangle$ represents a Dp'-brane, and $\mathcal{N}_{\text{B}p} = 2^{\frac{5}{2}}(4\pi^2\alpha')^{\frac{p-4}{2}}$ is a normalization factor obtained in Appendix 4.B.3. This result will be the starting point for our analysis in this section.

4.5.1 Matching non-torsion brane spectra

In this subsection we begin by rederiving the stable non-torsion brane spectra of the eight Pin^- Type 0 theories via the boundary state formalism. The analysis of the torsion brane spectra will be carried out in Section 4.5.2.

To understand the spectrum of branes in the theory with n copies of ABK, we need to understand the action of the worldsheet parity operator Ω on D-brane states in the presence of the invertible phase. We begin by understanding the action of Ω on the constituent boundary states $|\mathrm{B}p,\eta\rangle$. In Section 4.3.2, we described the action of Ω on the ground states in the theory with n copies of ABK. From this and (4.141) it easily follows that the action of Ω on the boundary states is given by

$$\Omega|\mathrm{B}p,\eta\rangle_{\mathrm{NSNS}} = |\mathrm{B}p,\eta\rangle_{\mathrm{NSNS}} \ , \qquad \Omega|\mathrm{B}p,\eta\rangle_{\mathrm{RR}} = i^{\eta\nu}|\mathrm{B}p,\eta\rangle_{\mathrm{RR}} \ , \tag{4.87}$$

with the parameter $\nu = \eta n - k$ defined in Section 4.4.

The branes which survive the orientifolding are those which are left invariant by Ω; i.e. those for which ν is zero modulo 4. Therefore, the non-torsion Dp-branes are in one-to-one correspondence with non-torsion elements of $\widetilde{KO}^n(S^k)$, while the non-torsion Dp'-branes are in one-to-one correspondence with non-torsion elements of $\widetilde{KO}^{-n}(S^k)$, as listed in Table 4.3.

Although ν is a mod 8 parameter, the presence of non-torsion branes depends on ν only mod 4. Indeed, this is to be expected since (4.87) was obtained by considering only the values of ABK on the Klein bottle K_2. However, as discussed in Section 4.3.2, K_2 is not the generating manifold for $\mathfrak{O}^2_{\mathrm{Pin}^-}(pt) = \mathbb{Z}_8$. Rather, the generating manifold is $\mathbb{RP}^2$, and since $K_2 \cong \mathbb{RP}^2\#\mathbb{RP}^2$ we currently have access to only a $\mathbb{Z}_4$ of the full $\mathbb{Z}_8$.

In contrast, the open string states *do* depend on ν mod 8. This is because the action of Ω on open string ground states comes from the Möbius strip amplitude. The Möbius strip M_2 contains a single $\mathbb{RP}^2$, whose amplitude is $e^{i\pi\mathrm{ABK}(\mathbb{RP}^2)/4} = e^{\pm i\pi/4}$, as we saw in Section

4.2.2. Then we have the schematic action

$$\Omega|0;ij\rangle \sim e^{\pm in\pi/4}|0;ji\rangle \tag{4.88}$$

where i, j are Chan-Paton indices. Therefore shifting $n \to n+4$ changes the action of Ω on the Chan-Paton factors by a minus sign, between symmetric and anti-symmetric. This is precisely as expected when going between O9$^-$- and O9$^+$-planes, and in agreement with the fact that $\widetilde{KO}^{n+4}(X) \cong \widetilde{KSp}^n(X)$.

4.5.2 Matching torsion brane spectra

We now use the boundary state formalism to check that the torsion brane spectra predicted by $\widetilde{KO}^n(X) \oplus \widetilde{KO}^{-n}(X)$ are reproduced by the theory with n copies of ABK. The study of torsion branes [325, 353, 354] in the boundary state formalism for unoriented theories was first done in [355–357]. Here we will adapt these methods to the Pin$^-$ Type 0 theories.

In contrast to the generic Type 0 non-torsion brane (4.86), the generic torsion branes of Type 0 consists of only the NSNS portion,

$$|\widetilde{\mathrm{D}p},\eta\rangle = \frac{\lambda_\nu}{\mathcal{N}_{Bp}}\frac{\eta}{\sqrt{2}}|\mathrm{B}p,\eta\rangle_{\mathrm{NSNS}}\ , \qquad\qquad \eta = \pm 1 \tag{4.89}$$

where $\lambda_\nu > 0$ is a normalization factor related to the tension of the torsion brane, which will be shown to depend only on ν. This state, though GSO invariant, is not stable in the oriented Type 0 theory since the tachyon is not projected out. This can be detected by computing the overlap of two boundary states in the closed string tree-channel, and then doing a modular transformation to the open string loop-channel, where a tachyon appears. However, in the unoriented theory the gauging of Ω can project out the tachyon. This is seen at the level of the amplitude by cancellation of the tachyon piece of the cylinder amplitude with the analogous piece of the Möbius strip amplitude.

To determine the spectrum of stable torsion branes, we begin by computing the closed string cylinder diagram in tree-channel. Using the results of (4.154), we have

$$\mathcal{A}_{C_2} = \int_0^\infty dl\, \langle \widetilde{\mathrm{D}p}, \eta | e^{-2\pi l H_{\rm cl}} | \widetilde{\mathrm{D}p}, \eta \rangle = \frac{\lambda_\nu^2}{2^6} v_{p+1} \int_0^\infty \frac{d\ell}{\ell^{\frac{9-p}{2}}} \frac{f_3^8(2i\ell)}{f_1^8(2i\ell)} \ . \tag{4.90}$$

The functions $f_i(\tau)$ are defined in (4.143) in terms of Jacobi theta functions and the Dedekind eta function. We can translate the tree-channel amplitude to loop-channel using the transformation $l = 1/2t$ and the modular S transformations in (4.144), which yields

$$\mathcal{A}_{C_2} = \frac{1}{2}\lambda_\nu^2\, v_{p+1} \int_0^\infty \frac{dt}{(2t)^{\frac{p+3}{2}}} \frac{f_3^8(it)}{f_1^8(it)} \ , \tag{4.91}$$

with the answer independent of η and n. Using the q-expansions of the $f_i(\tau)$ given in (4.143), we may isolate the tachyon contribution,

$$\mathcal{A}_{C_2}\big|_{\rm tachyon} = \frac{1}{2}\lambda_\nu^2\, v_{p+1} \int_0^\infty \frac{dt}{(2t)^{\frac{p+3}{2}}}\, e^{\pi t} \ . \tag{4.92}$$

We must now check under which circumstances this can be cancelled by a contribution from the Möbius strip. In order to calculate the Möbius strip amplitude, we use the orientifold state $|\mathrm{O}p\rangle$ introduced in (4.173) and calculate in the loop-channel

$$\begin{aligned}
\mathcal{A}_{M_2} &= \int_0^\infty dl \left(\langle \mathrm{O9} | e^{-2\pi \ell H_{\rm cl}} | \widetilde{\mathrm{D}p}, \eta \rangle + \langle \widetilde{\mathrm{D}p}, \eta | e^{-2\pi \ell H_{\rm cl}} | \mathrm{O9} \rangle \right) \\
&= -\lambda_\nu v_{p+1} \int_0^\infty d\ell \left[e^{i\frac{\pi n \eta}{4}} \left(\frac{f_3^8 f_4^{2(9-p)}}{f_1^{p-1}} \right) \left(2i\ell + \frac{1}{2} \right) \right. \\
&\qquad\qquad \left. - e^{-i\frac{\pi n \eta}{4}} \left(\frac{f_4^8 f_3^{2(9-p)}}{f_1^{p-1}} \right) \left(2i\ell + \frac{1}{2} \right) \right] \\
&= -\frac{\lambda_\nu}{2} v_{p+1} \int_0^\infty \frac{dt}{(2t)^{\frac{p+3}{2}}} \left[e^{i\frac{\pi}{4}(9-p-n\eta)} \left(\frac{f_3^8 f_4^{2(9-p)}}{f_1^{p-1}} \right) \left(it + \frac{1}{2} \right) \right. \\
&\qquad\qquad \left. - e^{-i\frac{\pi}{4}(9-p-n\eta)} \left(\frac{f_4^8 f_3^{2(9-p)}}{f_1^{p-1}} \right) \left(it + \frac{1}{2} \right) \right] \ .
\end{aligned} \tag{4.93}$$

Isolating the tachyon contribution yields

$$\mathcal{A}_{M_2}\big|_{\text{tachyon}} = \lambda_\nu \sin\left[\frac{\pi}{4}\nu\right]\ v_{p+1}\int_0^\infty \frac{dt}{(2t)^{\frac{p+3}{2}}}\, e^{\pi t}\ . \tag{4.94}$$

Combining (4.92) and (4.94), we have

$$(\mathcal{A}_{C_2}+\mathcal{A}_{M_2})\big|_{\text{tachyon}} = \frac{1}{2}\lambda_\nu\left(\lambda_\nu + 2\sin\left[\frac{\pi}{4}\nu\right]\right)\ v_{p+1}\int_0^\infty \frac{dt}{(2t)^{\frac{p+3}{2}}} e^{\pi t}\ . \tag{4.95}$$

Since λ_ν is positive, the values of p for which the tachyon can be cancelled are those such that $\sin\left[\frac{\pi}{4}\nu\right] < 0$. The tension of the corresponding torsion brane is then $\lambda_\nu T_p^0$, where $\lambda_\nu = -2\sin\left[\frac{\pi}{4}\nu\right]$ and T_p^0 is the tension of a stable non-torsion p-brane in Type 0. For example, when $n=0$ we conclude that cancellation is possible if $p\in\{-1,0,7,8\}$, regardless of $\eta=\pm1$. The corresponding branes have tension $2T_p^0$ for $p=-1,7$ and tension $\sqrt{2}T_p^0$ for $p=0,8$. These are in one-to-one correspondence with the torsion classes in $\widetilde{KO}^n(S^k)\oplus\widetilde{KO}^{-n}(S^k)$. The tensions determined here also match exactly with the ones listed in Table 4.5.

Note that in this example, it would naively seem that $p=6$ yields an acceptable torsion brane as well. However, this is not the case. To understand this, recall that before orientifolding these branes are unstable due to a tachyon in the p-p strings — these in particular are in the $(-1)^{\mathsf{f}}$ odd part of the spectrum, and are built out of a certain vacuum $|0\rangle_{pp}^{odd}$. One then notes that, without the presence of Chan-Paton factors [356],

$$\Omega|0\rangle_{pp}^{odd} = e^{-i\frac{\pi}{4}p}|0\rangle_{pp}^{odd}\ . \tag{4.96}$$

Hence for $p=2,6$ we see that $\Omega^2=-1$ on the vacuum. To compensate, we need to introduce at least a two-dimensional Chan-Paton index $i=1,2$, in the doublet representation of $Sp(1)$. Then the Ω projection keeps the antisymmetric combination $[ij]$ of the tachyon, and thus there is no stable torsion D6-brane. Indeed this class is absent from $\widetilde{KO}^n(S^k)\oplus\widetilde{KO}^{-n}(S^k)$.

The generalization of this condition for non-zero n is as follows. The goal is to check that

$\Omega^2 \neq -1$ on the relevant ground state, lest $\frac{1}{2}(1+\Omega)$ not be a valid projector for removing the tachyon. We know that non-zero n modifies the open string ground states such that the action of Ω is modified by (4.88). The cases with n even descend from Type 0B, in which case we have p even, whereas the cases with n odd descend from Type 0A, in which case we have p odd. Thus we conclude that Ω^2 on the $|0;n\rangle_{pp}^{odd}$ ground state is given by $e^{-i\frac{\pi}{2}\eta n}e^{-i\frac{\pi}{2}p}$, and hence we must exclude cases for which $p+\eta\, n = \pm 2, 6, 10, 14, \ldots$.

To summarize, the conditions that must be satisfied by torsion $(9-k)$-branes of type η in the theory with n copies of ABK are the following,

$$\sin\left[\frac{\pi}{4}\nu\right] < 0 \ , \qquad\qquad 9+\nu \neq \pm 2 \mod 8 \ . \tag{4.97}$$

Note that the combination of n, k appearing here, namely $\nu = \eta n - k \mod 8$, is the same one appearing in Section 4.4 and Section 4.5.1. We have already checked above that the analysis via boundary states is in agreement with the previous analysis via boundary fermions when $n = 0$. Since the results (4.97) only depend on ν, this agreement is simply extended to the general case.

4.5.3 Pin^+ Type 0 theories

We may now briefly turn to the analysis of the brane spectra in Pin^+ Type 0 theories. Using the action of Ω given in (4.87) (with $\nu \to -k$) and the action of $(-1)^{\mathsf{f}_L}$ given in (4.140), one finds

$$\Omega_{\mathsf{f}}|\mathrm{B}p,\eta\rangle_{\mathrm{NSNS}} = -|\mathrm{B}p,-\eta\rangle_{\mathrm{NSNS}} \ , \qquad \Omega_{\mathsf{f}}|\mathrm{B}p,\eta\rangle_{\mathrm{RR}} = i^{-\eta k}|\mathrm{B}p,-\eta\rangle_{\mathrm{RR}} \ . \tag{4.98}$$

in the trivial phase. In the non-trivial phase, one gets an extra sign in the action of Ω_{f} on RR ground states, so more generally

$$\Omega_{\mathsf{f}}|\mathrm{B}p,\eta\rangle_{\mathrm{NSNS}} = -|\mathrm{B}p,-\eta\rangle_{\mathrm{NSNS}} \ , \qquad \Omega_{\mathsf{f}}|\mathrm{B}p,\eta\rangle_{\mathrm{RR}} = i^{2n-\eta k}|\mathrm{B}p,-\eta\rangle_{\mathrm{RR}} \ . \tag{4.99}$$

with $n = 0, 1$ labelling the trivial or non-trivial phase. The stable D-brane states which are invariant under Ω_{f} then take the form

$$|\mathrm{D}p\rangle = \frac{1}{\mathcal{N}_{\mathrm{B}p}}\frac{1}{2}(|\mathrm{B}p,+\rangle_{\mathrm{NSNS}} - |\mathrm{B}p,-\rangle_{\mathrm{NSNS}} + |\mathrm{B}p,+\rangle_{\mathrm{RR}} + i^{2n-k}|\mathrm{B}p,-\rangle_{\mathrm{RR}}) \ , \tag{4.100}$$

reminiscent of the Type II states obtained in (4.158). In fact, these states are invariant under Ω_{f} for *any* value of $k = 9 - p$, both odd and even. On the other hand, the fully physical D-brane states must also be invariant under $(-1)^{\mathsf{f}}$. It is easy to see that this requires $2n - k$ to be even. Thus for both $n = 0, 1$, we keep all states with p odd, reproducing the full spectrum of non-torsion branes in Type IIB.

We may now ask about torsion branes. These would take the same form as in Type I, given by

$$|\widetilde{\mathrm{D}p}\rangle = \frac{\lambda}{\mathcal{N}_{\mathrm{B}p}}\frac{1}{2}(|\mathrm{B}p,+\rangle_{\mathrm{NSNS}} - |\mathrm{B}p,-\rangle_{\mathrm{NSNS}}) \tag{4.101}$$

with $\lambda > 0$ a normalization factor. In order for such a brane to be stable, we require the open string tachyon contributions from the cylinder and Möbius strip amplitudes to cancel. In order to calculate the Möbius strip amplitude, one must make use of the appropriate orientifold plane state, which is obtained in Section 4.B.4 and shown in (4.178). Importantly, note that the Pin^+ structure forces this state to be entirely in the RR sector. This means that the Möbius strip amplitude consists only of terms of the form ${}_{\mathrm{NSNS}}\langle \mathrm{B}p|\ldots|\mathrm{B}p\rangle_{\mathrm{RR}}$, which vanish. There is thus no Möbius strip contribution at all, and hence we cannot expect any cancellation of tachyons, and so no stable torsion branes. In conclusion, the spectrum of

stable branes in these theories is precisely the same as for oriented Type IIB, and is classified by the complex K-group $K(X)$.

4.6 No new Type I theories

In this final section we classify unoriented Type II (i.e. Type I) strings. Unlike Type 0 strings for which one may consider $\mathrm{Pin}^{\pm}$ theories separately, the unoriented Type II strings possess a more complicated spin extension of $\mathrm{O}(d)$, which contains both $\mathrm{Pin}^{\pm}(d)$ as subgroups. We refer to this as DPin structure, since it is a "doubled" Pin structure, and we define it precisely in Section 4.6.1. That such a thing is necessary is to be expected: as explained in Section 4.2.2, for Pin^{-} structure the boundary circle of the Möbius strip is automatically in the NS sector, whereas for Pin^{+} structure the boundary circle is automatically in the R sector. In contrast, we know that Type I strings allow both NS and R boundary conditions on the Möbius strip, so it is clear that these worldsheets must incorporate both $\mathrm{Pin}^{\pm}$.

In order to understand possible anomalies and invertible phases on the worlsheet of unoriented Type II theories, it is necessary to calculate the groups $\mathfrak{O}^{d}_{\mathrm{DPin}}(pt)$ for $d = 2, 3$. This may be done using the Atiyah-Hirzebruch spectral sequence for twisted spin bordism, as will be recalled in Section 4.6.2. Details of the calculation are relegated to Appendix 4.E. The final result is that $\mathfrak{O}^{2}_{\mathrm{DPin}}(pt) = (\mathbb{Z}_2)^2$ and $\mathfrak{O}^{3}_{\mathrm{DPin}}(pt) = \mathbb{Z}_8$. The latter implies that the unoriented Type II string is anomaly-free in ten dimensions. The former would naively suggest a quartet of string worldsheet theories, but as we discuss in Section 4.6.3 only two of these theories are physically distinct. The two distinct options are the traditional Type I and $\tilde{\mathrm{I}}$ strings, corresponding to orientifoldings by orientifold $\mathrm{O9}^{\mp}$-planes.

4.6.1 'Spin structure' on the Type I worldsheet

The oriented Type II worldsheet has separate spin structures for left- and right-movers, necessitating a $\mathrm{Spin} \times \mathbb{Z}_2$ structure. We would now like to understand the unoriented lift

of this structure. We note that the $\mathbb{Z}_2$ part of the Spin $\times\, \mathbb{Z}_2$ structure acts on $(\psi, \tilde{\psi})$ by $\mathrm{diag}(+1, -1)$, and should therefore be mapped to $\mathrm{diag}(-1, +1)$ under orientation reversal. To formalize, we then need an extension of $\mathrm{O}(d)$ by $\mathbb{Z}_2 \times \mathbb{Z}_2$,

$$0 \to \mathbb{Z}_2 \times \mathbb{Z}_2 \to G \to \mathrm{O}(d) \to 0 \tag{4.102}$$

such that the orientation reversal part of $\mathrm{O}(d)$ exchanges the two $\mathbb{Z}_2$ factors, and such that when restricted to $\mathrm{SO}(d)$ the extension class is given by (w_2, w_2). Another way of saying this is that we would like a spin structure on the orientation double cover of the worldsheet. Note that for the worldsheet we have $d = 2$, but we will work more generally for the moment.

We now consider the effect of the homomorphism $s : \mathbb{Z}_2 \times \mathbb{Z}_2 \to \mathbb{Z}_2$, $(a, b) \mapsto ab$ in the extension. Over $\mathrm{SO}(d)$, the extension class of the image is $w_2 + w_2 = 0$. The image is also invariant under the orientation reversal part of $\mathrm{O}(d)$. Therefore the extension

$$0 \to s(\mathbb{Z}_2 \times \mathbb{Z}_2) \to s(G) \to \mathrm{O}(d) \to 0 \tag{4.103}$$

is trivial and can be split: $s(G) \simeq \mathrm{O}(d) \times \mathbb{Z}_2$. There are two natural splitting; once there is a splitting, we can compose it with

$$\begin{aligned} \mathrm{O}(d) \times \mathbb{Z}_2 &\to \mathrm{O}(d) \times \mathbb{Z}_2 \\ (g, c) &\mapsto (g, c \det g) \end{aligned} \tag{4.104}$$

to get another. So G can also be put in the following sequence,

$$0 \to \mathbb{Z}_2 \to G \to \mathrm{O}(d) \times \mathbb{Z}_2 \to 0\ . \tag{4.105}$$

Its extension class is a linear combination of w_2, w_1^2, aw_1, and a^2, where a is the generator of $H^1(B\mathbb{Z}_2, \mathbb{Z}_2)$. To determine which linear combination, we may argue as follows. First, since

$\mathbb{Z}_2$ is not extended to $\mathbb{Z}_4$ within G, the term a^2 is not involved. Second, since the entire group is not $\mathrm{Pin}^{\pm} \times \mathbb{Z}_2$, we need the term aw_1. Finally, since the extension is $\mathrm{Spin}(d) \times \mathbb{Z}_2$ over $\mathrm{SO}(d) \times \mathbb{Z}_2$, the class w_2 must be involved. This means that the extension class is either $w_2 + w_1 a$ or $w_2 + w_1^2 + w_1 a$. These two are exchanged by the change of the splitting, since (4.104) sends $a \mapsto a + w_1$. Let us pick $w_2 + w_1^2 + w_1 a$ for definiteness, and write $c : G \to \mathbb{Z}_2$ for the projection to the $\mathbb{Z}_2$ factor. The kernel of c is $\mathrm{Pin}^-(d)$. The kernel of $\det g : G \to \mathrm{O}(d) \to \mathbb{Z}_2$ is $\mathrm{Spin}(d) \times \mathbb{Z}_2$, and the kernel of $c \det g$ is $\mathrm{Pin}^+(d)$. So G is an interesting mixture of all three groups — as mentioned before, we refer to it as $G = \mathrm{DPin}(d)$.

For $d = 2$ we can construct the group $\mathrm{DPin}(2)$ more directly. We first let $\mathrm{Spin}(2)$ act on $(\psi, \tilde{\psi})$ via $\mathrm{diag}(e^{i\theta/2}, e^{-i\theta/2})$. Next we supplement this with a chiral $\mathbb{Z}_2$ acting via

$$Z = \mathrm{diag}(+1, -1) \ , \tag{4.106}$$

and then further include orientation-reversing elements of $\mathrm{Pin}^-(2)$, which can be chosen to be elements of the Clifford algebra $\mathrm{Cl}(-2)$,

$$\gamma_0 = \begin{pmatrix} 0 & i \\ i & 0 \end{pmatrix} \ , \qquad \gamma_1 = \begin{pmatrix} 0 & -1 \\ 1 & 0 \end{pmatrix} \ . \tag{4.107}$$

Note that we have

$$\gamma_0 \gamma_1 = \mathrm{diag}(i, -i) \tag{4.108}$$

which is a lift of a 180° rotation. This means that $\gamma_0 \gamma_1 Z = i\,\mathbb{1}$ is also a lift of a 180° rotation. Then we see that

$$\tilde{\gamma}_0 := i\gamma_1 \ , \qquad \tilde{\gamma}_1 := -i\gamma_0 \tag{4.109}$$

are also in the group $\mathrm{DPin}(2)$. Together with $\mathrm{Spin}(2)$, these elements of $\mathrm{Cl}(+2)$ can be used to form $\mathrm{Pin}^+(2)$. In this way, we see explicitly how $\mathrm{DPin}(2)$ contains all three of $\mathrm{Spin}(2) \times \mathbb{Z}_2$, $\mathrm{Pin}^-(2)$, and $\mathrm{Pin}^+(2)$.

Now consider the Möbius strip M_2. As discussed above, the boundary circle of M_2 is automatically in the NS sector for Pin^- since $\gamma_i^2 = -1$, whereas for Pin^+ structure the boundary circle of M_2 is automatically in the NS sector since $\tilde{\gamma}_i^2 = 1$. We may now contrast this with the case of DPin structure. In that case, we can use either γ_i or $\tilde{\gamma}_i$ to construct M_2, and depending on this choice we can have NS or R on the boundary circle. From the boundary state point of view, this means that the orientifold plane states should have both NS and R sector contributions, which matches the well-known result (4.180).

4.6.2 The group $\mathfrak{O}^d_{\mathrm{DPin}}(pt)$

To understand the anomalies and invertible phases present on unoriented Type II worldsheets, we must calculate $\mathfrak{O}^d_{\mathrm{DPin}}(pt)$ for $d = 2, 3$. These groups may be calculated by using the Atiyah-Hirzebruch spectral sequence (AHSS) for twisted spin bordism groups.

We first recall twisted spin structures. We consider a space X with a real vector bundle V over it. Take a manifold M. A spin structure on M twisted by V is a pair

$$(f : M \to X \,,\, \text{spin structure on } TM \oplus f^*(V)). \tag{4.110}$$

We can then consider the corresponding bordism group $\Omega_d^{\mathrm{Spin}}(X; V)$. Note that we have

$$w_1(TM) = f^*(w_1(V)), \qquad w_2(TM) = f^*(w_1(V)^2 + w_2(V)) \tag{4.111}$$

since we have a spin structure on $TM \oplus f^*(V)$.

For example, when when V is a zero-dimensional trivial bundle this reduces to an ordinary spin bordism of X. As another set of examples, take L to be the real line bundle over $B\mathbb{Z}_2$

such that $w_1(L)$ is the generator of $H^1(B\mathbb{Z}_2, \mathbb{Z}_2) = \mathbb{Z}_2$. Then we have

$$\Omega_d^{\text{Spin}}(B\mathbb{Z}_2; L^{\oplus n}) = \begin{cases} \Omega_d^{\text{Spin}} \quad (B\mathbb{Z}_2) & n = 0, \\ \Omega_d^{\text{Pin}^-} \quad (pt) & n = 1, \\ \Omega_d^{\text{Spin}^{\mathbb{Z}_4}} (pt) & n = 2, \\ \Omega_d^{\text{Pin}^+} \quad (pt) & n = 3 \end{cases} \tag{4.112}$$

where $\text{Spin}^{\mathbb{Z}_4} = (\text{Spin} \times \mathbb{Z}_4)/\mathbb{Z}_2$.

The group DPin described above corresponds to taking $X = B\mathbb{Z}_2 \times B\mathbb{Z}_2$ and using $V = (L_1 \otimes L_2) \oplus L_2^{\oplus 3}$. Here L_1 and L_2 are real line bundles such that $w_1(L_1) = w$ and $w_1(L_2) = a$, where we denote the generators of $H^1(B\mathbb{Z}_2 \times B\mathbb{Z}_2, \mathbb{Z}_2) = \mathbb{Z}_2 \times \mathbb{Z}_2$ by w and a. Then

$$w_1(V) = w, \qquad\qquad w_2(V) = wa. \tag{4.113}$$

Let us now recall the basics of the AHSS. This review will not be comprehensive — for more thorough introductions to the AHSS, the reader can consult e.g. [312, 315, 319, 358]. The basic ingredients in the AHSS are the E_2 page and a set of differentials. For twisted spin bordism, the E_2 page consists of $E_2^{p,q} = H^p(X, \underline{\mathfrak{O}^q_{\text{Spin}}(pt)})$. The underline in the group $\mathfrak{O}^q_{\text{Spin}}(*)$ denotes the fact that the coefficient system is twisted by $w_1(V) \in H^1(X, \mathbb{Z}_2)$. The differentials on the E_2 page are as follows:

- $d_2^2 : E_2^{p,2} = H^p(X, \mathbb{Z}_2) \to E_2^{p+2,1} = H^{p+2}(X, \mathbb{Z}_2)$ is given by

$$d_2^2(x) = \text{Sq}^2 x + w_1(V)\,\text{Sq}^1 x + w_2(V)x \tag{4.114}$$

- $d_2^1 : E_2^{p,1} = H^p(X, \mathbb{Z}_2) \to E_2^{p+2,0} = H^{p+2}(X, \underline{U(1)})$ is given by

$$d_2^1(x) = \iota\left(\text{Sq}^2 x + w_1(V)\,\text{Sq}^1 x + w_2(V)x\right) = \iota\left(\text{Sq}^2 x + w_2(V)x\right) \tag{4.115}$$

where ι is the inclusion $\mathbb{Z}_2 \overset{\iota}{\hookrightarrow} U(1)$.[10]

These differentials, together with d_2^3, were determined in [359]. They were also deduced previously in [360, 361] when $w_1(V)$ is trivial. Alternatively, they can be deduced using the identity

$$\Omega_d^{\mathrm{Spin}}(X;V) = \tilde{\Omega}^{\mathrm{Spin}}_{d+\dim V}(\mathrm{Thom}(V)) \tag{4.116}$$

where $\mathrm{Thom}(V)$ is the Thom space of V. Indeed, denoting the Thom class by U, this equality implies

$$d_2^2(x)U = \mathrm{Sq}^2(xU), \qquad d_2^1(x)U = \iota(\mathrm{Sq}^2(xU)). \tag{4.117}$$

We then simply use the Cartan formula for the action of the Steenrod square, and the definition of the Stiefel-Whitney classes as $\mathrm{Sq}^d U = w_d(V)U$.

Details on our calculation will be given in Appendix 4.E, where we demonstrate how one computes $\mathfrak{O}_X^{2,3}(pt)$ not only for $X = \mathrm{DPin}$ but also for $X = \mathrm{Spin} \times \mathbb{Z}_2$ and $\mathrm{Pin}^{\pm}$ to illustrate the methods involved. The results of the computation are that $\mathfrak{O}^2_{\mathrm{DPin}}(pt) = (\mathbb{Z}_2)^2$ and $\mathfrak{O}^3_{\mathrm{DPin}}(pt) = \mathbb{Z}_8$, precisely as for the oriented Type II strings.

4.6.3 Invertible phases for DPin structure

As in the case of oriented Type II strings, the fact that $\mathfrak{O}^3_{\mathrm{DPin}}(pt) = \mathbb{Z}_8$ means that worldsheet anomalies conveniently cancel in ten dimensions. Also as for oriented Type II strings, the result $\mathfrak{O}^2_{\mathrm{DPin}}(pt) = (\mathbb{Z}_2)^2$ implies four worldsheet theories, though two of these will be physically indistinct from the others. The generators of $\mathfrak{O}^2_{\mathrm{DPin}}(pt)$ can be taken to be $\{(-1)^{\int w_1^2}, (-1)^{\mathrm{Arf}(\hat{\Sigma})}\}$, where $\hat{\Sigma}$ is the orientation double cover of Σ. The generator $(-1)^{\int w_1^2}$ is a bosonic invertible phase, which was discussed in detail in Section 4.2.2. The generator $(-1)^{\mathrm{Arf}(\hat{\Sigma})}$ was discussed in the context of Pin^+ in Section 4.2.2.

[10] The second term in $d_2^1(x)$ can be dropped since the twisted Bockstein associated to $0 \to \mathbb{Z}_2 \to \underline{U(1)} \to \underline{U(1)} \to 0$ is $\mathrm{Sq}^1 + w(V)$, which implies that $\iota \circ (\mathrm{Sq}^1 + w(V)) = 0$. Therefore $\iota(w(V)\,\mathrm{Sq}^1 x) = \iota(\mathrm{Sq}^1\,\mathrm{Sq}^1 \overline{x}) = 0$. The authors thank R. Thorngren for this point.

The effects of these phases on the Type I theory are easy to read off. We know that the presence of the phase $(-1)^{\int w_1^2}$, which has the effect of assigning -1 to Möbius strip amplitudes and $+1$ to cylinder and Klein bottle amplitudes, corresponds to the choice of O9$^{\pm}$-planes, i.e. it distinguishes between Type I and Type $\tilde{\text{I}}$ theories. On the other hand, adding $(-1)^{\text{Arf}(\hat{\Sigma})}$ leads to physically indistinct theories. To see this, note that on an oriented worldsheet Σ, the partition function contribution $(-1)^{\text{Arf}(\hat{\Sigma},\sigma)}$ can be interpreted as

$$(-1)^{\text{Arf}(\Sigma,\sigma_L)} \times (-1)^{\text{Arf}(\Sigma,\sigma_R)} \tag{4.118}$$

and can thus be absorbed for example by flipping ψ^9 and $\tilde{\psi}^9$ at the same time, i.e. by a spacetime parity flip in one direction, as explained in Section 4.3.1. So in fact the theory obtained from the non-trivial invertible phase $\text{Arf}(\hat{\Sigma})$ is not physically distinct from the one with the trivial phase, and the two are instead related in the same way that Type IIA/B and Type IIA/B$'$ were related.

4.A NSR formalism

Throughout this chapter we work in the NSR formalism, where the worldsheet fields for the closed string consist of scalars X^μ and left- and right-moving Majorana-Weyl fermions $\psi^\mu, \tilde{\psi}^\mu$, all of which are vectors in the ten-dimensional target space [73, 362].

Closed strings:

We choose our conventions such that the worldsheet spatial coordinate $\sigma \in [0, 2\pi)$. For simplicity we work in light-cone gauge, with $\mu = 0, 1$ being the light-cone coordinates. In this gauge the worldsheet action is

$$\frac{1}{4\pi}\int dt\, d\sigma \left(\frac{1}{\alpha'}\left(\partial_t X^\mu \partial_t X_\mu - \partial_\sigma X^\mu \partial_\sigma X_\mu\right) + i\psi^\mu(\partial_t + \partial_\sigma)\psi_\mu + i\tilde{\psi}^\mu(\partial_t - \partial_\sigma)\tilde{\psi}_\mu\right) \tag{4.119}$$

with $\mu = 2, \cdots, 9$. The oscillator expansions for these fields are

$$X^\mu(t,\sigma) = x^\mu + \alpha' t\, p^\mu + i\sqrt{\frac{\alpha'}{2}} \sum_n \frac{1}{n} \left(\alpha_n^\mu e^{-in(t-\sigma)} + \tilde{\alpha}_n^\mu e^{-in(t+\sigma)}\right) , \tag{4.120}$$

$$\psi^\mu(t,\sigma) = \sum_r \psi_r^\mu e^{-ir(t-\sigma)} , \qquad \tilde{\psi}^\mu(t,\sigma) = \sum_r \tilde{\psi}_r^\mu e^{-ir(t+\sigma)} , \tag{4.121}$$

where $r \in \mathbb{Z}$ or $\mathbb{Z} + \frac{1}{2}$ for R or NS boundary conditions, respectively.

We are mainly interested in the fermionic sector, and in particular in its zero-modes. There are no zero-modes for NS boundary conditions, and hence the left- and right-moving ground states, $|0\rangle_{\rm NS}$ and $|\tilde{0}\rangle_{\rm NS}$, are unique in this sector. It is easy to write fermion number operators in terms of the operators that count the number of modes, $\mathsf{N} = \sum_{r,\mu} r\, \psi_{-r}^\mu \psi_r^\mu$ and $\tilde{\mathsf{N}} = \sum_{r,\mu} r\, \tilde{\psi}_{-r}^\mu \tilde{\psi}_r^\mu$, as $(-1)^{\mathsf{f_L}} = (-1)^{\mathsf{N}-1}$ and $(-1)^{\mathsf{f_R}} = (-1)^{\tilde{\mathsf{N}}-1}$. The ground states are odd, i.e.

$$(-1)^{\mathsf{f_L}} |0\rangle_{\rm NS} = -|0\rangle_{\rm NS} , \qquad (-1)^{\mathsf{f_R}} |\tilde{0}\rangle_{\rm NS} = -|\tilde{0}\rangle_{\rm NS} . \tag{4.122}$$

On the other hand, fermions with R boundary conditions do allow zero-modes, which satisfy the anticommutation relations

$$\{\psi_0^\mu, \psi_0^\nu\} = \delta^{\mu\nu} , \qquad \{\tilde{\psi}_0^\mu, \tilde{\psi}_0^\nu\} = \delta^{\mu\nu} , \qquad \{\psi_0^\mu, \tilde{\psi}_0^\nu\} = 0 . \tag{4.123}$$

Left- and right-moving zero-modes then separately furnish representations of the Clifford algebra Cl(8). These representations act on the degenerate ground states, which can be spinors $|0\rangle_{\rm R}^a, |\tilde{0}\rangle_{\rm R}^a \in \mathbf{8}_s$ or conjugate spinors $|0\rangle_{\rm R}^{\dot{a}}, |\tilde{0}\rangle_{\rm R}^{\dot{a}} \in \mathbf{8}_c$ of the little group $SO(8)$. The two irreducible representations are distinguished by the eigenvalue of the left- and right-moving fermion numbers

$$(-1)_0^{\mathsf{f_L}} = \prod_\mu \sqrt{2}\, \psi_0^\mu , \qquad (-1)_0^{\mathsf{f_R}} = \prod_\mu \sqrt{2}\, \tilde{\psi}_0^\mu . \tag{4.124}$$

The full fermion number operators are obtained by combining these with the operators

counting the number of massive modes,

$$(-1)^{\mathsf{f}_{\mathsf{L}}} = (-1)^{\mathsf{f}_{\mathsf{L}}}_0 (-1)^{\mathsf{N}}\,, \qquad (-1)^{\mathsf{f}_{\mathsf{R}}} = (-1)^{\mathsf{f}_{\mathsf{R}}}_0 (-1)^{\tilde{\mathsf{N}}}\,. \tag{4.125}$$

Worldsheet parity Ω acts on the worldsheet fields as in (4.42), from which it follows that the action on the oscillator modes in (4.120) and (4.121) is

$$\Omega\alpha_n\Omega = \tilde{\alpha}_n\,, \qquad \Omega\psi_r\Omega = e^{2\pi r}\tilde{\psi}_r\,, \qquad \Omega\tilde{\psi}_r\Omega = -e^{2\pi r}\psi_r\,. \tag{4.126}$$

Next we review the low-lying spectra of the closed superstring. We will use the usual notation [73] and denote each of the low-lying states by $(A\pm, B\pm)$, where A, B can be R or NS and denote respectively the left- and right-moving sectors, while the signs indicate the fermion parity. The NSNS sector ground state is

$$(\mathrm{NS}-,\mathrm{NS}-): \quad |0\rangle_{\mathrm{NSNS}} = |0\rangle_{\mathrm{NS}} \otimes |\tilde{0}\rangle_{\mathrm{NS}}\,, \tag{4.127}$$

and is a scalar tachyon. The massless NSNS spectrum is given by the level one states,

$$(\mathrm{NS}+,\mathrm{NS}+): \quad \tilde{\psi}^{\mu}_{-1/2}\tilde{\psi}^{\nu}_{-1/2}|0\rangle_{\mathrm{NSNS}} \in \mathbf{8}_v \otimes \mathbf{8}_v = \mathbf{1} \oplus \mathbf{28} \oplus \mathbf{35}_v \tag{4.128}$$

and consist of a dilaton, $\mathbf{1}$, 2-form, $\mathbf{28}$, and graviton, $\mathbf{35}_v$. The RR sector ground states transform in the product of spinor representations of the little group $SO(8)$,

$$\begin{aligned}
&(\mathrm{R}+,\mathrm{R}+): \quad |0\rangle^{ab}_{\mathrm{RR}} = |0\rangle^{a}_{\mathrm{R}} \otimes |\tilde{0}\rangle^{b}_{\mathrm{R}} \in \mathbf{8}_s \otimes \mathbf{8}_s = \mathbf{1} \oplus \mathbf{28} \oplus \mathbf{35}_-,\\
&(\mathrm{R}-,\mathrm{R}-): \quad |0\rangle^{\dot{a}\dot{b}}_{\mathrm{RR}} = |0\rangle^{\dot{a}}_{\mathrm{R}} \otimes |\tilde{0}\rangle^{\dot{b}}_{\mathrm{R}} \in \mathbf{8}_c \otimes \mathbf{8}_c = \mathbf{1} \oplus \mathbf{28} \oplus \mathbf{35}_+,\\
&(\mathrm{R}+,\mathrm{R}-): \quad |0\rangle^{a\dot{b}}_{\mathrm{RR}} = |0\rangle^{a}_{\mathrm{R}} \otimes |\tilde{0}\rangle^{\dot{b}}_{\mathrm{R}} \in \mathbf{8}_s \otimes \mathbf{8}_c = \mathbf{8}_v \oplus \mathbf{56},\\
&(\mathrm{R}-,\mathrm{R}+): \quad |0\rangle^{\dot{a}b}_{\mathrm{RR}} = |0\rangle^{\dot{a}}_{\mathrm{R}} \otimes |\tilde{0}\rangle^{b}_{\mathrm{R}} \in \mathbf{8}_c \otimes \mathbf{8}_s = \mathbf{8}_v \oplus \mathbf{56}\,.
\end{aligned} \tag{4.129}$$

All of these states are massless and can be identified as the RR scalar $\mathbf{1}$, vector $\mathbf{8}_v$, two-form $\mathbf{28}$, three-form $\mathbf{56}$, and (anti)self-dual four-form $\mathbf{35}_{(-)+}$. Finally, the NSR states are

$$\begin{aligned} (\mathrm{NS}+,\mathrm{R}+): &\quad \psi^\mu_{-1/2}|0\rangle_{\mathrm{NS}} \otimes |\tilde{0}\rangle^a_{\mathrm{R}} \in \mathbf{8}_v \otimes \mathbf{8}_s = \mathbf{8}_c \oplus \mathbf{56}_s \,, \\ (\mathrm{NS}+,\mathrm{R}-): &\quad \psi^\mu_{-1/2}|0\rangle_{\mathrm{NS}} \otimes |\tilde{0}\rangle^{\dot{a}}_{\mathrm{R}} \in \mathbf{8}_v \otimes \mathbf{8}_c = \mathbf{8}_s \oplus \mathbf{56}_c \,, \end{aligned} \tag{4.130}$$

which include the dilatinos, $\mathbf{8}_s$ and $\mathbf{8}_c$, and gravitinos, $\mathbf{56}_s$ and $\mathbf{56}_c$. The RNS states are conjugate to these.

Open strings:

When considering open strings, one can have Dirichlet (D) or Neumann (N) boundary conditions on each end, which relate the left- and right-moving oscillators. We define the NN, DD, and ND directions of the open string as in (4.70). Though only the relative sign in those conditions is important, the conventions shown there are such that $\eta_{1,2} = +1$ represents a Dp-brane at $\sigma = 0, \pi$, while $\eta_{1,2} = -1$ represents a Dp'-brane at $\sigma = 0, \pi$.[11] That this is so will be discussed in the beginning of Appendix 4.B.

Note that the relative choice of $\eta_{1,2}$ is related to the choice of NS or R sectors on the open string. In particular, the string is in the NS sector for $\eta_1 = \eta_2$ and in the R sector for $\eta_1 = -\eta_2$. This may be seen as follows. First, we may replace the left- and right-moving fermions on $\sigma \in [0, \pi]$ with a single chiral fermion on $\sigma \in [0, 2\pi]$ by defining

$$\psi(t, \sigma) = \eta_2 \, \tilde{\psi}(t, 2\pi - \sigma) \,, \qquad \pi \leq \sigma \leq 2\pi \,. \tag{4.131}$$

The question of NS vs. R is then a question about the (anti-)periodicity of this extended fermion. In particular, say that $\tilde{\psi}(t, 2\pi) = \eta_3 \, \tilde{\psi}(t, 0)$ where $\eta_3 = +1$ for R and -1 for NS.

[11] Note that the extra sign in (4.70) is needed to encode the *same* physical boundary condition at $\sigma = \pi$ as at $\sigma = 0$, as explained e.g. in footnote 69 of [340]. To summarize, because the boundaries at $\sigma = 0, \pi$ have opposite orientation, imposing the same boundary condition on the two boundaries involves a reflection of one of them $t \to -t$, under which $\psi^\mu \to e^{i\pi/2}\psi^\mu$ and $\tilde{\psi}^\mu \to e^{-i\pi/2}\tilde{\psi}^\mu$.

Then we have

$$\psi(t,0) = \eta_2\, \tilde{\psi}(t,2\pi) = \eta_2\eta_3\, \tilde{\psi}(t,0)\ . \tag{4.132}$$

But from (4.70), we also have $\psi(t,0) = -\eta_1\, \tilde{\psi}(t,0)$ and hence we conclude that $\eta_1\eta_2 = -\eta_3$. The anti-periodic NS case then corresponds to $\eta_1 = \eta_2$, while the periodic R case corresponds to $\eta_1 = -\eta_2$. From (4.70) we then conclude that NS sector fermions can have zero modes along ND and DN directions, whereas R sector fermions can have zero modes along NN and DD directions. In constructing the open string fermion number operator $(-1)^{\mathsf{f}}$ one must take these zero modes into account, as was done above for the RR sector of the closed string.

As for the open string spectrum, let us just mention that the ground state in the NS sector, $|0\rangle_{\rm NS}$, is an open string tachyon with $(-1)^{\mathsf{f}}\,|0\rangle_{\rm NS} = -|0\rangle_{\rm NS}$. We will not review the massless spectrum here.

4.B Boundary state formalism

Here we review the boundary state formalism — for more details, the reader may consult [340, 362, 363].

4.B.1 Basics

From the closed string point of view, D-branes correspond to states in the closed string Hilbert space. Beginning with the boundary conditions (4.70), one can transition to Euclidean signature $t \to -it_E$, and then do a rotation of the worldsheet to interchange the t_E and σ directions, thereby going from the open string to the closed string picture. In particular, rotation by $\frac{\pi}{2}$ takes $(t_E, \sigma) \to (\sigma, -t_E)$. Under this transformation, the fermions

transform as

$$\psi^\mu(t_E + i\sigma) \to e^{i\pi/4}\,\psi^\mu(t_E + i\sigma)\ , \qquad \tilde{\psi}^\mu(t_E - i\sigma) \to e^{-i\pi/4}\,\tilde{\psi}^\mu(t_E - i\sigma)\ . \tag{4.133}$$

The boundary conditions at fixed σ then become conditions at fixed time — for example, on the slice $t_E = 0$ the initial conditions are

$$\begin{aligned} \mathrm{N}: \quad \psi^\mu(0,\sigma) &= +i\eta_1\,\tilde{\psi}^\mu(0,\sigma)\ , \\ \mathrm{D}: \quad \psi^\mu(0,\sigma) &= -i\eta_1\,\tilde{\psi}^\mu(0,\sigma)\ , \qquad \sigma \in [0, 2\pi)\ . \end{aligned} \tag{4.134}$$

The conditions at $t_E = \pi$ look the same, but with η_1 replaced by η_2 — note that we no longer have the relative minus sign for the same condition on the two boundaries, c.f. footnote 11. Let us now focus on the slice at $t_E = 0$. We will denote $\eta_1 = \eta$ for simplicity. We define the boundary states $|\mathrm{B}p,\eta\rangle$ to be the operator statement of the boundary conditions (4.134) on the closed string Hilbert space. Writing things in terms of Fourier modes and including bosonic constraints as well, these boundary states are then defined by

$$\begin{aligned} \mathrm{N}: \quad & (\alpha^\mu_n - \tilde{\alpha}^\mu_{-n})|\mathrm{B}p,\eta\rangle = (\psi^\mu_r - i\eta\tilde{\psi}^\mu_{-r})|\mathrm{B}p,\eta\rangle = 0\ , \\ \mathrm{D}: \quad & (\alpha^\mu_n + \tilde{\alpha}^\mu_{-n})|\mathrm{B}p,\eta\rangle = (\psi^\mu_r + i\eta\tilde{\psi}^\mu_{-r})|\mathrm{B}p,\eta\rangle = 0\ , \end{aligned} \tag{4.135}$$

where r is integer/half-integer for the R/NS sector. The general solution to these conditions can be written as a coherent state,

$$\begin{aligned} |\mathrm{B}p,\eta\rangle \propto \exp\Bigg\{ & \sum_{n=1}^{\infty}\left[-\frac{1}{n}\sum_{\mu=2}^{p+2}\alpha^\mu_{-n}\tilde{\alpha}^\mu_{-n} + \frac{1}{n}\sum_{\mu=p+3}^{9}\alpha^\mu_{-n}\tilde{\alpha}^\mu_{-n}\right] \\ & + i\eta\sum_{r>0}^{\infty}\left[-\sum_{\mu=2}^{p+2}\psi^\mu_{-r}\tilde{\psi}^\mu_{-r} + \sum_{\mu=p+3}^{9}\psi^\mu_{-r}\tilde{\psi}^\mu_{-r}\right]\Bigg\}\,|\mathrm{B}p,\eta\rangle^{(0)} \end{aligned} \tag{4.136}$$

up to a normalization factor which we discuss in Appendix 4.B.3. Here $|\mathrm{B}p,\eta\rangle^{(0)}$ is the ground state, which depends on the sector. In the NSNS sector the ground state is just the usual one

$$|\mathrm{B}p,\eta\rangle^{(0)}_{\mathrm{NSNS}} = |0\rangle_{\mathrm{NSNS}} \ . \tag{4.137}$$

In the RR sector there is an extra subtlety because we need to solve the gluing conditions for the zero-modes. This is easily done by noticing that $|\mathrm{B}7,\eta\rangle^{(0)}_{\mathrm{RR}}$ need only satisfy conditions of the kind

$$(\psi_0^\mu - i\eta\tilde{\psi}_0^\mu)|\mathrm{B}7,\eta\rangle^{(0)}_{\mathrm{RR}} = 0\,. \tag{4.138}$$

We can then build the rest of the boundary ground states as

$$|\mathrm{B}p,\eta\rangle^{(0)}_{\mathrm{RR}} = \prod_{\mu=p+3}^{9}(\psi_0^\mu + i\eta\tilde{\psi}_0^\mu)|\mathrm{B}7,\eta\rangle^{(0)}_{\mathrm{RR}}\,. \tag{4.139}$$

It is not entirely trivial to see the relation between $|\mathrm{B}7,\eta\rangle^{(0)}_{\mathrm{RR}}$ and the usual RR vacuum. This is explained, for instance, in Appendix B of [363]. The key feature is that the relation involves an even number of RR zero-mode operators. With this in mind it follows that

$$\begin{aligned}
(-1)^{\mathsf{f}_\mathsf{L}}|\mathrm{B}p,\eta\rangle_{\mathrm{NSNS}} &= -|\mathrm{B}p,-\eta\rangle_{\mathrm{NSNS}}\ , & (-1)^{\mathsf{f}_\mathsf{L}}|\mathrm{B}p,\eta\rangle_{\mathrm{RR}} &= (-1)^{7-p}|\mathrm{B}p,-\eta\rangle_{\mathrm{RR}}\ ,\\
(-1)^{\mathsf{f}_\mathsf{R}}|\mathrm{B}p,\eta\rangle_{\mathrm{NSNS}} &= -|\mathrm{B}p,-\eta\rangle_{\mathrm{NSNS}}\ , & (-1)^{\mathsf{f}_\mathsf{R}}|\mathrm{B}p,\eta\rangle_{\mathrm{RR}} &= |\mathrm{B}p,-\eta\rangle_{\mathrm{RR}}\ ,
\end{aligned} \tag{4.140}$$

where $(-1)^{\mathsf{f}_\mathsf{L}}$ and $(-1)^{\mathsf{f}_\mathsf{R}}$ are the left- and right-moving worldsheet fermion numbers. Similarly using (4.126) and (4.139) one can check that

$$\Omega|\mathrm{B}p,\eta\rangle_{\mathrm{NSNS}} = |\mathrm{B}p,\eta\rangle_{\mathrm{NSNS}}\ , \quad \Omega|\mathrm{B}p,\eta\rangle_{\mathrm{RR}} = -(-i\eta)^{7-p}|\mathrm{B}p,\eta\rangle_{\mathrm{RR}} = i^{-\eta k}|\mathrm{B}p,\eta\rangle_{\mathrm{RR}}. \tag{4.141}$$

where $k = 9-p$.

4.B.2 Theta functions, partition functions and boundary state amplitudes

In the remainder of this appendix, we will be calculating amplitudes for closed strings propagating between boundary states. In order to do so, some preliminary data will be needed. We now review our conventions for the different theta functions that appear in one-loop string partition functions, and give a few useful formulas for partition functions and boundary state amplitudes.

First, note that we will use the usual shorthand for theta functions with characteristic,

$$\begin{aligned}
\vartheta_1(z|\tau) &= \vartheta \begin{bmatrix} \frac{1}{2} \\ \frac{1}{2} \end{bmatrix} (z|\tau)\,, & \vartheta_2(z|\tau) &= \vartheta \begin{bmatrix} \frac{1}{2} \\ 0 \end{bmatrix} (z|\tau)\,, \\
\vartheta_3(z|\tau) &= \vartheta \begin{bmatrix} 0 \\ 0 \end{bmatrix} (z|\tau)\,, & \vartheta_4(z|\tau) &= \vartheta \begin{bmatrix} 0 \\ \frac{1}{2} \end{bmatrix} (z|\tau)\,,
\end{aligned} \tag{4.142}$$

and the notation $\vartheta_i(\tau) = \vartheta_i(0|\tau)$, where τ is the modular parameter of a torus. Recall that ϑ_1 is odd and vanishes at the origin, i.e. $\vartheta_1(\tau) = 0$. For convenience we define the following combinations,

$$\begin{aligned}
f_1(\tau) &= \eta(\tau) = q^{1/12} \prod_{n=1}^{\infty} (1 - q^{2n})\,, & f_2(\tau) &= \sqrt{\frac{\vartheta_2(\tau)}{\eta(\tau)}} = \sqrt{2} q^{1/12} \prod_{n=1}^{\infty} (1 + q^{2n})\,, \\
f_3(\tau) &= \sqrt{\frac{\vartheta_3(\tau)}{\eta(\tau)}} = q^{-1/24} \prod_{n=1}^{\infty} (1 + q^{2n-1})\,, & f_4(\tau) &= \sqrt{\frac{\vartheta_4(\tau)}{\eta(\tau)}} = q^{-1/24} \prod_{n=1}^{\infty} (1 - q^{2n-1})\,,
\end{aligned} \tag{4.143}$$

where $q = e^{i\pi\tau}$ and $\eta(\tau) = (\vartheta_1'(0|\tau)/2\pi)^{1/3}$ is the Dedekind eta function. It will be useful to

know the modular S transformations,

$$\begin{aligned} f_1\left(i/t\right) &= \sqrt{t} f_1(it)\,, \quad & f_2\left(i/t\right) &= f_4(it)\,, \\ f_3\left(i/t\right) &= f_3(it)\,, & f_4\left(i/t\right) &= f_2(it)\,, \end{aligned} \tag{4.144}$$

and the T transformations,

$$\begin{aligned} f_1\left(it+1\right) &= e^{i\frac{\pi}{12}} f_1(it)\,, & f_2\left(it+1\right) &= e^{i\frac{\pi}{12}} f_2(it)\,, \\ f_3\left(it+1\right) &= e^{-i\frac{\pi}{24}} f_4(it)\,, & f_4\left(it+1\right) &= e^{-i\frac{\pi}{24}} f_3(it)\,, \end{aligned} \tag{4.145}$$

as well as the more unfamiliar $P = T^{\frac{1}{2}} S T^2 S T^{\frac{1}{2}}$ transformation,

$$\begin{aligned} f_1\left(\frac{i}{4t}+\frac{1}{2}\right) &= \sqrt{2t} f_1\left(it+\frac{1}{2}\right)\,, \quad & f_2\left(\frac{i}{4t}+\frac{1}{2}\right) &= f_2\left(it+\frac{1}{2}\right)\,, \\ f_3\left(\frac{i}{4t}+\frac{1}{2}\right) &= e^{i\frac{\pi}{8}} f_4\left(it+\frac{1}{2}\right)\,, & f_4\left(\frac{i}{4t}+\frac{1}{2}\right) &= e^{-i\frac{\pi}{8}} f_3\left(it+\frac{1}{2}\right)\,, \end{aligned} \tag{4.146}$$

where $t \in \mathbb{R}$. The Jacobi "abstruse" and "triple product" identities

$$f_2(\tau)^8 - f_3(\tau)^8 + f_4(\tau)^8 = 0\,, \qquad\qquad f_2(\tau) f_3(\tau) f_4(\tau) = \sqrt{2} \tag{4.147}$$

will be used to simplify results.

The functions $f_i(\tau)$ introduced above are useful since the open and closed string sector traces are written naturally in terms of them. Denote the boundary state amplitudes in the tree-channel in sector S as follows

$$\tilde{Z}_{\mathrm{S}}^{\mathrm{LR}} = {}_{\mathrm{S,L}}\langle \mathrm{B}| e^{-2\pi l H_{\mathrm{cl}}} |\mathrm{B}\rangle_{\mathrm{S,R}} \tag{4.148}$$

where for fermionic sectors $|\mathrm{B}\rangle = |\mathrm{B}, \eta\rangle$ and L, R denote the boundary conditions — either Neumann (N) or Dirichlet (D) — on each boundary. The amplitudes with opposite η on either side are given by exchanging $\mathrm{N} \leftrightarrow \mathrm{D}$ on one boundary state, as can be seen in (4.135).

In terms of the $f_i(\tau)$, the bosonic contributions are found to be [362]

$$\tilde{Z}_{\rm B}^{\rm NN} = \frac{1}{f_1(2il)}\,, \qquad \tilde{Z}_{\rm B}^{\rm ND} = \frac{\sqrt{2}}{f_2(2il)}\,, \qquad \tilde{Z}_{\rm B}^{\rm DD} = \frac{1}{\sqrt{4\pi^2\alpha' l}}\frac{1}{f_1(2il)}\,, \tag{4.149}$$

the fermionic contributions in the NSNS sector are

$$\tilde{Z}_{\rm NSNS}^{\rm NN} = f_3(2il)\,, \qquad \tilde{Z}_{\rm NSNS}^{\rm ND} = f_4(2il)\,, \qquad \tilde{Z}_{\rm NSNS}^{\rm DD} = f_3(2il)\,, \tag{4.150}$$

and in the RR sector

$$\tilde{Z}_{\rm RR}^{\rm NN} = -f_2(2il)\,, \qquad \tilde{Z}_{\rm RR}^{\rm ND} = 0\,, \qquad \tilde{Z}_{\rm RR}^{\rm DD} = -f_2(2il)\,. \tag{4.151}$$

Consider parallel Bp and Bq boundary states with $q > p$. Note that there are $p-1$ NN, $9-q$ DD, and $q-p$ ND directions. Also recall that changing $\eta \to -\eta$ is equivalent to exchanging the boundary conditions N $\leftrightarrow$ D. The amplitudes for exchanging closed strings between these states then take the simple form

$$\begin{aligned}
{}_{\rm NSNS}\langle {\rm B}p,\eta|e^{-2\pi l H_{\rm cl}}|{\rm B}q,\eta\rangle_{\rm NSNS} &= \frac{V_{p+1}}{(4\pi^2\alpha' l)^{\frac{9-q}{2}}}\frac{f_3(2il)^8 f_4(2il)^{2(q-p)}}{f_1(2il)^{8-q+p}}\,, \\
{}_{\rm NSNS}\langle {\rm B}p,\eta|e^{-2\pi l H_{\rm cl}}|{\rm B}q,-\eta\rangle_{\rm NSNS} &= \frac{V_{p+1}}{(4\pi^2\alpha' l)^{\frac{9-q}{2}}}\frac{f_4(2il)^8 f_3(2i\ell)^{2(q-p)}}{f_1(2il)^{8-q+p}}\,, \\
{}_{\rm RR}\langle {\rm B}p,\eta|e^{-2\pi l H_{\rm cl}}|{\rm B}q,\eta\rangle_{\rm RR} &= -\frac{V_{p+1}}{(4\pi^2\alpha' l)^{\frac{9-q}{2}}}\frac{f_2(2il)^8}{f_1(2il)^8}\,, \\
{}_{\rm RR}\langle {\rm B}p,\eta|e^{-2\pi l H_{\rm cl}}|{\rm B}q,-\eta\rangle_{\rm RR} &= 0\,,
\end{aligned} \tag{4.152}$$

where V_{p+1} is the regularized volume of the p-brane, which comes from the zero-modes of the scalars parallel to its worldvolume. Note that we have used the Jacobi triple product identity (4.147) to remove some factors of $\sqrt{2}/f_2(2il)$ from these results. The last amplitude vanishes because $\eta_L = -\eta_R$ corresponds to Ramond boundary conditions in the direction orthogonal to the boundary, for which there is a fermion zero-mode.

4.B.3 D-brane boundary states

Boundary state normalization

In order to calculate tensions or tadpole contributions, we will want to find the proper normalization for the boundary states. The way to do this is to impose matching of the tree- and loop-channel cylinder amplitudes. That is, we want to impose the following identities

$$\begin{aligned}
\frac{1}{\mathcal{N}_{\mathrm{B}p}^2}\int_0^\infty dl\ {}_{\mathrm{NSNS}}\langle \mathrm{B}p,\eta|e^{-2\pi l H_{\mathrm{cl}}}|\mathrm{B}p,\eta\rangle_{\mathrm{NSNS}} &= \int_0^\infty \frac{dt}{2t}\,\mathrm{Tr}_{\mathrm{NS}}\left[e^{-2\pi t H_{\mathrm{op}}}\right]\,,\\
\frac{1}{\mathcal{N}_{\mathrm{B}p}^2}\int_0^\infty dl\ {}_{\mathrm{NSNS}}\langle \mathrm{B}p,\eta|e^{-2\pi l H_{\mathrm{cl}}}|\mathrm{B}p,-\eta\rangle_{\mathrm{NSNS}} &= \int_0^\infty \frac{dt}{2t}\,\mathrm{Tr}_{\mathrm{R}}\left[e^{-2\pi t H_{\mathrm{op}}}\right]\,,\\
\frac{1}{\mathcal{N}_{\mathrm{B}p}^2}\int_0^\infty dl\ {}_{\mathrm{RR}}\langle \mathrm{B}p,\eta|e^{-2\pi l H_{\mathrm{cl}}}|\mathrm{B}p,\eta\rangle_{\mathrm{RR}} &= \int_0^\infty \frac{dt}{2t}\,\mathrm{Tr}_{\mathrm{NS}}\left[e^{-2\pi t H_{\mathrm{op}}}(-1)^{\mathsf{f}}\right]\,,\\
\frac{1}{\mathcal{N}_{\mathrm{B}p}^2}\int_0^\infty dl\ {}_{\mathrm{RR}}\langle \mathrm{B}p,\eta|e^{-2\pi l H_{\mathrm{cl}}}|\mathrm{B}p,-\eta\rangle_{\mathrm{RR}} &= \int_0^\infty \frac{dt}{2t}\,\mathrm{Tr}_{\mathrm{R}}\left[e^{-2\pi t H_{\mathrm{op}}}(-1)^{\mathsf{f}}\right]=0\,.
\end{aligned}$$

We may for instance focus on the first one, which in loop-channel gives the result

$$\int_0^\infty \frac{dt}{2t}\,\mathrm{Tr}_{\mathrm{NS}}\left[e^{-2\pi t H_{\mathrm{op}}}\right] = v_{p+1}\int_0^\infty \frac{dt}{(2t)^{\frac{p+3}{2}}}\,\frac{f_3(it)^8}{f_1(it)^8} \tag{4.153}$$

where $v_{p+1}=V_{p+1}/(4\pi^2\alpha')^{\frac{p+1}{2}}$ is the regularized volume of the brane, in units of the string length. On the other hand, in tree-channel we have

$$\frac{1}{\mathcal{N}_{\mathrm{B}p}^2}\int_0^\infty dl\ {}_{\mathrm{NSNS}}\langle \mathrm{B}p,\eta|e^{-2\pi l H_{\mathrm{cl}}}|\mathrm{B}p,\eta\rangle_{\mathrm{NSNS}} = \frac{(4\pi^2\alpha')^{p-4}}{\mathcal{N}_{\mathrm{B}p}^2}\,v_{p+1}\int_0^\infty \frac{dl}{l^{\frac{9-p}{2}}}\,\frac{f_3(2il)^8}{f_1(2il)^8}\,. \tag{4.154}$$

We can translate the tree-channel amplitude to loop-channel using the transformation $l=\frac{1}{2t}$ and the modular S transformations in (4.144), which yields

$$\frac{(4\pi^2\alpha')^{p-4}}{\mathcal{N}_{\mathrm{B}p}^2}\,v_{p+1}\int_0^\infty \frac{dt}{2t^2}\,\frac{1}{(2t)^{\frac{p-9}{2}}}\,\frac{f_3(it)^8}{(t)^{\frac{8}{2}}f_1(it)^8} = \frac{2^5(4\pi^2\alpha')^{p-4}}{\mathcal{N}_{\mathrm{B}p}^2}\,v_{p+1}\int_0^\infty \frac{dt}{(2t)^{\frac{p+3}{2}}}\,\frac{f_3(it)^8}{f_1(it)^8} \tag{4.155}$$

Comparing (4.153) and (4.155), we find that the proper normalization for the boundary state is

$$\mathcal{N}_{\mathrm{B}p} = 2^{\frac{5}{2}}(4\pi^2\alpha')^{\frac{p-4}{2}} \ . \tag{4.156}$$

One can check that imposing the other identities gives the same result.

Type II and I

The states $|\mathrm{B}p,\eta\rangle$ must be assembled into a D-brane state such that they give the right open string amplitudes. Let us begin by finding the D-brane state in Type II. Since the open string sector includes both NS and R strings we must have

$$\begin{aligned}\int_0^\infty dl\, \langle \mathrm{D}p|e^{-2\pi l H_{\mathrm{cl}}}|\mathrm{D}p\rangle \\ = \int_0^\infty \frac{dt}{2t}\left(\mathrm{Tr}_{\mathrm{NS}}\left[e^{-2\pi t H_{\mathrm{op}}}\frac{1}{2}(1+(-1)^{\mathsf{f}})\right] - \mathrm{Tr}_{\mathrm{R}}\left[e^{-2\pi t H_{\mathrm{op}}}\frac{1}{2}(1+(-1)^{\mathsf{f}})\right]\right) .\end{aligned} \tag{4.157}$$

A brief calculation then shows that the proper normalization for the D-brane state is

$$|\mathrm{D}p\rangle = \frac{1}{\mathcal{N}_{\mathrm{B}p}}\frac{1}{2}\left(|\mathrm{B}p,+\rangle_{\mathrm{NSNS}} - |\mathrm{B}p,-\rangle_{\mathrm{NSNS}} + |\mathrm{B}p,+\rangle_{\mathrm{RR}} + |\mathrm{B}p,-\rangle_{\mathrm{RR}}\right) \tag{4.158}$$

with $\mathcal{N}_{\mathrm{B}p}$ as defined in (4.156). The choice of relative sign of the NSNS and RR contributions differentiates branes and anti-branes.

Recall that for Type II theories we wish to gauge both $(-1)^{\mathsf{f}_{\mathsf{L},\mathsf{R}}}$, so we should keep only states invariant under projection by

$$P^{\mathrm{II}}_{\mathrm{NSNS}} = \frac{1}{4}\left(1+(-1)^{\mathsf{f}_{\mathsf{L}}}\right)\left(1+(-1)^{\mathsf{f}_{\mathsf{R}}}\right) \ , \qquad P^{\mathrm{II}}_{\mathrm{RR}} = \frac{1}{4}\left(1+(-1)^{\mathsf{f}_{\mathsf{L}}}\right)\left(1\pm(-1)^{\mathsf{f}_{\mathsf{R}}}\right) \ , \tag{4.159}$$

with the two choices of sign corresponding to Type IIB $(+)$ and Type IIA $(-)$. Using (4.140) it is easy to see that the boundary states in Eq. (4.158) are invariant when p is odd for Type

IIB and when p is even for Type IIA.

In the presence of multiple branes the boundary state acquires an extra overall group theory factor G that accounts for the trace over the Chan-Paton space,

$$|\mathrm{D}p\rangle \to G|\mathrm{D}p\rangle \quad \text{where} \quad G = \begin{cases} N & \text{for } U(N)\,, \\ 2N & \text{for } Sp(N),\ SO(2N) \end{cases} \tag{4.160}$$

The latter implies that in Type I the D-brane states for even a single brane are normalized with an extra factor of 2.

Type 0

We now do the same analysis for D-branes in Type 0. In Type 0 the open strings stretching between two branes of the same (different) type are in the NS (R) sector, so we must have

$$\int_0^\infty dl\, \langle \mathrm{D}p, \eta | e^{-2\pi l H_{\mathrm{cl}}} | \mathrm{D}p, \eta \rangle = \int_0^\infty \frac{dt}{2t}\, \mathrm{Tr}_{\mathrm{NS}} \left[e^{-2\pi t H_{\mathrm{op}}} \frac{1}{2}(1 + (-1)^{\mathsf{f}}) \right] , \tag{4.161}$$

$$\int_0^\infty dl\, \langle \mathrm{D}p, \eta | e^{-2\pi l H_{\mathrm{cl}}} | \mathrm{D}p, -\eta \rangle = -\int_0^\infty \frac{dt}{2t}\, \mathrm{Tr}_{\mathrm{R}} \left[e^{-2\pi t H_{\mathrm{op}}} \frac{1}{2}(1 + (-1)^{\mathsf{f}}) \right] . \tag{4.162}$$

From this and the relations above it follows that the properly normalized Type 0 D-brane state is

$$|\mathrm{D}p, \eta\rangle = \frac{1}{\mathcal{N}_{\mathrm{B}p}} \frac{1}{\sqrt{2}} (\eta |\mathrm{B}p, \eta\rangle_{\mathrm{NSNS}} + |\mathrm{B}p, \eta\rangle_{\mathrm{RR}}) \ , \qquad \eta = \pm 1 \ . \tag{4.163}$$

The factor of η in front of $|\mathrm{B}p, \eta\rangle_{\mathrm{NSNS}}$ is needed so that the force between the branes is attractive. To see this, consider the NSNS contribution to the amplitude,

$$\int_0^\infty dl\, {}_{NSNS}\langle \mathrm{D}p, \eta | e^{-2\pi l H_{\mathrm{cl}}} | \mathrm{D}p, -\eta \rangle_{\mathrm{NSNS}} = -\frac{v_{p+1}}{2^6} \int_0^\infty dl \frac{dl}{l^{\frac{9-p}{2}}} \frac{f_4(2il)^8}{f_1(2il)^8} \,. \tag{4.164}$$

The contribution from the massless states can be extracted from the constant term in the expansion

$$\frac{f_4(2il)^8}{f_1(2il)^8} = \frac{1}{q} - 8 + \mathcal{O}(q^1) \tag{4.165}$$

where now $q = e^{-2\pi l}$. The minus sign cancels with the overall sign in (4.164), yielding a positive contribution and hence an attractive force.

Recall that for Type 0 strings we gauge only a diagonal spin structure $(-1)^{\mathsf{f_L}+\mathsf{f_R}}$, and hence we keep only states invariant under projection by

$$P^0_{\rm NSNS} = \frac{1}{2}\left(1 + (-1)^{\mathsf{f_L}+\mathsf{f_R}}\right) \ , \qquad P^0_{\rm RR} = \frac{1}{2}\left(1 \pm (-1)^{\mathsf{f_L}+\mathsf{f_R}}\right) \ , \tag{4.166}$$

with the two choices of sign corresponding to Type 0B (+) and Type 0A (−). Using (4.140), we see that (4.163) are invariant for p odd in Type 0B and p even in Type 0A.

In contrast to (4.158) then, for each such p there are now two boundary states for the Type 0 strings [363], which we will call Dp and Dp' for $|{\rm D}p,+\rangle$ and $|{\rm D}p,-\rangle$ respectively. Note that Dp'-branes are *not* anti Dp-branes.

Finally, note that the normalizations of Type 0 and Type II branes differ by a factor of $\sqrt{2}$. On the other hand, the amplitude for exchanging closed strings in Type II receives an extra contribution corresponding to R strings in the loop channel. This implies that the tensions of the Type 0 branes are smaller than those of Type II, in particular $T^0_p = T^{\rm II}_p/\sqrt{2}$ [364, 365]. Finally, as stated before, when there are multiple branes the boundary state acquires an extra group theory factor (4.160).

4.B.4 O-plane boundary states

Crosscap state normalization

In analogy to the discussion above, we can find the correct normalization of the crosscap states that correspond to O-planes by requiring that the tree-channel amplitude for exchanging a closed string between a D-brane and a crosscap state matches the loop-channel Möbius strip amplitude. We know that the crosscap states are related to the usual boundary state by a $\pi/2$ translation in imaginary time, so we normalize them as

$$|\mathrm{C}q,\eta\rangle = -\frac{n_{\mathrm{C}q}}{\mathcal{N}_{\mathrm{B}q}}\, i^{H_{\mathrm{cl}}}|\mathrm{B}q,\eta\rangle \tag{4.167}$$

where $n_{\mathrm{C}q}$ is the normalization relative to the usual boundary state, and the minus sign is required to get negative tension. Then, the relations we must impose are

$$\begin{aligned}
\frac{1}{\mathcal{N}_{\mathrm{B}p}}\int_0^\infty dl\ \left({}_{\mathrm{NSNS}}\langle \mathrm{C}q,\eta|e^{-2\pi l H_{\mathrm{cl}}}|\mathrm{B}p,\eta\rangle_{\mathrm{NSNS}} - {}_{\mathrm{NSNS}}\langle \mathrm{B}p,\eta|e^{-2\pi l H_{\mathrm{cl}}}|\mathrm{C}q,-\eta\rangle_{\mathrm{NSNS}}\right) \\
= \int_0^\infty \frac{dt}{2t}\,\mathrm{Tr}_{\mathrm{NS}}\left[e^{-2\pi t H_{\mathrm{op}}}\Omega\right]\ , \\
\frac{1}{\mathcal{N}_{\mathrm{B}p}}\int_0^\infty dl\ \left({}_{\mathrm{NSNS}}\langle \mathrm{B}p,\eta|e^{-2\pi l H_{\mathrm{cl}}}|\mathrm{C}q,\eta\rangle_{\mathrm{NSNS}} - {}_{\mathrm{NSNS}}\langle \mathrm{C}q,-\eta|e^{-2\pi l H_{\mathrm{cl}}}|\mathrm{B}p,\eta\rangle_{\mathrm{NSNS}}\right) \\
= \int_0^\infty \frac{dt}{2t}\,\mathrm{Tr}_{\mathrm{NS}}\left[e^{-2\pi t H_{\mathrm{op}}}(-1)^{\mathrm{f}}\Omega\right]\ , \\
\frac{1}{\mathcal{N}_{\mathrm{B}p}}\int_0^\infty dl\ \left({}_{\mathrm{RR}}\langle \mathrm{B}p,\eta|e^{-2\pi l H_{\mathrm{cl}}}|\mathrm{C}q,\eta\rangle_{\mathrm{RR}} - {}_{\mathrm{RR}}\langle \mathrm{C}q,-\eta|e^{-2\pi l H_{\mathrm{cl}}}|\mathrm{B}p,\eta\rangle_{\mathrm{RR}}\right) \\
= \int_0^\infty \frac{dt}{2t}\,\mathrm{Tr}_{\mathrm{R}}\left[e^{-2\pi t H_{\mathrm{op}}}\Omega\right]\ , \\
\frac{1}{\mathcal{N}_{\mathrm{B}p}}\int_0^\infty dl\ \left({}_{\mathrm{RR}}\langle \mathrm{C}q,\eta|e^{-2\pi l H_{\mathrm{cl}}}|\mathrm{B}p,\eta\rangle_{\mathrm{RR}} - {}_{\mathrm{RR}}\langle \mathrm{B}p,\eta|e^{-2\pi l H_{\mathrm{cl}}}|\mathrm{C}q,-\eta\rangle_{\mathrm{RR}}\right) \\
= \int_0^\infty \frac{dt}{2t}\,\mathrm{Tr}_{\mathrm{R}}\left[e^{-2\pi t H_{\mathrm{op}}}(-1)^{\mathrm{f}}\Omega\right]\ .
\end{aligned}$$

As before, we can fix the normalization using any of these relations by first writing the

loop-channel Möbius strip amplitude

$$\int_0^\infty \frac{dt}{2t}\,\mathrm{Tr}_{\mathrm{NS}}\left[e^{-2\pi t H_{\mathrm{op}}}\Omega\right] = -v_{p+1}\int_0^\infty \frac{dt}{(2t)^{\frac{p+3}{2}}}\,e^{i\frac{\pi}{4}(q-p)}\left[\frac{f_3^8 f_4^{2(q-p)}}{f_1^{8-q+p}}\right]\left(it+\frac{1}{2}\right), \tag{4.168}$$

and then calculating the corresponding tree-channel amplitude using the boundary states

$$\begin{aligned}
&\frac{1}{\mathcal{N}_{\mathrm{B}p}}\int_0^\infty dl\ \left({}_{\mathrm{NSNS}}\langle \mathrm{C}q,\eta|e^{-2\pi l H_{\mathrm{cl}}}|\mathrm{B}p,\eta\rangle_{\mathrm{NSNS}} - {}_{\mathrm{NSNS}}\langle \mathrm{B}p,\eta|e^{-2\pi l H_{\mathrm{cl}}}|\mathrm{C}q,-\eta\rangle_{\mathrm{NSNS}}\right)\\
&\quad = -\frac{n_{\mathrm{C}q}}{2^5}v_{p+1}\int_0^\infty \frac{dl}{l^{\frac{9-q}{2}}}\left[\left(\frac{f_3^8 f_4^{2(q-p)}}{f_1^{8-q+p}}\right)\left(2il-\frac{1}{2}\right)-\left(\frac{f_4^8 f_3^{2(q-p)}}{f_1^{8-q+p}}\right)\left(2il+\frac{1}{2}\right)\right]\\
&\quad = \frac{n_{\mathrm{C}q}}{2^4}v_{p+1}\int_0^\infty \frac{dl}{l^{\frac{9-q}{2}}}\left[\frac{f_4^8 f_3^{2(q-p)}}{f_1^{8-q+p}}\right]\left(2il+\frac{1}{2}\right)
\end{aligned} \tag{4.169}$$

where in the second equality we used the modular T transformations in (4.145). Next, we translate the tree-channel amplitude to the loop channel using the transformation $l = 1/8t$ and the modular P transformations in (4.146) to get

$$\begin{aligned}
&\frac{n_{\mathrm{O}q}}{2^4}v_{p+1}\int_0^\infty \frac{dt}{8t^2}\frac{1}{(8t)^{\frac{q-9}{2}}}\left[\frac{-f_3^8 e^{i\frac{\pi}{4}(q-p)}f_4^{2(q-p)}}{(2t)^{\frac{8-q+p}{2}}f_1^{8-q+p}}\right]\left(it+\frac{1}{2}\right)\\
&\quad = -\frac{n_{\mathrm{O}q}}{2^{q-4}}v_{p+1}\int_0^\infty \frac{dt}{(2t)^{\frac{p+3}{2}}}e^{i\frac{\pi}{4}(q-p)}\left[\frac{f_3^8 f_4^{2(q-p)}}{f_1^{8-q+p}}\right]\left(it+\frac{1}{2}\right).
\end{aligned} \tag{4.170}$$

Comparing with the previous result, we find that the normalization of the $|\mathrm{C}q,\eta\rangle$ crosscap state relative to the boundary state is

$$n_{\mathrm{C}q} = 2^{q-4}\ . \tag{4.171}$$

Pin$^-$ Type 0

Finally, we must assemble the crosscap states into physical orientifold plane states. For the Pin$^-$ theories, the Pin$^-$ structure on the worldsheet requires the boundary of the Möbius strip to have NS boundary conditions. Thus we expect the Oq-plane state to be purely in

the NSNS sector. In addition, we know that the open strings on the orientifold are in the NS sector, so the O-plane state must give the following loop channel result

$$\int_0^\infty dl\,(\langle \mathrm{D}p,\eta|e^{-2\pi l H_{\mathrm{cl}}}|\mathrm{O}q\rangle + \langle \mathrm{O}q|e^{-2\pi l H_{\mathrm{cl}}}|\mathrm{D}p,\eta\rangle) \\ = \int_0^\infty \frac{dt}{2t}\,\mathrm{Tr}_{\mathrm{NS}}\left[e^{-2\pi t H_{\mathrm{op}}}\frac{1}{2}(1+(-1)^{\mathsf{f}})\Omega\right]\,. \tag{4.172}$$

Thus the physical orientifold boundary state is

$$|\mathrm{O}q\rangle = \frac{1}{\sqrt{2}}\left(|\mathrm{C}q,+\rangle_{\mathrm{NSNS}} - |\mathrm{C}q,-\rangle_{\mathrm{NSNS}}\right)\,. \tag{4.173}$$

Importantly, the crosscap state carries crucial information about the presence of n copies of ABK. To see this, it is easiest to consider the Klein bottle amplitude. Requiring that the tree-channel amplitudes for exchanging closed strings between two crosscaps match the loop-channel Klein bottle amplitudes gives for example

$$\int_0^\infty dl\ {}_{\mathrm{NSNS}}\langle \mathrm{C}p,-\eta|e^{-2\pi l H_{\mathrm{cl}}}|\mathrm{C}p,\eta\rangle_{\mathrm{NSNS}} = \int_0^\infty \frac{dt}{2t}\,\mathrm{Tr}_{\mathrm{RR}}\left[e^{-2\pi t H_{\mathrm{cl}}}\Omega\right]\,, \tag{4.174}$$

$$\int_0^\infty dl\ {}_{\mathrm{NSNS}}\langle \mathrm{C}p,\eta|e^{-2\pi l H_{\mathrm{cl}}}|\mathrm{C}p,-\eta\rangle_{\mathrm{NSNS}} = \int_0^\infty \frac{dt}{2t}\,\mathrm{Tr}_{\mathrm{RR}}\left[e^{-2\pi t H_{\mathrm{cl}}}(-1)^{\mathsf{f}}\Omega\right]\,. \tag{4.175}$$

If we use these to calculate the normalization of the crosscap state as was done for the Möbius strip, then for $n = 0 \mod 8$ both (4.174) and (4.175) yield the same result (4.171).

For generic n, however, (4.174) and (4.175) are unequal complex conjugates and the result in (4.171) needs to be modified. This may be seen seen as follows. In the presence of n copies of ABK, we know that the action of Ω on the closed string RR Hilbert space is modified by a factor of i^n when the Pin^- structure is $q(a,b) = (2,1)$ or $(2,3)$, see (4.47). These Pin^- structures are exactly the ones captured by the right-hand sides of (4.174) and (4.175), and hence for non-zero n the left-hand side must change by i^n. In other words, we should redefine $|\mathrm{C}p,\eta\rangle$ by a phase $e^{i\theta(n,\eta)}$ such that $e^{-i\theta(n,-\eta)}e^{i\theta(n,\eta)} = i^n$, a solution of which

is $\theta(n,\eta) = \frac{\pi}{4}\eta n \mod 2\pi$. The correct crosscap states for the theory with $n \neq 0 \mod 8$ can then be taken to be

$$|\mathrm{C}q,\eta\rangle = -\frac{2^{q-4}}{\mathcal{N}_{\mathrm{B}q}} e^{\frac{i\pi n\eta}{4}}\, i^{H_{\mathrm{cl}}} |\mathrm{B}q,\eta\rangle\,. \tag{4.176}$$

This is what we must insert into (4.173) to obtain the physical orientifold plane state.

Pin^+ Type 0

Similarly, for unoriented Pin^+ Type 0 we know that the Oq-plane state must give the following loop channel results

$$\begin{aligned}\int_0^\infty dl\, (\langle \mathrm{D}p,\eta|e^{-2\pi l H_{\mathrm{cl}}}|\mathrm{O}q\rangle + \langle \mathrm{Oq}|e^{-2\pi l H_{\mathrm{cl}}}|\mathrm{D}p,\eta\rangle) \\ = \int_0^\infty \frac{dt}{2t}\,\mathrm{Tr}_{\mathrm{R}}\left[e^{-2\pi t H_{\mathrm{op}}}\frac{1}{2}(1+(-1)^{\mathsf{f}})\Omega\right]\,.\end{aligned} \tag{4.177}$$

The physical orientifold state is then found to be

$$|\mathrm{O}q\rangle = -\frac{1}{\sqrt{2}}\left(|\mathrm{C}q,+\rangle_{\mathrm{RR}} + |\mathrm{C}q,-\rangle_{\mathrm{RR}}\right)\,. \tag{4.178}$$

The fact that this contains only RR sector contributions is the boundary state formulation of the fact that fermions on the boundary of the Pin^+ Möbius strip are automatically in the R sector.

Type I

For completeness, we finally describe the physical orientifold plane states for Type I. These are obtained by requiring

$$\int_0^\infty dl\ \left(\langle \mathrm{D}p|e^{-2\pi l H_{\mathrm{cl}}}|\mathrm{O}q\rangle + \langle \mathrm{O}q|e^{-2\pi l H_{\mathrm{cl}}}|\mathrm{D}p\rangle\right) \tag{4.179}$$
$$= \int_0^\infty \frac{dt}{2t}\left(\mathrm{Tr}_{\mathrm{NS}}\left[e^{-2\pi t H_{\mathrm{op}}}\frac{1}{2}(1+(-1)^{\mathsf{f}})\Omega\right] - \mathrm{Tr}_{\mathrm{R}}\left[e^{-2\pi t H_{\mathrm{op}}}\frac{1}{2}(1+(-1)^{\mathsf{f}})\Omega\right]\right) .$$

The correct combination is found to be

$$|\mathrm{O}q\rangle = \frac{1}{2}\left(|\mathrm{C}q,+1\rangle_{\mathrm{NSNS}} - |\mathrm{C}q,-1\rangle_{\mathrm{NSNS}} + |\mathrm{C}q,+1\rangle_{\mathrm{RR}} + |\mathrm{C}q,-1\rangle_{\mathrm{RR}}\right) .$$

The fact that this contains both NSNS and RR contributions means that DPin structure on the worldsheet must allow the boundary of the Möbius strip to be in the NS or R sectors, and thus must contain both $\mathrm{Pin}^{\pm}$ as subgroups.

As an aside, let us note that the normalization of the O9 state relative to a Type I D9 state has an extra factor of 32, as expected by the usual Type I tadpole cancellation.

4.C Tadpole Cancellation

In this appendix we discuss the issue of tadpole cancellation in the unoriented Type 0 theories.

We begin by considering the Pin^- Type 0 theory with n copies of ABK. Before beginning any calculations it is important to recall that in this case the orientifold state corresponding to the O9-plane does not have an RR contribution; see (4.173). This means that the orientifold does not carry RR charge, and hence we will only be encountering NSNS tadpoles. Such tadpoles are not fatal since they can be cancelled by the Fischler-Susskind mechanism [366, 367], but this introduces a spacetime dependent coupling. We thus ask in which cases these NSNS tadpoles can be cancelled without resorting to this mechanism.

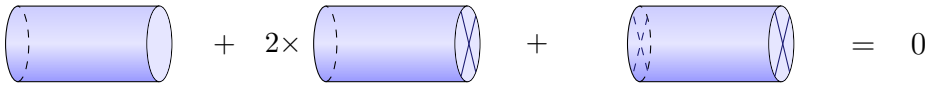

Figure 4.4: The tadpole cancellation condition. The Möbius strip is represented by a cylinder with one crosscap (the "X" at the end) and we must include separate contributions from crosscaps on the left and right ends. The Klein bottle is represented by a cylinder with two crosscaps.

The goal is to calculate the cylinder, Möbius strip, and Klein bottle amplitudes and check that the tadpole contributions cancel amongst them (Fig. 4.4). Furthermore, since the putative tadpoles are in the closed string sector we must focus on the amplitudes in the tree-channel. For the moment we will focus on the cases with n even, which are orientifolds of Type 0B.

First we will consider the cylinder amplitude. We recall that in Type 0B we have two different kinds of nine-branes, with corresponding boundary states

$$|\mathrm{D9},\eta\rangle = \frac{G}{\mathcal{N}_{\mathrm{B9}}}\frac{1}{\sqrt{2}}(\eta\,|\mathrm{B9},\eta\rangle_{\mathrm{NSNS}} + |\mathrm{B9},\eta\rangle_{\mathrm{RR}})\ , \tag{4.180}$$

where G is a group theory factor which equals $G = N$ for unitary gauge group and $G = 2N$ for orthogonal or symplectic gauge group; see (4.160). The corresponding antibranes are

$$|\overline{\mathrm{D9}},\eta\rangle = \frac{G}{\mathcal{N}_{\mathrm{B9}}}\frac{1}{\sqrt{2}}(\eta\,|\mathrm{B9},\eta\rangle_{\mathrm{NSNS}} - |\mathrm{B9},\eta\rangle_{\mathrm{RR}})\ . \tag{4.181}$$

In order to avoid introducing RR tadpoles, we must only introduce brane-antibrane pairs, with boundary state

$$|\mathrm{D}\overline{\mathrm{D}}9,\eta\rangle = |\mathrm{D9},\eta\rangle + |\overline{\mathrm{D9}},\eta\rangle = \frac{G}{\mathcal{N}_{\mathrm{B9}}}\sqrt{2}\,\eta\,|\mathrm{B9},\eta\rangle_{\mathrm{NSNS}}\ . \tag{4.182}$$

In terms of such boundary states the cylinder amplitude is given by

$$\mathcal{A}_{C_2} = \int_0^\infty dl\, \langle \mathrm{D}\overline{\mathrm{D}}9, \eta | e^{-2\pi l H_{\mathrm{cl}}} | \mathrm{D}\overline{\mathrm{D}}9, \eta \rangle \ , \tag{4.183}$$

which can be evaluated using the results collected in Appendix 4.B to give

$$\mathcal{A}_{C_2} = \frac{G^2}{16}\, v_{10} \int_0^\infty dl\, \frac{f_3^8(2il)}{f_1^8(2il)} \ . \tag{4.184}$$

Worldsheet parity does not affect this amplitude so the result does not depend on n. We can easily extract the massless NSNS tadpole contribution using the q-expansions in (4.143), giving

$$\mathcal{A}_{C_2}\big|_{\mathrm{tadpole}} = \frac{G^2}{2}\, v_{10} \int_0^\infty dl\,. \tag{4.185}$$

Next we calculate the Möbius strip amplitude. The O9-plane state was given in (4.173); crucially, it was argued to be n-dependent. Using the result obtained there, the Möbius strip amplitude can be evaluated to give

$$\begin{aligned} \mathcal{A}_{M_2} &= \int_0^\infty dl\, \left(\langle \mathrm{D}\overline{\mathrm{D}}9, \eta | e^{-2\pi l H_{\mathrm{cl}}} | \mathrm{O}9 \rangle + \langle \mathrm{O}9 | e^{-2\pi l H_{\mathrm{cl}}} | \mathrm{D}\overline{\mathrm{D}}9, \eta \rangle \right) \\ &= -2\, G\, v_{10} \int_0^\infty dl \left[\frac{e^{i\eta\frac{\pi}{4}n} f_3^8 - e^{-i\eta\frac{\pi}{4}n} f_4^8}{f_1^8} \right] \left(2il + \frac{1}{2} \right) \ , \end{aligned} \tag{4.186}$$

with the tadpole being

$$\mathcal{A}_{M_2}\big|_{\mathrm{tadpole}} = -2^5\, G\, \cos\left[\frac{\pi\eta n}{4}\right]\, v_{10} \int_0^\infty dl\,. \tag{4.187}$$

Finally, the Klein bottle amplitude amplitude is

$$\begin{aligned}\mathcal{A}_{K_2} &= \int_0^\infty dl\, \langle \mathrm{O9}|e^{-2\pi l H_{\mathrm{cl}}}|\mathrm{O9}\rangle \\ &= 16\, v_{10} \int_0^\infty dl \left[\frac{2f_3^8 - \left(e^{-i\eta\frac{\pi}{2}n} + e^{i\eta\frac{\pi}{2}n}\right) f_4^8}{f_1^8}\right](2il)\,, \end{aligned} \tag{4.188}$$

with tadpole

$$\begin{aligned}\mathcal{A}_{K_2}\big|_{\mathrm{tadpole}} &= 16^2 \left(1 + \cos\left[\frac{\pi\eta n}{2}\right]\right) v_{10} \int_0^\infty dl \\ &= 2^9 \cos\left[\frac{\pi\eta n}{4}\right]^2 v_{10} \int_0^\infty dl \end{aligned} \tag{4.189}$$

Putting all the contributions together we find that the total tadpole is

$$(\mathcal{A}_{C_2} + \mathcal{A}_{M_2} + \mathcal{A}_{K_2})\big|_{\mathrm{tadpole}} = \frac{1}{2}\left(G - 32\cos\left[\frac{\pi\eta n}{4}\right]\right)^2 v_{10} \int_0^\infty dl\ . \tag{4.190}$$

We may now read off the tadpole cancellation conditions. For $n = 0$ one can cancel the NSNS tadpole by adding sixteen 9-$\overline{9}$ pairs. If we choose these to consist of m D9-$\overline{\mathrm{D9}}$ pairs and $16-m$ D9′-$\overline{\mathrm{D9}}'$ pairs, the resulting gauge group is $[SO(2m)\times SO(32-2m)]^2$. The cases with $m = 0, 16$ are purely bosonic and have gauge group $SO(32)\times SO(32)$. For $n = 4$, we have the symplectic version of $n = 0$ and the tadpole cannot be cancelled. For $n = 2, 6$ we have zero tadpole contribution, and would seemingly not require addition of any nine-branes.

Next we discuss cases with n odd, which are orientifolds of Type 0A. In Type 0A there do not exist any stable 9-branes, but there are unstable ones. These unstable branes do not couple to RR fields, and are purely in the NSNS sector. Hence the corresponding states may be written as

$$|\widetilde{\mathrm{D9}}, \eta\rangle = \frac{G}{\mathcal{N}_{\mathrm{B9}}}\eta|\mathrm{B9}, \eta\rangle_{\mathrm{NSNS}} \tag{4.191}$$

with $\mathcal{N}_{\mathrm{B9}}$ the usual normalization factor accompanying $|\mathrm{B9}, \eta\rangle$ and G the corresponding group theory factor. This result differs from (4.182) only by a factor of $\sqrt{2}$. Then by a similar calculation as above we conclude that tadpole cancellation requires $G = 32\sqrt{2}\cos\left[\frac{\pi\eta n}{4}\right]$. The case of $n = 1$ allows the tadpole to be cancelled by the addition of sixteen 9-branes. If we choose these to consist of m D9-branes and $16 - m$ D9′-branes, the resulting gauge group is $SO(2m) \times SO(32 - 2m)$. Similar statements hold for $n = 7$. The $n = 5, 3$ cases are the corresponding symplectic cases, for which the NSNS tadpole cannot be cancelled by the addition of branes.

Finally, we discuss the issue of tadpole cancellation for Pin^+ strings. In contrast to the Pin^- theories studied above, for these theories the orientifold only has contributions from the RR sector; see (4.178). Hence one has an RR tadpole which must be cancelled. A calculation analogous to the one above shows that the tadpole can be cancelled by adding 32 D9 and 32 D9′-branes, giving total gauge group $U(32)$. Though this introduces NSNS tadpoles [85, 89], these do not render the theory inconsistent and can be removed via the Fischler-Susskind mechanism [366, 367].

Note that it makes sense to talk about tadpoles in the Pin^+ theories despite $\mathbb{RP}^2$ not admitting a Pin^+ structure. The reason for this is that the tadpole is given by a one-point function on $\mathbb{RP}^2$, which corresponds to a punctured $\mathbb{RP}^2$. The latter manifold is conformally equivalent to the Möbius strip, which does in fact admit a Pin^+ structure.

As a final note, whenever tadpole cancellation requires the addition of D9-branes, the question of stability of Dp-branes must be revisited to account for the possibility of tachyonic modes of the strings stretched between the Dp- and D9-branes. In this case, the K-theory classification outlined in Sections 4.4 and 4.5 will be modified, and branes which were previously stable may become unstable.

4.D Arf and ABK from index theory

In this appendix we rephrase many of the results on the Arf and ABK invariants given in Section 4.2 in terms of index theory. The majority of this appendix is due to E. Witten [332]. The authors thank him for very kindly allowing them to reproduce the content here. Four-dimensional analogs of many of these results can be found in Appendix C of [81].

4.D.1 η-invariants: generalities

Our normalization of the eta invariant is

$$\eta(\Sigma, \sigma) = \sum_E \mathrm{sgn}(E) \tag{4.192}$$

where E are the eigenvalues of the Dirac operator on Σ with spin structure σ, and the sum is to be appropriately regularized. We work in the convention that $\mathrm{sgn}(0) = 1$, so that $\eta(\Sigma, \sigma)$ also counts zero-modes. Often we will omit Σ from the argument of $\eta(\Sigma, \sigma)$.

Because the Arf and ABK invariants can be expressed as ratios of massive fermion path integrals as in (4.6) and (4.23), they are examples of η-invariants. For example, for the Arf invariant we have

$$(-1)^{\mathrm{Arf}(\Sigma,\sigma)} = \frac{Z_{\mathrm{ferm}}(m \gg 0)}{Z_{\mathrm{ferm}}(m \ll 0)} = \prod_E \frac{iE + m}{iE - m} = e^{i\frac{\pi}{2}\eta(\sigma)}. \tag{4.193}$$

An analogous result holds for the ABK invariant.

The η-invariant is not necessarily a bordism invariant, but in the case of two-dimensional theories the η-invariant modulo some integer is. This can be seen by appealing to the APS index theorem, which states that the index of the Dirac operator on a manifold Y_{d+1} with

boundary $\partial Y_{d+1} = X_d$ is given in terms of the η-invariant as[12]

$$\operatorname{ind} iD_{Y_{d+1}} = -\frac{1}{2}\eta(X_d, \sigma) + \int_{Y_{d+1}} \hat{A}(R)\operatorname{ch}(F) \ . \tag{4.194}$$

Note that when d is even, the local term on the right-hand side vanishes, and as a result the η-invariant can be a bordism invariant. Combined with the fact that the left-hand side is an integer, we see that the η-invariant modulo 2 is a bordism invariant. This can be refined further.

Assume that the fermion system whose Dirac operator is used in the definition of the η-invariant admits a mass term. This provides an invariant anti-symmetric bilinear form on the eigenfunctions, and therefore introduce a quaternionic structure. Therefore the index is in fact an even number, and η modulo 4 is a bordism invariant.

Let us now consider a spin 2-manifold. Then there exists a globally well-defined chirality matrix Γ satisfying $\Gamma^2 = 1$ and $\{iD, \Gamma\} = 0$, and hence for any state of non-zero eigenvalue E there is also a state with eigenvalue $-E$. Then the contributions to the η-invariant from nonzero eigenvalues simply cancel out. Denoting the number of positive chirality zero-modes with spin structure σ by $\zeta(\sigma)$, we have

$$\eta(\sigma) = 2\zeta(\sigma) \mod 4 \tag{4.195}$$

where the factor of 2 arises because $\eta(\sigma)$ counts both chiralities. This means that

$$(-1)^{\mathrm{Arf}(\Sigma,\sigma)} = e^{i\frac{\pi}{2}\eta(\sigma)} = (-1)^{\zeta(\sigma)} \tag{4.196}$$

generates at most a $\mathbb{Z}_2$, as expected by our previous definitions of the Arf invariant.

We next consider the Pin^- case. As argued above, the η-invariant is a mod 4 bordism invariant. Let us now show that η takes half-integer values, and thus provides us with a mod

[12] In the original notation of APS [368], what we are calling η is instead called 2ξ.

8 invariant. The half-integrality is proven as follows. Given a Pin^- structure $\sigma \in H^2(\Sigma, \mathbb{Z}_2)$, there exists a "complementary" Pin^- structure $\sigma' := \sigma + w_1$ which is obtained by twisting by the orientation bundle. Then note that[13]

$$\eta(\sigma) + \eta(\sigma') = 0 \mod 4 \ . \tag{4.197}$$

We also have generally that

$$4\eta(\sigma + a) - 4\eta(\sigma) = 0 \mod 4 \tag{4.198}$$

for any $a \in H^1(\Sigma, \mathbb{Z}_2)$.[14] In the case that $a = w_1$ we have $\sigma + a = \sigma'$, and thus combining (4.197) and (4.198) we conclude that $\eta(\sigma)$ is generically half-integral. As a result, we have that $e^{i\pi \mathrm{ABK}(\Sigma,\sigma)} = e^{i\frac{\pi}{2}\eta(\Sigma,\sigma)}$ generates at most $\mathbb{Z}_8$, as expected.

4.D.2 η-invariants: examples

We now offer some explicit calculations of the Arf and ABK invariants in terms of their definitions in this appendix.

T^2:

A trivial example is that of the Arf invariant on T^2 with spin structure σ. In that case we know that for the NSNS, RNS, and NSR spin structures we have $\zeta(\sigma) = 0$, whereas for RR we have $\zeta(\sigma) = 1$. This together with (4.196) then reproduces the results of (4.13).

[13] This equality is true because the left-hand side is the η-invariant of the spin structure on the oriented double cover $\hat{\Sigma}$. Note that $\hat{\Sigma}$ is the boundary of the total space X of the unit disk bundle of the orientation line bundle of Σ. That Σ is Pin^- is equivalent to X being spin. These facts together imply that $\hat{\Sigma}$ is null-bordant, and so the right-hand side is 0 modulo 4.

[14] To see this, note that $4\eta(\sigma)$ is the η-invariant of the Dirac operator with Pin^- structure σ acting on a rank 4 trivial real vector bundle V, whereas $4\eta(\sigma + a)$ is the η-invariant of the Dirac operator with Pin^- structure σ acting on a rank 4 real vector bundle $V' = A^{\oplus 4}$, where A has the property that $w_1(A) = a$. Because the Stiefel-Whitney classes of V' all vanish, V' is trivial and has the same mod 4 η-invariant as V, thereby giving (4.198).

$\mathbb{RP}^2$**:**

A less trivial result is to reproduce the values of ABK on $\mathbb{RP}^2$. We compute it in two ways. The first is to consider an orbifold of the three-torus $T^3/\mathbb{Z}_2$ where $\mathbb{Z}_2$ acts as $x_i \to -x_i$ for $i = 1, 2, 3$. The resulting space has eight fixed points at $x_i \in \frac{1}{2}\mathbb{Z}$. We may remove a small ball around each of these points to obtain a smooth manifold, with the boundary of this manifold being eight copies of $\mathbb{RP}^2$. Then by the APS index theorem (4.194) for $d = 2$ we conclude that $\eta(\mathbb{RP}^2) = -\frac{1}{4}\text{ind}iD$, with iD the Dirac operator on the $T^3/\mathbb{Z}_2$ with points removed. Using conformal invariance, it is possible to argue that the index of the Dirac operator on this manifold is the same as that on the original $T^3/\mathbb{Z}_2$, so we need only compute this quantity. Let us define $\mathcal{H}_\pm$ to be the spaces of spinors on T^3 which satisfy $\psi(-x) = \pm\psi(-x)$. The Dirac operator maps $\mathcal{H}_\pm \to \mathcal{H}_\mp$, and the index of the Dirac operator on $T^3/\mathbb{Z}_2$ is then just defined to be the number of zero-modes in $\mathcal{H}_+$ minus those in $\mathcal{H}_-$. These numbers are easily obtained: depending on the Pin^- structure, the zero-modes are the 2-dimensional space of constant spinors in either $\mathcal{H}_+$ or $\mathcal{H}_-$, with no zero modes in the remaining space. Hence we have $\text{ind}iD = \pm 2$, and consequently $\eta(\mathbb{RP}^2) = \pm\frac{1}{2}$. We may finally calculate the ABK invariant to be $e^{i\pi\text{ABK}(\mathbb{RP}^2)} = e^{\pm i\frac{\pi}{4}}$, matching the previous results in (4.27).

The second derivation of this result is a direct computation from the spectrum of the Dirac operator. Instead of directly studying the Dirac equation on unoriented manifolds Σ we will consider their orientable double covers $\hat{\Sigma}$. These are equipped with an orientation-reversing involution τ such that $\Sigma = \hat{\Sigma}/\tau$. We will make use of the following morphism

$$\text{Pin}^- \text{ structures on } \Sigma = \hat{\Sigma}/\tau \quad \longrightarrow \quad \tau\text{-invariant spin structures on } \hat{\Sigma}\,. \tag{4.199}$$

induced by the projection. This map is not injective, but rather two-to-one since given a Pin^- structure σ, both σ and its twist by the orientation bundle σ' lift to the same spin structure on the orientable double cover. It is not surjective either, since there are spin structures on $\hat{\Sigma}$ which are not the lift of any Pin^- structure. The τ-invariance of the spin structures

on $\hat{\Sigma}$ implies that $[\tau, iD] = 0$. Hence there is a basis of eigenspinors with a well-defined eigenvalue of τ. The different eigenvalues of τ correspond to different Pin^- structures σ and σ'. In summary, we can extract the spectrum of the Dirac operator iD on Σ from that on the orientable double cover $\hat{\Sigma}$ by considering eigenspinors of iD on the latter with a fixed eigenvalue of τ.

Let us apply this strategy to $\mathbb{RP}^2$. Its orientable double cover is a two-sphere S^2, which has a single spin structure. The spectrum of the Dirac operator on the two-sphere is well known and is given by[15]

$$E = \pm(n+1) \quad \text{with multiplicity} \quad 2(n+1) \quad \text{and} \quad \tau = \mp(-1)^n \ . \tag{4.200}$$

with $n \geq 0$. For convenience we will regularize the sum over eigenvalues (4.192) as follows

$$\eta = \lim_{\epsilon \to 0^+} \sum_E \mathrm{sgn}(E)\, e^{-\epsilon |E|} \ . \tag{4.201}$$

From this information we can readily calculate the η-invariant of $\mathbb{RP}^2$ for either Pin^- structure,

$$\tau = \pm 1 : \quad \eta = \lim_{\epsilon \to 0^+} \left(\mp \sum_{n \in 2\mathbb{N}} 2(n+1)\, e^{-\epsilon(n+1)} \pm \sum_{n \in 2\mathbb{N}+1} 2(n+1)\, e^{-\epsilon(n+1)} \right) = \mp \frac{1}{2} \tag{4.202}$$

reproducing our previous result.

The Klein bottle:

We now obtain the values for the η-invariant on the Klein bottle K_2. A trivial way to do so is to note that the η-invariant factorizes under connected sums, $\eta(\Sigma_1 \# \Sigma_2) = \eta(\Sigma_1) + \eta(\Sigma_2)$.

[15]The eigenspace decomposition is simply the spinor spherical harmonics. One way to quickly derive the eigenvalues is to use the operator-state correspondence of a free massless Dirac fermion in dimension $d+1$. There, the (absolute value of the) eigenvalues of the Dirac operator on S^d are the dilatation eigenvalues of the single-particle operators of the form $\partial \cdots \partial \psi$, which are therefore given by $n + d/2$.

Then recalling that $K_2 = \mathbb{RP}^2 \# \mathbb{RP}^2$, our previous results imply that $\eta(K_2) = 0, 0, \pm 1$ depending on the choice of Pin^- structure. This reproduces the results of (4.28) for the ABK invariant.

A more fulfilling derivation of this result is to again consider the explicit Dirac spectrum. The orientable double cover in this case is the torus T^2, which we take to be rectangular with side lengths 1 and 2. That is, $T^2 = \mathbb{R}^2/\Gamma$ for the lattice $\Gamma = \mathbb{Z} \oplus 2\mathbb{Z}$. Taking $x^i = (x, y)$ to be the coordinates on the torus, we have $(x, y) = (x+1, y) = (x+1, y+2)$. The orientation-reversing involution is $\tau(x, y) = (-x, y + 1)$. As was discussed in Section 4.2.2, of the four torus spin structures only those which are periodic in the y-direction descend in the quotient.

We first consider the spin structure periodic in x. We begin by finding the eigenspinors of the square of the Dirac operator, which is just the Laplacian, $(iD)^2 = -\Delta$. These can be easily constructed as

$$u_p(x^i) = f_p(x^i)\,\Psi, \quad f_p(x^i) = e^{2\pi i\, x^i p_i} \quad \text{with} \quad p_i \in \Gamma^* = \mathbb{Z} \oplus \frac{1}{2}\mathbb{Z} \tag{4.203}$$

where $f_p(x^i)$ are the eigenfunctions of the Laplacian, with momenta taking values in the dual lattice Γ^*, and Ψ a covariantly constant spinor. We can also construct eigenfunctions for the spin structure antiperiodic in x by letting the momenta take values in $\tilde{\Gamma}^* = (\mathbb{Z} + \frac{1}{2}) \oplus \frac{1}{2}\mathbb{Z}$. In both cases it is easy to check that

$$(iD)^2 u(x^i) = 4\pi^2 p^2\, u(x^i)\ . \tag{4.204}$$

In terms of the $u(x^i)$ we can construct the eigenspinors of the Dirac operator as

$$v^{\pm}(x^i) = \pm 2\pi |p|\, u(x^i) + iD\, u(x^i)\ , \quad \text{with} \quad iD\, v^{\pm}(x^i) = \pm 2\pi |p|\, v^{\pm}(x^i)\ . \tag{4.205}$$

This spectrum is clearly symmetric, and hence if there are no zero-modes the η-invariant vanishes. The only case in which there are zero-modes is the case of periodic spin structure

in both directions, and then the multiplicity of the zero-mode is two so that $\eta(T^2, \sigma_{\rm RR}) = 2$, as we know.

To get the corresponding results for the Klein bottle, we now keep the portion of the spectrum with fixed τ eigenvalue. To do so, it is useful to choose an explicit representation for the gamma-matrices, say as $\gamma_1 = \sigma_3$ and $\gamma_2 = \sigma_1$. Then in addition to acting on (x, y) in the manner shown above, the involution τ acts as σ_1 on spinors. With this, it is easy to show that the eigenspinors with fixed eigenvalue under τ have $p_1 = 0$, and hence require periodic spin structure in the x-direction. Defining $n := 2p_2$, the remaining spectrum is

$$E = \pm\pi|n| \quad \text{with multiplicity} \quad 1 \quad \text{and} \quad \tau = \mp(-1)^n \ , \tag{4.206}$$

with the zero eigenvalue having multiplicity 2.

Two of the Pin^- structures of K_2 lift to antiperiodic spin structure in the x-direction, and consequently have vanishing η-invariant. The remaining two Pin^- structures lift to periodic spin structure in the x-direction, and correspond to the two different eigenvalues for τ. The resulting η-invariants are

$$\tau = \pm 1 : \qquad \eta(K_2) = \lim_{\epsilon \to 0^+} 2 \left(\mp \sum_{n \in 2\mathbb{N}} e^{-\epsilon\pi|n|} \pm \sum_{n \in 2\mathbb{N}+1} e^{-\epsilon\pi|n|} \right) = \mp 1 \ , \tag{4.207}$$

reproducing earlier results.

4.D.3 Quadratic forms and enhancements

Let us now make contact between index theory and the combinatoric definitions of Arf and ABK given in (4.10) and (4.24). In order to do so, we first rewrite the quadratic form $\tilde{q}(a)$ and enhancement $q(a)$ in terms of indices.

We start with the oriented case. We consider

$$\tilde{q}(a) := \zeta(\sigma + a) - \zeta(\sigma) \mod 2 \tag{4.208}$$

for a given spin structure σ, where $\zeta(\sigma)$ is the number of zero modes of the positive-chirality Dirac operator. We now verify that this is the quadratic refinement of the intersection form, i.e. the relation (4.9) is satisfied. To do so, we must check that

$$\zeta(\sigma + a + b) + \zeta(\sigma + a) + \zeta(\sigma + b) + \zeta(\sigma) = \int a \cup b \mod 2 \tag{4.209}$$

holds. We note that the left-hand side is $\zeta(V)$, the mod 2 index with spin structure σ for the Dirac operator acting on a positive chirality spinor valued in a rank 4 real vector bundle $V = \epsilon + A + B + AB$, where ϵ is a trivial real line bundle and we have $w_1(A) = a$, $w_1(B) = b$, and $w_1(AB) = a + b$. From this definition, it also follows that $w_1(V) = 0$ and $w_2(V) = a \cup b$. Therefore, V is topologically equivalent to $H \oplus L$, the direct sum of a rank 2 real trivial bundle H and a complex line bundle L with $c_1(L) = w_2(V) \mod 2$. This is because real vector bundles on a Riemann surface are classified topologically by their rank and Stiefel-Whitney classes. Clearly $\zeta(H) = 0$ modulo 0, so we have $\zeta(V) = \zeta(L)$. Under the $U(1)$ rotating L, the zero-modes of L have charge ± 1, with respective numbers $n_\pm$. We then have $\zeta(L) = n_+ + n_- \mod 2$. By complex conjugation, we can replace a charge -1 mode of positive chirality with a charge $+1$ mode of negative chirality. Let $m_\pm$ denote the number of positive/negative chirality modes of charge $+1$. Then we have $n_\pm = m_\pm$, and hence $\zeta(L) = m_+ - m_- \mod 2$. The right-hand side is now the index of the Dirac operator acting on L, which by the index theorem is $\int c_1(L) = \int w_2(V) = \int a \cup b \mod 2$. We then conclude that $\zeta(V) = \int a \cup b \mod 2$, thereby confirming (4.209).

With the definition (4.208), it is now simply to check that our combinatorial definition

(4.10) is consistent with the definition (4.196). We have

$$\begin{aligned}(-1)^{\mathrm{Arf}(\Sigma,\sigma)} &= \frac{1}{\sqrt{|H^1(\Sigma,\mathbb{Z}_2)|}}\sum_{a\in H^1(\Sigma,\mathbb{Z}_2)}(-1)^{\zeta(\sigma+a)-\zeta(\sigma)} \\ &= (-1)^{\zeta(\sigma)}\left(\frac{1}{\sqrt{|H^1(\Sigma,\mathbb{Z}_2)|}}\sum_{a\in H^1(\Sigma,\mathbb{Z}_2)}(-1)^{\zeta(a)}\right). \end{aligned} \tag{4.210}$$

The term in parenthesis can be shown to square to 1 using steps analogous to those used for the combinatorial definition, and one can then fix the result to +1 by checking an explicit example.

We now move on to the Pin^- case. In that case we define the quadratic enhancement $q(a)$ as

$$q(a) = \zeta(\sigma + a) - \zeta(\sigma) \mod 4 \tag{4.211}$$

where σ is now a Pin^- structure. We must check that (4.25) is satisfied by this definition. To do so, let us first prove this in the special case of $\Sigma = \mathbb{RP}^2$. There is then only one non-trivial possibility for a and b, namely w_1. The identity (4.25) is trivially satisfied unless $a = b = w_1$, so we focus on that case. Then noting that $q(0) = 0$, the identity we wish to prove is

$$q(w_1) = \int w_1^2 = 1 \mod 2\ . \tag{4.212}$$

We now use the fact that $q(w_1) = \eta(\sigma') - \eta(\sigma) \mod 2$. As we showed in the previous subsection, for $\mathbb{RP}^2$ one of the two η-invariants is $+\frac{1}{2}$, while the other is $-\frac{1}{2}$. Either way, we conclude that $q(w_1) = 1 \mod 2$, thereby confirming the identity.

To prove the identity in generality, we now make use of bordism invariance. What we

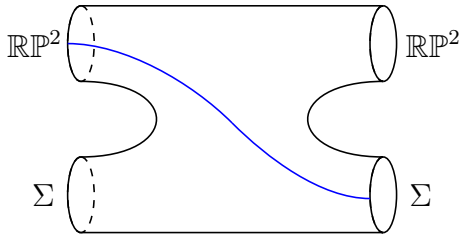

Figure 4.5: A bordism between $\mathbb{RP}^2 \times \Sigma$ and itself, with a real vector bundle V' on it. The blue line represents the Poincaré dual of $w_2(V')$.

would like to prove is

$$\zeta(\sigma + a + b) - \zeta(\sigma + a) - \zeta(\sigma + b) + \zeta(\sigma) = 2 \int a \cup b \mod 4 \,. \tag{4.213}$$

Equivalently, this is

$$\eta(V') - \eta(V) = 2 \int w_2(V') \mod 4 \tag{4.214}$$

where V is a rank 8 trivial bundle and V' is a rank 8 bundle with $w_1(V') = 0$ and $w_2(V') = a \cup b$. Recall that in two dimensions $w_2(V')$ is Poincaré dual to a point, while in three dimensions it is dual to a curve. Then consider a bordism from $\mathbb{RP}^2 \times \Sigma$ to itself by means of a connected sum, as shown in Fig. 4.5. In the figure, we have drawn a curve that starts at $\mathbb{RP}^2$ on the top left and goes down to Σ on the bottom right. Consider a real vector bundle V' such that $w_2(V')$ is Poincaré dual to this curve. This gives a bordism between $\mathbb{RP}^2 \times \Sigma$ with $w_2(V') = 1$ on $\mathbb{RP}^2$ and 0 on Σ, and $\mathbb{RP}^2 \times \Sigma$ with $w_2(V') = 0$ on $\mathbb{RP}^2$ and 1 on Σ. Because (4.214) is unchanged by this change in V', it must hold for any Σ, thus proving the claim.

4.E $\mathfrak{O}^d_{\mathrm{DPin}}(\mathrm{pt})$ via the Atiyah-Hirzebruch spectral sequence

In this appendix we analyze the Atiyah-Hirzebruch spectral sequence (AHSS) for $\mathfrak{O}_X^{d=2,3}(pt)$ for $X = \mathrm{Spin} \times \mathbb{Z}_2$, $\mathrm{Pin}^{\pm}$, and DPin. Except for the last case $X = \mathrm{DPin}$ the outcome is

well-known; we include the computations here just to illustrate the method.

To write down the E_2 page, we will need the groups $H^p(X, \underline{\mathfrak{O}^q_{\text{spin}}(pt)})$. More concretely, we need $H^*(B\mathbb{Z}_2 \times B\mathbb{Z}_2, \mathbb{Z}_2)$ and $H^*(B\mathbb{Z}_2 \times B\mathbb{Z}_2, \underline{U(1)})$, where the underline signifies that the first $\mathbb{Z}_2$ acts on $U(1)$ by complex conjugation and the second acts trivially. The first is standard: we have

$$H^*(B\mathbb{Z}_2 \times B\mathbb{Z}_2, \mathbb{Z}_2) = \mathbb{Z}_2[w, a] \tag{4.215}$$

where w and a are the generators of $H^1(B\mathbb{Z}_2 \times B\mathbb{Z}_2, \mathbb{Z}_2) = H^1(B\mathbb{Z}_2, \mathbb{Z}_2) \oplus H^1(B\mathbb{Z}_2, \mathbb{Z}_2)$. As for $H^*(B\mathbb{Z}_2 \times B\mathbb{Z}_2, \underline{U(1)})$, they are determined as an abstract group in e.g. Appendix J.6 of [369]; in particular all elements are annihilated by 2. For our purposes we will need more detailed data. We note that the short exact sequence

$$0 \longrightarrow \mathbb{Z}_2 \xrightarrow{\iota} \underline{U(1)} \xrightarrow{2\cdot} \underline{U(1)} \to 0 \tag{4.216}$$

leads to the long exact sequence

$$\begin{aligned} \cdots \xrightarrow{2\cdot} H^{d-1}(B\mathbb{Z}_2 \times B\mathbb{Z}_2, \underline{U(1)}) \xrightarrow{\beta} H^d(B\mathbb{Z}_2 \times B\mathbb{Z}_2, \mathbb{Z}_2) \\ \xrightarrow{\iota} H^d(B\mathbb{Z}_2 \times B\mathbb{Z}_2, \underline{U(1)}) \xrightarrow{2\cdot} H^d(B\mathbb{Z}_2 \times B\mathbb{Z}_2, \underline{U(1)}) \xrightarrow{\beta} \cdots \end{aligned} \tag{4.217}$$

Since $2\cdot$ annihilates everything, we see that $H^d(B\mathbb{Z}_2 \times B\mathbb{Z}_2, \underline{U(1)})$ is a quotient of $H^d(B\mathbb{Z}_2 \times$

$B\mathbb{Z}_2, \mathbb{Z}_2)$ by the image of the twisted Bockstein $\beta = \mathrm{Sq}^1 + w$. Therefore we find

$$H^0(B\mathbb{Z}_2 \times B\mathbb{Z}_2, \underline{U(1)}) = U(1) \ , \tag{4.218}$$

$$H^1(B\mathbb{Z}_2 \times B\mathbb{Z}_2, \underline{U(1)}) = \mathbb{Z}_2 = \frac{\langle w, a\rangle}{\langle w\rangle} \ , \tag{4.219}$$

$$H^2(B\mathbb{Z}_2 \times B\mathbb{Z}_2, \underline{U(1)}) = \mathbb{Z}_2^2 = \frac{\langle w^2, wa, a^2\rangle}{\langle a(a+w)\rangle} \ , \tag{4.220}$$

$$H^3(B\mathbb{Z}_2 \times B\mathbb{Z}_2, \underline{U(1)}) = \mathbb{Z}_2^2 = \frac{\langle w^3, w^2a, wa^2, a^3\rangle}{\langle w^3, wa^2\rangle} \ , \tag{4.221}$$

$$H^4(B\mathbb{Z}_2 \times B\mathbb{Z}_2, \underline{U(1)}) = \mathbb{Z}_2^3 = \frac{\langle w^4, w^3a, w^2a^2, wa^3, a^4\rangle}{\langle w^2a(a+w), a^3(a+w)\rangle} \ . \tag{4.222}$$

This data can be checked e.g. by noticing that in this low degree range $H^d(B\mathbb{Z}_2 \times BG, \underline{U(1)})$ with $T : \mathbb{Z}_2 \times G \to \mathbb{Z}_2$ given by $T = w$ equals $\mathfrak{V}^d_{\text{unoriented}}(BG)$. The generators of $\Omega_d^{\text{unoriented}}(B\mathbb{Z}_2)$ can be taken to be e.g. S^1 with nontrivial $\mathbb{Z}_2$ bundle for $d = 1$, $\mathbb{RP}^2$ with and without nontrivial $\mathbb{Z}_2$ bundle for $d = 2$, ($\mathbb{RP}^2$ with and without nontrivial $\mathbb{Z}_2$ bundle) $\times$ (S^1 with nontrivial $\mathbb{Z}_2$ bundle) for $d = 3$, and $\mathbb{RP}^4$ with and without nontrivial $\mathbb{Z}_2$ bundle, and $\mathbb{RP}^2 \times \mathbb{RP}^2$ with nontrivial $\mathbb{Z}_2$ on the first factor for $d = 4$. We can then evaluate all elements of $\mathbb{Z}_2[w, a]$ on the generators with the identification that w is w_1 of the manifold and a is w_1 of the $\mathbb{Z}_2$ bundle.

With this information, we can now proceed to the calculation of the relevant groups. Before computing $\mathfrak{V}^d_{\text{DPin}}(pt)$, we illustrate the technique in the known examples of $\mathfrak{V}^d_{\text{Spin}}(B\mathbb{Z}_2)$ and $\mathfrak{V}^d_{\text{Pin}^\pm}(pt)$. Below, the image of $\iota : \mathbb{Z}_2 \hookrightarrow \underline{U(1)}$ is denoted by prefixing by $\frac{1}{2}$, since $\{0, \frac{1}{2}\} \subset U(1)$.

$\underline{\mathfrak{O}_{\text{Spin}}(B\mathbb{Z}_2)}$

The E_2 page needed for obtaining $\mathfrak{O}_{\text{Spin}}(B\mathbb{Z}_2)$ is

q						
3						
2	$\mathbb{Z}_2$	$\mathbb{Z}_2$	$\mathbb{Z}_2$	$\mathbb{Z}_2$	$\mathbb{Z}_2$	
1	$\mathbb{Z}_2$	$\mathbb{Z}_2$	$\mathbb{Z}_2$	$\mathbb{Z}_2$	$\mathbb{Z}_2$	
0	$U(1)$	$\frac{1}{2}\mathbb{Z}_2$		$\frac{1}{2}\mathbb{Z}_2$		
	0	1	2	3	4	p

(4.223)

This can be found from the data given above by forgetting the pieces involving w. The differential d_2 starting from $E_2^{p,q}$ with $p+q \leq 4$ turns out to be zero. The E_3 page is then

q						
3						
2	$\mathbb{Z}_2$	$\mathbb{Z}_2$	?	?	?	
1	$\mathbb{Z}_2$	$\mathbb{Z}_2$	$\mathbb{Z}_2$	?	?	
0	$U(1)$	$\frac{1}{2}\mathbb{Z}_2$		$\frac{1}{2}\mathbb{Z}_2$		
	0	1	2	3	4	p

(4.224)

The only possibly nontrivial d_3 is $d_3 : E_3^{0,2} \to E_3^{3,0}$ but a special property of untwisted bordism says that every d_n starting from $E^{0,q}$ is zero. (This fact is explained below Theorem 9.10 of [358].) Then this is also the E_4 page, and $E^{p,q}$ with $p+q \leq 3$ cannot change any further.

From this we read off that $\mathfrak{O}^d_{\text{Spin}}(pt)$ for $d = 1, 2, 3$ contains $4, 4$, and 8 elements, respec-

tively. This agrees with known results.

$\underline{\mathfrak{O}_{\mathrm{Pin}^-}(pt)}$

The E_2 page in this case is

q						
3						
2	$\mathbb{Z}_2$	w	w^2	w^3	w^4	
1	$\mathbb{Z}_2$	w	w^2	w^3	w^4	
0	$U(1)$		$\frac{1}{2}w^2$		$\frac{1}{2}w^4$	
	0	1	2	3	4	p

(4.225)

This can be found from the data given above by forgetting the part involving a. For d_2 starting from $q = 2$, one has $d_2^2 = \mathrm{Sq}^2 + w_1(V)\,\mathrm{Sq}^1 + w_2(V) = \mathrm{Sq}^2 + w\,\mathrm{Sq}^1$. Then since $\mathrm{Sq}^2(w^2) = (\mathrm{Sq}^1 w)(\mathrm{Sq}^1 w) = w^4$ and $\mathrm{Sq}^1(w) = w^2$, we find

$$d_2^2(1) = d_2^2(w^3) = 0\ , \qquad d_2^2(w) = w^3\ , \qquad d_2^2(w^2) = w^4\ . \tag{4.226}$$

On the other hand we have $d_2^1 = \frac{1}{2}\,\mathrm{Sq}^2$, and hence

$$d_2^1(1) = d_2^1(w) = d_2^1(w^3) = 0\ , \qquad d_2^1(w^2) = \frac{1}{2}w^4\ . \tag{4.227}$$

Then the E_3 page is

q						
3						
2	$\mathbb{Z}_2$			?	?	
1	$\mathbb{Z}_2$	w			?	
0	$U(1)$		$\frac{1}{2}w^2$			
	0	1	2	3	4	p

(4.228)

This predicts $|\mathfrak{O}^d_{\mathrm{Pin}^-}(pt)| = 2, 8, 0$ for $d = 1, 2, 3$, in agreement with known results.

$\underline{\mathfrak{O}_{\mathrm{Pin}^+}(pt)}$

The E_2 page in this case is

q						
3						
2	$\mathbb{Z}_2$	w	w^2	w^3	w^4	
1	$\mathbb{Z}_2$	w	w^2	w^3	w^4	
0	$U(1)$		$\frac{1}{2}w^2$		$\frac{1}{2}w^4$	
	0	1	2	3	4	p

(4.229)

This is obtained from the previous data by setting $w = a$. We then have $d_2^2 = \mathrm{Sq}^2 + w_1\,\mathrm{Sq}^1 + w_2 = \mathrm{Sq}^2 + w\,\mathrm{Sq}^1 + w^2$, and so

$$d_2^2(1) = w^2\ , \qquad d_2^2(w) = d_2^2(w^2) = 0\ , \qquad d_2^2(w^3) = w^5\ . \tag{4.230}$$

On the other hand $d_2^1 = \frac{1}{2}\,\mathrm{Sq}^2 + \frac{1}{2}w^2$ and hence

$$d_2^1(1) = \frac{1}{2}w^2\ , \qquad d_2^1(w) = \frac{1}{2}w^3\ , \qquad d_2^1(w^2) = 0\ , \qquad d_2^1(w^3) = \frac{1}{2}w^5\ . \quad (4.231)$$

Then the E_3 page is

q						
3						
2		w	w^2	?	?	
1		w		w^3	?	
0	$U(1)$				$\frac{1}{2}w^4$	
	0	1	2	3	4	p

(4.232)

This predicts $|\mathfrak{O}^d_{\mathrm{Pin}^+}(pt)| = 0, 2, 2$ for $d = 1, 2, 3$, in agreement with known results.

$\underline{\mathfrak{O}_{\mathrm{DPin}}(pt)}$

We finally arrive at the case of interest. The E_2 page is

q						
3						
2	$\mathbb{Z}_2$	w, a	w^2, wa, a^2	w^3, w^2a, wa^2, a^3	$w^4, \ldots$	
1	$\mathbb{Z}_2$	w, a	w^2, wa, a^2	w^3, w^2a, wa^2, a^3	$w^4, \ldots$	
0	$U(1)$	$\frac{1}{2}a$	$\frac{1}{2}w^2, \frac{1}{2}wa = \frac{1}{2}a^2$	$\frac{1}{2}w^2a, \frac{1}{2}a^3$	$\frac{1}{2}w^4, \frac{1}{2}w^3a = \frac{1}{2}w^2a^2, \frac{1}{2}wa^3 = \frac{1}{2}a^4$	
	0	1	2	3	4	q

(4.233)

We have $d_2^2 = \mathrm{Sq}^2 + w\,\mathrm{Sq}^1 + wa$ and $d_2^1 = \frac{1}{2}\,\mathrm{Sq}^2 + \frac{1}{2}wa$. Then the E_3 page is

q						
3						
2		a	?	?	?	
1		a	a^2	?	?	
0	$U(1)$	$\frac{1}{2}a$	$\frac{1}{2}w^2$	$\frac{1}{2}a^3$	$\frac{1}{2}w^4 = \frac{1}{2}w^3a = \frac{1}{2}w^2a^2, \frac{1}{2}wa^3 = \frac{1}{2}a^4$	
	0	1	2	3	4	q

(4.234)

At this point we see that there can be at most four elements in $\mathfrak{O}^2_{\mathrm{DPin}}(pt)$ and eight elements in $\mathfrak{O}^3_{\mathrm{DPin}}(pt)$. We already know a subgroup $\mathbb{Z}_2 \times \mathbb{Z}_2$ of $\mathfrak{O}^2_{\mathrm{DPin}}(pt)$, generated by $(-1)^{\int w_1^2}$ and $(-1)^{\mathrm{Arf}(\hat{\Sigma})}$, and thus we conclude that $\mathfrak{O}^2_{\mathrm{DPin}}(pt) = (\mathbb{Z}_2)^2$. We also know that the anomaly of Majorana fermion on unoriented surfaces form $\mathbb{Z}_8$, so we conclude that $\mathfrak{O}^3_{\mathrm{DPin}}(pt) = \mathbb{Z}_8$.

4.F $\mathfrak{O}^d_{\mathrm{DPin}}(\mathrm{pt})$ via the Adams spectral sequence

In this appendix[16], we compute $\mathfrak{O}^d_{\mathrm{DPin}}(\mathrm{pt})$ for $d \leq 6$ a different way, using the Adams spectral sequence. Though computations with the Adams spectral sequence are often difficult, the problem simplifies greatly when computing twisted spin bordism groups Ω_d^X, thanks to a technique that first appears in Davis' thesis [370] and builds on work of Stong [371] and Anderson-Brown-Peterson [372].

We highly recommend Beaudry and Campbell's paper [373] for a detailed introduction to this method of computation and the ingredients that go into it, as well as several worked examples. We assume familiarity with the definitions and notation they give.

[16]This appendix was contributed by Arun Debray.

Theorem 4.235. *The low-degree dpin bordism groups are:* $\Omega_0^{\mathrm{DPin}} \cong \mathbb{Z}/2$, $\Omega_1^{\mathrm{DPin}} \cong \mathbb{Z}/2$, $\Omega_2^{\mathrm{DPin}} \cong \mathbb{Z}/2 \oplus \mathbb{Z}/2$, $\Omega_3^{\mathrm{DPin}} \cong \mathbb{Z}/8$, $\Omega_4^{\mathrm{DPin}} \cong \mathbb{Z}/2 \oplus \mathbb{Z}/2$, $\Omega_5^{\mathrm{DPin}} \cong 0$, *and* $\Omega_6^{\mathrm{DPin}} \cong \mathbb{Z}/2 \oplus \mathbb{Z}/2$.

For any finite abelian group A, there is a (noncanonical) isomorphism $A \cong \mathrm{Hom}(A, \mathrm{U}(1))$, so this also computes $\mho^d_{\mathrm{DPin}}(\mathrm{pt})$ for $0 \leq d \leq 6$, and agrees with the calculations made in Appendix 4.E. Recall from Sec. 4.6.2 that a dpin structure is equivalent to a choice of two real line bundles $L_1, L_2 \to M$ and a spin structure on

$$TM \oplus (L_1 \otimes L_2) \oplus (L_2)^{\oplus 3}. \tag{4.236}$$

One consequence is that if *MTDPin* denotes the Thom spectrum for dpin structures, so that $\pi_k(MTDPin) \cong \Omega_k^{\mathrm{DPin}}$, then

$$MTDPin \simeq MTSpin \wedge (B\mathbb{Z}/2 \times B\mathbb{Z}/2)^{L_1 L_2 + 3L_2 - 4}. \tag{4.237}$$

The second summand, $(B\mathbb{Z}/2 \times B\mathbb{Z}/2)^{L_1 L_2 + 3L_2 - 4}$, which we denote X to tame the notation, is the Thom spectrum of the virtual vector bundle

$$V \coloneqq (L_1 \otimes L_2) \oplus (L_2)^{\oplus 3} - \mathbb{R}^4 \longrightarrow B\mathbb{Z}/2 \times B\mathbb{Z}/2. \tag{4.238}$$

By (4.237), $\Omega_k^{\mathrm{DPin}} \cong \widetilde{\Omega}_k^{\mathrm{Spin}}(X)$.

We will compute $\widetilde{\Omega}_k^{\mathrm{Spin}}(X)$ for $0 \leq k \leq 6$ for our X using the Adams spectral sequence, employing a standard trick to work over $\mathcal{A}(1) \coloneqq \langle \mathrm{Sq}^1, \mathrm{Sq}^2 \rangle$ rather than the entire Steenrod algebra. For details on how this works and many worked examples, see Beaudry-Campbell [373], who carefully explain and summarize how to use the Adams spectral sequence for these kinds of computations. The idea is that we must determine $\widetilde{H}^*(X; \mathbb{F}_2)$ as an $\mathcal{A}(1)$-module. Then, the E_2-page of this Adams spectral sequence is

$$E_2^{s,t} = \mathrm{Ext}^{s,t}_{\mathcal{A}(1)}(\widetilde{H}^*(X; \mathbb{F}_2), \mathbb{F}_2). \tag{4.239}$$

(Definitions and notation are as in [373].) The spectral sequence converges to $\widetilde{ko}_{t-s}(X) \otimes \hat{\mathbb{Z}}_2$, where ko denotes connective real K-theory and $\hat{\mathbb{Z}}_2$ denotes the 2-adic integers. Furthermore, when $t - s \leq 7$, $\widetilde{ko}_{t-s}(X)$ is isomorphic to $\widetilde{\Omega}^{\text{Spin}}_{t-s}(X)$ [372]. We will show, for our particular choice of X, $\widetilde{\Omega}^{\text{Spin}}_*(X)$ lacks torsion for odd primes. Therefore tensoring it with $\hat{\mathbb{Z}}_2$ does not lose any information. (In general, information can be lost when tensoring with $\hat{\mathbb{Z}}_2$, but that information can be computed by other means.) This allows us to use the spectral sequence above to compute $\widetilde{\Omega}^{\text{Spin}}_{t-s}(X)$ in the degrees of our interest.

Proof of Theorem 4.235. First we argue $\widetilde{\Omega}^{\text{Spin}}_*(X)$ has no p-torsion for odd primes p. In fact, we will show that if p is an odd prime, $\widetilde{\Omega}^{\text{Spin}}_*(X) \otimes \mathbb{F}_p = 0$. For any finitely generated abelian group A, the p-torsion subgroup of A includes into the p-torsion subgroup of $A \otimes \mathbb{F}_p$, so this suffices.

By definition, $\widetilde{\Omega}^{\text{Spin}}_k(X) \cong \widetilde{H}_k(MTSpin \wedge X)$. Tensoring with $\mathbb{F}_p$, the map

$$\widetilde{H}_k(MTSpin \wedge X) \otimes \mathbb{F}_p \longrightarrow \widetilde{H}_k(MTSpin \wedge X; \mathbb{F}_p) \tag{4.240}$$

is injective, by the universal coefficient theorem. The Künneth theorem computes $\widetilde{H}_*(MTSpin \wedge X; \mathbb{F}_p)$ as a sum of tensor products of the form $\widetilde{H}_i(MTSpin; \mathbb{F}_p) \otimes \widetilde{H}_j(X; \mathbb{F}_p)$, so it suffices to show $\widetilde{H}_j(X; \mathbb{F}_p)$ vanishes for all j. The twisted-coefficients Thom isomorphism tells us there is a (in this case nontrivial) $\mathbb{Z}[\mathbb{Z}/2 \times \mathbb{Z}/2]$-module structure $\widetilde{\mathbb{F}}_p$ on $\mathbb{F}_p$ such that

$$\widetilde{H}_j(X; \mathbb{F}_p) \cong H_j(\mathbb{Z}/2 \times \mathbb{Z}/2; \widetilde{\mathbb{F}}_p). \tag{4.241}$$

Maschke's theorem implies that since $\#(\mathbb{Z}/2 \times \mathbb{Z}/2)$ and p are coprime, and since $\widetilde{\mathbb{F}}_p$ is p-torsion, $H_j(\mathbb{Z}/2 \times \mathbb{Z}/2; \widetilde{\mathbb{F}}_p)$ vanishes in degrees $j > 0$. Using that 0^{th} group homology is the abelian group of coinvariants, one can check directly that $H_0(\mathbb{Z}/2 \times \mathbb{Z}/2; \widetilde{\mathbb{F}}_p) = 0$ as well. Thus $\widetilde{\Omega}^{\text{Spin}}_*(X)$ has no p-torsion.

On to the Adams spectral sequence. First we determine $\widetilde{H}^*(X; \mathbb{F}_2)$. As a graded abelian

group, this is characterized by the Thom isomorphism: if $U \in \widetilde{H}^0(X;\mathbb{F}_2)$ denotes the Thom class, cup product with U is an isomorphism

$$(U\cdot)\colon H^k(B\mathbb{Z}/2 \times B\mathbb{Z}/2;\mathbb{F}_2) \xrightarrow{\cong} \widetilde{H}^k(X;\mathbb{F}_2). \tag{4.242}$$

There is no degree shift because the virtual vector bundle $V \to B\mathbb{Z}/2 \times B\mathbb{Z}/2$ (from (4.238)) has rank zero. Let $w \coloneqq w_1(L_1)$ and $a \coloneqq w_1(L_2)$ in $H^1(B\mathbb{Z}/2 \times B\mathbb{Z}/2;\mathbb{F}_2)$; then

$$H^*(B\mathbb{Z}/2 \times B\mathbb{Z}/2;\mathbb{F}_2) \cong \mathbb{F}_2[w,a]. \tag{4.243}$$

The $\mathcal{A}(1)$-module structure on $\widetilde{H}^*(X;\mathbb{F}_2)$ is determined by the following rules.

1. $\mathrm{Sq}^i(U) = Uw_i(V)$, where w_i denotes the i^{th} Stiefel-Whitney class. In this case, $w_1(V) = w$ and $w_2(V) = wa$.

2. The Cartan formula determines the Steenrod squares of a product. We only need Sq^1 and Sq^2, for which the Cartan formula specializes to

$$\mathrm{Sq}^1(xy) = \mathrm{Sq}^1(x)y + x\,\mathrm{Sq}^1(y) \tag{4.244a}$$

$$\mathrm{Sq}^2(xy) = \mathrm{Sq}^2(x)y + \mathrm{Sq}^1(x)\,\mathrm{Sq}^1(y) + x\,\mathrm{Sq}^2(y). \tag{4.244b}$$

3. From the axiomatic properties of Steenrod squares, $\mathrm{Sq}^1(w) = w^2$, $\mathrm{Sq}^1(a) = a^2$, and $\mathrm{Sq}^2(w) = \mathrm{Sq}^2(a) = 0$.

Using these three rules one can determine the action of Sq^1 and Sq^2 on any cohomology class of X, as it is a sum of products of U, w, and a. This is routine, and indeed we used a computer program to make these calculations. The answer is displayed in Figure 4.6.

From this figure, we see that, as an $\mathcal{A}(1)$-module, $\widetilde{H}^*(X;\mathbb{F}_2)$ splits into several summands. All summands pictured except the orange summand are isomorphic to shifts of $\mathcal{A}(1)$. The orange summand, i.e. the one that contains Ua, continues above what we draw in Figure 4.6

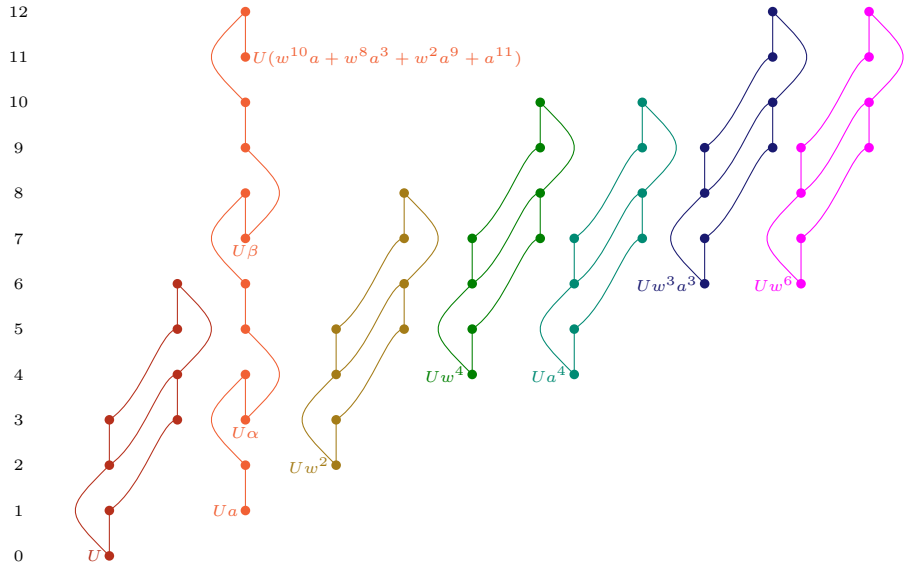

Figure 4.6: This $\mathcal{A}(1)$-submodule of $\widetilde{H}^*(X;\mathbb{F}_2)$ contains all elements of degree at most 7. Each dot represents an $\mathbb{F}_2$ summand, with its cohomological degree given by its height. The connecting lines, resp. curves, indicate an action by Sq^1, resp. Sq^2, carrying the lower dot to the upper dot. This $\mathcal{A}(1)$-module factors as several different summands; we give each summand a different color. In the generators of the orange summand, $\alpha := w^2a + a^3$ and $\beta := w^6a + w^4a^3 + w^2a^5 + a^7$.

and is isomorphic to the mod 2 cohomology of the spectrum $MO(1)$, the Thom spectrum of the tautological line bundle $\sigma \to B\mathrm{O}(1)$ (see [373, Figure 4]); therefore we denote that summand by $\widetilde{H}^*(MO(1))$.[17] Specifically,

$$\widetilde{H}^*(X;\mathbb{F}_2) \cong \mathcal{A}(1)\oplus\widetilde{H}^*(MO(1))\oplus\Sigma^2\mathcal{A}(1)\oplus\Sigma^4\mathcal{A}(1)\oplus\Sigma^4\mathcal{A}(1)\oplus\Sigma^6\mathcal{A}(1)\oplus\Sigma^6\mathcal{A}(1)\oplus P, \quad (4.245)$$

where P has no elements of degree less than 8. Hence, below degree $t - s = 8$, the E_2-page of the Adams spectral sequence (4.239) is the direct sum of the E_2-pages of the summands other than P, and these have all been calculated. For $\Sigma^k\mathcal{A}(1)$, there is a single $\mathbb{F}_2$ summand in bidegree $s = 0$, $t = k$; for $\widetilde{H}^*(MO(1))$, see [374, Example 6.3]. Putting these together, the E_2-page for this spectral sequence is

[17] Strictly speaking, we have only calculated this summand up to degree 12, and it could differ from $\widetilde{H}^*(MO(1))$ in larger degrees. This would only affect the E_2-page in degrees larger than we use and display in (4.246), so the calculation is the same in either case.

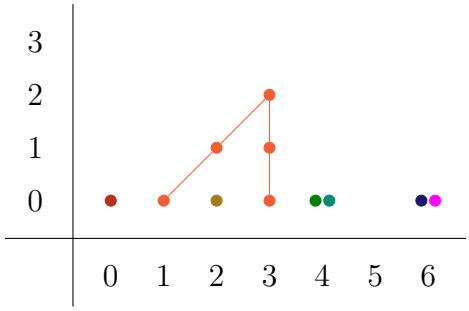

(4.246)

In this diagram, the x-axis is $t-s$ and the y-axis is s. Therefore a differential d_r moves one degree to the left and r degrees upwards. Each dot represents an $\mathbb{F}_2$ summand of the E_2-page; the different colors indicate which summands of $\widetilde{H}^*(X;\mathbb{F}_2)$ are responsible for which data on the E_2-page. The E_2-page carries an action by $\mathrm{Ext}^{*,*}_{\mathcal{A}(1)}(\mathbb{F}_2,\mathbb{F}_2)$. The vertical lines indicate action by an element $h_0 \in \mathrm{Ext}^{1,1}_{\mathcal{A}(1)}(\mathbb{F}_2,\mathbb{F}_2)$, and the diagonal lines indicate action by $h_1 \in \mathrm{Ext}^{2,1}_{\mathcal{A}(1)}(\mathbb{F}_2,\mathbb{F}_2)$; see [373, Example 4.1.1] for more on h_0 and h_1. All differentials are h_0- and h_1-linear, i.e. $d_r(h_i x) = h_i d_r(x)$ $(i=0,1)$. In this example, the only differential within the range displayed in (4.246) that could be nonzero is the d_2 from bidegree $(4,0)$ to bidegree $(3,2)$. Often, h_0- and h_1-linearity allow one to deduce that differentials vanish, but this does not provide any information about this d_2, so we have to do something different.

There will also be a question of extension problems: the line $t-s=k$ is the associated graded of a filtration, possibly nontrivial, on $\widetilde{\Omega}^{\mathrm{Spin}}_k(X)$. This in particular introduces an ambiguity in $\widetilde{\Omega}^{\mathrm{Spin}}_2(X)$: it could either be $\mathbb{Z}/2\oplus\mathbb{Z}/2$ or $\mathbb{Z}/4$. Fortunately, when we show this d_2 vanishes in Corollary 4.250, we will also be able to resolve this ambiguity.

Recall that a dpin structure on M is data of two line bundles $L_1, L_2 \to M$ and a spin structure on $TM \oplus (L_1 \otimes L_2) \oplus (L_2)^{\oplus 3}$. Computing w_1 and w_2 of this bundle with the Whitney sum formula shows that if (M, L_1, L_2) has a dpin structure, $w_1(M) = w_1(L_1)$ and $w_2(M) = w_1(M)(w_1(M) + w_1(L_2))$.

Lemma 4.247. *The assignment from (M, L_1, L_2) to a smooth representative of the Poincaré dual of $w_1(L_2) \in H^1(M;\mathbb{Z}/2)$ induces a map $D_{L_2}\colon \widetilde{\Omega}^{\mathrm{Spin}}_d(X) \to \Omega^{\mathrm{Pin}^-}_{d-1}$.*

Proof. These kinds of arguments are standard in bordism theory (e.g. [318, 319, 321]), so we will be succinct. Let $i\colon N \hookrightarrow M$ be a smooth representative for the Poincaré dual of $w_1(L_2)$ and $\nu \to N$ be the normal bundle; then $w(\nu) = 1 + w_1(L_2)$. Using the short exact sequence $0 \to TN \to \nu \to TM|_N \to 0$ and the Whitney sum formula, we get

$$w_1(N) = i^*(w_1(M) + w_1(L_2)) \tag{4.248a}$$

$$w_2(N) = i^*(w_2(M)) + w_1(N)w_1(\nu) \tag{4.248b}$$

$$= i^*(w_1(M)^2 + w_1(M)w_1(L_2) + (w_1(M) + w_1(L_2))w_1(L_2)) \tag{4.248c}$$

$$= i^*(w_1(M)^2 + w_1(L_2)^2) \tag{4.248d}$$

$$= w_1(N)^2, \tag{4.248e}$$

so N admits a pin$^-$ structure; a choice of pin$^-$ structure amounts to the additional data of a nullhomotopy of the map $w_2 + w_1^2\colon N \to K(\mathbb{Z}/2, 2)$. A choice of dpin structure on (M, L_1, L_2) includes (up to a contractible choice) data of nullhomotopies of the maps $w_1(M) + w_1(L_1)\colon M \to K(\mathbb{Z}/2, 1)$ and $w_2(M) + w_1(M)(w_1(M) + w_1(L_2))\colon M \to K(\mathbb{Z}/2, 2)$; via (4.248a), this induces a nullhomotopy of the map $w_1(N) + i^*(w_1(M) + w_1(L_2))\colon N \to K(\mathbb{Z}/2, 1)$, which then induces a nullhomotopy of $w_2 + w_1^2\colon N \to K(\mathbb{Z}/2, 2)$ via the rest of (4.248). The proof of bordism invariance of this construction is as usual. □

D_{L_2} is an example of a *Smith homomorphism*. For a general discussion of Smith homomorphisms, see e.g. [319, §4].

Lemma 4.249. *The image of* $D_{L_2}\colon \widetilde{\Omega}_3^{\mathrm{Spin}}(X) \to \Omega_2^{\mathrm{Pin}^-} \cong \mathbb{Z}/8$ *contains a generator of* $\Omega_2^{\mathrm{Pin}^-}$.

Proof. Let $a \in H^1(\mathbb{RP}^3; \mathbb{F}_2)$ be the generator. Let $L_1 \to \mathbb{RP}^3$ be trivial and $L_2 \to \mathbb{RP}^3$ be the tautological bundle, so $w_1(L_1) = 0$ and $w_1(L_2) = a$. Since $w(\mathbb{RP}^3) = (1 + a)^4 = 1 + a^4 = 0$, $w_1(\mathbb{RP}^3) = 0 = w_1(L_1)$ and $w_2(\mathbb{RP}^3) = 0 = w_1(\mathbb{RP}^3)(w_1(\mathbb{RP}^3)w_1(L_2))$. Hence $(\mathbb{RP}^3, L_1, L_2)$ admits a dpin structure; choose one.

The standard embedding $\mathbb{RP}^2 \hookrightarrow \mathbb{RP}^3$ represents the homology class Poincaré dual to a, so $D_{L_2}(\mathbb{RP}^3, L_1, L_2)$ is the pin$^-$ bordism class of $\mathbb{RP}^2$ with one of its two pin$^-$ structures. Kirby-Taylor [321, §3] describe how to show that $\mathbb{RP}^2$ with either choice of pin$^-$ structure generates $\Omega_2^{\mathrm{Pin}^-}$. □

Corollary 4.250.

1. $\widetilde{\Omega}_3^{\mathrm{Spin}}(X) \cong \mathbb{Z}/8$, *so the* d_2 *noted above vanishes.*

2. *The extension*

$$0 \longrightarrow \mathbb{Z}/2 \longrightarrow \widetilde{\Omega}_2^{\mathrm{Spin}}(X) \longrightarrow \mathbb{Z}/2 \longrightarrow 0, \tag{4.251}$$

which comes from the Adams filtration on $\widetilde{\Omega}_2^{\mathrm{Spin}}(X)$*, splits.*

Proof. For (1), let $\overline{x}, \overline{y}$ be elements on the E_∞-page, i.e. elements of the associated graded of the Adams filtration. It is a general fact about the Adams spectral sequence that if $h_0\overline{x} = \overline{y}$, then there are preimages $x, y \in \widetilde{\Omega}_*^{\mathrm{Spin}}(X)$ of $\overline{x}$, resp. $\overline{y}$, such that $2x = y$. For example, supposing the d_2 of interest were nonzero, the line $t - s = 3$ on the E_∞-page (i.e. the associated graded of $\widetilde{\Omega}_2^{\mathrm{Spin}}(X)$) would contain exactly two $\mathbb{Z}/2$ summands linked by an h_0; hence there would be nonzero $x_1, x_2 \in \widetilde{\Omega}_3^{\mathrm{Spin}}(X)$ with $x_1 = 2x_2$, so $\widetilde{\Omega}_3^{\mathrm{Spin}}(X) \cong \mathbb{Z}/4$. On the other hand, if $d_2 = 0$, there would be three $\mathbb{Z}/2$ summands linked by h_0s, so there would be nonzero $x_1, x_2 \in \widetilde{\Omega}_3^{\mathrm{Spin}}(X)$ with $x_1 = 4x_2$, and hence $\widetilde{\Omega}_3^{\mathrm{Spin}}(X)$ would be $\mathbb{Z}/8$. That is, $\widetilde{\Omega}_3^{\mathrm{Spin}}(X)$ is isomorphic to either $\mathbb{Z}/8$, if the d_2 in question vanishes, or $\mathbb{Z}/4$, if that d_2 does not vanish. Lemma 4.249 says $\widetilde{\Omega}_3^{\mathrm{Spin}}(X)$ admits a surjective map to $\mathbb{Z}/8$, so $\mathbb{Z}/4$ does not work.

On to (2). Like in the above case with h_0, it is a general fact about the Adams spectral sequence that if $h_1\overline{x} = \overline{y}$, then one can choose preimages x and y in $\widetilde{\Omega}_*^{\mathrm{Spin}}(X)$ such that $\eta \cdot x = y$, where η is the generator of $\pi_1\mathbb{S} \cong \mathbb{Z}/2$. (Concretely, if x is the dpin bordism class of some manifold M, then $\eta \cdot x$ is the bordism class of $S^1 \times M$, where S^1 has the dpin structure induced from the nonbounding framing.)

If the extension in (4.251) did not split, then $\widetilde{\Omega}_2^{\mathrm{Spin}}(X)$ would be $\mathbb{Z}/4$ rather than $\mathbb{Z}/2 \oplus \mathbb{Z}/2$. However, we can rule this out: suppose it were $\mathbb{Z}/4$, and let x be a generator. Then the image of x in the associated graded of $\widetilde{\Omega}_2^{\mathrm{Spin}}(X)$ (i.e. the $t-s=2$ line of the Adams E_∞-page) is the nontrivial element of the yellow $\mathbb{Z}/2$ summand in bidegree $(2,0)$, and the image of $2x$ is the nonzero element of the orange $\mathbb{Z}/2$ summand in bidegree $(2,1)$. The h_1-action carries this to the nonzero element of the orange $\mathbb{Z}/2$ summand in bidegree $(3,2)$, so $\eta \cdot 2x \neq 0$. Since $2\eta = 0$, however, this is a contradiction, forcing $\widetilde{\Omega}_2^{\mathrm{Spin}}(X) \cong \mathbb{Z}/2 \oplus \mathbb{Z}/2$. □

There can be no more nontrivial differentials or hidden extensions in the range shown in (4.246), so we are done. □

Bibliography

[1] Z. Bern, J. Parra-Martinez, and E. Sawyer, "Nonrenormalization and Operator Mixing via On-Shell Methods", Phys. Rev. Lett. **124**, 051601 (2020), arXiv:1910.05831 [hep-ph].

[2] Z. Bern, J. Parra-Martinez, and E. Sawyer, "Structure of two-loop SMEFT anomalous dimensions via on-shell methods", (2020), arXiv:2005.12917 [hep-ph].

[3] Z. Bern, H. Ita, J. Parra-Martinez, and M. S. Ruf, "Universality in the classical limit of massless gravitational scattering", Phys. Rev. Lett. **125**, 031601 (2020), arXiv:2002.02459 [hep-th].

[4] J. Parra-Martinez, M. S. Ruf, and M. Zeng, "Extremal black hole scattering at $O(G^3)$: graviton dominance, eikonal exponentiation, and differential equations", (2020), arXiv:2005.04236 [hep-th].

[5] J. Kaidi, J. Parra-Martinez, and Y. Tachikawa, "Classification of String Theories via Topological Phases", Phys. Rev. Lett. **124**, 121601 (2020), arXiv:1908.04805 [hep-th].

[6] J. Kaidi, J. Parra-Martinez, and Y. Tachikawa, "Topological Superconductors on Superstring Worldsheets", SciPost Phys. **9**, 10 (2020), arXiv:1911.11780 [hep-th].

[7] Z. Bern, M. Enciso, J. Parra-Martinez, and M. Zeng, "Manifesting enhanced cancellations in supergravity: integrands versus integrals", JHEP **05**, 137 (2017), arXiv:1703.08927 [hep-th].

[8] Z. Bern, J. Parra-Martinez, and R. Roiban, "Canceling the U(1) Anomaly in the S Matrix of N=4 Supergravity", Phys. Rev. Lett. **121**, 101604 (2018), arXiv:1712.03928 [hep-th].

[9] Z. Bern, A. Edison, D. Kosower, and J. Parra-Martinez, "Curvature-squared multiplets, evanescent effects, and the U(1) anomaly in $N = 4$ supergravity", Phys. Rev. D **96**, 066004 (2017), arXiv:1706.01486 [hep-th].

[10] Z. Bern, J. J. Carrasco, W.-M. Chen, A. Edison, H. Johansson, J. Parra-Martinez, R. Roiban, and M. Zeng, "Ultraviolet Properties of $\mathcal{N} = 8$ Supergravity at Five Loops", Phys. Rev. D **98**, 086021 (2018), arXiv:1804.09311 [hep-th].

[11] J. Henn, E. Herrmann, and J. Parra-Martinez, "Bootstrapping two-loop Feynman integrals for planar $\mathcal{N} = 4$ sYM", JHEP **10**, 059 (2018), arXiv:1806.06072 [hep-th].

[12] Z. Bern, D. Kosower, and J. Parra-Martinez, "Two-loop n-point anomalous amplitudes in N=4 supergravity", Proc. Roy. Soc. Lond. A **A476**, 20190722 (2020), arXiv:1905.05151 [hep-th].

[13] A. Edison, E. Herrmann, J. Parra-Martinez, and J. Trnka, "Gravity loop integrands from the ultraviolet", (2019), arXiv:1909.02003 [hep-th].

[14] E. Herrmann and J. Parra-Martinez, "Logarithmic forms and differential equations for Feynman integrals", JHEP **02**, 099 (2020), arXiv:1909.04777 [hep-th].

[15] W. Buchmuller and D. Wyler, "Effective Lagrangian Analysis of New Interactions and Flavor Conservation", Nucl. Phys. **B268**, 621 (1986).

[16] B. Grzadkowski, M. Iskrzynski, M. Misiak, and J. Rosiek, "Dimension-Six Terms in the Standard Model Lagrangian", JHEP **10**, 085 (2010), arXiv:1008.4884 [hep-ph].

[17] I. Brivio and M. Trott, "The Standard Model as an Effective Field Theory", Phys. Rept. **793**, 1 (2019), arXiv:1706.08945 [hep-ph].

[18] C. Grojean, E. E. Jenkins, A. V. Manohar, and M. Trott, "Renormalization Group Scaling of Higgs Operators and $\Gamma(h \to \gamma\gamma)$", JHEP **04**, 016 (2013), arXiv:1301.2588 [hep-ph].

[19] E. E. Jenkins, A. V. Manohar, and M. Trott, "Renormalization Group Evolution of the Standard Model Dimension Six Operators I: Formalism and lambda Dependence", JHEP **10**, 087 (2013), arXiv:1308.2627 [hep-ph].

[20] E. E. Jenkins, A. V. Manohar, and M. Trott, "Renormalization Group Evolution of the Standard Model Dimension Six Operators II: Yukawa Dependence", JHEP **01**, 035 (2014), arXiv:1310.4838 [hep-ph].

[21] R. Alonso, E. E. Jenkins, A. V. Manohar, and M. Trott, "Renormalization Group Evolution of the Standard Model Dimension Six Operators III: Gauge Coupling Dependence and Phenomenology", JHEP **04**, 159 (2014), arXiv:1312.2014 [hep-ph].

[22] R. Alonso, E. E. Jenkins, and A. V. Manohar, "Holomorphy without Supersymmetry in the Standard Model Effective Field Theory", Phys. Lett. **B739**, 95 (2014), arXiv:1409.0868 [hep-ph].

[23] J. Elias-Miro, J. R. Espinosa, and A. Pomarol, "One-loop non-renormalization results in EFTs", Phys. Lett. **B747**, 272 (2015), arXiv:1412.7151 [hep-ph].

[24] C. Cheung and C.-H. Shen, "Nonrenormalization Theorems without Supersymmetry", Phys. Rev. Lett. **115**, 071601 (2015), arXiv:1505.01844 [hep-ph].

[25] M. L. Mangano and S. J. Parke, "Multiparton amplitudes in gauge theories", Phys. Rept. **200**, 301 (1991), arXiv:hep-th/0509223 [hep-th].

[26] B. Abbott et al. (LIGO Scientific, Virgo), "Observation of Gravitational Waves from a Binary Black Hole Merger", Phys. Rev. Lett. **116**, 061102 (2016), arXiv:1602.03837 [gr-qc].

[27] B. Abbott et al. (LIGO Scientific, Virgo), "GW170817: Observation of Gravitational Waves from a Binary Neutron Star Inspiral", Phys. Rev. Lett. **119**, 161101 (2017), arXiv:1710.05832 [gr-qc].

[28] J. M. Antelis and C. Moreno, "Obtaining gravitational waves from inspiral binary systems using LIGO data", Eur. Phys. J. Plus **132**, 10 (2017), arXiv:1610.03567 [astro-ph.IM].

[29] Y. Iwasaki, "Quantum theory of gravitation vs. classical theory. - fourth-order potential", Prog. Theor. Phys. **46**, 1587 (1971).

[30] Y. Iwasaki, "Fourth-order gravitational potential based on quantum field theory", Lett. Nuovo Cim. **1S2**, 783 (1971).

[31] H. Okamura, T. Ohta, T. Kimura, and K. Hiida, "Perturbation calculation of gravitational potentials", Prog. Theor. Phys. **50**, 2066 (1973).

[32] S. Gupta and S. Radford, "Improved Gravitational Coupling of Scalar Fields", Phys. Rev. D **19**, 1065 (1979).

[33] J. F. Donoghue, "General relativity as an effective field theory: The leading quantum corrections", Phys. Rev. D **50**, 3874 (1994), arXiv:gr-qc/9405057.

[34] B. R. Holstein and J. F. Donoghue, "Classical physics and quantum loops", Phys. Rev. Lett. **93**, 201602 (2004), arXiv:hep-th/0405239.

[35] D. Neill and I. Z. Rothstein, "Classical Space-Times from the S Matrix", Nucl. Phys. B **877**, 177 (2013), arXiv:1304.7263 [hep-th].

[36] V. Vaidya, "Gravitational spin Hamiltonians from the S matrix", Phys. Rev. D **91**, 024017 (2015), arXiv:1410.5348 [hep-th].

[37] N. Bjerrum-Bohr, J. F. Donoghue, and P. Vanhove, "On-shell Techniques and Universal Results in Quantum Gravity", JHEP **02**, 111 (2014), arXiv:1309.0804 [hep-th].

[38] N. J. Bjerrum-Bohr, P. H. Damgaard, G. Festuccia, L. Planté, and P. Vanhove, "General Relativity from Scattering Amplitudes", Phys. Rev. Lett. **121**, 171601 (2018), arXiv:1806.04920 [hep-th].

[39] C. Cheung, I. Z. Rothstein, and M. P. Solon, "From Scattering Amplitudes to Classical Potentials in the Post-Minkowskian Expansion", Phys. Rev. Lett. **121**, 251101 (2018), arXiv:1808.02489 [hep-th].

[40] D. A. Kosower, B. Maybee, and D. O'Connell, "Amplitudes, Observables, and Classical Scattering", JHEP **02**, 137 (2019), arXiv:1811.10950 [hep-th].

[41] Z. Bern, C. Cheung, R. Roiban, C.-H. Shen, M. P. Solon, and M. Zeng, "Scattering Amplitudes and the Conservative Hamiltonian for Binary Systems at Third Post-Minkowskian Order", Phys. Rev. Lett. **122**, 201603 (2019), arXiv:1901.04424 [hep-th].

[42] Z. Bern, C. Cheung, R. Roiban, C.-H. Shen, M. P. Solon, and M. Zeng, "Black Hole Binary Dynamics from the Double Copy and Effective Theory", JHEP **10**, 206 (2019), arXiv:1908.01493 [hep-th].

[43] Z. Bern, L. J. Dixon, D. C. Dunbar, and D. A. Kosower, "One loop n point gauge theory amplitudes, unitarity and collinear limits", Nucl. Phys. **B425**, 217 (1994), arXiv:hep-ph/9403226 [hep-ph].

[44] Z. Bern, L. J. Dixon, D. C. Dunbar, and D. A. Kosower, "Fusing gauge theory tree amplitudes into loop amplitudes", Nucl. Phys. **B435**, 59 (1995), arXiv:hep-ph/9409265 [hep-ph].

[45] Z. Bern, L. J. Dixon, and D. A. Kosower, "One loop amplitudes for e+ e- to four partons", Nucl. Phys. **B513**, 3 (1998), arXiv:hep-ph/9708239 [hep-ph].

[46] R. Britto, F. Cachazo, and B. Feng, "Generalized unitarity and one-loop amplitudes in N=4 super-Yang-Mills", Nucl. Phys. **B725**, 275 (2005), arXiv:hep-th/0412103 [hep-th].

[47] Z. Bern, J. Carrasco, H. Johansson, and D. Kosower, "Maximally supersymmetric planar Yang-Mills amplitudes at five loops", Phys. Rev. D **76**, 125020 (2007), arXiv:0705.1864 [hep-th].

[48] H. Kawai, D. Lewellen, and S. Tye, "A Relation Between Tree Amplitudes of Closed and Open Strings", Nucl. Phys. B **269**, 1 (1986).

[49] Z. Bern, L. J. Dixon, M. Perelstein, and J. Rozowsky, "Multileg one loop gravity amplitudes from gauge theory", Nucl. Phys. B **546**, 423 (1999), arXiv:hep-th/9811140.

[50] Z. Bern, J. Carrasco, and H. Johansson, "New Relations for Gauge-Theory Amplitudes", Phys. Rev. D **78**, 085011 (2008), arXiv:0805.3993 [hep-ph].

[51] Z. Bern, J. J. M. Carrasco, and H. Johansson, "Perturbative Quantum Gravity as a Double Copy of Gauge Theory", Phys. Rev. Lett. **105**, 061602 (2010), arXiv:1004.0476 [hep-th].

[52] Z. Bern, J. J. Carrasco, M. Chiodaroli, H. Johansson, and R. Roiban, "The Duality Between Color and Kinematics and its Applications", (2019), arXiv:1909.01358 [hep-th].

[53] P. D'Eath, "High Speed Black Hole Encounters and Gravitational Radiation", Phys. Rev. D **18**, 990 (1978).

[54] S. Kovacs and K. Thorne, "The Generation of Gravitational Waves. 3. Derivation of Bremsstrahlung Formulas", Astrophys. J. **217**, 252 (1977).

[55] S. Kovacs and K. Thorne, "The Generation of Gravitational Waves. 4. Bremsstrahlung", Astrophys. J. **224**, 62 (1978).

[56] D. Amati, M. Ciafaloni, and G. Veneziano, "Superstring Collisions at Planckian Energies", Phys. Lett. B **197**, 81 (1987).

[57] G. 't Hooft, "Graviton Dominance in Ultrahigh-Energy Scattering", Phys. Lett. B **198**, 61 (1987).

[58] D. Amati, M. Ciafaloni, and G. Veneziano, "Classical and Quantum Gravity Effects from Planckian Energy Superstring Collisions", Int. J. Mod. Phys. A **3**, 1615 (1988).

[59] I. Muzinich and M. Soldate, "High-Energy Unitarity of Gravitation and Strings", Phys. Rev. D **37**, 359 (1988).

[60] S. B. Giddings, M. Schmidt-Sommerfeld, and J. R. Andersen, "High energy scattering in gravity and supergravity", Phys. Rev. D **82**, 104022 (2010), arXiv:1005.5408 [hep-th].

[61] D. Amati, M. Ciafaloni, and G. Veneziano, "Higher Order Gravitational Deflection and Soft Bremsstrahlung in Planckian Energy Superstring Collisions", Nucl. Phys. B **347**, 550 (1990).

[62] T. Damour, "High-energy gravitational scattering and the general relativistic two-body problem", Phys. Rev. D **97**, 044038 (2018), arXiv:1710.10599 [gr-qc].

[63] A. Buonanno and T. Damour, "Effective one-body approach to general relativistic two-body dynamics", Phys. Rev. D **59**, 084006 (1999), arXiv:gr-qc/9811091.

[64] A. Buonanno and T. Damour, "Transition from inspiral to plunge in binary black hole coalescences", Phys. Rev. D **62**, 064015 (2000), arXiv:gr-qc/0001013.

[65] T. Damour, "Classical and quantum scattering in post-Minkowskian gravity", Phys. Rev. D **102**, 024060 (2020), arXiv:1912.02139 [gr-qc].

[66] Y. Mino, M. Sasaki, and T. Tanaka, "Gravitational radiation reaction to a particle motion", Phys. Rev. D **55**, 3457 (1997), arXiv:gr-qc/9606018.

[67] T. C. Quinn and R. M. Wald, "An Axiomatic approach to electromagnetic and gravitational radiation reaction of particles in curved space-time", Phys. Rev. D **56**, 3381 (1997), arXiv:gr-qc/9610053.

[68] E. Cremmer, B. Julia, and J. Scherk, "Supergravity Theory in Eleven-Dimensions", Phys. Lett. **76B**, 409 (1978).

[69] E. Cremmer and B. Julia, "The N=8 Supergravity Theory. 1. The Lagrangian", Phys. Lett. **80B**, 48 (1978).

[70] E. Cremmer and B. Julia, "The SO(8) Supergravity", Nucl. Phys. **B159**, 141 (1979).

[71] F. Gliozzi, J. Scherk, and D. I. Olive, "Supergravity and the Spinor Dual Model", Phys. Lett. **65B**, 282 (1976).

[72] F. Gliozzi, J. Scherk, and D. I. Olive, "Supersymmetry, Supergravity Theories and the Dual Spinor Model", Nucl. Phys. **B122**, 253 (1977).

[73] J. Polchinski, *String Theory. Vol. 2: Superstring Theory and Beyond*, Cambridge Monographs on Mathematical Physics (Cambridge University Press, 2007).

[74] N. Seiberg and E. Witten, "Spin Structures in String Theory", Nucl. Phys. **B276**, 272 (1986).

[75] A. Y. Kitaev, "Unpaired Majorana fermions in quantum wires", Phys. Usp. **44**, 131 (2001), arXiv:cond-mat/0010440 [cond-mat.mes-hall].

[76] D. S. Freed, "Short-Range Entanglement and Invertible Field Theories", (2014), arXiv:1406.7278 [cond-mat.str-el].

[77] D. S. Freed and M. J. Hopkins, "Reflection Positivity and Invertible Topological Phases", (2016), arXiv:1604.06527 [hep-th].

[78] A. Kapustin, R. Thorngren, A. Turzillo, and Z. Wang, "Fermionic Symmetry Protected Topological Phases and Cobordisms", JHEP **12**, 052 (2015), arXiv:1406.7329 [cond-mat.str-el].

[79] K. Yonekura, "On the Cobordism Classification of Symmetry Protected Topological Phases", Commun. Math. Phys. **368**, 1121 (2019), arXiv:1803.10796 [hep-th].

[80] L. Fidkowski and A. Kitaev, "The effects of interactions on the topological classification of free fermion systems", Phys. Rev. **B81**, 134509 (2010), arXiv:0904.2197 [cond-mat.str-el].

[81] E. Witten, "Fermion Path Integrals And Topological Phases", Rev. Mod. Phys. **88**, 035001 (2016), arXiv:1508.04715 [cond-mat.mes-hall].

[82] M. Bianchi and A. Sagnotti, "On the Systematics of Open String Theories", Phys. Lett. **B247**, 517 (1990).

[83] A. Sagnotti, "Some properties of open string theories", in Supersymmetry and unification of fundamental interactions. Proceedings, International Workshop, SUSY 95, Palaiseau, France, May 15-19, 1995 (1995), pp. 473–484, arXiv:hep-th/9509080 [hep-th].

[84] A. Sagnotti, "Surprises in open string perturbation theory", Nucl. Phys. Proc. Suppl. **56B**, 332 (1997), arXiv:hep-th/9702093 [hep-th].

[85] R. Blumenhagen, A. Font, and D. Lust, "Nonsupersymmetric gauge theories from D-branes in type 0 string theory", Nucl. Phys. **B560**, 66 (1999), arXiv:hep-th/9906101 [hep-th].

[86] R. Blumenhagen, A. Font, A. Kumar, and D. Lust, "Aspects of type 0 string theory", Class. Quant. Grav. **17**, 989 (2000), arXiv:hep-th/9908155 [hep-th].

[87] R. Blumenhagen and A. Kumar, "A Note on orientifolds and dualities of type 0B string theory", Phys. Lett. **B464**, 46 (1999), arXiv:hep-th/9906234 [hep-th].

[88] I. R. Klebanov, N. A. Nekrasov, and S. L. Shatashvili, "An Orbifold of type 0B strings and nonsupersymmetric gauge theories", Nucl. Phys. **B591**, 26 (2000), arXiv:hep-th/9909109 [hep-th].

[89] O. Bergman and M. R. Gaberdiel, "Dualities of type 0 strings", JHEP **07**, 022 (1999), arXiv:hep-th/9906055 [hep-th].

[90] J. Distler, D. S. Freed, and G. W. Moore, "Orientifold Precis", 159 (2009), arXiv:0906.0795 [hep-th].

[91] J. Distler, D. S. Freed, and G. W. Moore, "Spin Structures and Superstrings", (2010), arXiv:1007.4581 [hep-th].

[92] E. Witten, "D-branes and K theory", JHEP **12**, 019 (1998), arXiv:hep-th/9810188 [hep-th].

[93] P. Horava, "Type IIA D-branes, K theory, and matrix theory", Adv. Theor. Math. Phys. **2**, 1373 (1999), arXiv:hep-th/9812135 [hep-th].

[94] M. Karoubi, *K-Theory: an Introduction*, Classics in Mathematics (Springer Berlin Heidelberg, Berlin, Heidelberg, 2008).

[95] M. Jiang, J. Shu, M.-L. Xiao, and Y.-H. Zheng, "New Selection Rules from Angular Momentum Conservation", (2020), arXiv:2001.04481 [hep-ph].

[96] N. Craig, M. Jiang, Y.-Y. Li, and D. Sutherland, "Loops and Trees in Generic EFTs", (2019), arXiv:2001.00017 [hep-ph].

[97] Z. Bern and A. G. Morgan, "Massive loop amplitudes from unitarity", Nucl. Phys. **B467**, 479 (1996), arXiv:hep-ph/9511336 [hep-ph].

[98] S. Caron-Huot and M. Wilhelm, "Renormalization group coefficients and the S-matrix", JHEP **12**, 010 (2016), arXiv:1607.06448 [hep-th].

[99] B. I. Zwiebel, "From Scattering Amplitudes to the Dilatation Generator in N=4 SYM", J. Phys. A **45**, 115401 (2012), arXiv:1111.0083 [hep-th].

[100] M. Wilhelm, "Amplitudes, Form Factors and the Dilatation Operator in $\mathcal{N} = 4$ SYM Theory", JHEP **02**, 149 (2015), arXiv:1410.6309 [hep-th].

[101] C. Berger, Z. Bern, L. Dixon, F. Febres Cordero, D. Forde, H. Ita, D. Kosower, and D. Maitre, "An Automated Implementation of On-Shell Methods for One-Loop Amplitudes", Phys. Rev. D **78**, 036003 (2008), arXiv:0803.4180 [hep-ph].

[102] R. Ellis, K. Melnikov, and G. Zanderighi, "W+3 jet production at the Tevatron", Phys. Rev. D **80**, 094002 (2009), arXiv:0906.1445 [hep-ph].

[103] C. Berger, Z. Bern, L. J. Dixon, F. Febres Cordero, D. Forde, T. Gleisberg, H. Ita, D. Kosower, and D. Maitre, "Precise Predictions for W + 4 Jet Production at the Large Hadron Collider", Phys. Rev. Lett. **106**, 092001 (2011), arXiv:1009.2338 [hep-ph].

[104] Z. Bern, C. Cheung, H.-H. Chi, S. Davies, L. Dixon, and J. Nohle, "Evanescent Effects Can Alter Ultraviolet Divergences in Quantum Gravity without Physical Consequences", Phys. Rev. Lett. **115**, 211301 (2015), arXiv:1507.06118 [hep-th].

[105] Z. Bern, H.-H. Chi, L. Dixon, and A. Edison, "Two-Loop Renormalization of Quantum Gravity Simplified", Phys. Rev. **D95**, 046013 (2017), arXiv:1701.02422 [hep-th].

[106] S. Abreu, F. Febres Cordero, H. Ita, M. Jaquier, B. Page, M. Ruf, and V. Sotnikov, "The Two-Loop Four-Graviton Scattering Amplitudes", Phys. Rev. Lett. **124**, 211601 (2020), arXiv:2002.12374 [hep-th].

[107] N. Arkani-Hamed and J. Trnka, "The Amplituhedron", JHEP **10**, 030 (2014), arXiv:1312.2007 [hep-th].

[108] S. Caron-Huot, L. J. Dixon, F. Dulat, M. von Hippel, A. J. McLeod, and G. Papathanasiou, "Six-Gluon amplitudes in planar $\mathcal{N} = 4$ super-Yang-Mills theory at six and seven loops", JHEP **08**, 016 (2019), arXiv:1903.10890 [hep-th].

[109] J. L. Bourjaily, E. Herrmann, C. Langer, A. J. McLeod, and J. Trnka, "All-Multiplicity Nonplanar Amplitude Integrands in Maximally Supersymmetric Yang-Mills Theory at Two Loops", Phys. Rev. Lett. **124**, 111603 (2020), arXiv:1911.09106 [hep-th].

[110] S. Caron-Huot, L. J. Dixon, J. M. Drummond, F. Dulat, J. Foster, Ö. Gürdoğan, M. von Hippel, A. J. McLeod, and G. Papathanasiou, "The Steinmann Cluster Bootstrap for N=4 Super Yang-Mills Amplitudes", in 19th Hellenic School and Workshops on Elementary Particle Physics and Gravity (May 2020), arXiv:2005.06735 [hep-th].

[111] Z. Bern, J. Carrasco, L. Dixon, H. Johansson, and R. Roiban, "Simplifying Multiloop Integrands and Ultraviolet Divergences of Gauge Theory and Gravity Amplitudes", Phys. Rev. D **85**, 105014 (2012), arXiv:1201.5366 [hep-th].

[112] N. Arkani-Hamed, P. Benincasa, and A. Postnikov, "Cosmological Polytopes and the Wavefunction of the Universe", (2017), arXiv:1709.02813 [hep-th].

[113] N. Arkani-Hamed and P. Benincasa, "On the Emergence of Lorentz Invariance and Unitarity from the Scattering Facet of Cosmological Polytopes", (2018), arXiv:1811.01125 [hep-th].

[114] P. Benincasa, "From the flat-space S-matrix to the Wavefunction of the Universe", (2018), arXiv:1811.02515 [hep-th].

[115] P. Benincasa, "Cosmological Polytopes and the Wavefuncton of the Universe for Light States", (2019), arXiv:1909.02517 [hep-th].

[116] N. Arkani-Hamed, D. Baumann, H. Lee, and G. L. Pimentel, "The Cosmological Bootstrap: Inflationary Correlators from Symmetries and Singularities", JHEP **04**, 105 (2020), arXiv:1811.00024 [hep-th].

[117] D. Baumann, C. Duaso Pueyo, A. Joyce, H. Lee, and G. L. Pimentel, "The Cosmological Bootstrap: Weight-Shifting Operators and Scalar Seeds", (2019), arXiv:1910.14051 [hep-th].

[118] D. Baumann, C. Duaso Pueyo, A. Joyce, H. Lee, and G. L. Pimentel, "The Cosmological Bootstrap: Spinning Correlators from Symmetries and Factorization", (2020), arXiv:2005.04234 [hep-th].

[119] S. Caron-Huot and Z. Zahraee, "Integrability of Black Hole Orbits in Maximal Supergravity", JHEP **07**, 179 (2019), arXiv:1810.04694 [hep-th].

[120] Z. Bern, A. Luna, R. Roiban, C.-H. Shen, and M. Zeng, "Spinning Black Hole Binary Dynamics, Scattering Amplitudes and Effective Field Theory", (2020), arXiv:2005.03071 [hep-th].

[121] N. Arkani-Hamed, T.-C. Huang, and Y.-t. Huang, "Scattering Amplitudes For All Masses and Spins", (2017), arXiv:1709.04891 [hep-th].

[122] Y. Shadmi and Y. Weiss, "Effective Field Theory Amplitudes the On-Shell Way: Scalar and Vector Couplings to Gluons", JHEP **02**, 165 (2019), arXiv:1809.09644 [hep-ph].

[123] T. Ma, J. Shu, and M.-L. Xiao, "Standard Model Effective Field Theory from On-shell Amplitudes", (2019), arXiv:1902.06752 [hep-ph].

[124] G. Durieux, T. Kitahara, Y. Shadmi, and Y. Weiss, "The electroweak effective field theory from on-shell amplitudes", JHEP **01**, 119 (2020), arXiv:1909.10551 [hep-ph].

[125] B. Bachu and A. Yelleshpur, "On-Shell Electroweak Sector and the Higgs Mechanism", (2019), arXiv:1912.04334 [hep-th].

[126] A. Adams, N. Arkani-Hamed, S. Dubovsky, A. Nicolis, and R. Rattazzi, "Causality, analyticity and an IR obstruction to UV completion", JHEP **10**, 014 (2006), arXiv:hep-th/0602178.

[127] G. N. Remmen and N. L. Rodd, "Consistency of the Standard Model Effective Field Theory", JHEP **12**, 032 (2019), arXiv:1908.09845 [hep-ph].

[128] G. N. Remmen and N. L. Rodd, "Flavor Constraints from Unitarity and Analyticity", (2020), arXiv:2004.02885 [hep-ph].

[129] J. Elias Miró, J. Ingoldby, and M. Riembau, "EFT anomalous dimensions from the S-matrix", (2020), arXiv:2005.06983 [hep-ph].

[130] P. Baratella, C. Fernandez, and A. Pomarol, "Renormalization of Higher-Dimensional Operators from On-shell Amplitudes", (2020), arXiv:2005.07129 [hep-ph].

[131] M. Jiang, T. Ma, and J. Shu, "Renormalization Group Evolution from On-shell SMEFT", (2020), arXiv:2005.10261 [hep-ph].

[132] G. Ossola, C. G. Papadopoulos, and R. Pittau, "Reducing full one-loop amplitudes to scalar integrals at the integrand level", Nucl. Phys. B **763**, 147 (2007), arXiv:hep-ph/0609007.

[133] D. Forde, "Direct extraction of one-loop integral coefficients", Phys. Rev. D **75**, 125019 (2007), arXiv:0704.1835 [hep-ph].

[134] E. Glover and M. Tejeda-Yeomans, "Two loop QCD helicity amplitudes for massless quark massless gauge boson scattering", JHEP **06**, 033 (2003), arXiv:hep-ph/0304169.

[135] E. Glover, "Two loop QCD helicity amplitudes for massless quark quark scattering", JHEP **04**, 021 (2004), arXiv:hep-ph/0401119.

[136] A. Smirnov, "Algorithm FIRE – Feynman Integral REduction", JHEP **10**, 107 (2008), arXiv:0807.3243 [hep-ph].

[137] A. V. Smirnov, "FIRE5: a C++ implementation of Feynman Integral REduction", Comput. Phys. Commun. **189**, 182 (2015), arXiv:1408.2372 [hep-ph].

[138] A. Smirnov and F. Chuharev, "FIRE6: Feynman Integral REduction with Modular Arithmetic", 10.1016/j.cpc.2019.106877 (2019), arXiv:1901.07808 [hep-ph].

[139] M. E. Peskin and D. V. Schroeder, *An Introduction to quantum field theory* (Addison-Wesley, Reading, USA, 1995).

[140] L. J. Dixon, "Calculating scattering amplitudes efficiently", in Theoretical Advanced Study Institute in Elementary Particle Physics (TASI 95): QCD and Beyond (Jan. 1996), pp. 539–584, arXiv:hep-ph/9601359.

[141] H. Elvang and Y.-t. Huang, "Scattering Amplitudes", (2013), arXiv:1308.1697 [hep-th].

[142] Z. Bern, L. J. Dixon, and D. A. Kosower, "One loop corrections to two quark three gluon amplitudes", Nucl. Phys. B **437**, 259 (1995), arXiv:hep-ph/9409393.

[143] N. Arkani-Hamed, F. Cachazo, and J. Kaplan, "What is the Simplest Quantum Field Theory?", JHEP **09**, 016 (2010), arXiv:0808.1446 [hep-th].

[144] Y.-t. Huang, D. A. McGady, and C. Peng, "One-loop renormalization and the S-matrix", Phys. Rev. D **87**, 085028 (2013), arXiv:1205.5606 [hep-th].

[145] T. Becher and M. Neubert, "Infrared singularities of scattering amplitudes in perturbative QCD", Phys. Rev. Lett. **102**, 162001 (2009), arXiv:0901.0722 [hep-ph].

[146] J.-y. Chiu, A. Fuhrer, R. Kelley, and A. V. Manohar, "Factorization Structure of Gauge Theory Amplitudes and Application to Hard Scattering Processes at the LHC", Phys. Rev. **D80**, 094013 (2009), arXiv:0909.0012 [hep-ph].

[147] A. J. Buras and P. H. Weisz, "QCD Nonleading Corrections to Weak Decays in Dimensional Regularization and 't Hooft-Veltman Schemes", Nucl. Phys. B **333**, 66 (1990).

[148] I. Jack, D. Jones, and K. Roberts, "Equivalence of dimensional reduction and dimensional regularization", Z. Phys. C **63**, 151 (1994), arXiv:hep-ph/9401349.

[149] S. Herrlich and U. Nierste, "Evanescent operators, scheme dependences and double insertions", Nucl. Phys. B **455**, 39 (1995), arXiv:hep-ph/9412375.

[150] R. Harlander, P. Kant, L. Mihaila, and M. Steinhauser, "Dimensional Reduction applied to QCD at three loops", JHEP **09**, 053 (2006), arXiv:hep-ph/0607240.

[151] M. J. Dugan and B. Grinstein, "On the vanishing of evanescent operators", Phys. Lett. B **256**, 239 (1991).

[152] G. F. Sterman, "Mass Divergences in Annihilation Processes. 1. Origin and Nature of Divergences in Cut Vacuum Polarization Diagrams", Phys. Rev. **D17**, 2773 (1978).

[153] G. F. Sterman, "Mass Divergences in Annihilation Processes. 2. Cancellation of Divergences in Cut Vacuum Polarization Diagrams", Phys. Rev. **D17**, 2789 (1978).

[154] L. Magnea and G. F. Sterman, "Analytic continuation of the Sudakov form-factor in QCD", Phys. Rev. **D42**, 4222 (1990).

[155] W. T. Giele and E. W. N. Glover, "Higher order corrections to jet cross-sections in e+ e- annihilation", Phys. Rev. **D46**, 1980 (1992).

[156] Z. Kunszt, A. Signer, and Z. Trocsanyi, "Singular terms of helicity amplitudes at one loop in QCD and the soft limit of the cross-sections of multiparton processes", Nucl. Phys. **B420**, 550 (1994), arXiv:hep-ph/9401294 [hep-ph].

[157] S. Catani, "The Singular behavior of QCD amplitudes at two loop order", Phys. Lett. **B427**, 161 (1998), arXiv:hep-ph/9802439 [hep-ph].

[158] L. J. Dixon and Y. Shadmi, "Testing gluon selfinteractions in three jet events at hadron colliders", Nucl. Phys. B **423**, 3 (1994), arXiv:hep-ph/9312363.

[159] A. Azatov, R. Contino, C. S. Machado, and F. Riva, "Helicity selection rules and noninterference for BSM amplitudes", Phys. Rev. D **95**, 065014 (2017), arXiv:1607.05236 [hep-ph].

[160] A. Helset and M. Trott, "On interference and non-interference in the SMEFT", JHEP **04**, 038 (2018), arXiv:1711.07954 [hep-ph].

[161] A. Brandhuber, M. Kostacinska, B. Penante, G. Travaglini, and D. Young, "The SU(2—3) dynamic two-loop form factors", JHEP **08**, 134 (2016), arXiv:1606.08682 [hep-th].

[162] A. Brandhuber, M. Kostacinska, B. Penante, and G. Travaglini, "Higgs amplitudes from $\mathcal{N} = 4$ super Yang-Mills theory", Phys. Rev. Lett. **119**, 161601 (2017), arXiv:1707.09897 [hep-th].

[163] A. Brandhuber, M. Kostacinska, B. Penante, and G. Travaglini, "Tr(F^3) supersymmetric form factors and maximal transcendentality Part I: $\mathcal{N} = 4$ super Yang-Mills", JHEP **12**, 076 (2018), arXiv:1804.05703 [hep-th].

[164] A. Brandhuber, M. Kostacinska, B. Penante, and G. Travaglini, "Tr(F^3) supersymmetric form factors and maximal transcendentality Part II: $0 < mathcalN < 4$ super Yang-Mills", JHEP **12**, 077 (2018), arXiv:1804.05828 [hep-th].

[165] G. F. Sterman, *An Introduction to quantum field theory* (Cambridge University Press, Aug. 1993).

[166] Z. Bern, L. J. Dixon, and D. A. Kosower, "On-Shell Methods in Perturbative QCD", Annals Phys. **322**, 1587 (2007), arXiv:0704.2798 [hep-ph].

[167] Z. Bern and Y.-t. Huang, "Basics of Generalized Unitarity", J. Phys. A **44**, 454003 (2011), arXiv:1103.1869 [hep-th].

[168] H. Ita, "Susy Theories and QCD: Numerical Approaches", J. Phys. A **44**, 454005 (2011), arXiv:1109.6527 [hep-th].

[169] L. J. Dixon, "A brief introduction to modern amplitude methods", in Theoretical Advanced Study Institute in Elementary Particle Physics: Particle Physics: The Higgs Boson and Beyond (2014), pp. 31–67, arXiv:1310.5353 [hep-ph].

[170] F. A. Berends, R. Kleiss, P. De Causmaecker, R. Gastmans, and T. T. Wu, "Single Bremsstrahlung Processes in Gauge Theories", Phys. Lett. B **103**, 124 (1981).

[171] F. A. Berends, R. Kleiss, P. De Causmaecker, R. Gastmans, W. Troost, and T. T. Wu, "Multiple Bremsstrahlung in Gauge Theories at High-Energies. 2. Single Bremsstrahlung", Nucl. Phys. B **206**, 61 (1982).

[172] Z. Xu, D.-H. Zhang, and L. Chang, "Helicity Amplitudes for Multiple Bremsstrahlung in Massless Nonabelian Gauge Theories", Nucl. Phys. B **291**, 392 (1987).

[173] Z. Bern, A. De Freitas, and L. J. Dixon, "Two loop helicity amplitudes for gluon-gluon scattering in QCD and supersymmetric Yang-Mills theory", JHEP **03**, 018 (2002), arXiv:hep-ph/0201161.

[174] J. C. Collins, A. V. Manohar, and M. B. Wise, "Renormalization of the vector current in QED", Phys. Rev. D **73**, 105019 (2006), arXiv:hep-th/0512187.

[175] H. Politzer, "Asymptotic Freedom: An Approach to Strong Interactions", Phys. Rept. **14**, 129 (1974).

[176] Y.-t. Huang, O. Schlotterer, and C. Wen, "Universality in string interactions", JHEP **09**, 155 (2016), arXiv:1602.01674 [hep-th].

[177] Z. Bern and D. A. Kosower, "The Computation of loop amplitudes in gauge theories", Nucl. Phys. B **379**, 451 (1992).

[178] Z. Kunszt, A. Signer, and Z. Trocsanyi, "One loop helicity amplitudes for all 2 —¿ 2 processes in QCD and N=1 supersymmetric Yang-Mills theory", Nucl. Phys. B **411**, 397 (1994), arXiv:hep-ph/9305239.

[179] B. Bertotti, "On gravitational motion", Nuovo Cim. **4**, 898 (1956).

[180] R. Kerr, "The Lorentz-covariant approximation method in general relativity I", Nuovo Cim. **13**, 469 (1959).

[181] B. Bertotti and J. Plebanski, "Theory of gravitational perturbations in the fast motion approximation", Annals Phys. **11**, 169 (1960).

[182] M. Portilla, "Momentum and Angular Momentum of Two Gravitating Particles", J. Phys. A **12**, 1075 (1979).

[183] K. Westpfahl and M. Goller, "Gravitational Scattering of Two Relativistic Particles in Postlinear Approximation", Lett. Nuovo Cim. **26**, 573 (1979).

[184] M. Portilla, "Scattering of Two Gravitating Particles: Classical Approach", J. Phys. A **13**, 3677 (1980).

[185] L. Bel, T. Damour, N. Deruelle, J. Ibanez, and J. Martin, "Poincaré-invariant gravitational field and equations of motion of two pointlike objects: The postlinear approximation of general relativity", Gen. Rel. Grav. **13**, 963 (1981).

[186] K. Westpfahl, "High-Speed Scattering of Charged and Uncharged Particles in General Relativity", Fortsch. Phys. **33**, 417 (1985).

[187] T. Ledvinka, G. Schaefer, and J. Bicak, "Relativistic Closed-Form Hamiltonian for Many-Body Gravitating Systems in the Post-Minkowskian Approximation", Phys. Rev. Lett. **100**, 251101 (2008), arXiv:0807.0214 [gr-qc].

[188] T. Damour, "Gravitational scattering, post-Minkowskian approximation and Effective One-Body theory", Phys. Rev. D **94**, 104015 (2016), arXiv:1609.00354 [gr-qc].

[189] B. Maybee, D. O'Connell, and J. Vines, "Observables and amplitudes for spinning particles and black holes", JHEP **12**, 156 (2019), arXiv:1906.09260 [hep-th].

[190] A. Antonelli, A. Buonanno, J. Steinhoff, M. van de Meent, and J. Vines, "Energetics of two-body Hamiltonians in post-Minkowskian gravity", Phys. Rev. **D99**, 104004 (2019), arXiv:1901.07102 [gr-qc].

[191] A. Koemans Collado and S. Thomas, "Eikonal Scattering in Kaluza-Klein Gravity", JHEP **04**, 171 (2019), arXiv:1901.05869 [hep-th].

[192] A. Cristofoli, P. H. Damgaard, P. Di Vecchia, and C. Heissenberg, "Second-order Post-Minkowskian scattering in arbitrary dimensions", JHEP **07**, 122 (2020), arXiv:2003.10274 [hep-th].

[193] R. J. Glauber, in *Lectures in theoretical physics*, edited by W. E. Brittin and L. G. Dunham (Interscience Publishers, Inc., New York, 1959), pp. 315–414.

[194] M. Levy and J. Sucher, "Eikonal approximation in quantum field theory", Phys. Rev. **186**, 1656 (1969).

[195] M. Soldate, "Partial Wave Unitarity and Closed String Amplitudes", Phys. Lett. **B186**, 321 (1987).

[196] D. N. Kabat and M. Ortiz, "Eikonal quantum gravity and Planckian scattering", Nucl. Phys. **B388**, 570 (1992), arXiv:hep-th/9203082 [hep-th].

[197] D. Amati, M. Ciafaloni, and G. Veneziano, "Towards an S-matrix description of gravitational collapse", JHEP **02**, 049 (2008), arXiv:0712.1209 [hep-th].

[198] E. Laenen, G. Stavenga, and C. D. White, "Path integral approach to eikonal and next-to-eikonal exponentiation", JHEP **03**, 054 (2009), arXiv:0811.2067 [hep-ph].

[199] S. Melville, S. Naculich, H. Schnitzer, and C. White, "Wilson line approach to gravity in the high energy limit", Phys. Rev. D **89**, 025009 (2014), arXiv:1306.6019 [hep-th].

[200] R. Akhoury, R. Saotome, and G. Sterman, "High Energy Scattering in Perturbative Quantum Gravity at Next to Leading Power", (2013), arXiv:1308.5204 [hep-th].

[201] P. Di Vecchia, A. Luna, S. G. Naculich, R. Russo, G. Veneziano, and C. D. White, "A tale of two exponentiations in $\mathcal{N} = 8$ supergravity", Phys. Lett. B **798**, 134927 (2019), arXiv:1908.05603 [hep-th].

[202] P. Di Vecchia, S. G. Naculich, R. Russo, G. Veneziano, and C. D. White, "A tale of two exponentiations in $\mathcal{N} = 8$ supergravity at subleading level", JHEP **03**, 173 (2020), arXiv:1911.11716 [hep-th].

[203] M. Kulaxizi, G. S. Ng, and A. Parnachev, "Subleading Eikonal, AdS/CFT and Double Stress Tensors", JHEP **10**, 107 (2019), arXiv:1907.00867 [hep-th].

[204] A. Koemans Collado, P. Di Vecchia, and R. Russo, "Revisiting the second post-Minkowskian eikonal and the dynamics of binary black holes", Phys. Rev. D **100**, 066028 (2019), arXiv:1904.02667 [hep-th].

[205] J. Blümlein, A. Maier, P. Marquard, and G. Schäfer, "Testing binary dynamics in gravity at the sixth post-Newtonian level", Phys. Lett. B **807**, 135496 (2020), arXiv:2003.07145 [gr-qc].

[206] D. Bini, T. Damour, and A. Geralico, "Binary dynamics at the fifth and fifth-and-a-half post-Newtonian orders", Phys. Rev. **D102**, 024062 (2020), arXiv:2003.11891 [gr-qc].

[207] J. Blümlein, A. Maier, P. Marquard, G. Schäfer, and C. Schneider, "From Momentum Expansions to Post-Minkowskian Hamiltonians by Computer Algebra Algorithms", Phys. Lett. **B801**, 135157 (2020), arXiv:1911.04411 [gr-qc].

[208] C. Cheung and M. P. Solon, "Classical gravitational scattering at $\mathcal{O}(\mathrm{G}^3)$ from Feynman diagrams", JHEP **06**, 144 (2020), arXiv:2003.08351 [hep-th].

[209] Z. Bern, L. J. Dixon, D. Dunbar, M. Perelstein, and J. Rozowsky, "On the relationship between Yang-Mills theory and gravity and its implication for ultraviolet divergences", Nucl. Phys. B **530**, 401 (1998), arXiv:hep-th/9802162 [hep-th].

[210] S. G. Naculich, H. Nastase, and H. J. Schnitzer, "Two-loop graviton scattering relation and IR behavior in N=8 supergravity", Nucl. Phys. B **805**, 40 (2008), arXiv:0805.2347 [hep-th].

[211] A. Brandhuber, P. Heslop, A. Nasti, B. Spence, and G. Travaglini, "Four-point Amplitudes in N=8 Supergravity and Wilson Loops", Nucl. Phys. B **807**, 290 (2009), arXiv:0805.2763 [hep-th].

[212] C. Boucher-Veronneau and L. Dixon, "N ¿- 4 Supergravity Amplitudes from Gauge Theory at Two Loops", JHEP **12**, 046 (2011), arXiv:1110.1132 [hep-th].

[213] H. Ita, "Two-loop Integrand Decomposition into Master Integrals and Surface Terms", Phys. Rev. D **94**, 116015 (2016), arXiv:1510.05626 [hep-th].

[214] S. Abreu, F. Febres Cordero, H. Ita, M. Jaquier, B. Page, and M. Zeng, "Two-Loop Four-Gluon Amplitudes from Numerical Unitarity", Phys. Rev. Lett. **119**, 142001 (2017), arXiv:1703.05273 [hep-ph].

[215] M. Ciafaloni and D. Colferai, "Rescattering corrections and self-consistent metric in Planckian scattering", JHEP **10**, 085 (2014), arXiv:1406.6540 [hep-th].

[216] J. M. Henn and B. Mistlberger, "Four-graviton scattering to three loops in $\mathcal{N} = 8$ supergravity", JHEP **05**, 023 (2019), arXiv:1902.07221 [hep-th].

[217] A. Bellini, M. Ademollo, and M. Ciafaloni, "Superstring one loop and gravitino contributions to Planckian scattering", Nucl. Phys. B **393**, 79 (1993), arXiv:hep-th/9207113.

[218] M. B. Green, J. H. Schwarz, and L. Brink, "N=4 Yang-Mills and N=8 Supergravity as Limits of String Theories", Nucl. Phys. **B198**, 474 (1982).

[219] Z. Bern, J. J. Carrasco, L. J. Dixon, H. Johansson, D. A. Kosower, and R. Roiban, "Three-Loop Superfiniteness of N=8 Supergravity", Phys. Rev. Lett. **98**, 161303 (2007), arXiv:hep-th/0702112 [hep-th].

[220] Z. Bern, J. J. M. Carrasco, L. J. Dixon, H. Johansson, and R. Roiban, "Manifest Ultraviolet Behavior for the Three-Loop Four-Point Amplitude of N=8 Supergravity", Phys. Rev. **D78**, 105019 (2008), arXiv:0808.4112 [hep-th].

[221] Z. Bern, J. J. Carrasco, L. J. Dixon, H. Johansson, and R. Roiban, "The Ultraviolet Behavior of N=8 Supergravity at Four Loops", Phys. Rev. Lett. **103**, 081301 (2009), arXiv:0905.2326 [hep-th].

[222] Z. Bern, J. J. M. Carrasco, W.-M. Chen, H. Johansson, R. Roiban, and M. Zeng, "Five-loop four-point integrand of $N = 8$ supergravity as a generalized double copy", Phys. Rev. **D96**, 126012 (2017), arXiv:1708.06807 [hep-th].

[223] Z. Bern, L. J. Dixon, and D. A. Kosower, "Two-loop $g \to gg$ splitting amplitudes in QCD", JHEP **08**, 012 (2004), arXiv:hep-ph/0404293 [hep-ph].

[224] Z. Bern, J. J. Carrasco, W.-M. Chen, H. Johansson, and R. Roiban, "Gravity Amplitudes as Generalized Double Copies of Gauge-Theory Amplitudes", Phys. Rev. Lett. **118**, 181602 (2017), arXiv:1701.02519 [hep-th].

[225] M. Beneke and V. A. Smirnov, "Asymptotic expansion of Feynman integrals near threshold", Nucl. Phys. **B522**, 321 (1998), arXiv:hep-ph/9711391 [hep-ph].

[226] A. V. Kotikov, "Differential equations method: New technique for massive Feynman diagrams calculation", Phys. Lett. **B254**, 158 (1991).

[227] Z. Bern, L. J. Dixon, and D. A. Kosower, "Dimensionally regulated pentagon integrals", Nucl. Phys. **B412**, 751 (1994), arXiv:hep-ph/9306240 [hep-ph].

[228] E. Remiddi, "Differential equations for Feynman graph amplitudes", Nuovo Cim. **A110**, 1435 (1997), arXiv:hep-th/9711188 [hep-th].

[229] T. Gehrmann and E. Remiddi, "Differential equations for two loop four point functions", Nucl. Phys. **B580**, 485 (2000), arXiv:hep-ph/9912329 [hep-ph].

[230] J. M. Henn, "Multiloop integrals in dimensional regularization made simple", Phys. Rev. Lett. **110**, 251601 (2013), arXiv:1304.1806 [hep-th].

[231] J. M. Henn, "Lectures on differential equations for Feynman integrals", J. Phys. **A48**, 153001 (2015), arXiv:1412.2296 [hep-ph].

[232] J. Ablinger, J. Blümlein, P. Marquard, N. Rana, and C. Schneider, "Automated Solution of First Order Factorizable Systems of Differential Equations in One Variable", Nucl. Phys. **B939**, 253 (2019), arXiv:1810.12261 [hep-ph].

[233] Z. Bern, N. E. J. Bjerrum-Bohr, and D. C. Dunbar, "Inherited twistor-space structure of gravity loop amplitudes", JHEP **05**, 056 (2005), arXiv:hep-th/0501137 [hep-th].

[234] N. E. J. Bjerrum-Bohr, D. C. Dunbar, and H. Ita, "Six-point one-loop N=8 supergravity NMHV amplitudes and their ir behaviour", Phys. Lett. **B621**, 183 (2005), arXiv:hep-th/0503102 [hep-th].

[235] N. E. J. Bjerrum-Bohr, D. C. Dunbar, H. Ita, W. B. Perkins, and K. Risager, "The No-Triangle Hypothesis for N=8 Supergravity", JHEP **12**, 072 (2006), arXiv:hep-th/0610043 [hep-th].

[236] Z. Bern, L. J. Dixon, and R. Roiban, "Is N = 8 supergravity ultraviolet finite?", Phys. Lett. **B644**, 265 (2007), arXiv:hep-th/0611086 [hep-th].

[237] Z. Bern, J. J. Carrasco, D. Forde, H. Ita, and H. Johansson, "Unexpected Cancellations in Gravity Theories", Phys. Rev. **D77**, 025010 (2008), arXiv:0707.1035 [hep-th].

[238] N. E. J. Bjerrum-Bohr and P. Vanhove, "Explicit Cancellation of Triangles in One-loop Gravity Amplitudes", JHEP **04**, 065 (2008), arXiv:0802.0868 [hep-th].

[239] G. Kälin and R. A. Porto, "From Boundary Data to Bound States", JHEP **01**, 072 (2020), arXiv:1910.03008 [hep-th].

[240] G. Kälin and R. A. Porto, "From boundary data to bound states. Part II. Scattering angle to dynamical invariants (with twist)", JHEP **02**, 120 (2020), arXiv:1911.09130 [hep-th].

[241] S. Weinberg, "Infrared photons and gravitons", Phys. Rev. **140**, B516 (1965).

[242] S. G. Naculich and H. J. Schnitzer, "Eikonal methods applied to gravitational scattering amplitudes", JHEP **05**, 087 (2011), arXiv:1101.1524 [hep-th].

[243] D. C. Dunbar and P. S. Norridge, "Calculation of graviton scattering amplitudes using string based methods", Nucl. Phys. B **433**, 181 (1995), arXiv:hep-th/9408014.

[244] Z. Bern, C. Cheung, H.-H. Chi, S. Davies, L. Dixon, and J. Nohle.

[245] Z. Bern, C. Boucher-Veronneau, and H. Johansson, "N ¿= 4 Supergravity Amplitudes from Gauge Theory at One Loop", Phys. Rev. D **84**, 105035 (2011), arXiv:1107.1935 [hep-th].

[246] G. 't Hooft and M. Veltman, "One loop divergencies in the theory of gravitation", Ann. Inst. H. Poincare Phys. Theor. A **20**, 69 (1974).

[247] M. H. Goroff and A. Sagnotti, "The Ultraviolet Behavior of Einstein Gravity", Nucl. Phys. B **266**, 709 (1986).

[248] A. van de Ven, "Two loop quantum gravity", Nucl. Phys. B **378**, 309 (1992).

[249] V. A. Smirnov, "Analytical result for dimensionally regularized massless on shell double box", Phys. Lett. B **460**, 397 (1999), arXiv:hep-ph/9905323.

[250] J. Tausk, "Nonplanar massless two loop Feynman diagrams with four on-shell legs", Phys. Lett. B **469**, 225 (1999), arXiv:hep-ph/9909506.

[251] N. Bjerrum-Bohr, J. F. Donoghue, B. R. Holstein, L. Planté, and P. Vanhove, "Bending of Light in Quantum Gravity", Phys. Rev. Lett. **114**, 061301 (2015), arXiv:1410.7590 [hep-th].

[252] N. Bjerrum-Bohr, J. F. Donoghue, B. R. Holstein, L. Plante, and P. Vanhove, "Light-like Scattering in Quantum Gravity", JHEP **11**, 117 (2016), arXiv:1609.07477 [hep-th].

[253] D. Bai and Y. Huang, "More on the Bending of Light in Quantum Gravity", Phys. Rev. D **95**, 064045 (2017), arXiv:1612.07629 [hep-th].

[254] H.-H. Chi, "Graviton Bending in Quantum Gravity from One-Loop Amplitudes", Phys. Rev. D **99**, 126008 (2019), arXiv:1903.07944 [hep-th].

[255] M. T. Grisaru, H. Pendleton, and P. van Nieuwenhuizen, "Supergravity and the S Matrix", Phys. Rev. D **15**, 996 (1977).

[256] M. T. Grisaru and H. Pendleton, "Some Properties of Scattering Amplitudes in Supersymmetric Theories", Nucl. Phys. B **124**, 81 (1977).

[257] L. Andrianopoli, R. D'Auria, S. Ferrara, P. Fre, and M. Trigiante, "E(7)(7) duality, BPS black hole evolution and fixed scalars", Nucl. Phys. **B509**, 463 (1998), arXiv:hep-th/9707087 [hep-th].

[258] G. Arcioni, A. Ceresole, F. Cordaro, R. D'Auria, P. Fre, L. Gualtieri, and M. Trigiante, "N=8 BPS black holes with 1/2 or 1/4 supersymmetry and solvable Lie algebra decompositions", Nucl. Phys. **B542**, 273 (1999), arXiv:hep-th/9807136 [hep-th].

[259] M. B. Green, J. H. Schwarz, and E. Witten, *Superstring Theory. Vol. 2: Loop Amplitudes, Anomalies And Phenomenology* (1988).

[260] V. P. Nair, "A Current Algebra for Some Gauge Theory Amplitudes", Phys. Lett. **B214**, 215 (1988).

[261] W. Beenakker and A. Denner, "Infrared Divergent Scalar Box Integrals With Applications in the Electroweak Standard Model", Nucl. Phys. **B338**, 349 (1990).

[262] R. Akhoury, R. Saotome, and G. Sterman, "Collinear and Soft Divergences in Perturbative Quantum Gravity", Phys. Rev. **D84**, 104040 (2011), arXiv:1109.0270 [hep-th].

[263] V. A. Smirnov, "Evaluating Feynman integrals", Springer Tracts Mod. Phys. **211**, 1 (2004).

[264] W. D. Goldberger and I. Z. Rothstein, "An Effective field theory of gravity for extended objects", Phys. Rev. **D73**, 104029 (2006), arXiv:hep-th/0409156 [hep-th].

[265] J. B. Gilmore and A. Ross, "Effective field theory calculation of second post-Newtonian binary dynamics", Phys. Rev. **D78**, 124021 (2008), arXiv:0810.1328 [gr-qc].

[266] K. G. Chetyrkin and F. V. Tkachov, "Integration by Parts: The Algorithm to Calculate beta Functions in 4 Loops", Nucl. Phys. **B192**, 159 (1981).

[267] M. Prausa, "epsilon: A tool to find a canonical basis of master integrals", Comput. Phys. Commun. **219**, 361 (2017), arXiv:1701.00725 [hep-ph].

[268] O. Gituliar and V. Magerya, "Fuchsia: a tool for reducing differential equations for Feynman master integrals to epsilon form", Comput. Phys. Commun. **219**, 329 (2017), arXiv:1701.04269 [hep-ph].

[269] P. V. Landshoff and J. C. Polkinghorne, "Iterations of regge cuts", Phys. Rev. **181**, 1989 (1969).

[270] S. Laporta, "High precision calculation of multiloop Feynman integrals by difference equations", Int. J. Mod. Phys. **A15**, 5087 (2000), arXiv:hep-ph/0102033 [hep-ph].

[271] S. Laporta and E. Remiddi, "The Analytical value of the electron $(g-2)$ at order α^3 in QED", Phys. Lett. **B379**, 283 (1996), arXiv:hep-ph/9602417 [hep-ph].

[272] A. B. Goncharov, "Multiple polylogarithms and mixed Tate motives", (2001), arXiv:math/0103059 [math.AG].

[273] A. B. Goncharov, M. Spradlin, C. Vergu, and A. Volovich, "Classical Polylogarithms for Amplitudes and Wilson Loops", Phys. Rev. Lett. **105**, 151605 (2010), arXiv:1006.5703 [hep-th].

[274] C. Duhr, "Hopf algebras, coproducts and symbols: an application to Higgs boson amplitudes", JHEP **08**, 043 (2012), arXiv:1203.0454 [hep-ph].

[275] S. Caron-Huot and J. M. Henn, "Iterative structure of finite loop integrals", JHEP **06**, 114 (2014), arXiv:1404.2922 [hep-th].

[276] D. A. Kosower and K. J. Larsen, "Maximal Unitarity at Two Loops", Phys. Rev. **D85**, 045017 (2012), arXiv:1108.1180 [hep-th].

[277] S. Caron-Huot and K. J. Larsen, "Uniqueness of two-loop master contours", JHEP **10**, 026 (2012), arXiv:1205.0801 [hep-ph].

[278] S. Abreu, R. Britto, C. Duhr, and E. Gardi, "Cuts from residues: the one-loop case", JHEP **06**, 114 (2017), arXiv:1702.03163 [hep-th].

[279] J. Bosma, M. Sogaard, and Y. Zhang, "Maximal Cuts in Arbitrary Dimension", JHEP **08**, 051 (2017), arXiv:1704.04255 [hep-th].

[280] M. Sogaard and Y. Zhang, "Unitarity Cuts of Integrals with Doubled Propagators", JHEP **07**, 112 (2014), arXiv:1403.2463 [hep-th].

[281] A. Primo and L. Tancredi, "On the maximal cut of Feynman integrals and the solution of their differential equations", Nucl. Phys. **B916**, 94 (2017), arXiv:1610.08397 [hep-ph].

[282] V. A. Smirnov, "Analytic tools for Feynman integrals", Springer Tracts Mod. Phys. **250**, 1 (2012).

[283] V. A. Smirnov, "Analytical result for dimensionally regularized massive on-shell planar double box", Phys. Lett. **B524**, 129 (2002), arXiv:hep-ph/0111160 [hep-ph].

[284] J. M. Henn and V. A. Smirnov, "Analytic results for two-loop master integrals for Bhabha scattering I", JHEP **11**, 041 (2013), arXiv:1307.4083 [hep-th].

[285] E. Remiddi and J. A. M. Vermaseren, "Harmonic polylogarithms", Int. J. Mod. Phys. **A15**, 725 (2000), arXiv:hep-ph/9905237 [hep-ph].

[286] T. Gehrmann and E. Remiddi, "Numerical evaluation of harmonic polylogarithms", Comput. Phys. Commun. **141**, 296 (2001), arXiv:hep-ph/0107173 [hep-ph].

[287] M. S. Bianchi and M. Leoni, "A $QQ \to QQ$ planar double box in canonical form", Phys. Lett. **B777**, 394 (2018), arXiv:1612.05609 [hep-ph].

[288] G. Heinrich and V. A. Smirnov, "Analytical evaluation of dimensionally regularized massive on-shell double boxes", Phys. Lett. **B598**, 55 (2004), arXiv:hep-ph/0406053 [hep-ph].

[289] I. Z. Rothstein and I. W. Stewart, "An Effective Field Theory for Forward Scattering and Factorization Violation", JHEP **08**, 025 (2016), arXiv:1601.04695 [hep-ph].

[290] S. Abreu, F. Febres Cordero, H. Ita, B. Page, and M. Zeng, "Planar Two-Loop Five-Gluon Amplitudes from Numerical Unitarity", Phys. Rev. D **97**, 116014 (2018), arXiv:1712.03946 [hep-ph].

[291] S. Abreu, J. Dormans, F. Febres Cordero, H. Ita, and B. Page, "Analytic Form of Planar Two-Loop Five-Gluon Scattering Amplitudes in QCD", Phys. Rev. Lett. **122**, 082002 (2019), arXiv:1812.04586 [hep-ph].

[292] M. Levi, A. J. Mcleod, and M. Von Hippel, "N^{3}LO gravitational spin-orbit coupling at order G^4", (2020), arXiv:2003.02827 [hep-th].

[293] M. Levi, A. J. Mcleod, and M. Von Hippel, "NNNLO gravitational quadratic-in-spin interactions at the quartic order in G", (2020), arXiv:2003.07890 [hep-th].

[294] J. Vines, "Scattering of two spinning black holes in post-Minkowskian gravity, to all orders in spin, and effective-one-body mappings", Class. Quant. Grav. **35**, 084002 (2018), arXiv:1709.06016 [gr-qc].

[295] J. Vines, J. Steinhoff, and A. Buonanno, "Spinning-black-hole scattering and the test-black-hole limit at second post-Minkowskian order", Phys. Rev. **D99**, 064054 (2019), arXiv:1812.00956 [gr-qc].

[296] A. Guevara, A. Ochirov, and J. Vines, "Scattering of Spinning Black Holes from Exponentiated Soft Factors", JHEP **09**, 056 (2019), arXiv:1812.06895 [hep-th].

[297] M.-Z. Chung, Y.-T. Huang, J.-W. Kim, and S. Lee, "The simplest massive S-matrix: from minimal coupling to Black Holes", JHEP **04**, 156 (2019), arXiv:1812.08752 [hep-th].

[298] A. Guevara, A. Ochirov, and J. Vines, "Black-hole scattering with general spin directions from minimal-coupling amplitudes", Phys. Rev. **D100**, 104024 (2019), arXiv:1906.10071 [hep-th].

[299] N. Arkani-Hamed, Y.-t. Huang, and D. O'Connell, "Kerr black holes as elementary particles", JHEP **01**, 046 (2020), arXiv:1906.10100 [hep-th].

[300] P. H. Damgaard, K. Haddad, and A. Helset, "Heavy Black Hole Effective Theory", JHEP **11**, 070 (2019), arXiv:1908.10308 [hep-ph].

[301] N. Siemonsen and J. Vines, "Test black holes, scattering amplitudes and perturbations of Kerr spacetime", Phys. Rev. **D101**, 064066 (2020), arXiv:1909.07361 [gr-qc].

[302] R. Aoude, K. Haddad, and A. Helset, "On-shell heavy particle effective theories", JHEP **05**, 051 (2020), arXiv:2001.09164 [hep-th].

[303] A. Neveu and J. H. Schwarz, "Factorizable Dual Model of Pions", Nucl. Phys. **B31**, 86 (1971).

[304] P. Ramond, "Dual Theory for Free Fermions", Phys. Rev. **D3**, 2415 (1971).

[305] L. Alvarez-Gaume, P. H. Ginsparg, G. W. Moore, and C. Vafa, "An O(16) x O(16) Heterotic String", Phys. Lett. **B171**, 155 (1986).

[306] L. D. Faddeev and S. L. Shatashvili, "Algebraic and Hamiltonian Methods in the Theory of Nonabelian Anomalies", Theor. Math. Phys. **60**, 770 (1985).

[307] C. G. Callan Jr. and J. A. Harvey, "Anomalies and Fermion Zero Modes on Strings and Domain Walls", Nucl. Phys. **B250**, 427 (1985).

[308] G. Katsianis, I. Papadimitriou, K. Skenderis, and M. Taylor, "Anomalous Supersymmetry", Phys. Rev. Lett. **122**, 231602 (2019), arXiv:1902.06715 [hep-th].

[309] O. S. An, J. U. Kang, J. C. Kim, and Y. H. Ko, "Quantum consistency in supersymmetric theories with R-symmetry in curved space", JHEP **05**, 146 (2019), arXiv:1902.04525 [hep-th].

[310] I. Papadimitriou, "Supercurrent Anomalies in 4D SCFTs", JHEP **07**, 038 (2017), arXiv:1703.04299 [hep-th].

[311] J. Gomis, Z. Komargodski, H. Ooguri, N. Seiberg, and Y. Wang, "Shortening Anomalies in Supersymmetric Theories", JHEP **01**, 067 (2017), arXiv:1611.03101 [hep-th].

[312] I. García-Etxebarria and M. Montero, "Dai-Freed anomalies in particle physics", JHEP **08**, 003 (2019), arXiv:1808.00009 [hep-th].

[313] Z. Wan, J. Wang, and Y. Zheng, "Quantum 4d Yang-Mills Theory and Time-Reversal Symmetric 5d Higher-Gauge Topological Field Theory", Phys. Rev. **D100**, 085012 (2019), arXiv:1904.00994 [hep-th].

[314] M. Guo, K. Ohmori, P. Putrov, Z. Wan, and J. Wang, "Fermionic Finite-Group Gauge Theories and Interacting Symmetric/Crystalline Orders via Cobordisms", (2018), arXiv:1812.11959 [hep-th].

[315] J. Davighi, B. Gripaios, and N. Lohitsiri, "Global anomalies in the Standard Model(s) and Beyond", (2019), arXiv:1910.11277 [hep-th].

[316] J. McNamara and C. Vafa, "Cobordism Classes and the Swampland", (2019), arXiv:1909.10355 [hep-th].

[317] C. Córdova and K. Ohmori, "Anomaly Obstructions to Symmetry Preserving Gapped Phases", (2019), arXiv:1910.04962 [hep-th].

[318] C. Cordova, K. Ohmori, S.-H. Shao, and F. Yan, "Decorated $\mathbb{Z}_2$ Symmetry Defects and Their Time-Reversal Anomalies", (2019), arXiv:1910.14046 [hep-th].

[319] I. Hason, Z. Komargodski, and R. Thorngren, "Anomaly Matching in the Symmetry Broken Phase: Domain Walls, CPT, and the Smith Isomorphism", (2019), arXiv:1910.14039 [hep-th].

[320] J. Wang, Y.-Z. You, and Y. Zheng, "Gauge Enhanced Quantum Criticality and Time Reversal Domain Wall: SU(2) Yang-Mills Dynamics with Topological Terms", (2019), arXiv:1910.14664 [cond-mat.str-el].

[321] R. C. Kirby and L. R. Taylor, "Pin structures on low-dimensional manifolds", in Geometry of low-dimensional manifolds, 2, Vol. 151, London Mathematical Society Lecture Note Series (1990), pp. 177–242.

[322] M. F. Atiyah, "Riemann surfaces and spin structures", Annales Scientifiques de L'École Normale Supérieure **4**, 47 (1971).

[323] C. Arf, "Untersuchungen über quadratische Formen in Körpern der Charakteristik 2. I", J. Reine Angew. Math. **183**, 148 (1941).

[324] D. Johnson, "Spin structures and quadratic forms on surfaces", Journal of the London Mathematical Society **2**, 365 (1980).

[325] A. Sen, "NonBPS states and Branes in string theory", in Supersymmetry in the theories of fields, strings and branes. Proceedings, Advanced School, Santiago de Compostela, Spain, July 26-31, 1999 (1999), pp. 187–234, arXiv:hep-th/9904207 [hep-th].

[326] F. Pollmann, E. Berg, A. M. Turner, and M. Oshikawa, "Symmetry protection of topological phases in one-dimensional quantum spin systems", Physical Review B **85**, 075125 (2012), arXiv:0909.4059 [cond-mat.str-el].

[327] M. Oshikawa, "The Haldane Phase as a Symmetry-Protected Topological Phase and Quantum Entanglement", (2010).

[328] S. Ryu and T. Takayanagi, "Topological Insulators and Superconductors from D-Branes", Phys. Lett. **B693**, 175 (2010), arXiv:1001.0763 [hep-th].

[329] S. Ryu and T. Takayanagi, "Topological Insulators and Superconductors from String Theory", Phys. Rev. **D82**, 086014 (2010), arXiv:1007.4234 [hep-th].

[330] A. Kitaev, "Periodic Table for Topological Insulators and Superconductors", AIP Conf. Proc. **1134**, 22 (2009), arXiv:0901.2686 [cond-mat.mes-hall].

[331] S. Ryu, A. P. Schnyder, A. Furusaki, and A. W. W. Ludwig, "Topological Insulators and Superconductors: Tenfold Way and Dimensional Hierarchy", New J. Phys. **12**, 065010 (2010).

[332] E. P. c. Witten.

[333] E. H. Brown Jr., "Generalizations of the Kervaire invariant", Ann. of Math. (2) **95**, 368 (1972).

[334] A. Turzillo, "Diagrammatic State Sums for 2D Pin-Minus TQFTs", (2018), arXiv:1811.12654 [math.QA].

[335] A. Debray and S. Gunningham, "The Arf-Brown TQFT of Pin$^-$ Surfaces", (2018), arXiv:1803.11183 [math-ph].

[336] R. Kobayashi, "Pin TQFT and Grassmann Integral", (2019), arXiv:1905.05902 [cond-mat.str-el].

[337] L. J. Dixon and J. A. Harvey, "String Theories in Ten-Dimensions Without Space-Time Supersymmetry", Nucl. Phys. **B274**, 93 (1986).

[338] E. Witten, "Global Anomalies in String Theory", in Symposium on Anomalies, Geometry, Topology Argonne, Illinois, March 28-30, 1985 (1985).

[339] Y. Tachikawa and K. Yonekura, "Why are Fractional Charges of Orientifolds Compatible with Dirac Quantization?", SciPost Phys. **7**, 058 (2019), arXiv:1805.02772 [hep-th].

[340] G. Y. Cho, K. Shiozaki, S. Ryu, and A. W. W. Ludwig, "Relationship between Symmetry Protected Topological Phases and Boundary Conformal Field Theories via the Entanglement Spectrum", J. Phys. **A50**, 304002 (2017), arXiv:1606.06402 [cond-mat.str-el].

[341] K. Shiozaki, H. Shapourian, and S. Ryu, "Many-body topological invariants in fermionic symmetry-protected topological phases", Phys. Rev. **B95**, 205139 (2017), arXiv:1609.05970 [cond-mat.str-el].

[342] R. Blumenhagen, A. Font, and D. Lust, "Tachyon free orientifolds of type 0B strings in various dimensions", Nucl. Phys. **B558**, 159 (1999), arXiv:hep-th/9904069 [hep-th].

[343] C. Angelantonj and A. Armoni, "Nontachyonic type 0B orientifolds, nonsupersymmetric gauge theories and cosmological RG flow", Nucl. Phys. **B578**, 239 (2000), arXiv:hep-th/9912257 [hep-th].

[344] A. Sen, "Tachyon condensation on the brane anti-brane system", JHEP **08**, 012 (1998), arXiv:hep-th/9805170 [hep-th].

[345] S. Gukov, "K theory, reality, and orientifolds", Commun. Math. Phys. **210**, 621 (2000), arXiv:hep-th/9901042 [hep-th].

[346] M. F. Atiyah, "K-THEORY AND REALITY", Quart. J. Math. Oxford Ser. **17**, 367 (1966).

[347] M. F. Atiyah, R. Bott, and A. Shapiro, "Clifford modules", Topology **3**, 3 (1964).

[348] C. T. C. Wall, "Graded Brauer groups", J. Reine Angew. Math. **213**, 187 (1963).

[349] D. Stanford and E. Witten, "JT Gravity and the Ensembles of Random Matrix Theory", (2019), arXiv:1907.03363 [hep-th].

[350] D. Gao and K. Hori, "On the Structure of the Chan-Paton Factors for D-Branes in Type II Orientifolds", (2010), arXiv:1004.3972 [hep-th].

[351] O. Bergman, "Tachyon condensation in unstable type I D-brane systems", JHEP **11**, 015 (2000), arXiv:hep-th/0009252 [hep-th].

[352] T. Asakawa, S. Sugimoto, and S. Terashima, "Exact description of D branes via tachyon condensation", JHEP **02**, 011 (2003), arXiv:hep-th/0212188 [hep-th].

[353] A. Sen, "Stable nonBPS states in string theory", JHEP **06**, 007 (1998), arXiv:hep-th/9803194 [hep-th].

[354] A. Sen, "Stable nonBPS bound states of BPS D-branes", JHEP **08**, 010 (1998), arXiv:hep-th/9805019 [hep-th].

[355] O. Bergman and M. R. Gaberdiel, "Stable nonBPS D particles", Phys. Lett. **B441**, 133 (1998), arXiv:hep-th/9806155 [hep-th].

[356] M. Frau, L. Gallot, A. Lerda, and P. Strigazzi, "Stable nonBPS D-branes in type I string theory", Nucl. Phys. **B564**, 60 (2000), arXiv:hep-th/9903123 [hep-th].

[357] M. R. Gaberdiel, "Lectures on nonBPS Dirichlet branes", Class. Quant. Grav. **17**, 3483 (2000), arXiv:hep-th/0005029 [hep-th].

[358] J. F. Davis and P. Kirk, *Lecture notes in algebraic topology*, Vol. 35, Graduate Studies in Mathematics (American Mathematical Society, Providence, RI, 2001), pp. xvi+367.

[359] R. Thorngren, "Anomalies and Bosonization", (2018), arXiv:1810.04414 [cond-mat.str-el].

[360] P. Teichner, "On the signature of four-manifolds with universal covering spin", Math. Ann. **295**, 745 (1993).

[361] A. V. Zhubr, in *Topology, ergodic theory, real algebraic geometry*, Vol. 202, Amer. Math. Soc. Transl. Ser. 2 (Amer. Math. Soc., Providence, RI, 2001), pp. 263–286.

[362] R. Blumenhagen, D. Lüst, and S. Theisen, *Basic concepts of string theory*, Theoretical and Mathematical Physics (Springer, Heidelberg, Germany, 2013).

[363] O. Bergman and M. R. Gaberdiel, "A Nonsupersymmetric open string theory and S duality", Nucl. Phys. **B499**, 183 (1997), arXiv:hep-th/9701137 [hep-th].

[364] I. R. Klebanov and A. A. Tseytlin, "D-branes and dual gauge theories in type 0 strings", Nucl. Phys. **B546**, 155 (1999), arXiv:hep-th/9811035 [hep-th].

[365] M. Billo, B. Craps, and F. Roose, "On D-branes in type 0 string theory", Phys. Lett. **B457**, 61 (1999), arXiv:hep-th/9902196 [hep-th].

[366] W. Fischler and L. Susskind, "Dilaton Tadpoles, String Condensates and Scale Invariance", Phys. Lett. **B171**, 383 (1986).

[367] W. Fischler and L. Susskind, "Dilaton Tadpoles, String Condensates and Scale Invariance. 2.", Phys. Lett. **B173**, 262 (1986).

[368] M. F. Atiyah, V. K. Patodi, and I. M. Singer, "Spectral asymmetry and Riemannian geometry 2", Math. Proc. Cambridge Phil. Soc. **78**, 405 (1976).

[369] X. Chen, Z.-C. Gu, Z.-X. Liu, and X.-G. Wen, "Symmetry protected topological orders and the group cohomology of their symmetry group", Phys. Rev. **B87**, 155114 (2013), arXiv:1106.4772 [cond-mat.str-el].

[370] D. Davis, "Generalized homology and the vector field problem", The Quarterly Journal of Mathematics **25**, 169 (1974).

[371] R. E. Stong, "Determination of $H^*(BO(k,\ldots,\infty),Z_2)$ and $H^*(BU(k,\ldots,\infty),Z_2)$", Transactions of the American Mathematical Society **107**, 526 (1963).

[372] D. W. Anderson, E. H. Brown Jr., and F. P. Peterson, "The structure of the Spin cobordism ring", Ann. of Math. (2) **86**, 271 (1967).

[373] A. Beaudry and J. Campbell, "A guide for computing stable homotopy groups", Contemporary Mathematics, 89 (2018), arXiv:1801.07530 [math.AT].

[374] J. A. Campbell, "Homotopy theoretic classification of symmetry protected phases", (2017), arXiv:1708.04264 [math.AT].